AP600 DOCUMENT COVER SHEET

TDC: _____ IDS: I _____ S _____

Form 58202G(5/94)

AP600 CENTRAL FILE USE ONLY:

0058.FRM

RFS#: RFS ITEM #:

AP600 DOCUMENT NO.	REVISION NO.		ASSIGNED TO
PCS-GSR-009	0	Page 1 of (XXX)	W-PIPLICA

ALTERNATE DOCUMENT NUMBER: WCAP-14383 WORK BREAKDOWN #: 3.1.1.9.7

DESIGN AGENT ORGANIZATION: WESTINGHOUSE

TITLE: WGOTHIC CODE DESCRIPTION AND VALIDATION

ATTACHMENTS: N/A	DCP #/REV. INCORPORATED IN THIS DOCUMENT REVISION: N/A
CALCULATION/ANALYSIS REFERENCE: 522	

ELECTRONIC FILENAME	ELECTRONIC FILE FORMAT	ELECTRONIC FILE DESCRIPTION
U:\(2026w).NON	WordPerfect 5.1 WINDOWS	DOCUMENT TEXT AND FIGURES

☐ WESTINGHOUSE PROPRIETARY CLASS 2

This document contains information proprietary to Westinghouse Electric Corporation; it is submitted in confidence and is to be used solely for the purpose for which it is furnished and returned upon request. This document and such information is not to be reproduced, transmitted, disclosed or used otherwise in whole or in part without prior written authorization of Westinghouse Electric Corporation, Energy Systems Business Unit, subject to the legends contained hereof.

☐ WESTINGHOUSE PROPRIETARY CLASS 2C

This document is the property of and contains Proprietary Information owned by Westinghouse Electric Corporation and/or its subcontractors and suppliers. It is transmitted to you in confidence and trust, and you agree to treat this document in strict accordance with the terms and conditions of the agreement under which it was provided to you.

☒ WESTINGHOUSE CLASS 3 (NON PROPRIETARY)

COMPLETE 1 IF WORK PERFORMED UNDER DESIGN CERTIFICATION OR COMPLETE 2 IF WORK PERFORMED UNDER FOAKE.

1 ☒ **DOE DESIGN CERTIFICATION PROGRAM** – GOVERNMENT LIMITED RIGHTS STATEMENT [See page 2]

Copyright statement: A license is reserved to the U.S. Government under contract DE-AC03-90SF18495.

☐ DOE CONTRACT DELIVERABLES (DELIVERED DATA)

Subject to specified exceptions, disclosure of this data is restricted until September 30, 1995 or Design Certification under DOE contract DE-AC03-90SF18495, whichever is later.

EPRI CONFIDENTIAL: NOTICE: 1 ☒ 2 ☐ 3 ☐ 4 ☐ 5 ☐ CATEGORY: A ☒ B ☐ C ☐ D ☐ E ☐ F ☐

2 ☐ **ARC FOAKE PROGRAM** – ARC LIMITED RIGHTS STATEMENT [See page 2]

Copyright statement: A license is reserved to the U.S. Government under contract DE-FC02-NE34267 and subcontract ARC-93-3-SC-001.

☐ ARC CONTRACT DELIVERABLES (CONTRACT DATA)

Subject to specified exceptions, disclosure of this data is restricted under ARC Subcontract ARC-93-3-SC-001.

ORIGINATOR	SIGNATURE/DATE	
R. P. Ofstun	R. P. Ofstun	
AP600 RESPONSIBLE MANAGER	SIGNATURE*	APPROVAL DATE
J. A. Gresham	J. A. Gresham	6/28/95

*Approval of the responsible manager signifies that document is complete, all required reviews are complete, electronic file is attached and document is released for use.

Form 58202G(5/94)

LIMITED RIGHTS STATEMENTS

DOE GOVERNMENT LIMITED RIGHTS STATEMENT

(A) These data are submitted with limited rights under government contract No. DE-AC03-90SF18495. These data may be reproduced and used by the government with the express limitation that they will not, without written permission of the contractor, be used for purposes of manufacturer nor disclosed outside the government; except that the government may disclose these data outside the government for the following purposes, if any, provided that the government makes such disclosure subject to prohibition against further use and disclosure:
(I) This "Proprietary Data" may be disclosed for evaluation purposes under the restrictions above.
(II) The "Proprietary Data" may be disclosed to the Electric Power Research Institute (EPRI), electric utility representatives and their direct consultants, excluding direct commercial competitors, and the DOE National Laboratories under the prohibitions and restrictions above.

(B) This notice shall be marked on any reproduction of these data, in whole or in part.

ARC LIMITED RIGHTS STATEMENT:

This proprietary data, furnished under Subcontract Number ARC-93-3-SC-001 with ARC may be duplicated and used by the government and ARC, subject to the limitations of Article H-17.F. of that subcontract, with the express limitations that the proprietary data may not be disclosed outside the government or ARC, or ARC's Class 1 & 3 members or EPRI or be used for purposes of manufacture without prior permission of the Subcontractor, except that further disclosure or use may be made solely for the following purposes:

This proprietary data may be disclosed to other than commercial competitors of Subcontractor for evaluation purposes of this subcontract under the restriction that the proprietary data be retained in confidence and not be further disclosed, and subject to the terms of a non-disclosure agreement between the Subcontractor and that organization, excluding DOE and its contractors.

DEFINITIONS

CONTRACT/DELIVERED DATA — Consists of documents (e.g. specifications, drawings, reports) which are generated under the DOE or ARC contracts which contain no background proprietary data.

EPRI CONFIDENTIALITY / OBLIGATION NOTICES

NOTICE 1: The data in this document is subject to no confidentiality obligations.

NOTICE 2: The data in this document is proprietary and confidential to Westinghouse Electric Corporation and/or its Contractors. It is forwarded to recipient under an obligation of Confidence and Trust for limited purposes only. Any use, disclosure to unauthorized persons, or copying of this document or parts thereof is prohibited except as agreed to in advance by the Electric Power Research Institute (EPRI) and Westinghouse Electric Corporation. Recipient of this data has a duty to inquire of EPRI and/or Westinghouse as to the uses of the information contained herein that are permitted.

NOTICE 3: The data in this document is proprietary and confidential to Westinghouse Electric Corporation and/or its Contractors. It is forwarded to recipient under an obligation of Confidence and Trust for use only in evaluation tasks specifically authorized by the Electric Power Research Institute (EPRI). Any use, disclosure to unauthorized persons, or copying this document or parts thereof is prohibited except as agreed to in advance by EPRI and Westinghouse Electric Corporation. Recipient of this data has a duty to inquire of EPRI and/or Westinghouse as to the uses of the information contained herein that are permitted. This document and any copies or excerpts thereof that may have been generated are to be returned to Westinghouse, directly or through EPRI, when requested to do so.

NOTICE 4: The data in this document is proprietary and confidential to Westinghouse Electric Corporation and/or its Contractors. It is being revealed in confidence and trust only to Employees of EPRI and to certain contractors of EPRI for limited evaluation tasks authorized by EPRI. Any use, disclosure to unauthorized persons, or copying of this document or parts thereof is prohibited. This Document and any copies or excerpts thereof that may have been generated are to be returned to Westinghouse, directly or through EPRI, when requested to do so.

NOTICE 5: The data in this document is proprietary and confidential to Westinghouse Electric Corporation and/or its Contractors. Access to this data is given in Confidence and Trust only at Westinghouse facilities for limited evaluation tasks assigned by EPRI. Any use, disclosure to unauthorized persons, or copying of this document or parts thereof is prohibited. Neither this document nor any excerpts therefrom are to be removed from Westinghouse facilities.

EPRI CONFIDENTIALITY / OBLIGATION CATEGORIES

CATEGORY "A" — (See Delivered Data) Consists of CONTRACTOR Foreground Data that is contained in an issued reported.

CATEGORY "B" — (See Delivered Data) Consists of CONTRACTOR Foreground Data that is not contained in an issued report, except for computer programs.

CATEGORY "C" — Consists of CONTRACTOR Background Data except for computer programs.

CATEGORY "D" — Consists of computer programs developed in the course of performing the Work.

CATEGORY "E" — Consists of computer programs developed prior to the Effective Date or after the Effective Date but outside the scope of the Work.

CATEGORY "F" — Consists of administrative plans and administrative reports.

WCAP-14383

W GOTHIC CODE DESCRIPTION AND VALIDATION

May 1995

by

M. Kennedy
R. Ofstun
D. Spencer
K. Howe
D. Paulsen
J. Woodcock

WESTINGHOUSE ELECTRIC CORPORATION
Energy Systems Business Unit
Nuclear Technology Division
P.O. Box 355
Pittsburgh, Pennsylvania 15230-0355

TABLE OF CONTENTS

TABLE OF CONTENTS (Continued)

TABLE OF CONTENTS (Continued)

LIST OF TABLES

LIST OF FIGURES

LIST OF FIGURES (Continued)

LIST OF FIGURES (Continued)

LIST OF FIGURES (Continued)

LIST OF FIGURES (Continued)

LIST OF FIGURES (Continued)

SUMMARY

Westinghouse's advanced nuclear plant concept uses a passive containment cooling system (PCS) that relies on natural forces, such as buoyancy-driven circulation, condensation, evaporation and radiation to remove heat released to the containment following postulated events, such as a loss-of-coolant accident (LOCA) or a main steam line break (MSLB). The containment pressure and temperature response following a design basis accident (DBA) must be calculated using a validated computer model to determine if the peak values will remain below the design criteria. The first step in producing a computer model that is capable of modeling the PCS is to identify the important phenomena that must be included in the model. This is described in Section 1.0.

Westinghouse reviewed the existing containment analysis codes to determine which most closely met the requirements identified in the phenomena identification and ranking table (PIRT). The GOTHIC computer code was selected for further development based on its impressive validation history and 3-D modeling capability. Section 2.0 of this report provides a description of the changes made to the GOTHIC code to incorporate mechanistic heat and mass transfer correlations and wall-to-wall radiant heat transfer for modeling the PCS.

The PCS has undergone an extensive testing program. Both separate effects tests and integral tests were performed to demonstrate the mechanisms of heat and mass transfer used in the passive containment cooling system. These test data, along with other publicly available test data, have been used to validate the PCS heat and mass transfer models and their integration into the GOTHIC code. The code validation requirements and PCS test program overview is provided in Section 3.0.

The separate effects validation is described in Section 4.0. The correlations selected for modeling heat and mass transfer in the PCS were found to yield acceptable results with mean predicted-to-measured heat and mass transfer ratios near 1.0 over the expected range of dimensionless parameters during DBA events in the AP600.

The development of the WGOTHIC distributed and lumped parameter models to be used in the integrated effects test comparison and noding sensitivity studies using these models are described in Sections 5.0 through 7.0. The AP600 containment distributed and lumped parameter noding structures to be used in the DBA evaluation model were developed based on the results of these noding sensitivity studies.

The results of the integrated effects code validation test comparison with data from the Westinghouse Large-Scale Test (LST) program are provided in Section 8.0. The distributed parameter model was found to yield acceptable results in all of the important validation parameters (pressure, local temperatures, local velocities, noncondensible gas concentrations, etc.). The lumped parameter model causes compensating errors with respect to velocity and the noncondensible gas distribution and as a result over-predicts the global pressure.

An assessment of the code uncertainty is presented in Section 9.0. Within the range of parameters characterizing the LST, the pressure at 95 percent confidence is 1.037 times the pressure predicted by the distributed parameter evaluation model and 0.975 times the pressure predicted by the lumped parameter model.

ACKNOWLEDGEMENTS

The authors gratefully acknowledge significant contributions from the following people: Dr. L. E. Hochreiter for ground breaking development of the methodology applied; P. Shipe for his painstaking verification of the WGOTHIC coding; A. Forgie for his efforts in producing the large-scale test data comparison plots; and P. Kennevan and T. Miele for their efforts in reducing the large-scale test data.

DIMENSIONLESS GROUPS

Grashof Number

$$Gr = \frac{g\beta\rho_f^2 (T_w - T_\infty) L^3}{\mu^2} \quad (1)$$

or

$$Gr = \frac{g\rho_f (\rho_\infty - \rho_w) L^3}{\mu^2} \quad (2)$$

Nusselt Number

$$Nu = \frac{h_c L}{k} \quad (3)$$

Prandtl Number

$$Pr = \frac{\mu C_p}{k} \quad (4)$$

Reynolds Number

$$Re = \frac{\rho_f v L}{\mu} \quad (5)$$

Schmidt Number

$$Sc = \frac{\mu}{\rho_f D_v} \tag{6}$$

Sherwood Number

$$Sh = \frac{k_G R T p_{BM} L}{D_v P} \tag{7}$$

where:

C_p = specific heat of gas mixture (Btu/lb_m/°F)
D_v = air-water vapor diffusion coefficient ($ft.^2$/sec.)
g = gravitational acceleration (ft./$sec.^2$)
h_c = convective heat transfer coefficient (Btu/$ft.^2$/sec./°F)
k = thermal conductivity of gas mixture in volume (Btu/ft./sec./°F)
k_G = gas mass transfer coefficient (lb-mol/hr/$ft.^2$/atm)
L = characteristic length (ft.)
P = total pressure (psi)
p_{BM} = log mean pressure of noncondensible gas
R = universal gas constant (psi-ft^3/lb-mol/R)
T = temperature (°F)
T_w = temperature of conductor surface (°F)
T_∞ = reference temperature (°F)
v = bulk velocity (ft./sec.)
β = thermal expansion coefficient (1/R)
μ = gas mixture viscosity (lb_m/ft./sec.)
ρ_f = density of mixture at boundary layer (lb_m/$ft.^3$)
ρ_w = density of mixture at the wall (lb_m/$ft.^3$)
ρ_∞ = reference mixture density (lb_m/$ft.^3$)

1.0 INTRODUCTION

Westinghouse's advanced nuclear plant concept uses a passive containment cooling system (PCS) to remove heat released to the containment following postulated events, such as a loss-of-coolant accident (LOCA) or a main steam line break (MSLB). The system uses passive or natural draft air cooling to transfer heat from the containment vessel to the environment, along with provisions for wetting the exterior of the shell to allow evaporative cooling. Air enters an annular space between the containment vessel and the concrete shield building through inlets in the shield building wall. The exterior heat transfer may be enhanced by covering the surface exposed to the air flow with a thin evaporating water film, which is deposited on the surface by passive means. The air then rises in the annulus as a result of the natural draft developed as the air is heated by the containment surface. The heated air exits the shield building through an outlet (chimney) located above the containment shell. Heat is transferred from the containment vessel and the shield building surfaces by natural convection and by evaporation on wetted surfaces. Heat is also transferred from the containment vessel to the adjacent wall inner surface by radiation.

Current requirements for containment analyses, arising from the reliance on passive cooling, have led to a need for computer models that can calculate the fluid distributions within a containment volume and the heat and mass transfer through external annuli. In such models, steam and noncondensibles within the containment volume can be tracked separately, and fluid conditions in the regions near the structures are available. Since heat and mass transfer to structures (internal heat sinks and the containment shell) are governed by local conditions within the given boundary layer, heat transfer should be correlated to conditions as near the boundary layer as possible.

The correlations to model heat transfer in containments are inseparable from the formulation of the computer code in which they are used. The correlations typically used by containment-pressurization transient-analysis codes, such as the Tagami[1] correlation for internal condensation, have a test basis. These types of correlations are intended for use in containment analysis codes based on conservation equations written for a single, large control volume representing the entire containment. The use of a single containment control volume requires that the heat transfer correlations themselves inherently include the effects of flow fields within the containment. Computations with such an approach are straightforward, however, such an approach raises questions when finer detail is required for internal containment modeling. Another difficulty in using a total heat transfer coefficient, such as Tagami's, is determining how to apportion the total heat transfer between convective and condensing heat transfer. Treating the containment interior as a single volume does not allow explicit calculation of the distribution of noncondensibles and the resulting surface temperature and heat flux distributions. Therefore, a methodology has been developed that includes a more complete formulation of the thermal-hydraulic equations linked with correlations based on bulk fluid conditions relatively near a surface to provide spatially distributed conditions within containment.

The computer code and the associated noding structure that were developed for modeling a PCS-type containment are described in this report. This report also provides a summary of the separate effects validation tests of the code (to validate the selected heat and mass transfer correlations in the code) and detailed results from the integral validation tests of the computer model.

The first step in producing this computer model is to identify the important phenomena that must be considered in the application. This is summarized in the next section.

1.1 Summary of Passive Cooling System (PCS) Phenomena Identification and Ranking Table (PIRT)

The mass, momentum, and energy transport processes important to the AP600 containment pressure during a loss-of-coolant accident (LOCA) or main steam-line break (MSLB) transient were identified and ranked by their relative importance in the scaling analysis.[2,3] It was determined that the processes and components of primary importance are the following:

- Transfer processes
  - Condensation mass transfer inside containment.
  - Evaporation mass transfer outside containment.
  - The energy carried by the condensed liquid on the internal shell and heat sinks.
  - The subcooled heat capacity of the external liquid is of primary importance for some of the large-scale tests and is second-order for AP600.
  - Conduction heat transfer through the shell and its coatings.
  - The convective air flow rate between subcompartments and up the riser.
  - The velocity, temperature, and concentration fields as they influence the mass transfer process.
- Components
  - Containment atmosphere.
  - Area of the external shell surface that is wetted by the external water film.
  - The transient heat capacity of the shell and internal heat sinks.
  - The break pool in the bottom of reactor and steam generator cavities may become a modest steam source after several thousand seconds.

When it is postulated that the external shell is not wetted and the resulting containment pressure is required, the dominant heat rejection mechanisms for the external shell are the following:

- Convection heat transfer to the riser air
- Radiation heat transfer to the baffle with subsequent baffle heat transfer

The baffle will release energy by forced convection heat transfer to the riser and downcomer air and by radiation to the inner surface of the shield building. The shield building will release energy by forced convection heat transfer to the downcomer air and free convection heat transfer to the ambient air.

2.0 WGOTHIC CODE DESCRIPTION

The passive containment cooling system (PCS) phenomena were identified and ranked by order of importance in determining the vessel pressure in a phenomena identification and ranking table (PIRT). The important phenomena were summarized in Section 1.1. Existing containment analysis codes were reviewed to determine which most closely met the requirements identified in the PIRT. Although none of the codes met all of the requirements, the GOTHIC code was selected for further development based on its impressive validation history and 3-D modeling capability. This section describes the changes made to the GOTHIC code to incorporate the special heat and mass transfer correlations and wall-to-wall radiation model for performing design-basis analyses for PCS-type containments.

2.1 GOTHIC Code Overview

The GOTHIC code[32, 33] is a state-of-the-art program for modeling multi-phase flow. The GOTHIC code has been developed through a long history from other qualified thermal-hydraulic computer codes (as shown in Figure 2-1). GOTHIC actually consists of three separate programs. The preprocessor allows the user to rapidly create and modify an input model. The solver performs the numerical solution for the problem. The postprocessor, in conjunction with the preprocessor, allows the user to rapidly create graphical and tabular outputs for virtually any parameter in the model.

GOTHIC solves the integral form of the conservation equations for mass, momentum, and energy for multicomponent, two-phase flow. The conservation equations are solved for three fields; continuous liquid, liquid drops, and the steam/gas phase. The three fields may be in thermal nonequilibrium within the same computational cell. This would allow the modeling of subcooled drops (for example, containment spray) falling through an atmosphere of saturated steam. The gas component of the steam/gas field can be comprised of up to eight different noncondensable gases with mass balances performed for each component. Relative velocities are calculated for each field as well as the effects of two-phase slip on pressure drop. Heat transfer between the phases, surfaces, and the fluid are also allowed.

The GOTHIC code is capable of performing calculations in three modes. The code can be used in the lumped-parameter nodal-network mode, the two-dimensional distributed parameter mode, and the three-dimensional distributed parameter mode. Each of these modes may be used within the same model (as shown in Figure 2-2). The capability of multi-dimensional analyses greatly enhances the ability to study noncondensables and stratification as well as allowing the calculation of flow field details within any given volume. The flexible noding and conservation equation solutions in the GOTHIC code allow its application to a wide variety of problems, not necessarily just containment pressure and temperature calculations. A more detailed discussion of how these features are used in containment modeling is given in Section 5-1.

The GOTHIC code also contains the options to model a large number of structures and components. These include, but are not limited to, heated and unheated conductors, pumps, fans, a variety of heat

exchangers, and ice condensers. These components can be coupled to represent the various systems found in any typical containment.

The GOTHIC containment analysis code was modified by Westinghouse to include mechanistic convective heat and mass transfer correlations, a liquid film tracking model, a one-dimensional wall conduction model, and wall-to-wall radiant heat transfer to model heat removal by the PCS. The code with modifications is called Westinghouse-GOTHIC and abbreviated as WGOTHIC.

The three programs that make up the WGOTHIC code—solver version 1.2, pre-processor version number 2.0 and post-processor version 1.0—are based on GOTHIC code version 3.4d as described in NAI 8907-06[4]. The pre-processor (input handler) and solver (numerical solution) programs contain the code modifications to incorporate the PCS models. Changes were made to the pre-processor program to assist the user in setting up model input. These changes were verified by hand. Changes to the solver program are described in the sections that follow.

2.2 The WGOTHIC Clime Model

A solution technique that includes wall-to-wall radiation necessitates a close coupling between the involved walls. This coupling is accomplished by assigning boundaries that define the portions of the various walls that radiate to each other. In keeping with the GOTHIC formulation[32,33], which considers conductors, or heat sinks, to be energy source (or sink) terms, the core modifications made to include wall-to-wall radiant heat transfer can be thought of as the addition of a special type of conductor group. This new conductor group consists of a set of walls that radiate to each other and interface with GOTHIC fluid cells through mass and energy source terms. To distinguish this type of conductor from the existing GOTHIC terminology, the term *Clime*, meaning a *region*, is used.

A Clime is depicted in Figure 2-3. This Clime is a horizontal slice consisting of the heat and mass transfer source terms from the vessel volume to the wall, conduction through the vessel wall, heat and mass transfer source terms from the vessel wall to the air-flow channel, radiation from the vessel wall to the baffle wall, heat transfer source terms from the baffle wall to the air flow channel, conduction through the baffle wall, and radiation and convective heat transfer from the baffle wall to the environment. The vessel volume, air-flow channel volume and environment volume are separate computational cells (fluid volumes) in WGOTHIC. The vessel and baffle wall are one-dimensional conductors representing solid walls between the computational cells. These conductors may be subdivided into regions of different materials, of different solution mesh size, or both.

Climes may be stacked on top of one another in a model. The change in liquid flow rate on the conductor surfaces is tracked from Clime-to-Clime in a stack. For example, two stacked sets of Climes are used in the PCS model to simulate the wetting of the containment shell by an applied external film. A water flow is input to the shell conductor surface of the top Clime of one stack (the "wet" stack) while the Clime shell conductor surfaces of the other stack are kept dry. The film flow rate between the Clime shell conductor surfaces in the wet stack is reduced as water evaporates.

The radiation boundary conditions implicitly couple the temperature of Clime surfaces that face each other, such as the outer surface of the vessel wall with the inner surface of the baffle wall. All other surface temperatures are coupled to a boundary temperature. All Clime surfaces are coupled explicitly to the computational cells (fluid volumes) for convective heat and mass transfer.

Figure 2-3 also illustrates the wall heat source terms that represent the heat and mass transfer within a Clime. Positive heat flow is defined as moving from left to right. Convective heat transfer, steam condensation, conduction, liquid film evaporation, wall-to-wall radiation, and film enthalpy transport are modeled in a Clime. The details of the Clime conductor are described in the sections that follow.

2.3 Clime Heat and Mass Transfer Models

Heat transfer is driven by a temperature gradient, and mass transfer is driven by a concentration gradient. Given a mixture of gases A and B, where B is noncondensible and A is transferred to (or from) the bulk gas from (or to) the liquid film, the mass transfer equation for gas A is shown below:

$$G = k_G M_A (p_{Ai} - p_{AG}) \qquad (2\text{-}1)$$

where:

G	=	condensing or evaporating mass flux	(lbm/hr-ft.^{2})
k_G	=	mass transfer coefficient	(lbm-mole/hr-ft.^{2}-psi)
M_A	=	molecular weight of gas A	(lbm/lbm-mole)
p_{Ai}	=	partial pressure of gas A at the interface	(psi)
p_{AG}	=	partial pressure of gas A in the bulk gas mixture	(psi)

The mass transfer coefficient, k_G, can be predicted using empirical correlations similar to the heat transfer coefficient, h_C. The Sherwood number for mass transfer is analogous to the Nusselt number for heat transfer. The Sherwood number for gas-phase mass transfer is shown below.

$$Sh = \frac{k_G R T p_{BM} L}{D_v P} \qquad (2\text{-}2)$$

where:

R	=	universal gas constant	(ft.^{3}-psi/R-lbm-mole)
T	=	boundary layer temperature $(T_{film} + T_{bulk})/2$	(R)
p_{BM}	=	log mean partial pressure $(p_{BG} - p_{Bi})/\ln (p_{BG}/p_{Bi})$	(psi)
L	=	characteristic length	(ft.)
D_v	=	diffusion coefficient	(ft.^{2}/hr)
P	=	total pressure	(psi)

An empirical correlation for the Sherwood number, which is derived by dimensional analysis using the Reynolds analogy and Colburn j factors for heat and mass transfer, is shown below.

$$Sh = \frac{Nu}{(Pr/Sc)^{1/3}} \tag{2-3}$$

where:

Nu	=	Nusselt number based on the heat transfer correlation evaluated at the boundary layer temperature
Pr	=	Prandtl number evaluated at the boundary layer temperature
Sc	=	Schmidt number evaluated at the boundary layer temperature

This correlation is used in WGOTHIC to calculate both condensation and evaporation mass transfer from the heat transfer correlation.

The convective heat transfer in any large containment vessel will primarily be turbulent rather than laminar. Heat transfer from the small fraction of area in the laminar heat transfer regime will be underpredicted using the turbulent convection heat transfer correlations and therefore, a laminar heat transfer correlation has not been included in the WGOTHIC code. The flow regime for turbulent convective heat transfer is typically qualified as either free, forced, or mixed. The combination of free and forced convection in the mixed regime is either assisting (that is, they work in the same direction, as in upward flow in a hot pipe) or opposed (that is, they work against each other, as in downward flow in a hot pipe).

Based on a review of the literature, the free convection heat transfer correlation for gas mixtures has the form $Nu = C\,(GrPr)^N$, with the value of C varying between 0.09 and 0.15 and the value of N varying between 0.3 and 0.4. Approximately 95 percent of the condensing shell surface is expected to operate in the turbulent ($Gr > 10^{10}$) free convection range. Data in the turbulent free convection range are reasonably fit using a value of 1/3 for N. A value of 0.13 for C provides a reasonable fit for the large-scale PCS data, as shown in Section 4.3.

The McAdams[5] correlation, shown below, has been incorporated into WGOTHIC for calculating turbulent free convection heat transfer on the inside, condensing surface of the containment shell.

$$Nu_{free} = 0.13(Gr_x\ Pr)^{1/3} \tag{2-4}$$

The same correlation, with the characteristic length in the Grashof number based on channel diameter instead of the distance, is used to model turbulent free convection heat transfer in the PCS annulus. This correlation is widely used to calculate turbulent free convection heat transfer from both vertical and inclined flat plates with both constant temperature and constant heat flux boundary conditions.

The work of Vliet[6] shows that Equation (2-4) underpredicts the heat transfer from an inclined flat plate. Even though it may slightly underpredict heat transfer from the small fraction of the containment dome that can be considered a horizontal surface, Equation (2-4) will be used to conservatively calculate turbulent free convection heat transfer for the entire shell surface.

The Colburn[7] correlation, shown below, has been incorporated into WGOTHIC for calculating turbulent forced convection heat transfer in the PCS annulus.

$$Nu_{forc} = 0.023 Re_d^{4/5} Pr^{1/3} \qquad (2\text{-}5)$$

This correlation is applicable to both constant temperature and constant heat flux boundary conditions for fully developed flow in long ducts. This correlation is widely used to calculate turbulent forced convection heat transfer in long tubes and ducts. The annulus hydraulic diameter is used as the characteristic length in the Reynolds and Nusselt numbers.

The measured heat transfer coefficient at the entrance to a heated channel or plate is significantly higher than predicted by the Colburn forced convection heat transfer correlation. The increase in heat transfer at the entrance is attributed to the development of the boundary layer. The entrance effect is important in modeling heat transfer in short channels or plates (for example, some test assemblies), but is relatively unimportant for modeling heat transfer from a containment vessel due to its much larger L/d scale.

The correlation and coefficients recommended by Boelter, Young, and Iverson[8] are used to account for the entrance effect:

$$\frac{h_m}{h_\infty} = 1 + F_1 \frac{d}{L} \qquad (2\text{-}6)$$

where:

h_∞	=	the heat transfer coefficient calculated from the Colburn correlation
h_m	=	the mean or length average heat transfer coefficient over length L
F_1	=	a geometry-dependent constant multiplier from Burmeister[9]
d	=	channel diameter
L	=	channel length

An equation is needed that will give a length average heat transfer coefficient between x_1 and x_2. Given an equation for h(x), the average value of h on the interval (x_1,x_2) is

$$\bar{h}_{x_1,x_2} = \frac{1}{x_2-x_1}\int_{x_1}^{x_2} h(x)dx \qquad (2\text{-}7)$$

Analytically, $\bar{h}_{x_1,x_2}$ could be derived from the above definition over the interval (0, L), but the equation produces a singularity when this is attempted. A modest change to the exponent, however, results in

$$\frac{\bar{h}_{x_1,x_2}}{h_\infty} = 1 + F_1\frac{d\,(x_2^{.3}-x_1^{.3})}{L^{.3}(x_2-x_1)} \qquad (2\text{-}8)$$

a form that has the same average over length L, but with slightly lower values for small values of x, and with slightly higher values for higher values of x. Therefore, the calculated forced convection heat transfer coefficient multiplier is an input value that is dependent on the WGOTHIC model noding structure.

The flat plate correlation,[10] shown below, has been selected for calculating turbulent forced convection heat transfer inside containment.

$$Nu_{forc} = 0.0296Re_x^{4/5}Pr^{1/3} \qquad (2\text{-}9)$$

This correlation is applicable to an open geometry, therefore, the Re_x and Nu_x numbers are dependent on the heated length and not the channel hydraulic diameter.

For calculational purposes, a single correlation (or combination of free and forced convection correlations) is needed to cover the entire range of mixed convection. A method for calculating mixed free and forced convection heat transfer was recommended by Churchill[11] and is given below. For opposed free and forced convection,

$$Nu_c = (Nu_{free}^3+Nu_{forc}^3)^{1/3} \qquad (2\text{-}10)$$

and for assisting free and forced convection, Nu_c is the largest of the following three expressions:

$$\begin{matrix} \mathrm{abs}\left[\left(Nu_{free}^{3} - Nu_{forc}^{3}\right)\right]^{1/3} \\ Nu_{free} \\ 0.75Nu_{forc} \end{matrix} \qquad (2\text{-}11)$$

The lower limit in the latter equation, which prevents the value of Nu_c from going to zero when Nu_{free} and Nu_{forc} are equal, comes from Eckert and Diaguila.[12]

The method for calculating mixed convection heat transfer is asymptotic to both the individual free and forced convection correlations. Consequently, it is unnecessary to choose in advance whether the heat transfer regime is free, forced, or mixed in the analytical model.

2.4 Clime Film Model

The WGOTHIC Clime model tracks the temperature and thickness of water films that can form on or be applied to the various conductor surfaces of the Clime. A time-dependent water flow rate boundary condition can be specified for each surface of each conductor of the top Clime in a stack of Climes. The next Clime in the stack takes the film flow rate from each conductor surface of the previous Clime as input, then adds the local condensation rate or subtracts the local evaporation rate to determine the output water flow rate on each of its corresponding conductor surfaces. Liquid mass is conserved whenever a conductor surface dries out or the film reaches the bottom Clime in the stack. If a conductor surface of a Clime loses all of its liquid film flow (by evaporation, for example), the corresponding conductor surface of the next Clime on the stack will start with no flow. If a conductor surface of the bottom Clime in a stack of Climes were to have a water film remaining, this water would be added to the liquid field of the GOTHIC cell in contact with the wet surface or an alternate drain cell specified by user input.

A Reynolds number is used to characterize the different types of film flow regimes. The liquid film Reynolds number is given by

$$Re = \frac{4\Gamma}{\mu}$$

where:

Γ = flow film rate per unit length of perimeter
μ = fluid viscosity

The Chun and Seban[13] correlation for wavy laminar films ($Re \leq 5800\ Pr^{-1.06}$) is used to compute the mean film thickness given the fluid properties and flow rates.

$$\delta x_{film} = 1.33 Re^{-0.11} \left[\frac{3\nu\ \Gamma}{\rho\ g \sin\theta} \right]^{1/3}$$

The film thermal conductivity is needed in the film energy transport equation. For a wavy laminar film, the thermal conductivity is based on the film centerline temperature. However, for turbulent film flow ($Re > 5800\ Pr^{-1.06}$), the Chun and Seban liquid film heat transfer correlation is used to determine the effective thermal conductivity as follows:

$$k_{effective} = h_{turbulent}\ \delta x$$

$$h_{turbulent} = 3.8 \times 10^{-3} \left[\frac{4\Gamma}{\mu} \right]^{0.4} \left[\frac{\upsilon}{\alpha} \right]^{0.65} \left[\frac{\upsilon^2}{g\theta k^3} \right]^{-1/3}$$

where:

υ	=	fluid kinematic viscosity
ρ	=	fluid density
θ	=	angle of inclination from horizontal
α	=	fluid thermal diffusivity
g	=	gravitational acceleration
k	=	fluid thermal conductivity

2.5 General Clime Equations

The energy equation for the film must balance the heat from the wall into the film, the heat conduction through the film, and the heat and mass transfer from the film surface to the ambient, with the change in energy of the flowing film. Assuming constant fluid properties over the node surface, one-dimensional film flow along the wall, one-dimensional conduction across the film and that the viscous dissipation term can be neglected, the general energy transport equation for the film can be written in terms of temperature as

$$\frac{\partial T}{\partial t} = \frac{k}{\rho c_p} \frac{\partial^2 T}{\partial x^2} + v_z \frac{\partial T}{\partial Z}$$

For computational purposes, the water film is divided into two layers as shown in Figure 2-4. The inner boundary of the film touches the wall and its temperature equals the wall temperature. The outer boundary touches the atmosphere and its temperature is coupled to the temperature of the atmosphere through the heat and mass transfer boundary layer correlations. The temperature at the center line between the layers represents the average heat stored in the film. Referring to Figure 2-4, the film energy transport equation can be expressed in finite difference form as follows:

$$\frac{T_{avg} - T_{avg}^{old}}{\Delta t} = \frac{k_{film}}{\rho_{film} c_{p,film}} \frac{T_{surf,1} - 2T_{avg} + T_{wall}^{1}}{\delta x_{film}^{2}} + v_Z \frac{T_{in} - T_{out}}{\Delta Z}$$

where:

k_{film}	=	film thermal conductivity
δx_{film}	=	film thickness
$c_{p,film}$	=	film heat capacity
ρ_{film}	=	film density
T_{in}	=	inlet temperature of film at the top of the Clime
T_{out}	=	exit temperature of film at the bottom of the Clime
T_{avg}	=	temperature of the center of the film
T_{wall}^{1}	=	temperature of first wall node
$T_{surf,1}$	=	film surface temperature
ΔZ	=	height of the Clime
v_Z	=	film velocity

The film inlet temperature is given either from a boundary condition or from the outlet temperature of the preceding Clime in the stack. The film outlet temperature is defined to be the same as average temperature as a stability criterion.

$$T_{out} = T_{avg}$$

The inner film surface boundary condition forces the heat flux from the outer surface of the conductor wall to equal the heat flux into the inner layer of the film. The inner film surface boundary condition is

$$k_{wall} \frac{T_{wall}^{1} - T_{wall}^{2}}{\Delta x_{wall}} = 2k_{film} \frac{T_{avg} - T_{wall}^{1}}{\delta x_{film}}$$

where

Δx_{wall} = wall node layer thickness

T^2_{wall} = temperature of second wall node

k_{wall} = wall thermal conductivity

The outer film surface boundary condition equates the energy leaving the outer film layer surface to the energy entering the atmosphere. The energy leaving the film surface may enter the atmosphere through a combination of convection, evaporation, and radiation. The outer film surface boundary condition is

$$2k_{film}\frac{T_{surf,1} - T_{avg}}{\delta x_{film}} = h_c(T_{surf,1} - T_{air}) + h_M\, h_{fg}\,(P^{air}_{stm} - P^{film}_{g}) + \varepsilon\sigma\,(T^4_{surf,1} - T^4_{surf,2})$$

where:

h_c = convective heat transfer coefficient from the film to the air

T_{air} = air temperature

h_M = mass transfer coefficient

h_{fg} = latent heat of vaporization of the film

P^{air}_{stm} = partial pressure of steam in the air

P^{film}_{g} = saturation pressure of steam at the film surface temperature, $T_{surf,1}$

ε = emissivity of film surface

σ = Stefan-Bolzman constant

$T_{surf,2}$ = temperature of second radiative surface

The four film equations are

$$\frac{T_{avg} - T^{old}_{avg}}{\Delta t} = \frac{k_{film}}{\rho_{film} c_{p,film}}\,\frac{T_{surf,1} - 2T_{avg} + T^1_{wall}}{\delta x^2_{film}} + V_Z\,\frac{T_{in} - T_{out}}{\Delta Z} \qquad (2\text{-}12)$$

$$k_{wall}\frac{T^1_{wall} - T^2_{wall}}{\Delta x_{wall}} = 2k_{film}\frac{T_{avg} - T^1_{wall}}{\delta x_{film}} \qquad (2\text{-}13)$$

$$2k_{film}\frac{T_{surf,1}-T_{avg}}{\delta x_{film}} = h_c\,(T_{surf,1}-T_{air}) + h_M\,h_{fg}\,(P_{stm}^{air}-P_g^{film}) + \varepsilon\sigma\,(T_{surf,1}^4-T_{surf,2}^4) \quad (2\text{-}14)$$

$$T_{out} = T_{avg} \quad (2\text{-}15)$$

The wall conduction equation is tightly coupled to these film equations. For points within the wall, the conduction equation is simply a one-dimensional partial differential equation:

$$\frac{\partial T}{\partial t} = \frac{k}{\rho c_p}\frac{\partial^2 T}{\partial x^2} \quad (2\text{-}16)$$

By replacing the derivatives with finite differences, this partial differential equation is replaced with a system of algebraic equations. The superscript n identifies the point (node) at which the derivatives are to be calculated.

$$\frac{T_{wall}^{n}-T_{wall}^{n,old}}{\Delta t} = \frac{k_{wall}}{\rho_{wall}c_{p,wall}}\frac{T_{wall}^{n+1}-2T_{wall}^{n}+T_{wall}^{n-1}}{\Delta x_{wall}^2} \quad (2\text{-}17)$$

This equation, along with Equations (2-12) through (2-15), can be considered to be the system of equations for a Clime.

[

$$\left[\rho_{wall}c_{p,wall}\frac{\Delta x_{wall}}{2}+\rho_{film}c_{p,film}\frac{\delta x_{film}}{4}\right]\frac{dT_{wall}^{1}}{dt} = k_{wall}\frac{T_{wall}^{2}-T_{wall}^{1}}{\Delta x_{wall}} - 2k_{film}\frac{T_{wall}^{1}-T_{avg}}{\delta x_{film}} \quad (2\text{-}18)$$

]^{a,c}

[ ] a,b,c

(2-19)

Equations (2-12), (2-15), (2-17), (2-18), and (2-19) represent the complete system of equations for a Clime as used in WGOTHIC.

2.6 Clime Subroutine Descriptions and Integration into GOTHIC

The GOTHIC subroutines and structure of the solver are described in detail in Section 2 of the *GOTHIC Programmer's Manual.*[14] A set of subroutines have been added to GOTHIC to create WGOTHIC.

gshell is the main program of the WGOTHIC Clime model. It calls the routines to compute heat and mass transfer coefficients. It computes surface to surface radiation heat transfer and computes the conductor temperature distribution. It returns the heat and mass source terms for the GOTHIC mass and energy conservation equations.

The WGOTHIC program flow control outline is shown in Figure 2-5.

The addition of the Clime models to GOTHIC requires the following changes to be made in the GOTHIC solver logic:

1. Addition of a call to subroutine gshell, the routine containing the Clime model.
2. Addition of a call to the subroutine generating the ASCII text Clime output.
3. Addition of a call to the subroutine reading the Clime input.

The following GOTHIC common block arrays are also affected by the addition of the Clime models:

1. The Clime model calculates the vapor mass transfer rate to or from the conductor surface and updates the corresponding GOTHIC array variable. A GOTHIC subroutine adds smvap to the cell source term for the steam mass balance.

2. A GOTHIC subroutine initially computes the vapor energy transfer rate for each cell and stores the value in an array variable. The Clime model calculates the convective vapor energy transfer rate to or from the conductor surface and updates this GOTHIC array variable.

3. The bottom Clime in a stack of Climes must put any remaining liquid mass and energy from a conductor surface into the liquid field of the adjacent or user specified

GOTHIC cell. The Clime model calculates the remaining liquid mass and energy on each conductor surface and updates the corresponding GOTHIC array variables. A GOTHIC subroutine adds the mass to the cell source term for the liquid mass balance and adds the energy to the cell source term for the liquid energy balance.

GOTHIC Family Tree

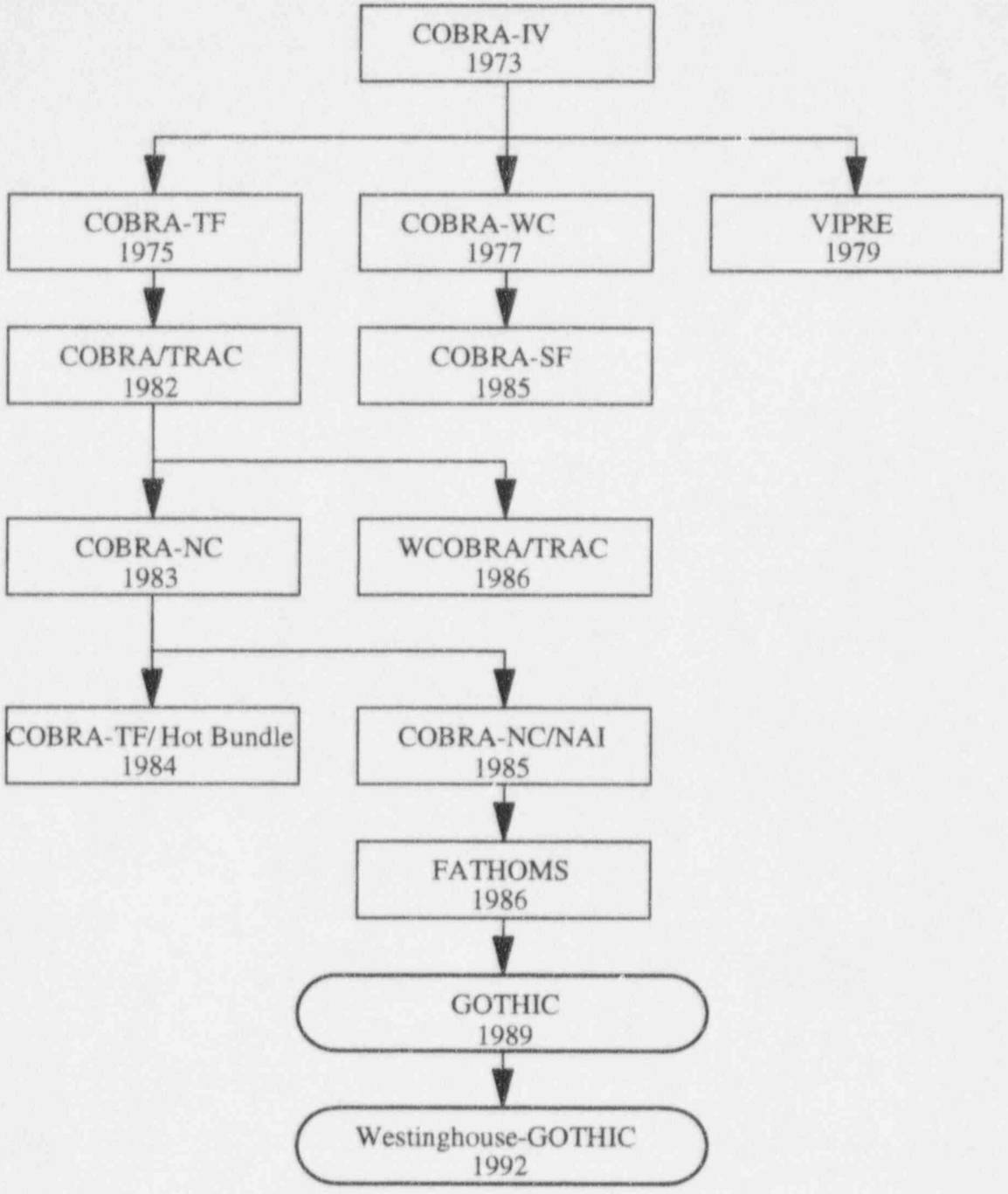

Figure 2-1 Summary of GOTHIC Historical Development

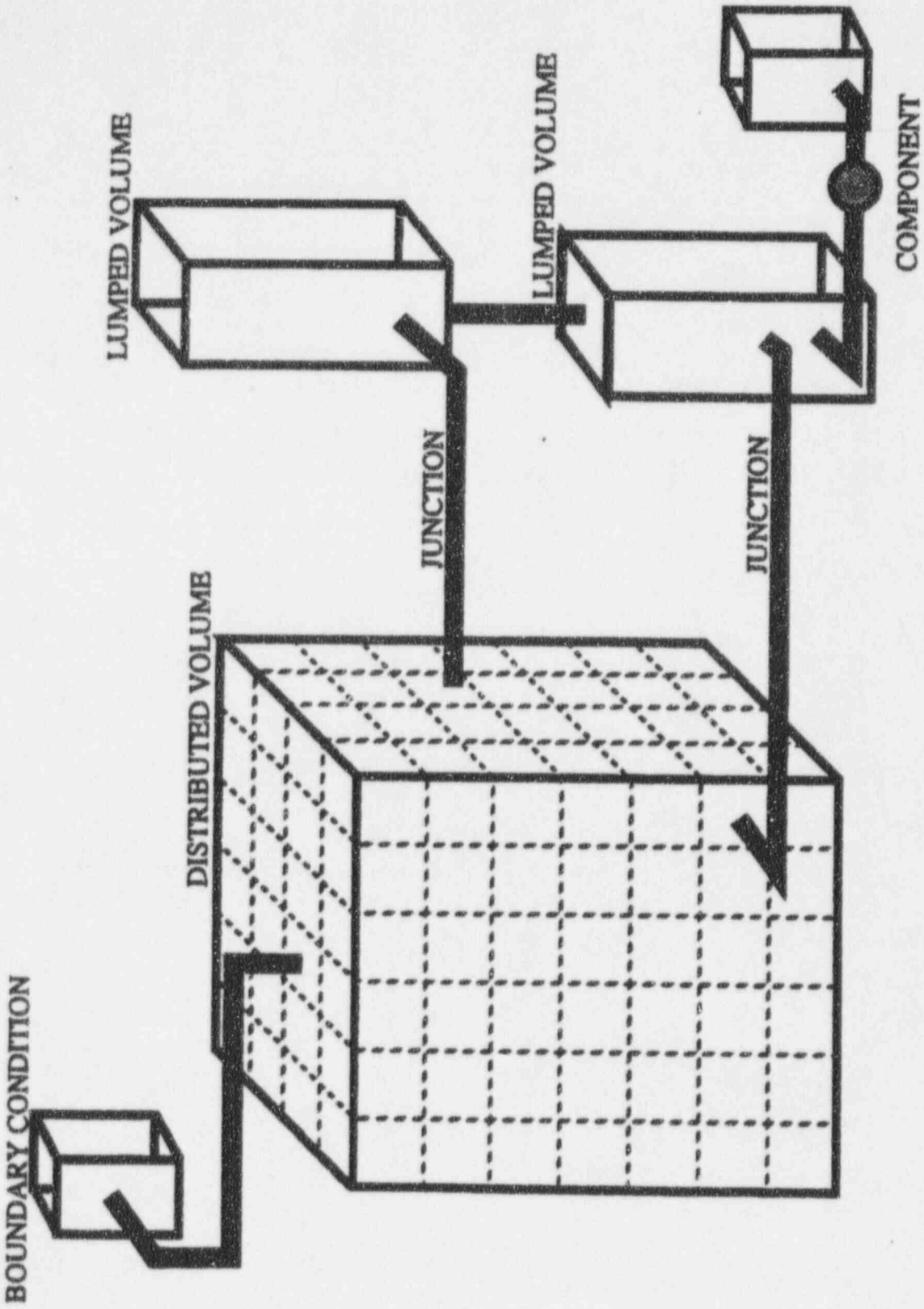

Figure 2-2 GOTHIC Modeling Features

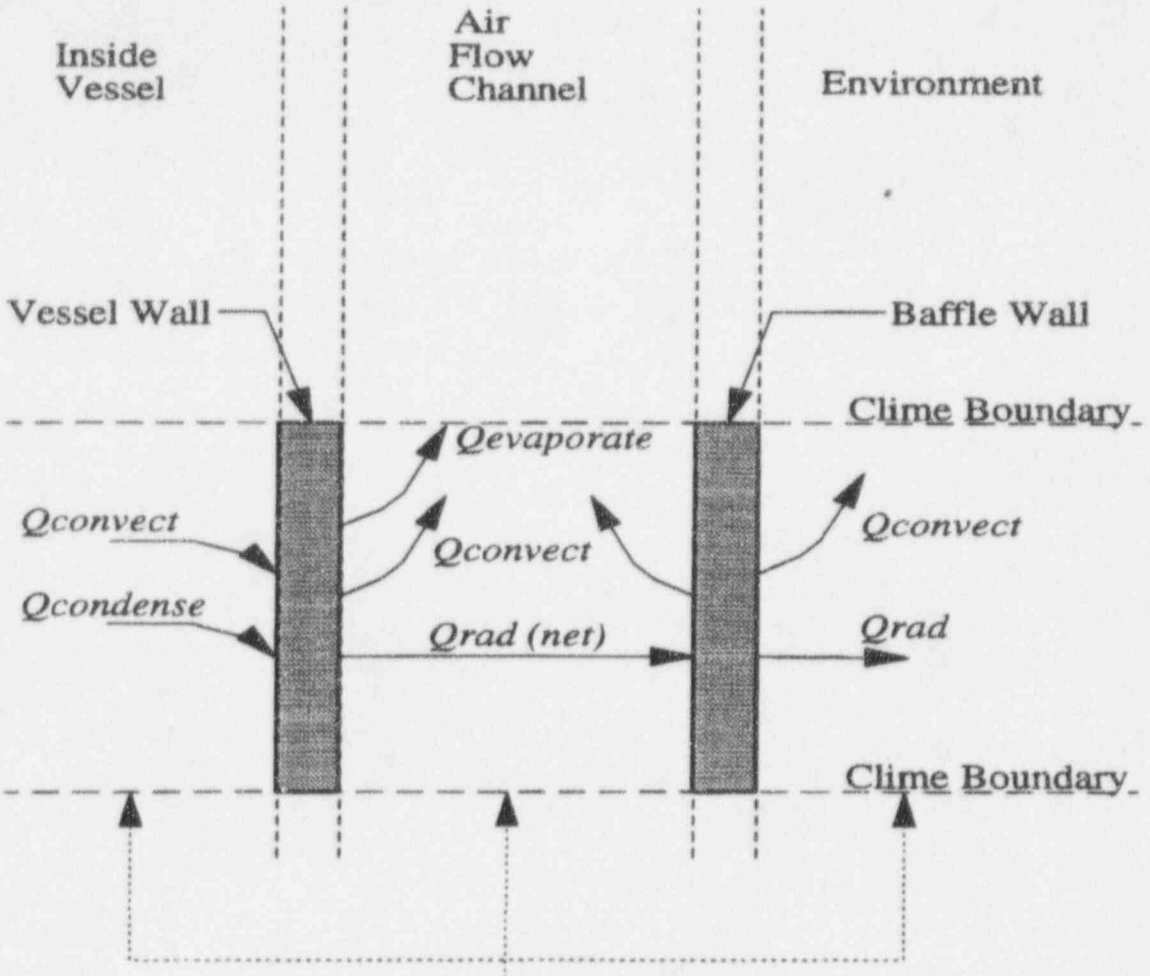

CLIME Heat and Mass Source Terms Interface with Westinghouse-GOTHIC Volumes, and the Volume Conditions Are Used in the CLIME Heat and Mass Transfer Correlations

Figure 2-3 Westinghouse-GOTHIC Clime Wall Source Term Models

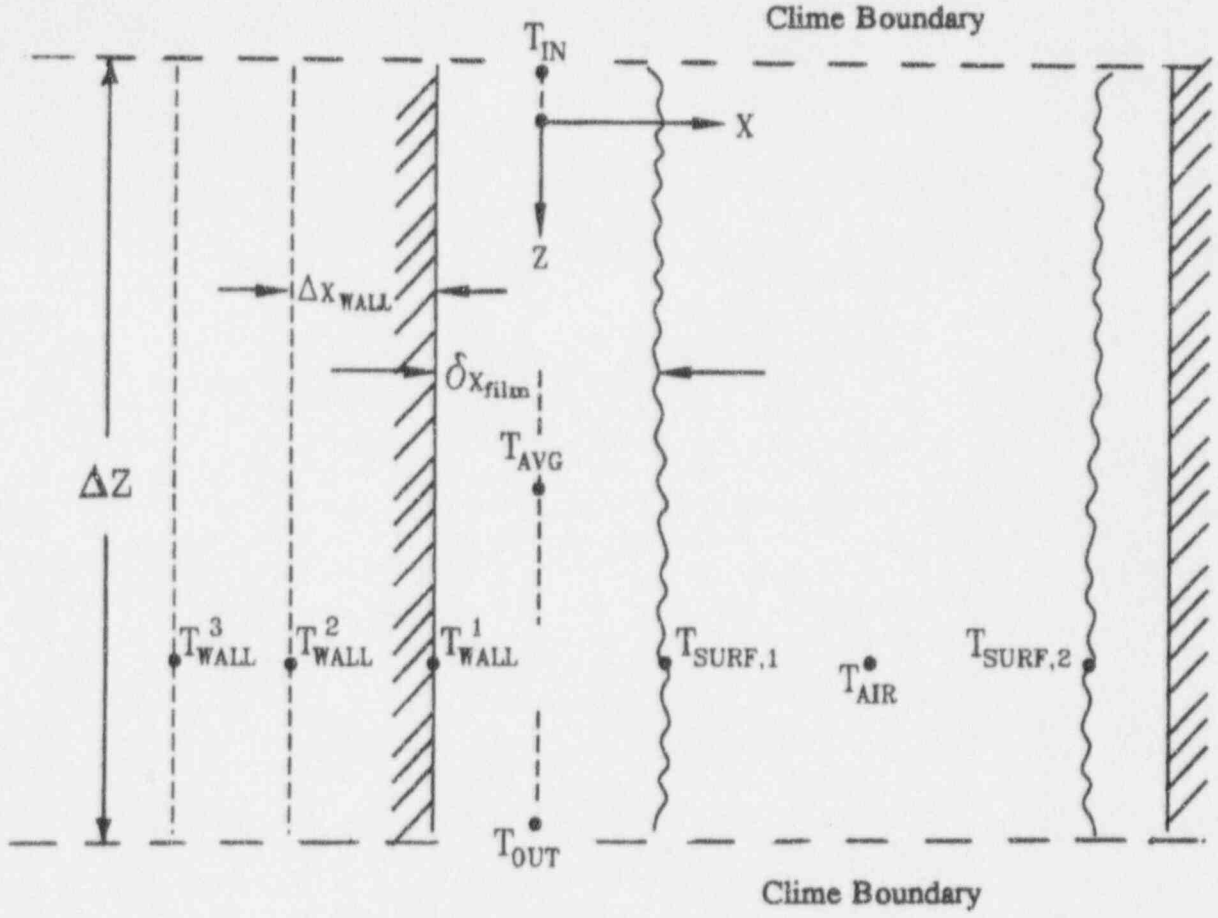

Figure 2-4 Clime Finite-Difference Model Definitions

a,b,c

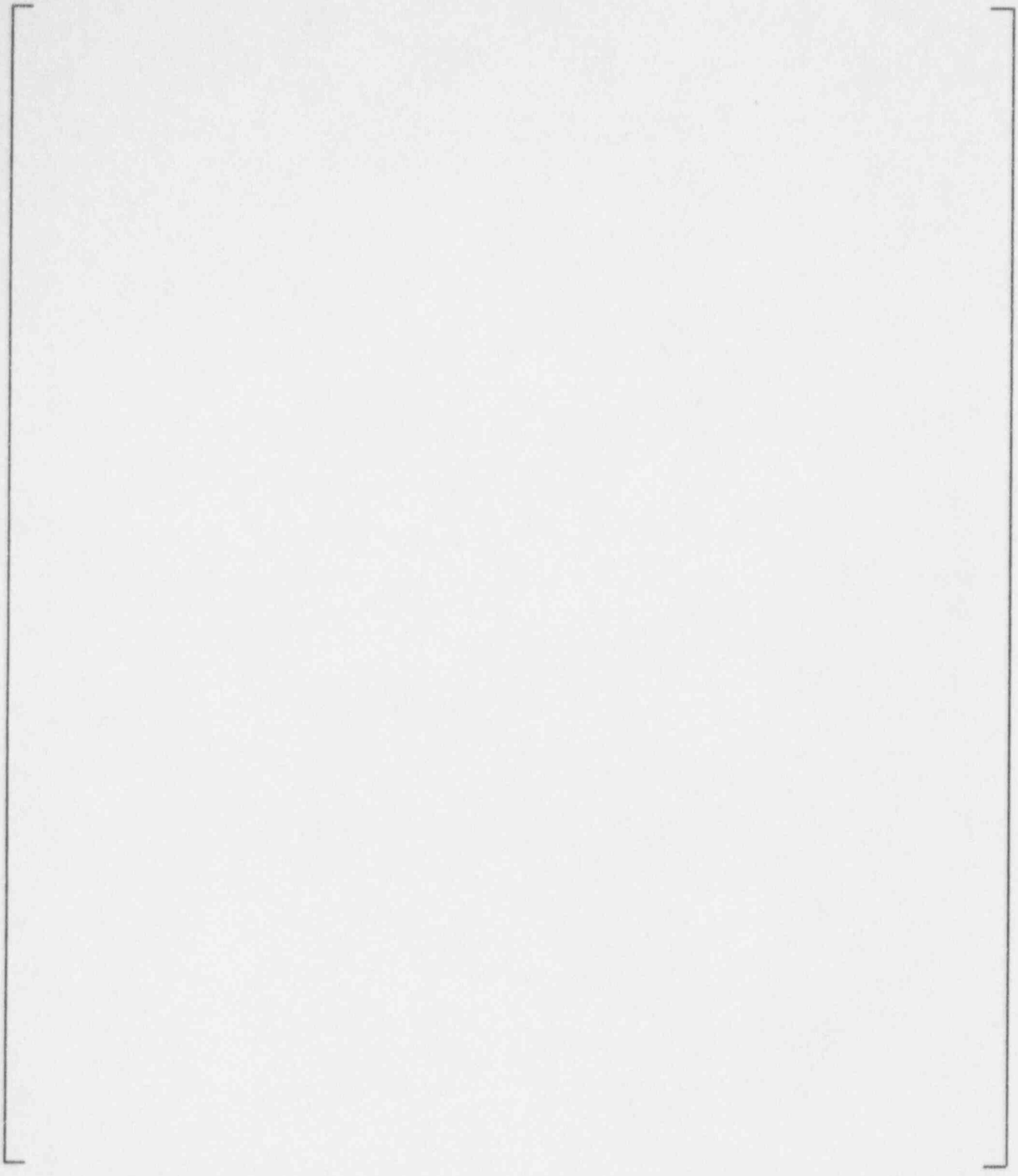

Figure 2-5 Clime Routines Flow Control Outline

3.0 WGOTHIC VALIDATION PROGRAM OVERVIEW

A validation program must demonstrate that the code can adequately model the phenomena required for a particular application. Typically, a validation program includes both a comparison of code-calculated results with analytical solutions to specified standard problems and a comparison of code-calculated results with experimental data.

For WGOTHIC, the required phenomena are identified in the phenomena identification ranking table (PIRT) which is summarized in Section 1.0. This section presents an overview of the WGOTHIC code validation program and the passive containment cooling system (PCS) test program, which provided most of the test data needed to validate the WGOTHIC code.

3.1 Validation Program Description

The GOTHIC code as an extensive validation history, which was an important criterion in the selection of the code for further development for modeling of the PCS. The results of the GOTHIC code validation program are presented in NAI 8907-09.[15] Table 3-1 lists some of the tests used in the GOTHIC code validation program. The phenomenological models validated by each test are cross-referenced and presented in Table 3-2.

After compiling and installing the GOTHIC code on the Westinghouse computer workstations, the entire set of GOTHIC validation tests was run to determine if changes in the computer platform or compiler would affect the results. No significant differences were observed in any of the parameters that were compared; however, in performing this initial testing, certain tests were discovered to be more sensitive than others to changes in the computer platform, compiler and/or the numerical solution time step. This subset of the GOTHIC validation tests was used to verify that the code changes that were made to incorporate the PCS heat and mass transfer and wall-to-wall radiation models would not affect the previous GOTHIC validation results.

As described in Section 2.0, WGOTHIC was created by incorporating the special Clime heat and mass transfer models into GOTHIC. The validation program for the newly created WGOTHIC code consisted of four parts:

1. The subset of GOTHIC validation tests that was identified as sensitive in the original acceptance tests was rerun with WGOTHIC. These tests were run with the same input options selected in the original GOTHIC validation calculation (that is, the PCS models were not exercised) to determine if any of the code changes made to incorporate the PCS models would affect the transient results. This comparison is presented in Appendix D.

2. The Clime one-dimensional conduction equation solution technique was validated by comparison with an analytical solution for a test problem. This comparison is presented in Section 4.1.

3. The Clime heat and mass transfer correlations were validated by comparison with separate effects test data from the Westinghouse Flat Plate Tests, the Westinghouse Large-Scale Tests, the Wisconsin Condensation Tests, and publicly available published reports. These comparisons were documented in WCAP-14326[16] and are summarized in Sections 4.2 through 4.4.

4. The WGOTHIC code, including the PCS models, was validated by comparison with transient test data from the Westinghouse Large-Scale tests. Comparison with test data from the large-scale tests validate the ability of WGOTHIC to represent internal flow fields and noncondensible gas distributions and to calculate the net heat removal from the vessel in an integral system.

3.2 Westinghouse Passive Containment Cooling System (PCS) Test Program

The PCS test program was conducted over a period of several years. The PCS test program provided data on the heat transfer performance of the passive containment cooling system under various operating conditions and included both separate effects and integral effects tests for assessing the performance of the PCS. As part of the program, laboratory scale tests were performed to separately represent convection and condensation on the inner surface and convection, evaporation, and radiation on the external surfaces. Integral effects tests were performed, using pressure vessels of two different sizes and aspect (height to width) ratios. The complete PCS test program is outlined in the *Standard Safety Analysis Report* (SSAR), Chapter 1.5, R&D Programs.[17] The results from the PCS test program were documented in a series of reports listed in Section 11.0.

In addition to providing data on the performance of the PCS, the test program provided data for WGOTHIC code validation. The following sections summarize the characteristics of each of the PCS tests, which were selected for code validation. Section 4.0 presents the results of the WGOTHIC comparisons to the separate effects validation tests, and Section 8.0 presents the results of comparisons to the integral effects validation tests.

3.2.1 Heated Flat Plate Tests

A series of forced convection heat transfer tests were performed at the Westinghouse Science and Technology Center (STC) and are described in detail in WCAP-12665.[18] The purpose for these tests was to provide heat and mass transfer data for channels with heat fluxes, liquid film flow rates, and cooling air velocities representative of the AP600 annulus during a design basis accident (DBA).

The test section (Figure 3-1) was a vertical, 6-ft. long heated flat steel plate that was coated with a highly wettable inorganic-zinc coating. The test section was inclined to examine behavior at angles other than vertical. A clear acrylic cover provided a channel for the forced air flow and allowed for observation of the applied liquid film. The plate temperature, applied liquid film temperature, and both the liquid and air flow rates were varied for each test.

3.2.2 Separate Effects Condensation Tests

A series of condensation tests were conducted at the University of Wisconsin and are described in detail in WCAP-13308.[19] These tests provided data on condensing heat and mass transfer in the presence of a noncondensible gas at various inclination angles, velocities, and steam/air concentrations. The test conditions were similar to what could be expected following a loss-of-coolant accident (LOCA) or main steam line break (MSLB) transient within the AP600 containment vessel.

The test section was 6.25-ft. long with a 2.75-ft. entrance length and a 3.5-ft. condensing surface length. The channel cross section was square with an area of 0.25 ft.^{2}. The top of the test section was covered with a thick aluminum plate coated with a highly wettable, protective, inorganic-zinc coating. Seven 0.5-ft. long coolant plates were attached to the back of the aluminum test plate to remove heat. Each coolant plate had both flux meters and cooling coils with thermocouples to provide redundant, diverse energy measurements. The test section could be inclined from any angle (0 to 90 degrees from horizontal). Plate number 1 was located at the end nearest the air/steam source and was always at the lowest level when the test section was inclined.

3.2.3 Integral Large-Scale Tests

The Westinghouse large-scale PCS test facility was built to provide integral test data for a geometrically similar model of the AP600 containment vessel and PCS. The tests provide experimental data that can be used for evaluating the physics in containment, determining the relative importance of various parameters that affect heat and mass transfer and validating computer codes. Three series of tests[20,21] were run at the Westinghouse large-scale PCS test facility. The steady-state pressure, annulus air flow rate, water coverage, steam flow rate, injection velocity, location and orientation, and noncondensible gas concentration were varied between the tests (summarized in Table 3-3).

The large-scale PCS test facility uses a 20-ft. tall, 15-ft. diameter pressure vessel to simulate the AP600 containment vessel. The geometry is approximately a 1/8-scale of the AP600 containment vessel. A plexiglas cylinder is installed around the vessel to form the air cooling annulus. Air flows upward through the annulus via natural convection to cool the vessel, resulting in condensation of the steam inside the vessel. A fan is located at the top of the annular shell to provide the capability of inducing higher air velocities than can be achieved during purely natural convection. A liquid film can be applied outside of the test vessel to provide additional evaporative cooling.

Test conditions (pressure, steam flow rate, cooling air flow rate, water coverage, etc.) were selected to provide heat and mass transfer validation over a range of conditions representative of a DBA.

For most of the tests, steam was injected through a diffuser located under a simulated steam generator compartment below the operating deck (Figure 3-2). The steam rises upward as a plume. Air is entrained in the rising plume, resulting in a natural circulation flow pattern and partial mixing within

the vessel. Variations in steam injection velocity and location were made to evaluate the effects on mixing and heat transfer (Figure 3-3).

Approximately 300 thermocouples are installed in the test facility. Thermocouples are embedded in both the inner and outer surfaces of the vessel at various angles at ten different elevations (Figure 3-4), to determine the temperature and flux distribution over the height and circumference of the vessel. Thermocouples are also placed inside the vessel on a movable rake to measure the bulk temperature at various locations.

The steam inlet pressure, temperature and flow; the vessel pressure; and condensate temperature and flow are measured to provide an accurate measurement of the total heat supplied to the vessel. The cooling air temperature and plexiglas surface temperature are measured at several locations in the annulus to determine the amount of convective and radiative heat removal. The external liquid film flow rate and temperature are measured at the inlet and exit to determine the amount of heat removed by evaporation and sensible heating of the liquid film.

A more detailed description of the large-scale PCS test facility and instrumentation locations is given in WCAP-14135.[20]

TABLE 3-1 GOTHIC VALIDATION TESTS	
Battelle-Frankfurt Tests D-1, D-15, D-16	Modeling: 7 lumped parameter volumes, junctions Phenomena: Blowdown transients, subcompartment pressurization, wall differential pressures
Battelle-Frankfurt Test 6	Modeling: 1 distributed parameter volume (55 cells), conductors, junctions Phenomena: Hydrogen transport by convection and diffusion
Battelle-Frankfurt Tests 12, 20	Modeling: Combination of 5 lumped and 1 distributed parameter volumes (2 cells), conductors, junctions Phenomena: Hydrogen transport by convection and diffusion
Battelle-Frankfurt Tests C-13, C-15	Modeling: 10 lumped parameter volumes, conductors, junctions Phenomena: Main steamline break, pressure/temperature response
Hanford Engineering Development Laboratory Tests HM-5, HM-6	Modeling: 1 distributed parameter volume (300 cells), conductors, junctions Phenomena: Hydrogen mixing in a large, simulated containment
Light Water Reactor Aerosol Containment Experiments Tests LA-5, LA-6	Modeling: Combination of 1 lumped and 1 distributed parameter (2 cells) volumes, conductors, junctions Phenomena: Severe accident response to sudden containment failure
Marviken Full-Scale Containment Tests 17, 24	Modeling: 21 lumped parameter volumes, conductors, junctions Phenomena: Pressurized high temperature steam blowdown
Carolina's Virginia Tube Reactor Tests 3, 4, 5	Modeling: 2 lumped volume and a 2 distributed parameter volume (20 cells) models, conductors, junctions Phenomena: Steam blowdowns (T31.5 includes hydrogen/helium)
Heissdampfreaktor Tests V21.1, T31.1, T31.5, V44	Modeling: 37 lumped parameter volumes, conductors, junctions Phenomena: Steam blowdowns (T31.5 includes hydrogen/helium)

TABLE 3-2 GOTHIC PHENOMENOLOGICAL MODELS VALIDATED BY TEST						
Item	**BFMC**	**HEDL**	**LACE**	**MARV**	**CVTR**	**HDR**
Fluid momentum	X		X	X		
Energy transport	X		X	X		
Noncondensible gases	X	X	X	X	X	X
Equations of state	X		X	X		
Pressure response	X	X	X	X	X	X
Temperature response	X	X	X	X	X	X
Humidity response	X	X	X	X	X	X
Hydrogen transport	X					
Energy sources	X	X	X		X	X
Subcompartment analysis	X			X		
High energy line breaks	X					
PWR standard containment			X			
BWR pressure suppression				X		
Fluid/structure interaction	X					
Conductors	X					
Subdivided volumes	X					
Turbulence	X					
3-D calculations	X	X		X		

TABLE 3-3
LARGE-SCALE PCS TEST MATRIX

Test Number	Pressure (psig)	Flow (lb_m/sec.)	Configuration	Air Flow (ft./sec.)	Water Coverage (% Area)	Long-Term Heat Sinks	Helium	Sampling
Baseline Tests without Internals								
201.1	10	-	C3D	9	100	NO	NO	NO
202.1	30	-	C3D	9	100	NO	NO	NO
203.1	40	-	C3D	9	100	NO	NO	NO
207.1	30	-	C3D	9	75-Quad	NO	NO	NO
207.2	30	-	C3D	9	75	NO	NO	NO
Baseline Tests with Internals								
201.2	10	-	DSG - NSG	12	100	NO	NO	NO
202.2	30	-	DSG - NSG	12	100	NO	NO	NO
203.2	40	-	DSG - NSG	12	100	NO	NO	NO
204.1	30	-	DSG - NSG	16	100	NO	NO	NO
205.1	30	-	DSG - NSG	8	100	NO	NO	NO
206.1	30	-	DSG - NSG	FREE	100	NO	NO	NO
207.3	30	-	DSG - NSG	12	75-Quad	NO	NO	NO
208.1	30	-	DSG - NSG	12	50-Quad	NO	NO	NO
207.4	30	-	DSG - NSG	12	75	NO	NO	NO
210.1	40	-	DSG - NSG	12	100-Heated	NO	NO	NO
211.1	40	-	DSG - NSG	FREE	100-Heated	NO	NO	NO

TABLE 3-3
LARGE-SCALE PCS TEST MATRIX (Cont.)

Test Number	Pressure (psig)	Flow (lb_m/sec.)	Configuration	Air Flow (ft./sec.)	Water Coverage (% Area)	Long-Term Heat Sinks	Helium	Sampling
Phase 2 Tests								
202.3	30	-	DSG	12	100	NO	NO	NO
203.3	40	-	DSG	12	100	NO	NO	NO
212.1A	-	0.25	DSG	12	75	NO	NO	YES
212.1B	-	0.50	DSG	12	75	NO	NO	YES
212.1C	-	0.75	DSG	12	75	NO	NO	YES
213.1A	-	0.25	DSG	12	25	NO	NO	NO
213.1B	-	0.50	DSG	12	25	NO	NO	NO
213.1C	-	0.75	DSG	12	25	NO	NO	NO
214.1A	-	1	DSG	FREE	75	NO	NO	NO
214.1B	-	1	DSG	12	75	NO	NO	NO
215.1A	-	1	DSG	FREE	75	NO	NO	NO
215.1B	-	1	DSG	12	75	NO	NO	NO
216.1A	-	0.50	DSG	12	75-Quad	NO	NO	NO
216.1B	-	0.50	DSG	12	25-Quad	NO	NO	NO
217.1A	-	1	DSG	12	75	NO	NO	YES
217.1B	-	1	DSG	12	75	NO	[ ]^{a,b}	YES
218.1A	-	1	DSG	12	75	YES	NO	YES
218.1B	-	1	DSG	12	75	YES	[ ]^{a,b}	YES

TABLE 3-3
LARGE-SCALE PCS TEST MATRIX (Cont.)

Test Number	Pressure (psig)	Flow (lbm/sec.)	Configuration	Air Flow (ft./sec.)	Water Coverage (% Area)	Long-Term Heat Sinks	Helium	Sampling
219.1A	-	0.20	DSG	12	DRY	YES	NO	YES
219.1B	-	0.20	DSG	12	DRY	YES	[ ]a,b	YES
219.1C	-	0.20	DSG	12	50	YES	[ ]a,b	YES
220.1	-	Blowdown	DSG	12	75	YES	NO	YES
221.1A	-	Blowdown	DSG	12	50	YES	[ ]a,b	YES
221.1B	-	Blowdown	DSG	12	DRY	YES	[ ]a,b	YES
Phase 3 Tests								
222.1	-	Blowdown	DSG	12	75	YES	NO	YES
222.2A	-	Blowdown	ADD	12	75	YES	NO	YES
222.2B	30	-	ADD	12	75	YES	NO	YES
222.3A	-	Blowdown	AD3S	12	75	YES	NO	YES
222.3B	30	-	AD3S	12	75	YES	NO	YES
222.4A	-	Blowdown	AD3U	12	75	YES	NO	YES
222.4B	30	-	AD3U	12	75	YES	NO	YES
223.1	-	1.5	DSG - Vac.	12	75	YES	NO	YES
224.1	-	0.25	DSG - 2 atm.	12	100	YES	NO	YES
224.2	-	0.50	DSG - 2 atm.	12	100	YES	NO	YES

C3D - Center of vessel, 3-in. pipe at deck elevation
DSG - Diffuser in steam generator compartment
NSG - No steam generator model
ADD - 6-ft. above deck, diffuser
AD3S - 6-ft. above deck, 3-in. pipe, pointed sideways
AD3U - 6-ft. above deck, 3-in. pipe, pointed upward

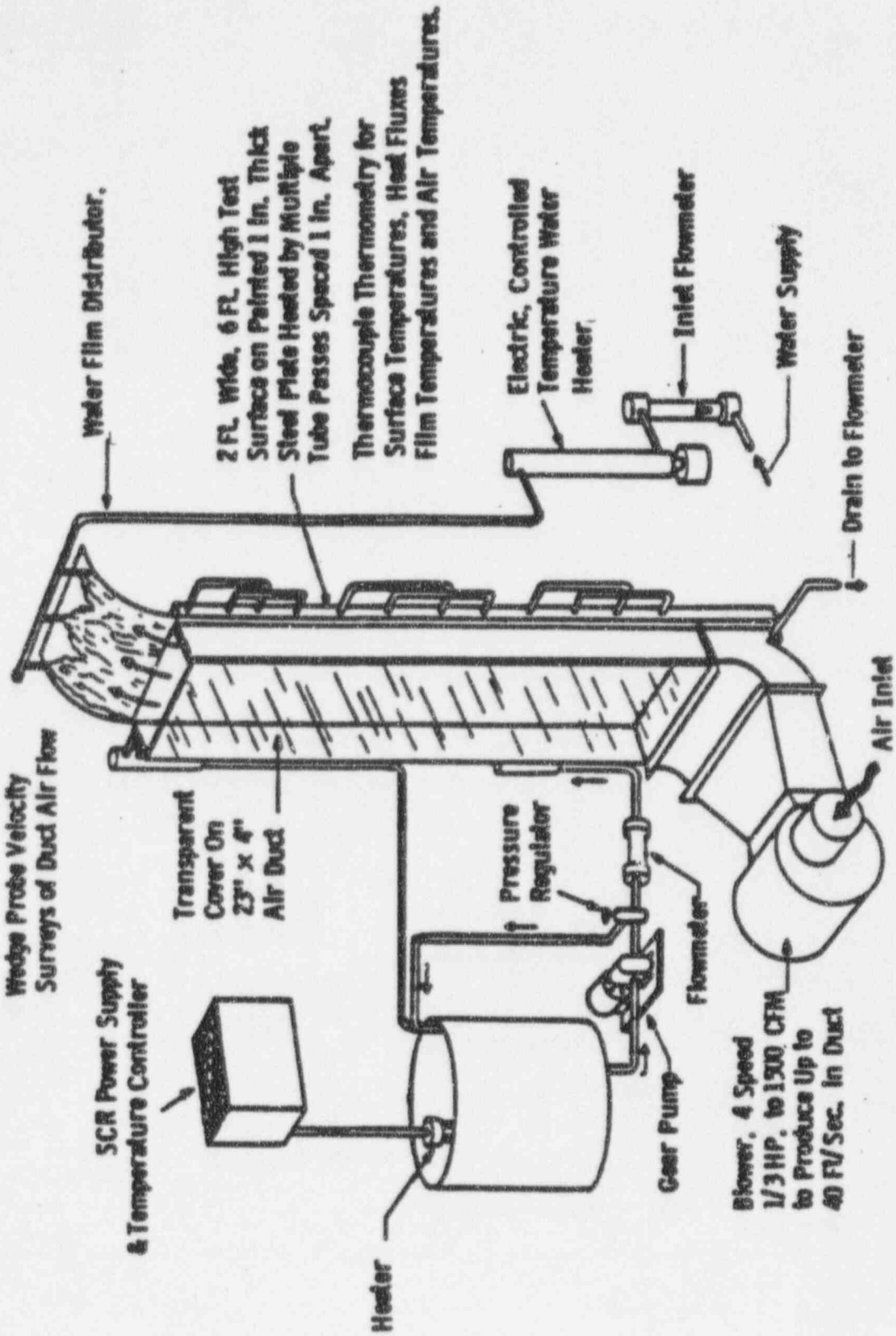

Figure 3-1 STC Heated Flat Plate Test Apparatus

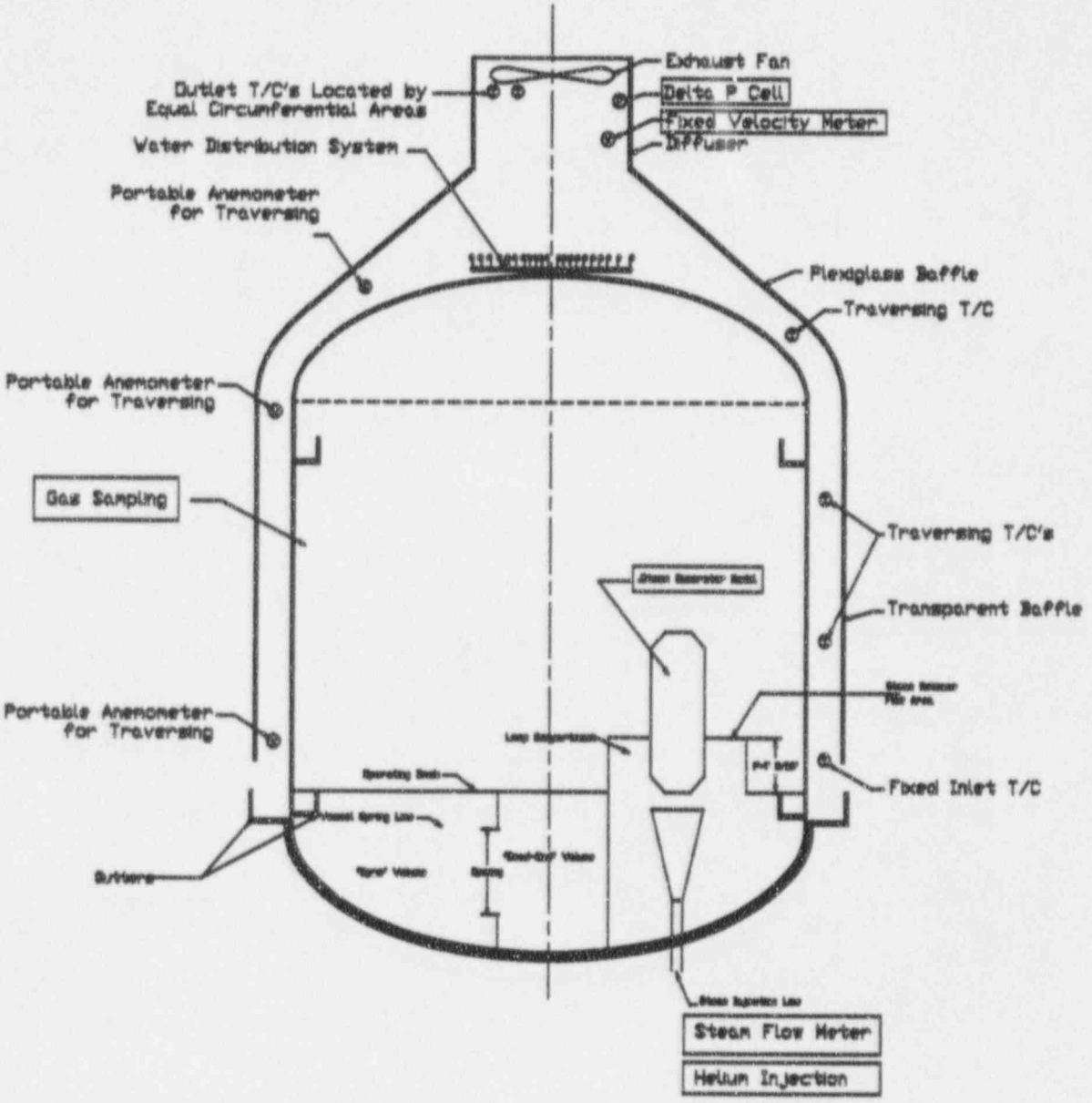

Figure 3-2 AP600 Large-Scale PCS Test Internals

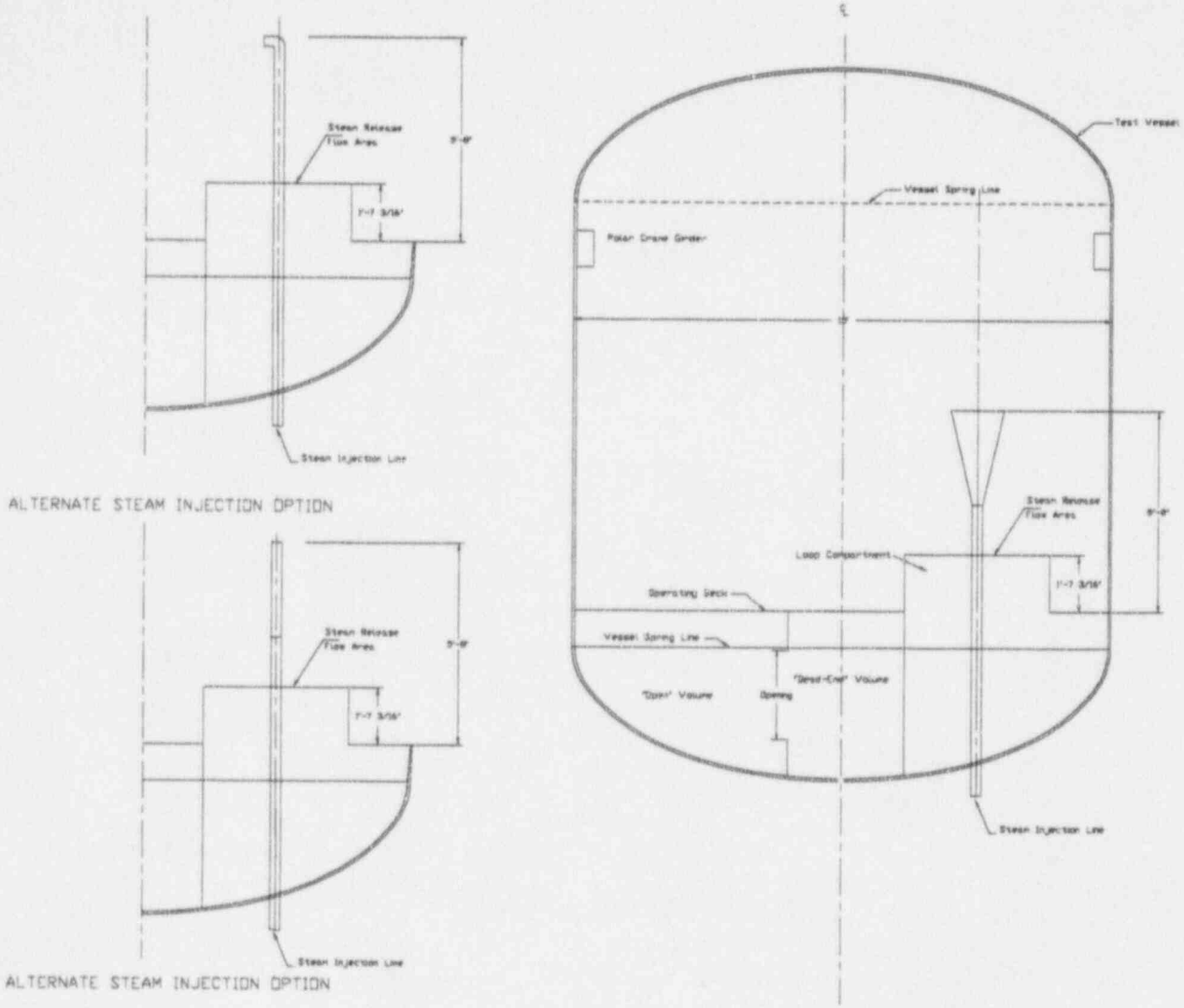

Figure 3-3 Alternate Steam Injection Locations

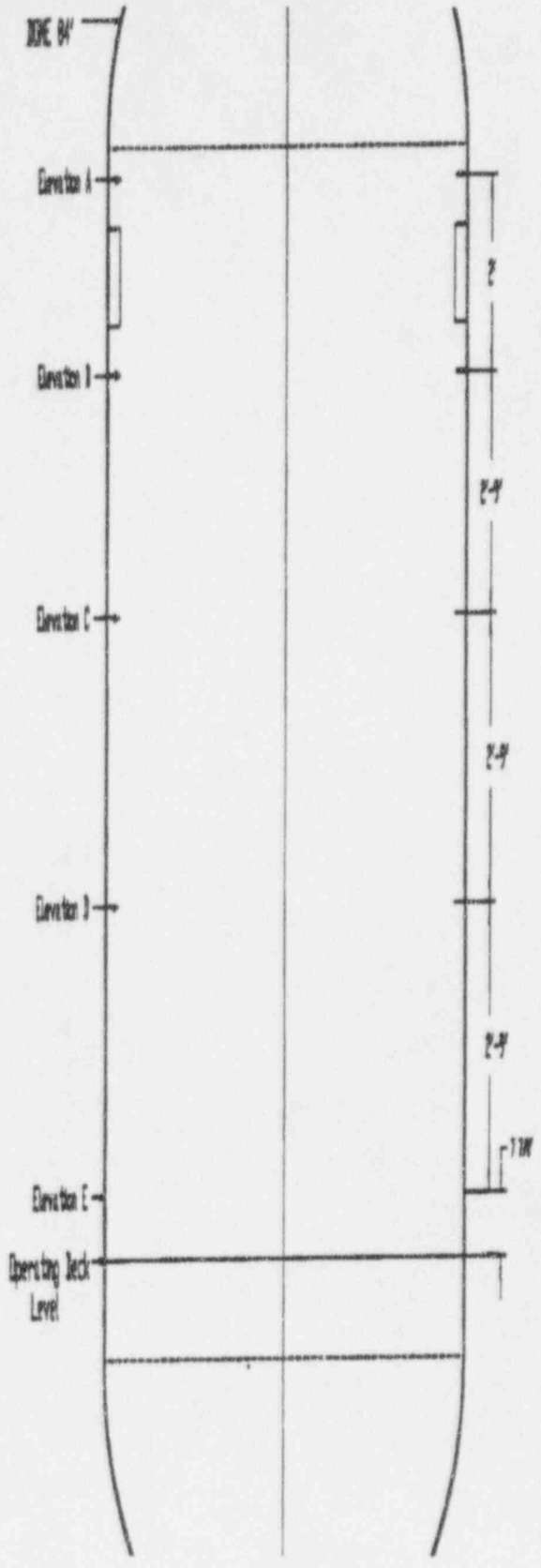

Figure 3-4 Large-Scale PCS Instrumentation Elevations

4.0 WESTINGHOUSE GOTHIC SEPARATE EFFECTS VALIDATION TESTS

Separate effects validation tests were performed to validate the method of solution of the transient conduction equation for the Clime wall and the heat and mass transfer correlations that were selected for modeling the passive containment cooling system (PCS). This section presents the results of the WGOTHIC separate effects validation tests.

4.1 Transient Wall Conduction

Validation of the Clime numerical solution method for transient wall conduction has been performed by comparison of code-calculated results with an analytical solution. Analytical solutions of the transient conduction equation can be obtained for a semi-infinite solid with convective boundary condition.[22] The solution is straightforward if the convective boundary condition considers a constant convective heat transfer coefficient and a constant environment temperature, where the semi-infinite solid is suddenly exposed to the environment as the initial condition. The analytical solution for such a case is

$$\frac{T(l,t) - T^i}{T_a - T^i} = 1 - erf\left[\frac{l}{(2\sqrt{\alpha t})}\right] - \left[\exp\left(\frac{h_c l}{k_c} + \frac{h_c^2 \alpha t}{k_c^2}\right)\right]\left[1 - erf\left(\frac{l}{(2\sqrt{\alpha t})} + \frac{h_c\sqrt{\alpha t}}{k_c}\right)\right]$$

where:

$T(l,t)$	=	temperature of conductor at time t and position l (°F)
T^i	=	initial temperature of the solid conductor (°F)
T_a	=	volume temperature (°F)
h_c	=	heat transfer coefficient (Btu/ft.^{2}-sec.-°F)
k_c	=	thermal conductivity of conductor (Btu/ft.-sec.°F)
l	=	position from edge of conductor (ft.)
t	=	time (sec.)
α	=	conductor thermal diffusivity (ft.^{2}/sec.)

A simple WGOTHIC model was created (shown in Figure 4.1-1). The model consisted of a single conductor, 1.667 ft. long with a coarse mesh width of 1/24 ft. The conductor temperature was initially 50°F. The conductor was exposed to two effectively infinite volumes; the volume on the left side was maintained at 70°F, and the volume on the right side was maintained at 50°F. Radiation heat transfer to the conductor surfaces was eliminated by setting the code emissivity input values to zero. Mass transfer did not occur for the conditions of the problem. The convective heat transfer coefficient was calculated by the code and remained at an essentially constant value throughout the time of interest.

The material properties and geometry used in the analytical and WGOTHIC solutions are summarized as follows:

Conductor

Surface area	1.0 $ft.^2$	
Length	1.667 ft.	
Mesh width, Δl	1/24 ft.	(1.667 ft./40 meshes)

k_c	0.002611 Btu/ft./sec./°F
ρ_c	501.0 $lbm/ft.^3$
c_p	0.12 Btu/lbm/°F
α	4.343×10^{-5} $ft.^2/sec$

Initial temperature 50°F

Boundary Conditions

h_c	1.740×10^{-4} $Btu/ft.^2/sec./°F$
T_a	70°F

The WGOTHIC numerical solution is compared with the analytical solution and is shown as a function of distance from the imposed boundary condition at a problem time of 500.5 seconds in Figure 4-2. The local error, relative to the analytical solution temperature, is shown in Figure 4-3. The maximum variation for the conservatively large mesh size is less than 0.06 percent, which is acceptable. Therefore, the numerical solution method for solving the transient wall conduction equation is valid.

4.2 Convection Heat Transfer

The convective heat transfer correlations that have been coded into WGOTHIC have been validated by comparison with test data from various sources. These sources include both publicly available test data from published papers by Hugot[23], Eckert and Diaguila[12], and Siegel and Norris[24] and proprietary test data from the Westinghouse passive containment cooling system (PCS) test program. The convective heat transfer test data covered a Reynolds number range of between 1.0E3 and 5.0E5 and a Grashof number range of between 1.0E6 and 1.0E11. During a design basis accident (DBA) event, the AP600 riser annulus Reynolds number can be as high as 1.0E5 and the riser Grashof number can be as high as 1.0E9 in the annulus region between the steel containment shell and the steel baffle. Therefore, the test data cover the expected range of both dimensionless groups within the annulus. A description of the test facilities and the comparison of WGOTHIC heat and mass transfer correlations with the test data from each source is presented in WCAP-14326[16]. The results are summarized here.

The mixed convection correlation has a nonlinear dependence on the Reynolds and Grashof numbers; therefore, it is necessary to present separate comparisons of the predicted-to-measured Nusselt numbers as functions of the Reynolds and Grashof numbers. The predicted-to-measured Nusselt number ratio is shown as a function of the Reynolds number in Figure 4-4 and as a function of the Grashof number in Figure 4-5. The mean predicted-to-measured Nusselt number ratio is 0.976 with a standard deviation of 0.278.

The mean predicted-to-measured Nusselt number value near 1.0 indicates that the mixed-convection heat-transfer correlation fits the measured data very well over both the Grashof and Reynolds number ranges. As discussed in Section 3.2, the convective heat-transfer correlation serves as the basis for the prediction of condensation and evaporation heat and mass transfer. Condensation and evaporation heat and mass transfer result in much higher heat fluxes than convection alone and, as shown in Sections 4.3 and 4.4, the standard deviation for the predicted-to-measured evaporation and condensation heat and mass transfer is much lower. Therefore, the relatively large standard deviation in the predicted-to-measured convective heat transfer is most likely due to the large uncertainty that results from taking the difference of two wall thermocouple temperature measurements, especially when the difference is small due to a low wall heat flux.

4.3 Condensation Heat and Mass Transfer

The data for validating the WGOTHIC mass transfer correlation for condensation was obtained from the Wisconsin condensation tests[19] and the Westinghouse large-scale passive containment cooling system (PCS) tests.[20,21] The Wisconsin condensation tests were performed under forced-convection (relatively high Reynolds number) conditions, while condensation on the inside of the Westinghouse large-scale PCS test facility took place under free convection conditions. The Wisconsin condensation tests covered a Reynolds number range of between 5.0E3 and 2.5E4 and the Westinghouse large-scale PCS tests covered a Grashof number range of between 1.0E10 and 1.0E13. A description of the test facilities and the comparison of WGOTHIC heat and mass transfer correlations with the test data from each source is presented in WCAP-14326.[14] The results are summarized here.

A comparison of the measured mass transfer with the correlation is presented as a function of the Reynolds number in Figures 4-6 (for the Wisconsin condensation tests) and as a function of the Grashof number in Figure 4-7 (for the Westinghouse large-scale PCS tests). The correlation fits the measured data.

The predicted-to-measured Sherwood ratio is shown as a function of the Reynolds number, Grashof number and dimensionless steam concentration in Figures 4-8 through 4-10. The mean predicted-to-measured Sherwood number ratio is 0.983 with a standard deviation of 0.187. Local Reynolds number values could not be consistently and accurately determined from the measured internal condensation data from the large-scale PCS tests, therefore, only the Wisconsin condensation test data are shown on Figure 4-8.

The Reynolds number will vary with time and position inside the AP600 containment vessel during a design basis accident (DBA). During the relatively short blowdown phase, the velocity and corresponding Reynolds number will be largest on the wall nearest the break location and decrease as the flow moves away from the break. A natural circulation flow pattern is expected to develop during the depressurization phase when the PCS is in operation. The Reynolds number along the wall will be small during natural circulation.

The upper bound of the Grashof number range (calculated using the AP600 inner vessel wall heated length as the length parameter) is estimated to be 1.0E15 during PCS operation. Even though the large-scale PCS test data do not extend into this range, the large-scale PCS test data show that the condensation mass transfer coefficient is independent of length and that the correlation matches the trend in the data over the three decades of measured Grashof numbers. Other investigators[25,26] have also concluded that the turbulent free convection condensation heat transfer coefficient is independent of the length. Therefore, it can be assumed that this correlation can be extrapolated to full-scale containment modeling.

4.4 Evaporation Heat and Mass Transfer

For most evaporation heat and mass transfer tests, the liquid mass flow rate is measured only at the entrance and exit of the test assembly. The difference in measured liquid mass flow rates between the entrance and exit of the test assembly is the total evaporation rate. The average measured Sherwood number, determined from the measured total evaporation rate, is representative of the local evaporation rate if the partial pressure difference between the film surface and air does not change significantly through the test assembly. The Westinghouse STC flat plate evaporation tests[18] met this criterion. Relatively high air-flow rates, in comparison to the mass transfer, were used in these tests. The Westinghouse STC flat plate evaporation test data covered a Reynolds number range up to 1.2E5 and a Grashof number range up to 7.0E10. The evaporation test data covers the expected range of both the Reynolds and Grashof numbers in the annulus during a design basis accident (DBA) event.

A comparison of the measured mass transfer for the Westinghouse STC flat-plate evaporation tests with the correlation is presented as a function of the Reynolds numbers in Figure 4-11. The correlation fits the data.

The predicted-to-measured Sherwood ratio for the Westinghouse STC flat plate evaporation tests is shown as a function of the Reynolds number, Grashof number and dimensionless steam concentration in Figures 4-12 through 4-13. The mean predicted-to-measured Sherwood number ratio is 0.936 with a standard deviation of 0.139.

The Gilliland and Sherwood evaporation tests[27] provided a comparison of the measured and predicted total evaporation rates at relatively low Reynolds and Grashof numbers. As shown in Section 3.5 of WCAP-14326,[16] the heat and mass transfer correlations predicted the measured total evaporation rates very well. However, local evaporation measurements were not made and internal variations in partial

pressure difference vary too much to be able to determine either a local, or a meaningful average Sherwood number for these tests.

The integral large-scale passive containment cooling system (PCS) tests have been evaluated using the WGOTHIC code to provide added confidence that evaporative heat and mass transfer are being well-modeled. The results of this evaluation are presented in Section 8.0 of this report.

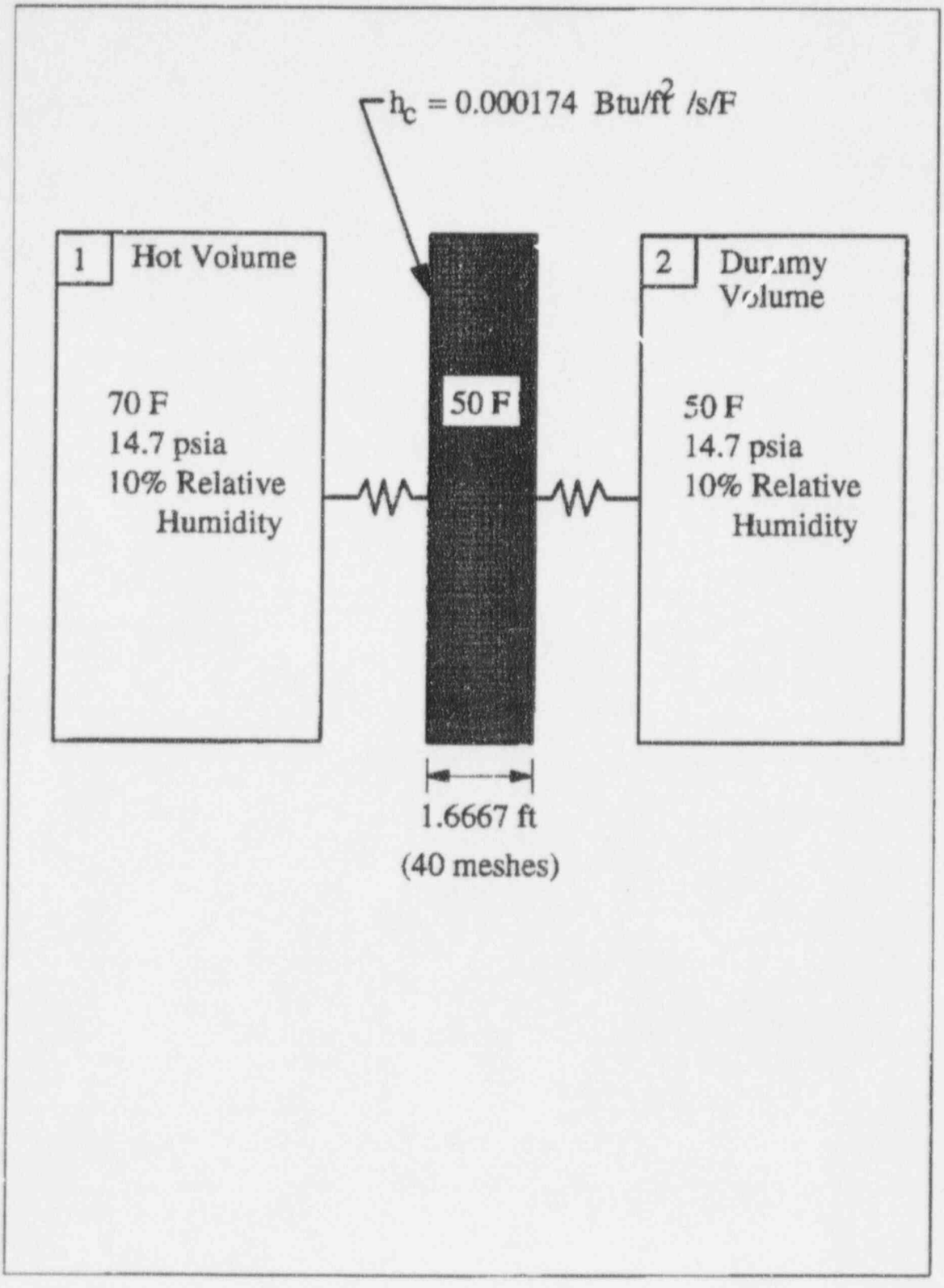

Figure 4-1 Westinghouse-GOTHIC Model of Transient Wall Conduction Problem

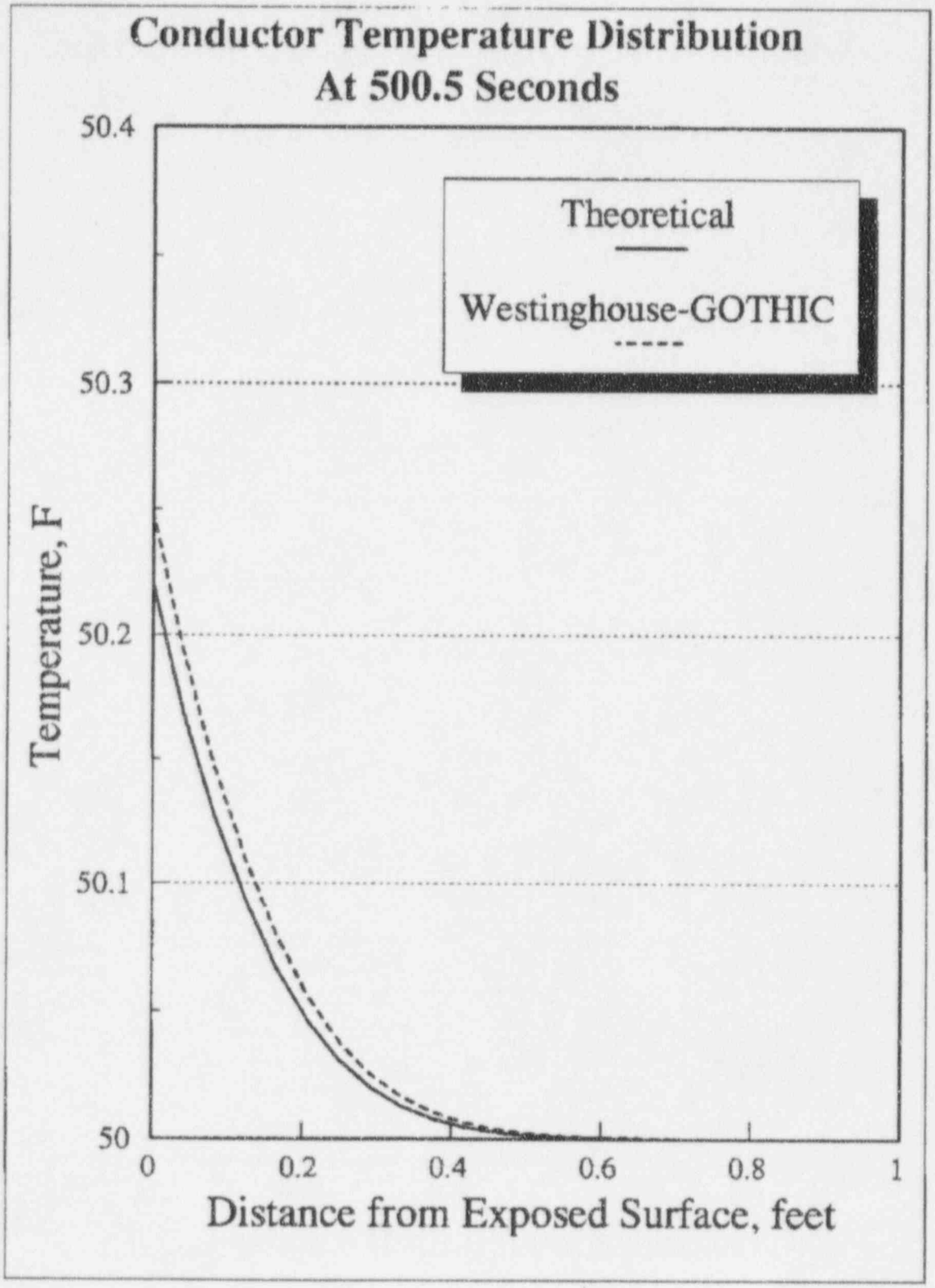

Figure 4-2 Comparison of Westinghouse-GOTHIC and Theoretical Transient Wall Conduction Solution

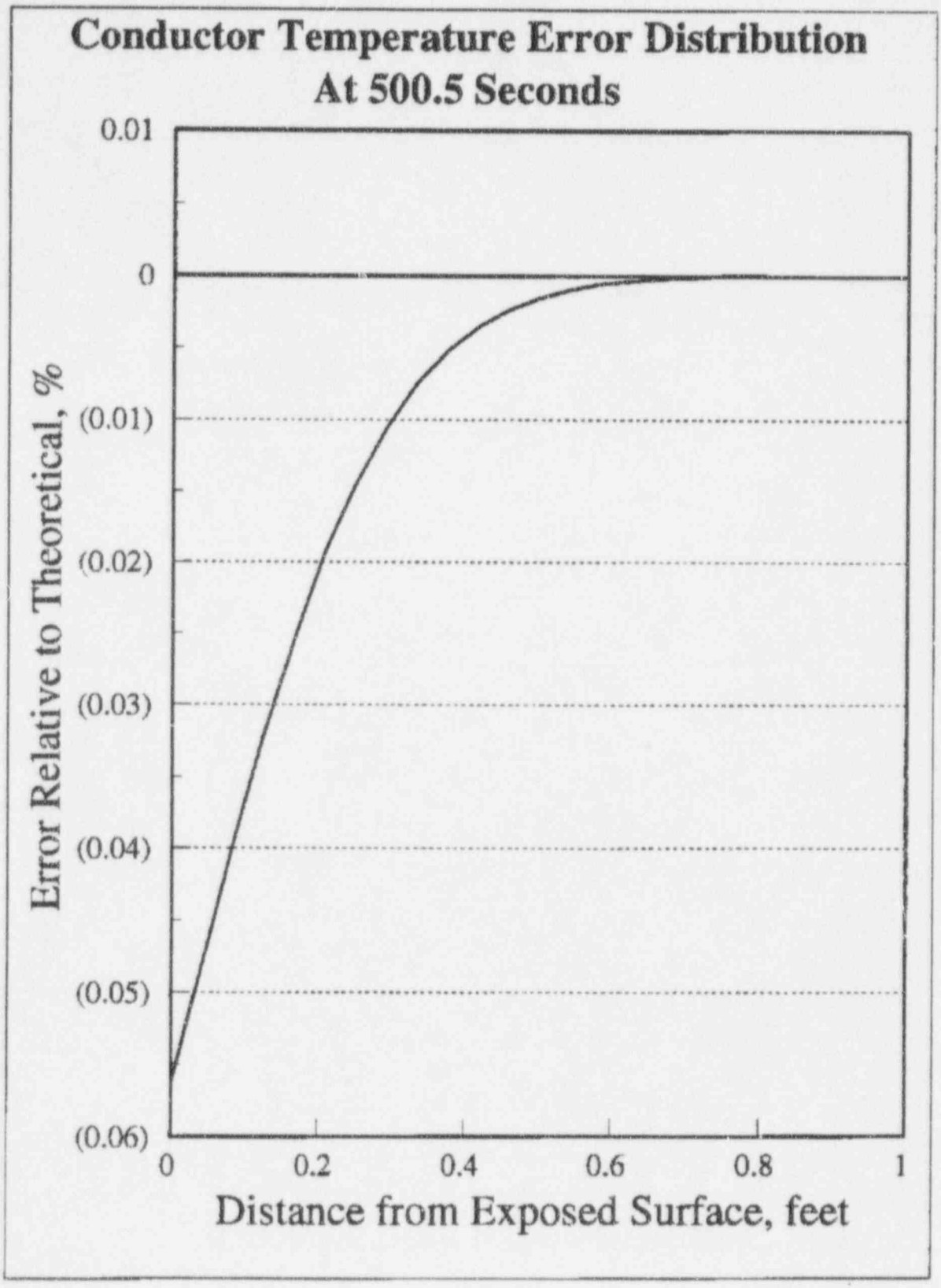

Figure 4-3 Temperature Error Relative to Theoretical Solution as a Function of Position

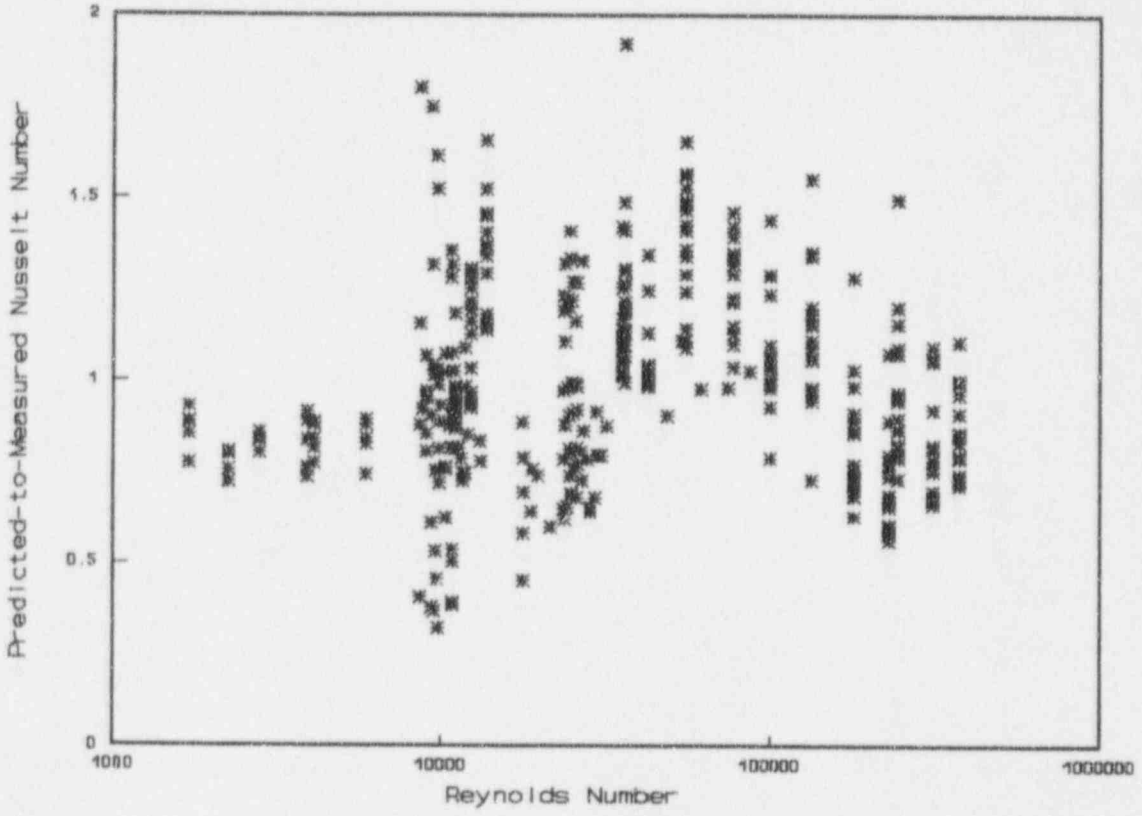

Figure 4-4 **Predicted-to-Measured Nusselt Numbers for Convection as a Function of the Reynolds Number**

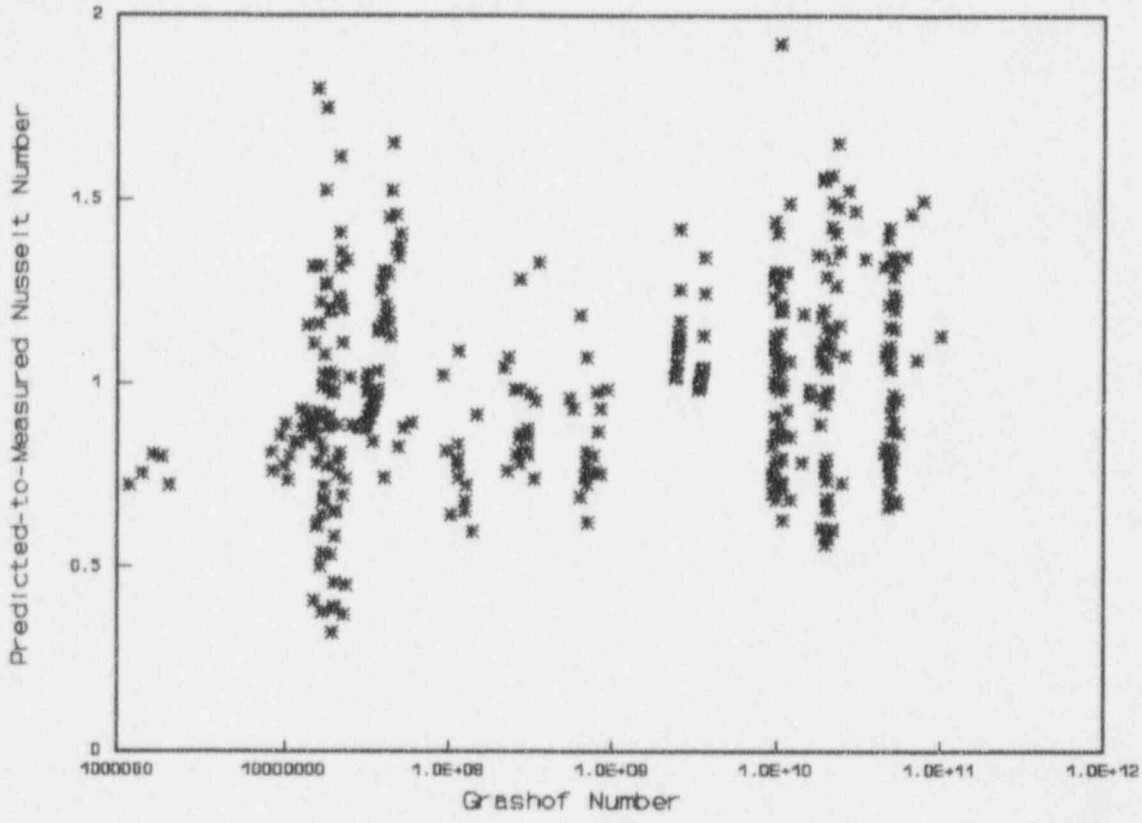

Figure 4-5 **Predicted-to-Measured Nusselt Numbers for Convection as a Function of the Grashof Number**

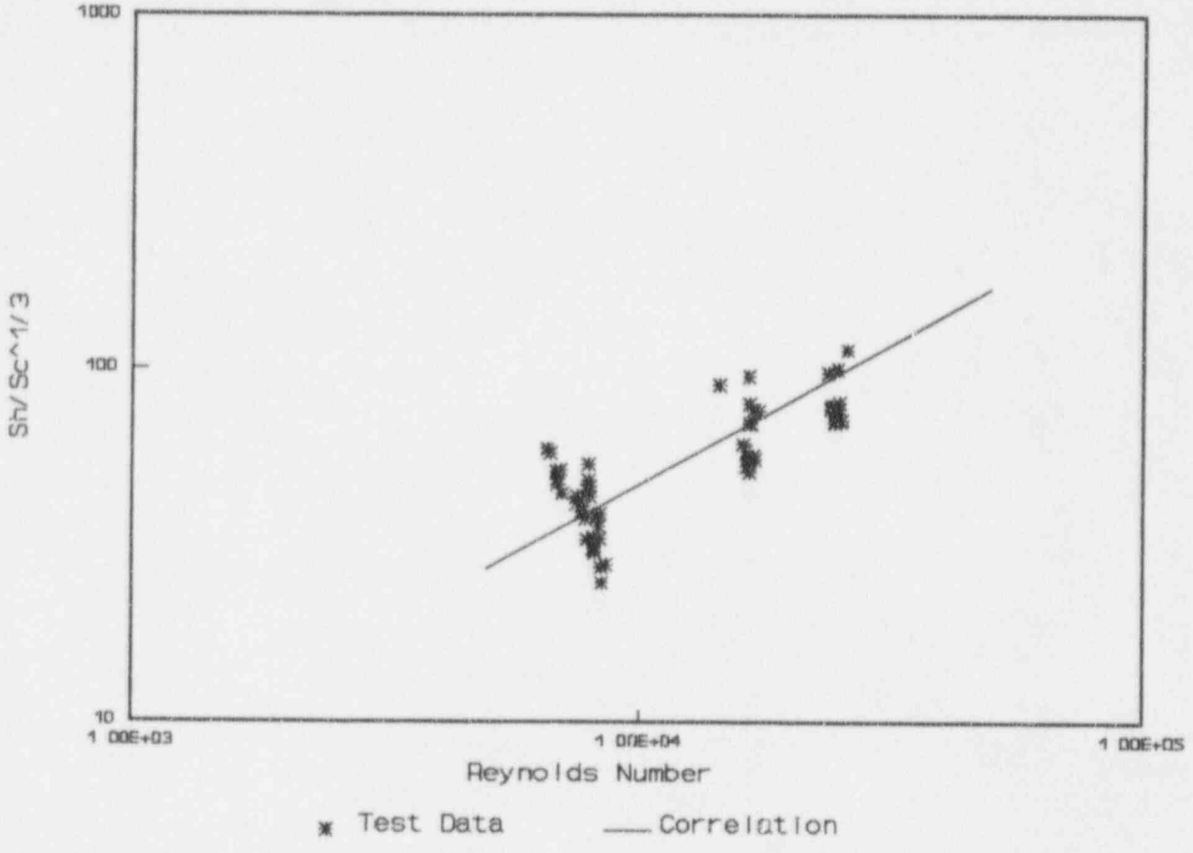

Figure 4-6 Correlated Mass Transfer Data for the Wisconsin Condensation Tests

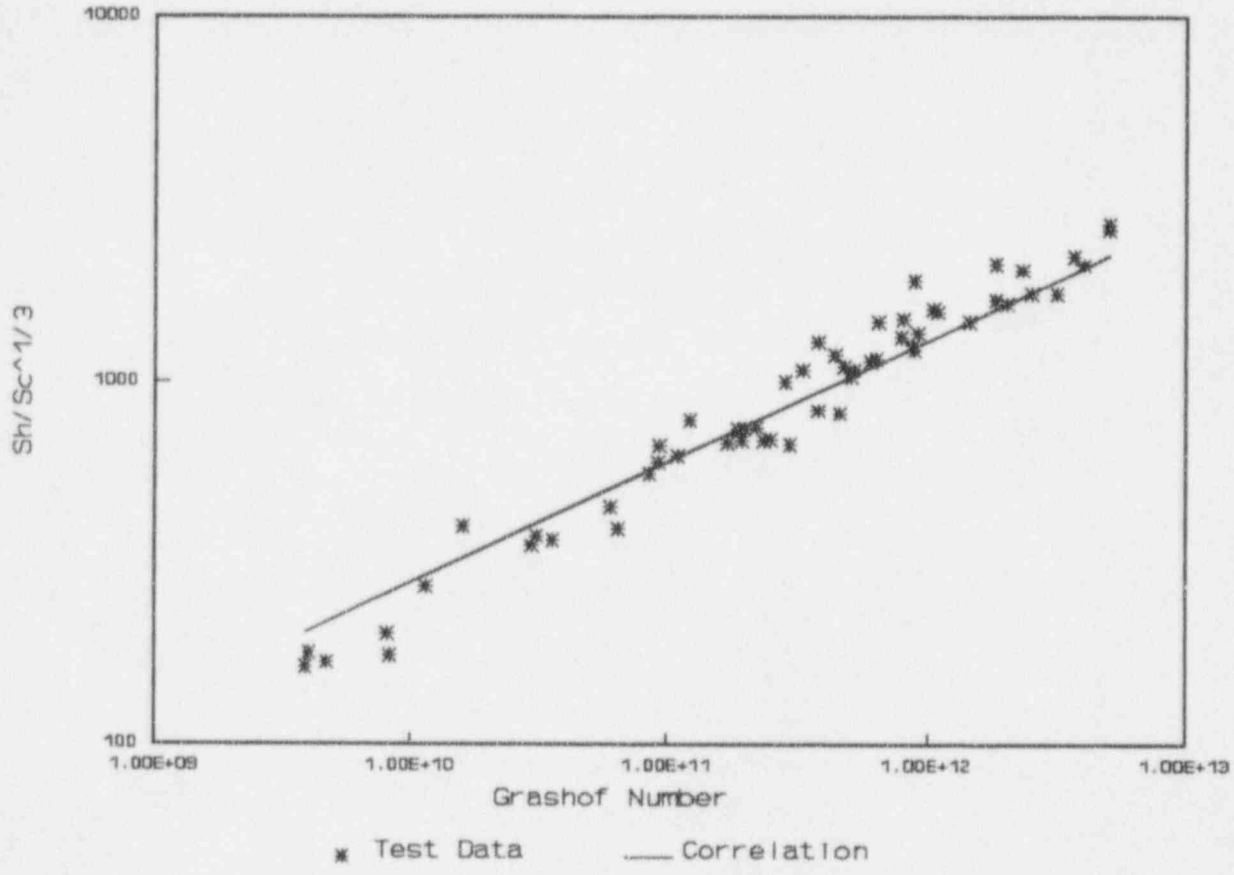

Figure 4-7 **Correlated Condensation Mass Transfer Data for the Westinghouse Large-Scale PCS Tests**

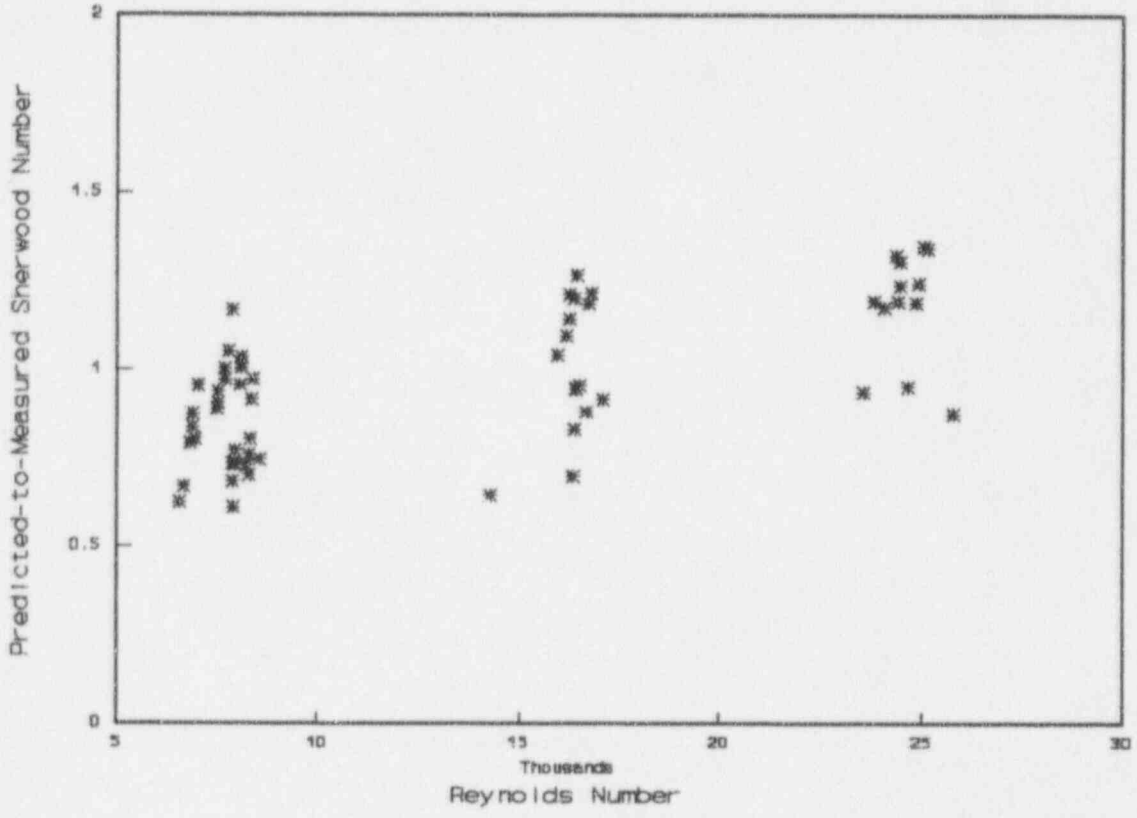

Figure 4-8 Predicted-to-Measured Sherwood Numbers for Condensation as a Function of the Reynolds Number

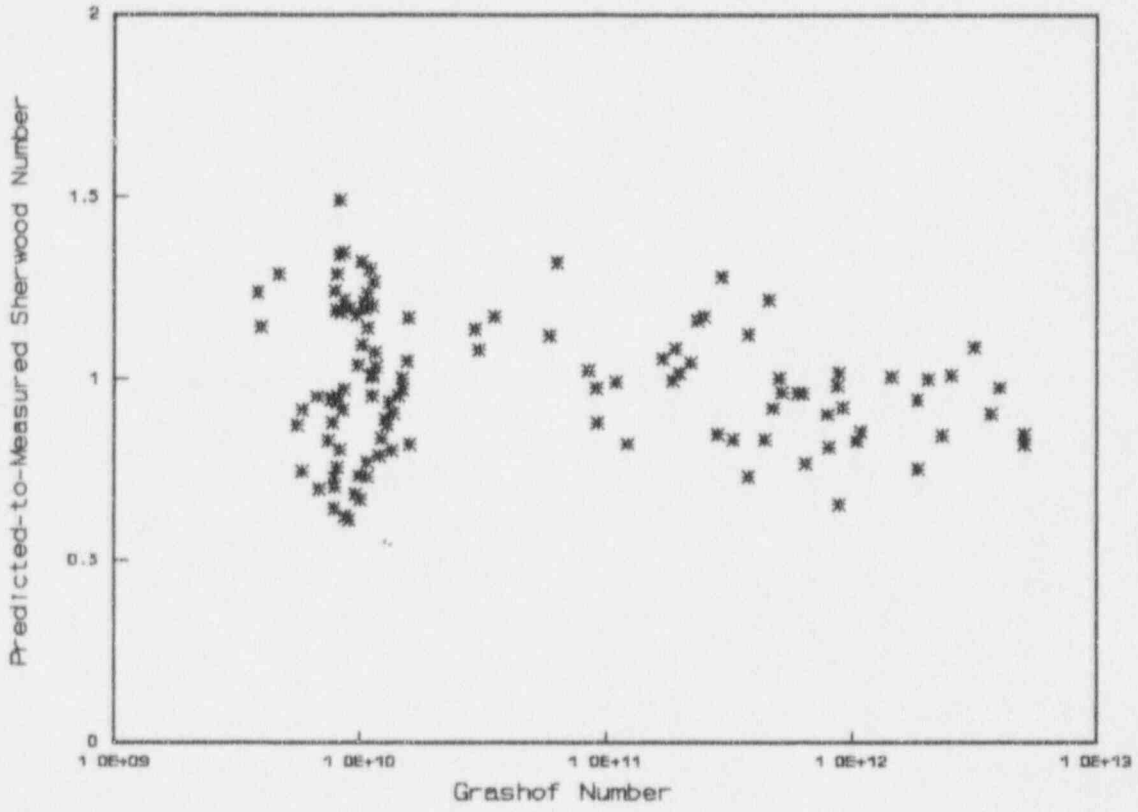

Figure 4-9 **Predicted-to-Measured Sherwood Numbers for Condensation as a Function of the Grashof Number**

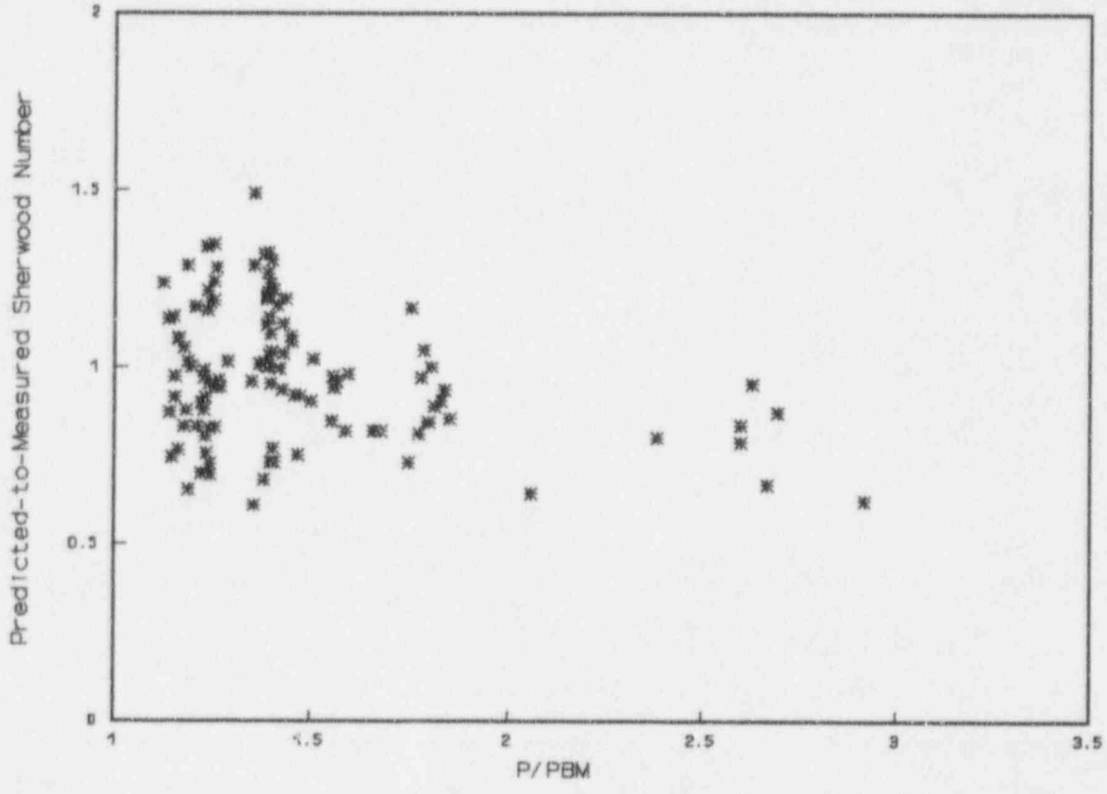

Figure 4-10 Predicted-to-Measured Sherwood Numbers for Condensation as a Function of Dimensionless Pressure

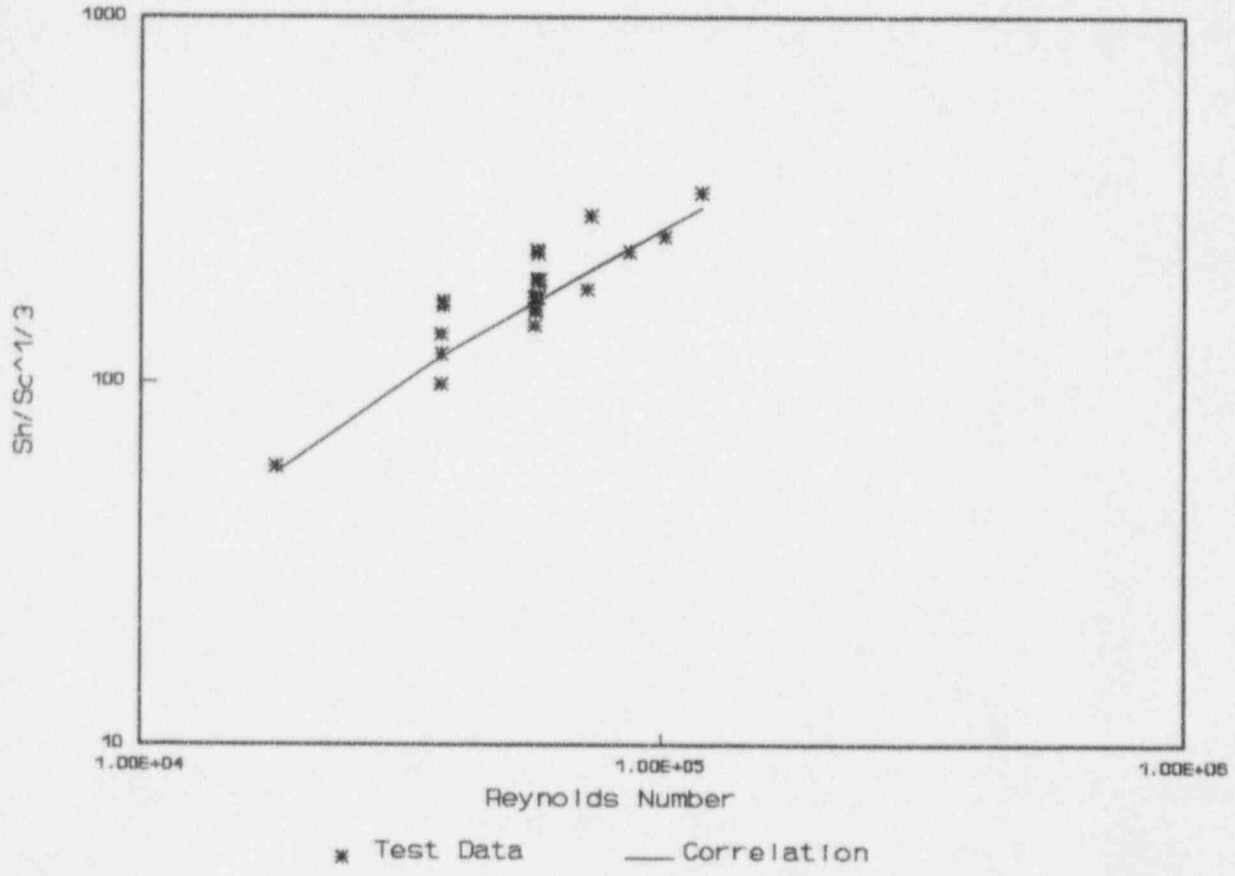

Figure 4-11 Correlated Mass Transfer Data for the STC Wet Flat-Plate Tests

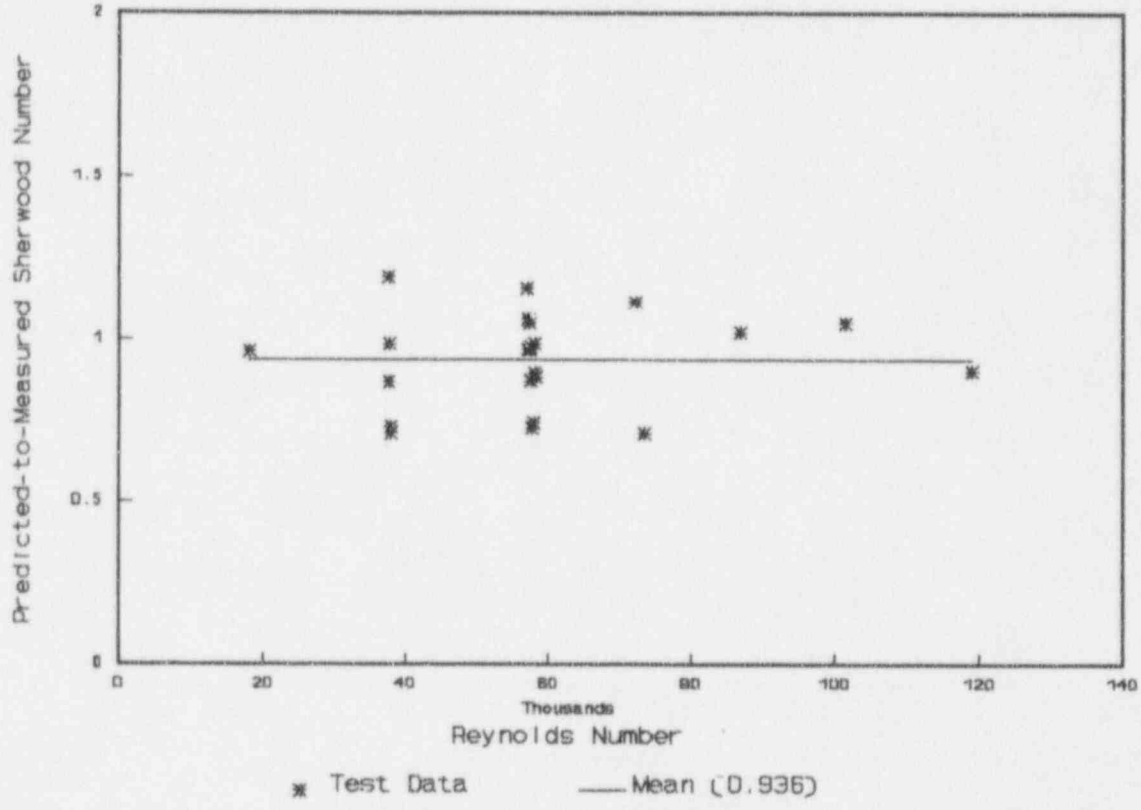

Figure 4-12 Predicted-to-Measured Sherwood Numbers for Evaporation as a Function of the Reynolds Number

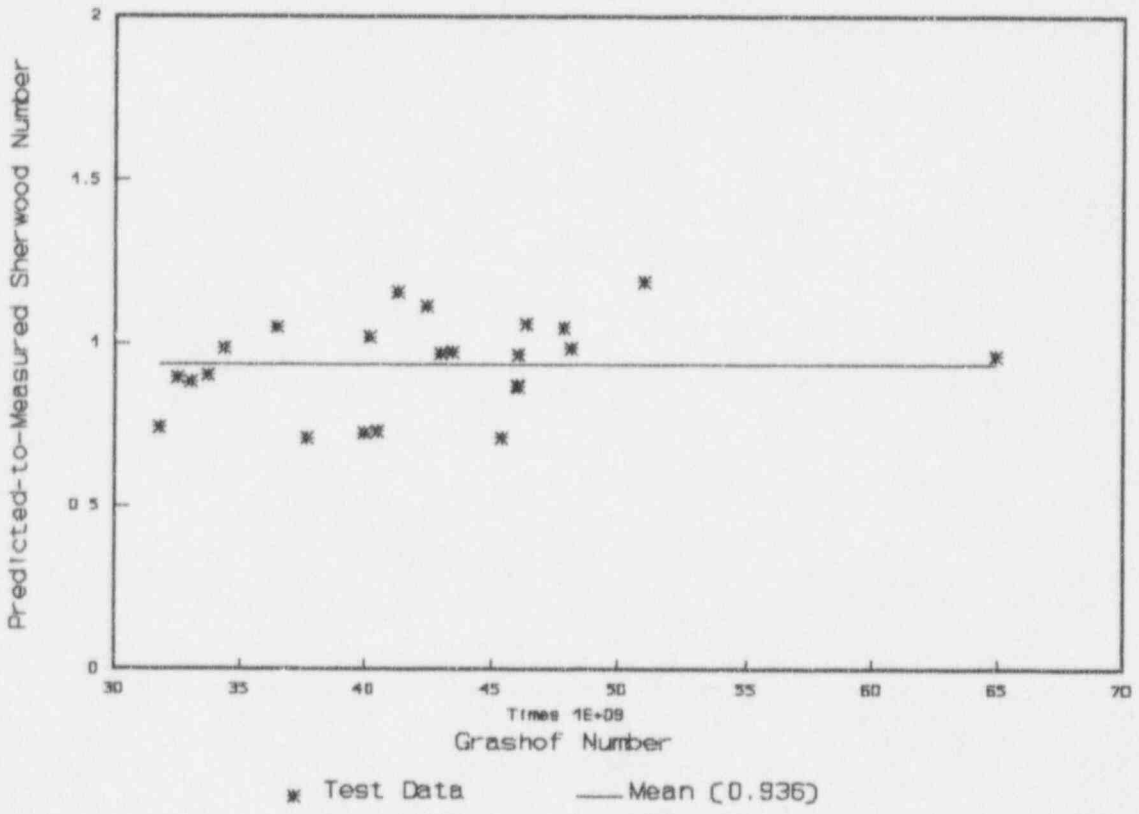

Figure 4-13 Predicted-to-Measured Sherwood Numbers for Evaporation as a Function of the Grashof Number

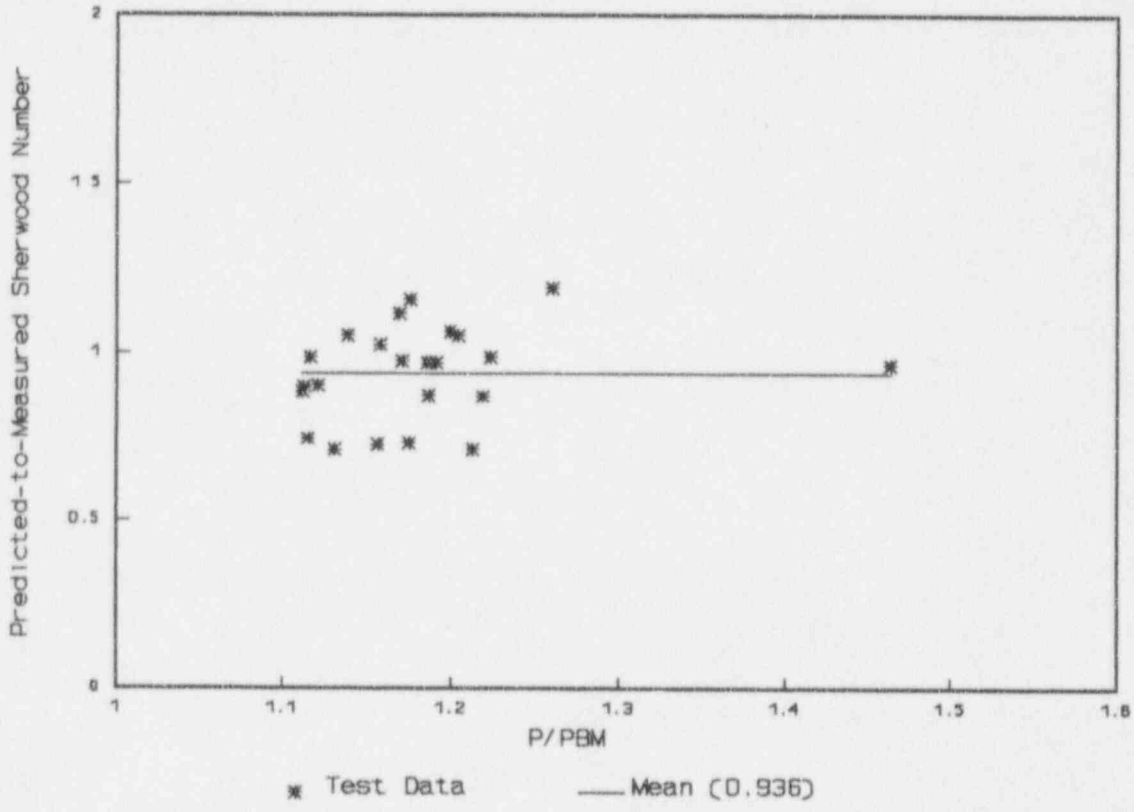

Figure 4-14 Predicted-to-Measured Sherwood Numbers for Evaporation as a Function of the Dimensionless Pressure

5.0 WGOTHIC MOMENTUM FORMULATION AND LARGE-SCALE TEST NODING STUDIES

The following section summarizes the modeling capabilities of the WGOTHIC transient momentum equation formulations and the effects of the formulation and noding on the ability to predict large-scale test (LST) performance.

5.1 WGOTHIC Momentum Formulation

The traditional single-node containment code and WGOTHIC formulations are compared and contrasted in Figure 5-1. In single node codes, the entire containment open volume is represented as one node and there can be no resolution of velocities or noncondensible distributions within the containment. WGOTHIC provides analysis capabilities beyond those of containment codes used for operating plants.

The following are definitions of key terms used in WGOTHIC discussions. For passive containment cooling system (PCS) design basis accident (DBA) evaluations, compartments below deck are modeled in WGOTHIC as lumped parameter volumes in a node-network solution, which is referred to as the *lumped parameter formulation*. The lumped parameter formulation in WGOTHIC differs from traditional single node codes. In this formulation, a transient momentum equation is solved[4] through the junctions joining nodes. The transient momentum equation for flow *junctions* linking lumped parameter volumes provides a coarse representation of transient fluid velocities, and the discretization of the containment allows coarse representation of steam/air concentrations throughout the containment.

An accurate representation of entrainment into a buoyant plume rising into an open volume requires a more detailed model than can be obtained with lumped parameter volumes. WGOTHIC includes a finite-difference solution to the transient momentum equation within an open volume[4] which, when taken with relatively large node sizes, is referred to as the *distributed parameter formulation*. The distributed parameter formulation is a user option to define a more detailed matrix of nodes within an open volume. Such a *subdivided volume* allows a better resolution of flow fields, such as those arising from plume entrainment. Subdivided volumes can be connected to lumped parameter volumes or other subdivided volumes using junctions.

The following discusses the bases for noding used in the evaluation models discussed in Section 6.0.

5.2 WGOTHIC Distributed Parameter LST Noding Studies

The WGOTHIC analysis results within this section discuss noding studies and the bases for the LST distributed parameter model noding.

5.2.1 Local Noding Studies

Local noding studies were performed on a WGOTHIC distributed parameter model of the dry baseline large-scale test. The purpose of the local noding sensitivities is to examine the effect of changing the noding in one region while other noding is left unchanged from a defined base case model. These

local noding studies were used to develop the detailed distributed-parameter model (discussed in Appendix A).

A brief description of the test, followed by a discussion of the noding studies performed and their results are given in this section. All results are given at steady-state conditions.

5.2.2 Baseline Large-Scale Test Facility Description

The baseline test configuration is shown in Figure 5-2. Steam is supplied to the vessel through a 3-inch pipe at the vessel axial centerline, with the vertical pipe exit located at the operating deck level. The vessel has no representation of the full-scale plant internals. Thus, the internal gases are free to move throughout the interior volume of the test vessel. The vessel contains an operating deck grating with 83 percent open area, approximately 57 inches from the bottom of the vessel.

In the baseline test series, steam is delivered to the centerline axis from a 3-inch pipe. At steady-state, the vessel pressure is not changing, and the condensate drain rate equals the steam flow rate.

The steam delivery pipe is axisymmetric and delivers steam at the operating deck level, an elevation similar to plant break flow exiting a steam generator compartment. Other than the grating and steam supply pipe, the vessel is empty (that is, the full-scale plant internals are not represented).

Outside, the vessel is surrounded by a plexiglass baffle with a chimney. Heated air rises from the chimney, and natural convective flow cools the vessel.

Steam is much less dense than air at the same temperature and pressure, so a strong buoyant force causes the steam plume to rise, entraining surrounding atmosphere over its height. An air-rich layer exists below the steam injection location.

The plume rises to the inner dome surface and turns, following the inner surface curvature (Figure 5-3). As the steam-rich bulk flow travels along the cooler dome and sidewall surfaces, steam condenses and forms a liquid film which runs down the wall.

Beneath and near the steam inlet, fluid travels primarily horizontally at the steam inlet elevation over to be entrained by the jet. Some flow from beneath the inlet also is entrained, which brings some of the air from the region below the grating back into the bulk flow field. At steady-state, the mass flow rate of air returned to the upper region by entrainment over the lower portion of the steam plume is equal to the rate at which air flows into the lower region around the vessel circumference.

Although the tests include no representation of the full-scale plant internals, these tests are useful for the WGOTHIC noding studies. The vessel without any flow blockages is a relatively stringent test of the code's ability to predict axial gradients of air/steam. Also, the empty containment vessel makes it easier to vary the noding and has a short run-time so that more cases can be run to contribute to the understanding of noding effects.

Test number 103.1 from the Heavy Water Reactor Facility (HWRF) Test Program[28] was used for this study. The tests completed under this HWRF program are similar to the AP600 baseline tests, except

the HWRF tests had no water applied to the outside of the vessel. Thus, the total condensate flow rate is lower than AP600 LST. This is factored into the noding used for the AP600 LST, as discussed in Section 5.2.6. The extent of instrumentation for this test is the same as was available for the AP600 baseline LST.

A brief data summary for this test is shown in Table 5-1. The air-flow annulus velocity is controlled by a fan. A low-steam flow rate is injected through a 3-inch pipe, creating a buoyant plume.

5.2.3 Baseline Large-Scale Test WGOTHIC Model - Base Case Model

The WGOTHIC baseline LST model developed for these studies uses distributed parameter noding for the pressure vessel. The air annulus is modeled in the lumped parameter formulation because the conditions are expected to be relatively homogeneous across the majority of the annulus gap width.

The LST is modeled on a ¼-symmetry bases. The vessel is modeled as a cylinder. The height was maintained and the radius was set to 6.22 ft. (74.6 in.) so the total vessel volume and surface area were maintained. The noding diagram for the base case model is given in Figure 5-4. Noding sensitivities will be compared to the results from this base case.

The predicted steady-state vessel pressure is 25.4 psia, less than 5 percent overpredicted. The predicted and measured inside vessel-wall temperature distribution as a function of vessel height is shown in Figure 5-5. There are several climes along the top and bottom of the vessel that are essentially at the same height. This is indicated in Figure 5-5 by several points at about 0 and 20 ft. Agreement between the measured and predicted trend in axial-wall temperatures is good, although there is an indication of too much mixing below to above the operating deck.

The base-case velocity field is shown in Figure 5-6. In the lower left corner of the velocity vector figure, Vmax is specified. Vmax is the maximum velocity in the figure. The largest arrow in the figure has the velocity Vmax. Typically, all other vectors are linearly scaled from Vmax. However, to see the entire flow field better, an exponent (0.3) has been used on the velocity ratio (local velocity/Vmax), which sets the lengths of the velocity vectors. This causes the lengths of the shortest vectors to increase relative to the longest vector. The velocity for the inlet plume, the velocity along the wall, and the velocity along the base are given for reference. As can be seen, the calculation predicts the plume rising at the center of the vessel up to the dome, then turning along the dome and moving down along the vessel wall. Flow is entrained into the plume just above and below the operating deck.

The incoming steam has a low velocity, producing a buoyant plume. Therefore, these noding studies are applicable to test with entrainment into buoyant plumes, such as the Phase 2 large-scale tests.

5.2.4 Local Noding Case Studies

Noding sensitivities were performed to study separately the effect of noding in three particular areas:

- Along the vessel wall
- In the vertical and radial direction near the steam inlet
- Vertical noding throughout vessel

The effect on the following predicted parameters will be assessed as the noding is changed:

- vessel pressure
- velocity field
- axial steam gradient

These three parameters were chosen because of their importance in the analysis. The vessel pressure is dependent on the heat and mass transfer and is a primary measure of code success. The velocity field affects the mixing of the steam and air within the vessel. The velocities along the vessel walls are used to calculate the local heat and mass transfer correlations. The axial steam gradient is an important parameter in calculating the internal mass transfer rates.

Noding Along the Vessel Wall

Since there is a downward velocity along the wall, the node near the wall must be small enough to allow a reasonable prediction of the downward convected flow. Because the heat and mass transfer correlations rely on differences between the film surface and bulk fluid properties, the node along the vessel wall must also be larger than the boundary layer thickness. These provide the basis for the range of node sizes studied.

Several node sizes along the vessel wall were studied. Figures 5-7, 5-8, 5-9, 5-10, 5-11, and 5-12 show the radial noding used for the base case, cases a.1, a.2, a.3, a.4, and a.5, respectively.

Cases a.1, a.2, and a.3 examine progressively larger node sizes. Cases a.4 and a.5 study the effect of the node size adjacent to the node along the wall. Case a.4 is a variation of case a.1. Case a.5 is a variation of case a.3.

To more clearly allow comparison of the sensitivity results, the vessel pressure, maximum wall velocity, and steam pressure ratio (steam partial pressure divided by the total vessel pressure) predicted for each case are shown in Table 5-2. As expected, as the node size along the wall increases, the velocity decreases. This is because the downward flow is averaged with more of the bulk flow as the node size increases. However, the velocity is not a strong function of node size within the range examined. For example, the node size along the wall from the base case to case a.3 was increased by a factor of [ ]^{a,c}, but the velocity along the wall only decreased by [ ]^{a,c}.

The flow fields for the base case and one of the largest noded cases, case a.5, are shown for illustration of the unchanged flow field in Figure 5-13. The overall flow field was essentially unchanged for the near wall noding sensitivity cases.

For the range of node sizes studied here, the node size along the vessel wall had a relatively small impact on the overall results. For all the cases, the magnitude of the predicted velocity along the vessel wall is so small that the heat and mass transfer to the vessel wall is dominated by free convection.

Noding Near Steam Inlet

The node size in the vertical and radial directions near the steam injection location was varied.

Vertical Noding

For the noding sensitivity in the vertical direction (case b.1), the node boundary at elevation [ ]^{a,c} (Figure 5-3) was deleted, [ ]^{a,c} the size of the node directly below the steam injection point. The results are shown in Table 5-3. This resulted in significantly less axial steam stratification in the vessel.

The velocity field for the base case and for case b.1 are shown in Figure 5-14. There is a subtle but important difference between the two velocity fields. In the base case, the inlet steam is entraining from [ ]^{a,c}. It is not entraining from [ ]^{a,c}. In case b.1, there is entrainment from [ ]^{a,c}. This noding structure causes better mixing of the noncondensible gases throughout the vessel.

Detailed axial noding just below the steam injection location into the containment atmosphere is important for predicting the noncondensible axial stratification. If the nodes are too big, the code entrains from a larger layer causing more mixing below the steam injection location.[29]

Radial Noding

Two cases study the sensitivity in the radial direction near the steam inlet. The node adjacent to the steam inlet (case b.2) and the steam inlet node (case b.3) were increased in size. The noding as a function of radius for cases b.2 and b.3, are shown in Figures 5-15 and 5-16, respectively. Since case b.3 is more coarsely noded, it will be discussed.

Figure 5-17 shows the velocity field for the base case and case b.3. Steam is injected into a node in which the vertical flow area has more than tripled, but the inlet plume velocity was only minimally impacted. This is because in case b.3 there is more mass flowing through the node caused by entrainment from the adjacent node. The vessel does not overmix the noncondensibles from below deck because it is entraining the additional flow from the adjacent node above deck, as compared to the effect of the vertical noding study which entrained from below the deck. The additional mass flow entrained is carried over to the vessel-side wall where the maximum wall velocity increased from 1.69 ft./sec. in the base case to 1.83 ft./sec. in case b.3 (Table 5-4).

The steam inlet buoyant plume is entraining more fluid in case b.3 from its adjacent node than the base case, but the overall impact is small, since it does not entrain additional flow from below the deck. Thus the internal velocity fields are a weak function of the radial noding near the plume within the ranges studied.

Vertical Noding Throughout Vessel

Several nodes in the vertical direction were combined (case c.1) to examine the sensitivity to noding in this direction. The node boundaries were removed with the intention of deleting the ones that were

thought to minimally affect the flow field. The boundaries at elevations [
]^{a,c} were removed, leaving a total of [ ]^{a,c} elevations in the vessel.

The velocity field for the base case and case c.1 are shown in Figure 5-18. The velocity field of case c.1 approximates the base case flow field. The magnitude of the velocity below the operating deck is higher than for the base case; however, the maximum wall velocity is smaller, as shown in Table 5-5. Mixing is minimally affected by the change in vertical noding.

5.2.5 Local Noding Studies Conclusions

Local noding studies have been completed using a model of the baseline LST with no internals. Noding sensitivities were performed in order to study, separately, the effect of noding in three particular areas to define the detailed distributed-parameter model to be used for the WGOTHIC code validation using Phase 2 LST data (Appendix A). Many of the noding modifications had a small impact on the predicted results. None of the cases had a major impact on the predicted vessel pressure or the overall velocity field. The model was most sensitive to a change in the node height directly below the steam injection point. A summary of the results are discussed below.

Noding Along the Vessel Wall

The node width along the vessel was varied from [ ]^{a,c}. As the node size along the wall increased, the velocity along the wall decreased due to averaging, as expected. However, in the range of node sizes studied, none of them had a significant impact on the results. There are two reasons for this. First, a significant increase in node width [ ]^{a,c} caused a relatively small decrease in velocity [ ]^{a,c}. Second, since the heat transfer is dominated by free convection; that is, the calculated velocities, even with a [ ]^{a,c} node width, did not get into a forced convection regime, the heat and mass transfer rates were not significantly affected by the change in wall velocity. Also, the mixing of air from below the injection location with steam and air in the upper containment was not strongly affected by the change in wall velocity, as indicated by the steam pressure ratio.

Noding Near the Steam Inlet

Deleting the noding elevation located just below the point of steam injection resulted in over-entrainment of air from below the operating deck and a significant increase in the mixing throughout the vessel.

Increasing the steam injection node width did not impact the overall results significantly. It did increase the entrainment into the buoyant plume from adjacent nodes, but it was not enough to significantly impact the vessel pressure, predicted flow field pattern, or the mixing results.

Vertical Noding Throughout the Vessel

Deleting several noding elevation planes from above and below the operating deck had a weak effect on the internal velocity field and did not strongly influence the vessel pressure or steam mixing.

5.2.6 Application of Local Noding Studies

The conclusions from the noding sensitivity studies on the baseline test were applied to the development of the detailed distributed parameter Phase 2 test model to be used for WGOTHIC integral validation. The baseline LST noding sensitivities are applicable to tests with a buoyant plume. They are, therefore, applicable to developing the noding to be used for the Phase 2 tests. The more complex internal geometry, the wider range of steam flow rates, and the external water applied to the vessel surface of the Phase 2 tests must also be taken into consideration.

The purpose of the detailed distributed-parameter model was to have an accurate representation of entrainment into a buoyant plume rising into an open volume and to provide a reasonable detailed resolution of the velocity and noncondensible gas distributions in the LST. When building the detailed distributed-parameter model, if there was a doubt as to whether it was necessary to have additional noding, the additional noding was used in the model.

The baseline LST noding sensitivity studies showed that elevational resolution is needed directly below the height at which the steam enters the containment atmosphere in order to model entrainment into the buoyant plume and predict axial noncondensible stratification. Although [ ]^{a,c} elevations were used in the baseline LST model just discussed, [ ]^{a,c} elevations below the steam injection into containment were used in the detailed distributed-parameter model. This [ ]^{a,c} was used since the Phase 2 tests have a wider range of steam inlet flow rates.

Within the range of node sizes studied, the node size along the wall was not of extreme importance. A node width of [ ]^{a,c} along the vessel wall, and a node width of [ ]^{a,c} adjacent to this was used (similar to case a.5). The noding in case a.5 had the smallest number of nodes in the "a" sensitivity cases. Since finer noding along the wall proved to be of no benefit, it was not used.

The baseline noding sensitivity studies showed an insignificant effect due to increasing the width of the node into which the steam enters. However, since the Phase 2 tests have a different steam inlet geometry due to the steam diffuser and the steam generator compartment, the node width for this test was modelled to be [ ]^{a,c}. Also, significant noding detail in and around the steam generator compartment was modelled.

The noding studies showed that decreasing the number of vertical elevations minimally affected the flow field and the mixing of noncondensible gas from below the injection location. However, since the steam entered the containment atmosphere at a higher elevation than it did for the baseline tests therefore making it necessary to model the heating an evaporation of the applied exterior water, which causes larger wall-heat fluxes, noding in the vertical direction was not spared.

The vessel internals' geometry in the Phase 2 tests was also used to determine node boundaries. For example, the specific location of several of the subvolume boundaries were determined based on the [ ]^{a,c}.

Further description of the detailed distributed-parameter noding and comparisons of results from this model with measured test data from two of the Phase 2 tests are given in Appendix A.

5.2.7 Noding Convergence

Once it was established that agreement between the detailed distributed parameter LST model and the measured data was very good (Appendix A), additional noding studies were performed on the detailed distributed parameter model. The purpose of these studies was to simplify the noding without distorting the flow field. Reducing the number of nodes will decrease the run time and will require less set up time. The resulting noding from this study will be used in the distributed parameter evaluation model for the WGOTHIC large-scale test evaluation model (Section 6.2) and corresponding noding structure will be used for the AP600 distributed-parameter evaluation model.

In the following sections, the noding convergence studies are discussed followed by a comparison of the resulting distributed parameter evaluation model to the detailed distributed parameter model.

5.2.8 Phase 2 Large-Scale Test WGOTHIC Model - Base Case Model

The base case is the detailed distributed parameter Phase 2 LST model for test number 212.1A. The model and the comparison results are discussed in Appendix A.

The detailed distributed-parameter noding is shown in Figures 5-19, 5-20, and 5-21. The hatching in Figure 5-21 shows the location of the simulated break. These figures will be referred to throughout this section.

5.2.9 Noding Convergence Case Studies

The following were varied in these noding convergence sensitivity studies:

- vertical noding
- steam generator compartment noding
- open and dead-ended compartment noding
- angular noding

To assess the effect of noding changes, the vessel pressure, the flow field, and the axial noncondensible distribution were examined. These three parameters were chosen because of their importance in the analysis. The vessel pressure is the primary measure of code success. The velocity field affects the mixing and the predicted velocities along the vessel walls, which are used in the WGOTHIC heat and mass transfer correlations. The axial noncondensible gradient affects the internal mass-transfer rates.

The first steady-state portion of test 212.1 (referred to as 212.1A) was used for the studies. Rather than showing multiple vector plots for each case study, the velocity field in the most influencing plane will be shown. This is the vertical plane that passes through the simulated break location. The plane is marked as A-A in Figure 5-22. The maximum wall velocity will also be tabulated, as well as the air-pressure ratio at the measurement locations in the dome and at elevation F.

In the lower left corner of the velocity vector figures, Vmax is specified. Vmax is the maximum velocity in the figure. The largest arrow in the figure has the velocity Vmax. All other arrows are

scaled linearly, so the size of the arrow is representative of the magnitude of the velocity. (This is different than the vector plots discussed in Section 5.2.3 in which the vector plots were not linearly scaled).

Vertical Noding

For the sensitivity in the vertical direction, the node boundaries at elevations [ ]^{a,c} (Figure 5-19) were removed (case d.1). The intent was to delete the node boundaries that were thought to minimally affect the flow field. In fact, the results showed that the flow field and noncondensible gradient were minimally affected (Table 5-6).

The predicted velocity field in the plane containing the simulated break location for the base case and case d.1 are shown in Figure 5-23. There are some slight differences between the flow fields, but the flow patterns are the same. Case d.1 is a good representation of the base case with fewer nodes.

Steam Generator Compartment Noding

Based on the local noding sensitivity studies (Section 5.2.4), the vertical noding directly below the steam injection location is important for predicting noncondensible gas concentration, therefore, elevation boundaries at [ ]^{a,c} shown in Figure 5-19 were not modified.

Noding in and around the steam generator compartment was modified as shown in Figure 5-24 (Case e.1). The predicted velocity fields in the plane containing the simulated-break compartment for the base case and case e.1 are shown in Figure 5-25. There are significant differences between the flow fields. In case e.1, all the flow is upward from the top of the steam generator model to the dome, even along the vessel wall. Also, the overall velocity magnitude in case e.1 is greater. This is evident from the bigger arrows in the velocity field figure for case e.1.

The vessel pressure and noncondensible pressure ratio in the dome and at the F elevation are shown in Table 5-7. The noding for case e.1 increased the noncondensible mixing of noncondensible gas from below the operating deck with steam and air above the deck.

Open and Dead-ended Compartment Noding

The open and dead-ended compartment were each modeled as a single lumped-parameter volume.

The velocity field for the plane across the steam generator compartment was not affected, as expected (Figure 5-26). An additional plane for the base case and case f.1 is shown in Figure 5-27. This shows the flow field in the plane across the open compartment (Figure 5-28 marked as B-B). There is no flow field for case f.1 below the operating deck because the open compartment is modeled as a lumped volume. It is obvious that the flow field above the operating deck is essentially unchanged. The entire vessel velocity field above the operating deck was insignificantly affected by this change. The noncondensible pressure ratios for the base case and case f.1 are shown in Table 5-8. The differences between the results of the cases are minimal.

Angular Noding

The node boundary at the [ ]^{a,c} position was removed, combining two planes in the base case into a single plane. The resulting noding is shown in the plan view of the LST model in Figure 5-29 (case g.1). The number of elevations was unchanged from the base case.

Figure 5-30 shows the flow field in the simulated-break location plane for the base case and case g.1. This flow field is essentially unaffected.

Figures 5-31 and 5-32 show the flow fields for the base case and case g.1 in the planes that were modified. The single plane in case g.1 is approximately equal to the average of the two planes that it replaced from the base case. The results for case g.1 are summarized in Table 5-9.

5.2.10 Noding Convergence Studies Conclusions

Noding studies have been completed using a detailed distributed parameter model of the Phase 2 LST as the base case. In the four areas studied,

- vertical noding
- steam generator compartment noding
- open and dead-ended compartment noding
- angular noding

only the change in the number of nodes in and around the steam generator compartment produced significant differences between the base case and the modified case. The number of elevations in the steam generator compartment was reduced during the vertical noding study, but this did not significantly affect the results.

5.2.11 Application of Noding Convergence Studies

The conclusions from the noding convergence studies completed using the Phase 2 LST model were applied to reduce the number of nodes in the detailed distributed parameter model (Appendix A). The number of elevations was reduced (case d.1). Noding in and around the steam generator compartment was left unchanged (case e.1). The open and dead-ended compartments were modeled using the lumped-parameter formulation (case f.1). Although, the noding study showed that deleting the angular division at [ ]^{a,c} had a negligible effect (case g.1), this division was left in the final model, primarily to provide a more consistent node size distribution throughout the vessel.

There were two additional changes made to the detailed distributed-parameter model. One was to extend the radial divisions at a radius of [ ]^{a,c} through the entire vessel as shown in Figure 5-33. This actually simplifies the set up for the model because in the detailed distributed-parameter model, the containment vessel was modeled [ ]^{a,c} having a different number of subvolumes in the radial direction. These [ ]^{a,c} subdivided volumes were connected with junctions. [

]^{a,c}

The second change was to model the dome as a cylinder. Due to the rectangular coordinate system in the distributed-parameter formulation, modeling curved geometries required special attention. The detailed distributed-parameter model dome was modeled by taking small downward rectangular steps from the top of the dome to the spring line. With a reduction in the number of elevations in the dome, this becomes impractical because the steps become large and do not provide a good representation of the dome. Modeling the dome as a cylinder greatly simplifies the calculational input required to build the AP600 plant evaluation model with corresponding noding. In order to model the dome as a cylinder and maintain the correct vessel volume and surface area, the LST vessel height is reduced as shown in Figure 5-34. The total dome surface area and volume are preserved and the flow field is not distorted.

Figure 5-35 shows the elevation view of the vessel and air annulus. The vessel volume above the operating deck is divided into [ ]^{a,c} using the distributed-parameter formulation. The vessel is modeled by coupling the distributed-parameter above the deck and the lumped-parameter below the deck. The air annulus is modeled with the lumped parameter volumes. More details on the noding are given in Section 6.2.

The resulting flow field in the plane containing the simulated break location for the detailed distributed-parameter model (base case) and the modified distributed-parameter model are shown in Figure 5-36. The flow pattern is essentially the same. There is a small difference between the maximum velocity predicted, similar to Case d.1 which also had the number of elevations below the operating deck reduced. This is because the velocity is averaged over a larger area.

Table 5-10 shows a summary of the final case. There is some difference between the base case and the final case noncondensible gas concentration distribution. However, it is small enough not to significantly affect the over-all results. The maximum wall velocity is greater than the detailed distributed-parameter model, but is still within the range of measured velocities of [ ]^{a,c}.

Comparisons to additional LST using this model are shown in Section 8.0. Differences between the measured and predicted results will be assessed in the uncertainty analysis (Section 9.0).

5.3 WGOTHIC Lumped Parameter Model Development

Noding for the lumped-parameter model is shown in Figure 5-37. Details on the noding are given in Section 6.3.

Results obtained by comparison to Phase 2 test 212.1 showed that the lumped parameter model had a tendency to overentrain results in two competing effects:

- Overmixing of noncondensibles in the vessel penalizes the heat and mass transfer rates by moving noncondensible gas to regions near PCS heat removal.

- Overpredicting the velocity in the vessel, which enhances the heat and mass transfer rates. The predicted velocities were [ ]^{a,c}. The measurements show the velocities are [ ]^{a,c} along the vessel wall.[20]

These competing effects resulted in a slight over-prediction in vessel pressure as shown in Table 5.11 (case 1) for Test 212.1A. Preliminary noding studies showed that increasing the number of nodes did not reduce the competing effects.

To eliminate the competing effect due to velocity, only free convection was used to model heat and mass transfer inside the vessel. This conservatively biases the results toward a higher predicted vessel pressure. The resulting predicted vessel pressure is tabulated in Table 5-11 for Test 212.1A (case 2).

a,b

TABLE 5-1 DATA SUMMARY FOR TEST 103.1	
Steady State Conditions	
Ambient Temperature (°F)	
Ambient Pressure (in Hg)	
Ambient Relative Humidity (%)	
Vessel Internal Pressure (psia)	
Steam Inlet Temperature (°F)	
Condensate Flow Rate (lbm/hr)	
Annulus Velocity (ft/s)	

TABLE 5-2
SUMMARY OF NODE SIZE ALONG WALL SENSITIVITIES

Case	Vessel Pressure (psia)	Maximum Wall Velocity (ft./sec.)	Steam Pressure Ratio in Dome	Steam Pressure Ratio Below Deck
base	25.4	1.69	0.33	0.11
a.1	26.54	1.16	0.35	0.07
a.2	26.2	0.9	0.34	0.10
a.3	25.23	0.68	0.33	0.04
a.4	25.74	1.59	0.34	0.08
a.5	26.35	0.92	0.34	0.03

TABLE 5-3
SUMMARY OF NODE SIZE VERTICAL VARIATION NEAR STEAM INJECTION

Case	Vessel Pressure (psia)	Maximum Wall Velocity (ft./sec.)	Steam Pressure Ratio in Dome	Steam Pressure Ratio Below Deck
base	25.4	1.69	0.33	0.11
b.1	24.97	1.84	0.29	0.22

TABLE 5-4 SUMMARY OF NODE SIZE RADIAL VARIATION NEAR STEAM INJECTION				
Case	Vessel Pressure (psia)	Maximum Wall Velocity (ft./sec.)	Steam Pressure Ratio in Dome	Steam Pressure Ratio Below Deck
base	25.4	1.69	0.33	0.11
b.2	25.30	1.65	0.34	0.08
b.3	25.23	1.83	0.32	0.09

TABLE 5-5 SUMMARY OF VERTICAL NODING VARIATION (Local Noding)				
Case	Vessel Pressure (psia)	Maximum Wall Velocity (ft./sec.)	Steam Pressure Ratio in Dome	Steam Pressure Ratio Below Deck
base	25.4	1.69	0.33	0.11
c.1	25.37	1.36	0.35	0.04

TABLE 5-6 SUMMARY OF VERTICAL NODING VARIATION (Noding Convergence)				
Case	Vessel Pressure (psia)	Maximum Wall Velocity (ft./sec.)	Air P.R. at Dome-90°-63"	Air P.R. at F-0°
base	25.8	1.67	0.58	0.97
d.1	26	1.70	0.56	0.96

TABLE 5-7 SUMMARY OF STEAM GENERATOR COMPARTMENT NODING				
Case	Vessel Pressure (psia)	Maximum Wall Velocity (ft./sec.)	Air P.R. at Dome-90°-63"	Air P.R. at F-0°
base	25.8	1.67	0.58	0.97
e.1	27.5	2.70	0.63	0.78

TABLE 5-8 SUMMARY OF OPEN AND DEAD-ENDED COMPARTMENT NODING				
Case	Vessel Pressure (psia)	Maximum Wall Velocity (ft./sec.)	Air P.R. at Dome-90°-63"	Air P.R. at F-0°
base	25.8	1.67	0.58	0.97
f.1	26.1	1.68	0.58	0.94

TABLE 5-9 SUMMARY OF ANGULAR NODING				
Case	Vessel Pressure (psia)	Maximum Wall Velocity (ft./sec.)	Air P.R. at Dome-90°-63"	Air P.R. at F-0°
base	25.8	1.67	0.58	0.97
g.1	25.8	1.68	0.56	0.97

TABLE 5-10 SUMMARY OF DISTRIBUTED PARAMETER FINAL NODING				
Case	Vessel Pressure (psia)	Maximum Wall Velocity (ft./sec.)	Air P.R. at Dome-90°-63"	Air P.R. at F-0°
base	25.8	1.67	0.58	0.97
f.1	26.0	2.49	0.61	0.87

TABLE 5-11 TEST 212.1A VESSEL PRESSURES	
	Vessel Pressure (psia)
measured	[ ]^{a,b}
case 1	26.1
case 2	28.7

Traditional Plant Containment Analysis
(Single Node Lumped Parameter)

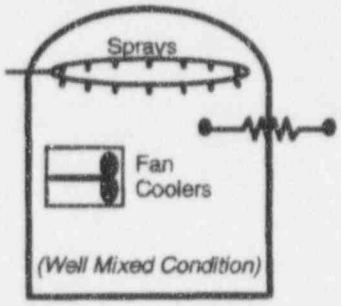

*WGOTHIC Lumped Parameter **
(Node-Network)

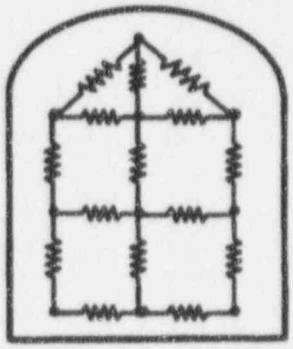

*WGOTHIC Distributed Parameter **
(Finite Difference, Large Mesh)

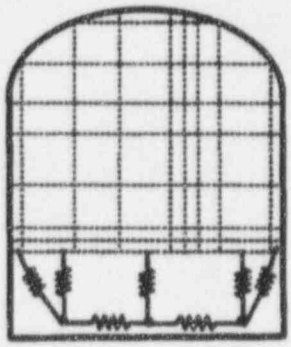

** Not actual noding. For illustration only.*

Figure 5-1 Comparison of Traditional Lumped Parameter Containment Codes to WGOTHIC Momentum Formulations

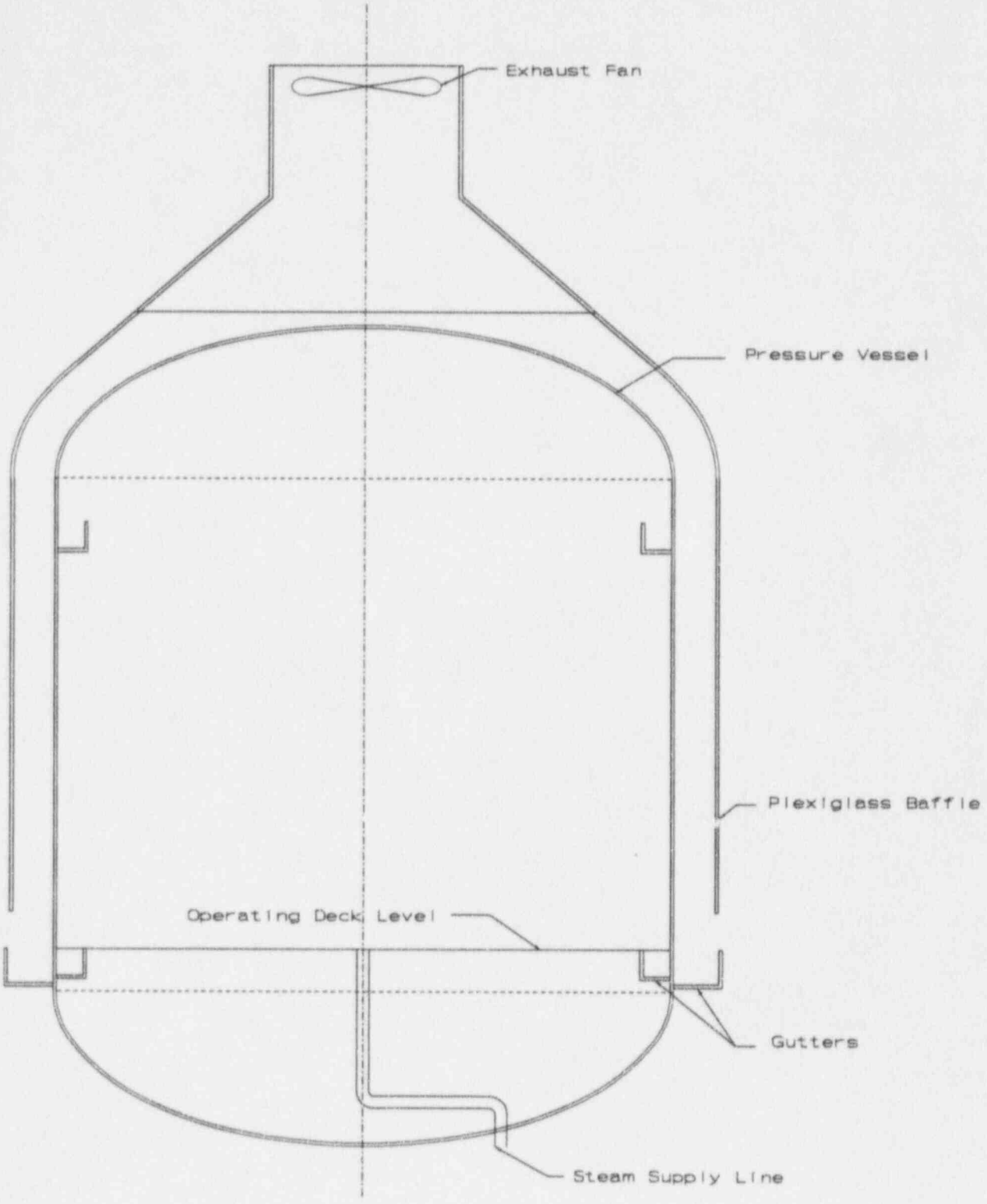

Figure 5-2 Section View of Baseline Large-Scale Test

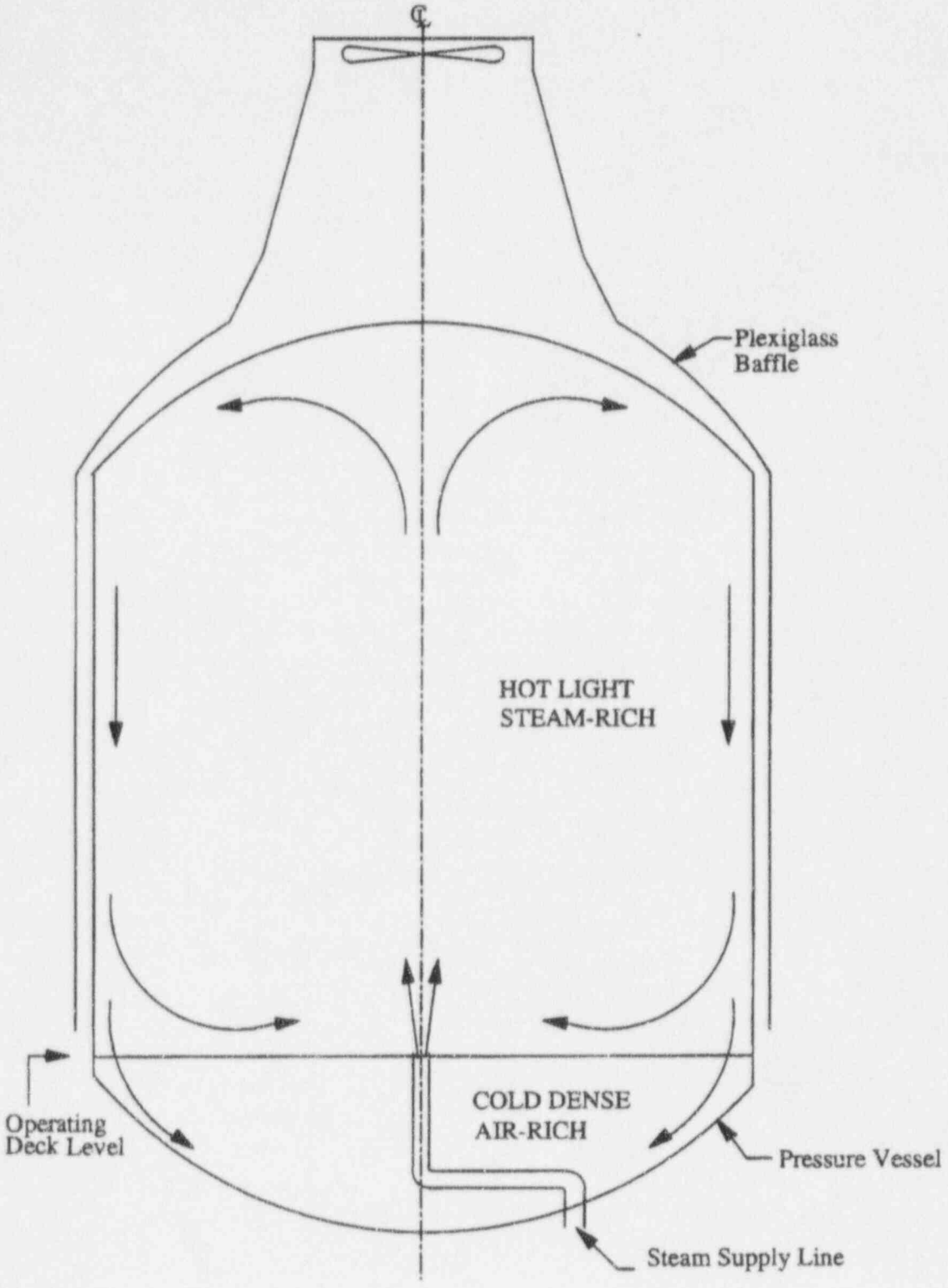

Figure 5-3 Baseline Large-Scale Test Characteristics

a,c

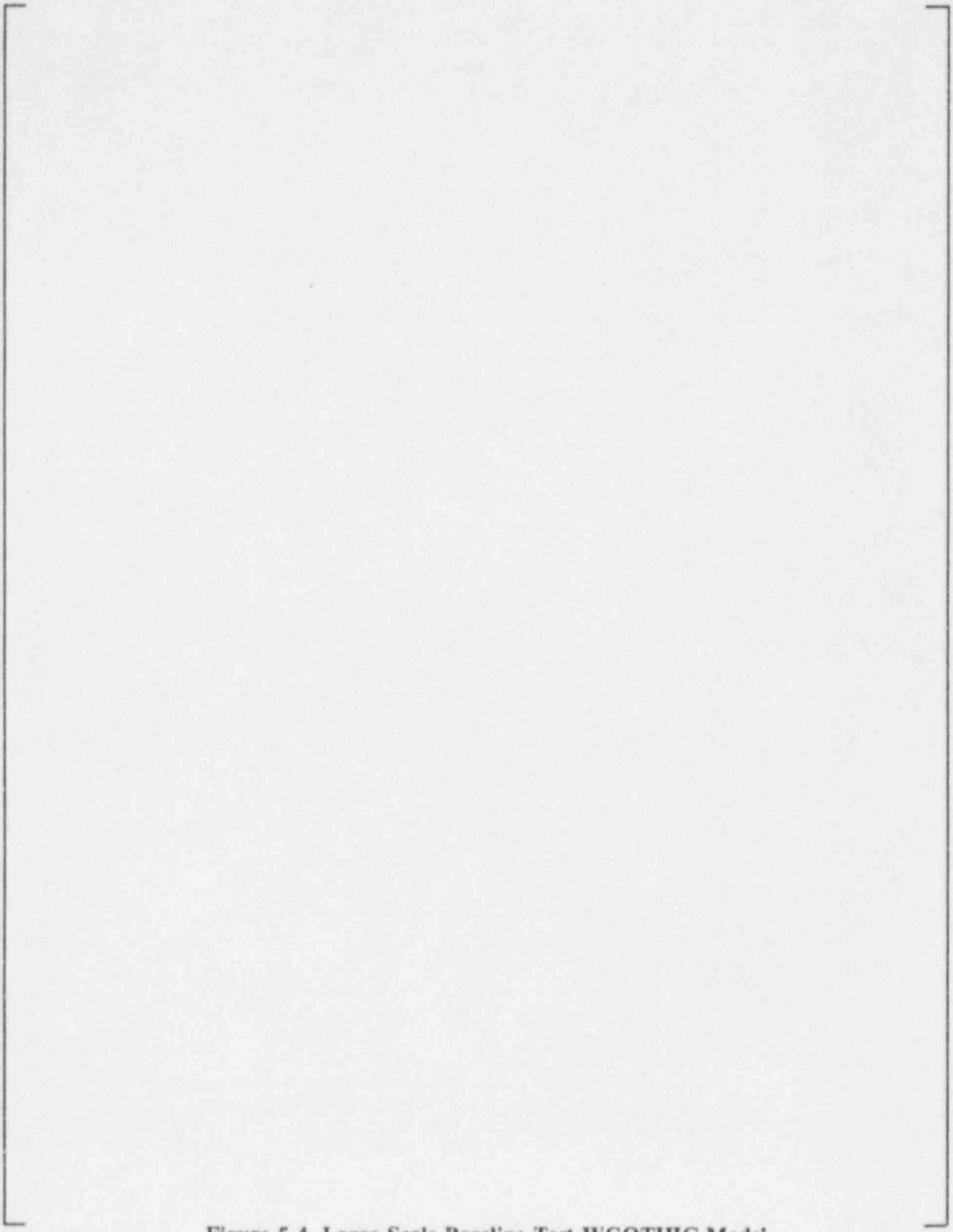

Figure 5-4 Large-Scale Baseline Test WGOTHIC Model

a,c

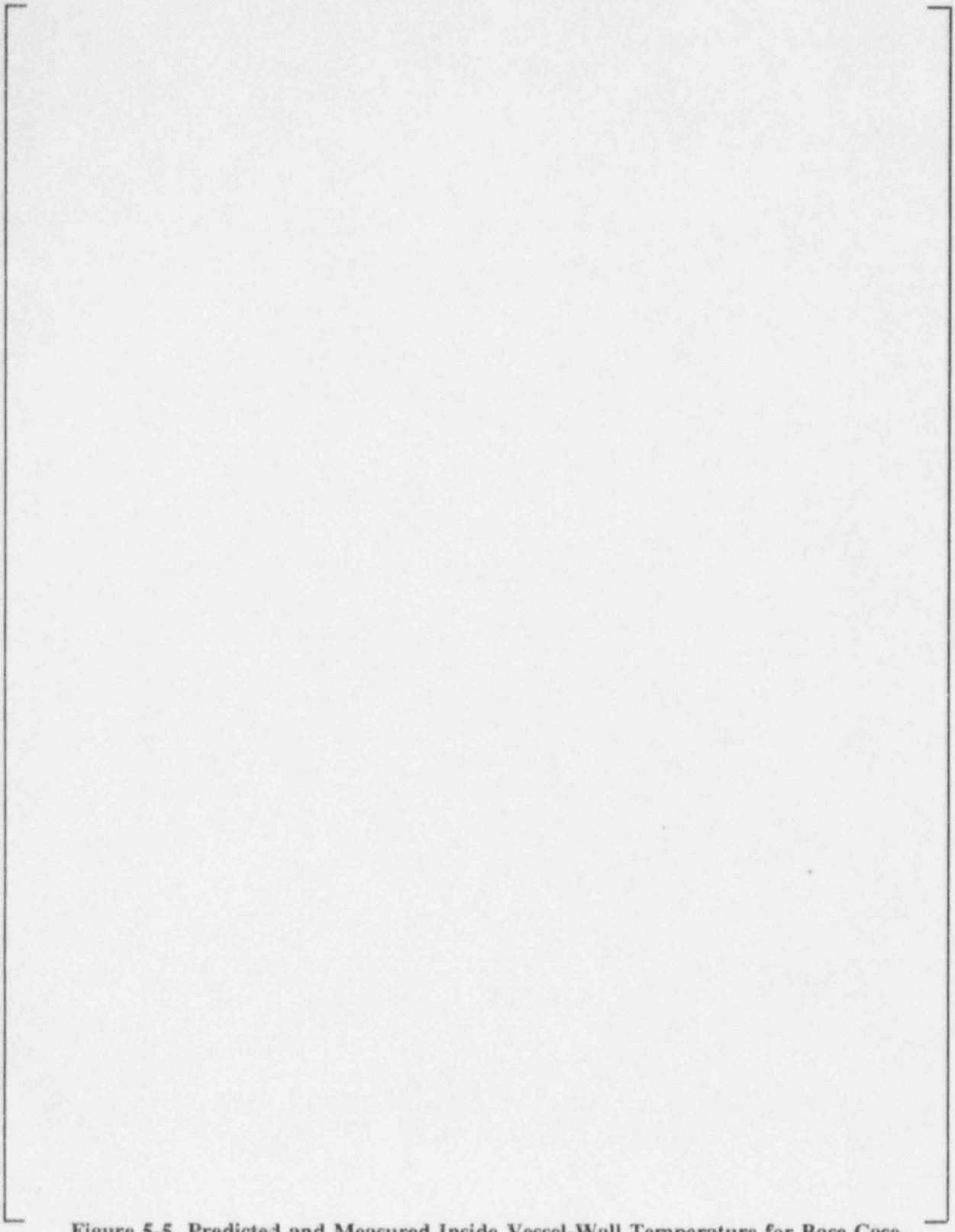

Figure 5-5 Predicted and Measured Inside Vessel-Wall Temperature for Base Case

a,c

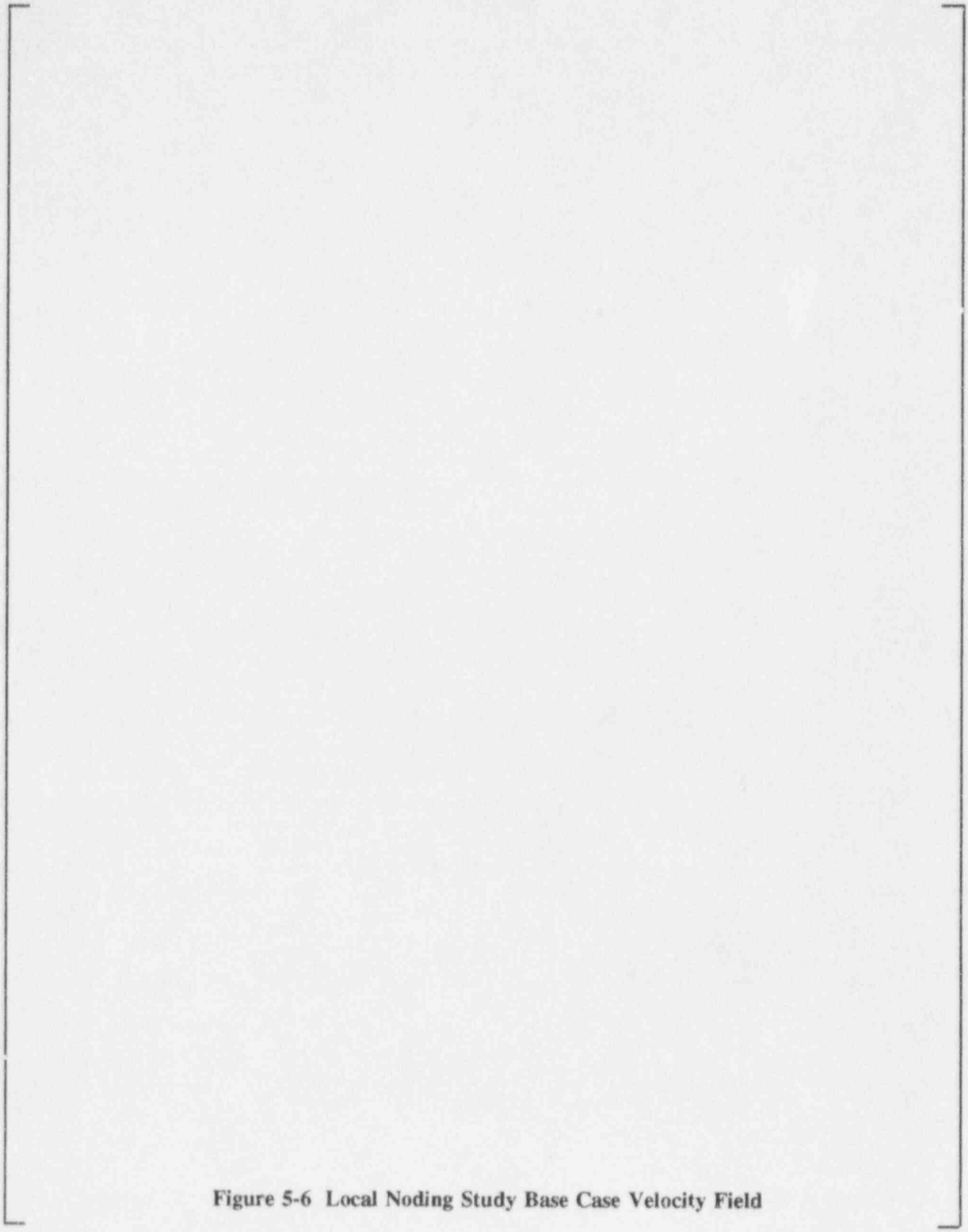

Figure 5-6 Local Noding Study Base Case Velocity Field

Figure 5-7 Radial Noding Base Case

a,c

Figure 5-8 Radial Noding for Case a.1

a,c

Figure 5-9 Radial Noding for Case a.2

a,c

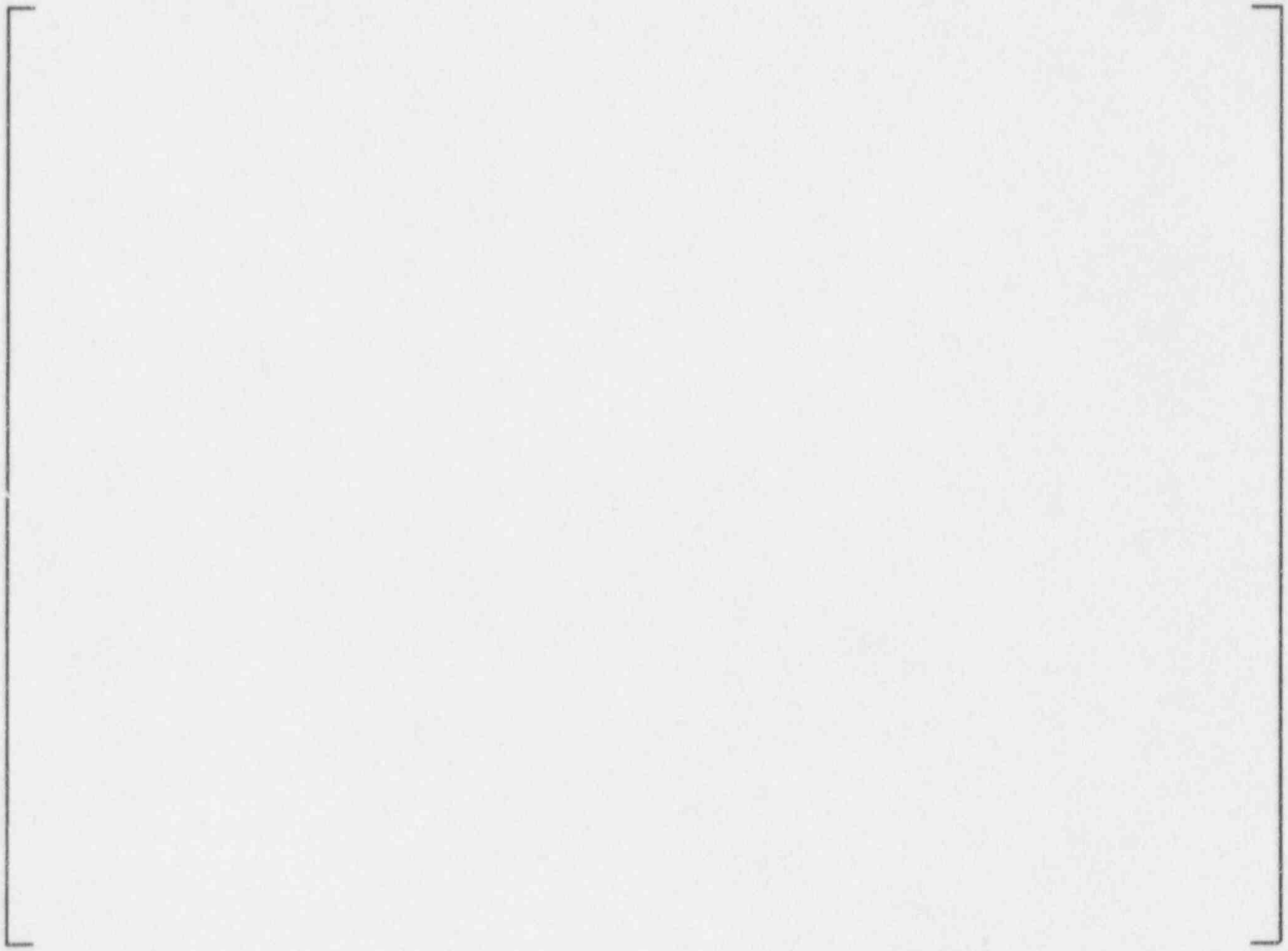

Figure 5-10 Radial Noding for Case a.3

Figure 5-11 Radial Noding for Case a.4

a,c

Figure 5-12 Radial Noding for Case a.5

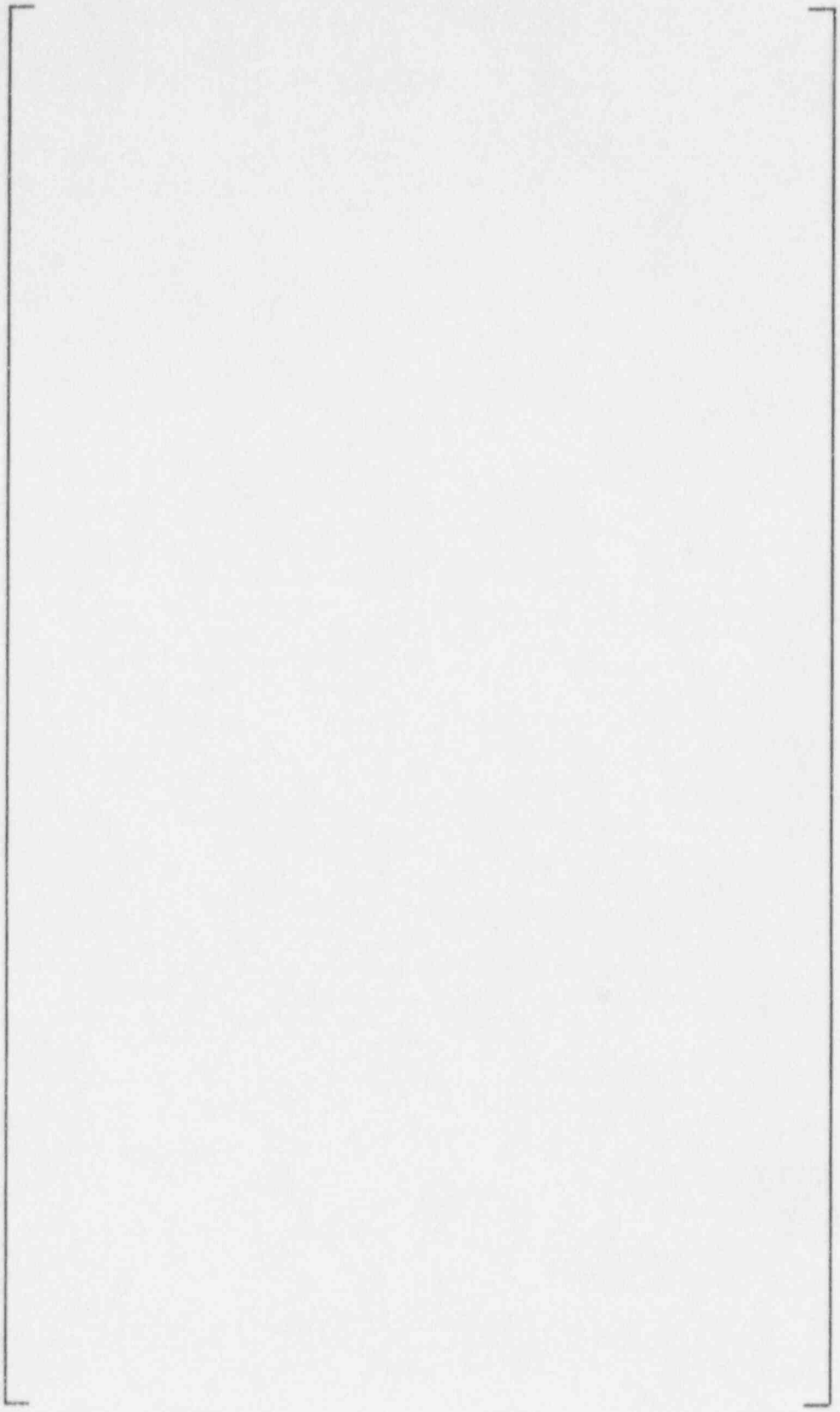

a,c

Figure 5-13 Base Case and Case a.5 Velocity Fields

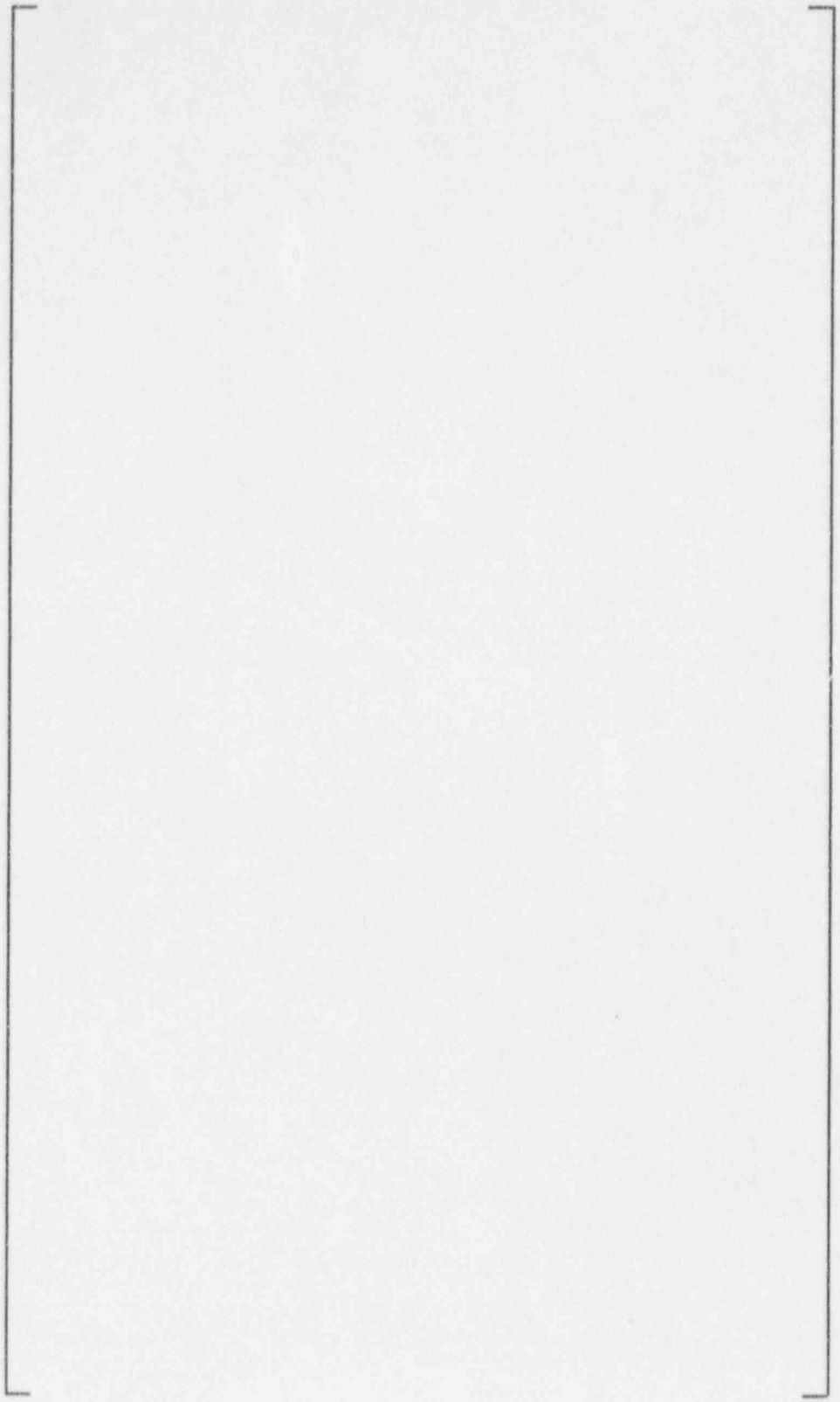

a,c

Figure 5-14 Base Case and Case b.1 Velocity Fields

Figure 5-15 Radial Noding for Case b.2

a,c

Figure 5-16 Radial Noding for Case b.3

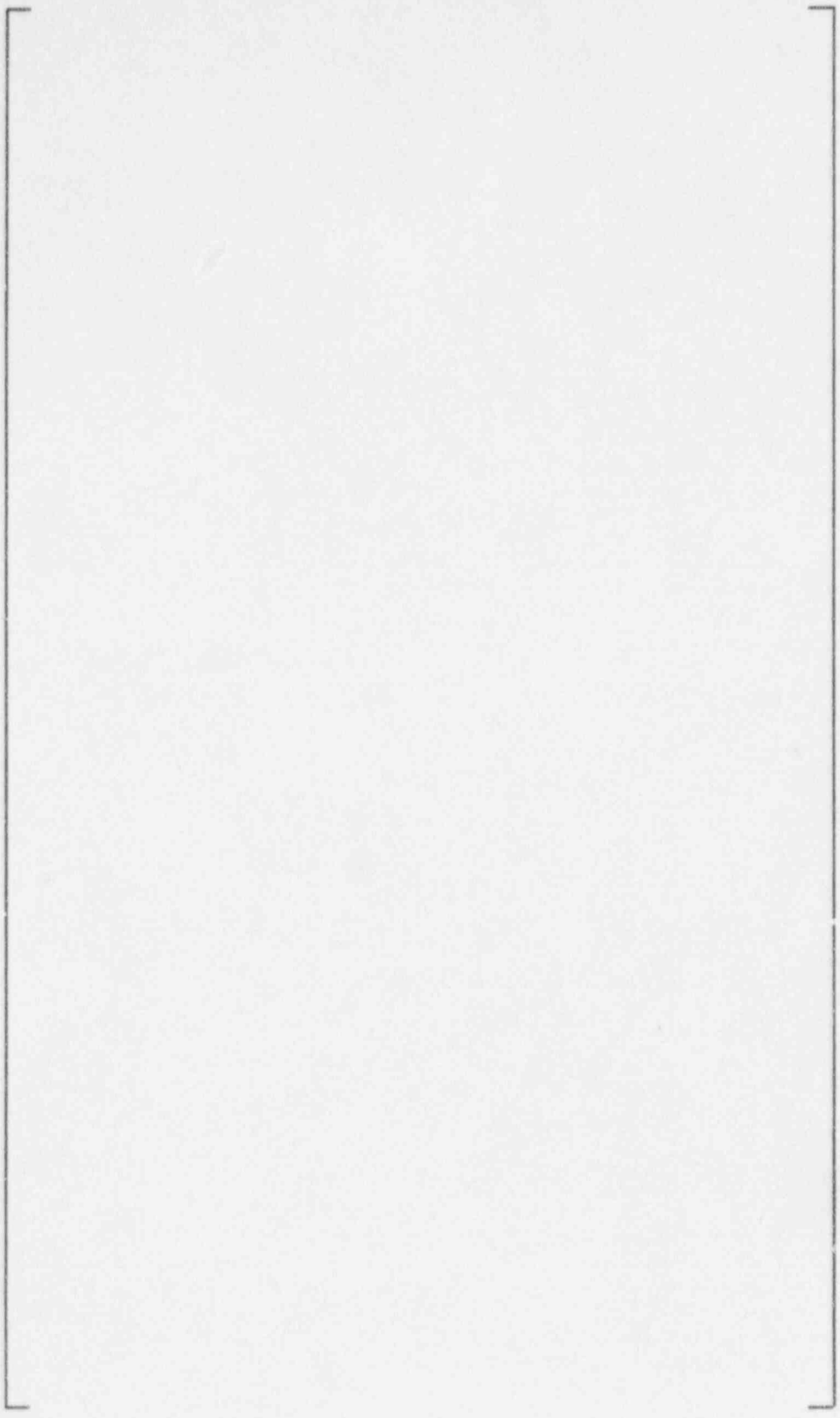

Figure 5-17 Base Case and Case b.3 Velocity Fields

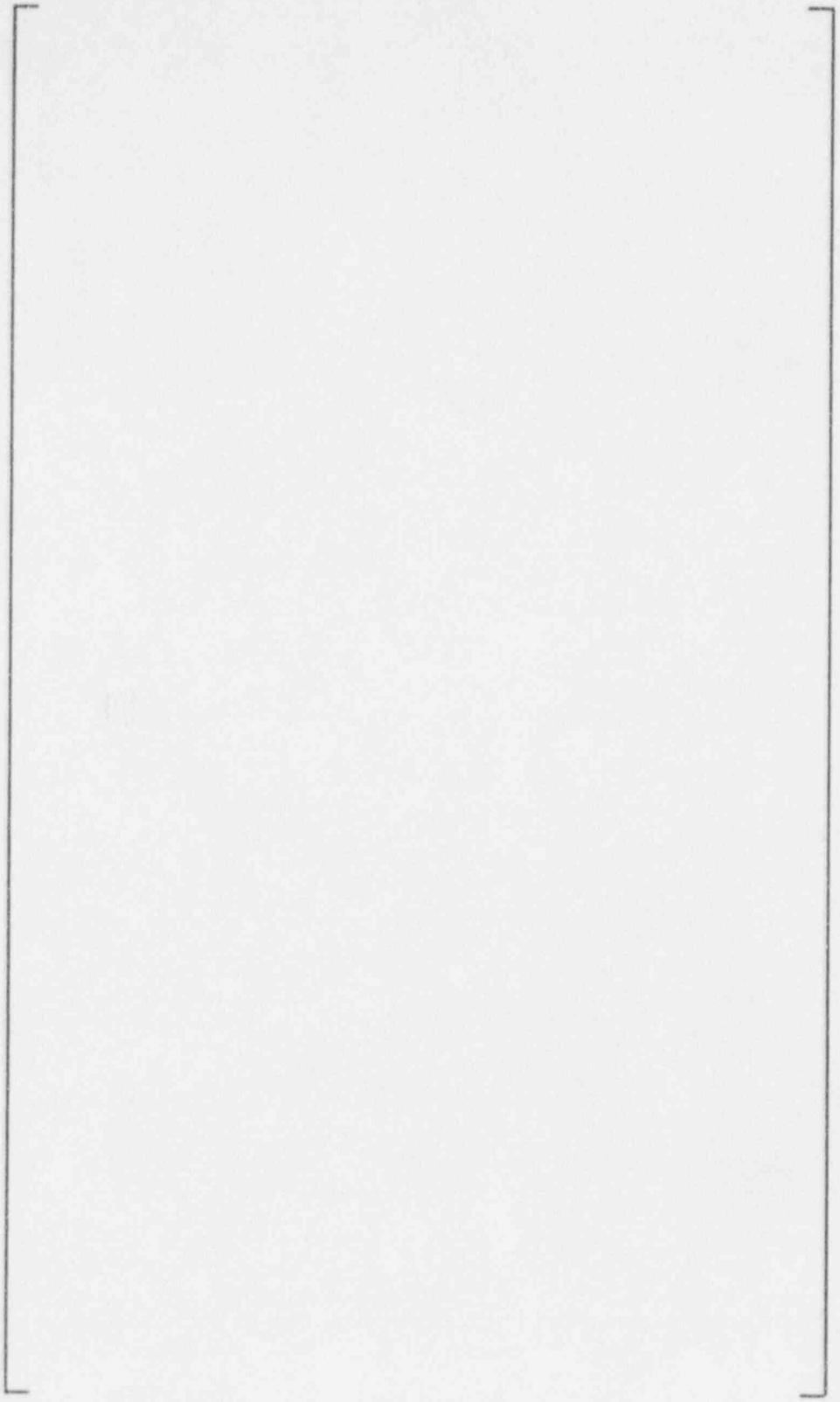

a,c

Figure 5-18 Base Case and Case c.1 Velocity Fields

a,c

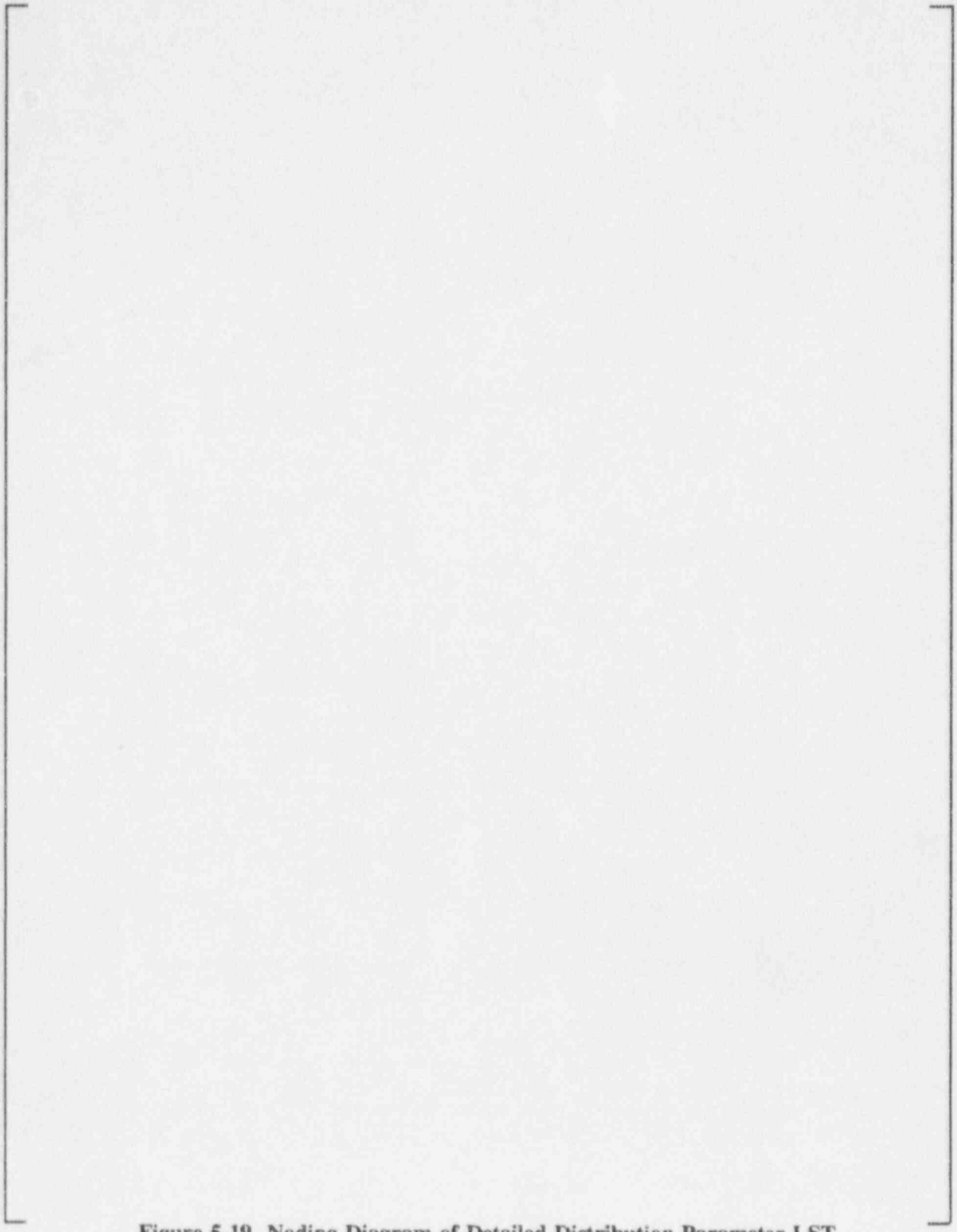

Figure 5-19 Noding Diagram of Detailed Distribution Parameter LST

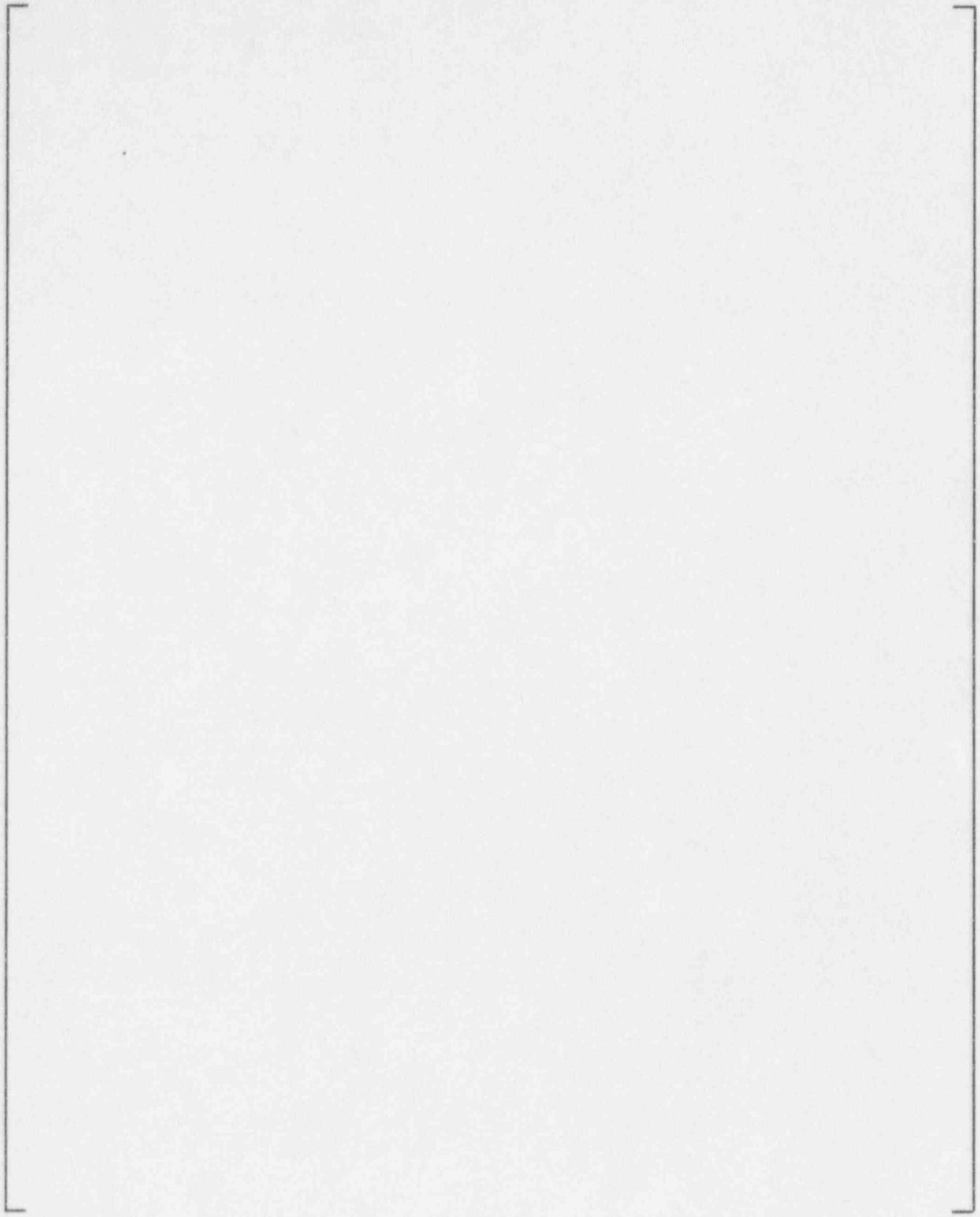

a,c

Figure 5-20 Plan View Detailed Distributed Parameter Model above Operating Deck

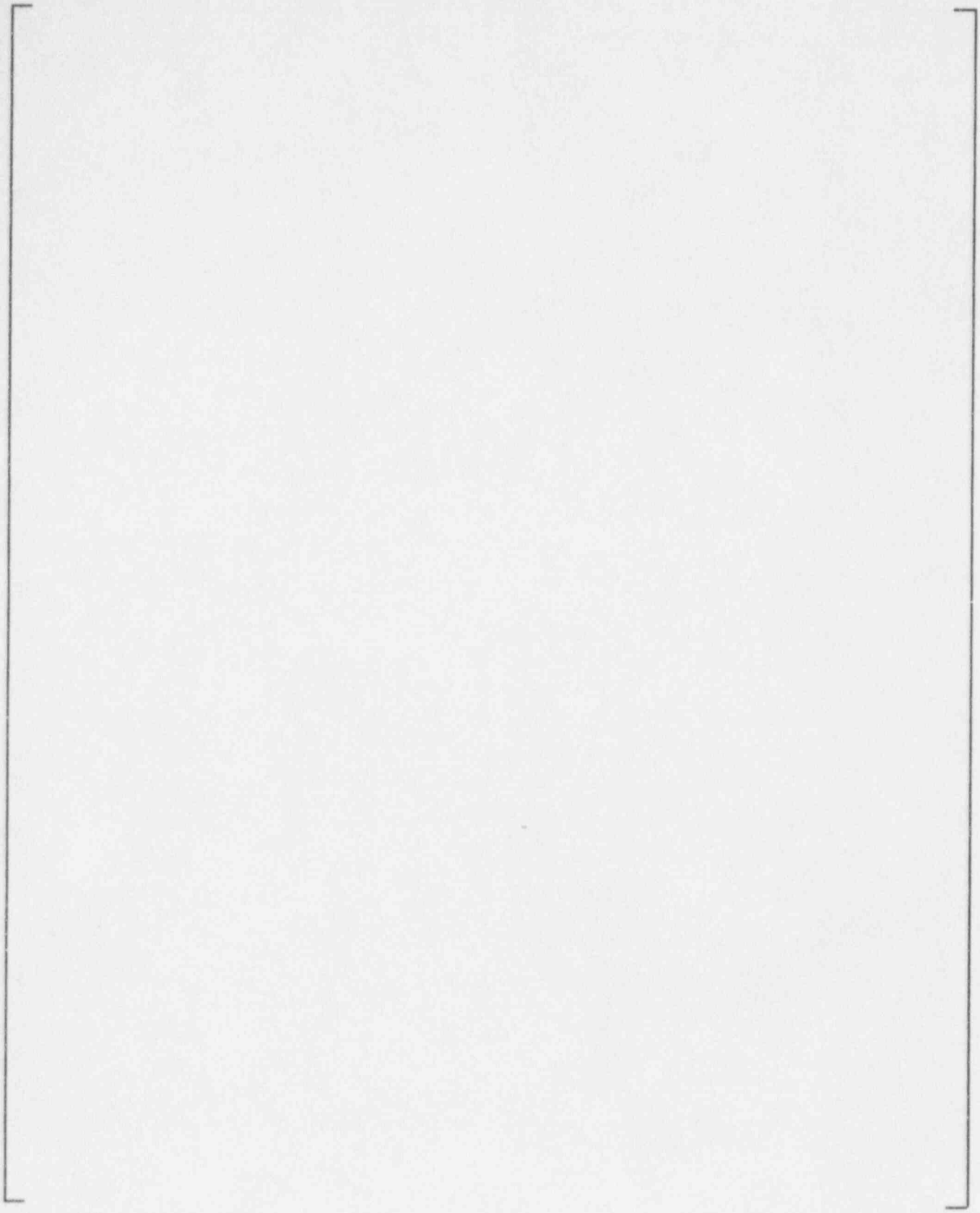

a,c

Figure 5-21 Plan View of Detailed Distribution Parameter Model at Operating Deck Level

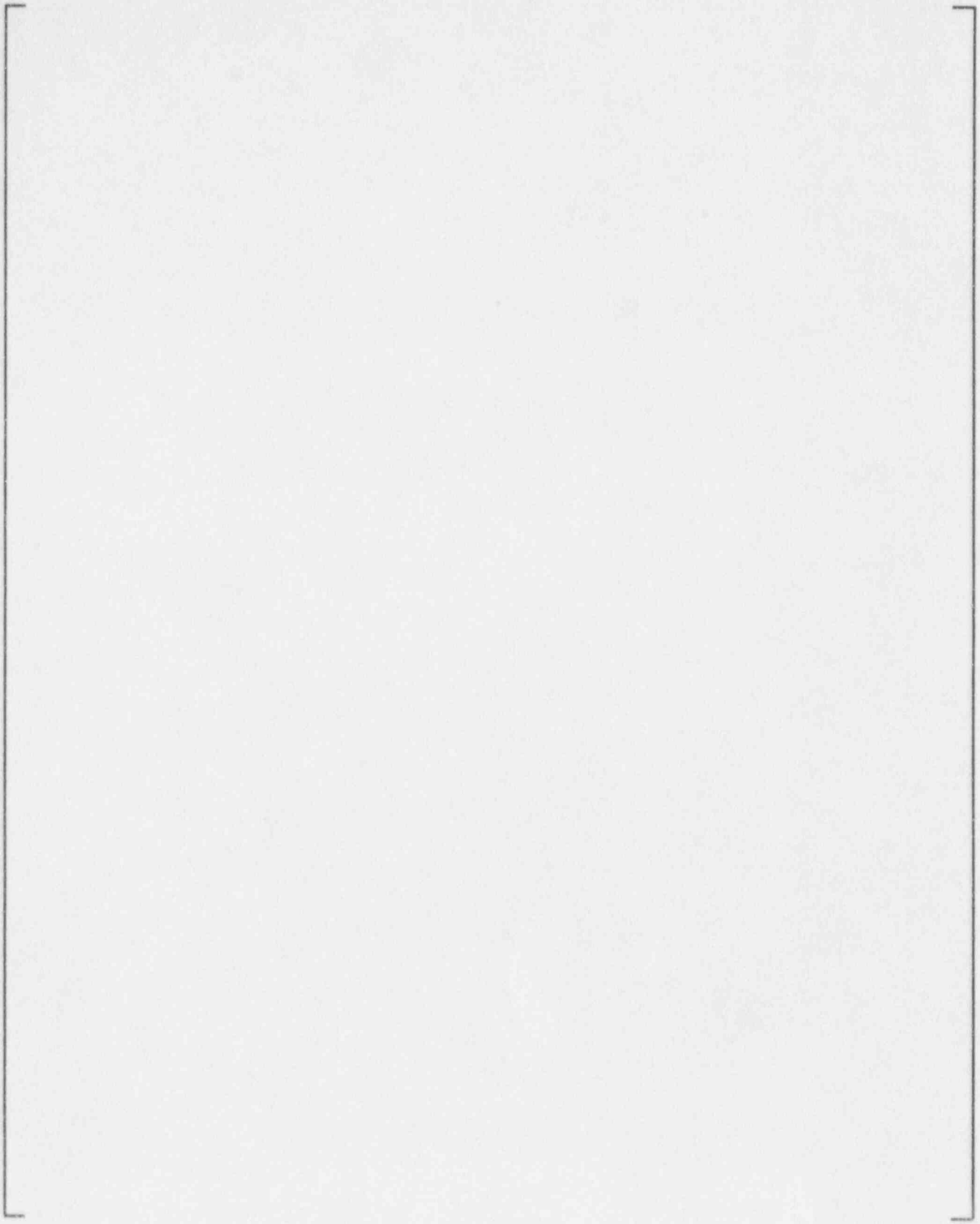

a,c

Figure 5-22 Plane A-A through Steam Generator Break Location

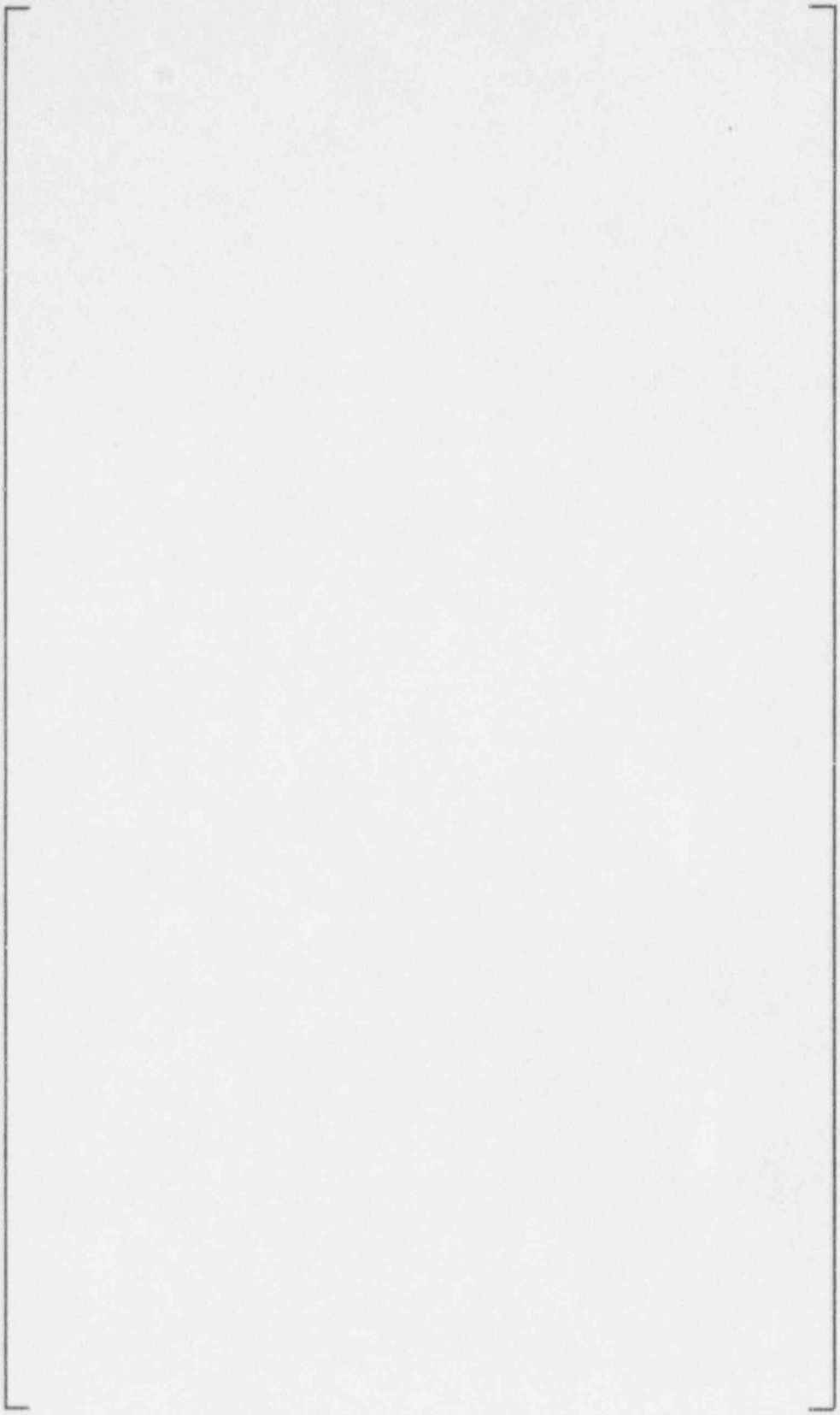

a,c

Figure 5-23 Base Case and Case d.1 Velocity Fields

a,c

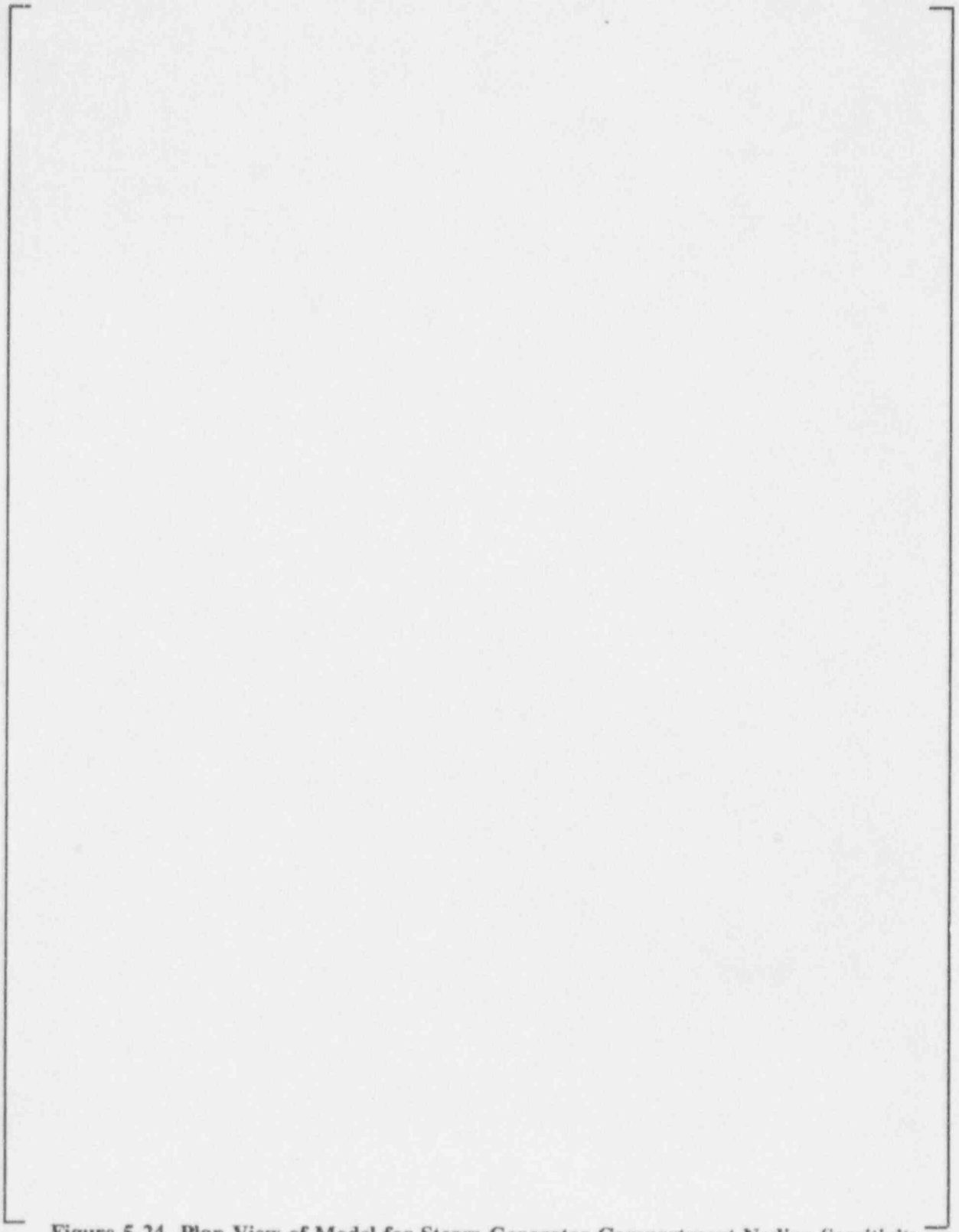

Figure 5-24 Plan View of Model for Steam Generator Compartment Noding Sensitivity

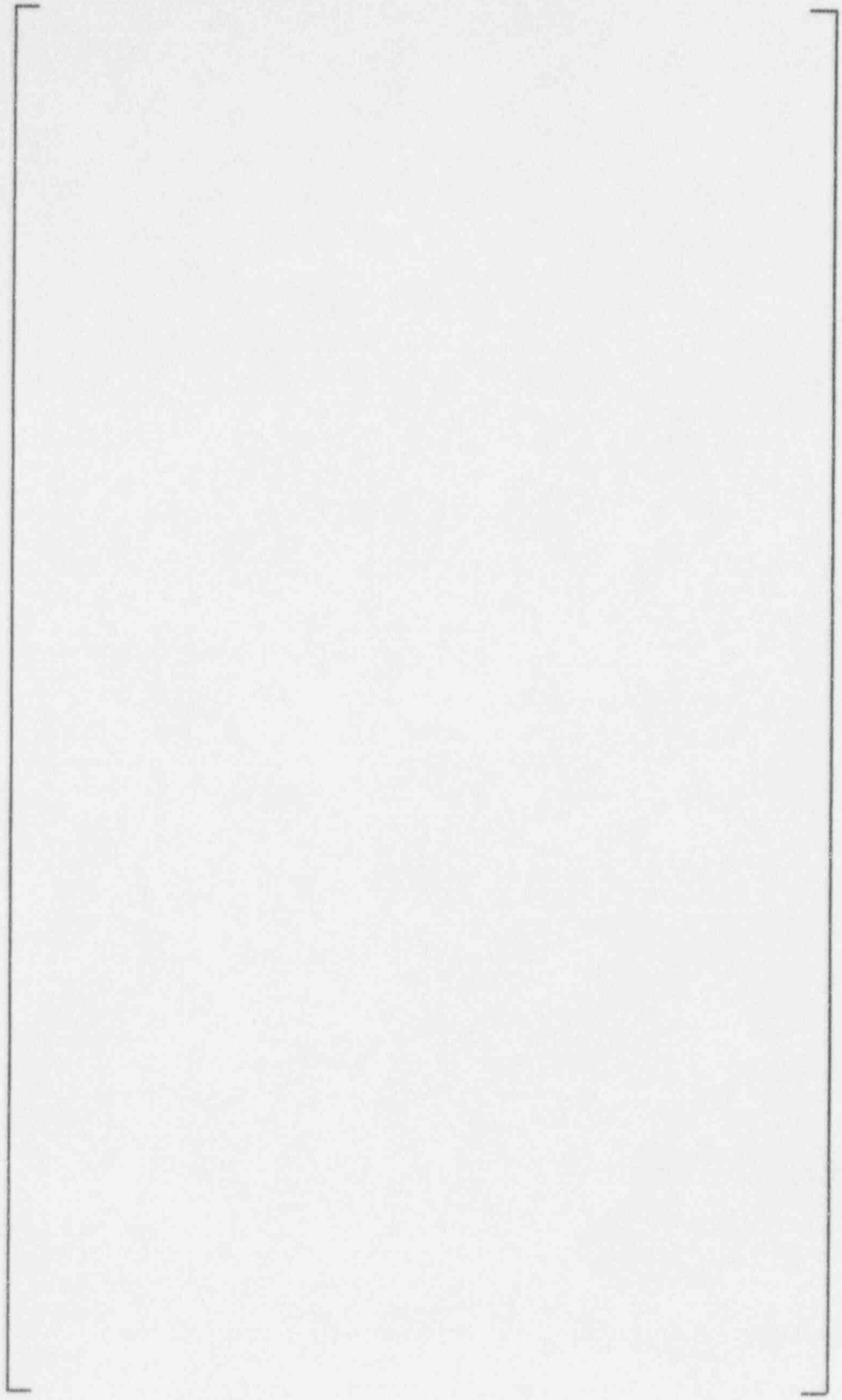

a,c

Figure 5-25 Base Case and Case e.1 Velocity Fields

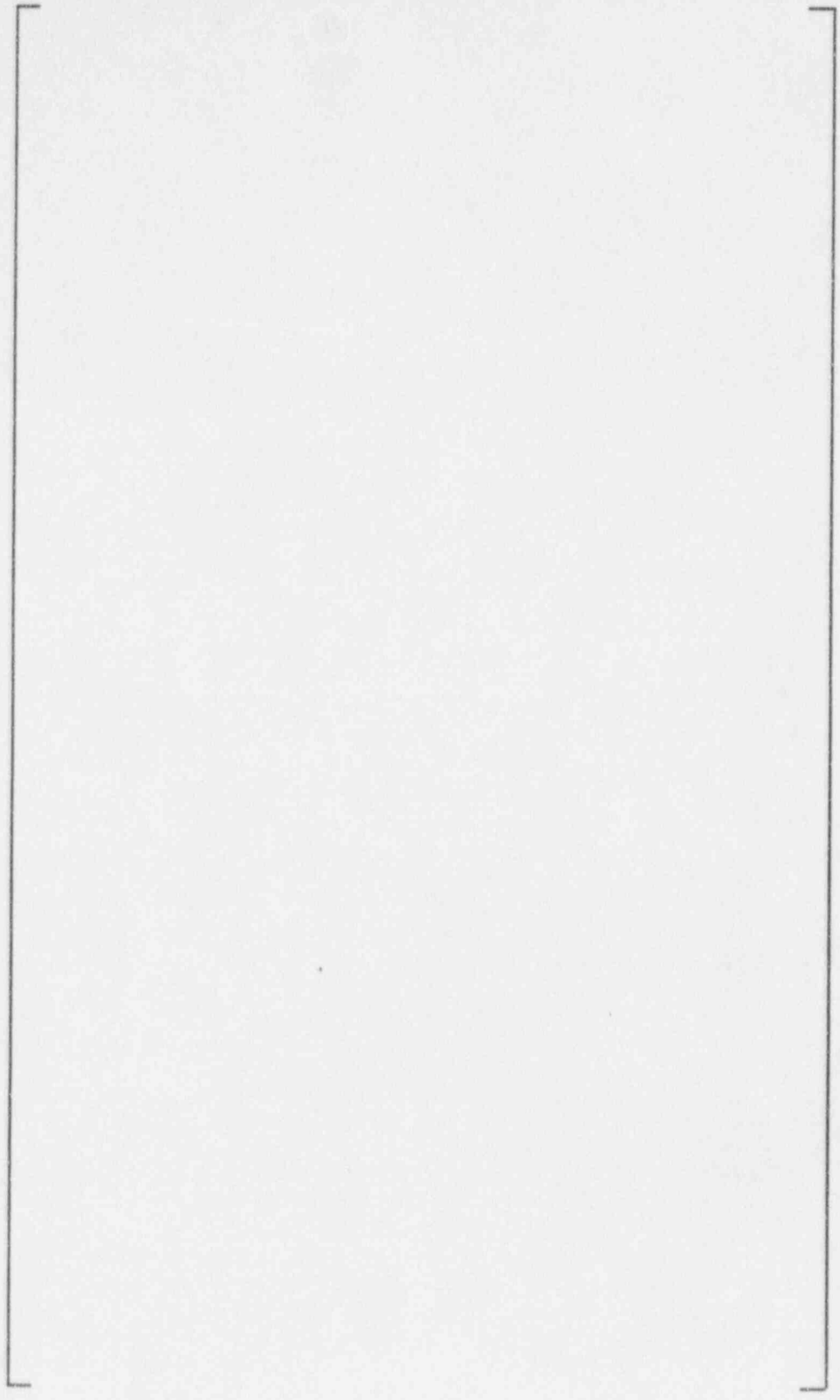

a,c

Figure 5-26 Base Case and Case f.1 Velocity Fields

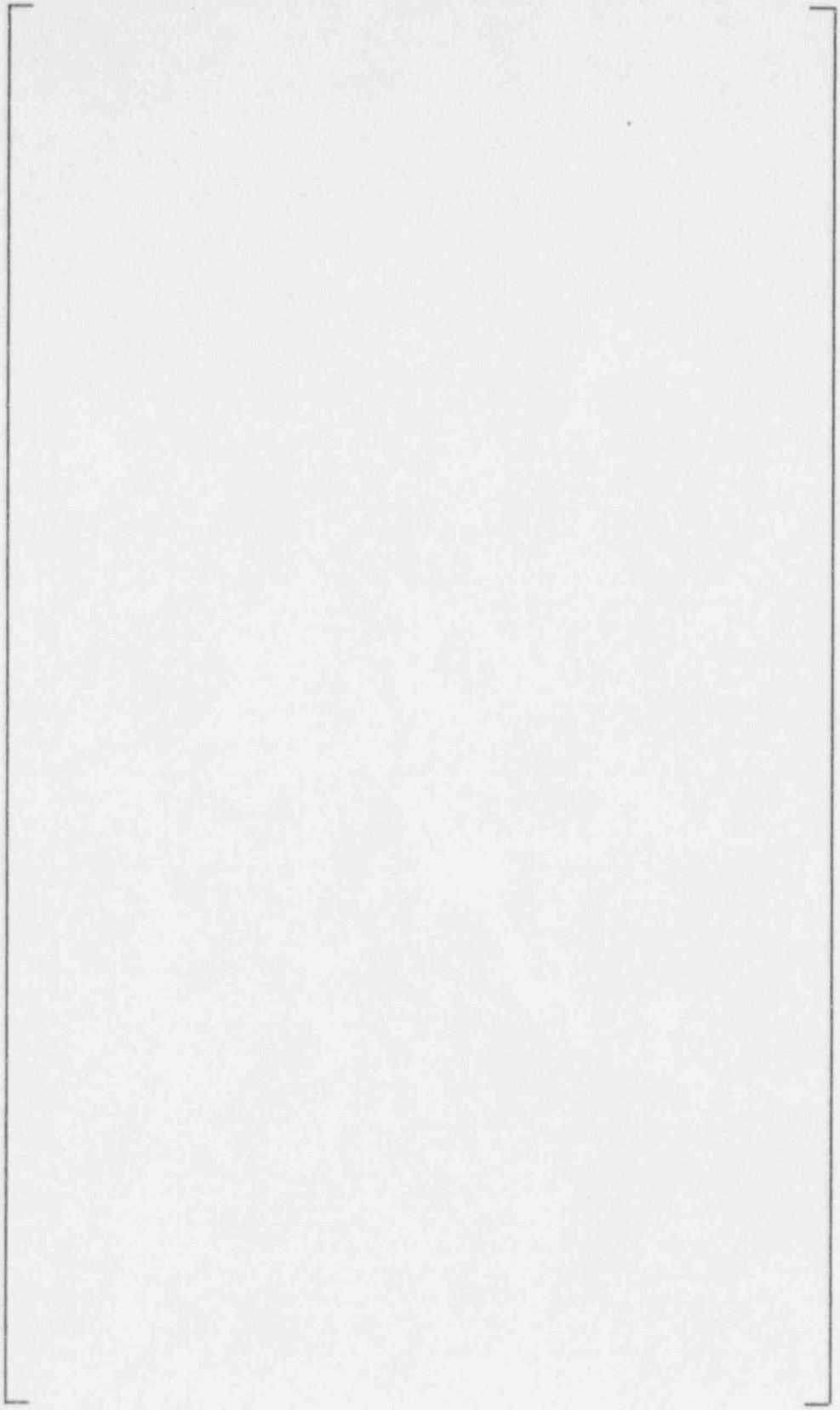

a,c

Figure 5-27 Base Case and Case f.1 Velocity Field across Open Compartment Plane

a,c

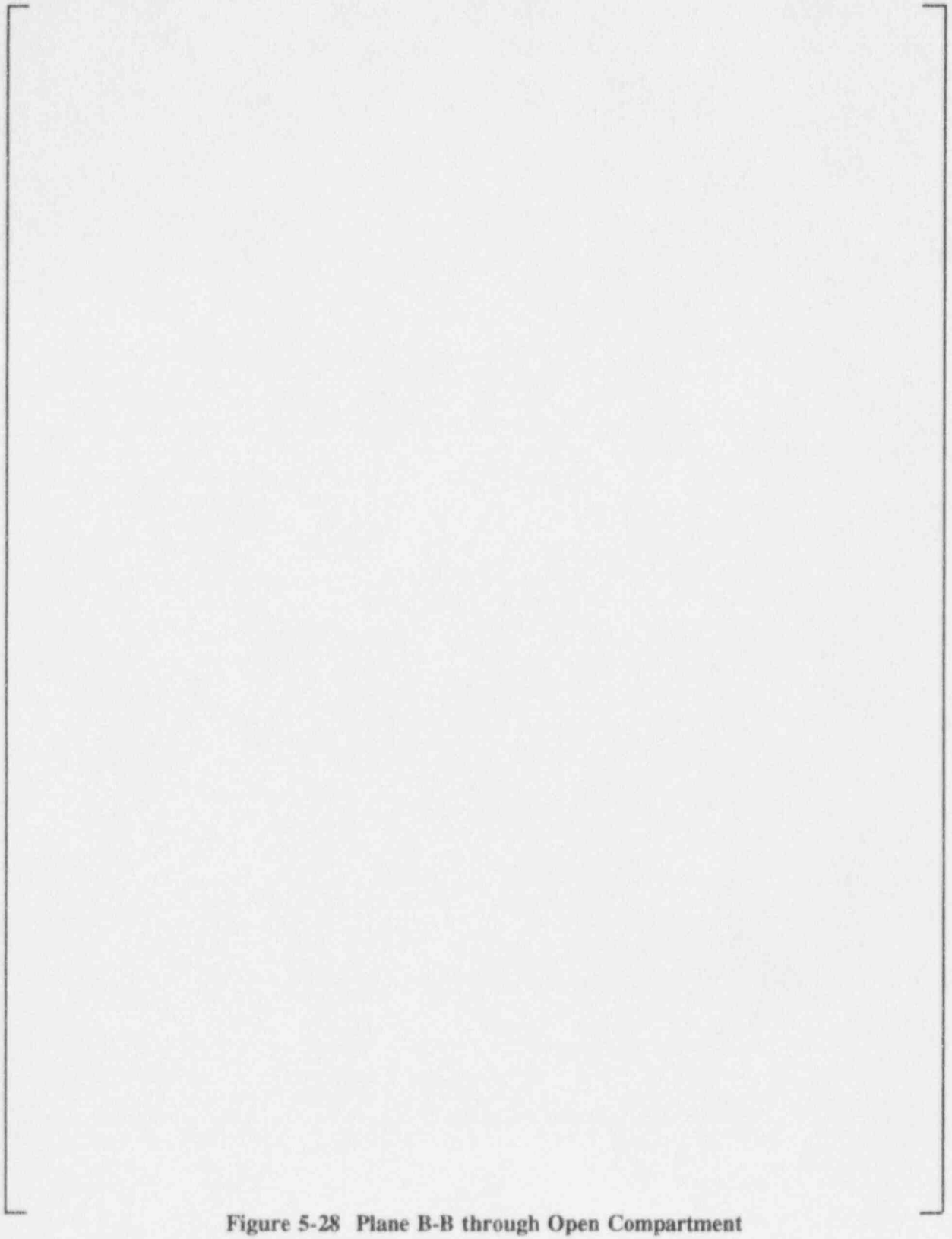

Figure 5-28 Plane B-B through Open Compartment

a,c

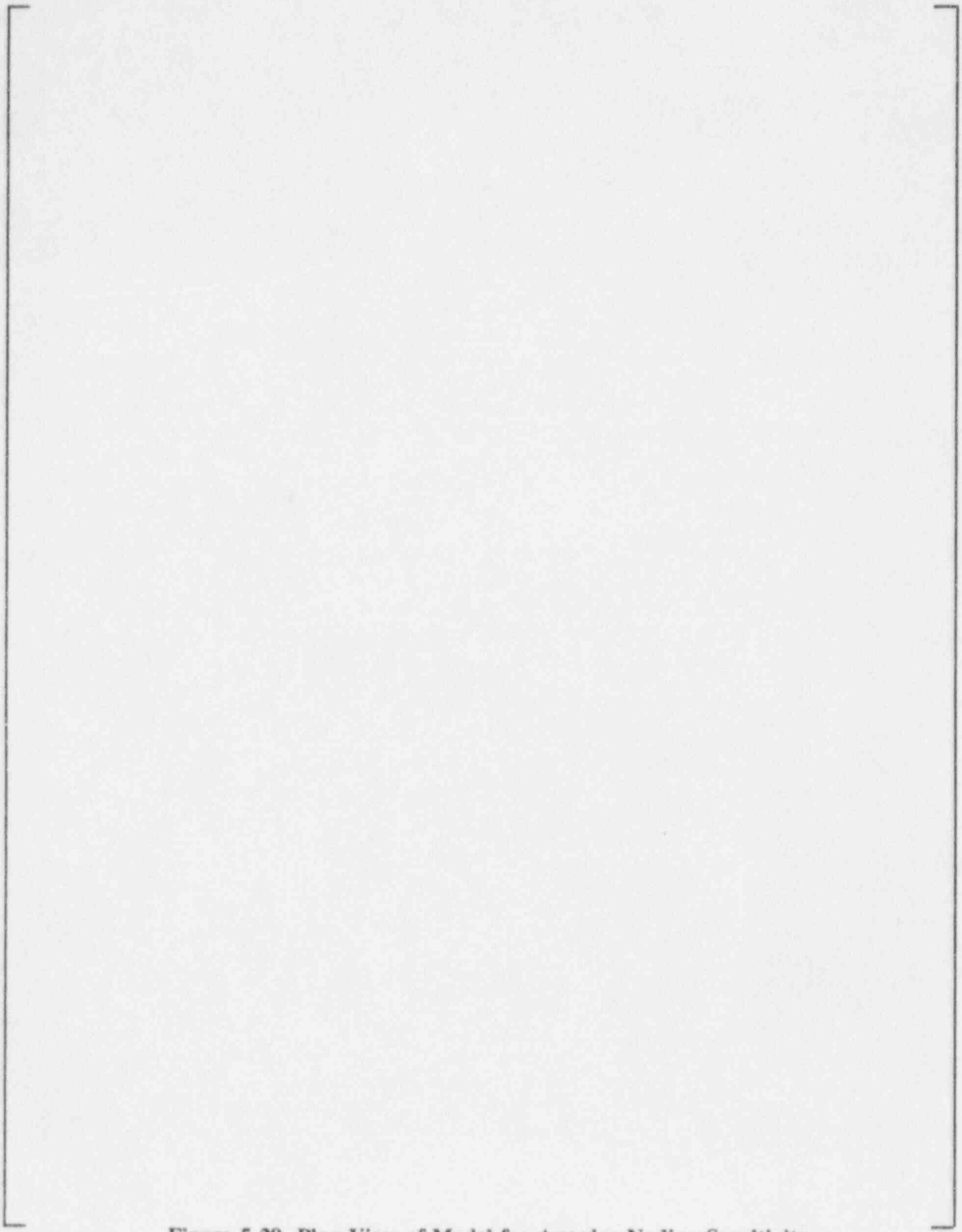

Figure 5-29 Plan View of Model for Angular Noding Sensitivity

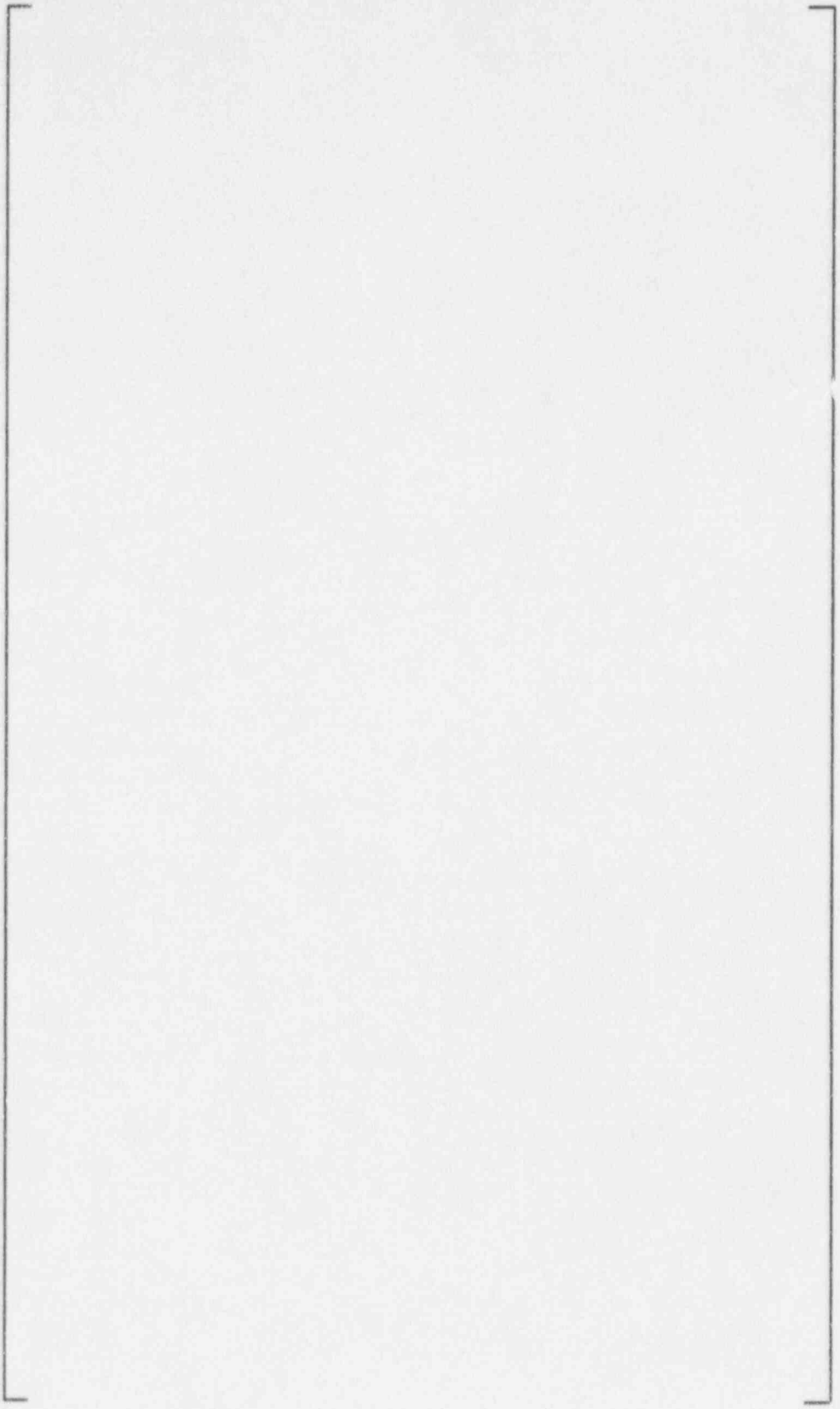

a,c

Figure 5-30 Base Case and Case g.1 Velocity Field

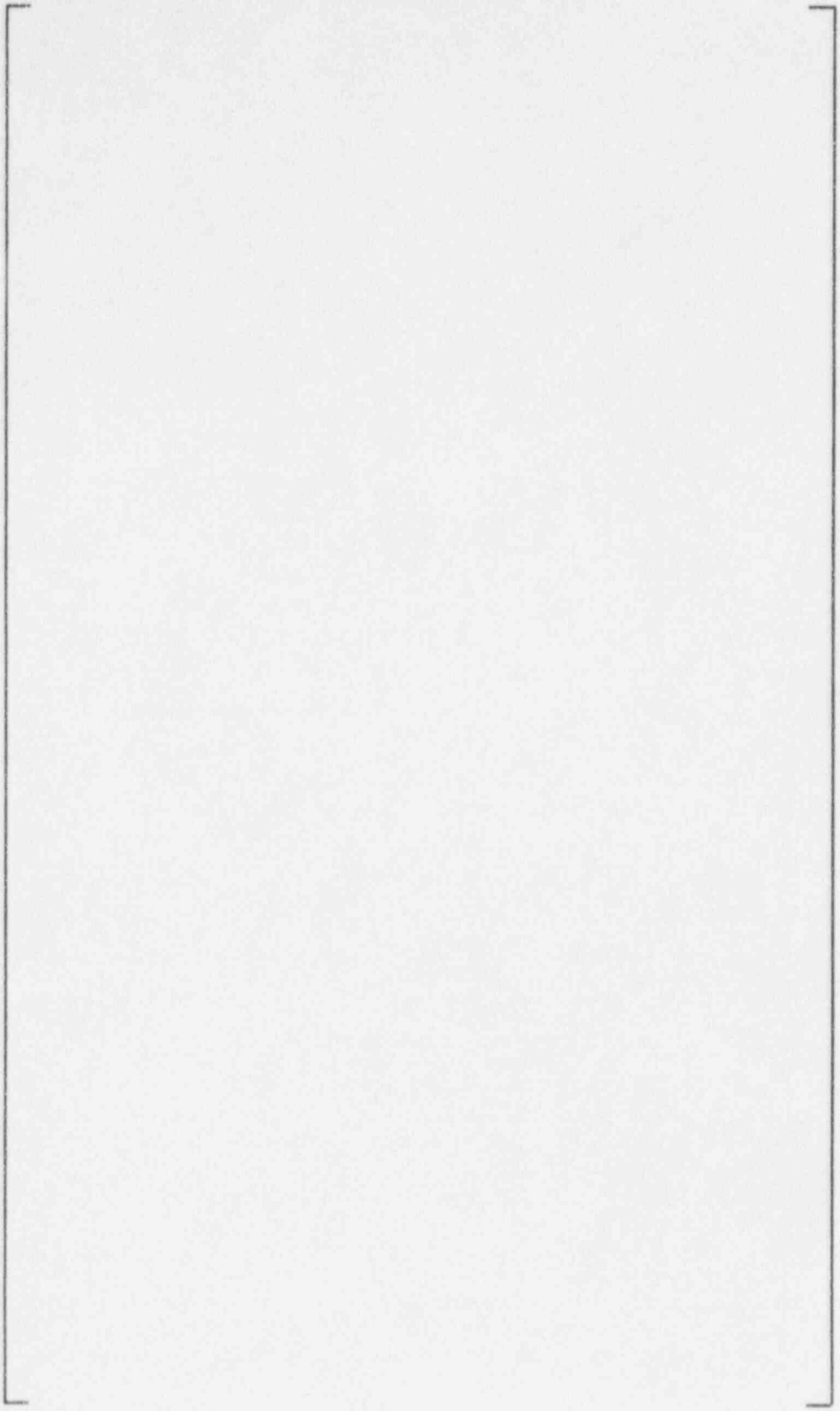

a,c

Figure 5-31 Base Case and Case g.1 Velocity Field in Modified Plane

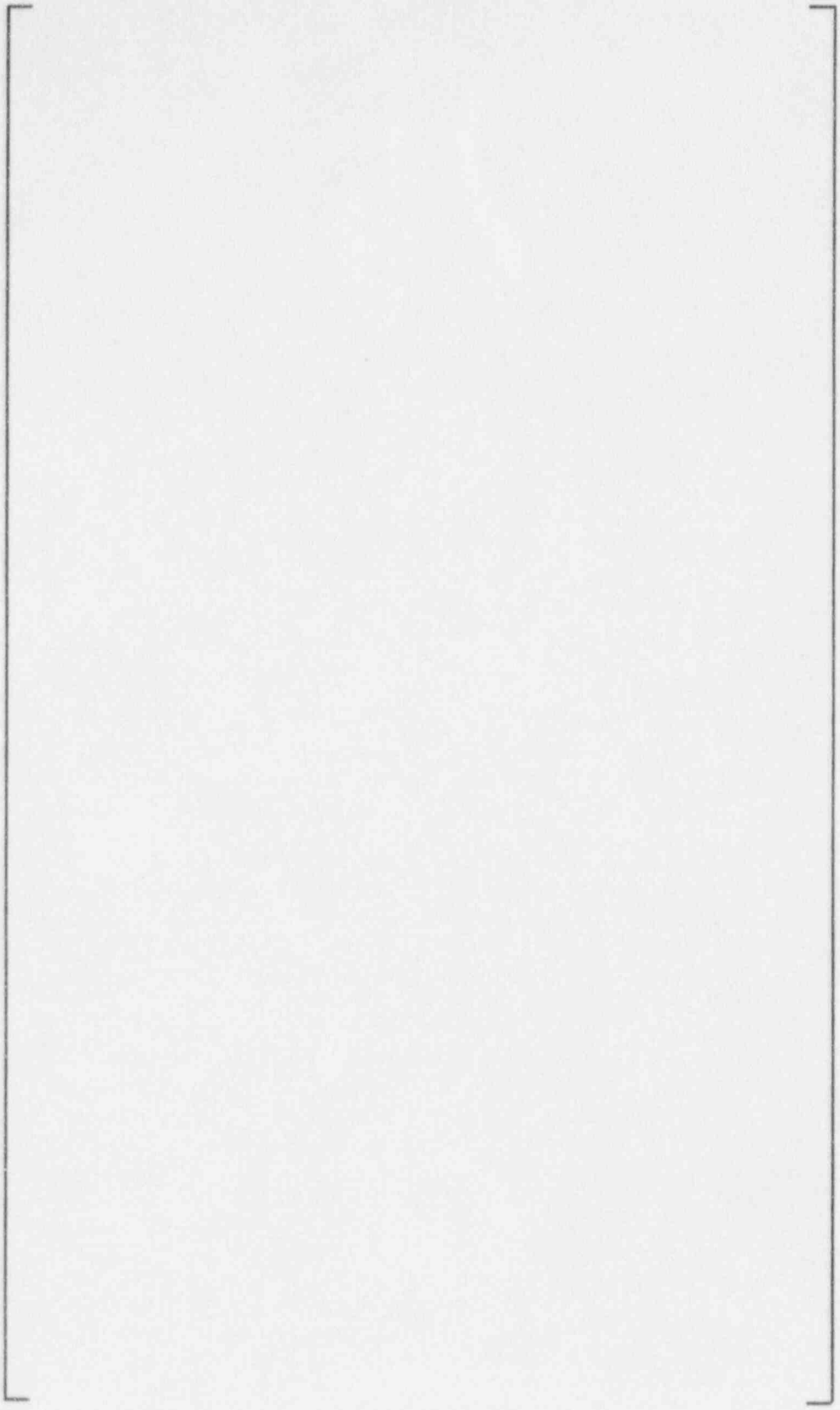

a,c

Figure 5-32 Base Case and Case g.1 Velocity Field in Modified Plane

a,c

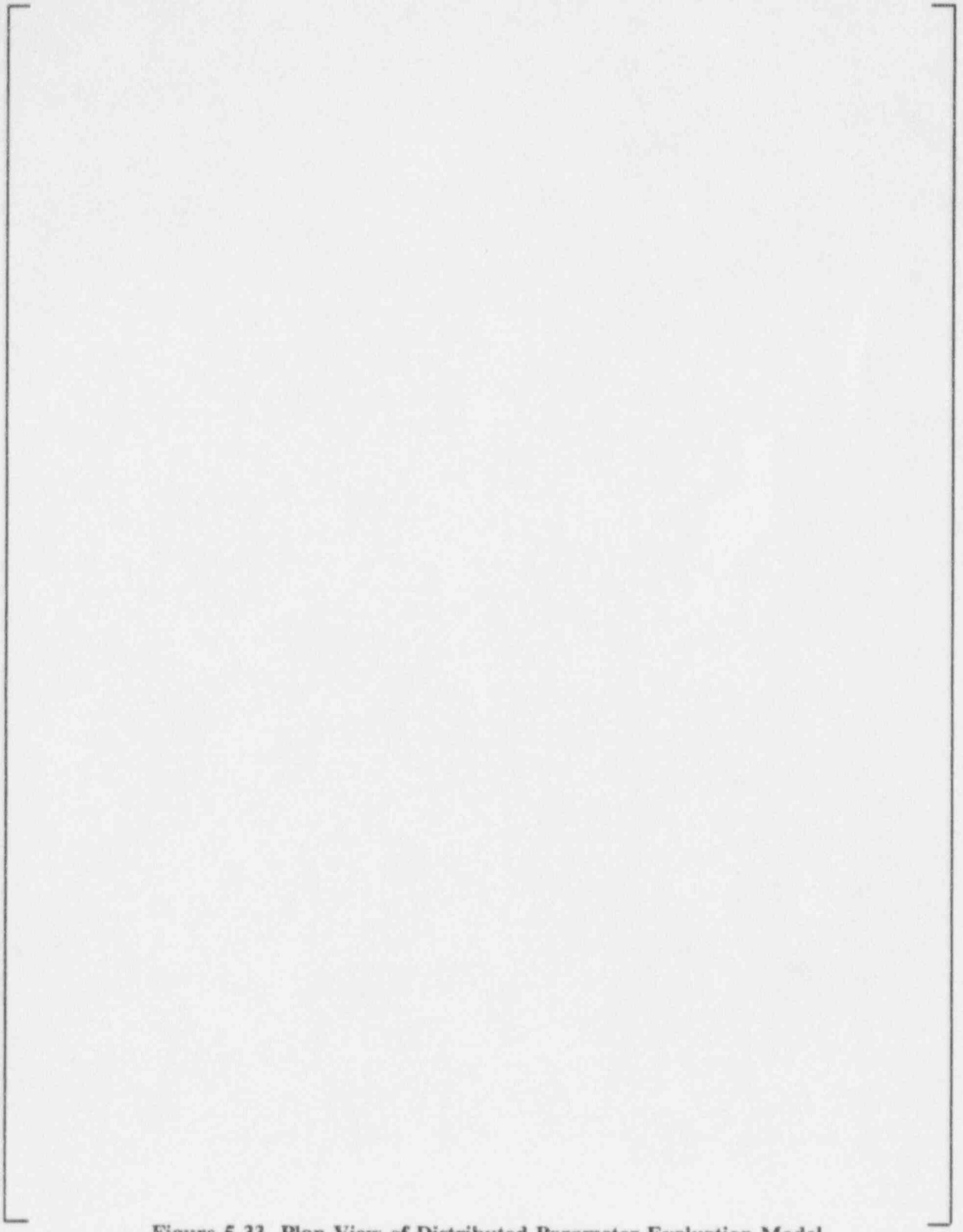

Figure 5-33 Plan View of Distributed Parameter Evaluation Model

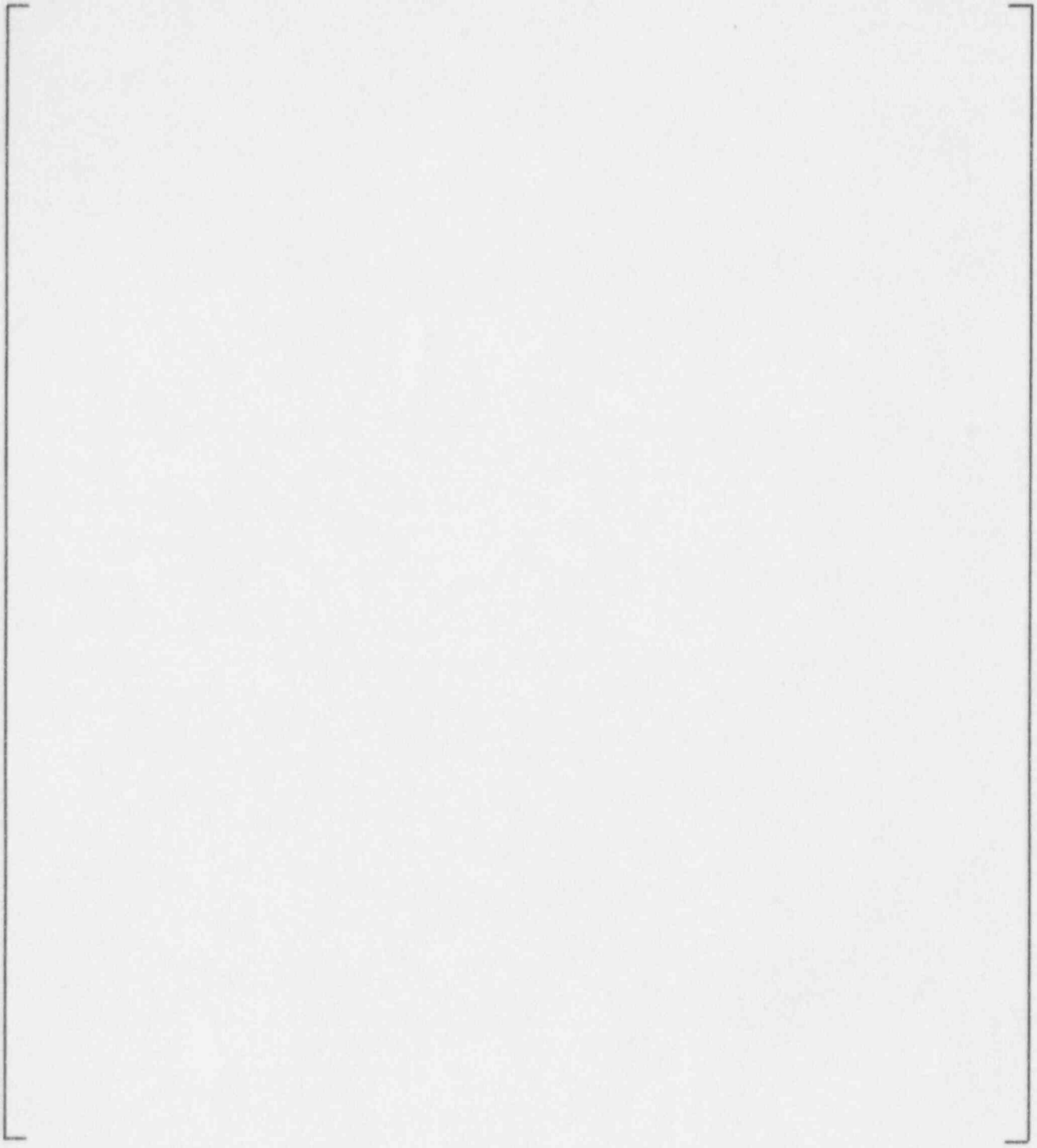

Figure 5-34 Distributed Parameter Axial Noding for Vessel

a,c

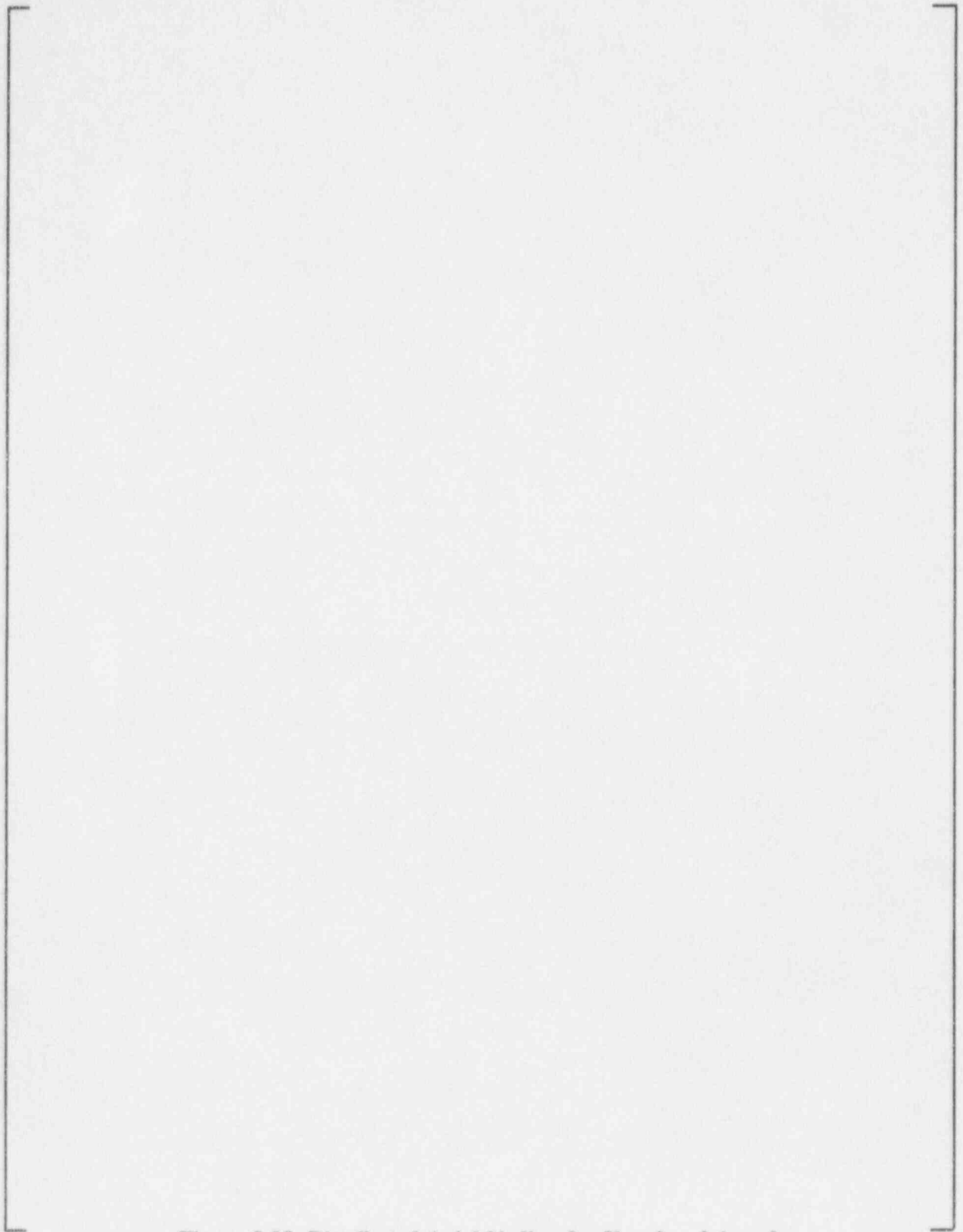

Figure 5-35 Distributed Axial Noding for Vessel and Annulus

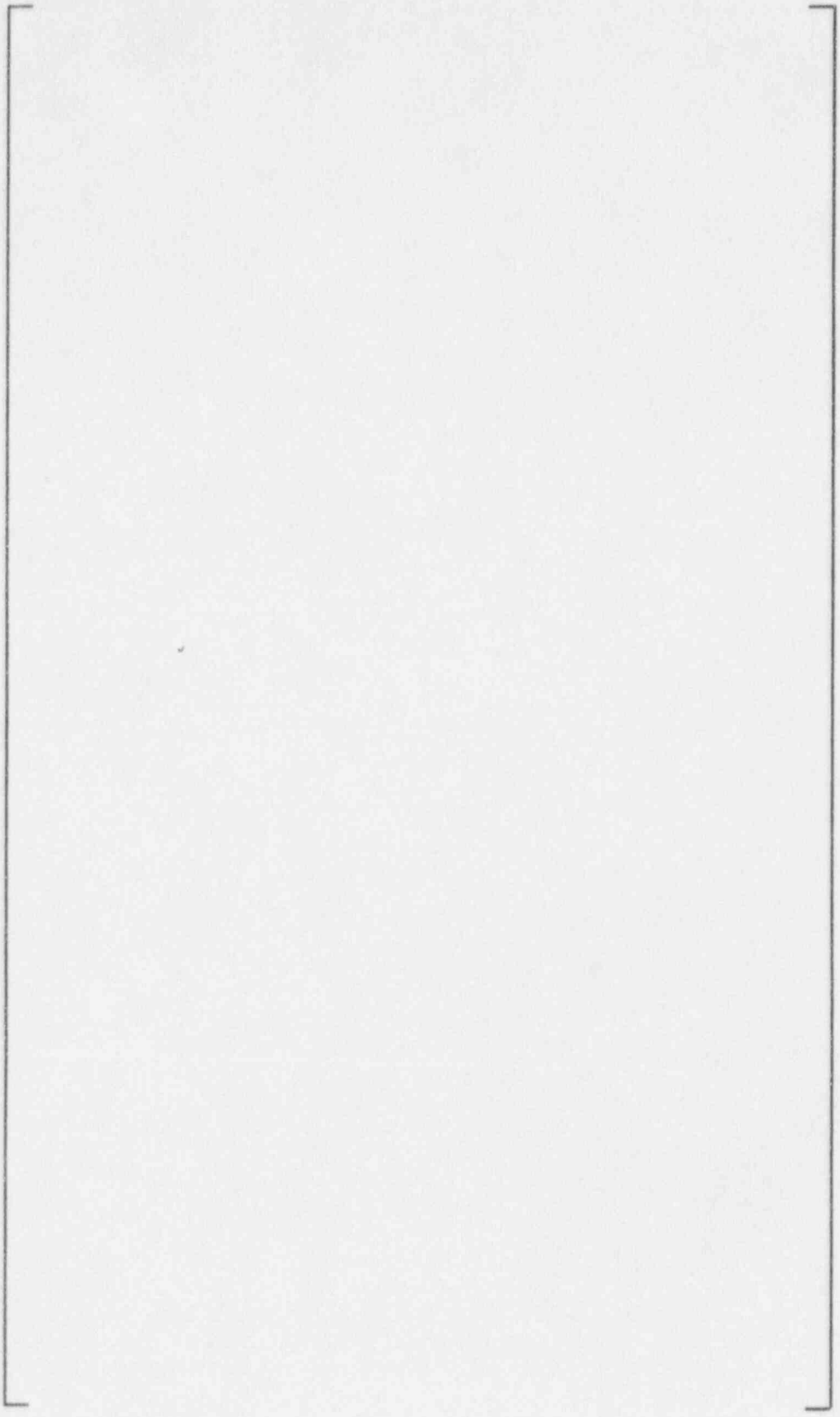

a,c

Figure 5-36 Base Case and Final Case Velocity Field

a,c

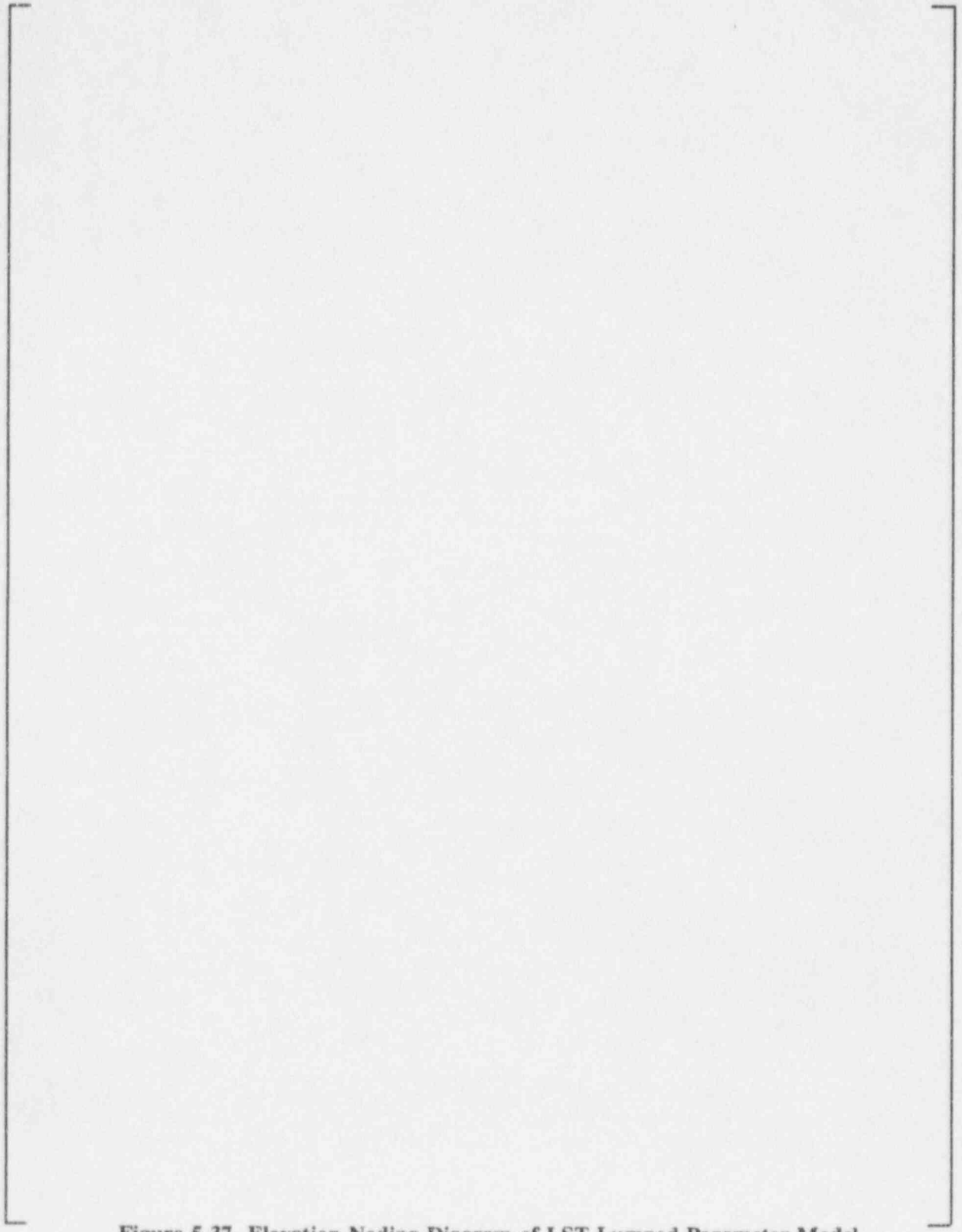

Figure 5-37 Elevation Noding Diagram of LST Lumped Parameter Model

6.0 WGOTHIC LARGE-SCALE TEST EVALUATION MODELS AND APPLICATION TO AP600

The lumped parameter and distributed parameter large-scale test (LST) evaluation models will be described in this section. The evaluation models will be used to validate the WGOTHIC code using data from the Phase 2 and Phase 3 large-scale test series.

The AP600 lumped and distributed parameter evaluation models will have a noding structure corresponding to the LST lumped and distributed parameter noding, respectively.

6.1 Input Common to the Distributed and Lumped Parameter Models

The same initial and boundary conditions are defined for the lumped and distributed parameter models. Of course, the initial and boundary conditions vary for each test and are input into the code as reported in WCAP-14135.[20]

The boundary conditions are steam flow rate, enthalpy and pressure; ambient pressure, temperature, and humidity; external water flow rate, applied temperature, and coverage; and air annulus boundary condition. The air annulus flow for tests with natural draft is modeled with pressure boundary conditions that represent the environmental density gradient, the appropriate flow area, and a total loss coefficient. For tests in which the annulus flow velocity is controlled by a fan, the annulus flow is modeled with a flow boundary condition that represents the measured flow rate, the appropriate flow area, loss coefficient, and frictional loss.

The initial conditions are the initial ambient pressure, temperature, and humidity; the initial vessel pressure, temperature, and humidity; and the heat sinks, vessel wall, and baffle wall initial temperatures.

A single loss coefficient is used inside the vessel to model the loss across the operating deck grating. The grating loss coefficient based on the unblocked area is [ ]^{a,c}. The total air flow loss coefficient in the annulus and chimney is [ ]^{a,c} based on the air flow area.

The mechanistic correlations discussed in Section 2.0 are used to model the passive containment heat and mass transfer from the vessel internal atmosphere, through the walls, and out to the ultimate heat sink (the environment). The Uchida correlation is used for the internal heat sinks, such as the internal compartment walls, the aluminum heat sink plates, and the operating deck.

6.2 Distributed Parameter LST Input Model

Noding and input specific for the distributed parameter model are discussed in this section.

6.2.1 Distributed Parameter Noding Methodology

The noding is derived from the detailed distributed parameter model discussed in Appendix A. Its development from the detailed distributed parameter model is discussed in Section 5.2.11.

The distributed parameter evaluation model has the following noding characteristics:

- The model is a 1/2 symmetry representation of the LST vessel, dividing the facility through the 0° - 180° plane (See Figure 6-1).

- The vessel is modeled by coupling distributed parameter above deck and lumped parameter below deck. The vessel model includes one distributed parameter volume having approximately 375 subdivided nodes and two lumped parameter volumes. Figure 7-2 shows the elevation view of the vessel. The volume above the operating deck is divided into [ ]^{a,c} elevations using the distributed parameter formulation.

- The air annulus is modeled using lumped parameter volumes. [ ]^{a,c} volumes are used to model the air annulus and chimney as shown in Figure 6-6.

The elevation planes are based on internal geometry and the noding studies discussed in Section 5.0. The elevation planes shown in Figure 6-7 are:

[ ]^{a,c}

[ ]^{a,c}

[ ]^{a,c}

[ ]^{a,c}

[ ]^{a,c}

[ ]^{a,c}

[ ]^{a,c}

Due to the rectangular coordinate system in the distributed parameter formulation, modeling curved geometries requires special attention. In this input model, the top of the vessel is modeled as a flat top. This greatly simplifies the calculational input required to build the AP600 plant model with corresponding noding. The total dome surface area and volume are preserved and as shown in Section 5.2.11, the flow field is not distorted.

The plan view for the vessel above the operating deck is shown in Figure 6-3. The radial divisions are based on the following:

[ ]^{a,c}

[ ]^{a,c}

[ ]^{a,c}

[ ]^{a,c}

[

]^{a,c}

[ ]^{a,c}

The angular divisions are based on the following:

[ ]^{a,c}

[ ]^{a,c}

[

]^{a,c}

[

]^{a,c}

[

]^{a,c}

[ ]^{a,c}

Noding below the operating deck is described below:

- The steam generator compartment below the operating deck is divided into [ ]^{a,c} elevations using the distributed parameter formulation. The distributed parameter formulation was used because it provides a more detailed representation of the flow field within the steam generator compartment.

- The open compartment is also divided into [ ]^{a,c} elevations. The top [ ]^{a,c} elevations are modeled in the distributed parameter formulation. The bottom elevation is modeled as a

lumped parameter node. The compartment was modeled in this manner in order to aid in predicting the noncondensible distribution.

- The dead-ended compartment is modeled as a single lumped parameter node.

The elevation plane view of the vessel at the operating deck level is shown in Figure 6-4. The hatching shows the location of the steam generator model. A plane view of the vessel at an elevation of [ ]^{a,c} is shown (Figure 6-5) to illustrate the noding change from distributed to lumped in the open compartment.

The air annulus noding elevation view is shown in Figure 6-6. In most cases, it has the same elevations as the vessel. The annulus is modeled with lumped parameter volumes. Each vertical slice represents one volume. The elevation plane view for the air annulus is shown in Figure 6-7.

The noding in the distributed parameter model was developed and is applicable to the Phase 2 and Phase 3 tests with the steam diffuser. The noding described above is not, in general applicable to tests with high velocity jets, such as some of the Phase 3 tests in which the steam enters containment through a 3-inch pipe. Modeling of these tests is discussed in Section 8.2.1.

6.2.2 Distributed Parameter Unique Input

The following input items are unique to the distributed parameter model as compared to the lumped parameter model.

The viscous and turbulent shear and diffusion options were activated for the subdivided vessel. A Prandtl mixing length of [ ]^{a,c} was specified for the anisotropic turbulence model for every test modeled.

6.3 Lumped Parameter LST Input Model

Noding and input specific for the lumped parameter model are discussed in this section.

6.3.1 Lumped Parameter Noding Methodology

The lumped parameter model has the following noding characteristics:

- The vessel is modeled with [ ]^{a,c} lumped parameter volumes.
- The air annulus is modeled with [ ]^{a,c} lumped parameter volumes.

The noding is derived from the baseline large-scale test model in WCAP-13246,[30] taking into consideration the vessel internals that exist in the Phase 2 and 3 tests.

Figure 6-1 is an elevation diagram of the noding. It has [ ]^{a,c} elevations above the operating deck. This is the same number of elevations as the lumped parameter baseline large scale test model[30] but the elevations are located in slightly different positions. [

]^{a,c}

Figure 6-9 is the plan view of the model between the operating deck and the upper internal gutter [ ]^{a,c} elevations have this plan view per Figure 6-8). [ ]^{a,c} separate nodes are identified with circled letters. The angles shown are determined based on the internal geometry. [

]^{a,c}

The radial divisions are determined based on internal geometry also.

[ ]^{a,c}
[ ]^{a,c}
[ ]^{a,c}

Figure 6-3 presents the noding diagram for the [ ]^{a,c} elevations above the upper internal gutter. [ ]^{a,c} nodes are identified with circled letters. More detailed noding was used in the [ ]^{a,c} elevations below the internal gutter to model the plume area. That detail is deemed unnecessary at the top of the vessel.

6.3.2 Lumped Parameter Unique Input

Climes with the correlations discussed in Section 2.0 are used to model the passive containment heat and mass transfer from the vessel internal atmosphere, through the walls, and out to the ultimate heat sink (the environment). However, the forced convection component in Equation (2-10) of Section 2.0 is set to essentially zero when modeling the heat and mass transfer to the inside vessel wall, so that the internal heat and mass transfer rates in the lumped parameter model are calculated using free convection.

As discussed in Section 5.3, the use of a free convection correlation and the lumped parameter model conservatively biases the results toward a higher predicted pressure for a Phase 2 test which has a buoyant plume induced by steam injection through a diffuser. It will also predict a conservative pressure for the Phase 3 tests in which the steam is injected through a 3-inch pipe producing a jet. In this case, the forced convection component is dominant; however, since forced convection is neglected as described above, a conservative pressure is predicted (Section 8.2.1).

6.4 Application of LST Vessel Noding to Full-Scale Plant Modeling

The noding characteristics of the WGOTHIC LST distributed and lumped parameter evaluation models provide guidance for setting up the full-scale AP600 plant evaluation models.

6.4.1 Noding of the AP600 Distributed Parameter Evaluation Model

The AP600 distributed parameter evaluation model should have the following characteristics consistent with the LST distributed parameter evaluation model:

- The LST analysis was based on a 1/2-symmetry model in order to decrease the run time; however, the entire AP600 will be modeled as full symmetry to account for the asymmetric plant layout.
- The containment should be modeled by coupling distributed parameter above deck and lumped parameter below deck.
- The upcomer, downcomer, and chimney should be modeled using the lumped parameter formulation of the code.
- The elevation, radial, and azimuthal nodalization should correspond with the LST distributed parameter evaluation model.

There should be the same number of elevations in the LST model and the AP600 model. The AP600 upper dome should be modeled as a cylinder similar to the LST model. The AP600 elevations should be defined by passing lines through the same geometrical locations as the LST model when possible. The following guidance is given to determine elevation boundaries:

[ ]^{a,c}

[

]^{a,c}

[ ]^{a,c}

[ ]^{a,c}

[ ]^{a,c}

[ ]^{a,c}

The following should be used to determine the radial divisions for the AP600 model:

[ ]a,c

[ ]a,c

[ ]a,c

[ ]a,c

[

]a,c

The following guidance is given for determining the azimuthal divisions in the AP600 distributed parameter evaluation model. For this discussion, the break is located at approximately the 180-degree azimuthal location.

The asymmetry of plant must be accommodated in determining the azimuthal boundaries. Since the entire vessel is modeled, the AP600 model will have approximately twice the number of azimuthal locations of the LST model:

[

]a,c

[

]a,c

[

]a,c

6.4.2 Noding of the AP600 Lumped Parameter Evaluation Model

The AP600 lumped parameter evaluation model should have the following characteristics:

- The containment vessel should be modeled using lumped parameter volumes.
- The upcomer, downcomer, and chimney should be modeled using the lumped parameter formulation of the code.

- The elevation, radial, and azimuthal nodalization should correspond with the LST lumped parameter evaluation model.

The same number of elevations in the LST lumped parameter model should be used in the AP600 lumped parameter model. The following AP600 lumped parameter elevation boundaries are recommended:

[ ]^{a,c}
[ ]^{a,c}
[ ]^{a,c}
[ ]^{a,c}
[ ]^{a,c}
[ ]^{a,c}

The plan view of the model between the operating deck and the crane rail should look very similar to the LST lumped parameter model. There should be [ ]^{a,c} radial rings and their boundary determination should use the same basis as the LST lumped parameter model:

[ ]^{a,c}

[ ]^{a,c}

[

]^{a,c}

From the crane rail to the top of the vessel [ ]^{a,c} radial rings should be in the AP600 lumped parameter model. [

]^{a,c}

Between the operating deck and the top of the vessel there should be [ ]^{a,c} azimuthal sections. Determination of the azimuthal divisions for the AP600 should use the same basis as the LST lumped parameter model. [

]^{a,c}

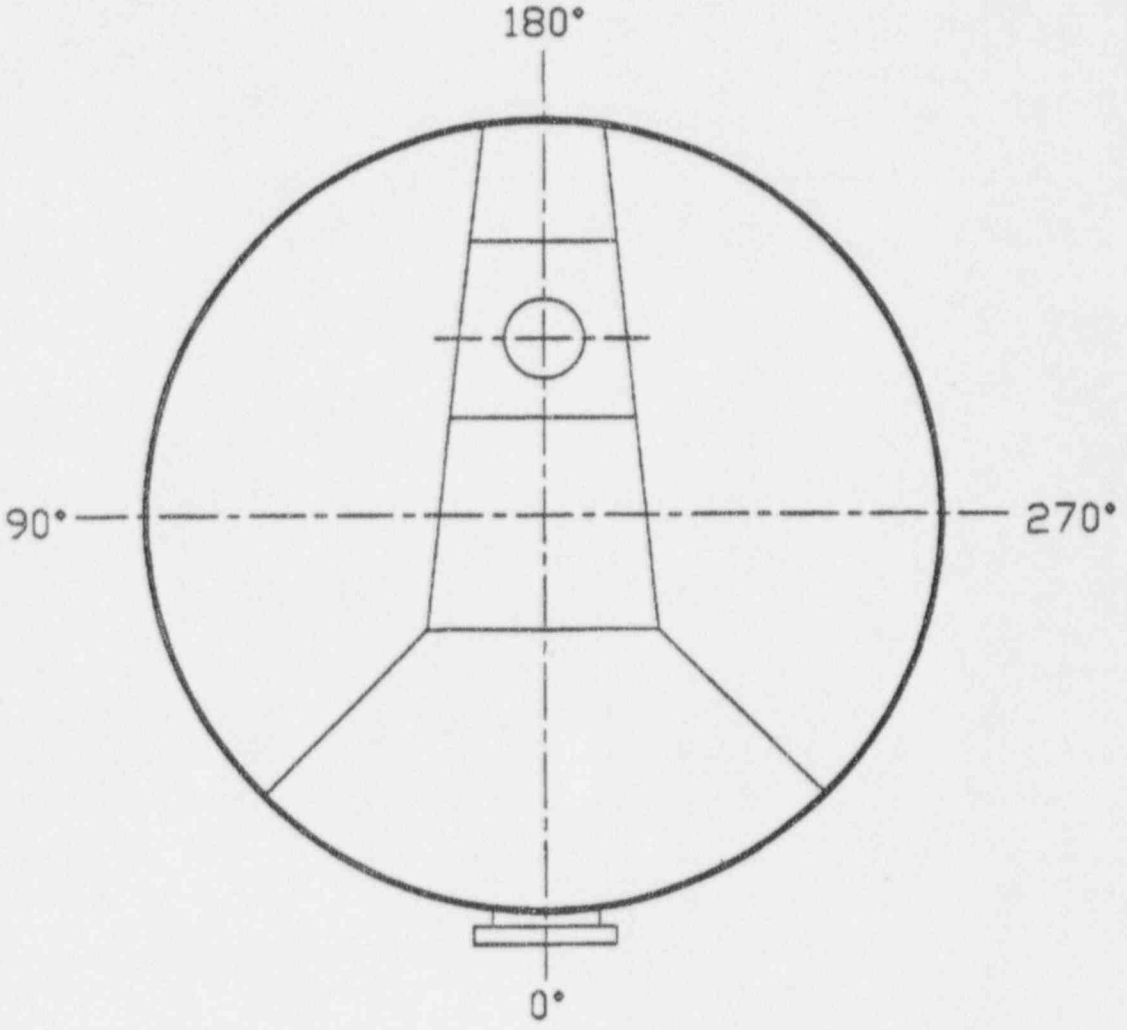

Figure 6-1 Cross-Section Orientation Convention

a,c

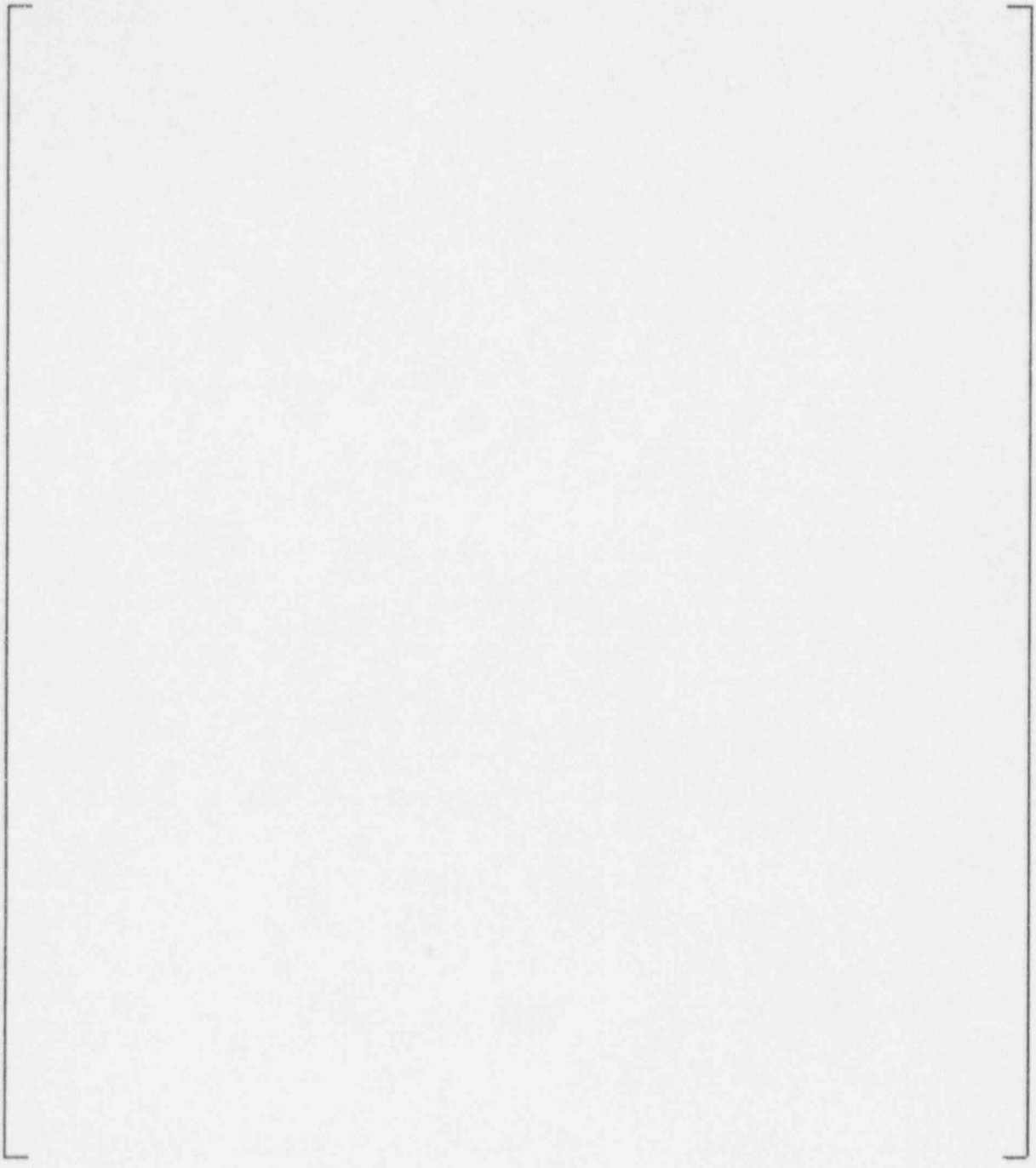

Figure 6-2 Elevation Noding Diagram of LST Distributed Parameter Model

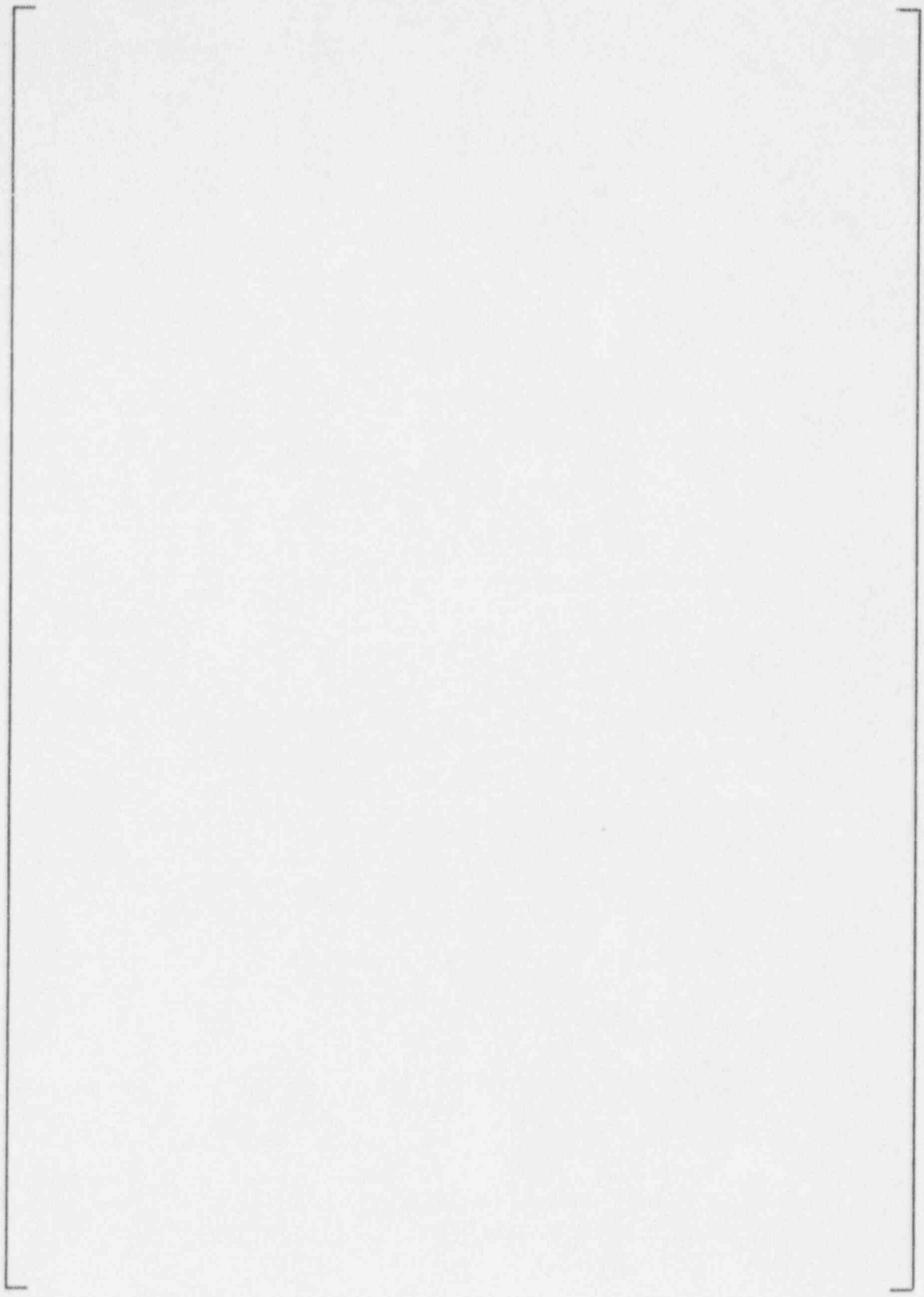

Figure 6-3 Plan View of LST Vessel Distributed Parameter Noding from Operating Deck (4.8 feet) to Top of Vessel

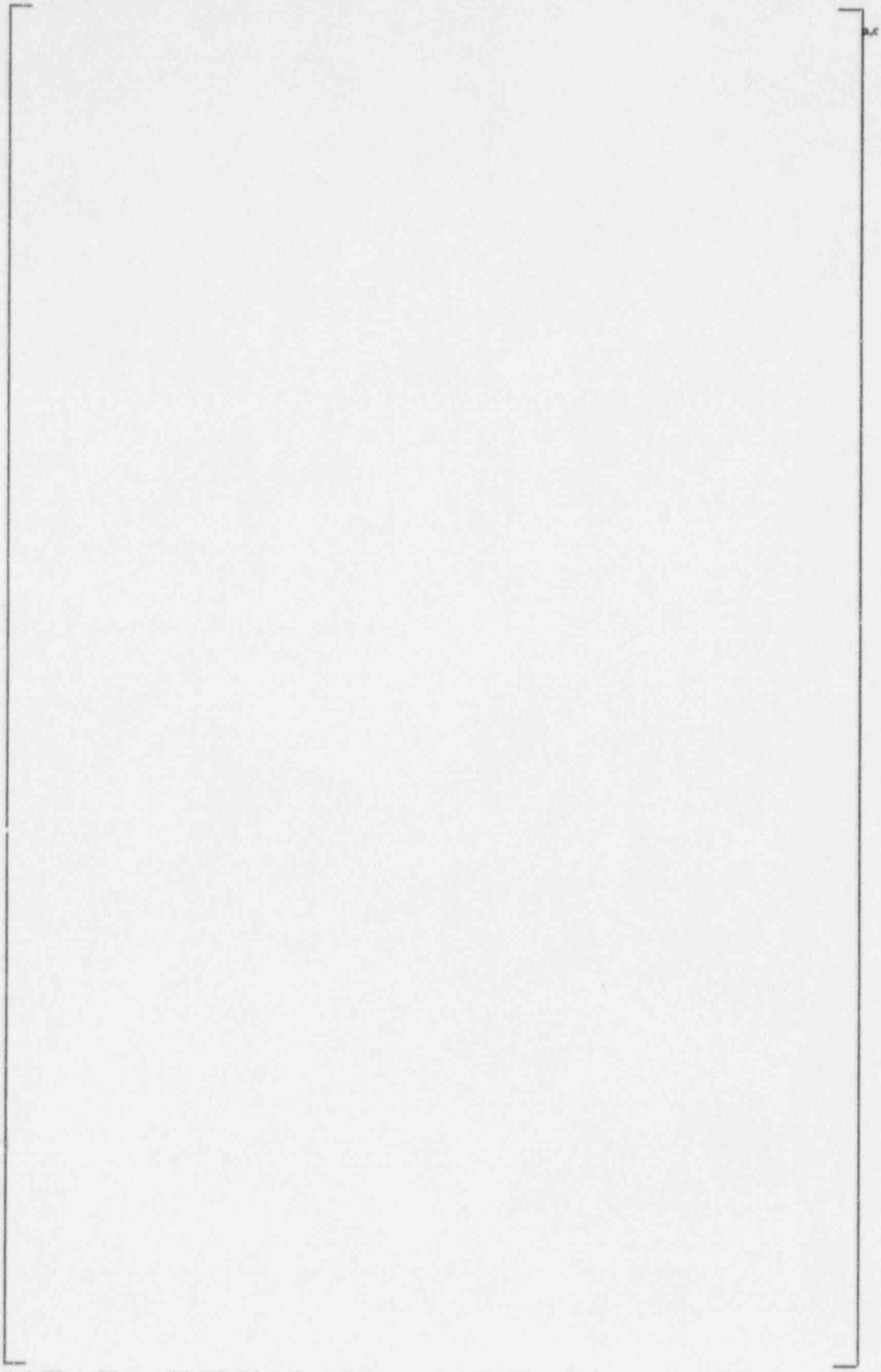

Figure 6-4 Plan View of LST Distributed Parameter Noding at the Operating Deck (4.8 feet)

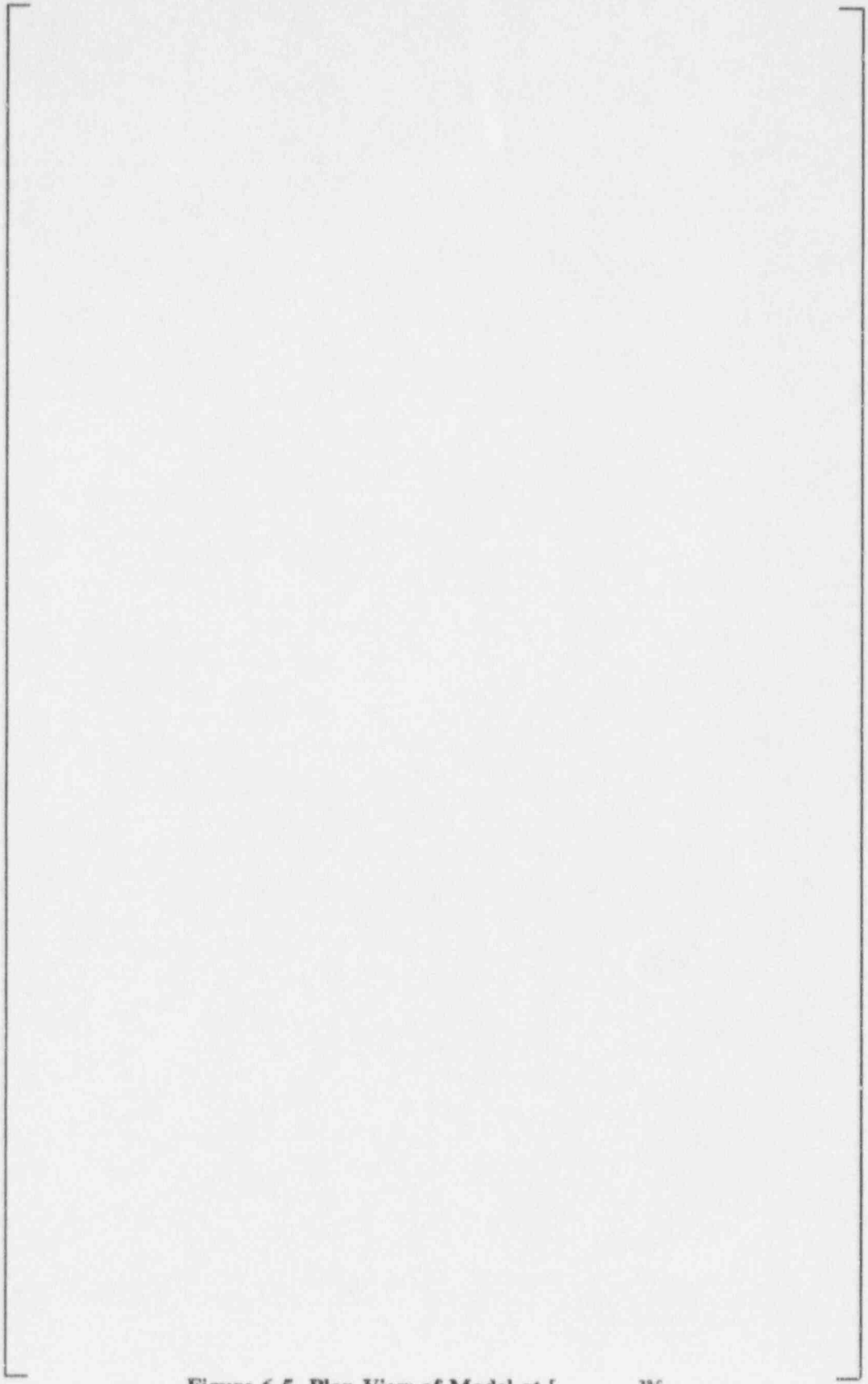

a,c

Figure 6-5 Plan View of Model at [ ]^{a,c}

a,c

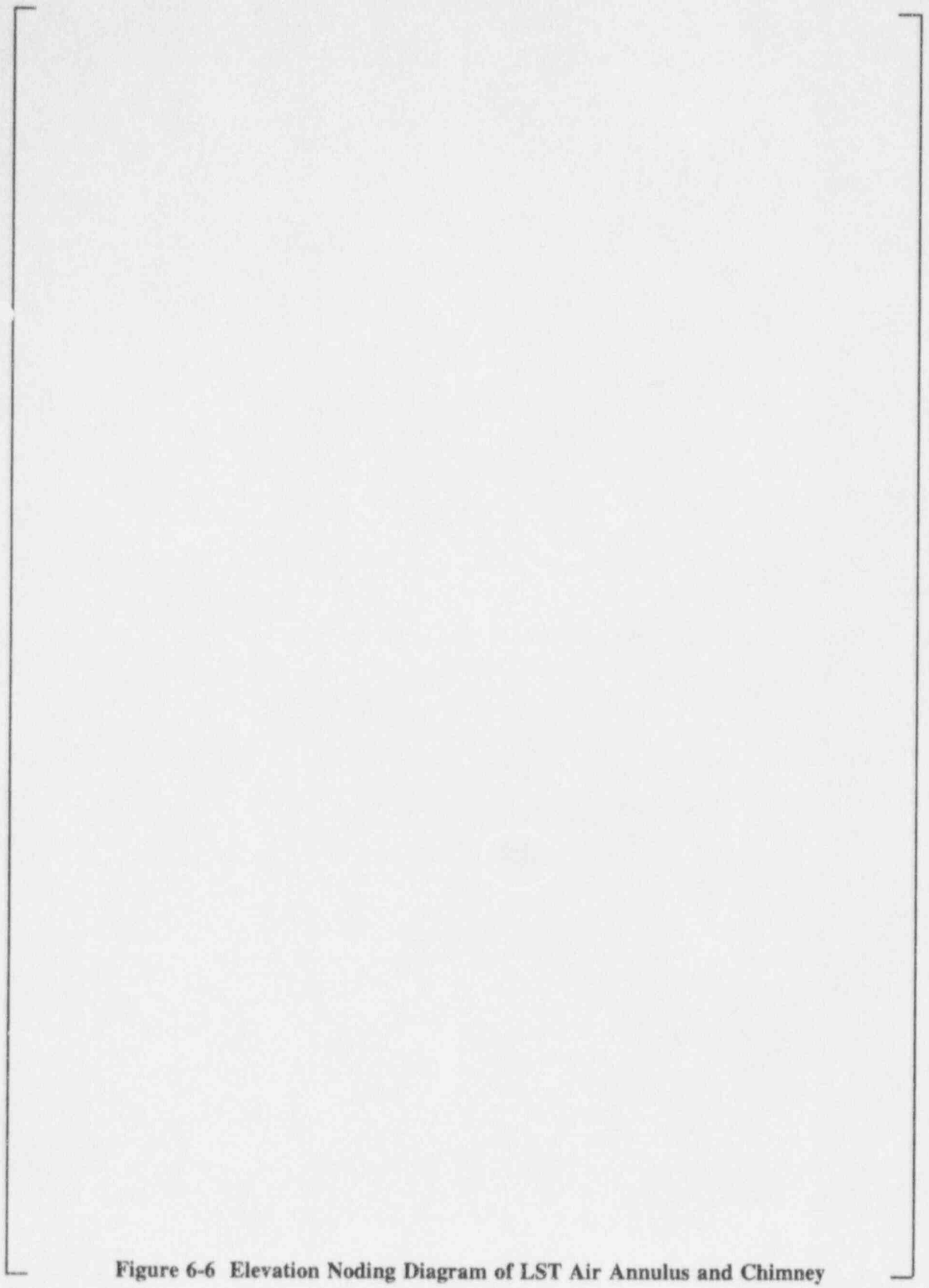

Figure 6-6 Elevation Noding Diagram of LST Air Annulus and Chimney

a,c

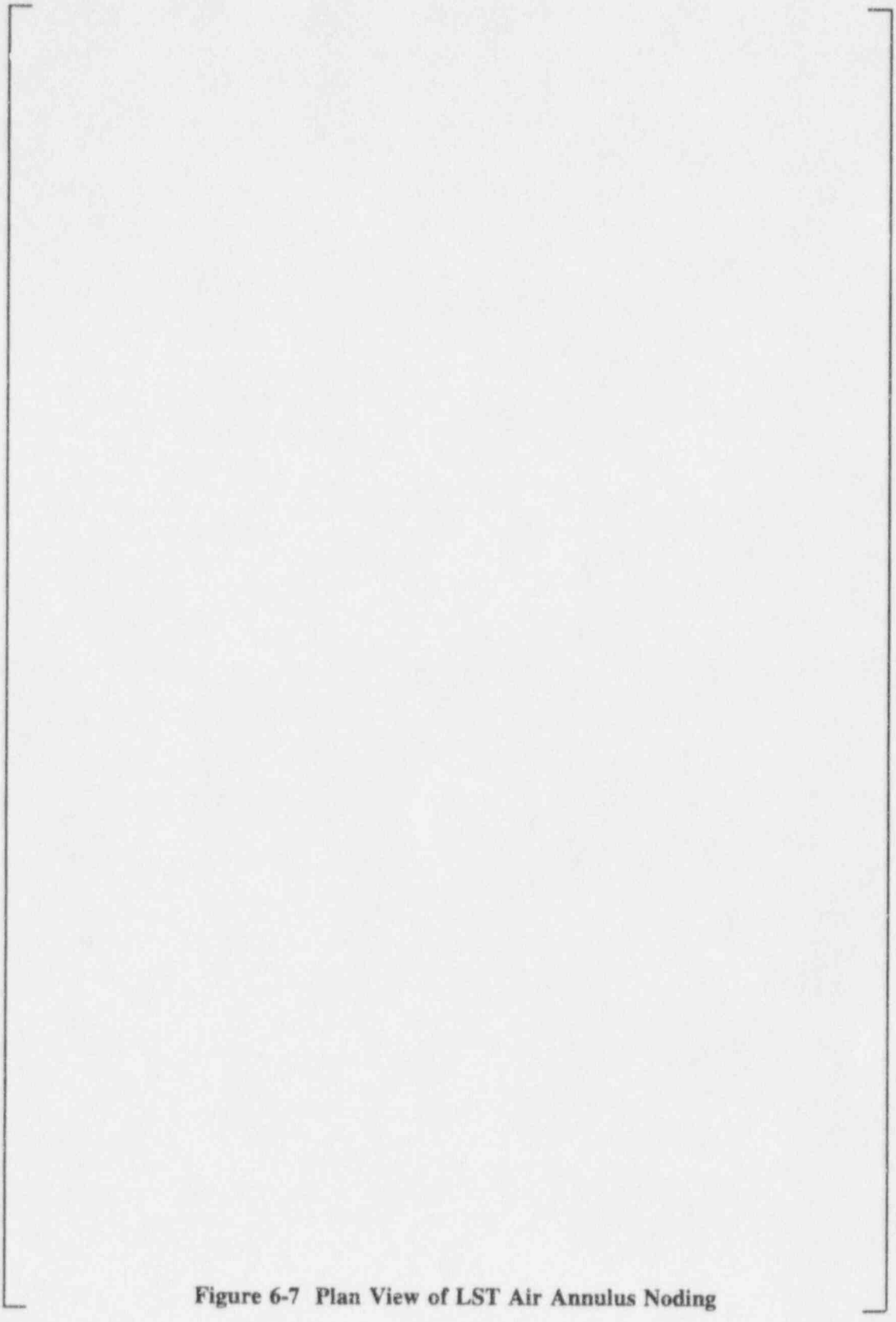

Figure 6-7 Plan View of LST Air Annulus Noding

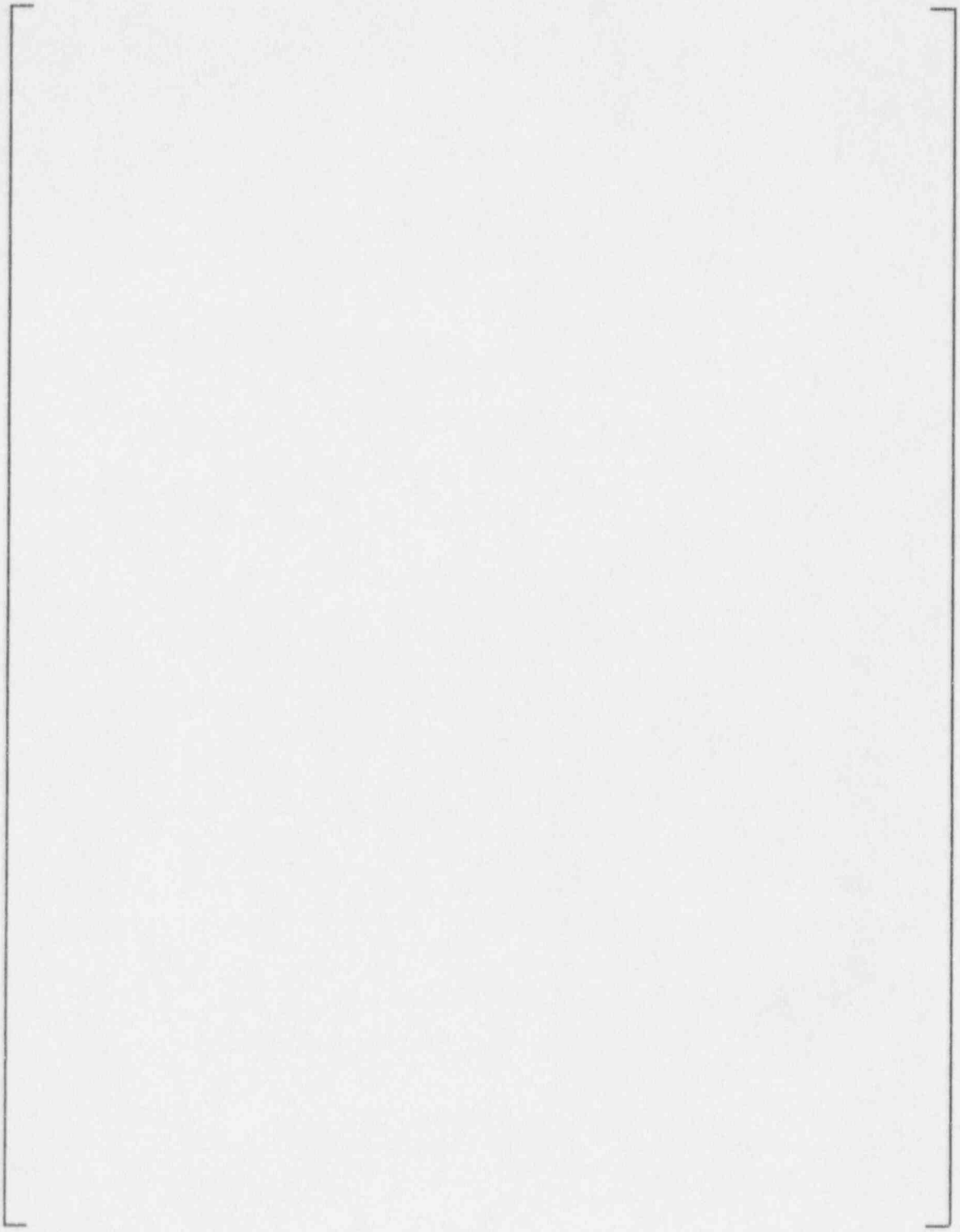

a,c

Figure 6-8 Elevation Noding Diagram of LST Lumped Parameter Model

a,c

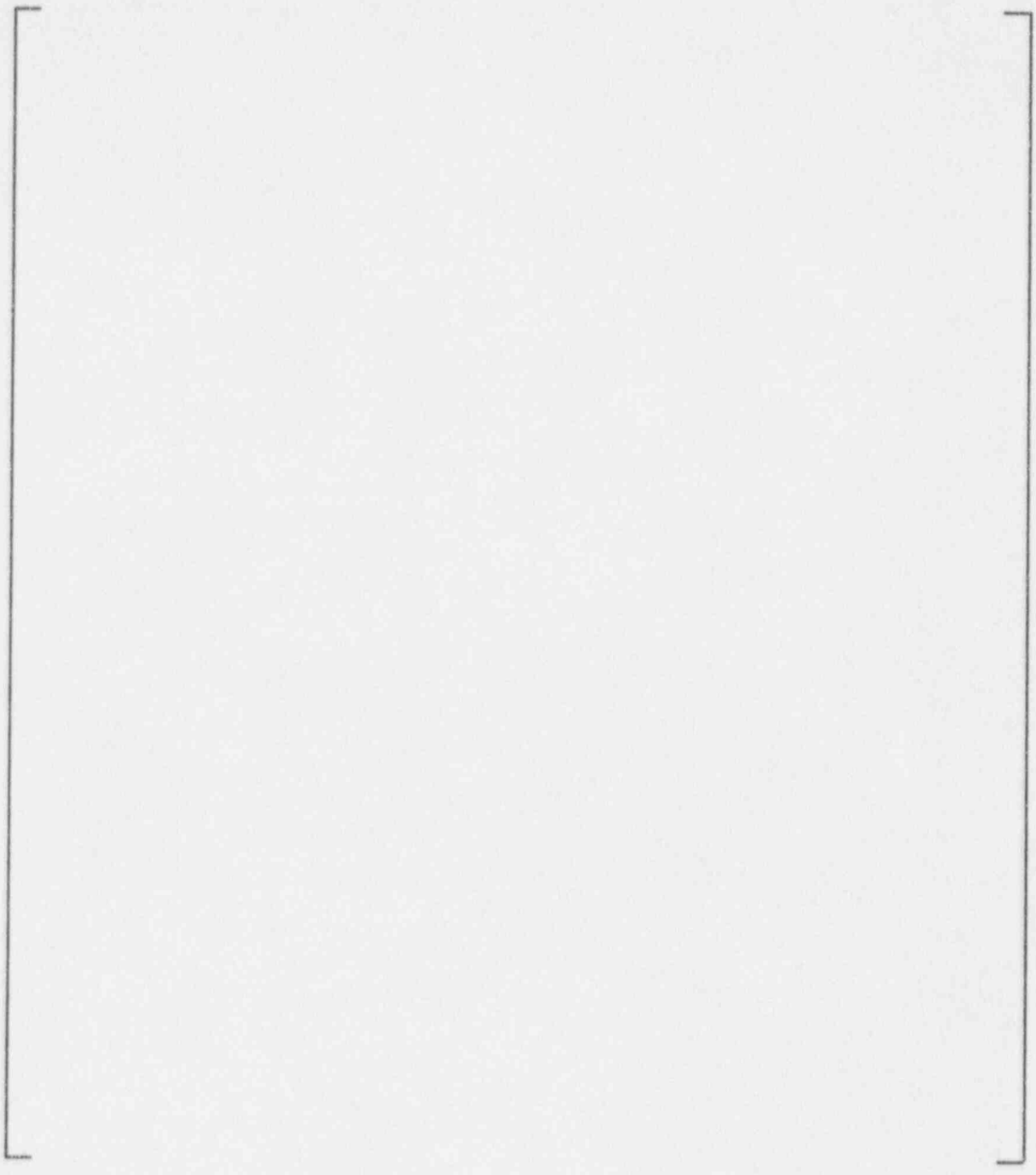

Figure 6-9 Plan View of LST Vessel Lumped Parameter Noding from Operating Deck (4.8 Feet) to Upper Internal Gutter (14.3 Feet)

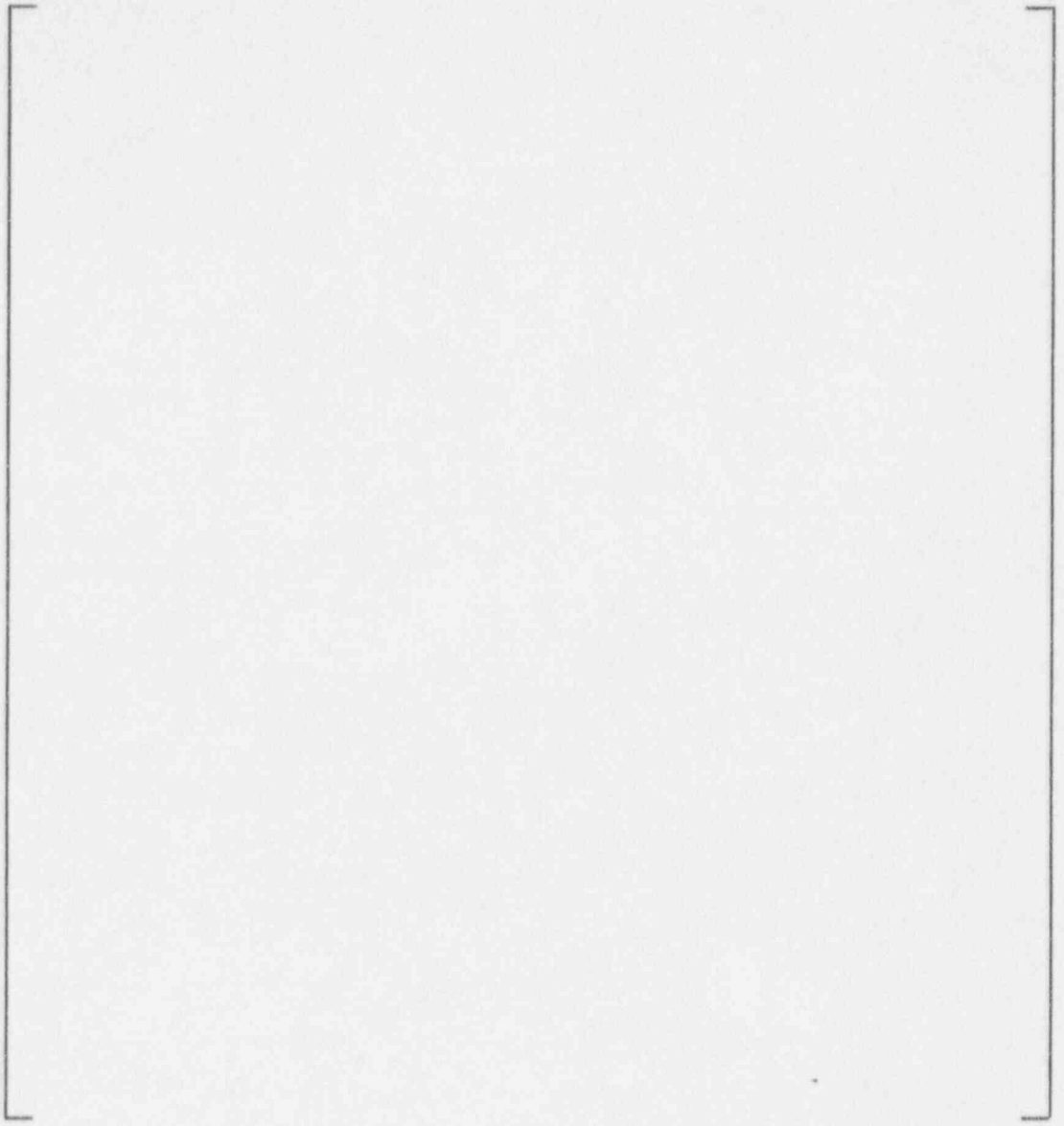

a,c

Figure 6-10 **Plan View of LST Vessel Lumped Parameter Noding from Upper Internal Gutter (14.3 Feet) to Top of Vessel**

7.0 SELECTION OF PRIORITY LARGE-SCALE TESTS FOR WGOTHIC VALIDATION

The large-scale test (LST) facility examines the thermal-hydraulic phenomena expected in the AP600. The tests performed at the LST facility also provide data to validate the WGOTHIC code over a range of prototypic conditions.

Data from the LST have been used to examine several topics in the AP600 passive containment cooling system analysis. Local data obtained from the LST have been used to confirm the validity of the boundary layer correlations selected for modeling condensation heat and mass transfer in the AP600.[16] Evaluations of the LST data have also been used to describe containment physics and quantify effects, such as sensible heating of subcooled films, evaporation, and mixing and stratification within the vessel in support of scaling studies.[2] A global evaluation of the LST data has examined the relative importance of the various parameters that affect heat removal from the vessel[31]. Finally, data from the LST facility are used to support validation of the WGOTHIC computer code, which is the emphasis of this report.

This section discusses the Phase 2 and Phase 3 large-scale test series that have been chosen for the priority tests to be used for integral validation of the WGOTHIC code. The basis for the selection of tests is also discussed.

7.1 Priority Phase 2 and Phase 3 Large-Scale Tests

The large-scale tests that have been selected for code validation cover a range of parameters with special attention placed on the parameters that have the largest effect on vessel pressure, as shown in the scaling analysis and test data evaluation. They also address the important phenomena as identified in a phenomena identification and ranking table (PIRT).[2]

The tests chosen are listed in Table 7-1. The priority tests include tests with the steam injected through the diffuser and through an elevated 3-inch pipe simulating loss-of-coolant accident (LOCA) and main steam line break (MSLB) transient conditions, respectively. The 13 steady-state conditions, as well as the transients leading to the steady states, cover a wide range of parameters. Table 7-2 shows the range of steady-state parameters covered by the priority tests and by the Phase 2 and 3 tests.

Table 7-3 is the PIRT. All the phenomena are addressed by the priority tests.

The purpose of choosing priority tests was to establish the most important tests for validation and the tests to be run with WGOTHIC first. All other Phase 2 and 3 tests will be referred to as nonpriority tests. Some of the nonpriority tests were also run with WGOTHIC in Section 8.0 and used for the uncertainty evaluation in Section 9.0, along with the priority tests.

7.2 Priority Tests' Description and Application to Validation

This section briefly describes of the priority tests (tests 212.1A, 212.1B, 212.1C, 214.1A, 214.1B, 216.1A, 216.1B, 219.1A, 219.1B, 219.1C, 222.1, 222.4A and 222.4B). The descriptions are useful for understanding the measured and predicted results in Section 8.0. This section also discusses how each test will be used to validate the WGOTHIC code.

Table 7-1 gives a summary of the priority tests, including the steam inlet configuration and the steady-state measured water coverage.

7.2.1 Tests 212.1A, 212.1B, and 212.1C

Large-scale test 212.1 was conducted by establishing a constant steam flow and maintaining the flow until the vessel arrived at a constant pressure with the air cooling fan on and cooling water applied to the vessel exterior. The vessel exterior was initially 100 percent wetted.

After the vessel reached a constant steady-state pressure (test 212.1A), the steam flow was increased and maintained until the vessel again reached a steady pressure (test 212.1B). The steam flow was increased to a third level and was allowed to come to a third and final steady pressure (test 212.1C).

The passive containment cooling system (PCS) water coverage was measured at each steady state period. For the first and second steady-states (tests 212.1A and 212.1B), the water coverage was 100 percent. For the third steady-state (test 212.1C), the measured water coverage was 95.3 percent.

7.2.2 Tests 214.1A and 214.1B

Large-scale test 214.1 was a constant steam flow test that included an air flow transition between natural convection air flow and forced convection air flow. Initially the vessel exterior was 100 percent wetted.

A constant steam flow rate was maintained until the vessel arrived at constant pressure with the air cooling fan off (test 214.1A). After the vessel reached constant pressure the air cooling fan was turned on and it was maintained at a constant speed until the vessel again reached a steady-state pressure (test 214.1B).

Water coverage was measured at each steady state period. For test 214.1A, water coverage was [ ]^{a,b}. For test 214.1B, water coverage was [ ]^{a,b}.

7.2.3 Tests 216.1A and 216.1B

Large-scale test 216.1 was a constant steam flow test with the air cooling fan on and the exterior water coverage controlled by applying the water in quadrants. Initially, the water coverage was [ ]^{a,b} with three quadrants wet and the fourth dry.

With the constant steam flow rate and [ ]^{a,b} coverage, the vessel reached a steady-state pressure (test 216.1A). Then water coverage was reduced to [ ]^{a,b} by turning the water off to two wetted quadrants. The vessel then reached a second steady-state pressure (test 216.1B).

7.2.4 Tests 219.1A, 219.1B, and 219.1C

Large-scale test 219.1 was a constant steam flow test with the air cooling fan on. With the vessel exterior dry, the vessel reached a steady-state pressure (test 219.1A). Helium was then injected into the inlet steam line, and the vessel came to a second steady-state pressure (test 219.1B). Water was then applied to the exterior vessel surface, and the vessel came to a third steady-state pressure (test 219.1C).

7.2.5 Test 222.1

Large-scale test 222.1 had a steam blowdown followed by a constant steam flow rate. Initially the vessel exterior was 100 percent wetted. Forced convection air cooling was used for the entire test.

Maximum flow of steam attainable was provided to the vessel for a 15-second period of time. Flow was then reduced to approximately 3 lb/sec. for 30 seconds and then reduced to 0.5 lbm/sec. for the remainder of the test until the vessel arrived at a constant pressure.

The extent of water coverage was measured at two points in time. After blowdown the water coverage was [ ]^{a,b} At steady-state, the water coverage was [ ]^{a,b}

7.2.6 Tests 222.4A and 222.4B

Test 222.4 had a steam blowdown followed by two levels of constant steam flow rates.

Maximum steam flow attainable was provided to the vessel for a 15-second period. Flow was then reduced to approximately 3 lb/sec. for 30 seconds and then reduced to 0.9 lb/sec. where it remained until the vessel reached a constant vessel pressure (test 222.4A). The steam flow rate was then increased to 1.3 lbm/sec. This flow was maintained until the vessel reached a second steady-state pressure (test 222.4B). The steady-state water coverage measured for tests 222.4A and 222.4B was [ ]^{a,b} and [ ]^{a,b} respectively.

7.2.7 Test Application to Validation

Table 7-4 shows which tests will be compared to predictions from the distributed and lumped parameter LST evaluation models (Section 8.0) to validate the WGOTHIC code.

Test data from 222.4A and 222.4B will only be compared to the lumped parameter LST evaluation model. Using the lumped parameter LST model is a conservative modeling approach. As stated in Section 6.2.1, the distributed parameter model was developed for a buoyant plume. Since test 222.4

used a 3-inch injection pipe, steam entered the vessel as a jet having significant kinetic energy. The forced convection component of the heat and mass transfer to the inside of the vessel was significant for this test. Running the lumped parameter evaluation model, in which the forced convection component inside containment is ignored (Section 6.3.2), results in a conservative vessel pressure prediction as shown in Section 8.2.

TABLE 7-1
LARGE-SCALE PCS PRIORITY TESTS

Test Number	Flow (lbm/sec.)	Configuration	Air Flow (ft./sec.)	Water Coverage (% Area)	Helium	Sampling
Phase 2 Tests						
212.1A		DSG			NO	YES
212.1B		DSG			NO	YES
212.1C		DSG			NO	YES
214.1A		DSG			NO	NO
214.1B		DSG			NO	NO
216.1A		DSG			NO	YES
216.1B		DSG			NO	YES
219.1A		DSG			NO	YES
219.1B		DSG			YES	YES
219.1C		DSG			YES	YES
Phase 3 Tests						
222.1		DSG			NO	YES
222.4A		AD3U			NO	YES
222.4B		AD3U			NO	YES

DSG - Diffuser in SG compartment
AD3U - 6-ft. above deck, 3-in. pipe, pointed upward
NOTE: The table illustrates the measured conditions[20]

TABLE 7-2
TEST PARAMETER RANGES

Test Parameter	Priority Tests Range*	Phase 2 and 3 Tests Range*
Steam flow rate (lb/sec.)	0.1 - 1.3	0.1 - 1.6
Jet froude number	1.6×10^{-3} - 1.9×10^{4}	1.6×10^{-3} - 2.2×10^{4}
Volume froude number	5×10^{-6} - 5.9×10^{-1}	5×10^{-6} - 6.9×10^{-1}
Maximum flow for blow down (lb/sec.)	5.5	5.3 - 6.0
External water flow rate (lb/sec.)	0 (dry test) 0.5 - 2.8	0 (dry test) 0.4 - 3.4
External water coverage (%)	0 (dry test) 25 - 100	0 (dry test) 25 - 100
Air velocity (ft./sec.)	7.7 (free) - 14.8 (forced)	5.4 (free) - 15.2 (forced)
Helium flow rate (lb/sec.)	[ ]^{a,b}	[ ]^{a,b}

* For steady-state, unless otherwise indicated

TABLE 7-3
PCS PHENOMENA IDENTIFICATION
AND RANKING TABLE FOR AP600 LOCA AND MSLB

Component	Phenomena	Rank*	Test
Module Volume	Multi-component compressible gases	H	
	Buoyancy	H	
	Jet-plume mixing/entrainment	H	
	Steam source superheating	M	
	Flow field stability/stratification	H	
Module Surface	Liquid film heat transfer	M	
	Liquid film stability/coverage	H	All the phenomena are addressed by the following:
	Liquid film subcooling	M	
	Free convection heat transfer	M	
	Forced convection heat transfer	L	212.1 A,B,C; 214.1 A,B; 216.1 A,B;
	Radiation heat transfer	L	219.1 A,B,C; 222.1; 222.4 A,B
	Free convection mass transfer	H	
	Forced convection mass transfer	H	
Module Solids	One-dimensional transient conduction heat transfer	H	
	Two- or three-dimensional conduction	L	
Inter-Module	Convection	M	
	Conduction	H	
	Form and friction losses	H	

*H-High, M-Medium, L-Low

TABLE 7-4 PRIORITY TESTS VALIDATION APPLICABILITY		
Test Number	**Distributed Parameter**	**Lumped Parameter**
212.1A	YES	YES
212.1B	YES	YES
212.1C	YES	YES
214.1A	YES	YES
214.1B	YES	YES
216.1A	YES	YES
216.1B	YES	YES
219.1A	YES	YES
219.1B	YES	YES
219.1C	YES	YES
222.1	YES	YES
222.4A	NO	YES
222.4B	NO	YES

8.0 WGOTHIC INTEGRAL VALIDATION USING LARGE-SCALE TESTS

Noding for the distributed and lumped parameter large-scale test WGOTHIC models has been established (Section 6.0). This section discusses the validation of WGOTHIC_S Version 1.2 using the Phase 2 and 3 large-scale test (LST).

Measured data will be compared to the distributed parameter and lumped parameter model predictions. More detailed comparisons will be made to the distributed parameter model to show its ability to model the LST. As discussed in Section 6.0, the lumped parameter model is conservatively biased by ignoring forced convection inside containment.

8.1 Distributed Parameter WGOTHIC Validation

A detailed distributed parameter evaluation model of the LST has been developed through noding studies. Comparisons between the evaluation model predictions and the measured data from the LST will be shown in this section. The focus is on the priority tests, defined in Section 7.0; however, selected nonpriority tests are also considered.

8.1.1 Validation Using Priority Tests

The priority large-scale tests to be compared with predictions from the distributed parameter model are tests 212.1A, 212.1B, 212.1C, 214.1A, 214.1B, 216.1A, 216.1B, 219.1A, 219.1B, 219.1C, and 222.1. As discussed in Section 7.2.6, tests 222.4A and 222.4B will not be used for the WGOTHIC distributed parameter validation.

Several global and local parameters are compared for each priority validation test. The following global parameters are compared:

- Vessel pressure
- Condensate flow rate
- Excess external PCS water flow rate

The following local parameters will be compared to support predictions of heat and mass transfer through the PCS and implicitly address effects of three-dimension distributions:

- Noncondensible concentrations
- Velocity along vessel inner wall
- Temperature difference (ΔT) through vessel wall

The following parameter is compared to add confidence to the internal three-dimensional flow field predictions:

- Internal rake temperatures

Comparison of these parameters will provide a good assessment of the WGOTHIC code and distributed parameter model's performance. The global parameters are necessary to show the overall code and model performance. The local parameters give details about the model's ability to predict the flow field and mixing within the vessel to address the potential for competing errors, and to support the global comparison results (that is, the code is calculating the right pressure for the right reasons).

Global Comparisons

WGOTHIC comparison to measured vessel pressure, condensate flow rate, and excess external water flow rate will be discussed in this section.

Vessel Pressure

For design basis accident evaluation application, the vessel pressure is the primary measure of code success. The vessel pressures for the priority tests as a function of time are shown in Figures 8-1, 8-2, 8-3, 8-4, and 8-5.

The predicted transient pressures for tests 212.1A, 212.1B, and 212.1C; 214.1A and 214.1B; 216.1A, and 216.1B; and 219.1A, 219.1B, and 219.1C, follow the same trend as the measured pressure. The predicted transient pressure for test 222.1 requires special mention.

As recommended in WCAP-14135[19] for test 222.1, the condensate flow was used for the steam flow rate boundary condition during steady state because the vortex meter consistently read a value of 8 to 12 percent lower flow than indicated by the condensate. For the initial blowdown, the steam flow rate measured by the vortex meter was used for the WGOTHIC input since the condensate flow during transients is not available and/or reliable.

For test 222.1, the code is overpredicting the measured steady-state pressure by approximately 5 percent. The variation in the predicted vessel pressure as a function of time particularly between 8000 seconds and 12,000 seconds is due to the variation in condensate flow (Figure 8-10) which was used for the steam flow rate.

The dips in the measured vessel pressure for test 222.1 at about 9000 seconds and 11,300 seconds (Figure 8-5) are due to a direct discharge of condensate that had backed up into the test vessel. The vessel pressure transducer is closely coupled with the vessel sight gage line and is reacting to the localized decrease in pressure (WCAP-14135[19]).

The predicted vessel pressure in test 222.1 is underpredicted from approximately 400 seconds to 700 seconds (Figure 8-5). The predicted pressure reaches a minimum at approximately 550 seconds, at which time it is 13 percent less than measured pressure. This discrepancy between the measurement and prediction is attributed to the uncertainty in the vortex meter measurement. The lower limit on the

vortex meter's applicable range is 0.45 lb/sec. The vortex meter reading (0.05 lb/sec. to 0.1 lb/sec.) is significantly below its applicable range for approximately 5 minutes following the blowdown.

Table 8-1 shows the average steady-state measured and predicted pressures for the priority tests. The agreement between the predicted and measured vessel pressures is good.

Condensate Flow

The condensate flow rate for the priority tests are shown in Figures 8-6, 8-7, 8-8, 8-9, and 8-10. The agreement between the measure and predicted values is good.

At steady-state, the steam flow rate into the vessel is equal to the condensate flow rate out of the vessel. The measured condensate rates during a transient are not reliable because the measurements are not instantaneous. However, the change in predicted condensate flow rate is evident during transient periods. In Figure 8-7 at approximately 9500 seconds, the fan is turned on and there is an increase in the predicted condensation rate. The increase in the external forced convection heat and mass transfer enhances the heat and mass transfer to the inside of the vessel wall resulting in a temporary increase in the condensation rate. This is consistent with the decrease in vessel pressure shown in Figure 8-2.

Similarly, for test 216.1 (Figure 8-8), the condensation rate decreases when the external water flow rate and coverage are reduced, thus reducing the external vessel heat and mass transfer. This causes the vessel pressure to increase.

For test 219.1 (Figure 8-9), when the external water flow rate is applied at approximately 34,000 seconds, the condensation rate is increased due to the enhanced external heat and mass transfer.

Excess External PCS Water Flow Rate

The excess PCS water flow rate is an indirect measurement of the total evaporation rate from the vessel. The excess water collected at the external gutter elevation, is shown in Figures 8-11, 8-12, 8-13, 8-14, 8-15, and 8-16 for the priority tests. Figures 8-14 and 8-15 are for test 219.1, but with different time scales. The excess water is slightly overpredicted for a majority of the tests, indicating that the external evaporation rate is underpredicted by WGOTHIC.

The oscillating flow for the tests is caused by the applied exterior water flow rate having a similar oscillating characteristic. This is evident in Figure 8-17 where the external wall flow rate applied to the vessel is shown for test 214.1. The dip in the external excess water for test 214.1 (Figure 8-12) between 12,000 seconds and 15,000 seconds is due to a decrease in the applied external water flow rate. In comparing the measured initial flow rates in Figures 8-12 and 8-17, notice that the external excess water is greater than the applied cooling water flow rate. This is because there is a time difference between when the water is applied to the vessel and when the water is removed from the vessel at the external gutter elevation. The vessel is initially [ ]^{a,b} wet; in fact, the water is

applied to the vessel exterior before the steam enters the vessel at which time there is no evaporation. The measured excess water flow rate from the vessel is initially greater than the applied water flow rate because the measured excess water flow rate corresponds to a higher cooling water flow rate before measurements were taken. The initial measured excess water flow rate which is higher than the applied water flow rate is not predicted because the higher cooling water flow rate was not input to the code because the data was not available.

The water is applied to the vessel exterior at 34,044 seconds in test 219.1. The applied cooling water flow rate is shown in Figure 8-18 for tests 219.1B and 219.1C. When the cooling water is initially turned on (from 34,044 seconds to approximately 36,000 seconds), the measured water flow rate is highly oscillatory. It is believed that air is initially in the line and is causing some of the noise in the measurement. The measured excess water supports this. Figure 8-15 shows the measured excess water. Around 36,000 seconds, the measured excess water flow rate is not nearly as chaotic as the applied cooling water flow rate. However, the applied cooling water flow rate shown in Figure 8-18 was the flow rate that was used for the code input. Therefore, the predicted exterior excess water at around 36,000 seconds has many more spikes than predicted for the excess water. It is also interesting to note that although the water was applied at 34,044 seconds, no exterior water was collected until about 35,500 seconds for both the measured and predicted values. Therefore, all the cooling water applied was evaporated before it reaches the external gutter during this period.

Table 8-2 shows the average steady-state measured and predicted excess water flow rates. There does not seem to be a trend between the vessel pressure predictions and the external excess water flow rate overprediction.

Local Comparisons

WGOTHIC comparisons to measured noncondensible concentrations, internal rake temperatures, velocity along the inner vessel wall, and the temperature difference through the vessel wall will be discussed in this section.

Noncondensible Concentrations

Up to four gas sample locations were used to measure the noncondensible gas concentrations (see Figure 8-19 for LST instrumentation elevations):

- F-0°-6": The location is at elevation F at the 0° azimuthal position taken approximately 6 inches from the inside of the vessel wall.

- E-90°-6": The location is at elevation E at the 90° azimuthal location taken approximately 6 inches from the inside of the vessel wall.

- A-270°-6": The location is at elevation A at the 270° azimuthal location taken approximately 6 inches from the inside of the vessel wall.

- DO-90°-63"-3": The location is in the dome at a height corresponding to a 63" radius at the 90° azimuthal location. The noncondensible measurement was taken approximately 3 inches from the inside of the vessel wall.

Noncondensible measurements were not taken for test 214.1A and 214.1B. Noncondensible measurements were only taken at locations DO-90°-63"-3" and F-0°-6" for tests 212.1A, 212.1B, 212.1C, 216.1A, and 216.1B. Noncondensible measurements were taken at all 4 locations for the remaining priority tests.

The measurements and predictions are compared on a noncondensible pressure ratio basis. The air pressure ratio is defined as the air partial pressure divided by the total vessel pressure. The air steady state pressure ratios as a function of vessel height are shown in Figures 8-20 through 8-28 for the priority tests. Figures 8-29 and 8-30 show the helium pressure ratio (helium partial pressure divided by total pressure) for test 219.1B and 219.1C.

Both the tests and the code predictions show that the vessel is air rich at elevation F for tests 212.1A, 212.1B, 212.1C, 214.1A, 214.1B, 216.1A 216.1B, 219.1A, 219.1B and 222.1. For test 219.1C the predictions and measurements show that the air is relatively well mixed throughout the vessel. A comparison of Figures 8-26 and 8-27 shows that the air concentration at elevation F did not change significantly from 219.1B to 219.1C, but the concentrations of air at elevations E, A, and dome increased.

When the water is applied to the vessel exterior between 219.1B and 219.1C, the mass transfer above the operating deck increases. Steam is removed from the steam rich atmosphere above the operating deck and condensed on the inside vessel wall at a increased rate (Figure 8-9). Thus, the air concentration at elevations E and A and at the dome increases.

When the helium is initially injected, there is little helium below the operating deck. As the test continued, the helium began to mix and was completely mixed by the start of steady-state test 219.1C. Agreement between the code helium concentrations and the measurements is good (Figures 8-29 and 8-30).

Velocity Along Vessel Inner Wall

Five velocity sensors (vane-type anemometers) were used within the vessel to monitor the flow of gas. The locations are listed below. The elevation is listed followed by the azimuthal position in degrees.

- Dome-42"-165° (Hontzsch sensor, directional output available)
- A-90° (Hontzsch sensor, directional output available)
- Dome-42"-345° (Pacer sensor)
- D-180° (Pacer sensor)
- E-30° (Pacer sensor)

During testing, functional output was not always available from some of the velocity sensors (see Table 8-3). The aggregate measurements obtained gave an indication of the local bulk velocity along the wall. The velocity measurements were used in the WGOTHIC validation to show that the code can predict the proper range of velocities along the vessel wall.

The predictions are compared to the available measurements in Table 8-4. Since the meters at E-30° and D-180° were not functioning during the entire test (Table 8-3), they are not shown in Table 8-4. Although Table 8-3 shows that some data are available for the Dome locations of test 214.1, only information at the start of the test are available. Since the information in Table 8-4 is for steady-state, it shows no functional output for 214.1A and 214.1B.

The Hontzsch velocity meters have directional output. Both WGOTHIC and the measurements consistently show that the velocity at along the wall A-90° is in the downward direction and the velocity at above the plume Dome-42"-165°] is in the upward direction.

The magnitude and direction of the predicted velocities are consistent with the measured velocities.

The overall predicted velocity field shows that during steady-state the steam comes out of the steam generator compartment, flows up to the dome, turns and flows down the vessel walls. Flow also enters the steam generator compartment from the above deck containment atmosphere. Since the steam exiting the steam generator compartment is a buoyant plume and there is no communication between the steam generator compartment and other compartments below deck, as the hot steam-air mixture exits the steam generator compartment, cooler gas from above the deck replaces the air entrained into the plume (as shown in Figure 8-47 for test 212.1A).

ΔT Through Vessel Wall

At the LST instrumentation elevations (Figure 8-19), the temperature difference through the vessel wall is measured at several azimuthal locations. An average azimuthal temperature difference through the vessel wall at each elevation is used in the comparison with the WGOTHIC predicted value.

The average vessel wall temperature differences for tests 212.1 A, B, and C at the instrumentation elevations are shown in Figures 8-48 through 8-57. The vessel wall temperature differences are also shown for test 222.1 in Figures 8-58 through 8-67. This azimuthal average includes wet and dry portions of the vessel wall. Tests 212.1A and 212.1B are [ ]^{a,b} wet. Test 212.1C is [ ]^{a,b} wet, and test 222.1 is initially [ ]^{a,b} wet but was [ ]^{a,b} at steady-state.

The most significant discrepancy between the measured and predicted values occurs in the dome at DO-21 (at a 21 in. radius on dome). This discrepancy is due to the location of the PCS water film distributor and the way in which it is modelled.

Location DO-21 is in between the two sets of J-tube rings through which the water is supplied to the vessel (see Figure 8-68). In the WGOTHIC model, all the water is applied to the top center of the

vessel; however in reality the full water flow rate is not applied until after the second set of J-tube rings [ ]^{a,b} If for example, the measured water coverage was reported to be 100 percent [ ]^{a,b} the vessel at [ ]^{a,b} is not 100 percent wet. However, it is modeled as 100 percent wet, resulting in a higher predicted heat flux. The surface area affected by this modeling limitation is small (less than 1 percent of total surface area) and has a negligible impact on the overall results.

The trend in the wall temperature difference after 2,000 seconds for test 222.1, has the same trend as the condensate flow (Figure 8-10) which was used as the steam flow into the vessel. For all elevations in test 222.1, the temperature difference is underpredicted immediately following the blow down at the same time that the vessel pressure is underpredicted. This further supports the conclusion that the steam flow measured and input into the code during this time is too low (Section 9.1.1).

The temperature difference through the vessel wall will not be shown for the remaining tests. The results are expected to be similar to the results of test 212.1 and 222.1.

Internal Rake Temperatures

Thermocouples on an instrument rake mounted in the center of the test vessel provided temperature data on the internal fluid temperature distribution under the dome and at elevations A, B, C, and D at particular radial locations. The rake is shown in Figure 8-31.

The measured temperatures along the 0-degree to 180-degree plane (Figure 8-32) will be compared to the predicted temperatures in corresponding locations. The radial locations for each elevation are listed below. A negative radial location corresponds to a distance toward the 0-degree azimuthal location. A positive radial location corresponds to a distance toward the 180-degree azimuthal location.

Rake locations along the 0-degree to 180-degree plane are

- Dome at radial locations 18 in., 0 in., -18 in.
- A at radial locations 78 in., 66 in., 54 in., 36 in., 18 in., 0 in., -78 in.
- B at radial locations 78 in., 66 in., 54 in., 36 in., 18 in., 0 in., -78 in.
- C at radial locations 78 in., 66 in., 54 in., 36 in., 18 in., 0 in., -78 in.
- D at radial locations 78 in., 66 in., 54 in., 18 in., 0 in., -78 in.

The measured and predicted rake temperatures are shown in Figures 8-32 through 8-36 for tests 212.1A, 8-37 through 8-41 for test 212.1B, and 8-42 through 8-46 for test 212.1C. In each case, both the measured and predicted temperatures increase at a radial location over the steam injection point. The measured and predicted temperatures are fairly constant at other radial locations.

Rake temperatures for the remaining tests are not shown. The comparisons are expected to have results similar to tests 212.1A, 212.1B, and 212.1C.

8.1.2 Nonpriority Tests

Several of the nonpriority tests were also run with the distributed parameter evaluation model. These tests were run to strengthen the statistical analysis in support of the uncertainty evaluation (Section 9.0). The nonpriority tests run with the model are 213.1A, 213.1B, 218.1A, 218.1B, 224.2, 221.1A, 221.1B, 221.1C, and 202.2.

The predicted results from the nonpriority tests are consistent with the priority tests. No detailed comparisons will be shown for the non-priority tests. The steady-state predicted and measured pressures for the nonpriority tests are given in Table 8-5.

8.1.3 Distributed Parameter Evaluation Model Conclusions

The WGOTHIC distributed parameter formulation with the noding discussed in Section 6.0 provides a reasonably accurate and detailed resolution of velocity and noncondensible distributions within the LST.

Figure 8-69 shows the predicted and measured vessel pressures for all the LST run with the distributed parameter evaluation model. Agreement is very good. The uncertainty associated with the code predictions is assessed in Section 9.0.

8.2 Lumped Parameter Comparison Results

The noding for the lumped parameter evaluation model has been discussed in Section 6.0. This section will discuss the characteristics of the model. The predicted and measured vessel pressure will be compared for the pr ority and nonpriority tests.

8.2.1 Validation Using Priority Tests

The priority tests to be run with the lumped parameter evaluation model are tests 212.1A, 212.1B, 212.1C, 214.1A, 214.1B, 216.1A, 216.1B, 219.1A, 219.1B, 219.1C, 222.1, 222.4A and 222.4A.

The steam inlet configuration for tests 212.1A, 212.1B, 212.1C, 214.1A, 214.1B, 216.1A, 216.1B, 219.1A, 219.1B, 219.1C, and 222.1, is a steam diffuser within the simulated steam generator compartment. The steam enters the containment atmosphere as a buoyant plume, similar to a post-blowdown loss-of-coolant accident (LOCA) event.

The steam inlet configuration for tests 222.4A and 222.4B is a 3-in. diameter pipe located 5.5 ft. above the operating deck. The steam enters the containment atmosphere as a high velocity jet, similar to a main steamline break (MSLB) event.

Because the mixing and velocity magnitude inside containment differ significantly between the two configurations, they will be discussed separately within this section.

Buoyant Plume Tests

The large-scale tests conducted with the steam diffuser below deck simulate the post-blowdown portion of a LOCA.

The heat and mass transfer inside the LST vessel is dominated by free convection. The low-velocity steam injection results in relatively good mixing and small axial noncondensable concentration gradients above the injection location, but stratification below, causing air to be concentrated below the operating deck.

Test 222.1, which had noncondensible measurements at four locations within containment, will be discussed in some detail to explain the characteristics of the lumped parameter evaluation model.

The lumped parameter evaluation model overmixes the air from below the injection location noncondensibles and overpredicts the velocity in the vessel as shown in Figure 8-70 and Table 8-6 for test 222.1. The velocity meter along the wall at A-90° was the only meter functioning for this test. Although the measurement and prediction show that the velocity is in the downward direction, the predicted velocity is much higher than the measured velocity.

For the lumped parameter evaluation model, the forced convection component of mixed convection heat and mass transfer inside the vessel is neglected, but the vessel is also over-mixed. The overmixing carries air above the operating deck. Increasing the concentration of air above the operating deck degrades the mass transfer, and thereby reduces the heat removal from the vessel.

Figure 8-71 shows the measured and lumped parameter evaluation model predicted vessel pressure for test 222.1. As expected, the vessel pressure is overpredicted. Section 8.1.1 presents a discussion of the predicted vessel pressure trend and the dips in the measured pressure (at 9000 seconds and 11,300 seconds).

Figures 8-72 through 8-75 show the measured and predicted vessel pressure for tests 212.1A, 212.1B, 212.1C, 214.1A, 214.1B, 216.1A, 216.1B, 219.1A, 219.1B, and 219.1C. The vessel pressure is over predicted for all tests except the initial part of test 214.1A.

The initial underprediction for test 214.1A is caused by the modeling of the water coverage. The water coverage fraction on the exterior vessel surface is a code input parameter. Test 214.1 was initially [ ]^{a,b} wet, but the water fraction coverage measured during the latter part of test 214.1A was 78 percent.]^{a,b} The water coverage was changed from 100 percent to 78 percent at 3,000 seconds in the model, resulting in an underprediction of vessel pressure from approximately 1500 seconds to 3,000 seconds. The water coverage in the model should have been changed continuously, starting at an earlier time. However, since coverage was not continuously monitored, it was simply modeled by as step change.

High Velocity Jet Tests

The large-scale tests with a 3-in. steam source simulate the lower velocity portions of a MSLB.

The injection of the high velocity steam source resulted in a well-mixed containment based on noncondensible measurements. Based on measurements of internal velocity, the heat and mass transfer within containment have a significant forced convection component.

The lumped parameter evaluation model uses only free convection heat and mass transfer models, which conservatively biases the results because the test actually has a significant forced convection component. The vessel pressures calculated with the lumped parameter evaluation model are compared to the measured pressures for tests 222.4A and 222.4B in Figure 8-77.

In the evaluation model, the steam is injected at an elevated level as it was in the test. Figures 8-77 and 8-78 show the measured and predicted noncondensible gas concentration as a function of vessel height for test 222.4A and 222.4B. The model predicts a more stratified containment than the measurements. This is because the model entrains fluid into the jet from nodes at or above the steam injection point resulting in a well mixed atmosphere above the point of steam injection and air rich atmosphere below the steam injection point. This is contrary to the measurements which show the kinetic energy from the high velocity jet mixes the entire containment.

Table 8-7 shows the average steady state measured and predicted vessel pressures for all the priority tests. The lumped parameter evaluation model overpredicts the measured steady state vessel pressure for all the tests.

8.2.2 Nonpriority Tests

The nonpriority tests run with the lumped parameter evaluation model are tests 213.1A, 213.1B, 218.1A, 218.1B, 224.2, 221.1A, 221.1B, 202.2, 224.1, 217.1A, and 217.1B. These tests were run to strengthen the statistical analysis in support of the uncertainty evaluation (Section 9.0).

The predicted results for the priority tests are consistent with the nonpriority tests. The steady state predicted and measured pressure for the nonpriority tests are given in Table 8-8.

8.2.3 Lumped Parameter Evaluation Model Conclusions

The lumped parameter evaluation model overpredicts the vessel pressure for steam entering the vessel as either a buoyant plume or a high velocity jet. Figure 8-79 graphically illustrates the conservatism in the model. The uncertainty associated with the code predictions is assessed in Section 9.0

TABLE 8-1
MEASURED AND DISTRIBUTED PARAMETER PREDICTED
AVERAGE STEADY-STATE VESSEL PRESSURES FOR PRIORITY TESTS

Test Number	Measured Pressure (psia)	Predicted Pressure (psia)	Predicted/Measured
212.1A	[a,b]	[a,c]	1.04
212.1B			1.03
212.1C			1.04
214.1A			0.98
214.1B			1.00
216.1A			0.98
216.1B			1.01
219.1A			1.02
219.1B			1.05
219.1C			1.16
222.1			1.05

TABLE 8-2
MEASURED AND DISTRIBUTED PARAMETER PREDICTED
AVERAGE STEADY-STATE EXCESS EXTERNAL WATER FLOW RATE

Test Number	Measured Flow (lbm/sec.)	Predicted Flow (lbm/sec.)	Predicted/Measured
212.1A	[a,b]	[a,c]	1.03
212.1B			1.08
212.1C			1.07
214.1A			1.18
214.1B			1.17
216.1A			1.04
216.1B			1.13
219.1A			1.00
219.1B			1.00
219.1C			1.12
222.1			1.12

TABLE 8-3 INTERNAL VELOCITY METER MEASUREMENT PERFORMANCE					
Test Number	**E-30°**	**D-180°**	**Dome-42"-345°**	**A-90°**	**Dome-42"-165°**
212.1	NF	NF	FP	F	FP
214.1	NF	NF	FP	F	FP
216.1	NF	NF	NF	F	FP
219.1	NF	NF	NF	FP	NF
222.1	NF	NF	NF	F	NF

NF – Not functioning for entire test
FP – Functioning for part of test
F – Functioning for entire test

a,b,c

TABLE 8-4
MEASURED AND PREDICTED AVERAGE STEADY-STATE INTERNAL VELOCITIES

Test Number	Dome-42"-345° Measured	Dome-42"-345° Predicted	A-90° Measured	A-90° Predicted	Dome-42"-165° Measured	Dome -42"-165° Predicted
212.1A						
212.1B						
212.1C						
214.1A						
214.1B						
216.1A						
216.1B						
219.1A						
219.1B						
219.1C						
222.1						

TABLE 8-5
MEASURED AND DISTRIBUTED PARAMETER PREDICTED AVERAGE STEADY-STATE VESSEL PRESSURES FOR NONPRIORITY TESTS

Test Number	Measured Pressure (psia)	Predicted Pressure (psia)	Predicted/Measured
213.1A	[ ] a,b	[ ] a,c	1.01
213.1B	[ ]	[ ]	1.03
218.1A	[ ]	[ ]	1.00
218.1B	[ ]	[ ]	1.05
224.2	[ ]	[ ]	1.07
[illegible]1A	[ ]	[ ]	1.10
221.1B	[ ]	[ ]	1.12
221.1C	[ ]	[ ]	1.02
202.3	[ ]	[ ]	0.96

a,b,c

TABLE 8-6 MEASURED AND LUMPED PARAMETER PREDICTED AVERAGE STEADY-STATE INTERNAL VELOCITY		
Test Number	A-90° Measured Velocity (ft./sec.)	A-90° Predicted Velocity (ft./sec.)

TABLE 8-7 MEASURED AND LUMPED PARAMETER PREDICTED AVERAGE STEADY-STATE VESSEL PRESSURES FOR PRIORITY TESTS			
Test Number	Measured Pressure (psia)	Predicted Pressure (psia)	Predicted/Measured
212.1A	a,b	a,c	1.15
212.1B			1.17
212.1C			1.20
214.1A			1.03
214.1B			1.12
216.1A			1.11
216.1B			1.19
219.1A			1.03
219.1B			1.07
219.1C			1.31
222.1			1.18
222.4A			1.15
222.4B			1.28

TABLE 8-8
MEASURED AND LUMPED PARAMETER PREDICTED AVERAGE STEADY-STATE VESSEL PRESSURES FOR NONPRIORITY TESTS

Test Number	Measured Pressure (psia)	Predicted Pressure (psia)	Predicted/Measured
213.1A	[a,b]	[a,c]	1.13
213.1B			1.18
218.1A			1.11
218.1B			1.19
224.2			1.24
221.1A			1.22
221.1B			1.19
202.3			1.07
224.1			1.25
217.1A			1.06
217.1B			1.32

a,c

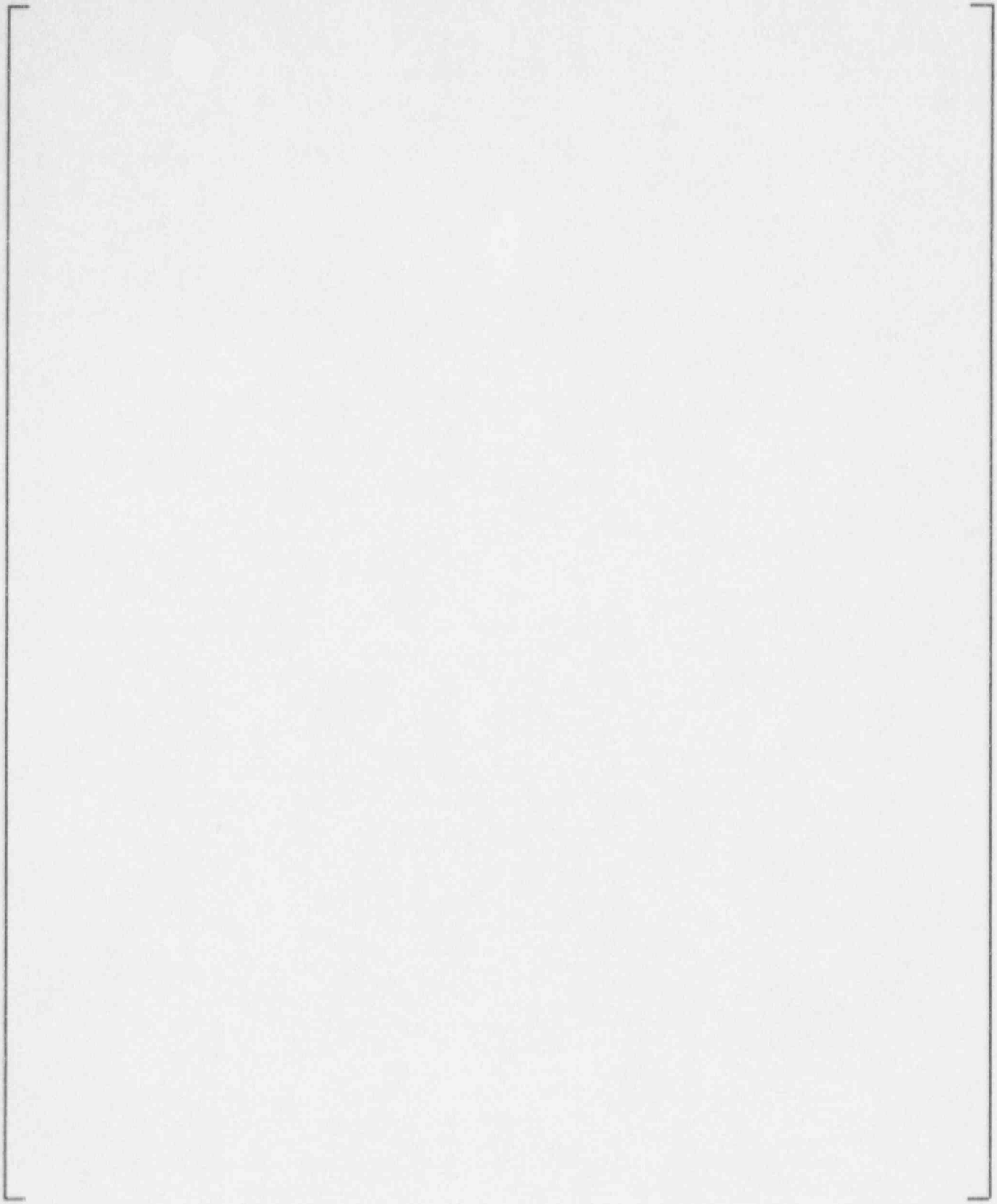

Figure 8-1 Measured and Distributed Parameter Predicted Vessel Pressure for Tests 212.1A, 212.1B, and 212.1C

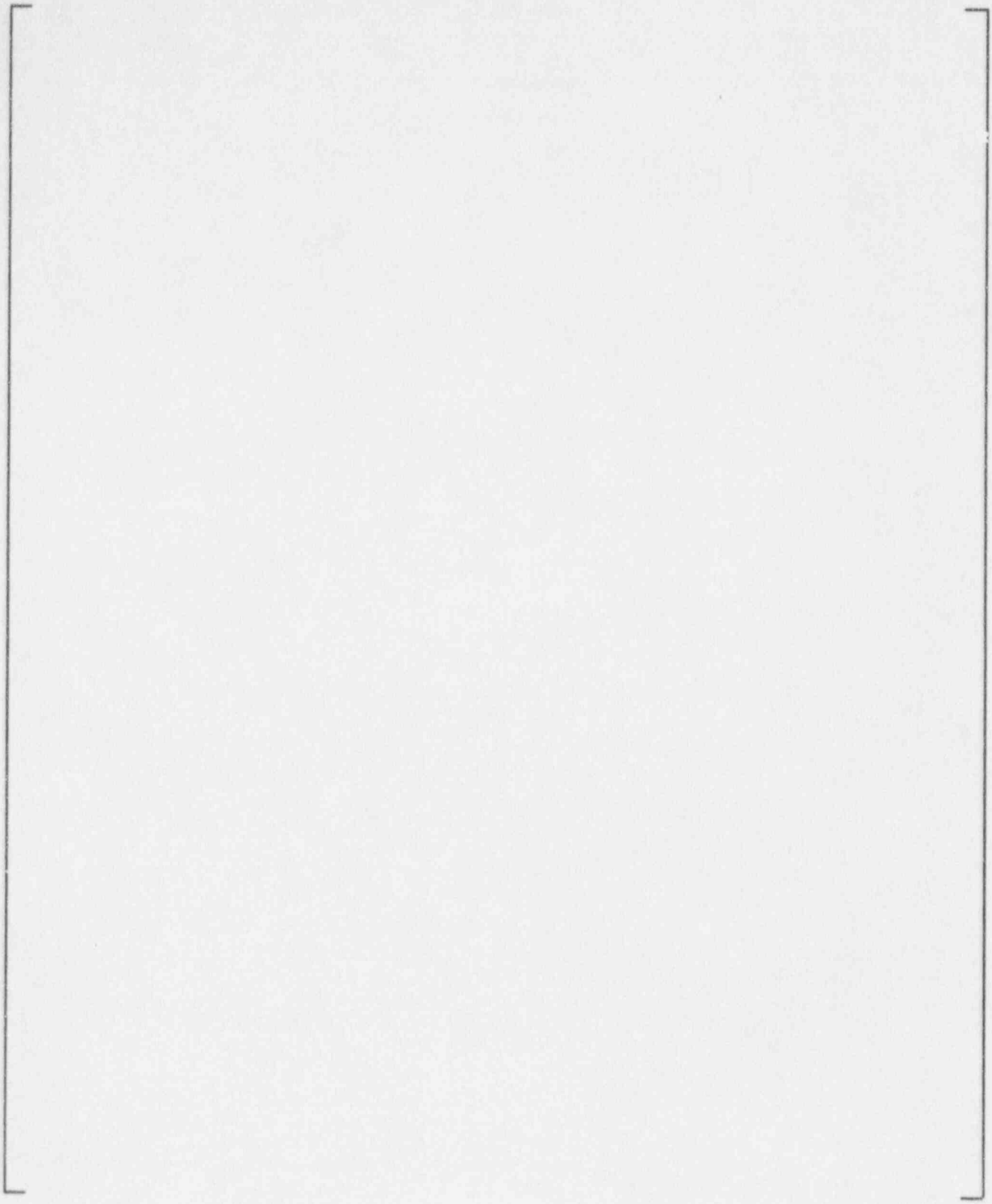

Figure 8-2 Measured and Distributed Parameter Predicted Vessel Pressure for Tests 214.1A and 214.1B

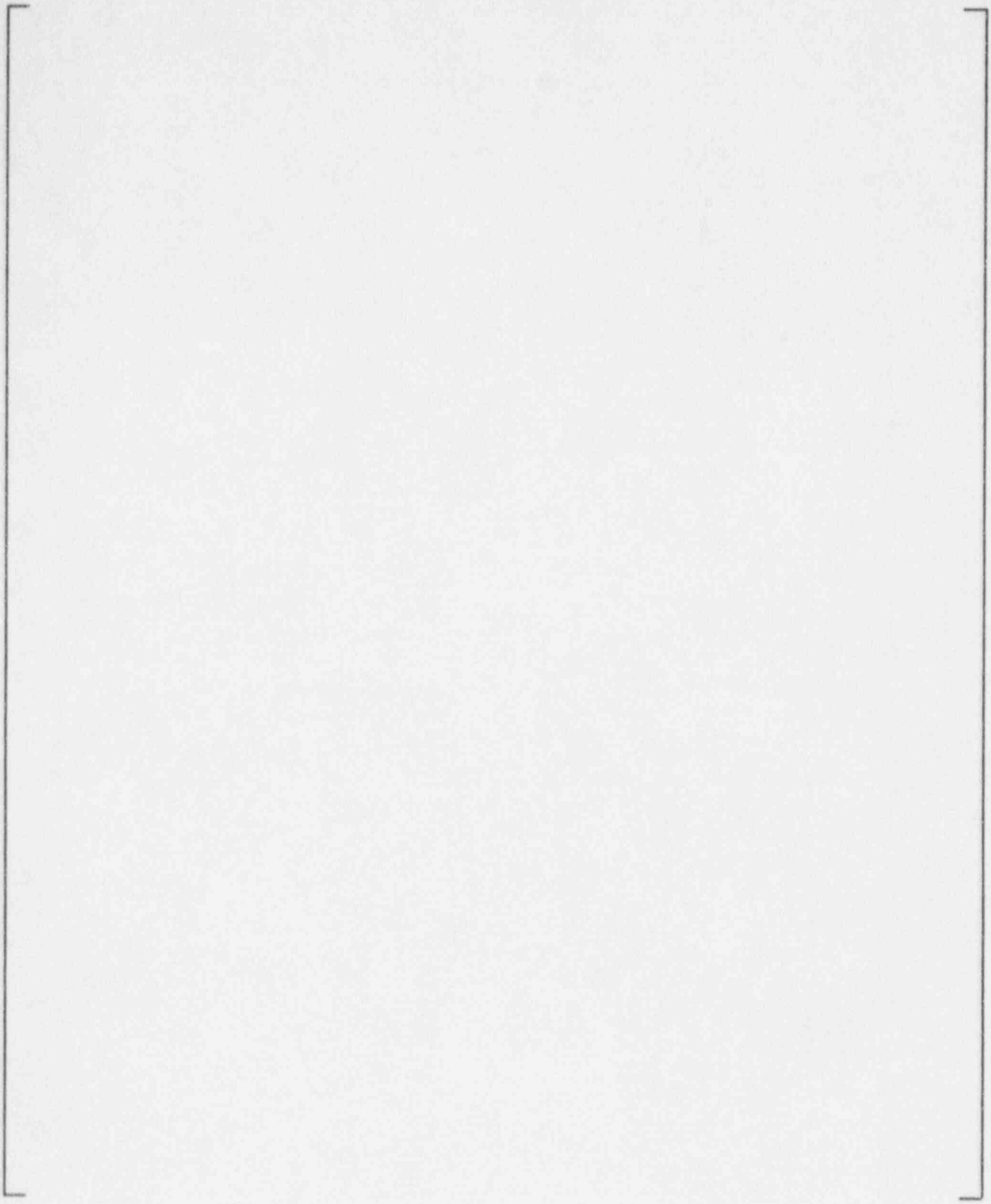

Figure 8-3 Measured and Distributed Parameter Predicted Vessel Pressure for Tests 216.1A and 216.1B

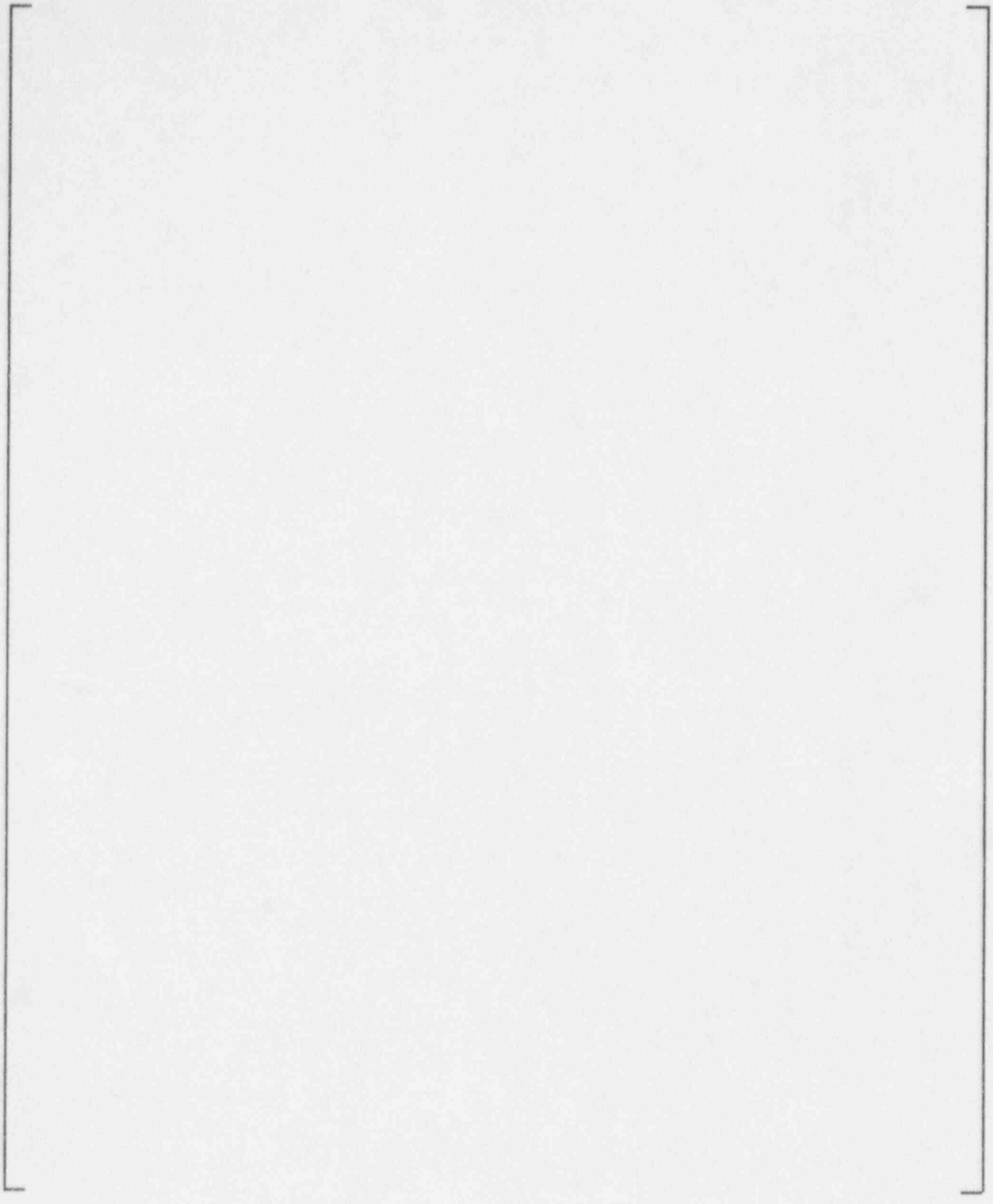

Figure 8-4 **Measured and Distributed Parameter Predicted Vessel Pressure for Tests 219.1A, 219.1B, and 219.1C**

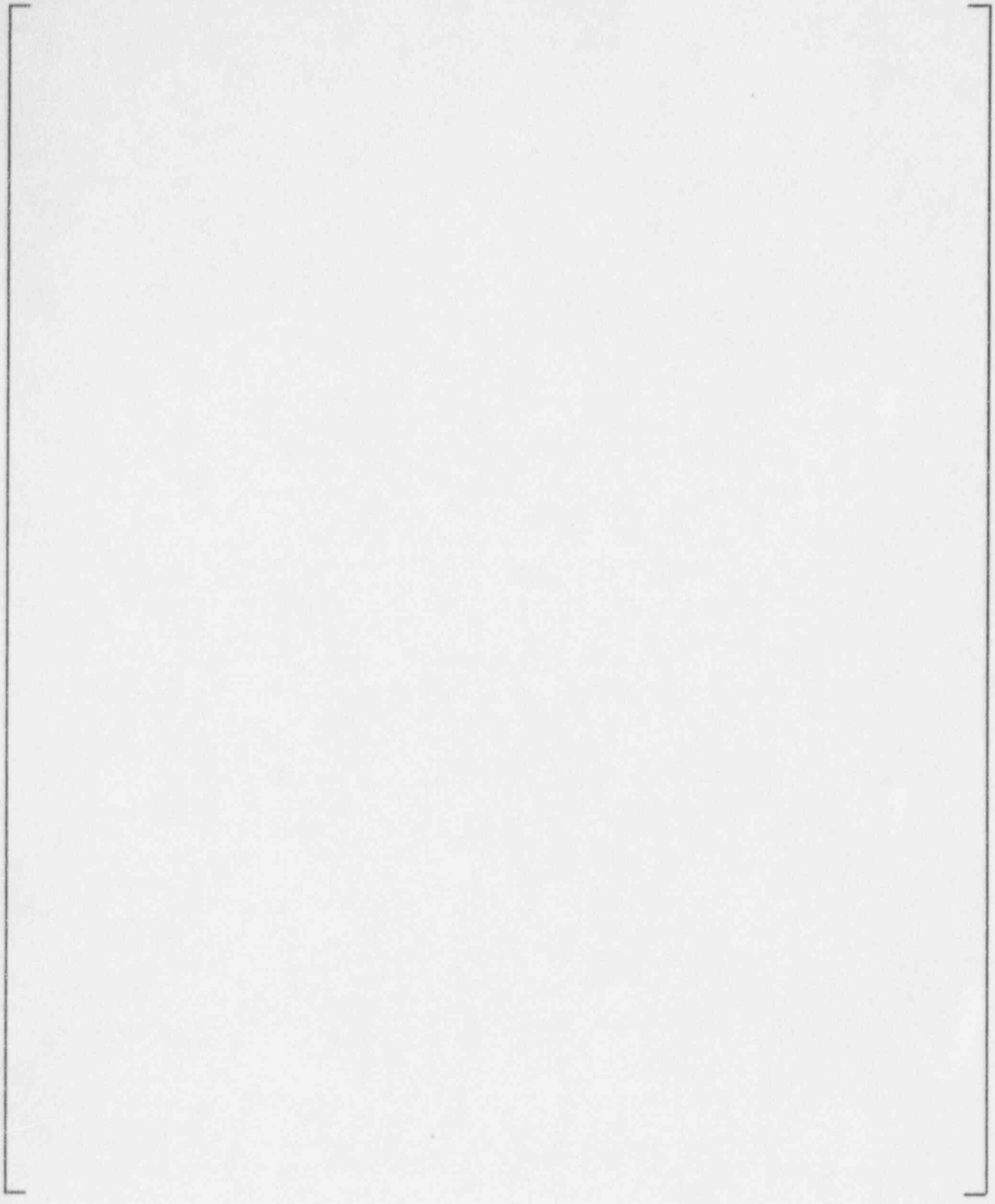

Figure 8-5 Measured and Distributed Parameter Predicted Vessel Pressure for Test 222.1

a,c

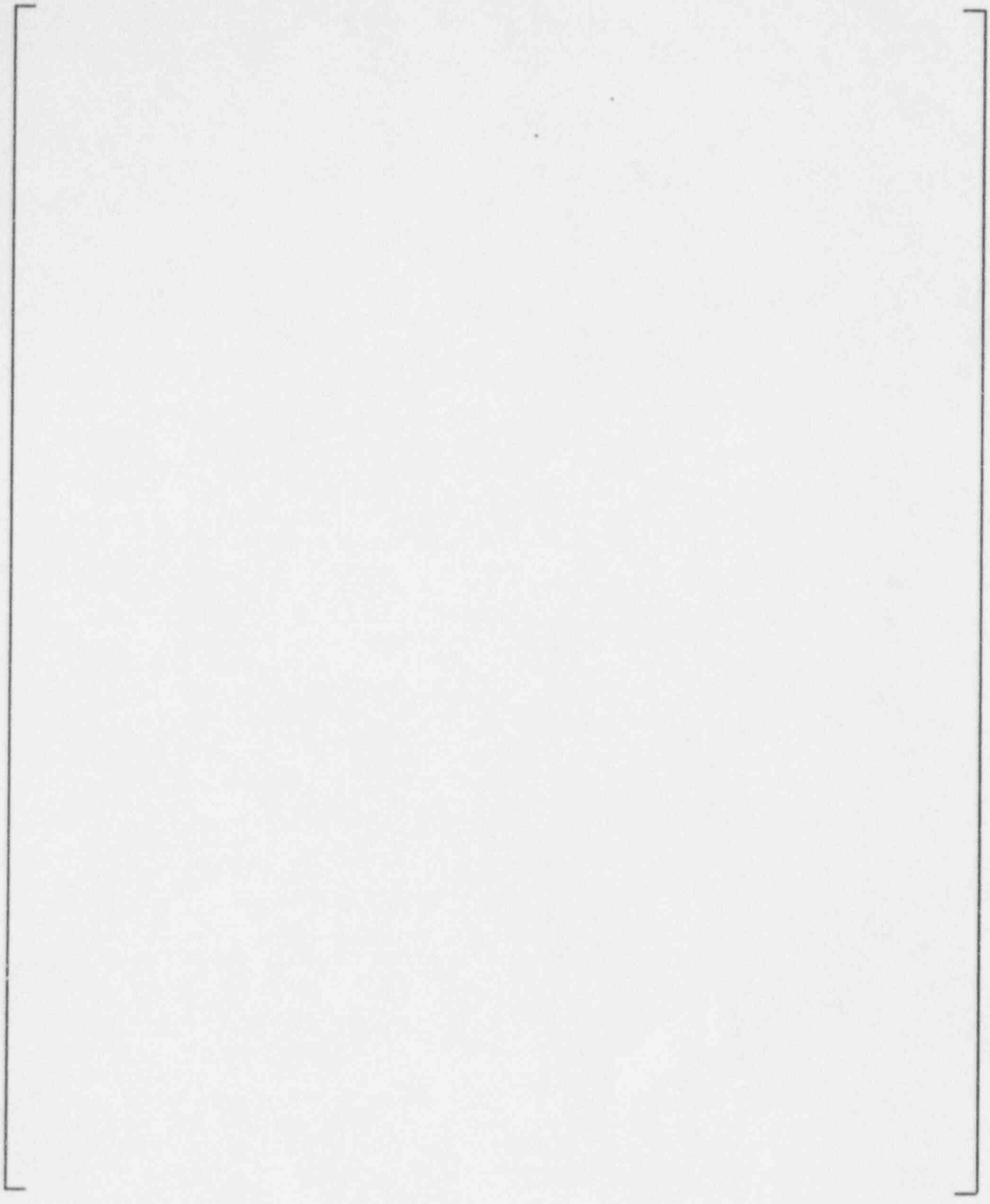

Figure 8-6 Measured and Distributed Parameter Predicted Condensate Flow for Tests 212.1A, 212.1B, and 212.1C

a,c

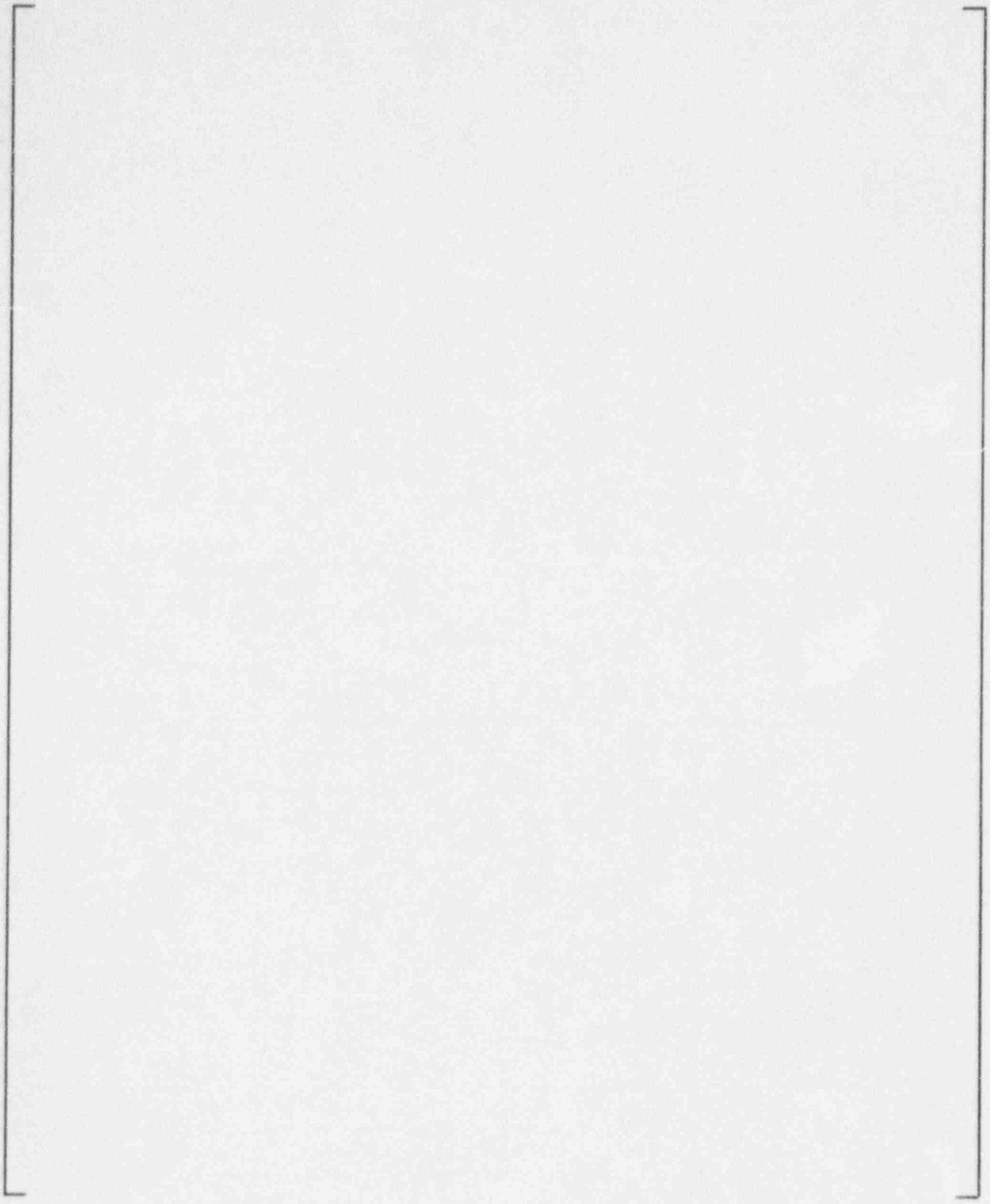

Figure 8-7 Measured and Distributed Parameter Predicted Condensate Flow for Tests 214.1A and 214.1B

a,c

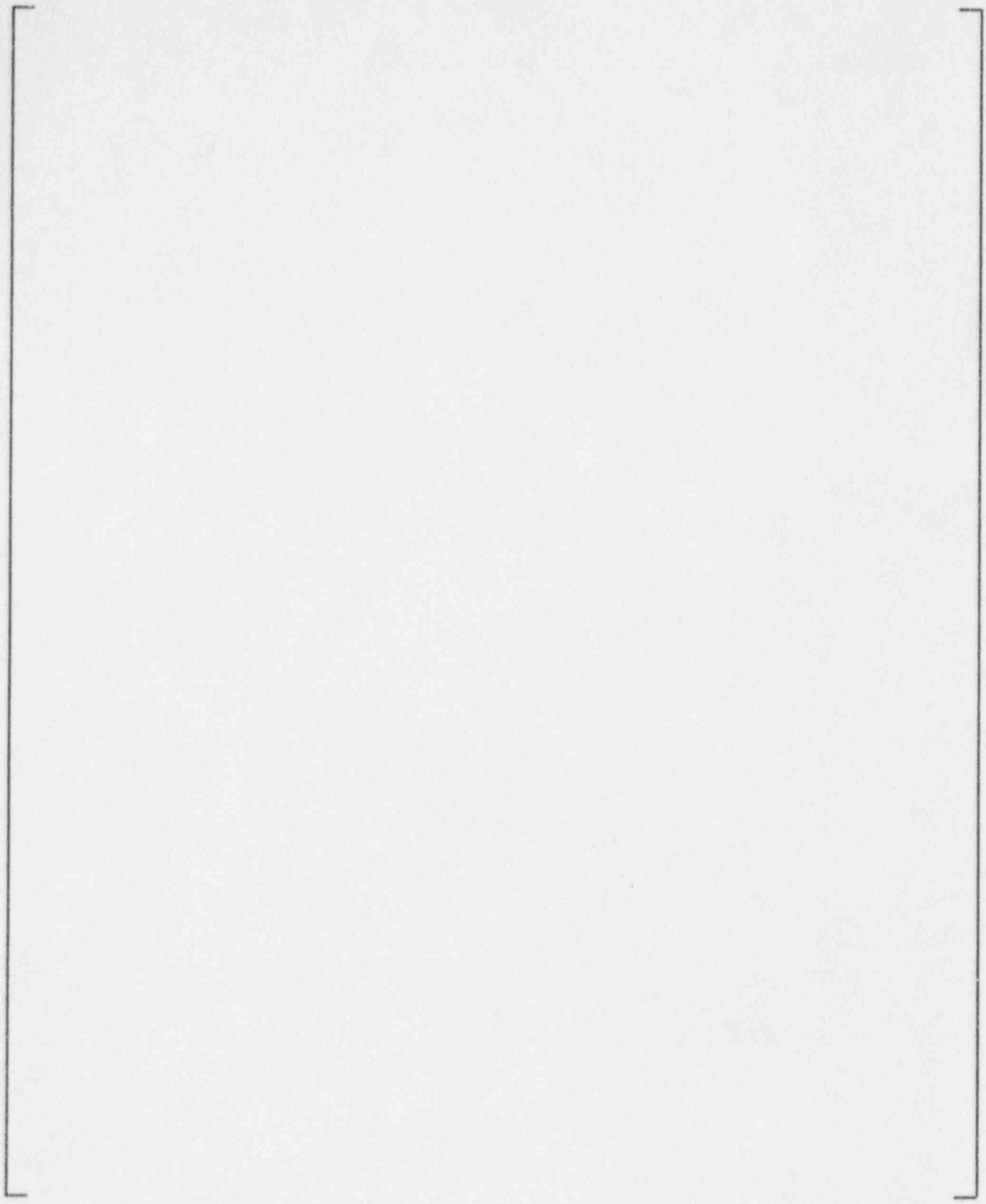

Figure 8-8 Measured and Distributed Parameter Predicted Condensate Flow for Tests 216.1A and 216.1B

a,c

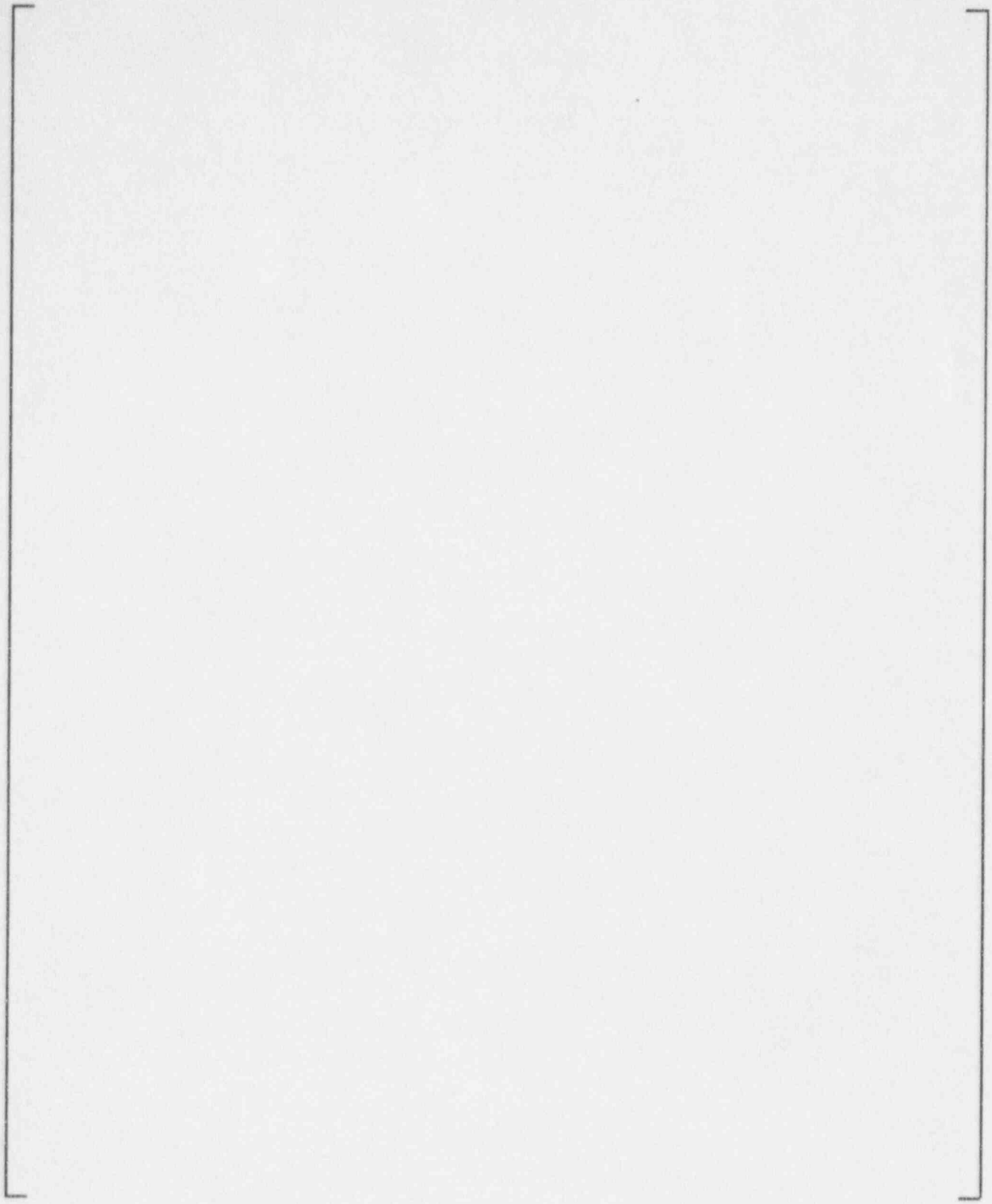

Figure 8-9 Measured and Distributed Parameter Predicted Condensate Flow for Tests 219.1A, 219.1B, and 219.1C

a,c

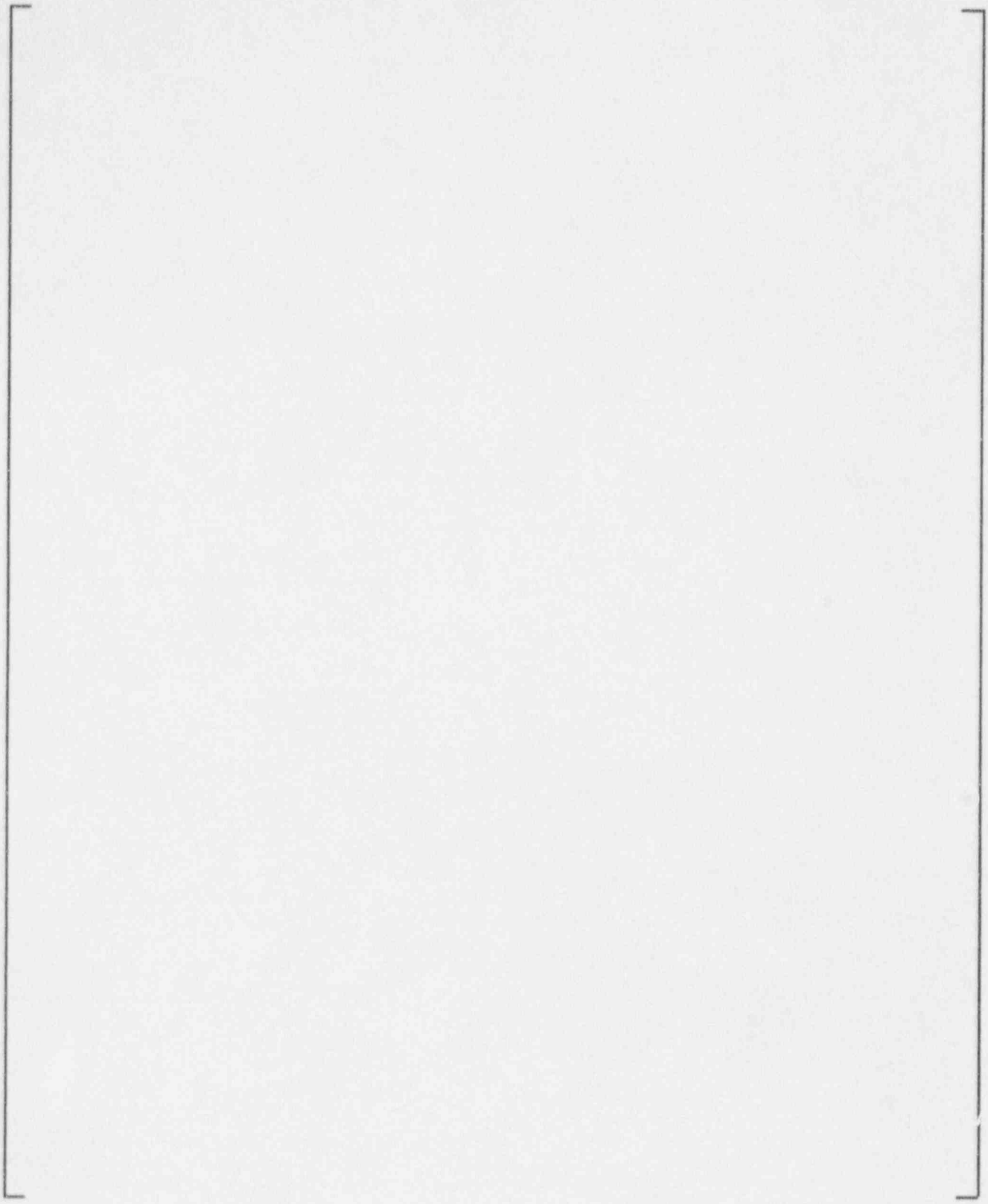

Figure 8-10 Measured and Distributed Parameter Predicted Condensate Flow for Test 222.1

a,c

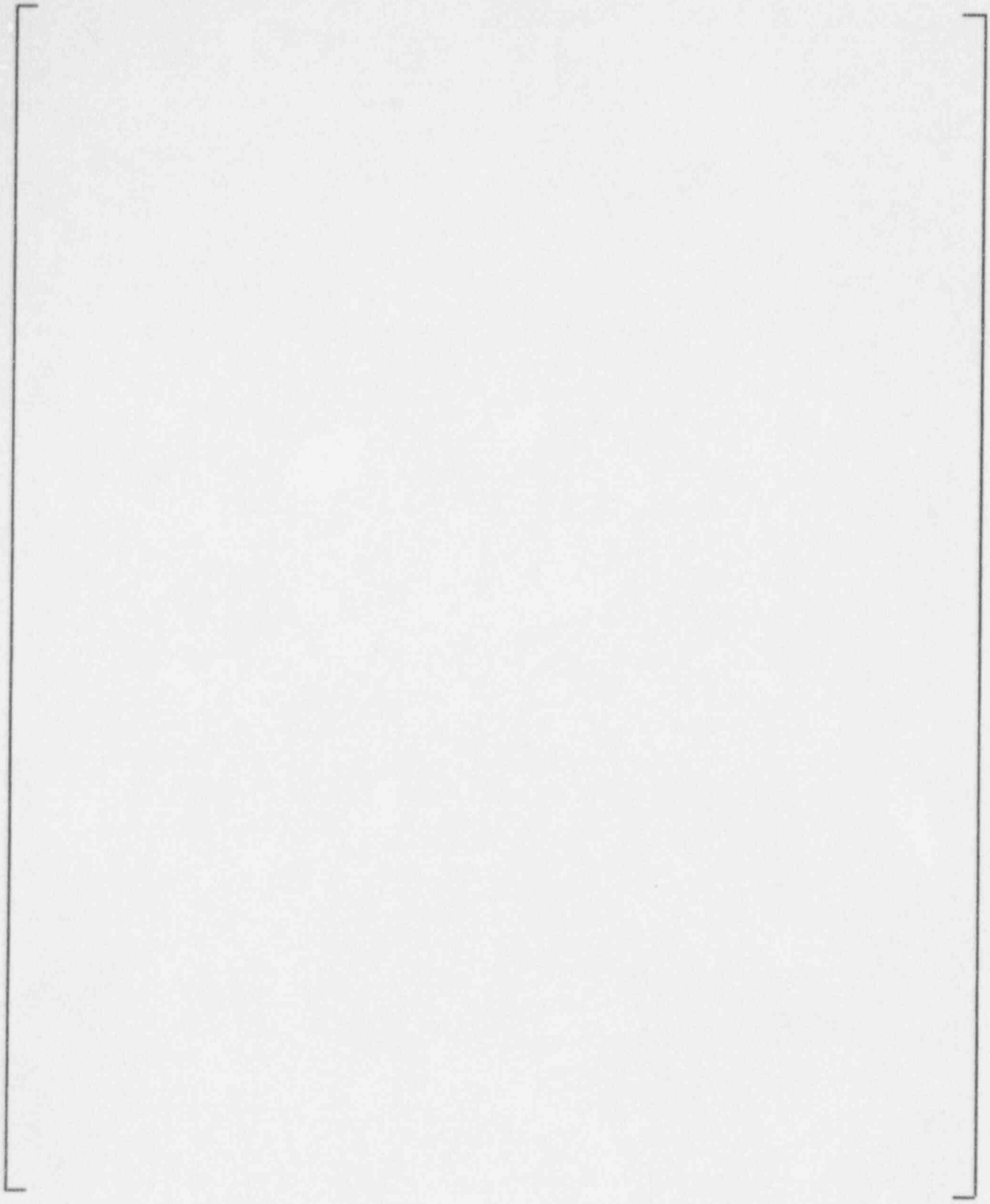

Figure 8-11 Measured and Distributed Parameter Predicted Excess Water Flow for Tests 212.1A, 212.1B, and 212.1C

a,c

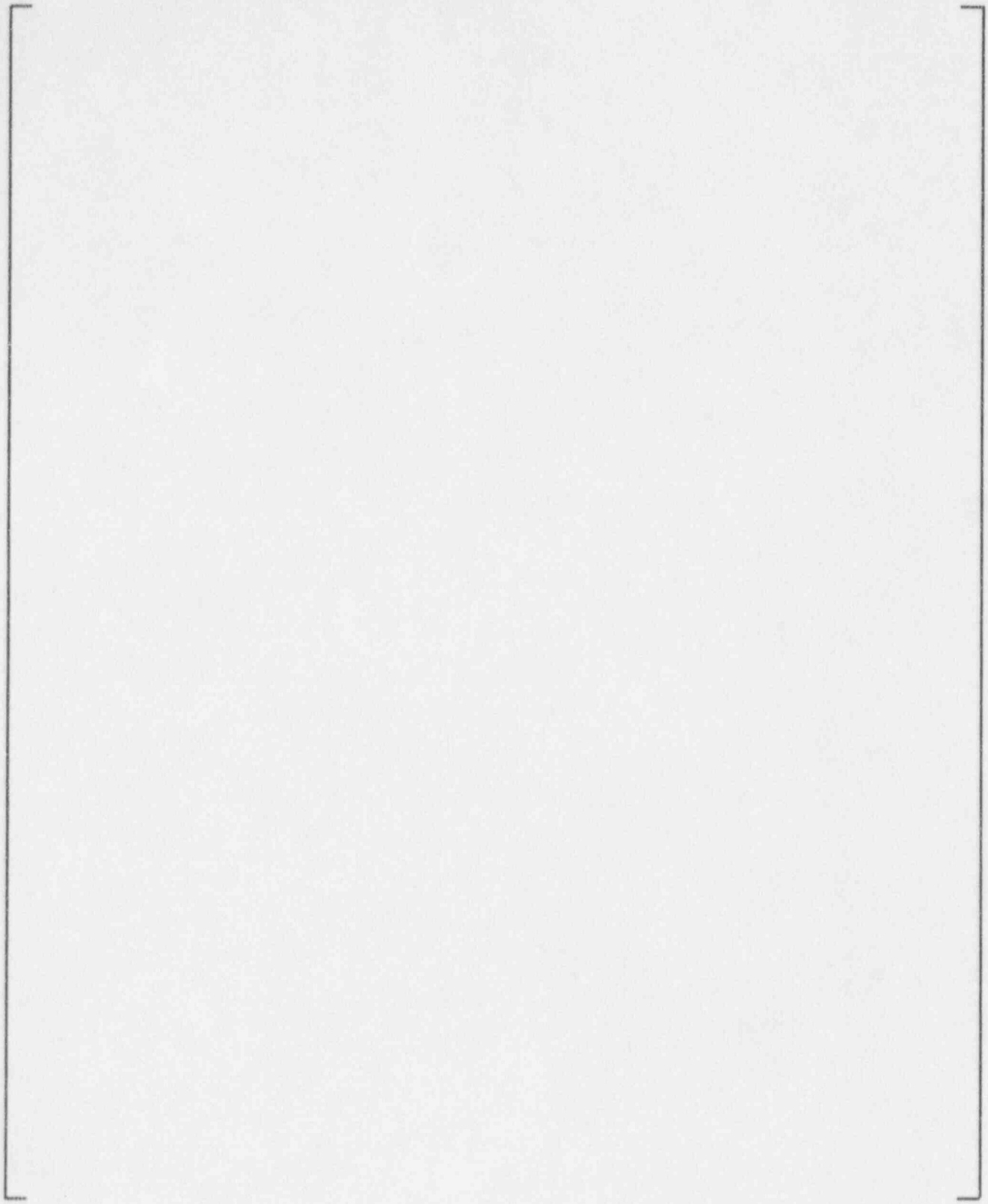

Figure 8-12 Measured and Distributed Parameter Predicted Excess Water Flow for Tests 214.1A and 214.1B

a,c

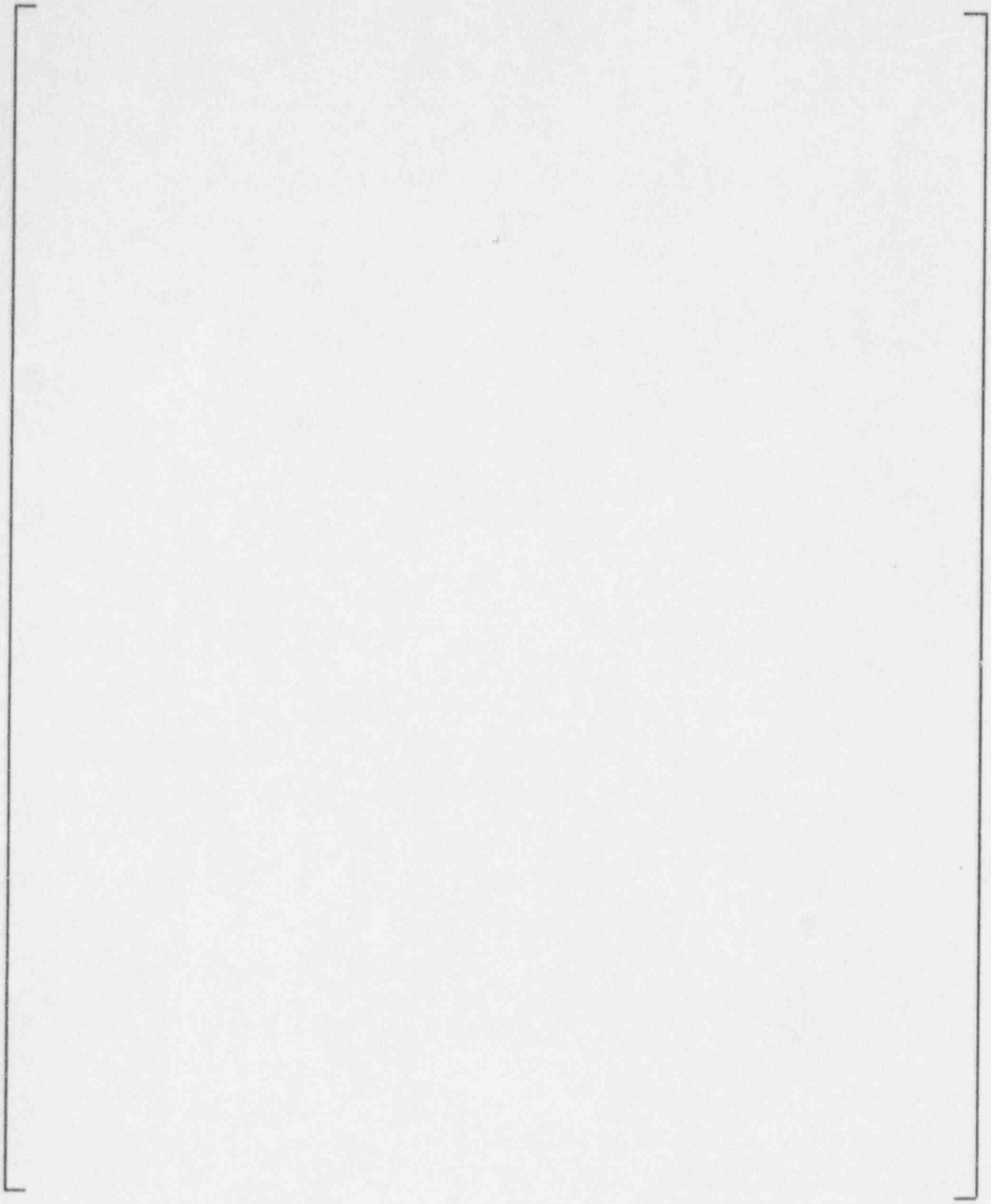

Figure 8-13 Measured and Distributed Parameter Predicted Excess Water Flow for Tests 216.1A and 216.1B

a,c

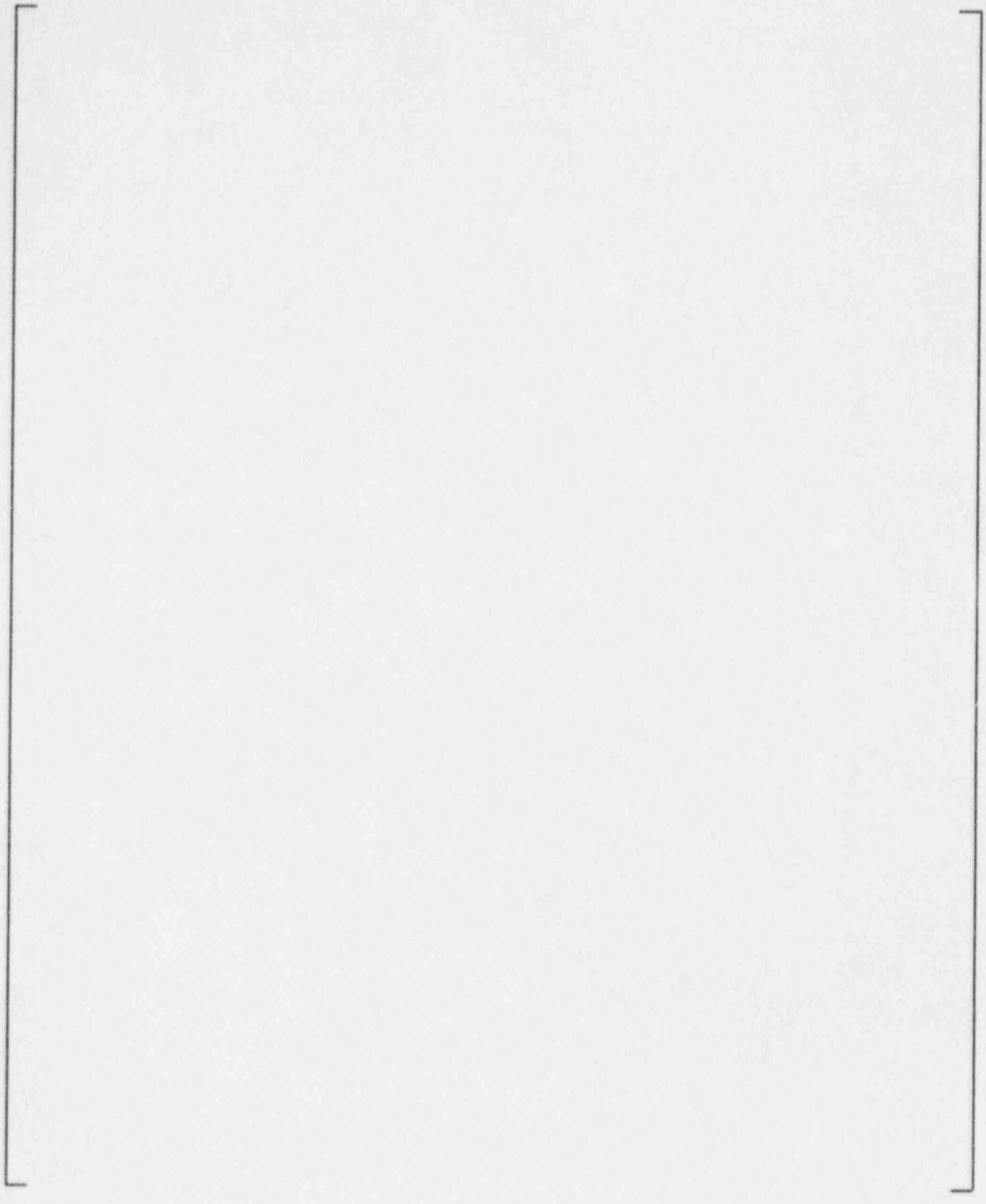

Figure 8-14 Measured and Distributed Parameter Predicted Excess Water Flow for Tests 219.1A, 219.1B, and 219.1C

a,c

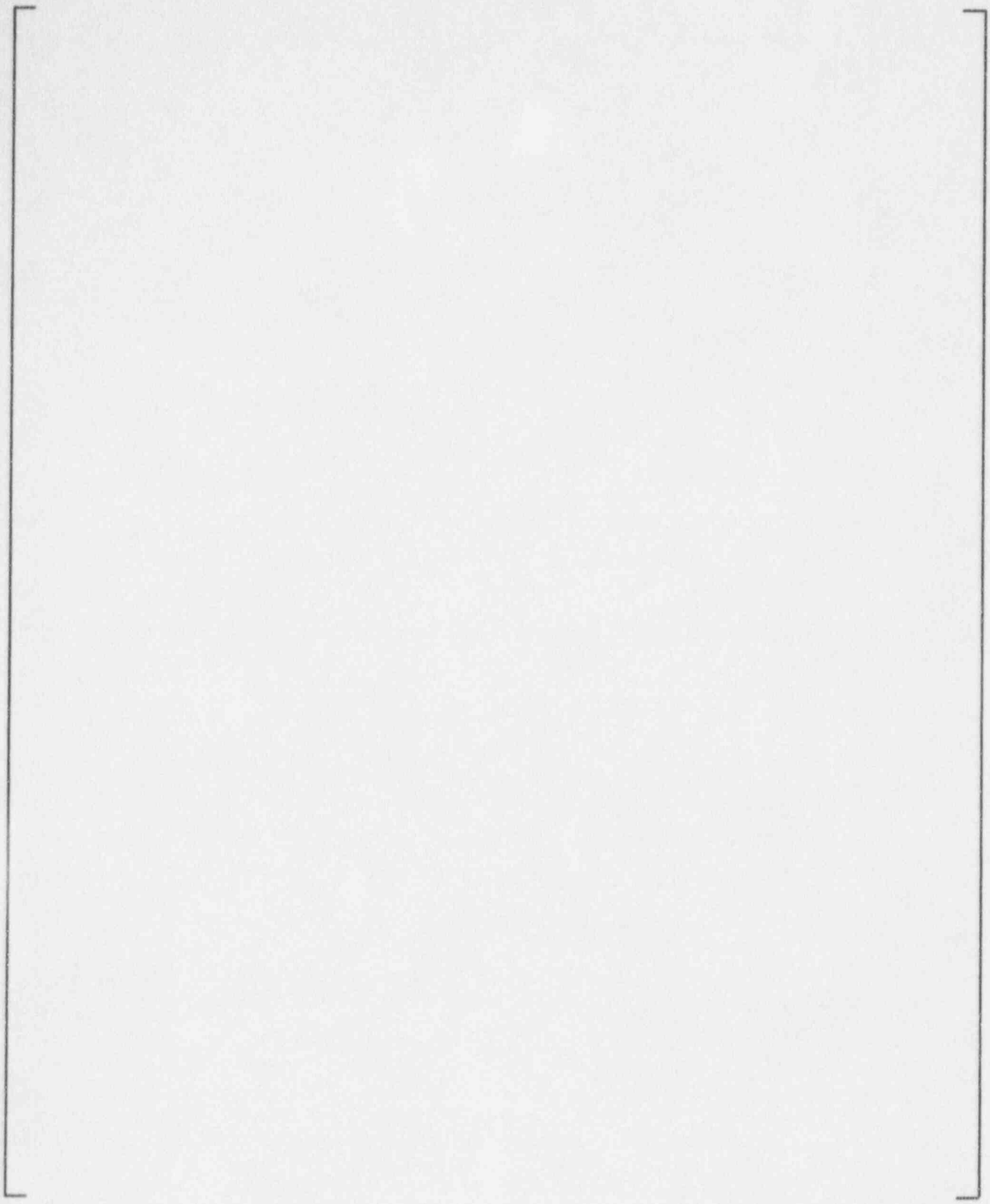

Figure 8-15 Measured and Distributed Parameter Predicted Excess Water Flow for Tests 219.1B and 219.1C

a,c

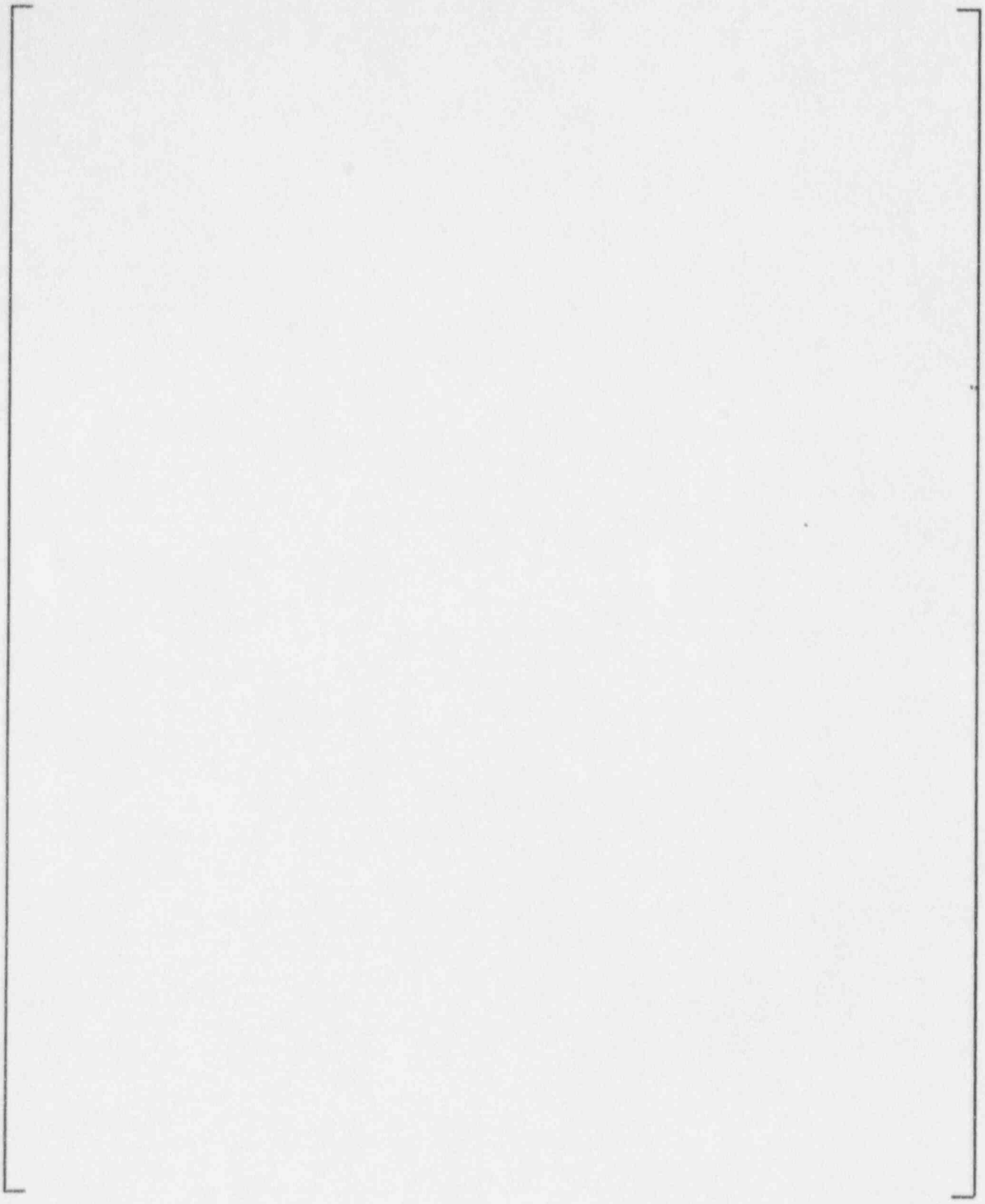

Figure 8-16 Measured and Distributed Parameter Predicted Excess Water Flow for Test 222.1

a,b

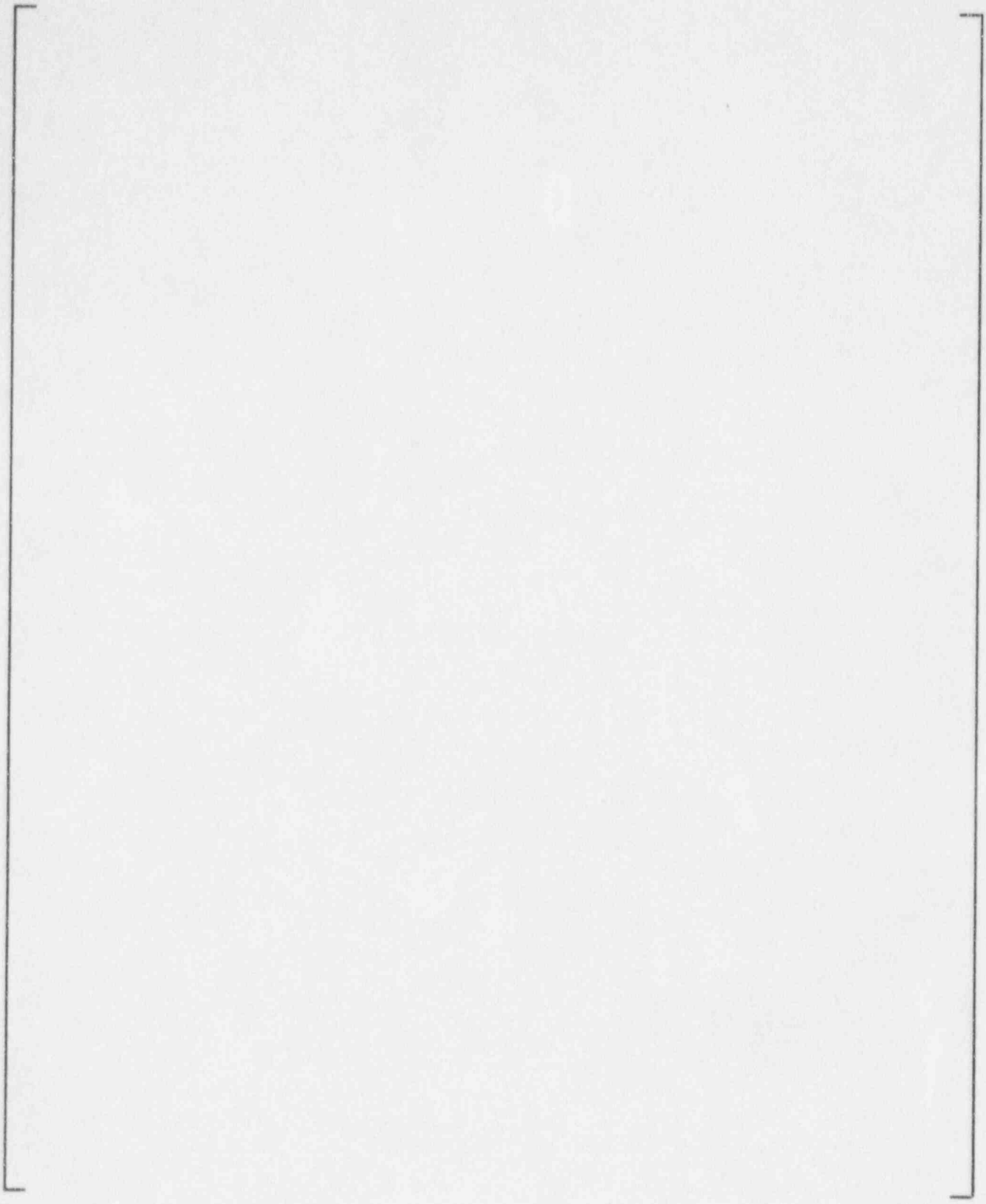

Figure 8-17 Measured Cooling Water Flow Applied to Vessel for Tests 214.1A and 214.1B

[a,b

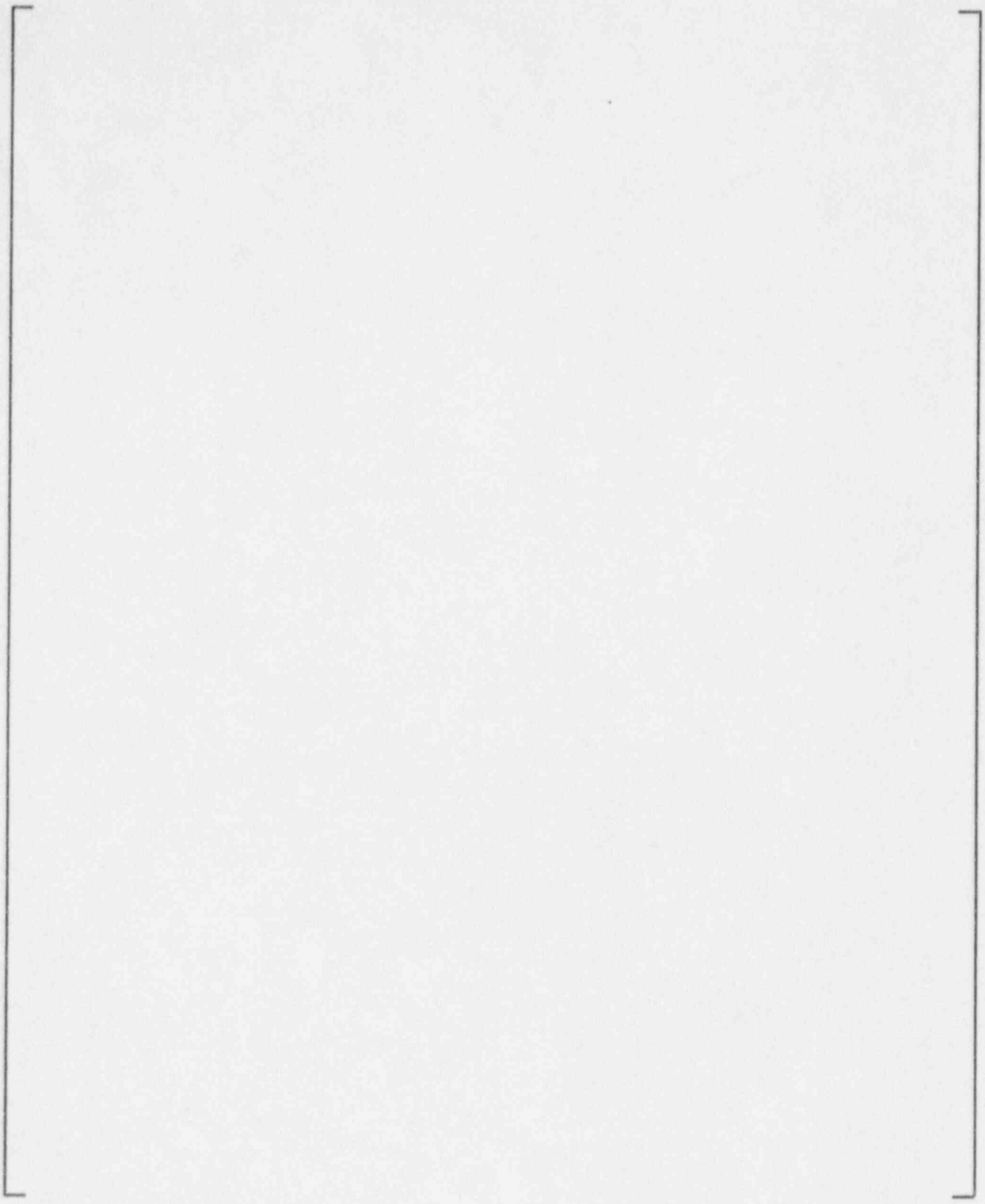

]

Figure 8-18 Measured Cooling Water Flow Rate Applied to Vessel for Tests 219.1B and 219.1C

a,c

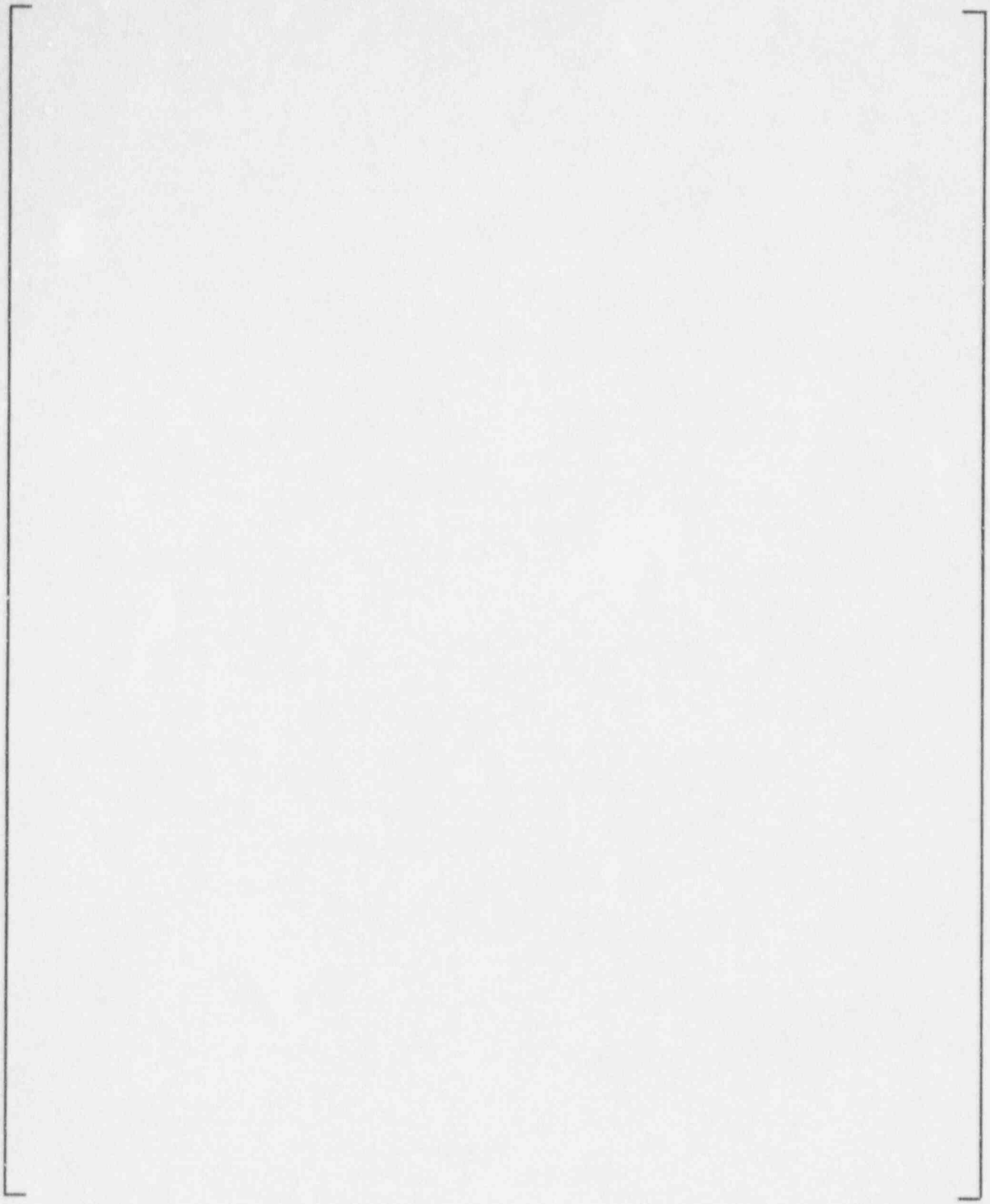

Figure 8-19 Large-Scale PCS Instrumentation Elevations

a,c

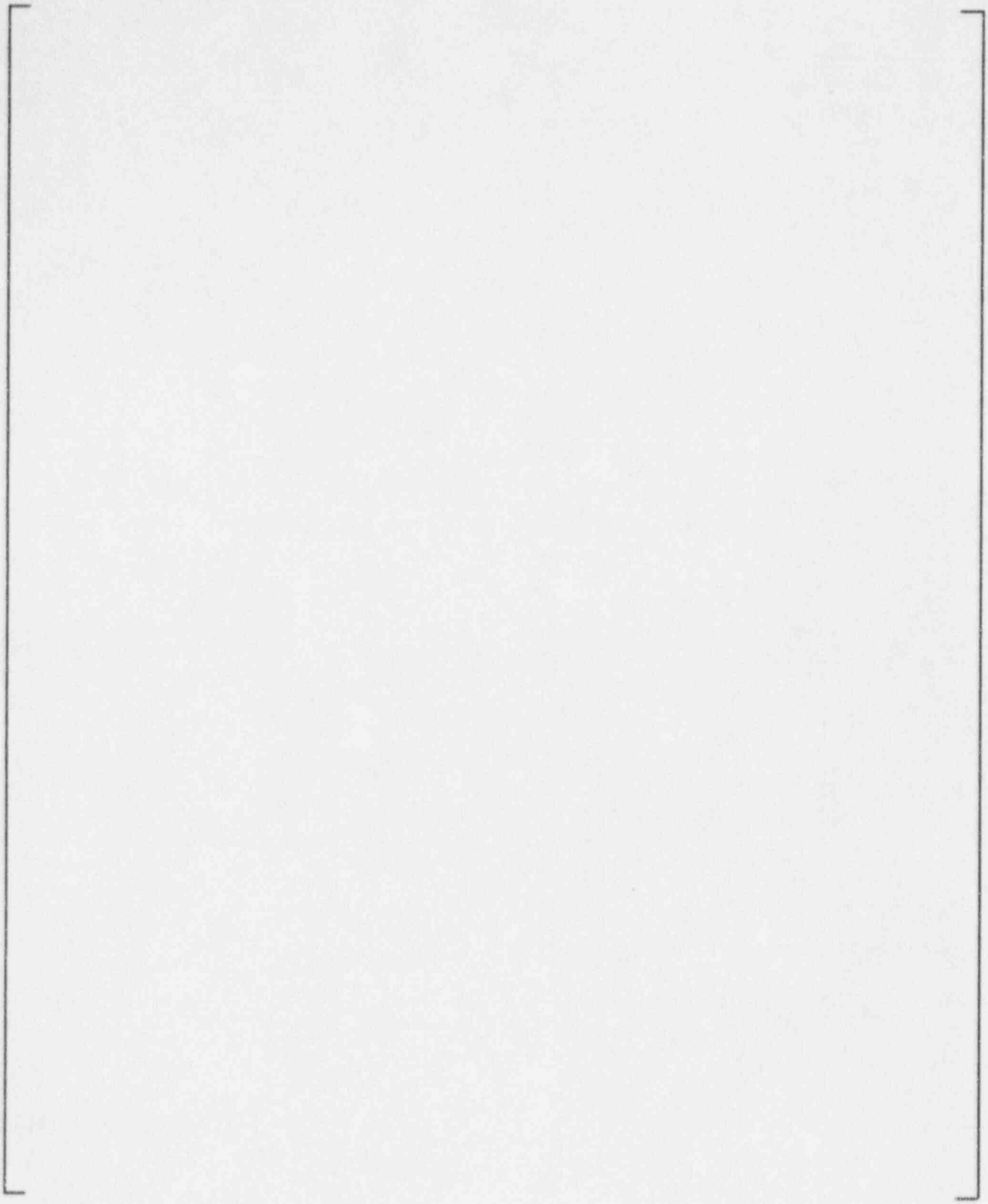

Figure 8-20 Measured and Distributed Parameter Predicted Air Pressure Ratios for Test 212.1A

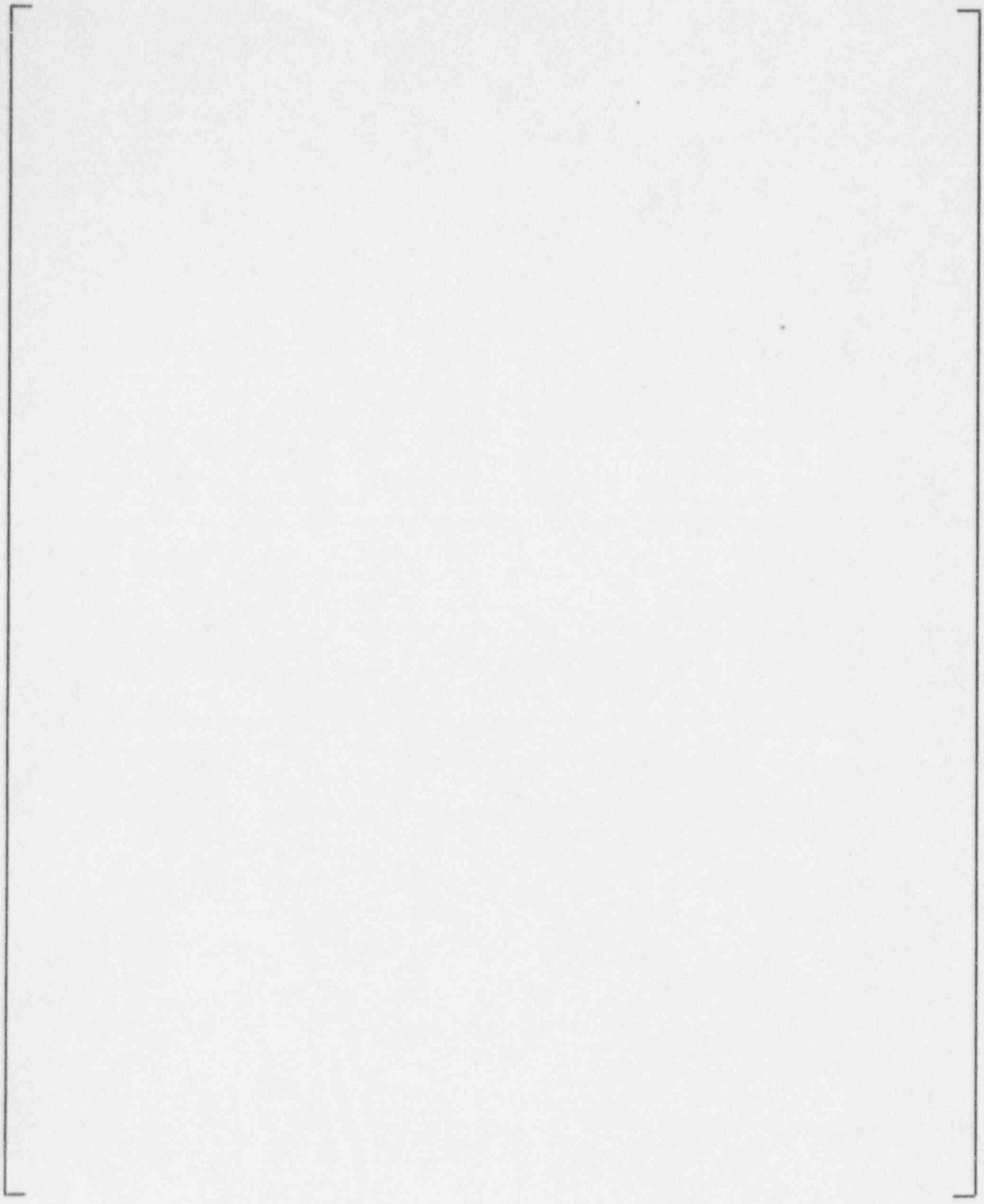

Figure 8-21 Measured and Distributed Parameter Predicted Air Pressure Ratios for Test 212.1B

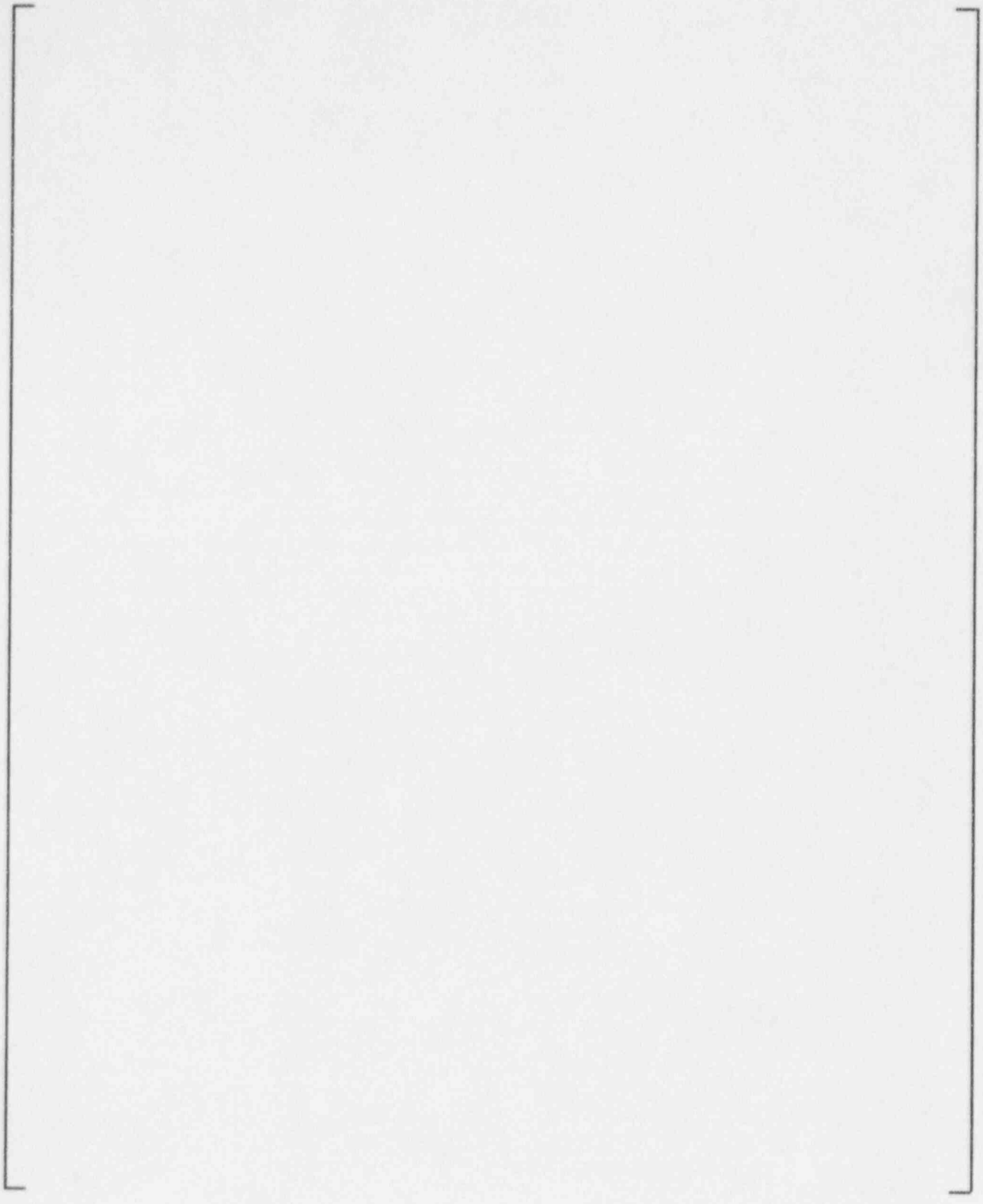

Figure 8-22 Measured and Distributed Parameter Predicted Air Pressure Ratios for Test 212.1C

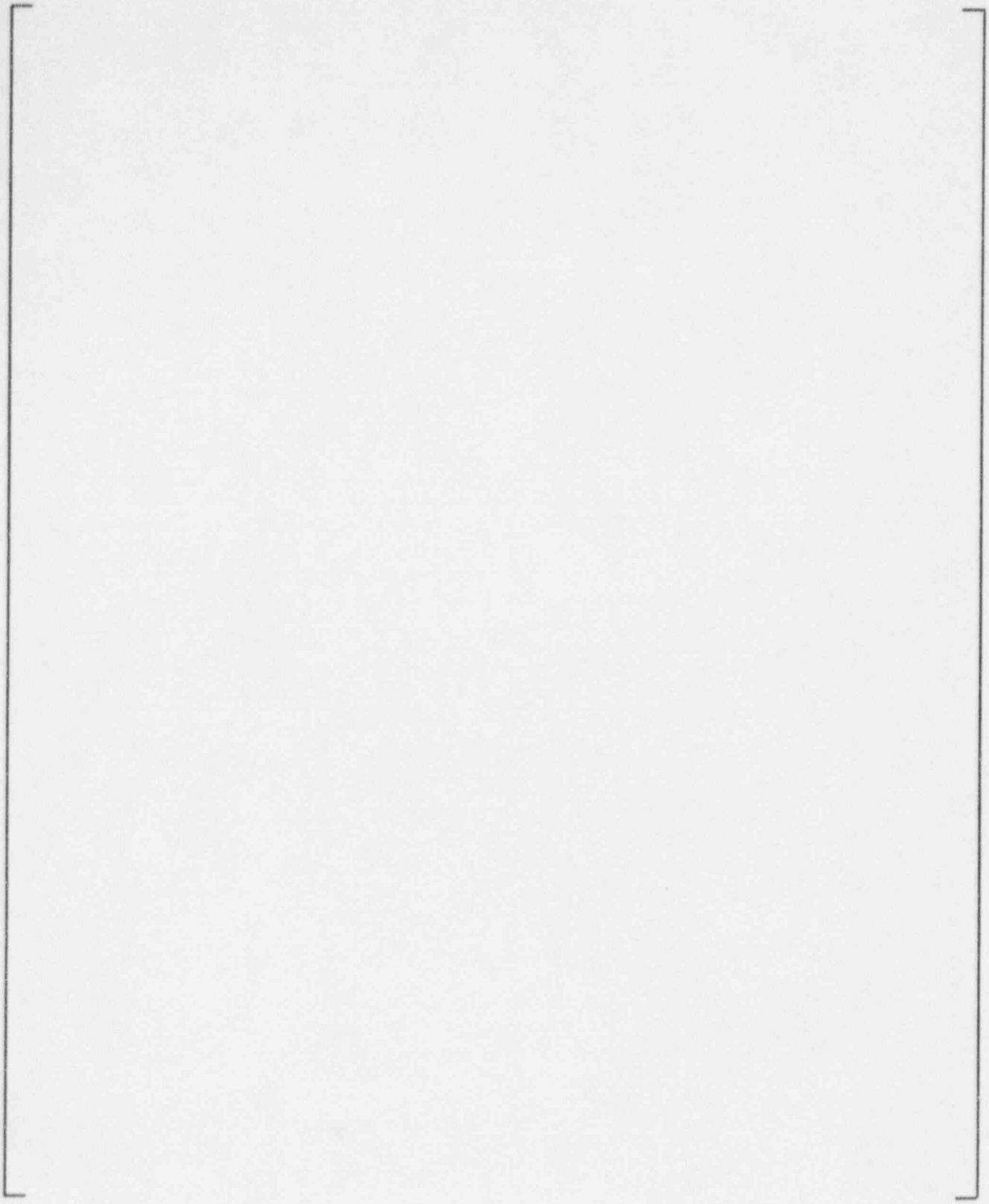

Figure 8-23 Measured and Distributed Parameter Predicted Air Pressure Ratios for Test 216.1A

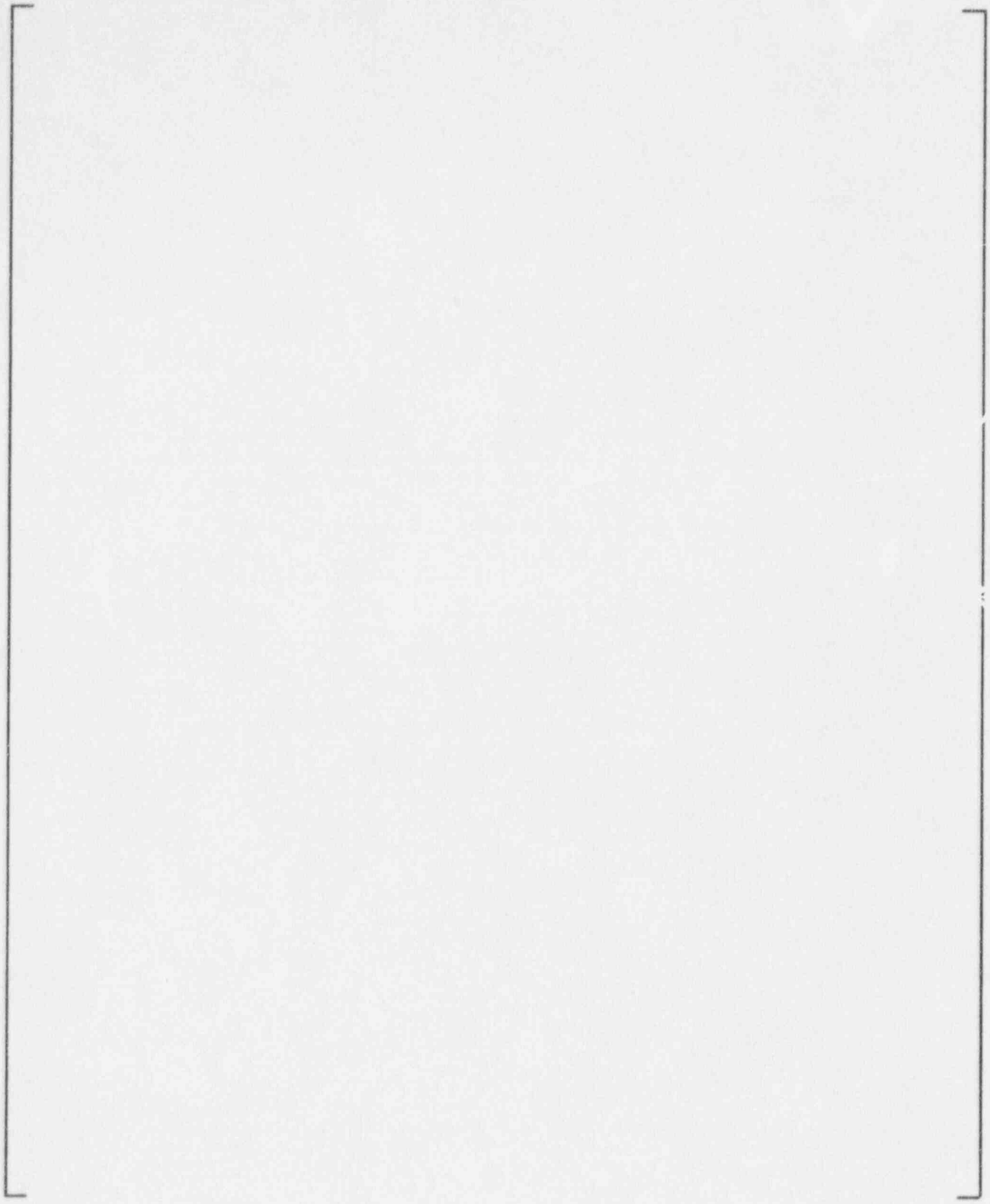

Figure 8-24 Measured and Distributed Parameter Predicted Air Pressure Ratios for Test 216.1B

a,c

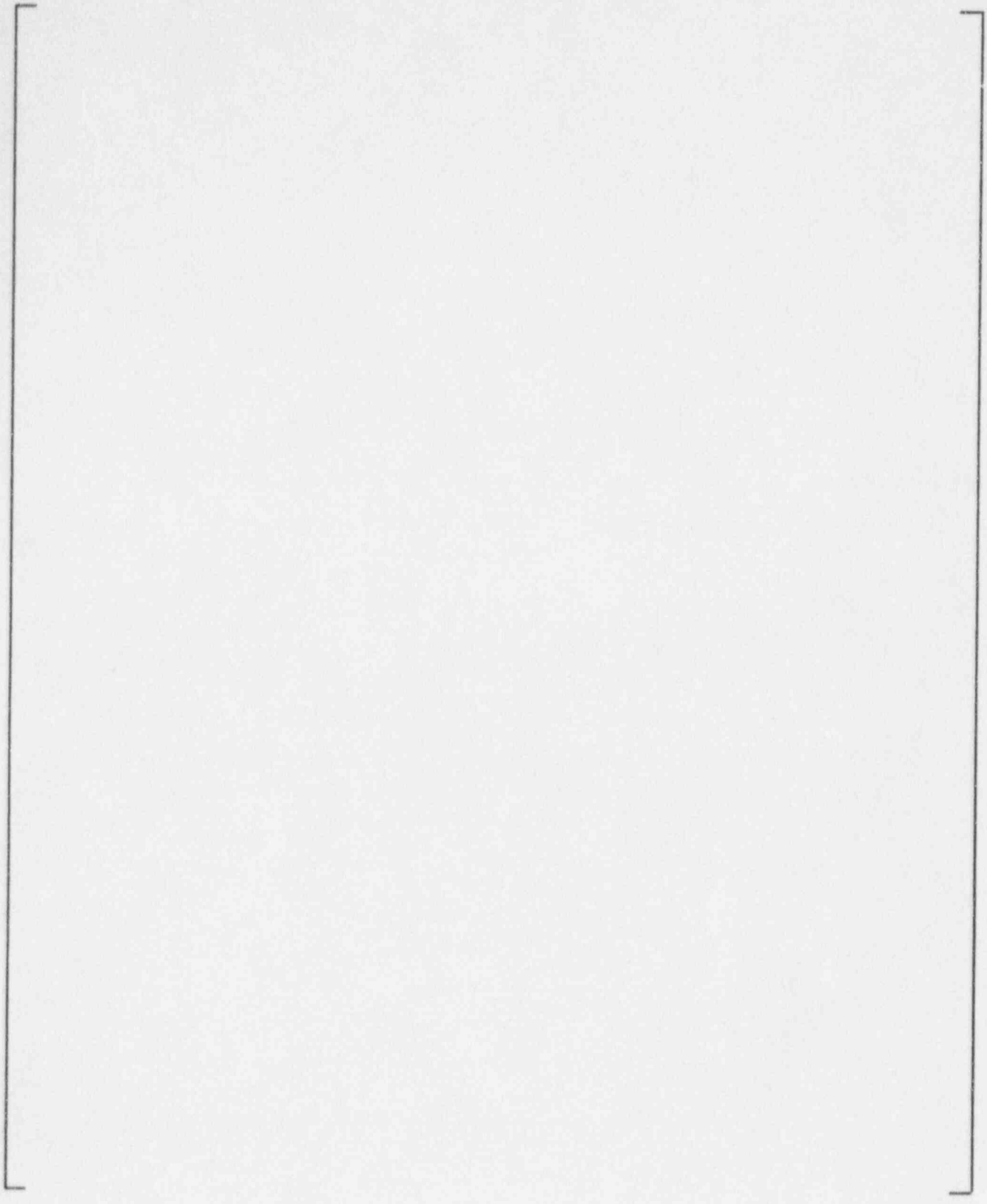

Figure 8-25 Measured and Distributed Parameter Predicted Air Pressure Ratios for Test 219.1A

a,c

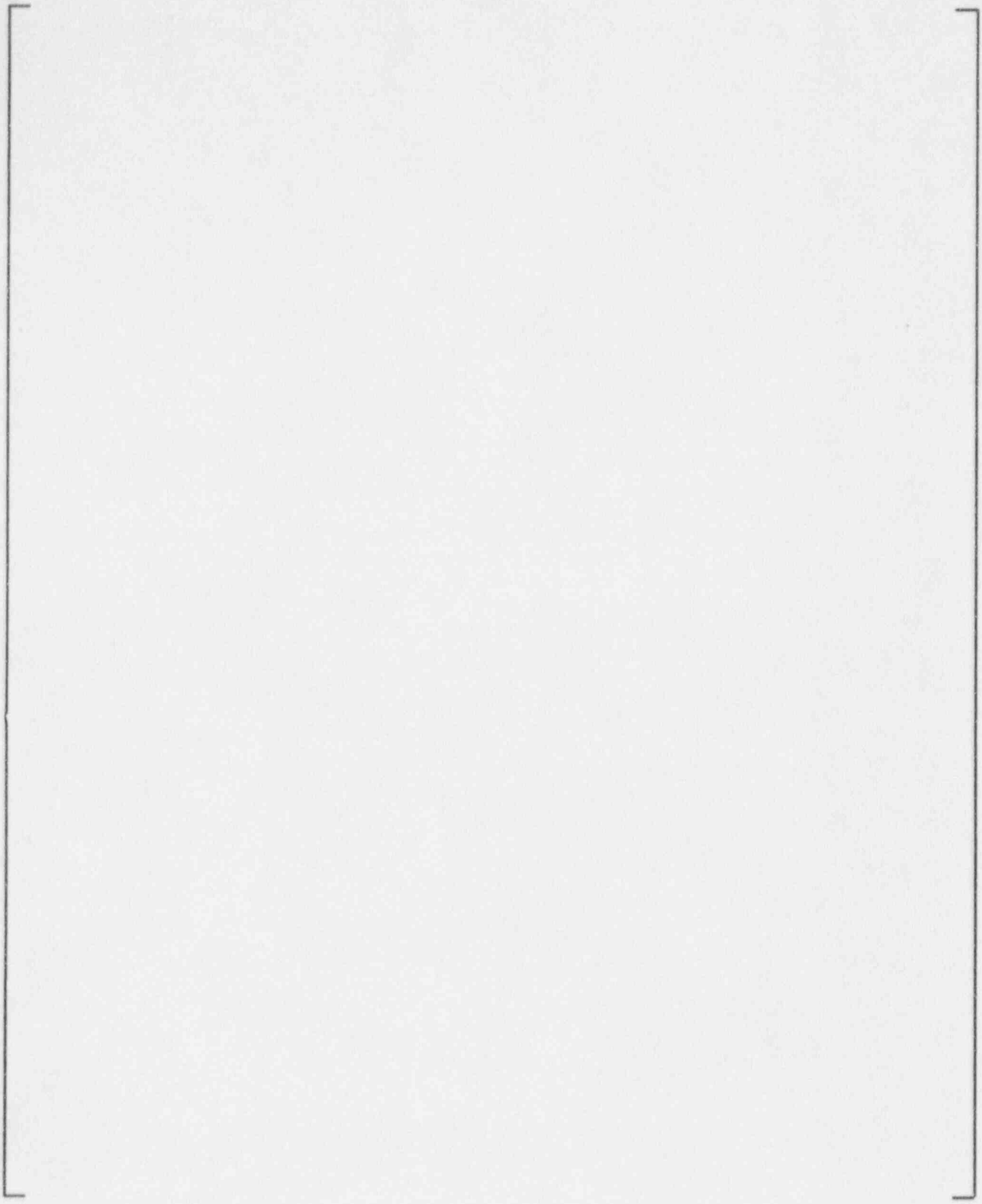

Figure 8-26 Measured and Distributed Parameter Predicted Air Pressure Ratios for Test 219.1B

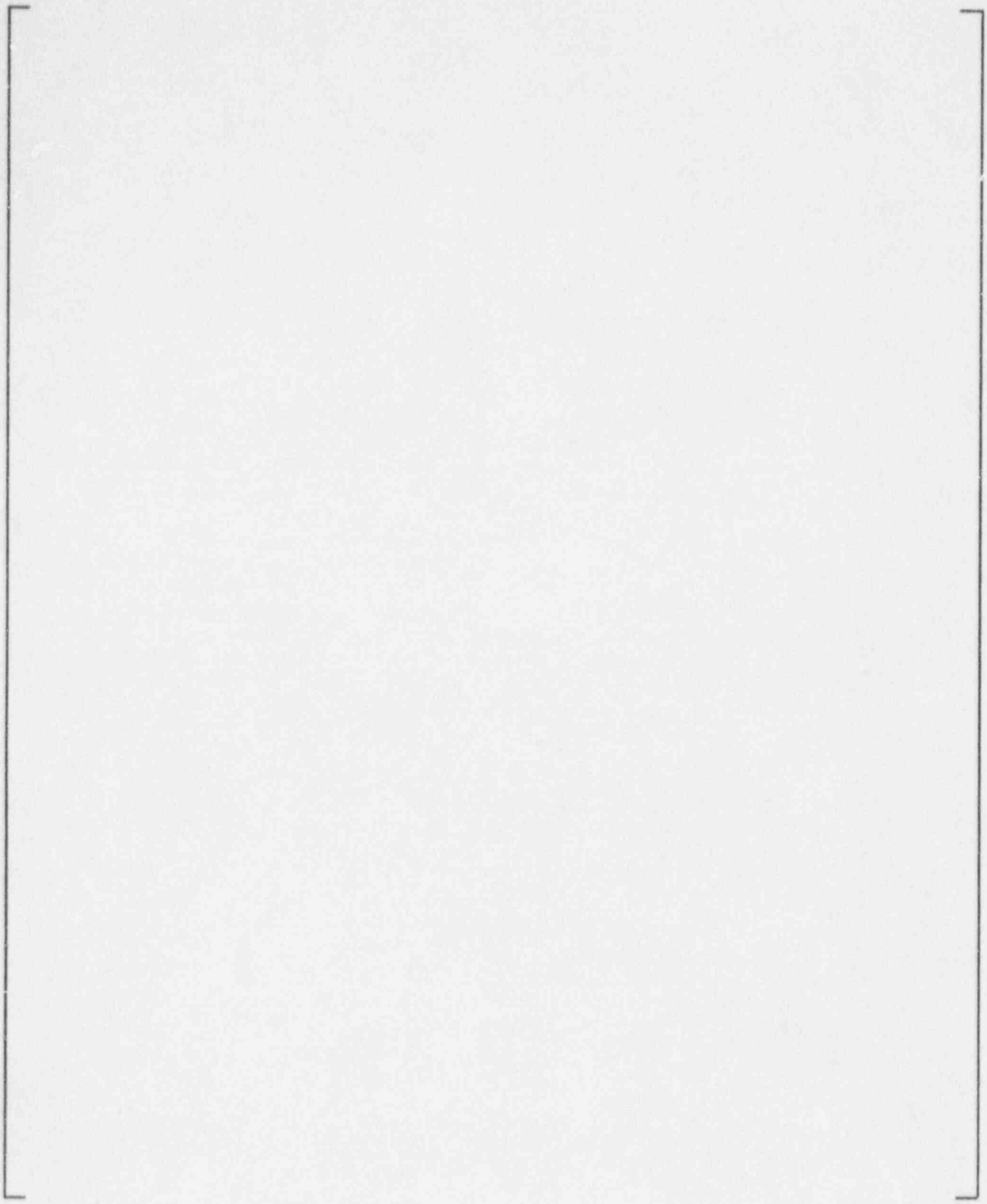

Figure 8-27 Measured and Distributed Parameter Predicted Air Pressure Ratios for Test 219.1C

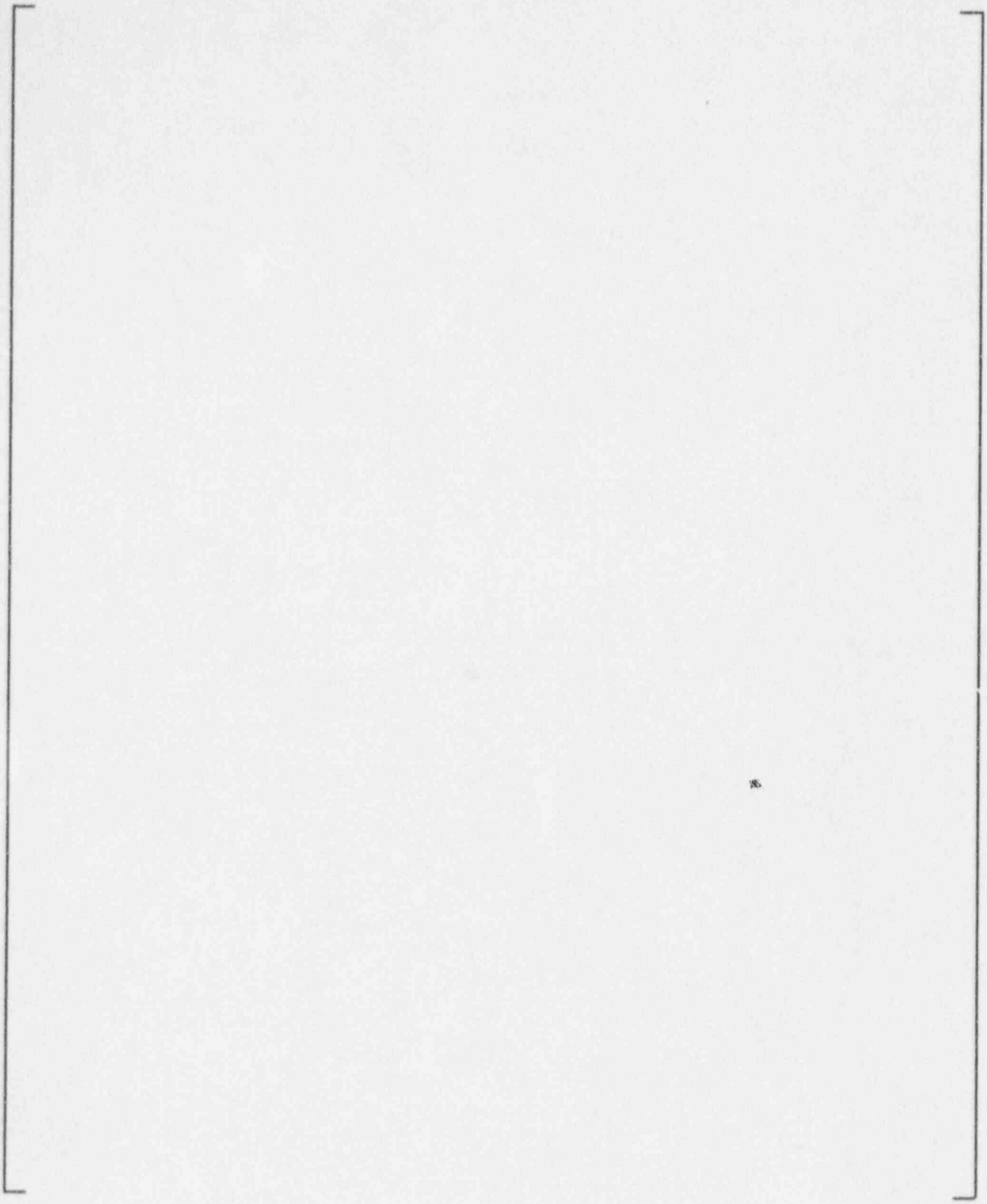

Figure 8-28 Measured and Distributed Parameter Predicted Air Pressure Ratios for Test 222.1

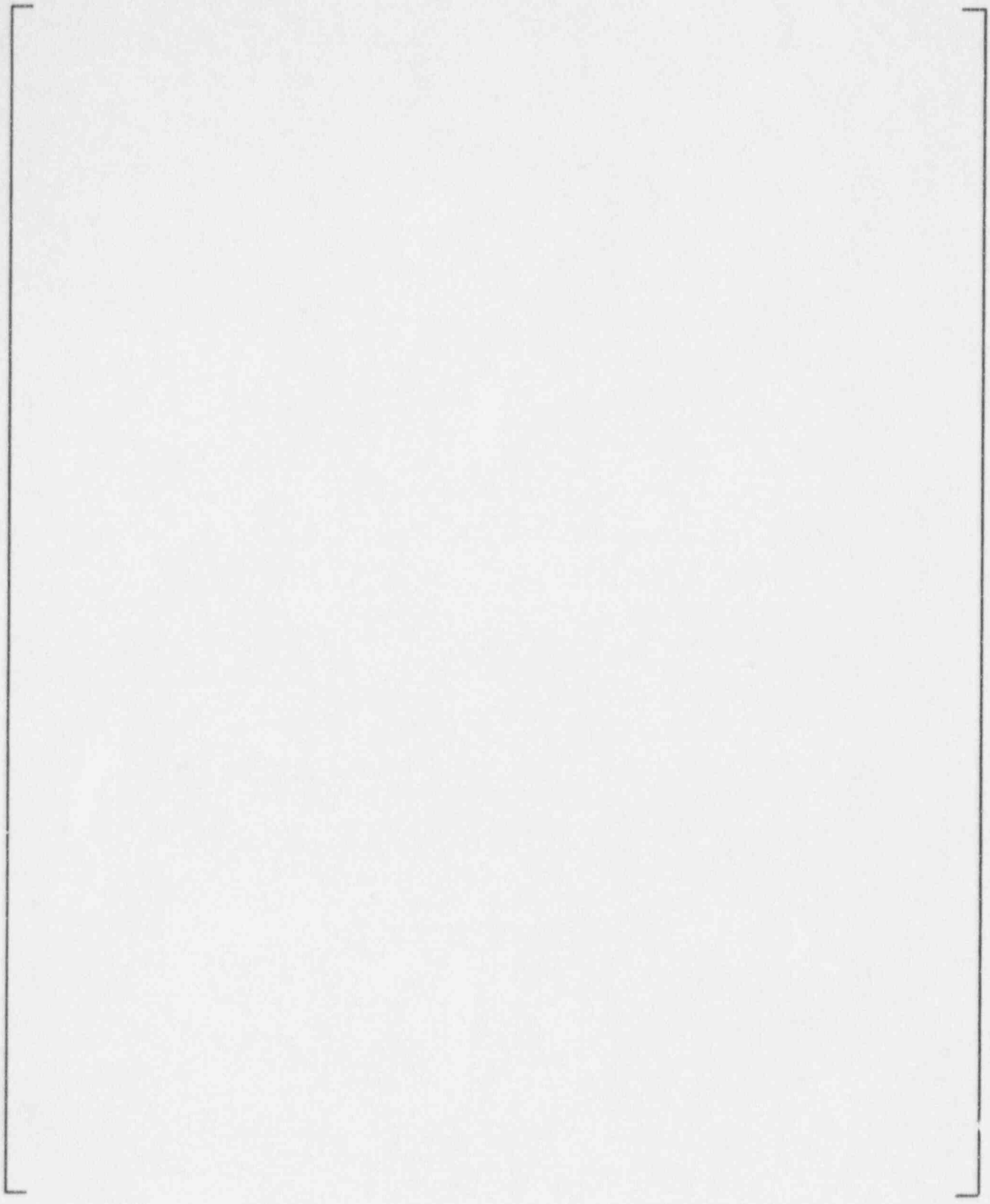

Figure 8-29 Measured and Distributed Parameter Predicted Helium Pressure Ratios for Test 219.1B

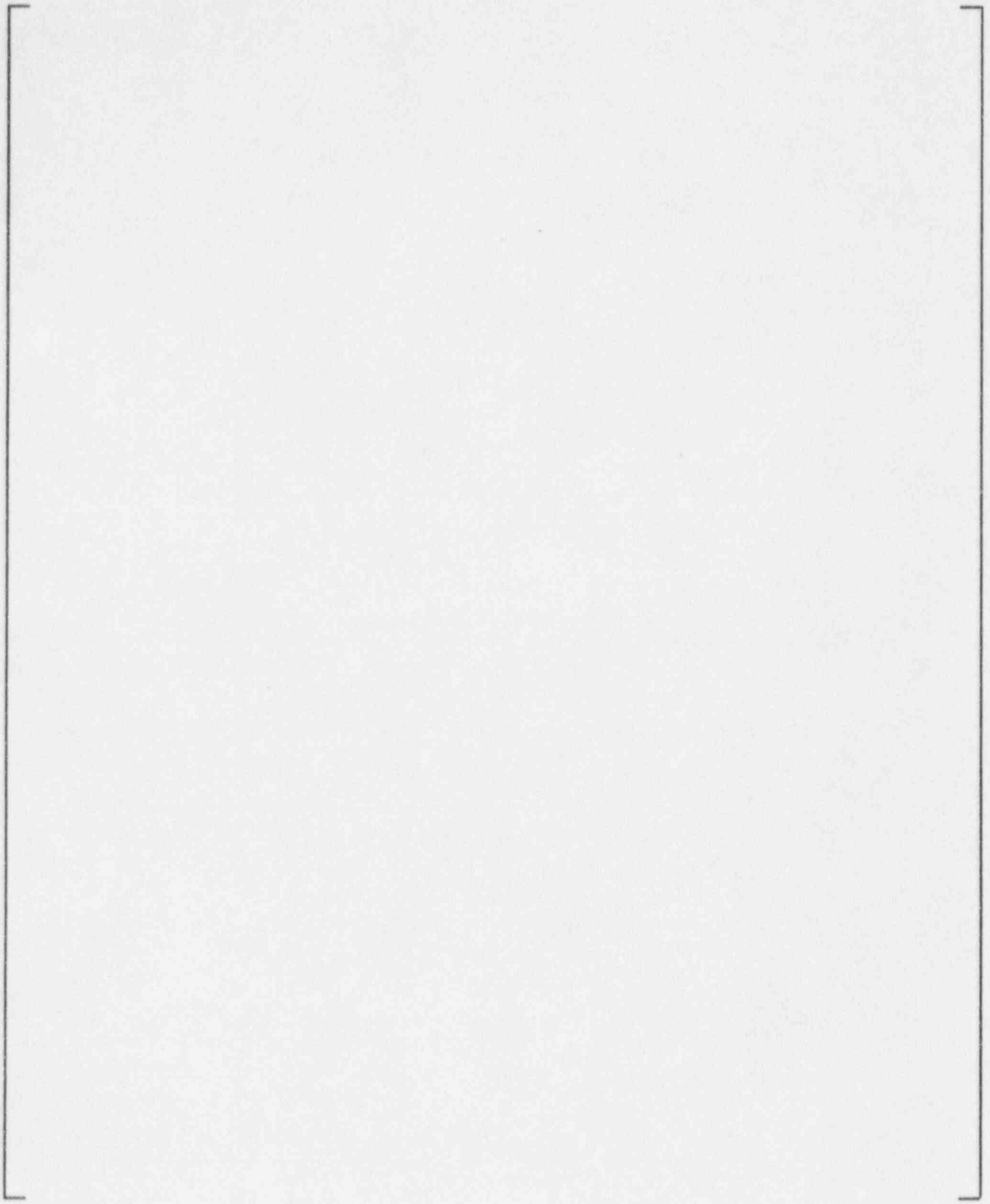

Figure 8-30 Measured and Distributed Parameter Predicted Helium Pressure Ratios for Test 219.1C

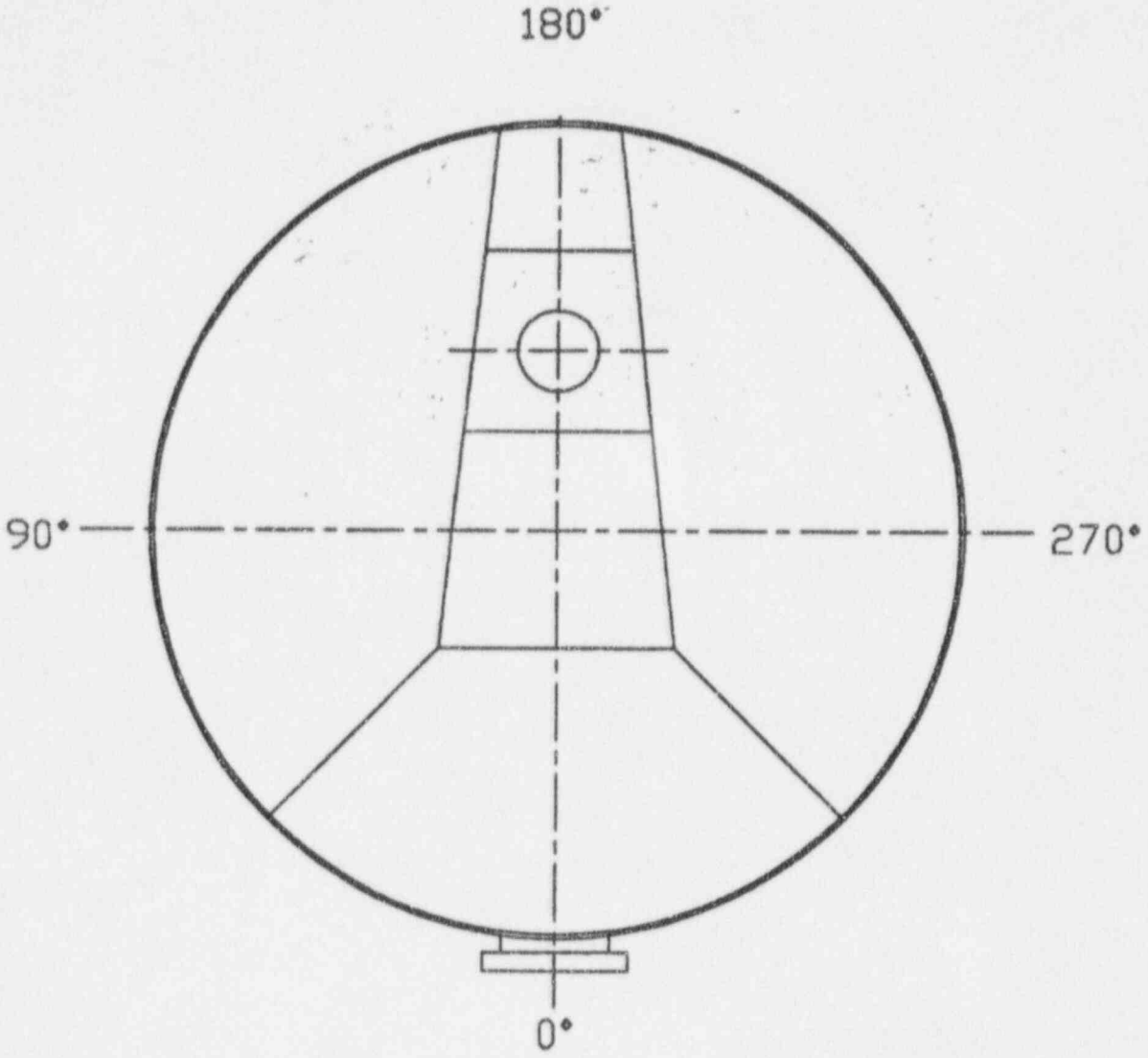

Figure 8-31 Cross-Section Orientation Convention

a,c

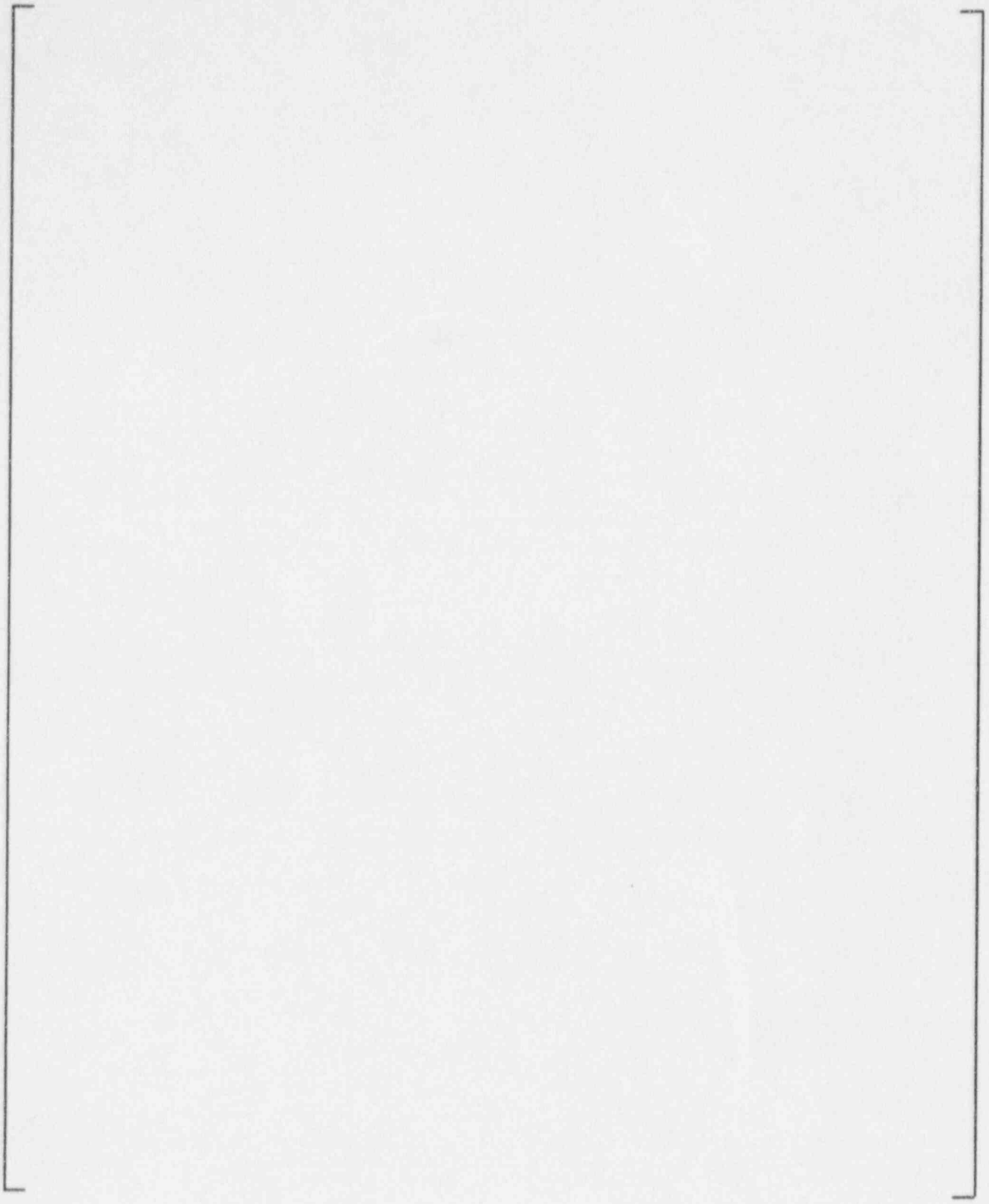

Figure 8-32 Measured and Distributed Parameter Predicted Rake Temperatures at Elevation D for Test 212.1A

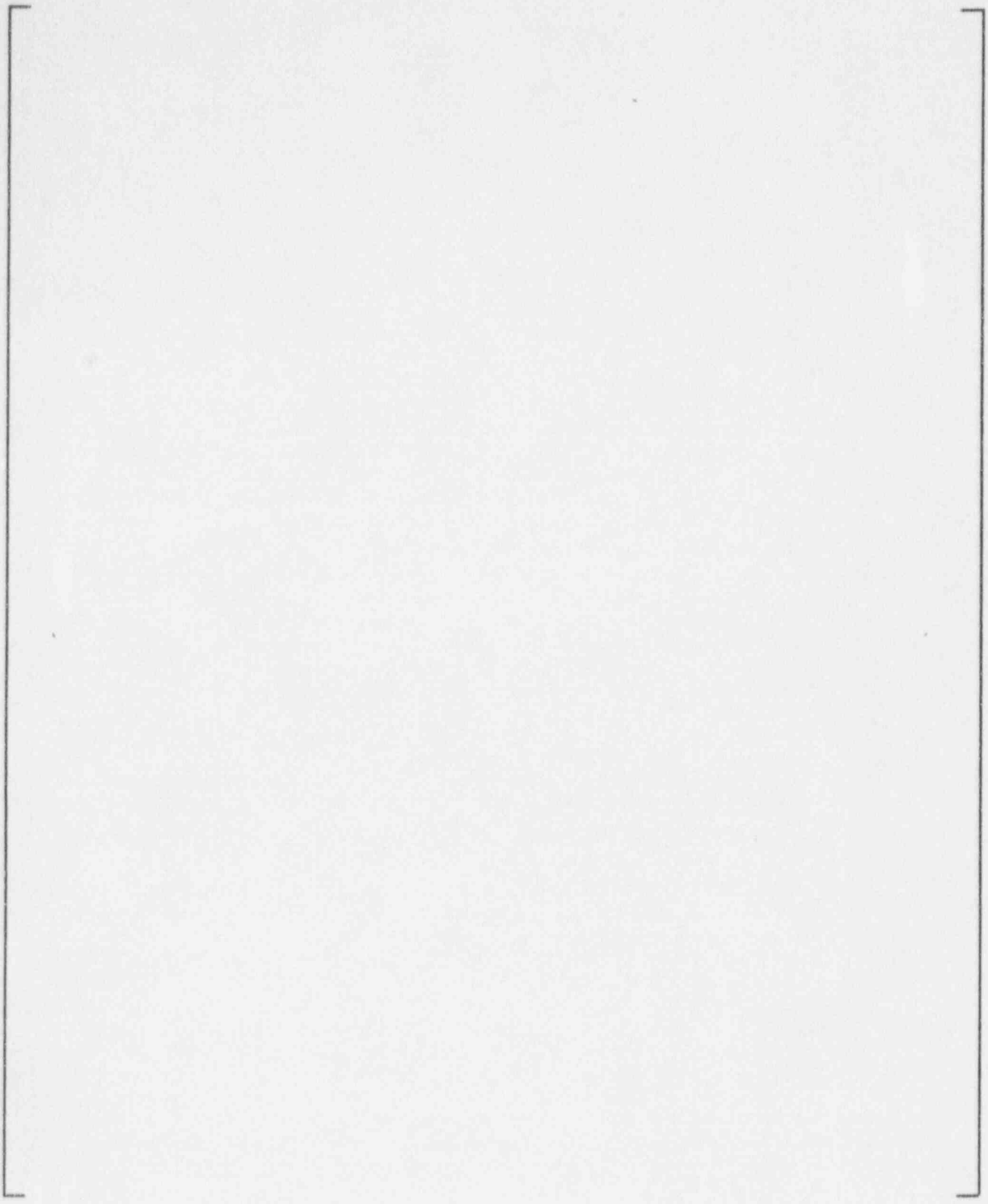

Figure 8-33 Measured and Distributed Parameter Predicted Rake Temperatures at Elevation C for Test 212.1A

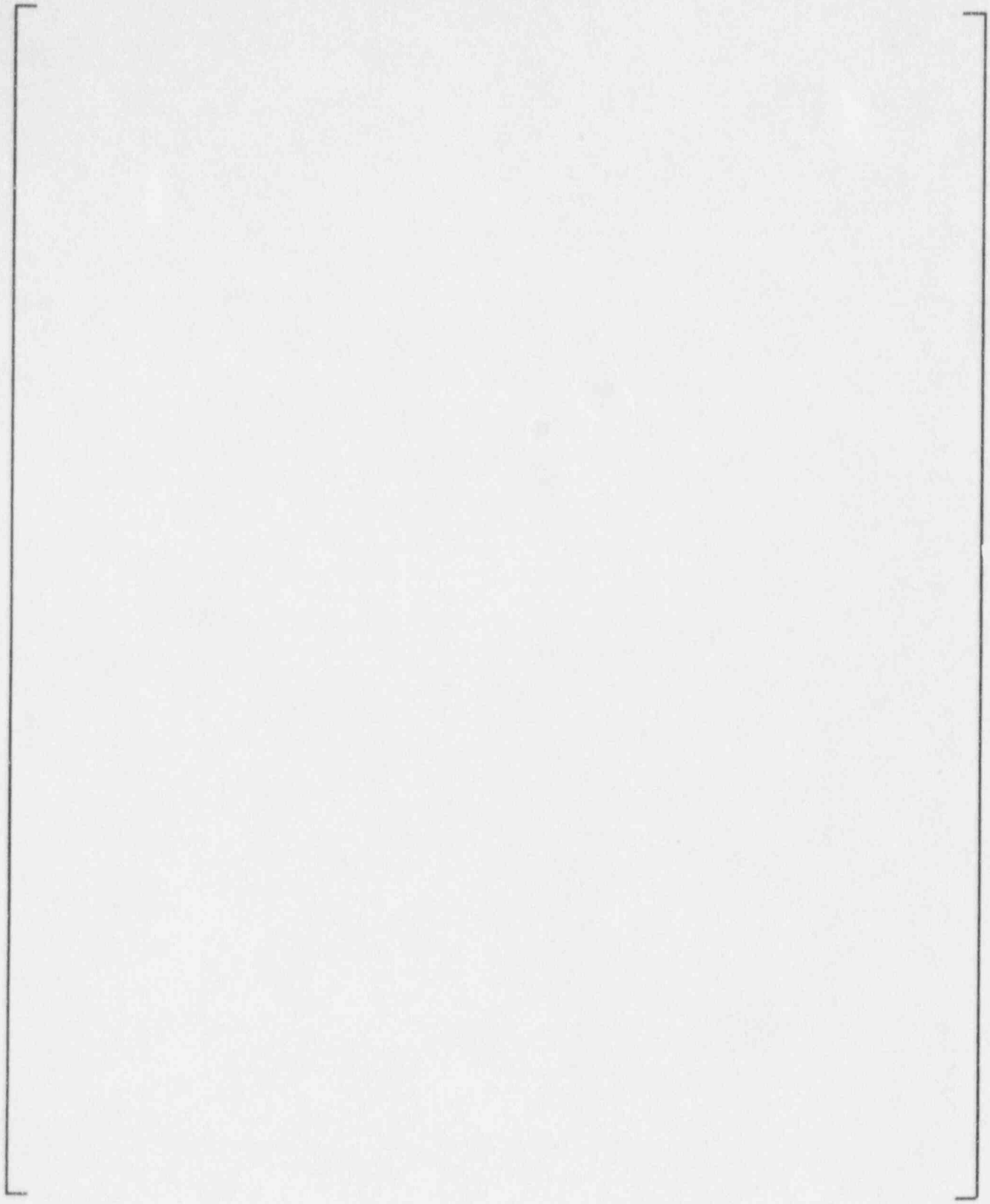

Figure 8-34 Measured and Distributed Parameter Predicted Rake Temperatures at Elevation B for Test 212.1A

a,c

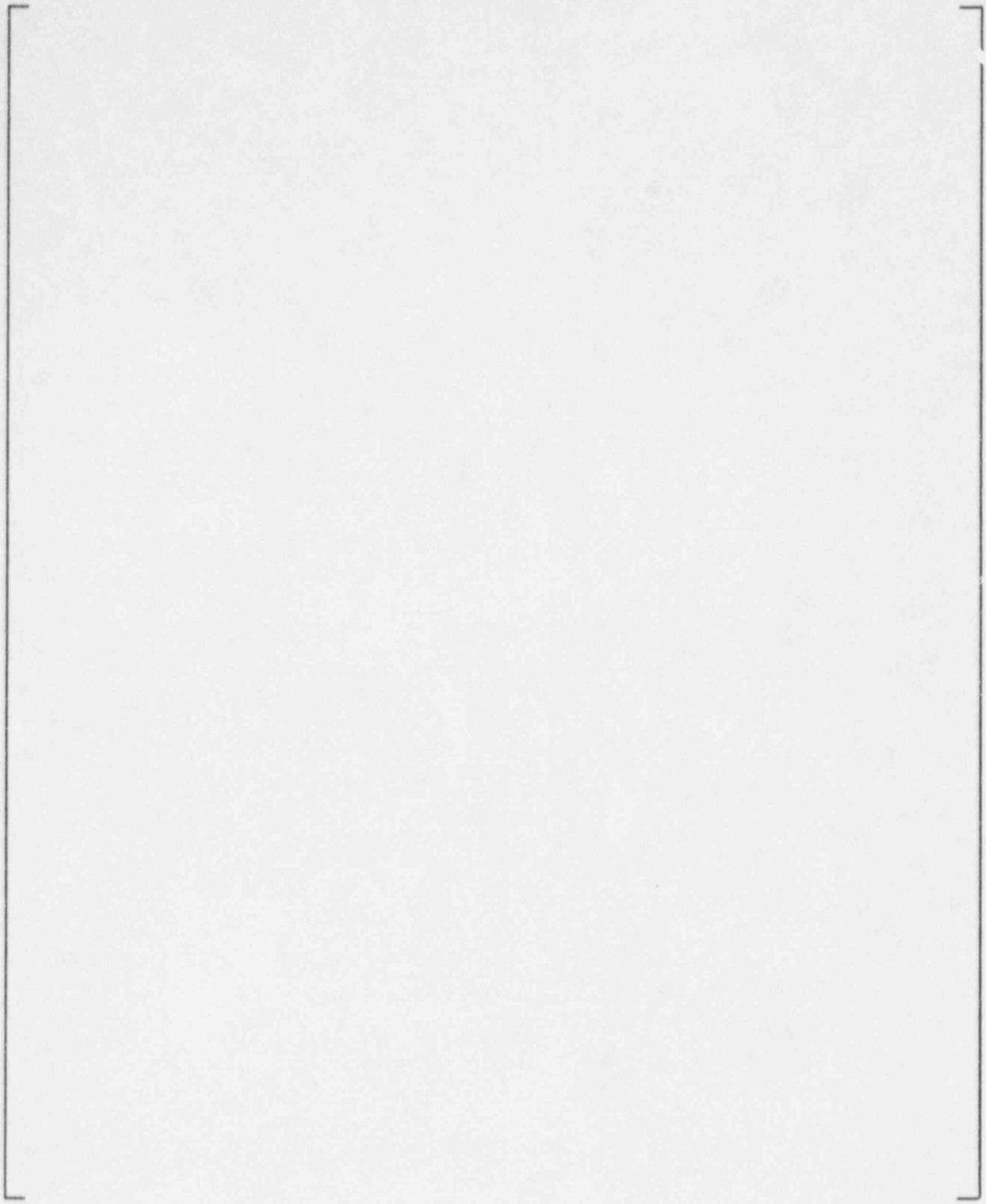

Figure 8-35 Measured and Distributed Parameter Predicted Rake Temperatures at Elevation A for Test 212.1A

a,c

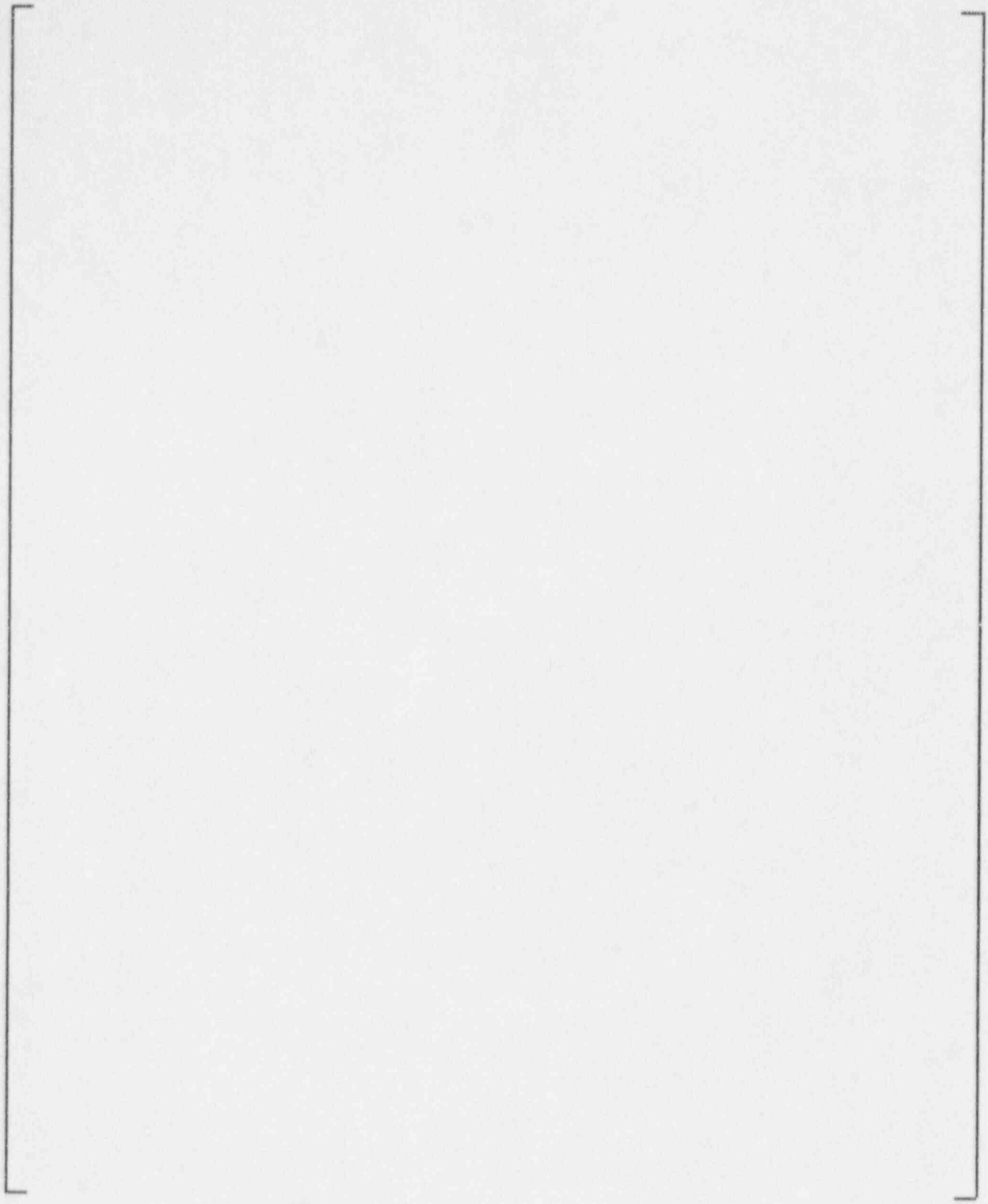

Figure 8-36 Measured and Distributed Parameter Predicted Rake Temperatures at Elevation Dome for Test 212.1A

a,c

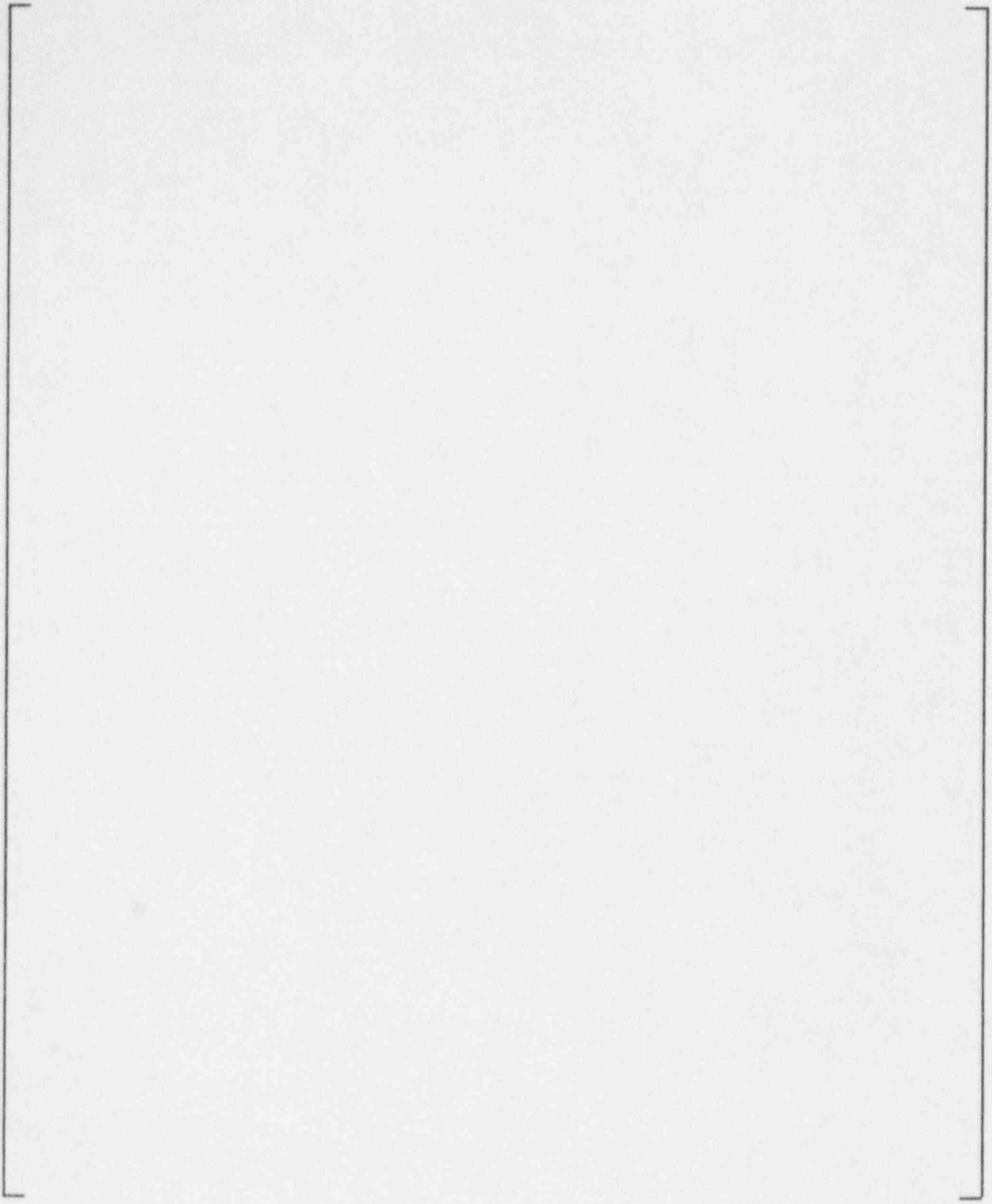

Figure 8-37 Measured and Distributed Parameter Predicted Rake Temperatures at Elevation D for Test 212.1B

a,c

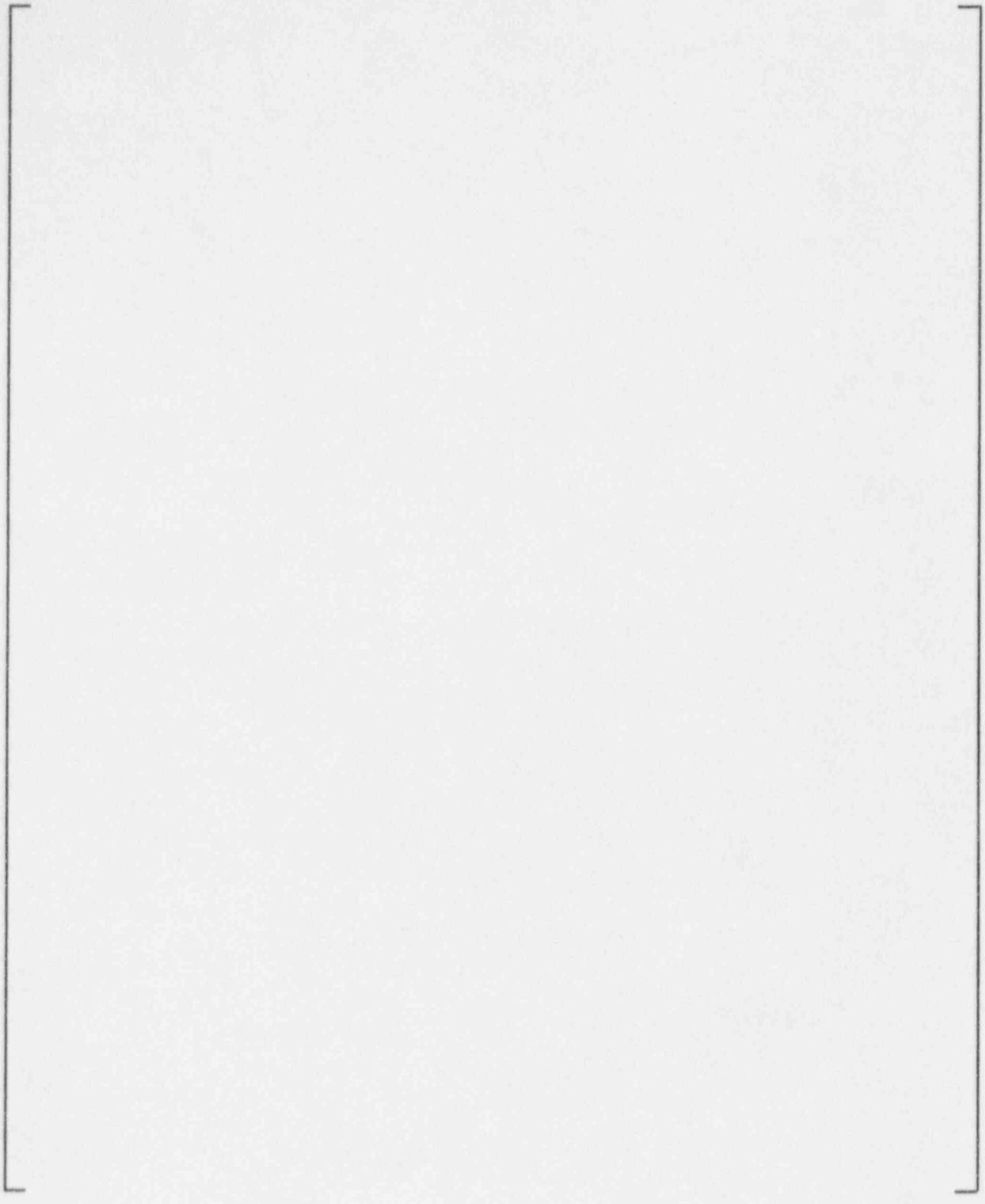

Figure 8-38 Measured and Distributed Parameter Predicted Rake Temperatures at Elevation C for Test 212.1B

a,c

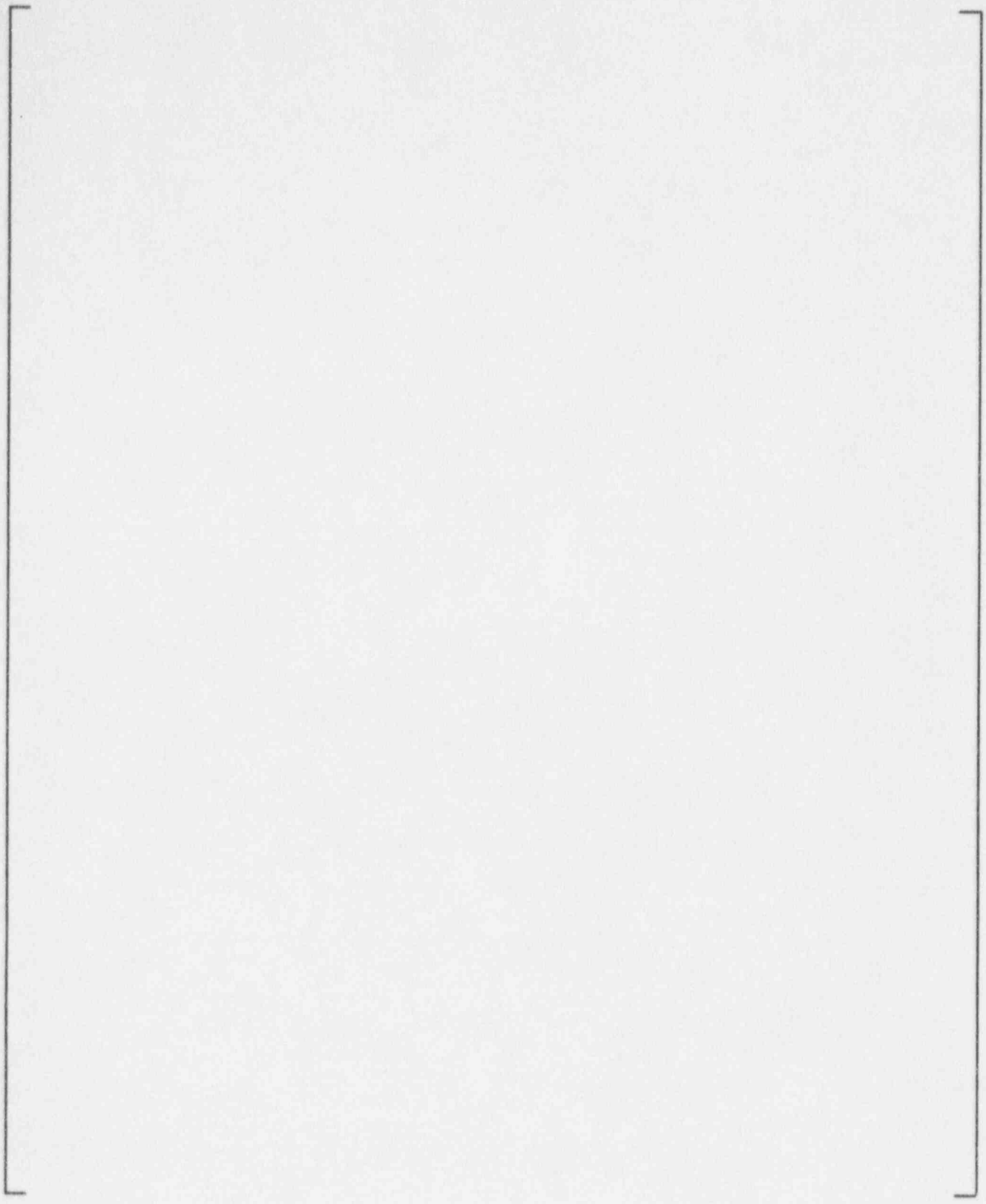

Figure 8-39 Measured and Distributed Parameter Predicted Rake Temperatures at Elevation B for Test 212.1B

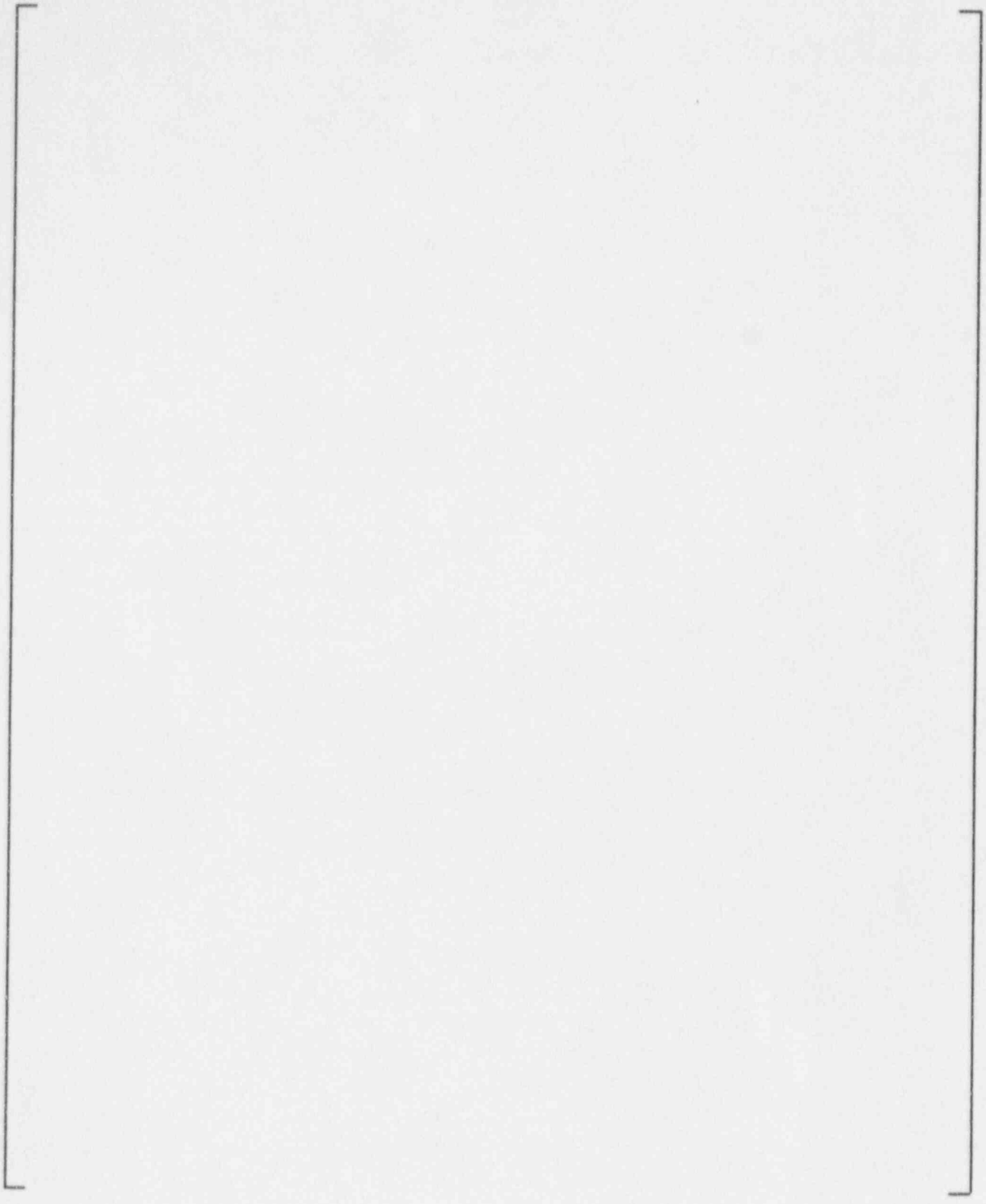

Figure 8-40 Measured and Distributed Parameter Predicted Rake Temperatures at Elevation A for Test 212.1B

a,c

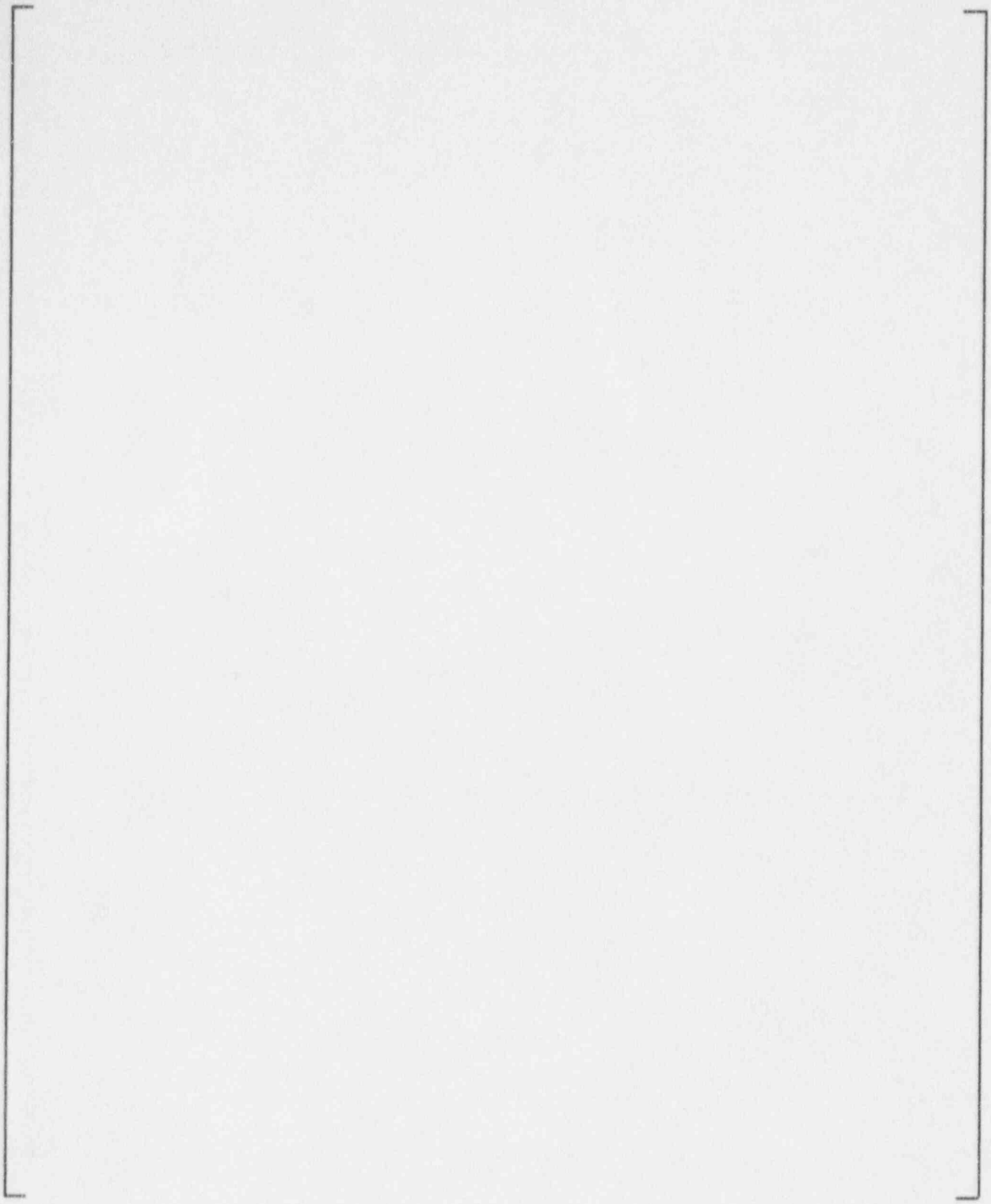

Figure 8-41 Measured and Distributed Parameter Predicted Rake Temperatures at Elevation Dome for Test 212.1B

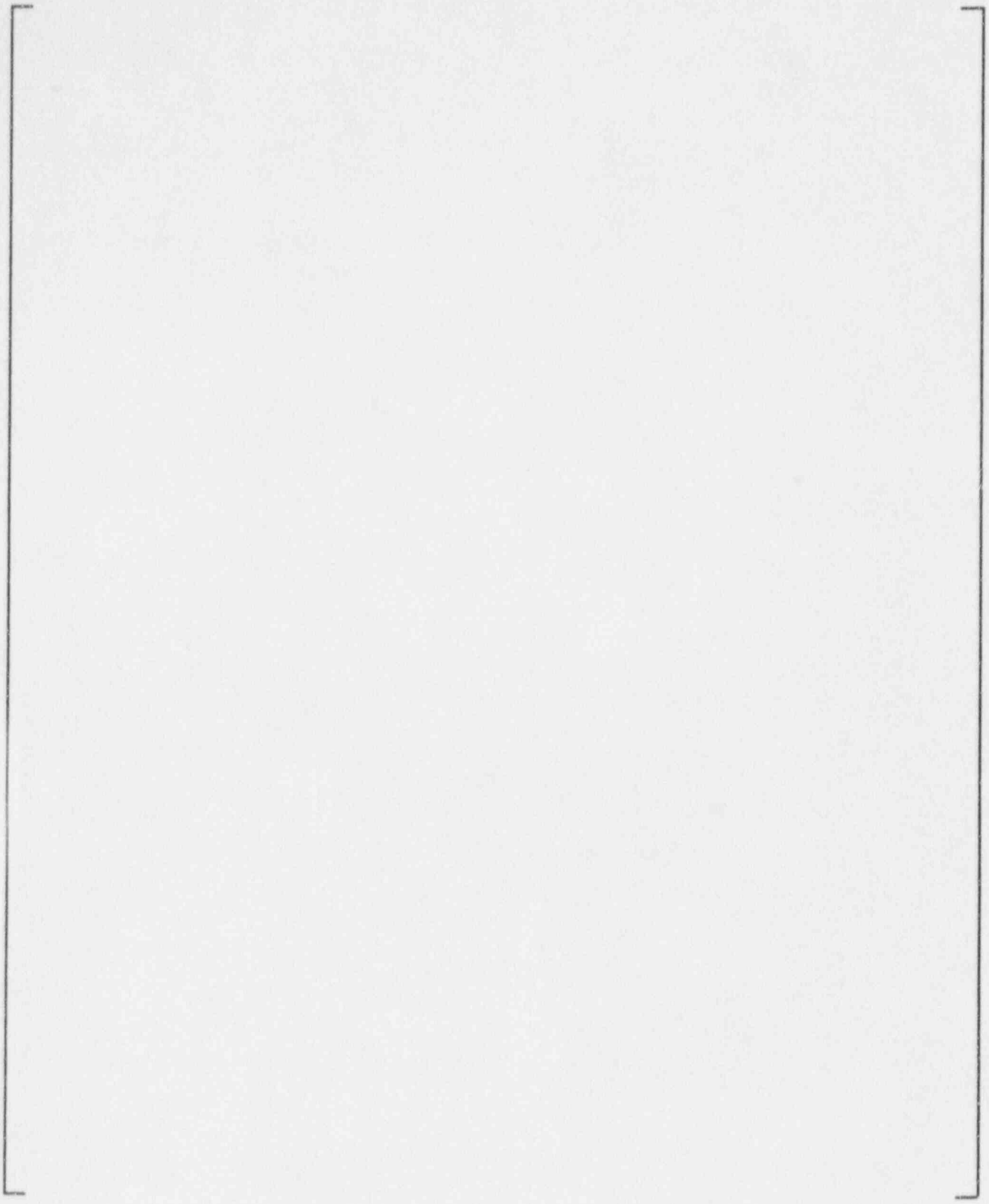

Figure 8-42 Measured and Distributed Parameter Predicted Rake Temperatures at Elevation D for Test 212.1C

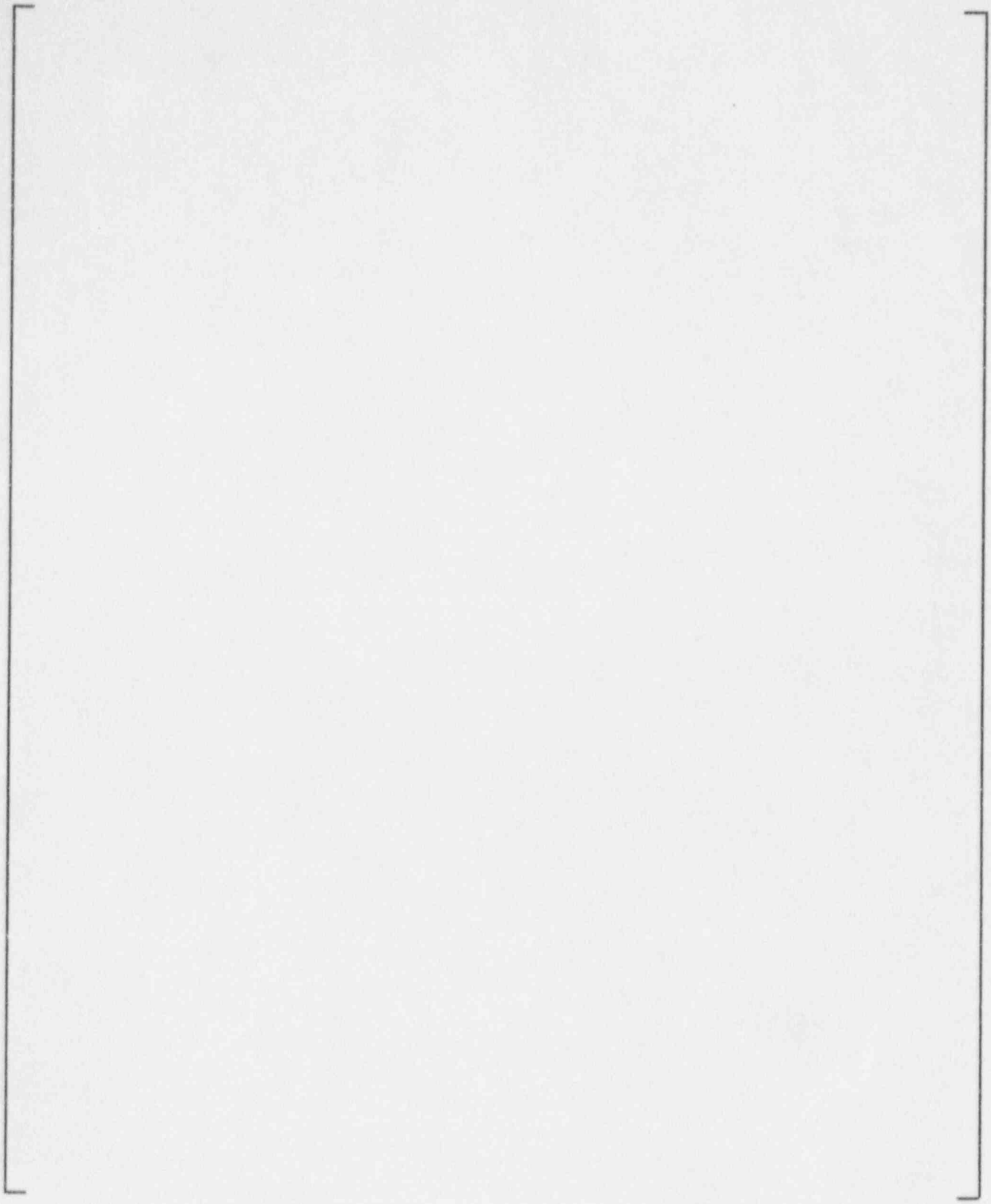

Figure 8-43 Measured and Distributed Parameter Predicted Rake Temperatures at Elevation C for Test 212.1C

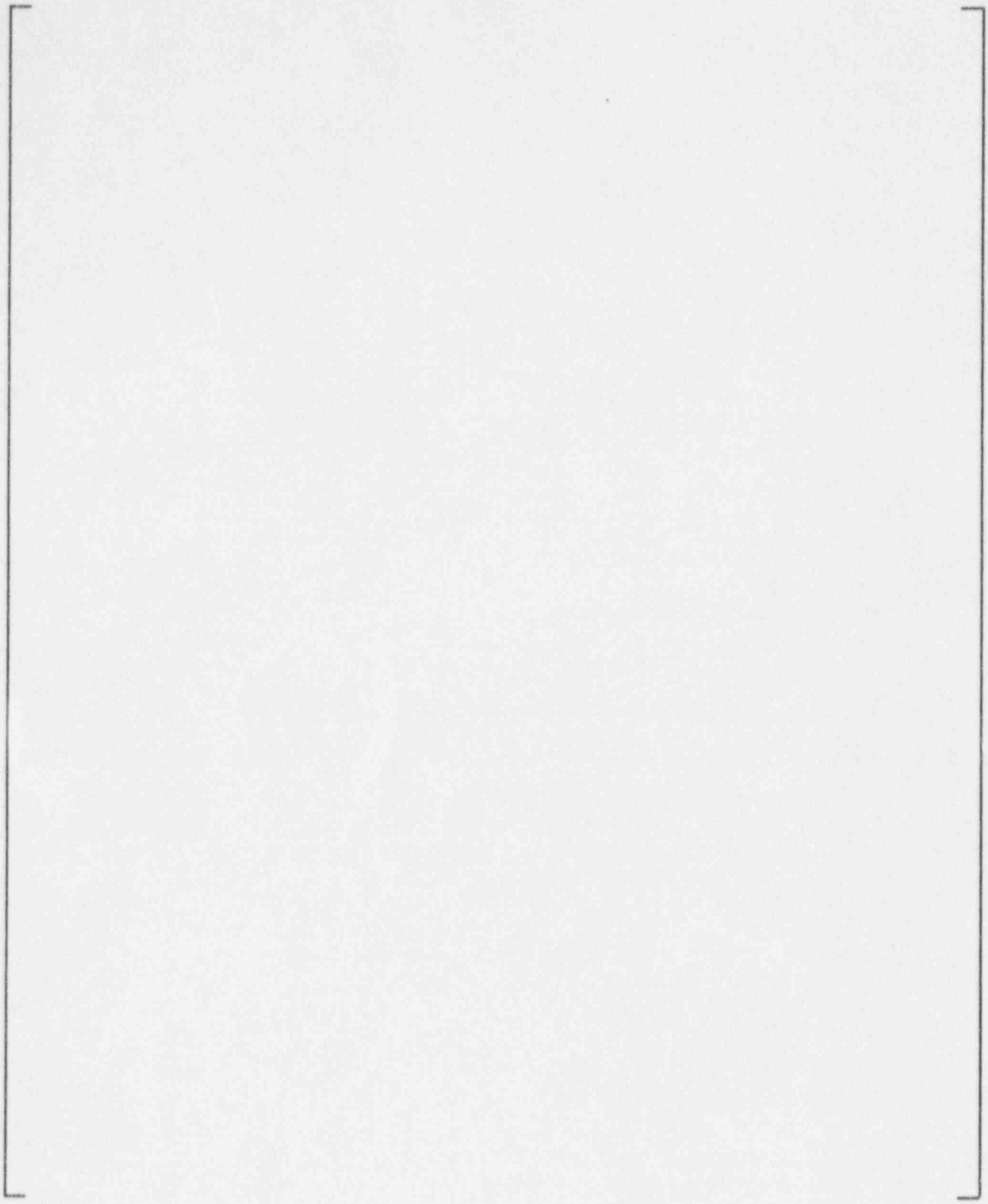

Figure 8-44 Measured and Distributed Parameter Predicted Rake Temperatures at Elevation B for Test 212.1C

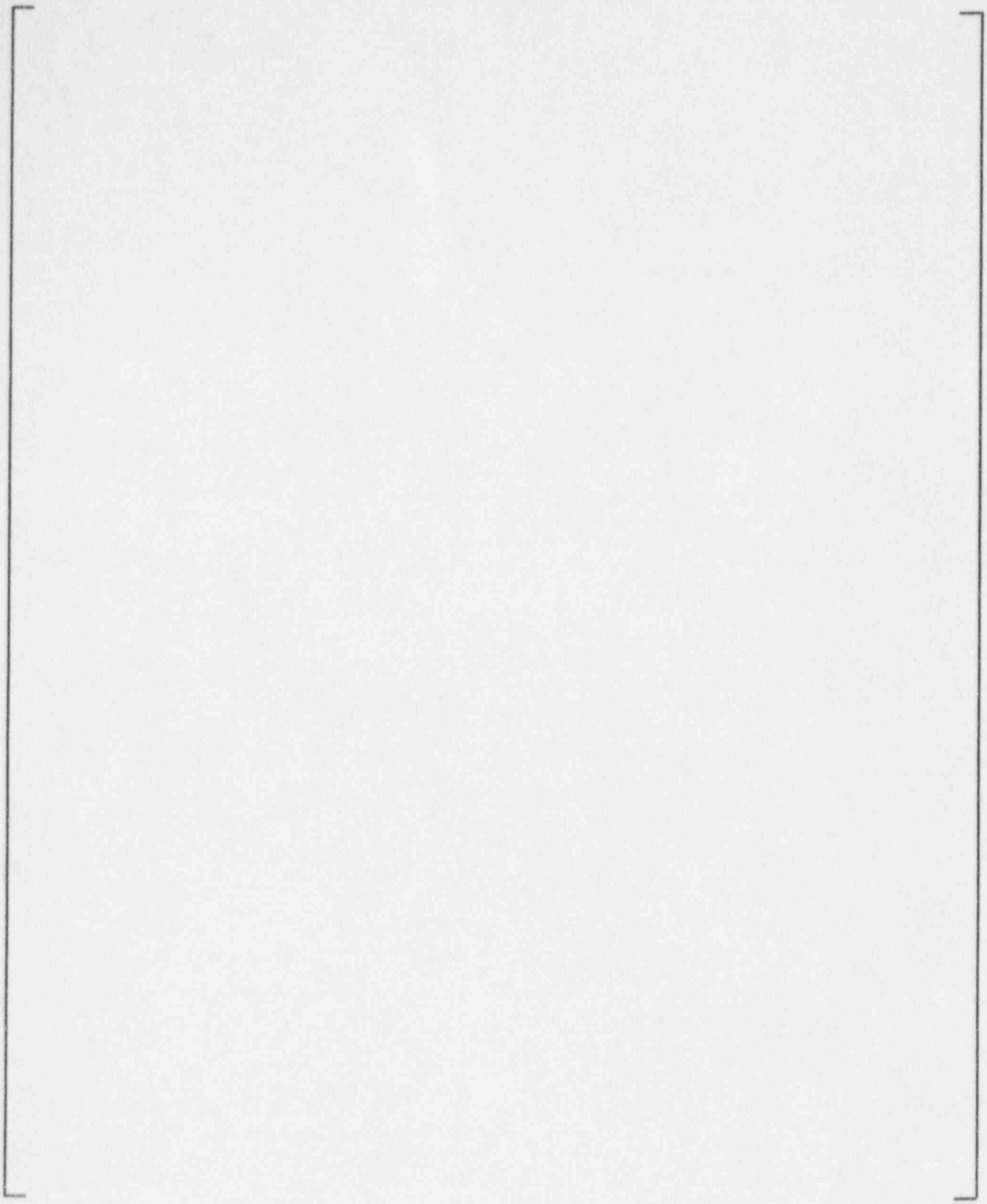

Figure 8-45 Measured and Distributed Parameter Predicted Rake Temperatures at Elevation A for Test 212.1C

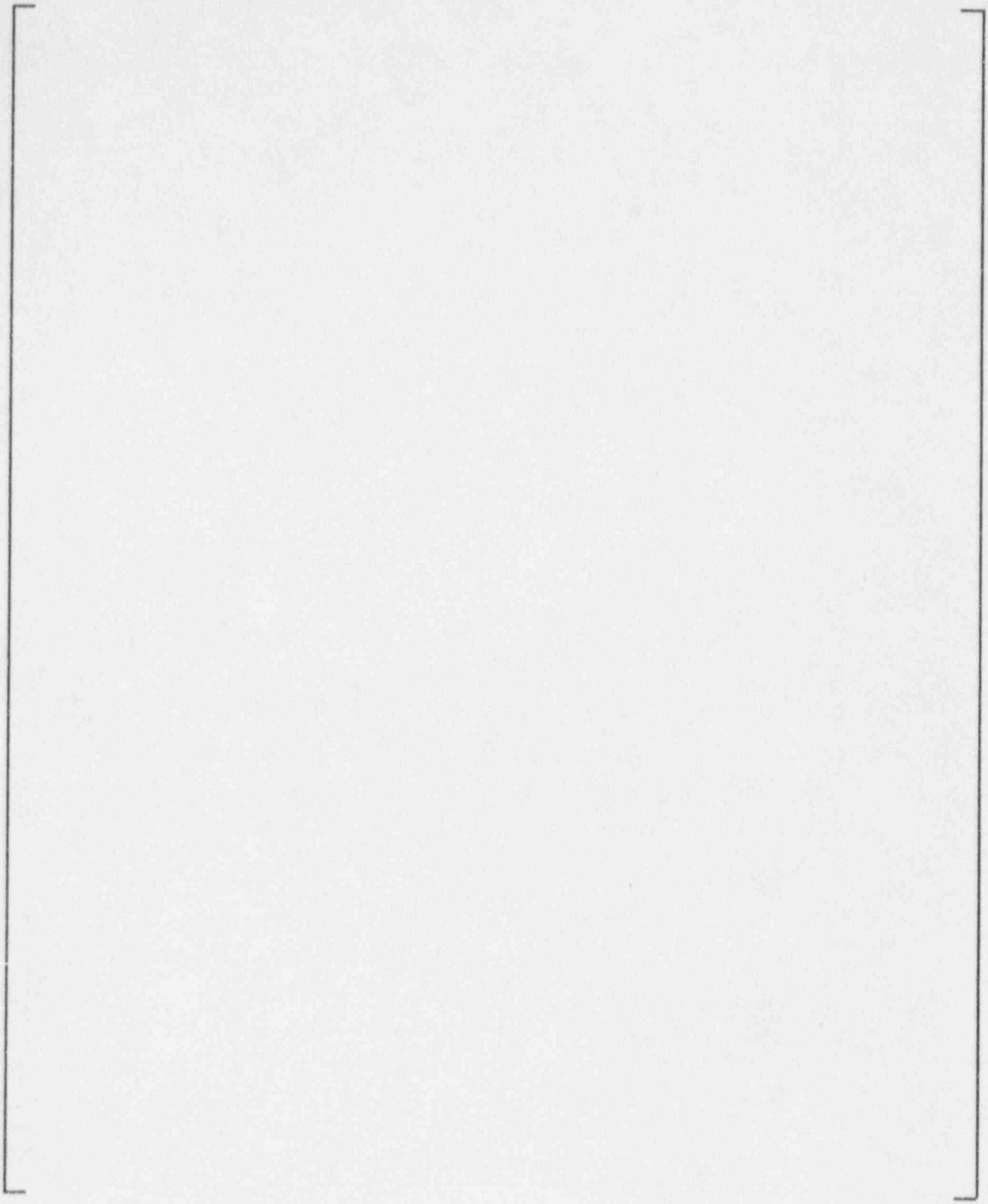

Figure 8-46 Measured and Distributed Parameter Predicted Rake Temperatures at Elevation Dome for Test 212.1C

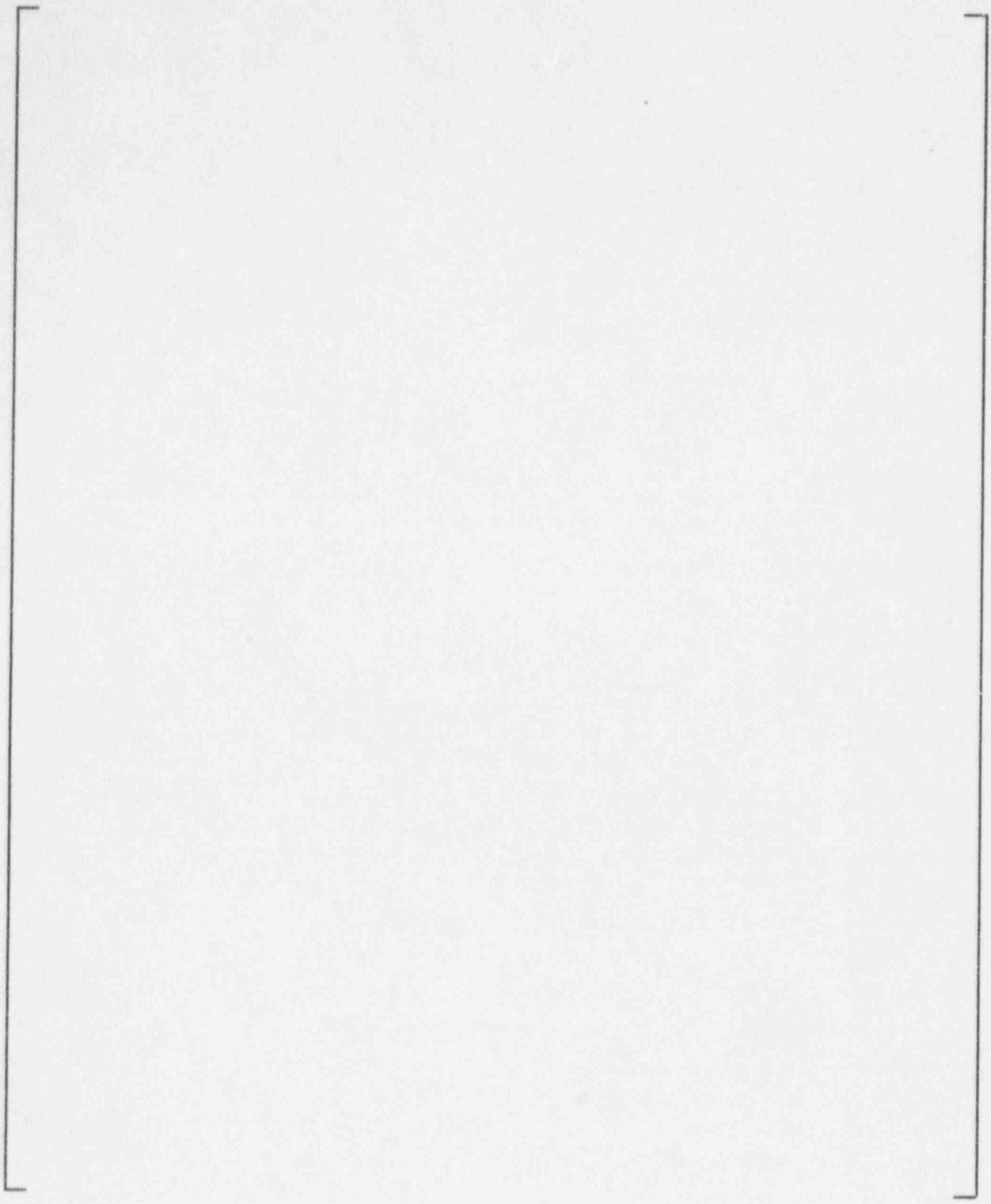

Figure 8-47 Velocity Field

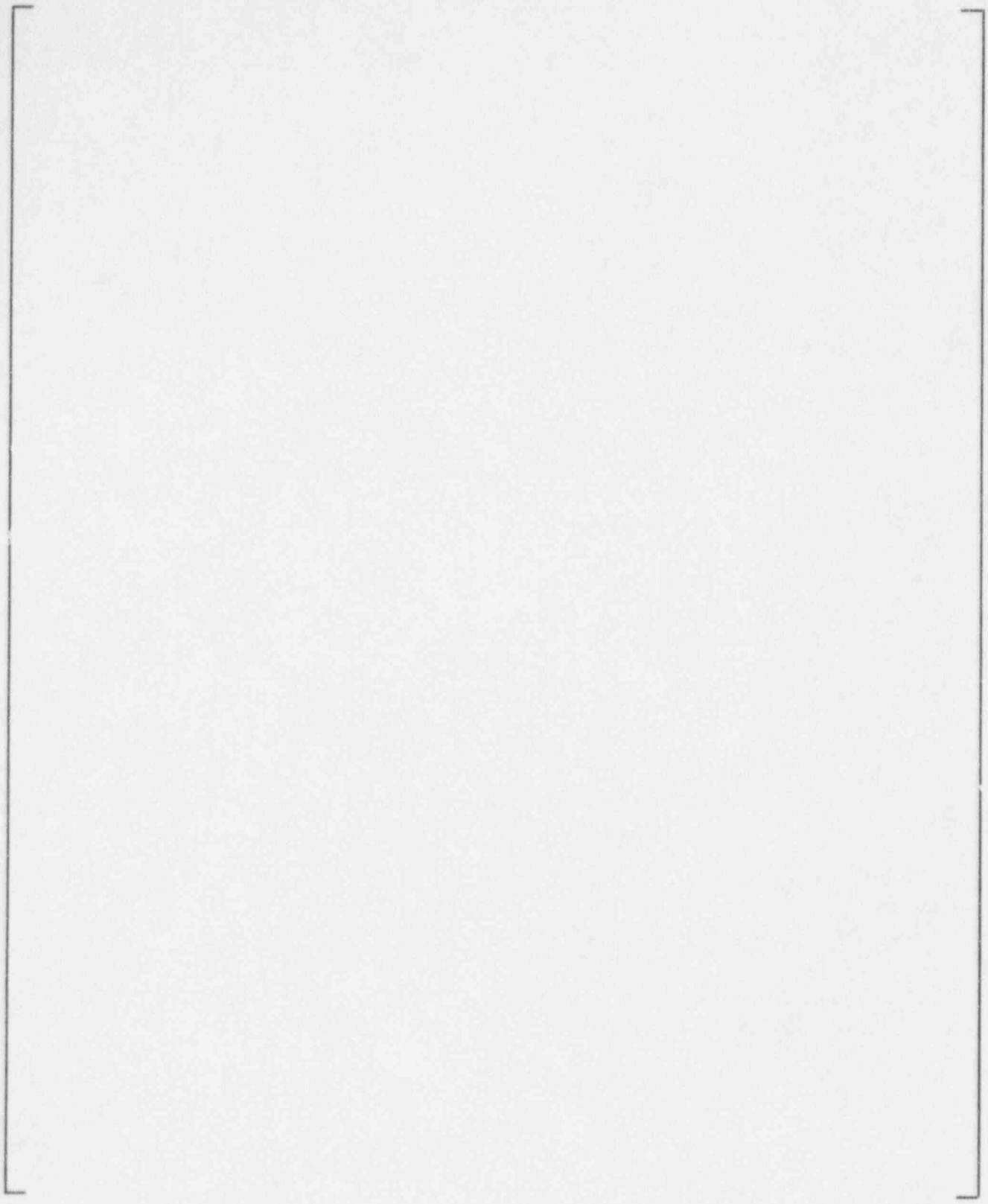

Figure 8-48 Measured and Distributed Parameter Predicted Temperature Difference at Elevation DO-21 forTests 212.1A, 212.1B, and 212.1C

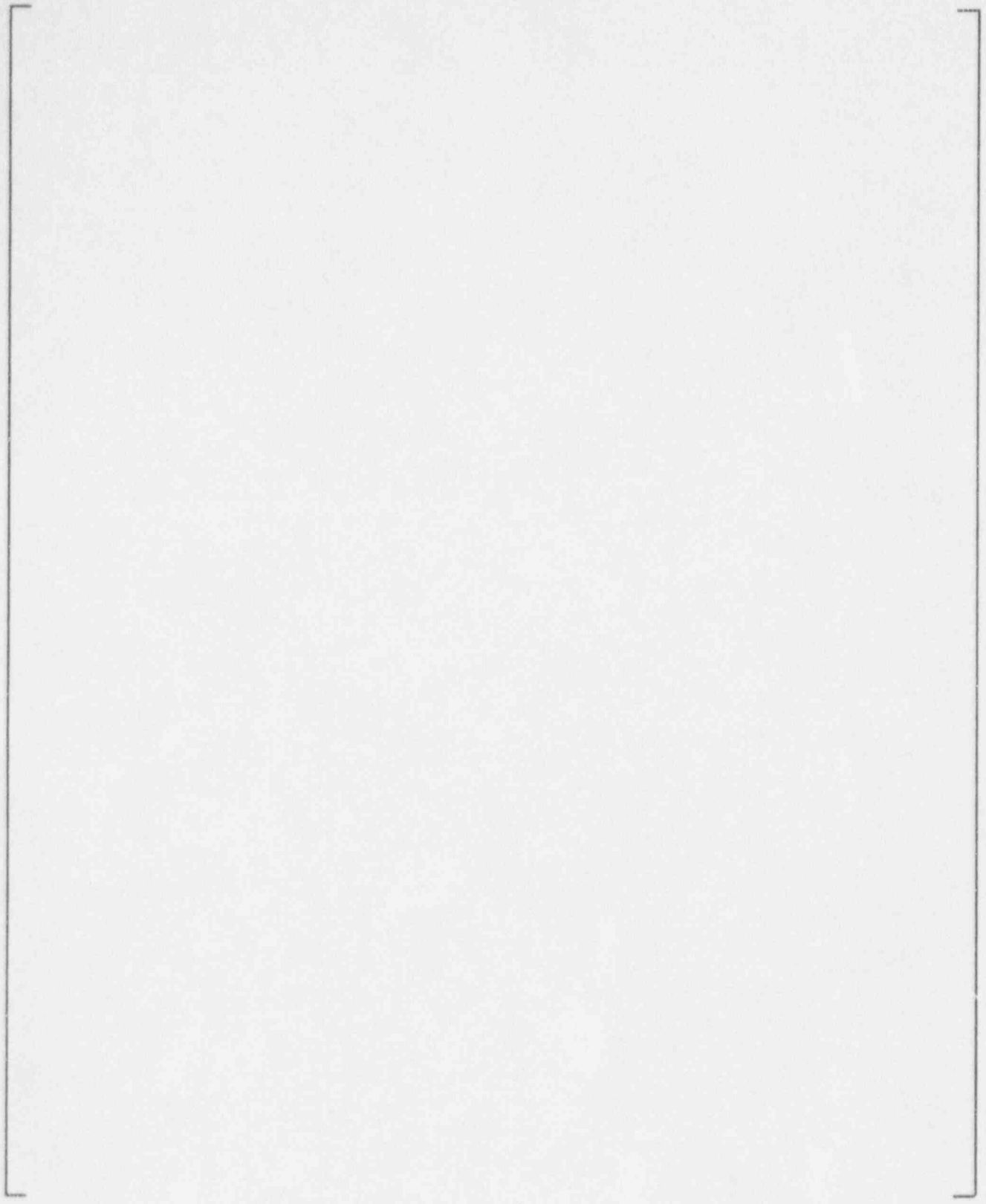

Figure 8-49 Measured and Distributed Parameter Predicted Temperature Difference at Elevation DO-42 for Tests 212.1A, 212.1B, and 212.1C

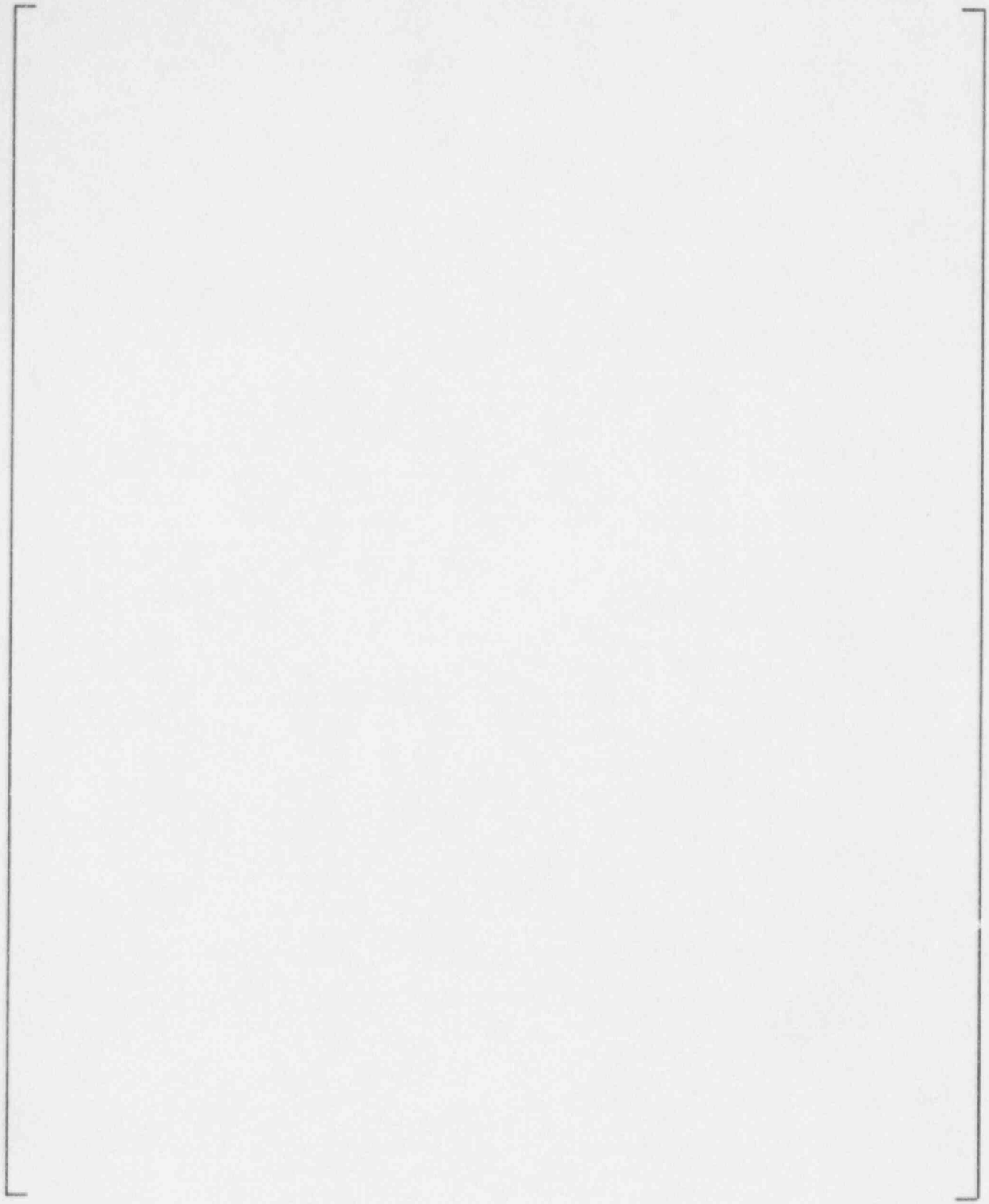

Figure 8-50 Measured and Distributed Parameter Predicted Temperature Difference at Elevation DO-63 for Tests 212.1A, 212.1B, and 212.1C

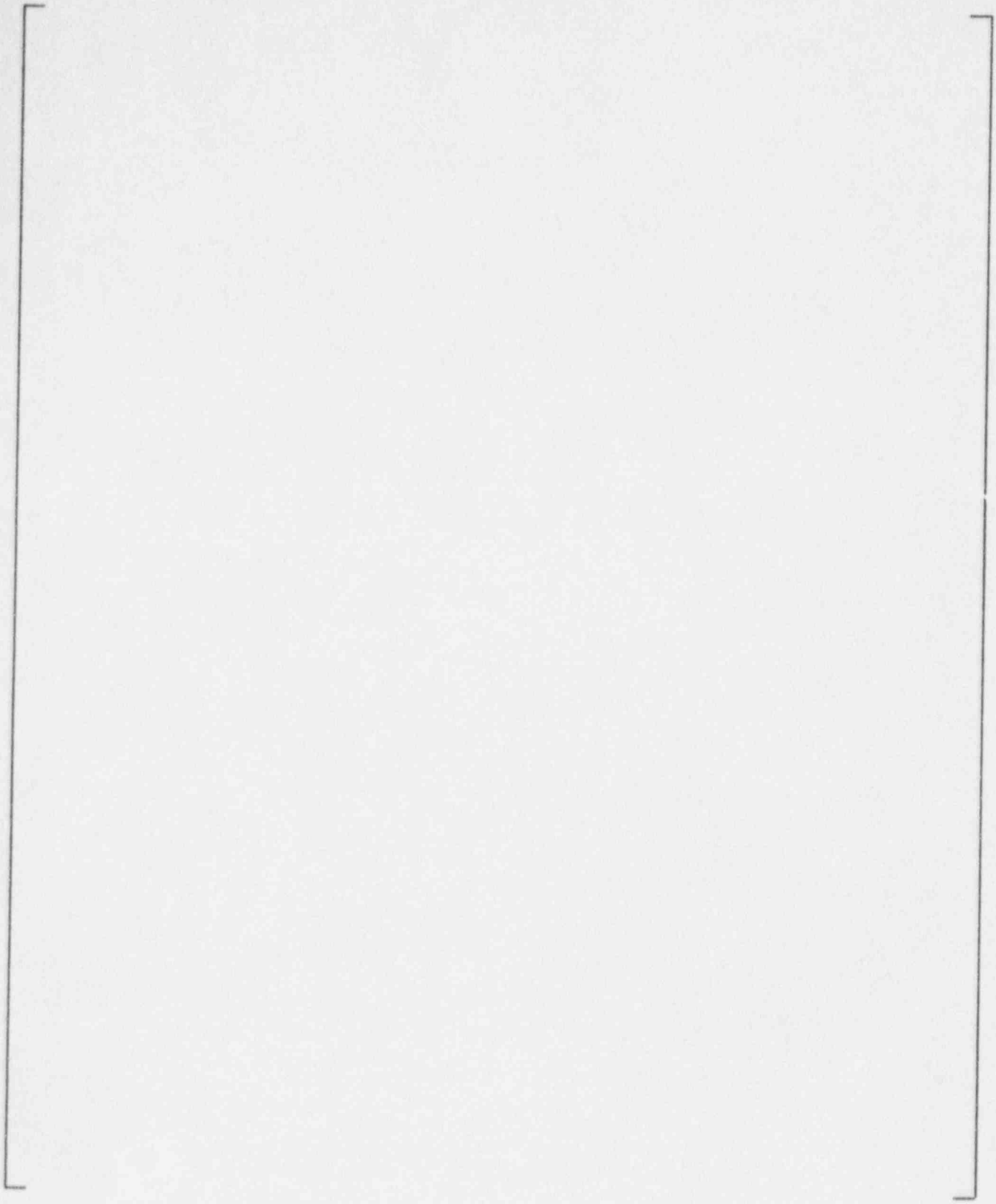

Figure 8-51 Measured and Distributed Parameter Predicted Temperature Difference at Elevation DO-84 for Tests 212.1A, 212.1B, and 212.1C

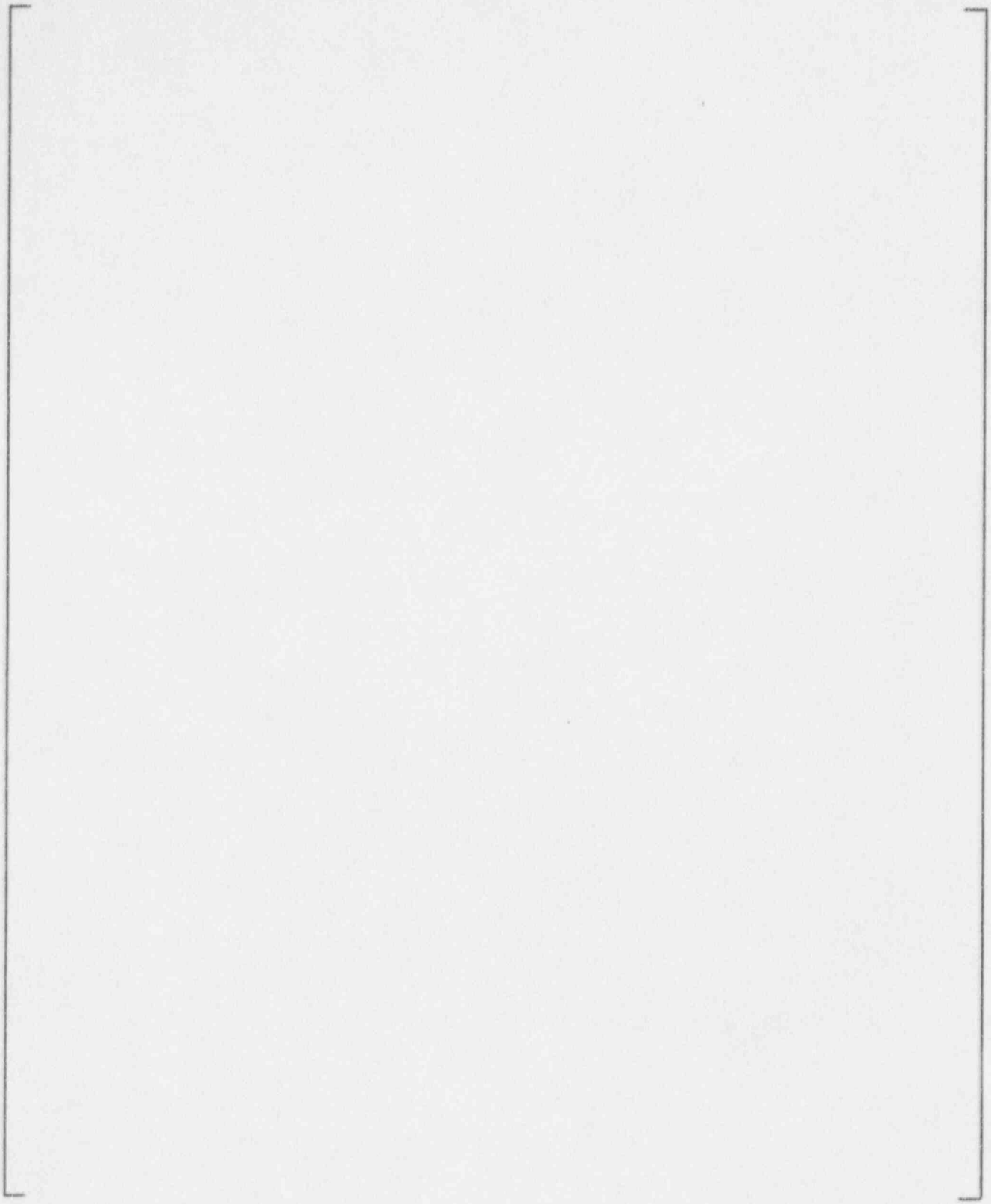

Figure 8-52 Measured and Distributed Parameter Predicted Temperature Difference at Elevation A for Tests 212.1A, 212.1B, and 212.1C

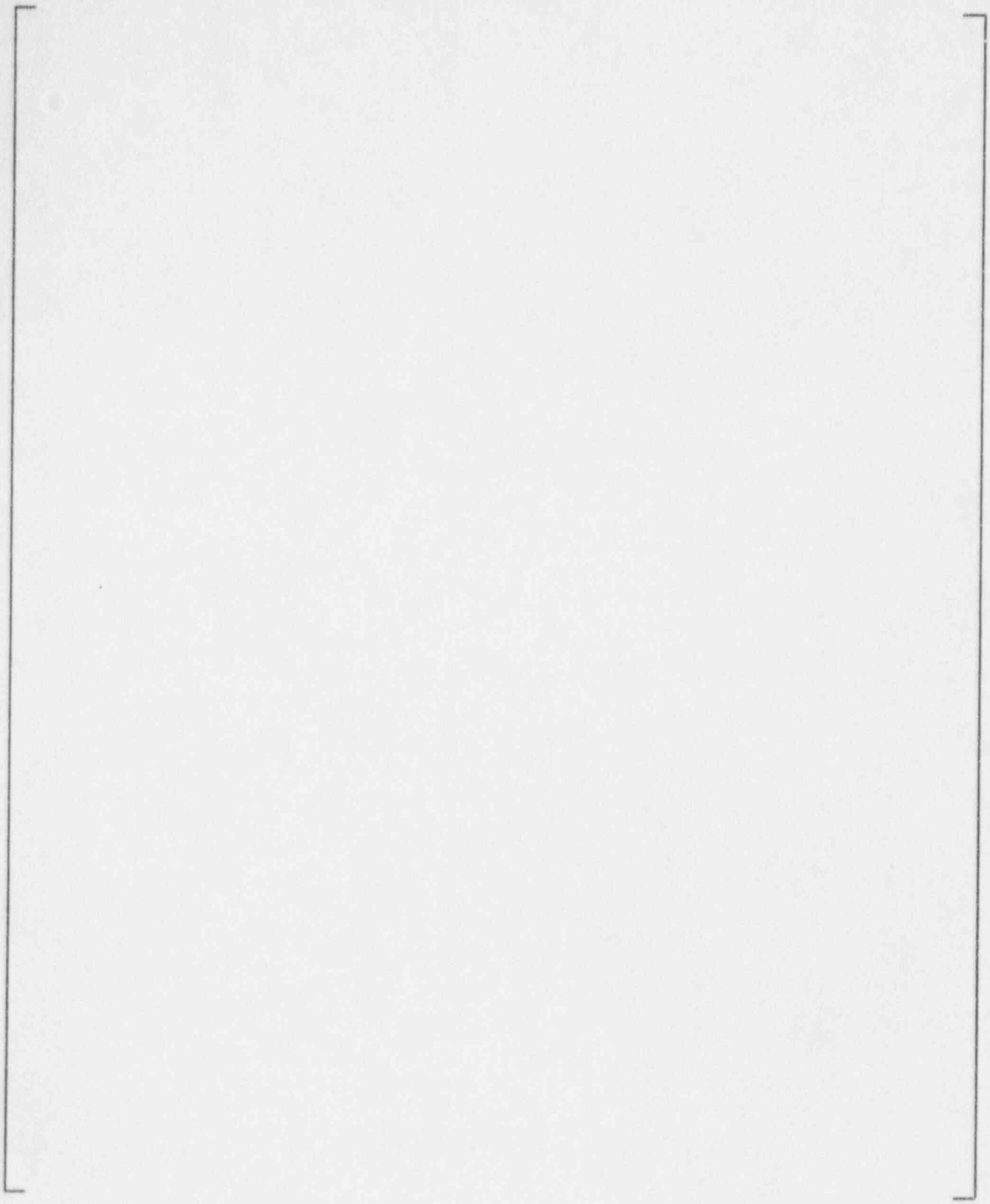

Figure 8-53 Measured and Distributed Parameter Predicted Temperature Difference for Elevation B for Tests 212.1A, 212.1B, and 212.1C

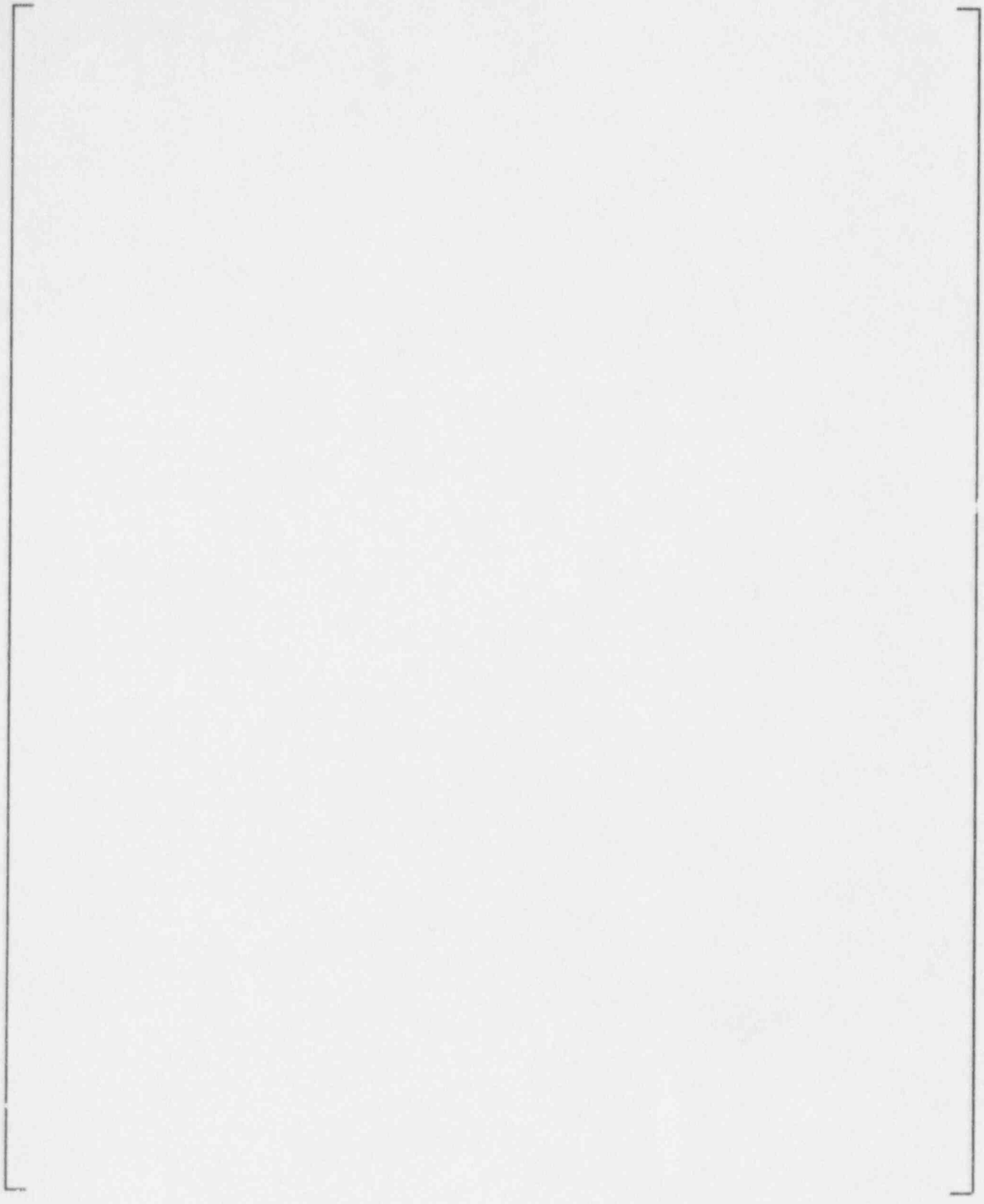

Figure 8-54 Measured and Distributed Parameter Predicted Temperature Difference at Elevation C for Tests 212.1A, 212.1B, and 212.1C

a,c

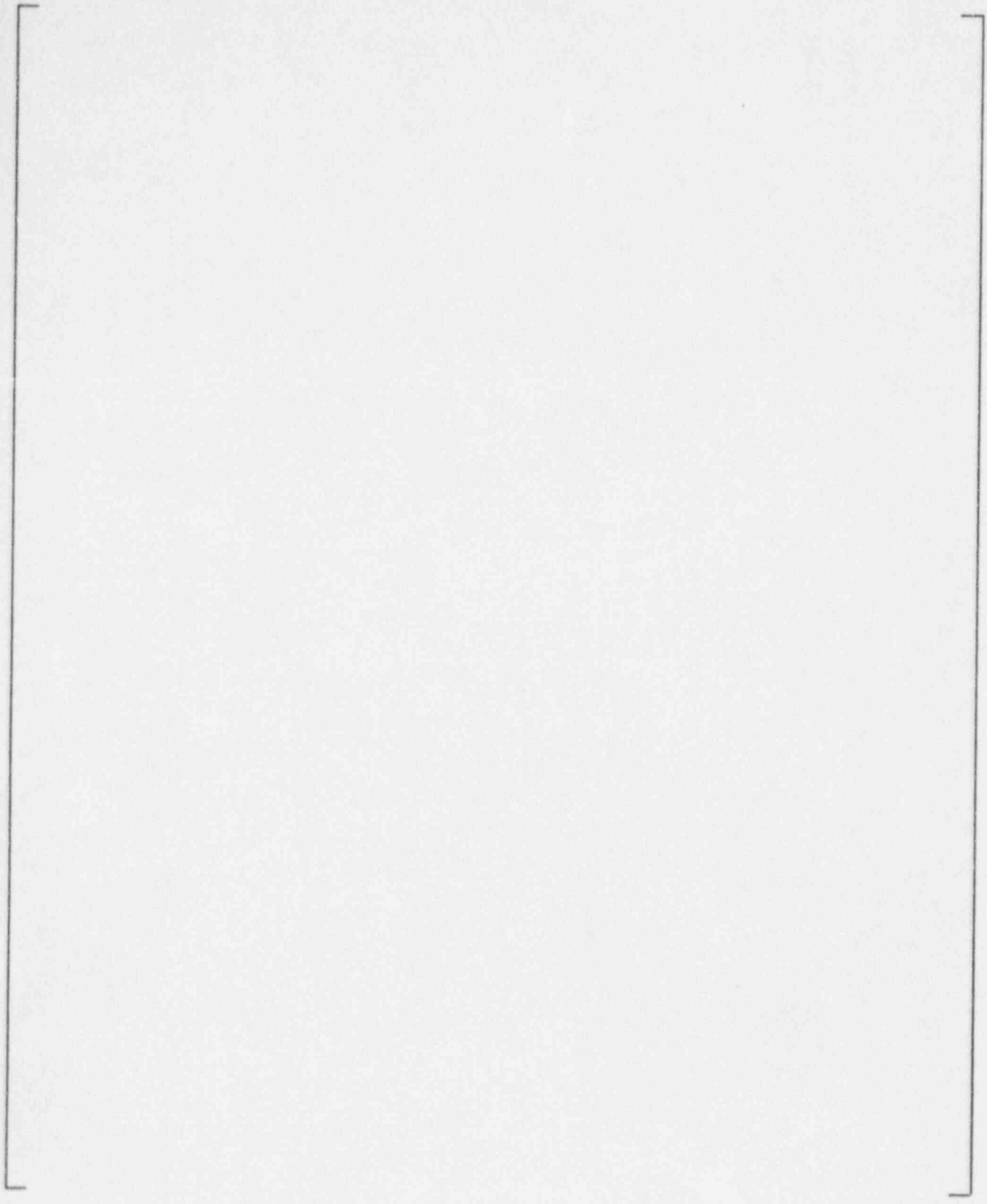

Figure 8-55 Measured and Distributed Parameter Predicted Temperature Difference at Elevation D for Tests 212.1A, 212.1B, and 212.1C

a,c

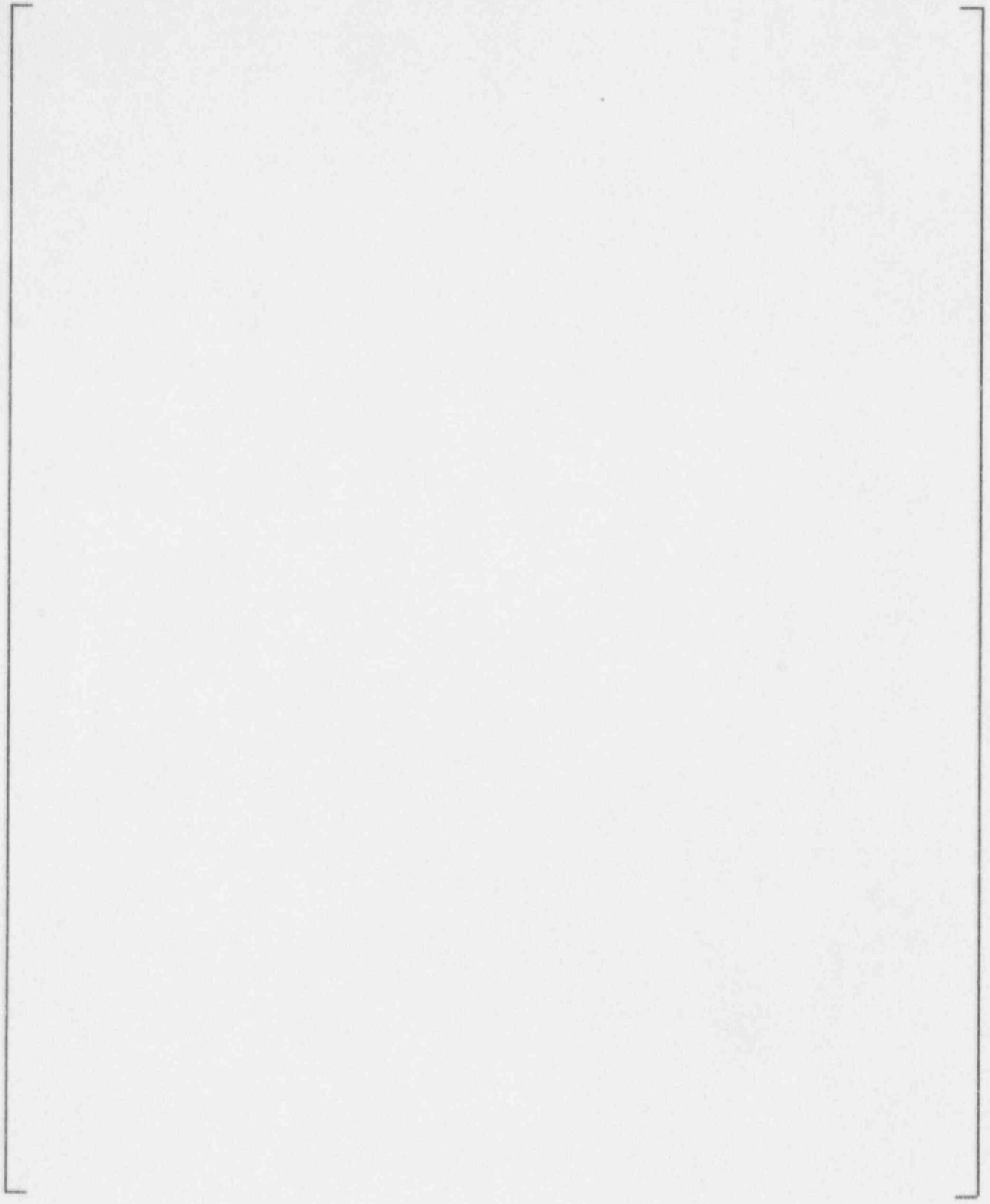

Figure 8-56 Measured and Distributed Parameter Predicted Temperature Difference at Elevation E for Tests 212.1A, 212.1B, and 212.1C

a,c

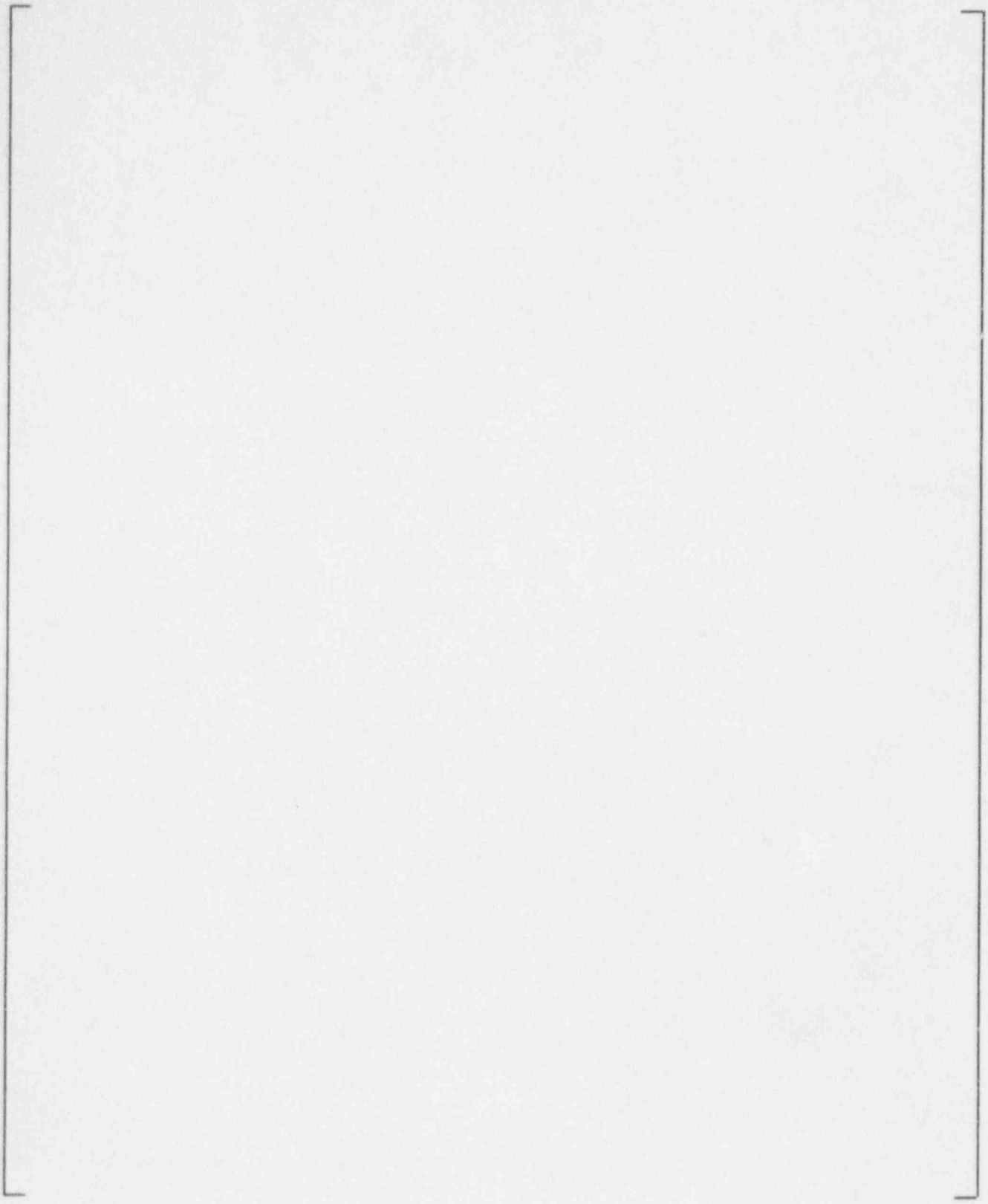

Figure 8-57 Measured and Distributed Parameter Predicted Temperature Difference at Elevation F for Tests 212.1A, 212.1B, and 212.1C

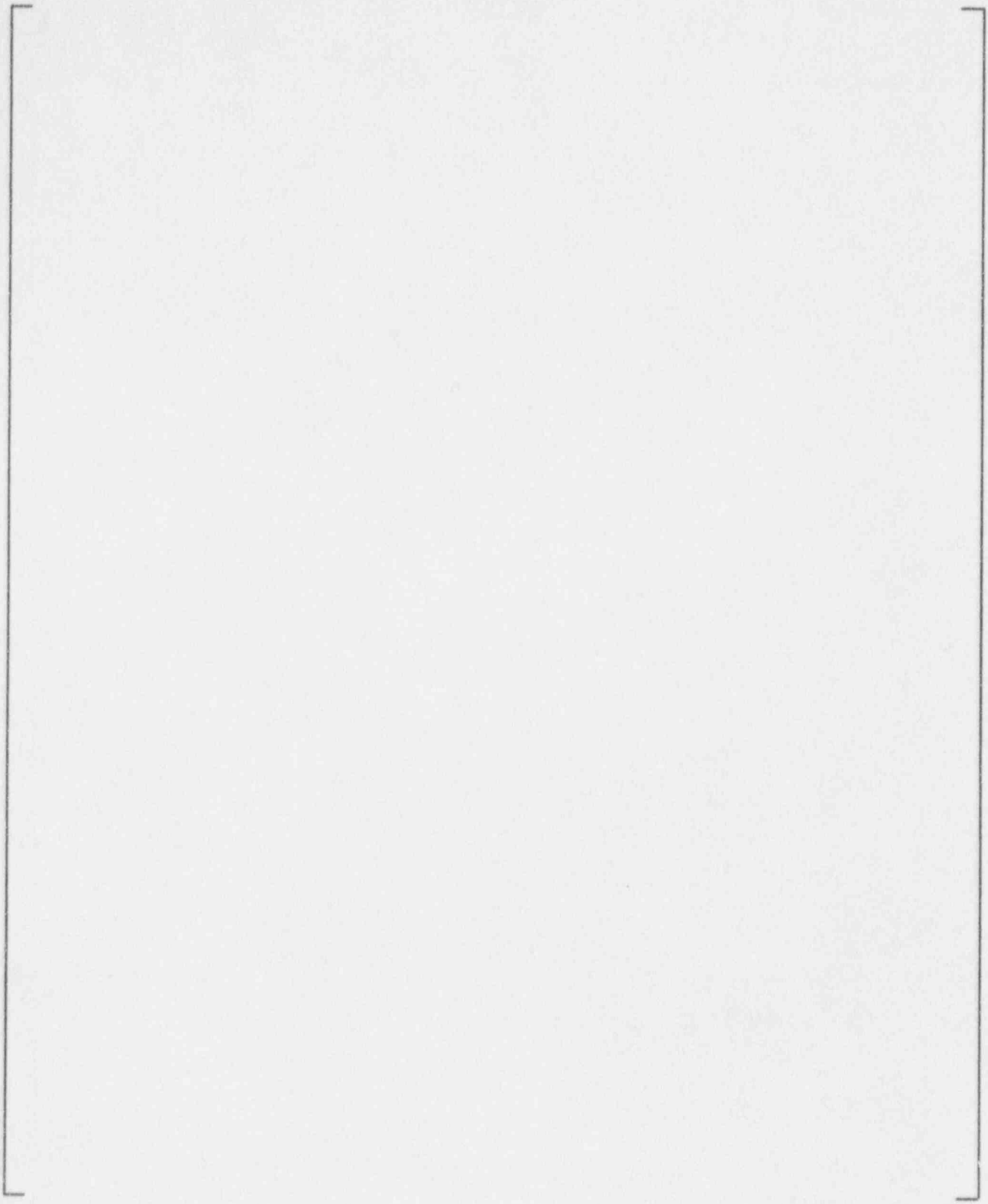

Figure 8-58 Measured and Distributed Parameter Predicted Temperature Difference at Elevation DO-21 for Test 222.1

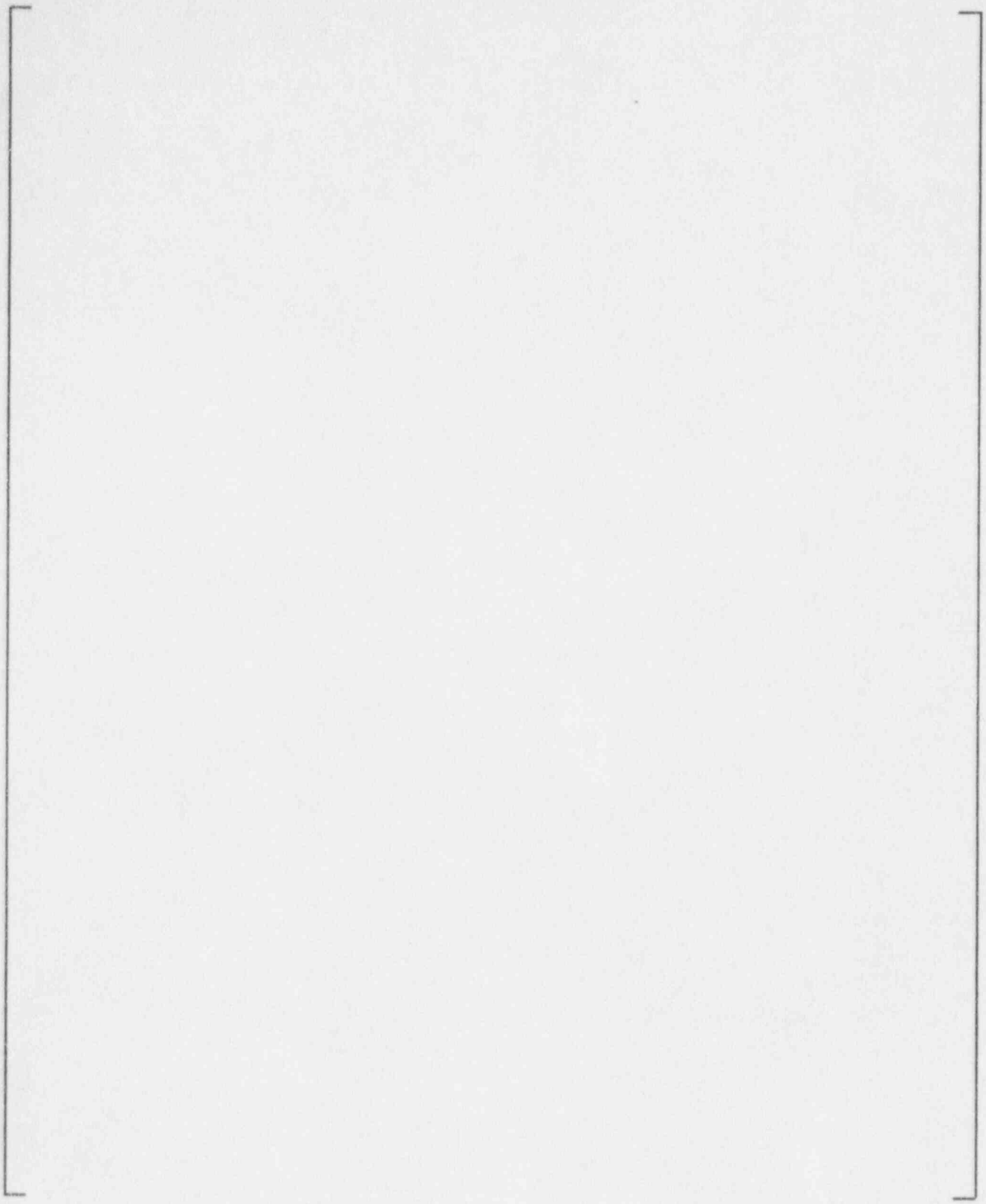

Figure 8-59 Measured and Distributed Parameter Predicted Temperature Difference at Elevation DO-42 for Test 222.1

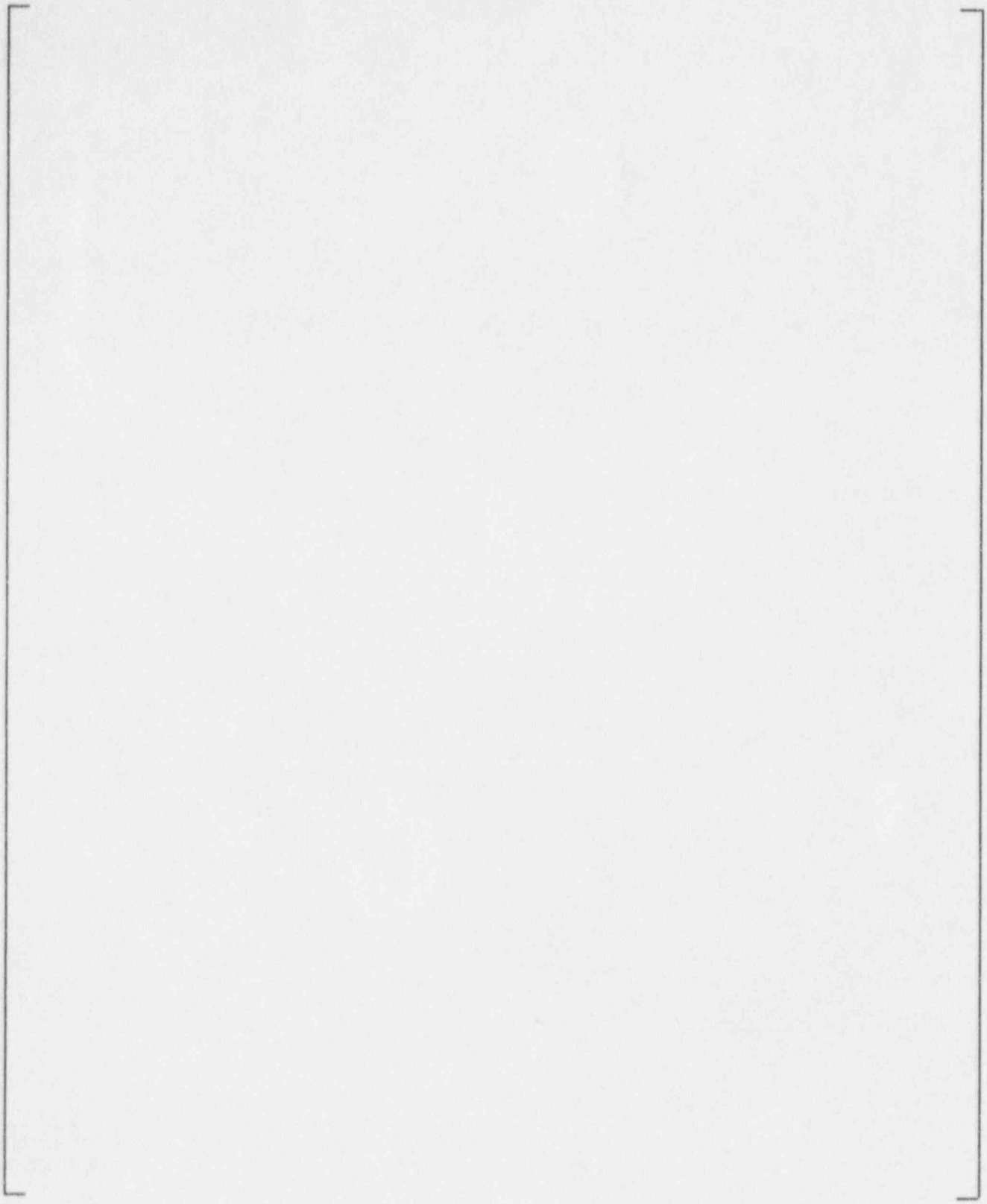

Figure 8-60 Measured and Distributed Parameter Predicted Temperature Difference at Elevation DO-63 for Test 222.1

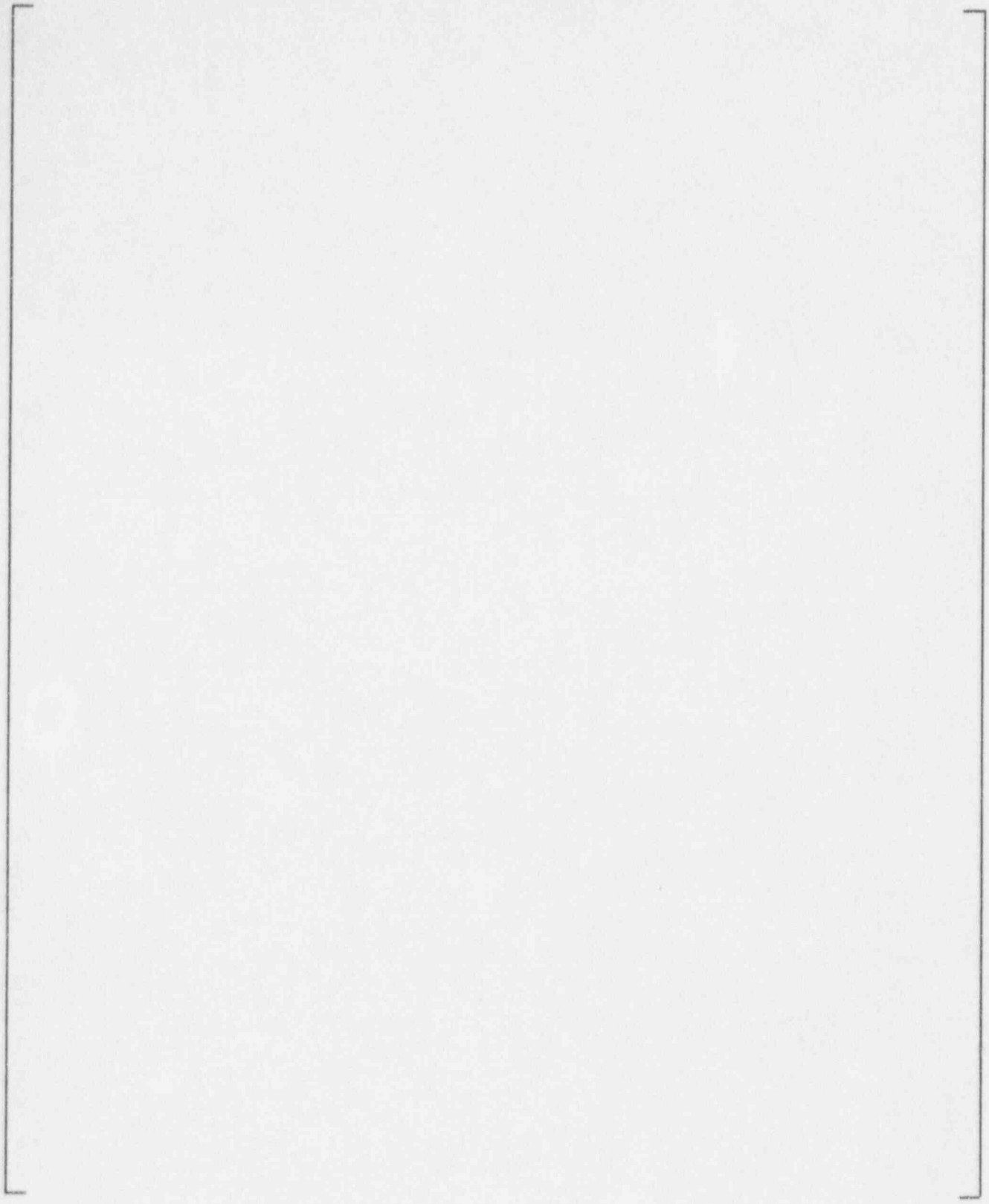

Figure 8-61 Measured and Distributed Parameter Predicted Temperature Difference at Elevation DO-84 for Test 222.1

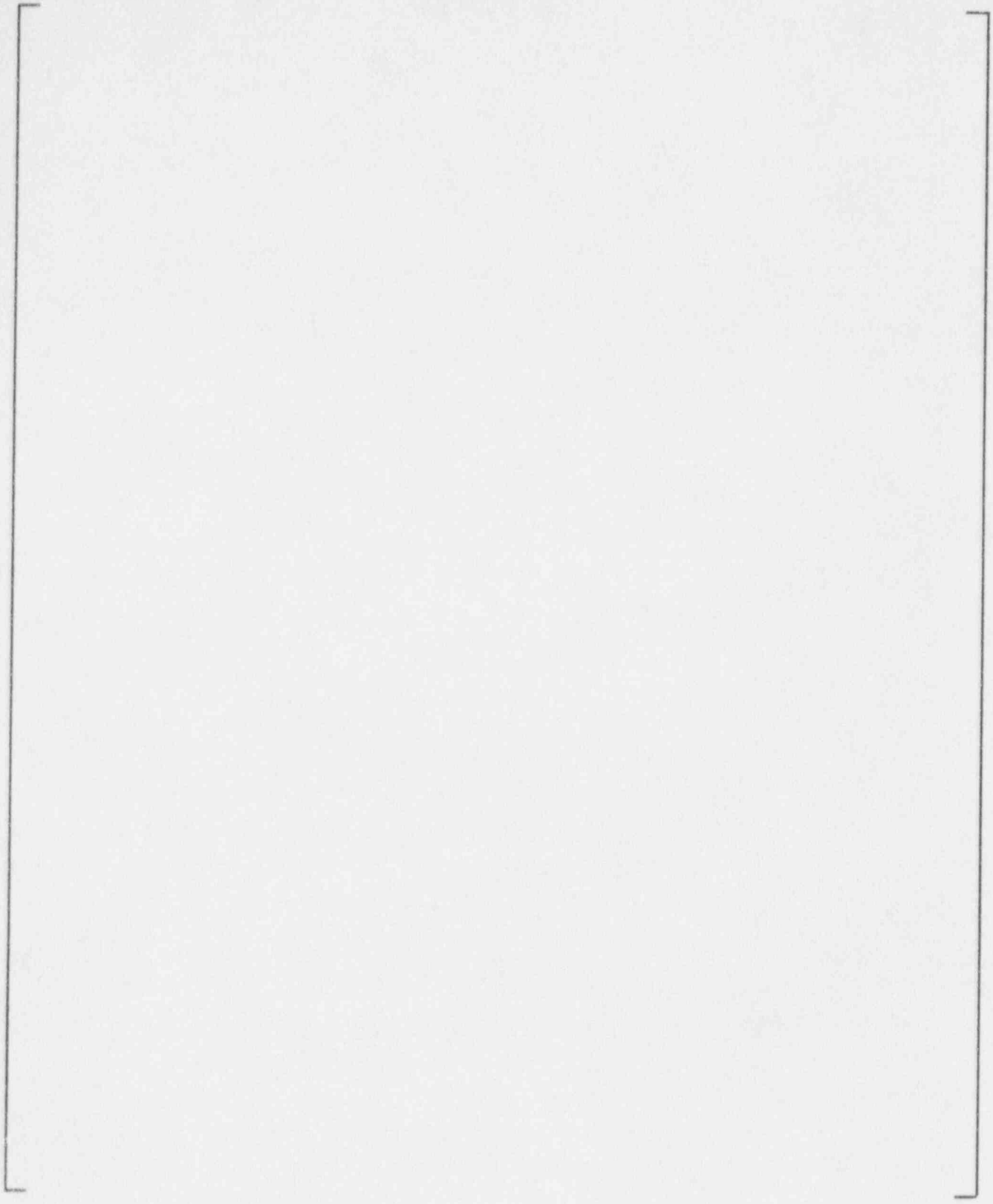

Figure 8-62 Measured and Distributed Parameter Predicted Temperature Difference at Elevation A for Test 222.1

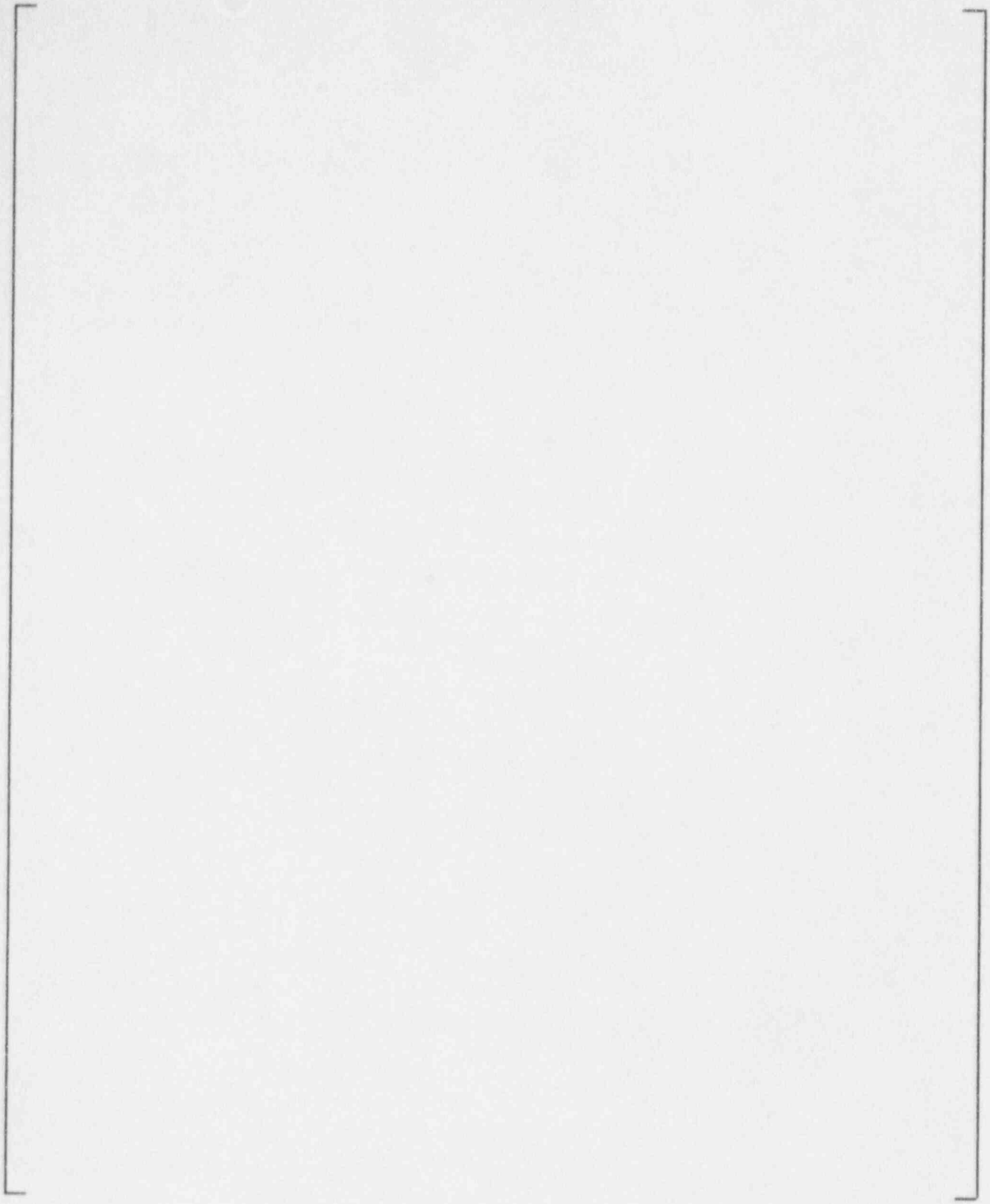

Figure 8-63 Measured and Distributed Parameter Predicted Temperature Difference at Elevation B for Test 222.1

a,c

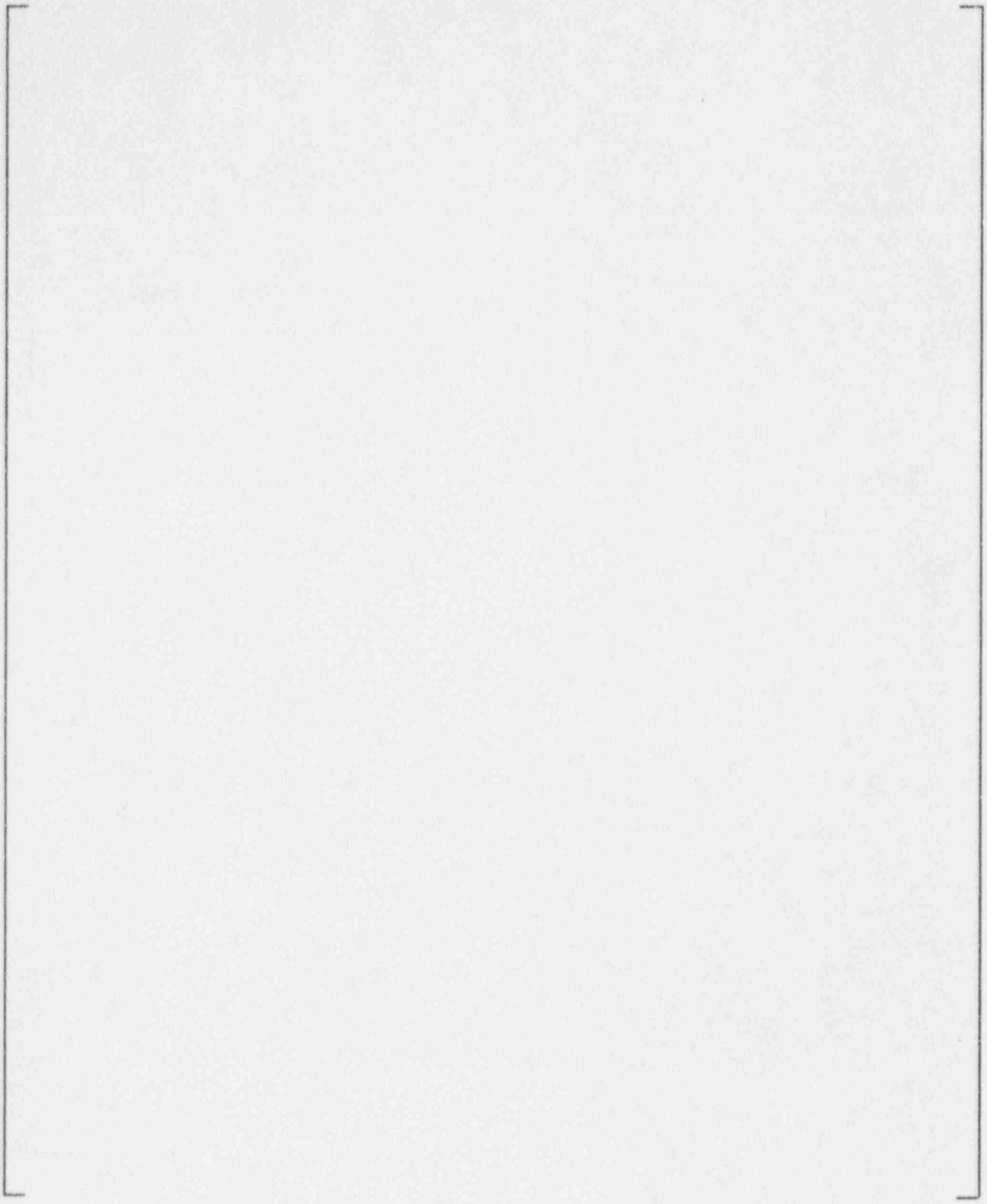

Figure 8-64 Measured and Distributed Parameter Predicted Temperature Difference at Elevation C for Test 222.1

a,c

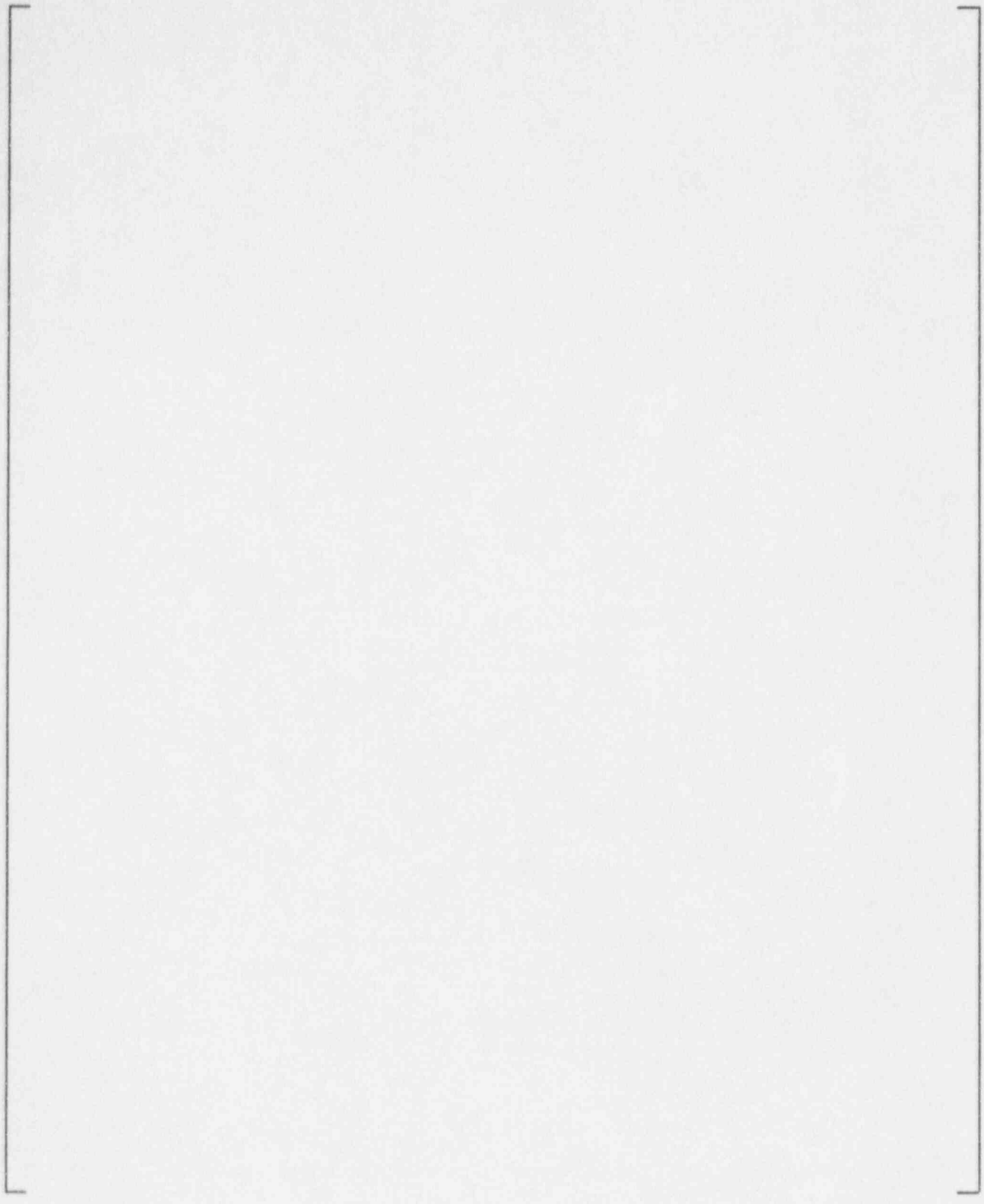

Figure 8-65 Measured and Distributed Parameter Predicted Temperature Difference at Elevation D for Test 222.1

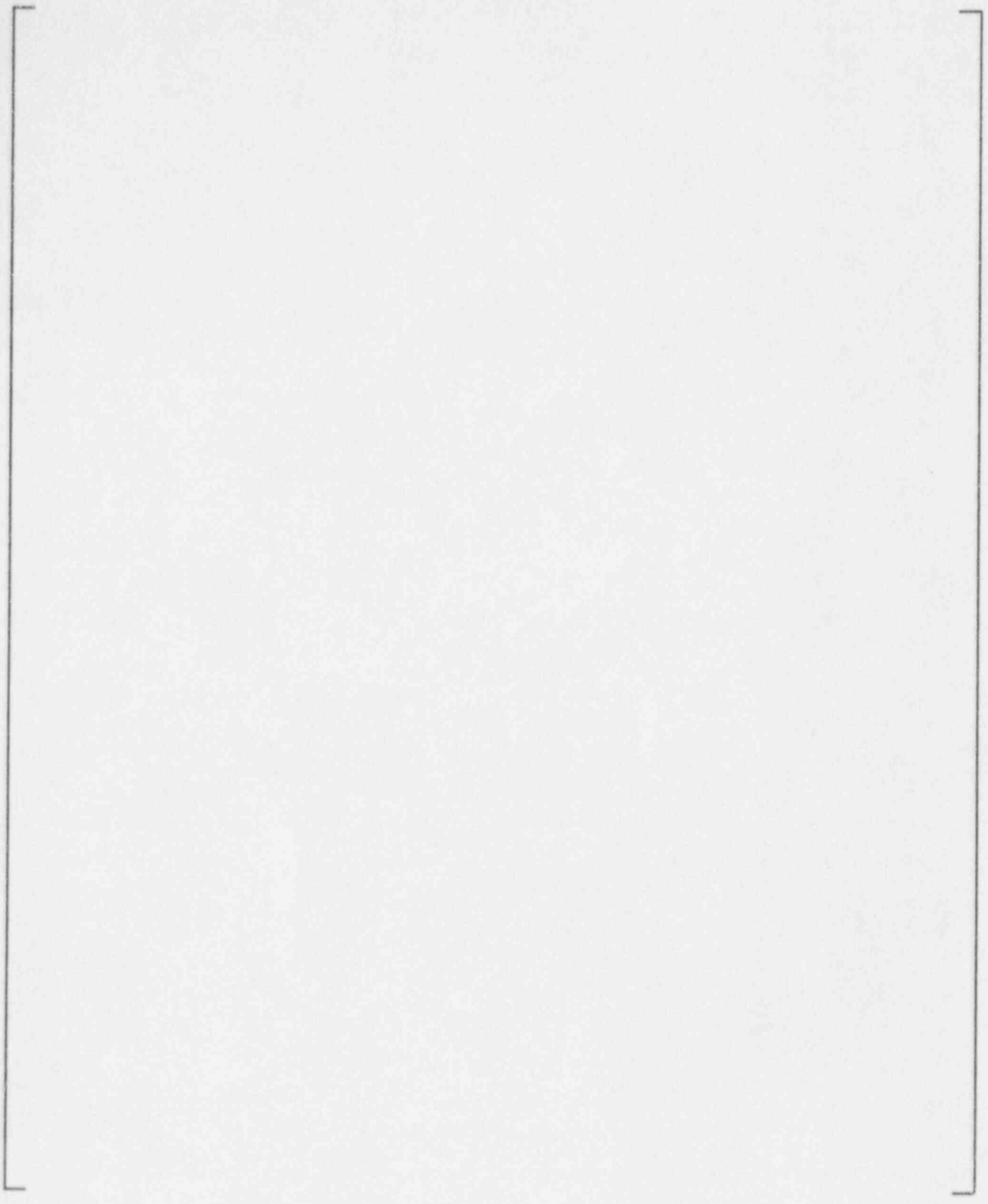

Figure 8-66 Measured and Distributed Parameter Predicted Temperature Difference at Elevation E for Test 222.1

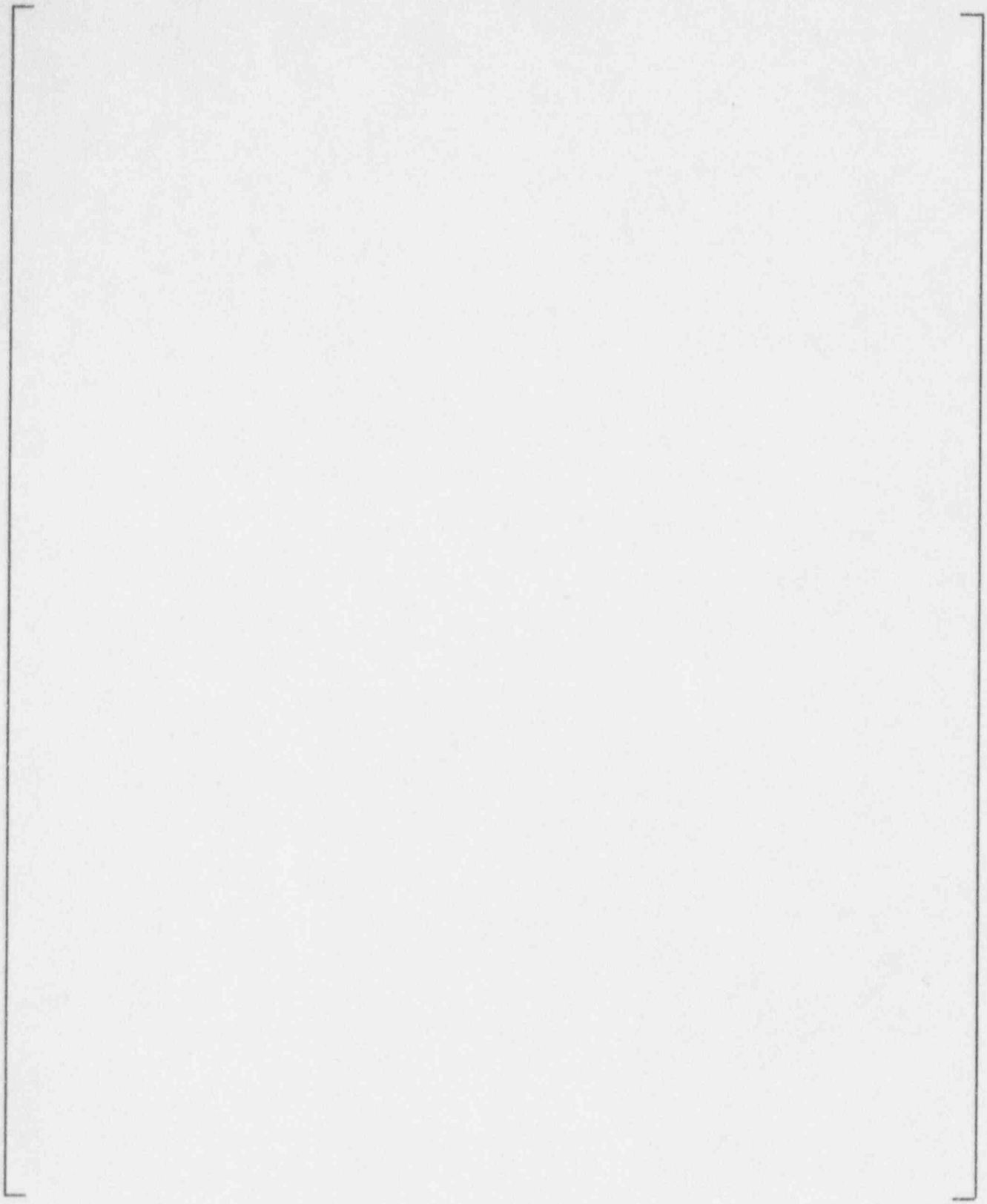

Figure 8-67 Measured and Distributed Parameter Predicted Temperature Difference at Elevation F for Test 222.1

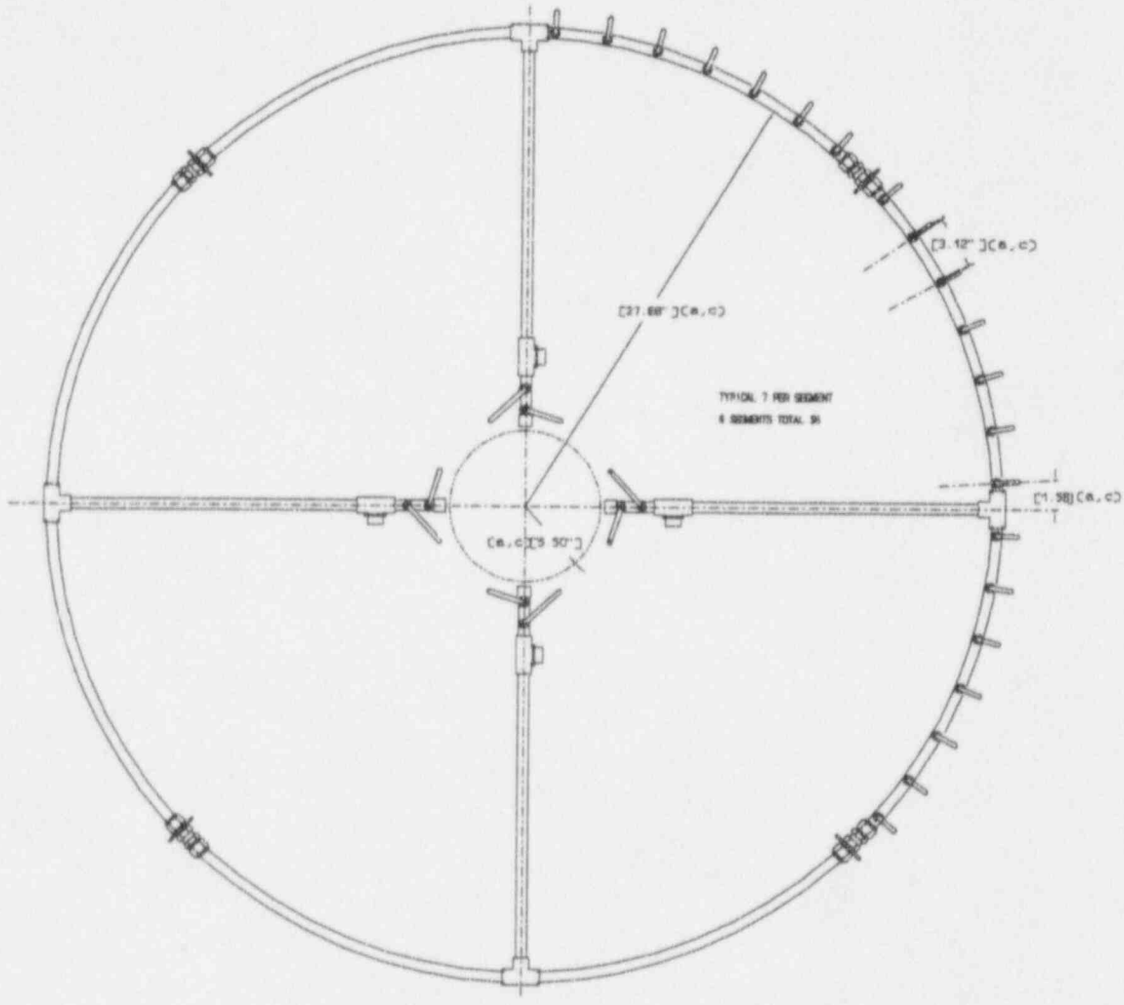

Figure 8-68 Large Scale Test Water Film Distributor

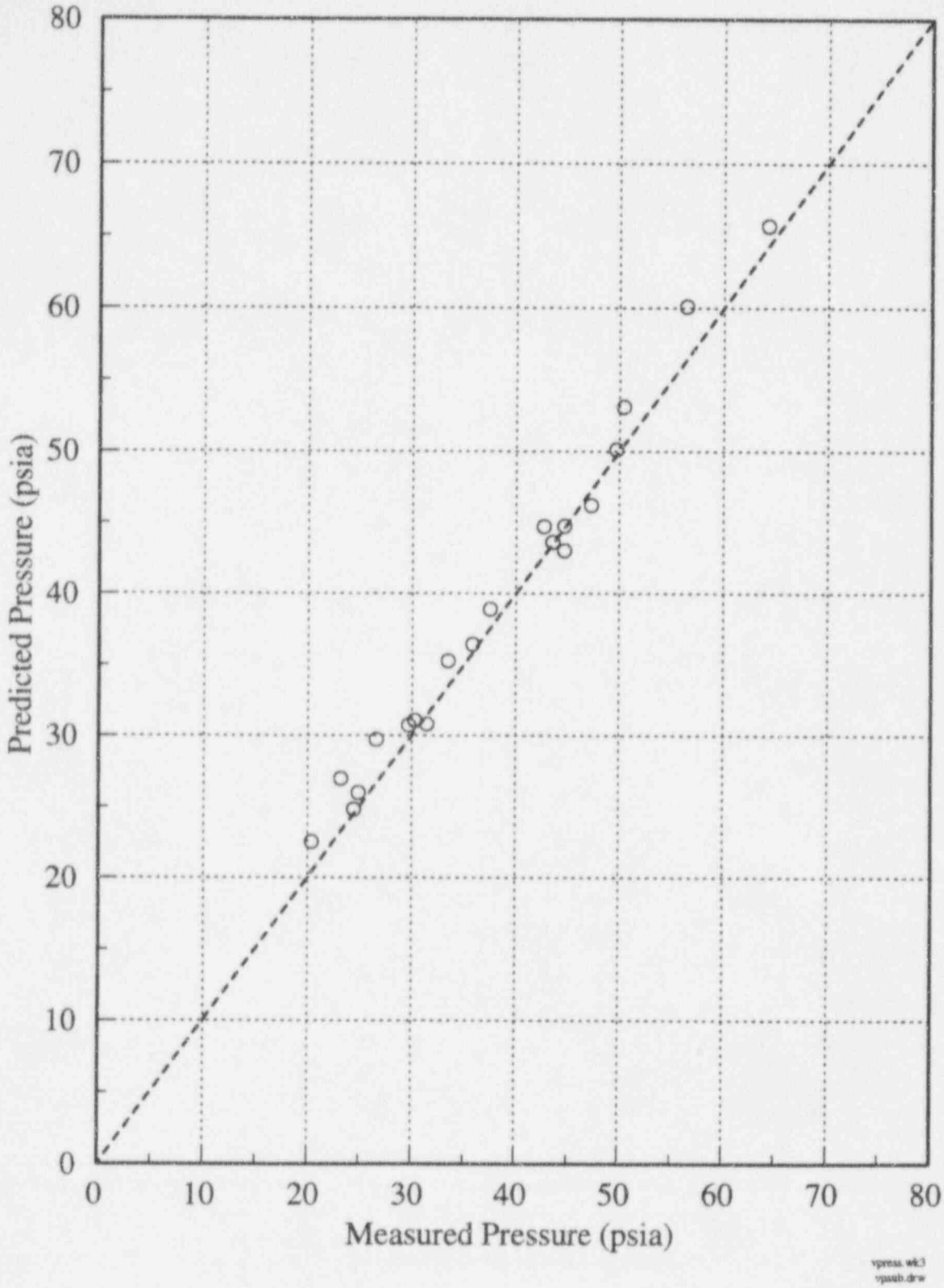

Figure 8-69 LST Distributed Parameter Predicted vs. Measured Steady-State Vessel Pressure

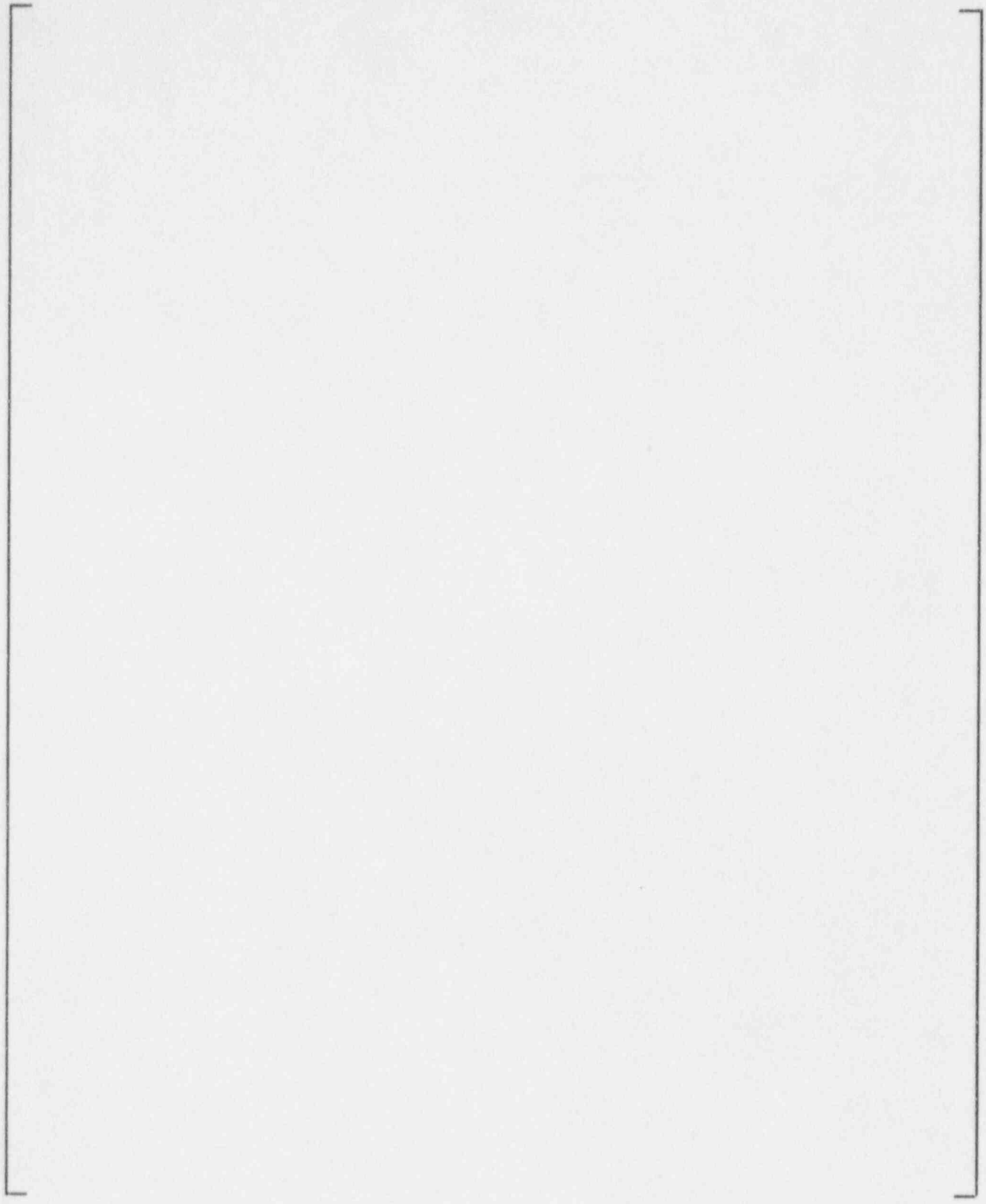

a,c

Figure 8-70 Measured and Lumped Parameter Predicted Air Pressure Ratios for Test 222.1

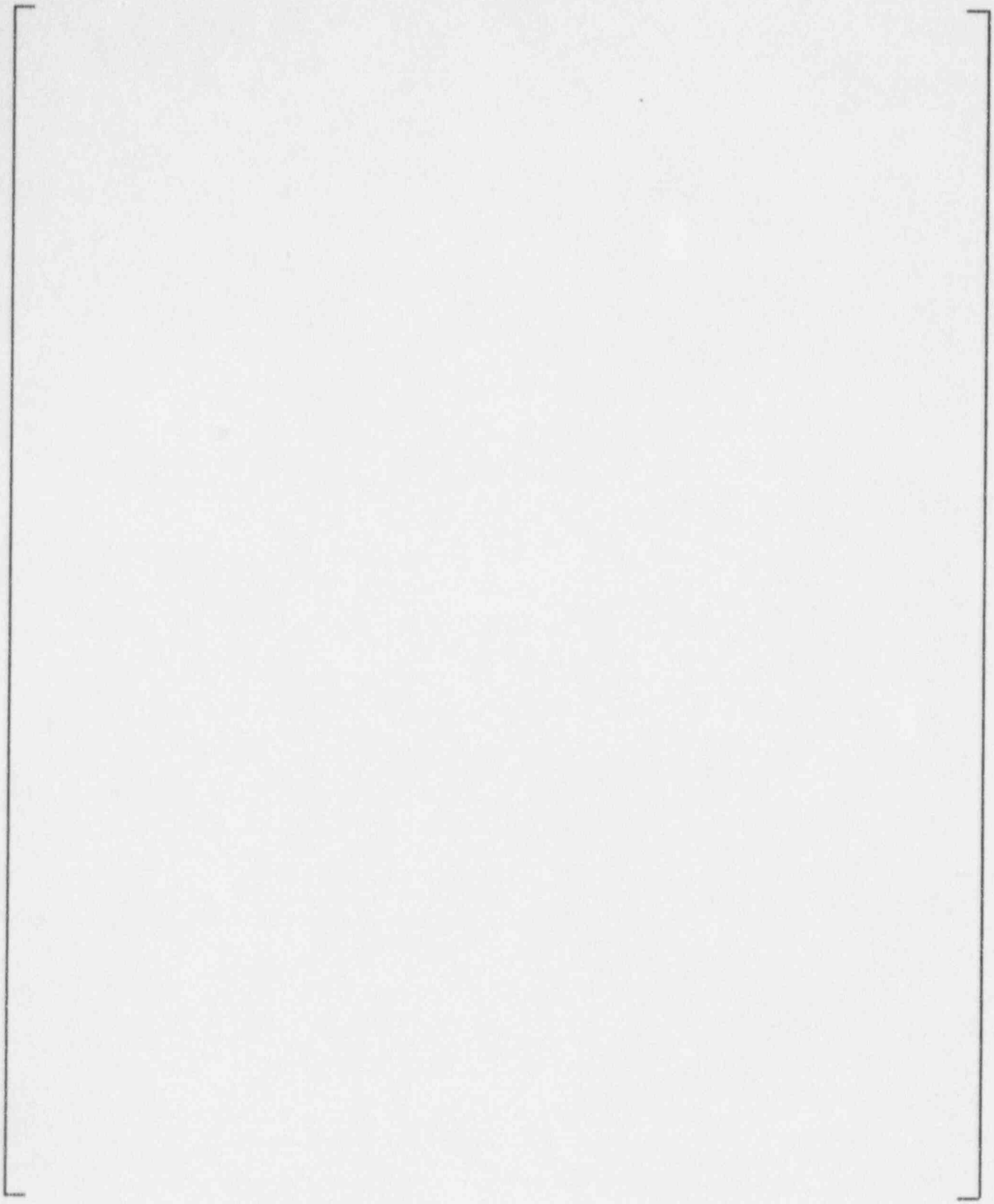

Figure 8-71 Measured and Lumped Parameter Predicted Vessel Pressure for Test 222.1

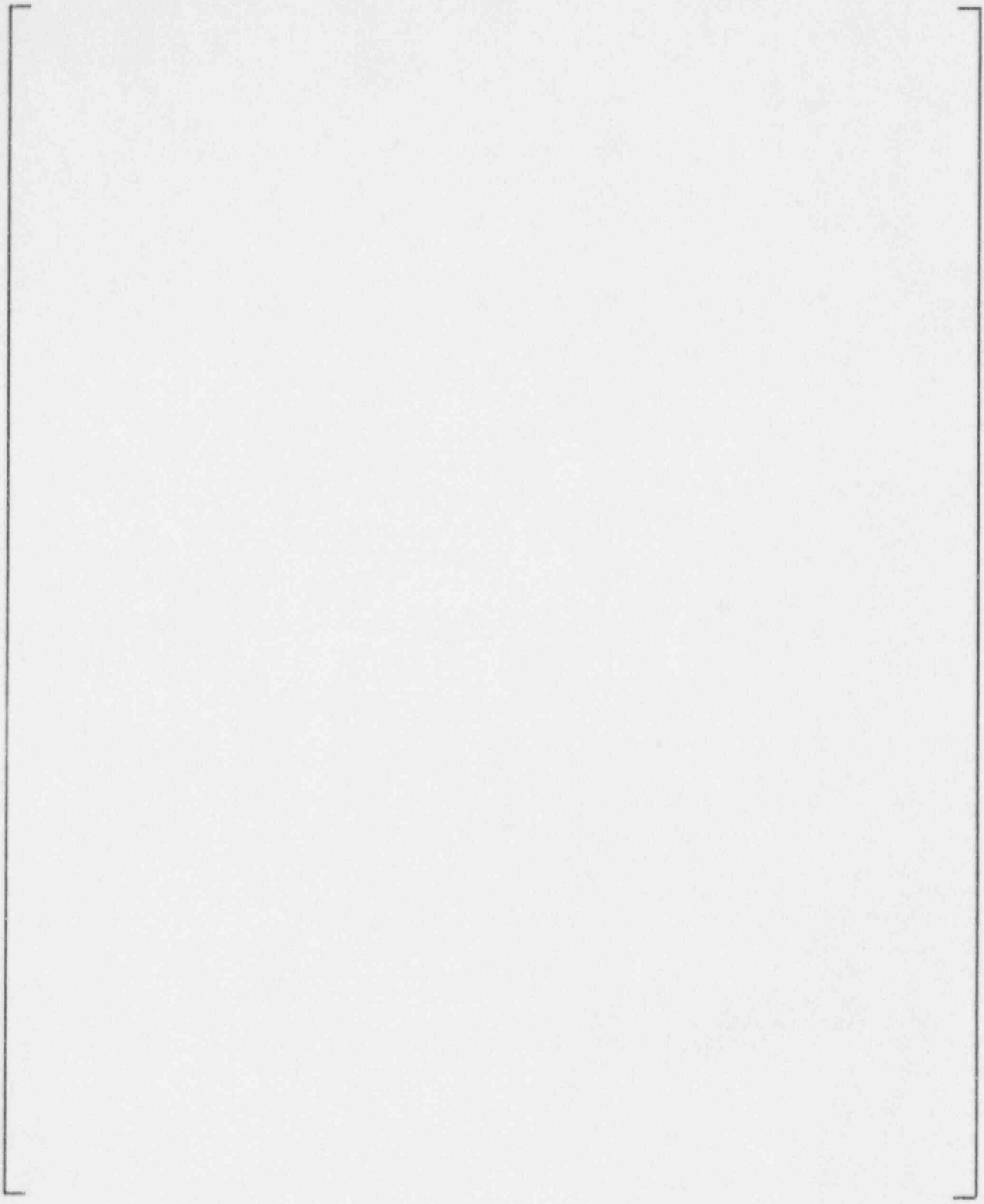

Figure 8-72 Measured and Lumped Parameter Predicted Vessel Pressure for Tests 212.1A, 212.1B, and 212.1C

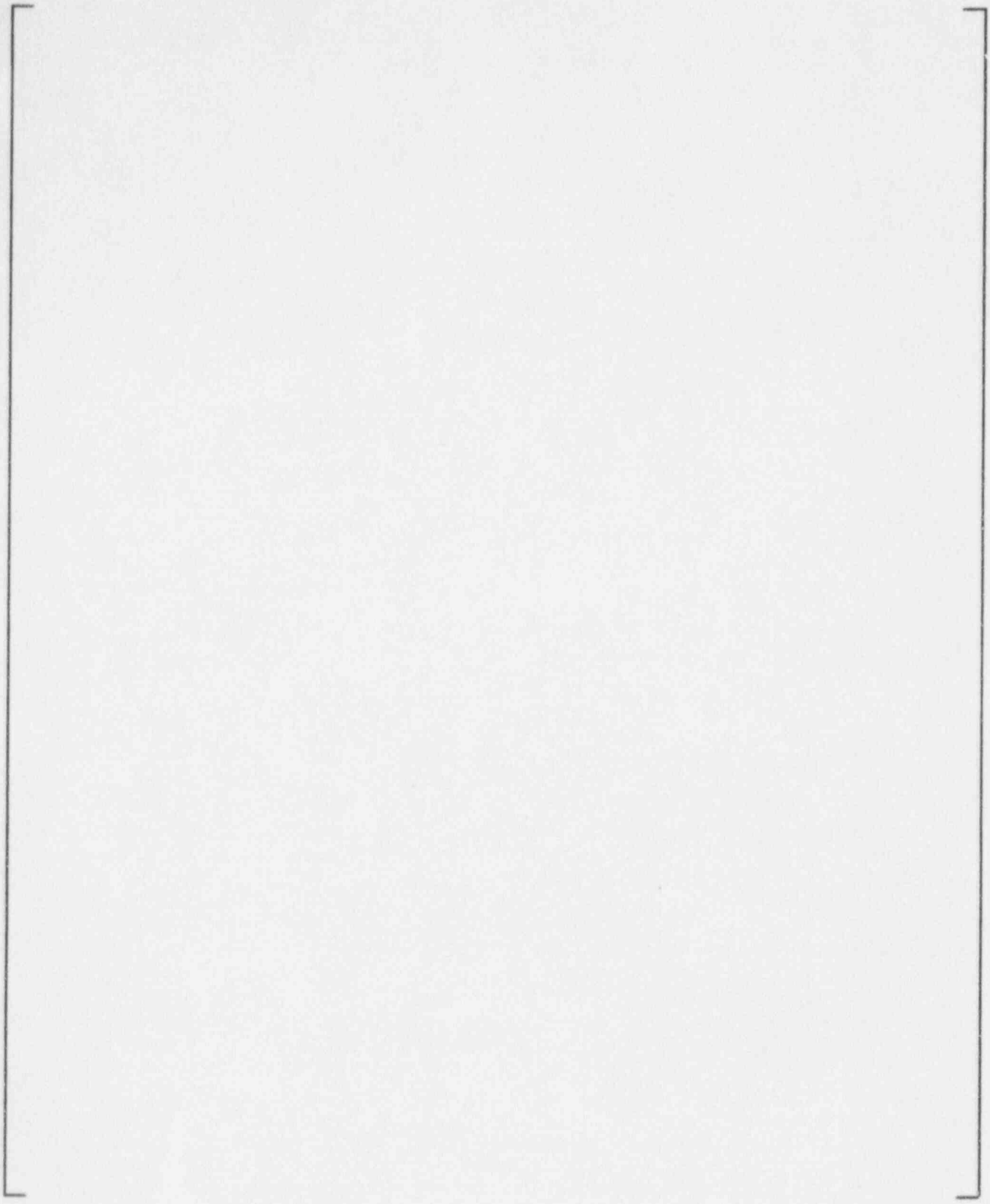

Figure 8-73 Measured and Lumped Parameter Predicted Vessel Pressure for Tests 214.1A and 214.1B

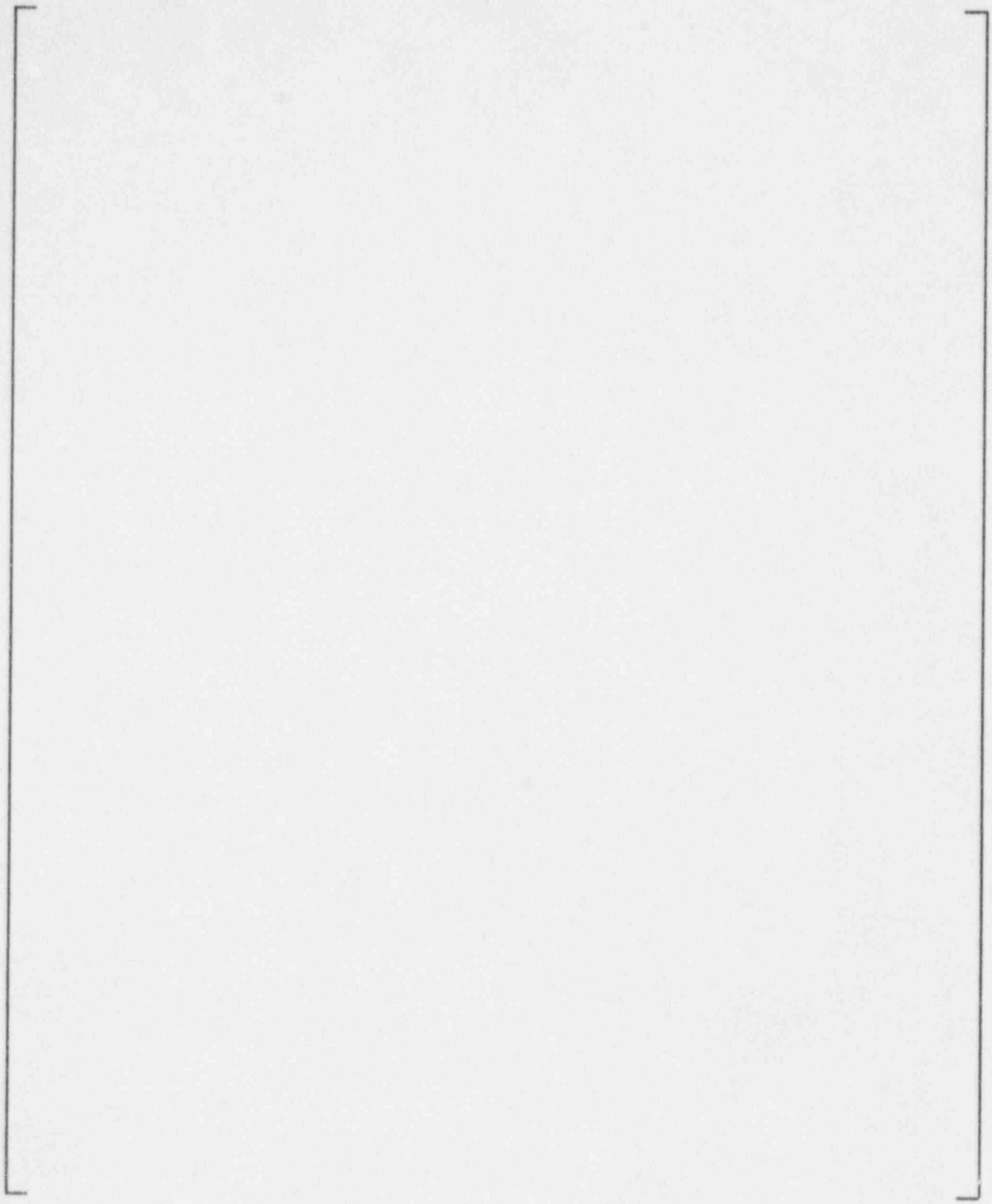

Figure 8-74 Measured and Lumped Parameter Predicted Vessel Pressure for Tests 216.1A and 216.1B

a,c

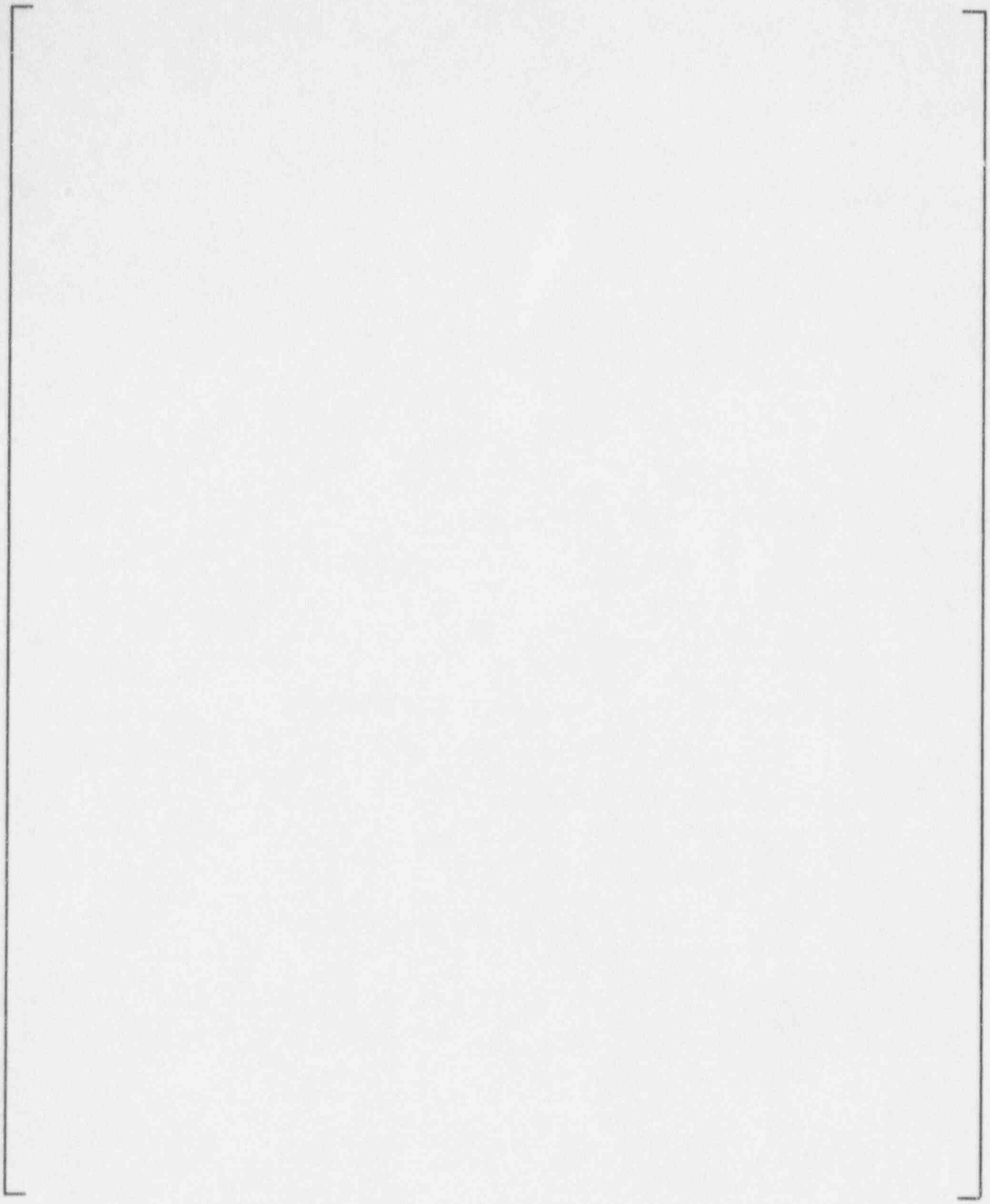

Figure 8-75 Measured and Lumped Parameter Predicted Vessel Pressure for Tests 219.1A and 219.1B, and 219.1C

a,c

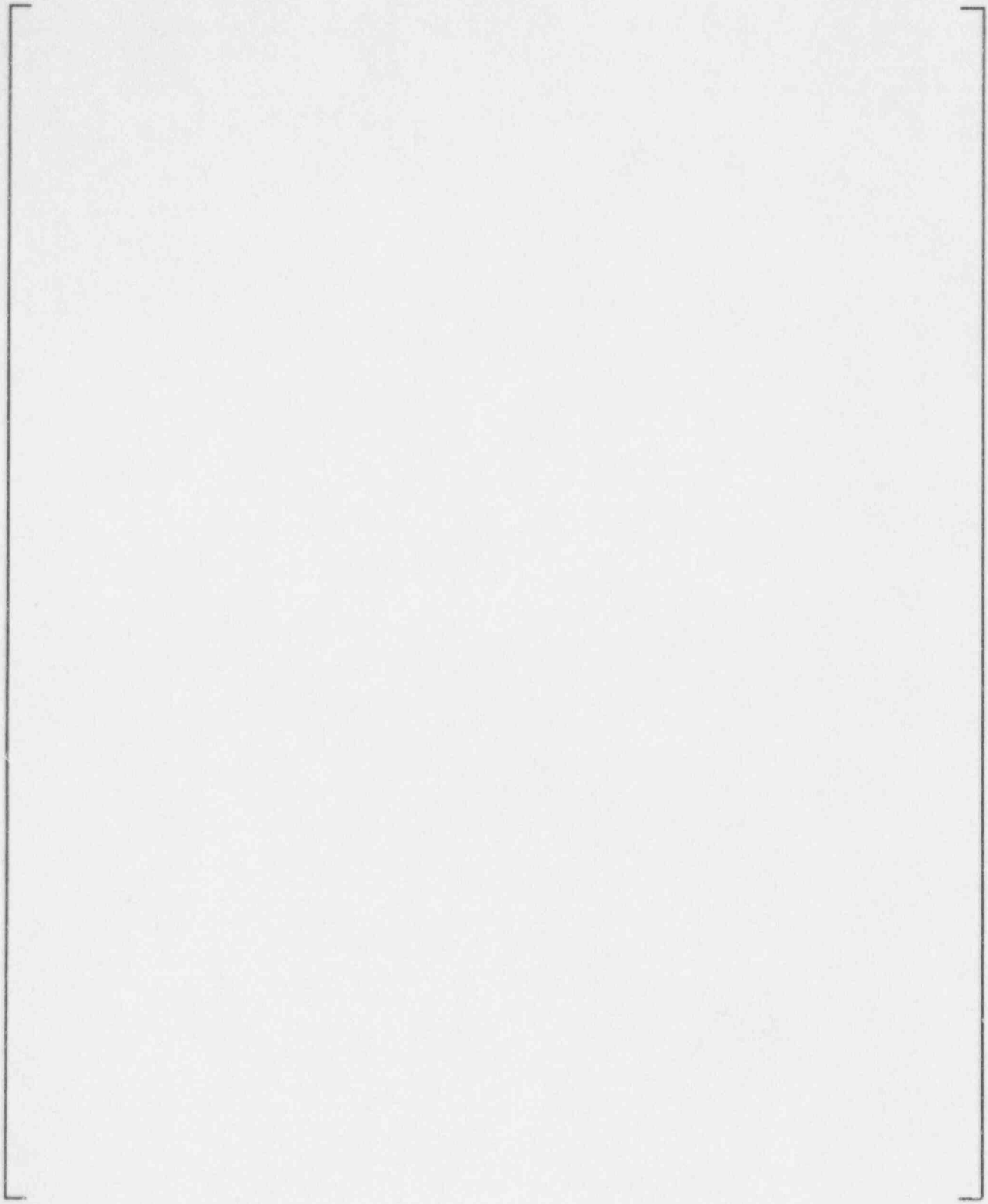

Figure 8-76 Measured and Lumped Parameter Predicted Vessel Pressure for Tests 222.4A and 222.4B

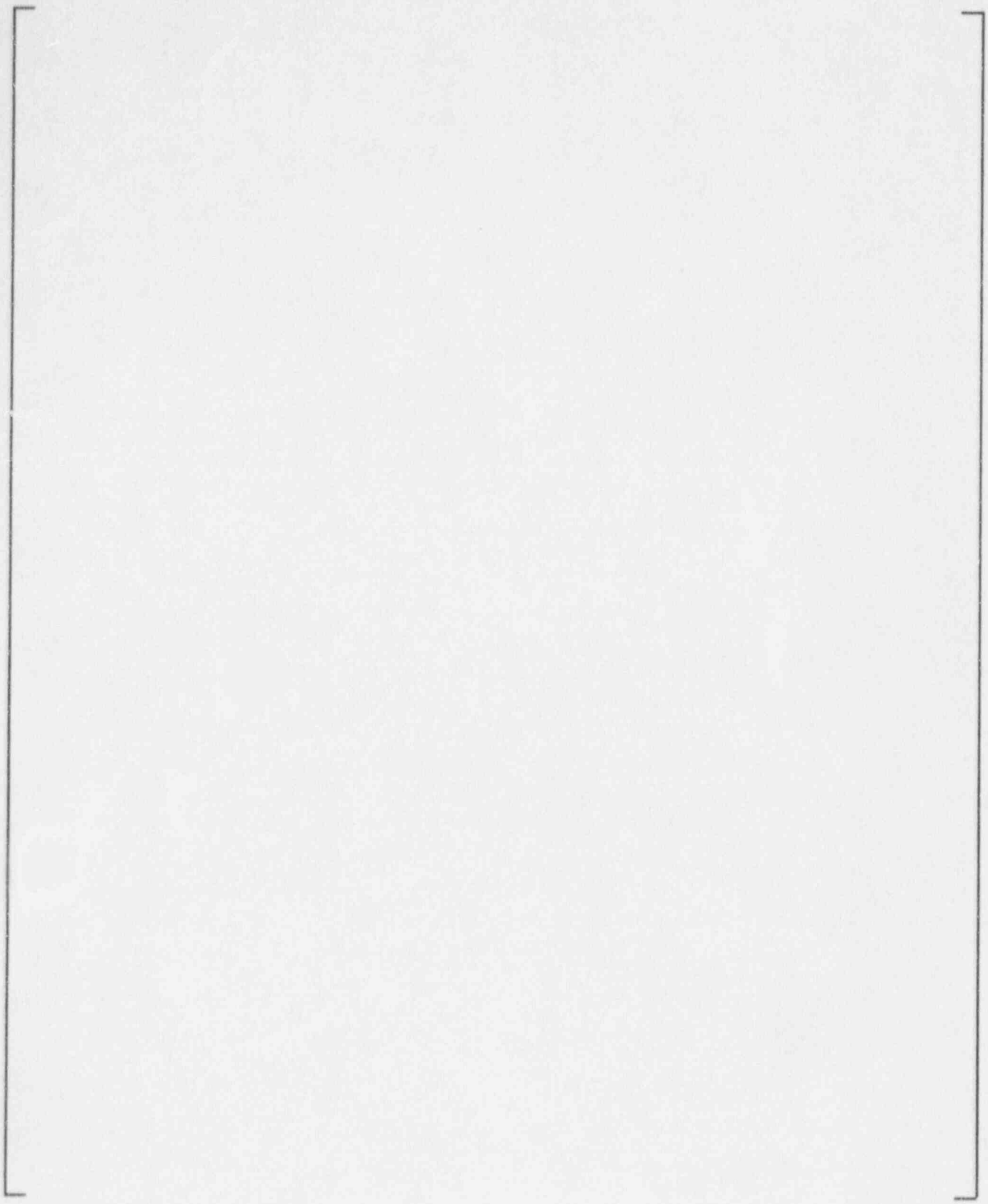

Figure 8-77 Measured and Lumped Parameter Predicted Air Pressure Ratios for Test 222.4A

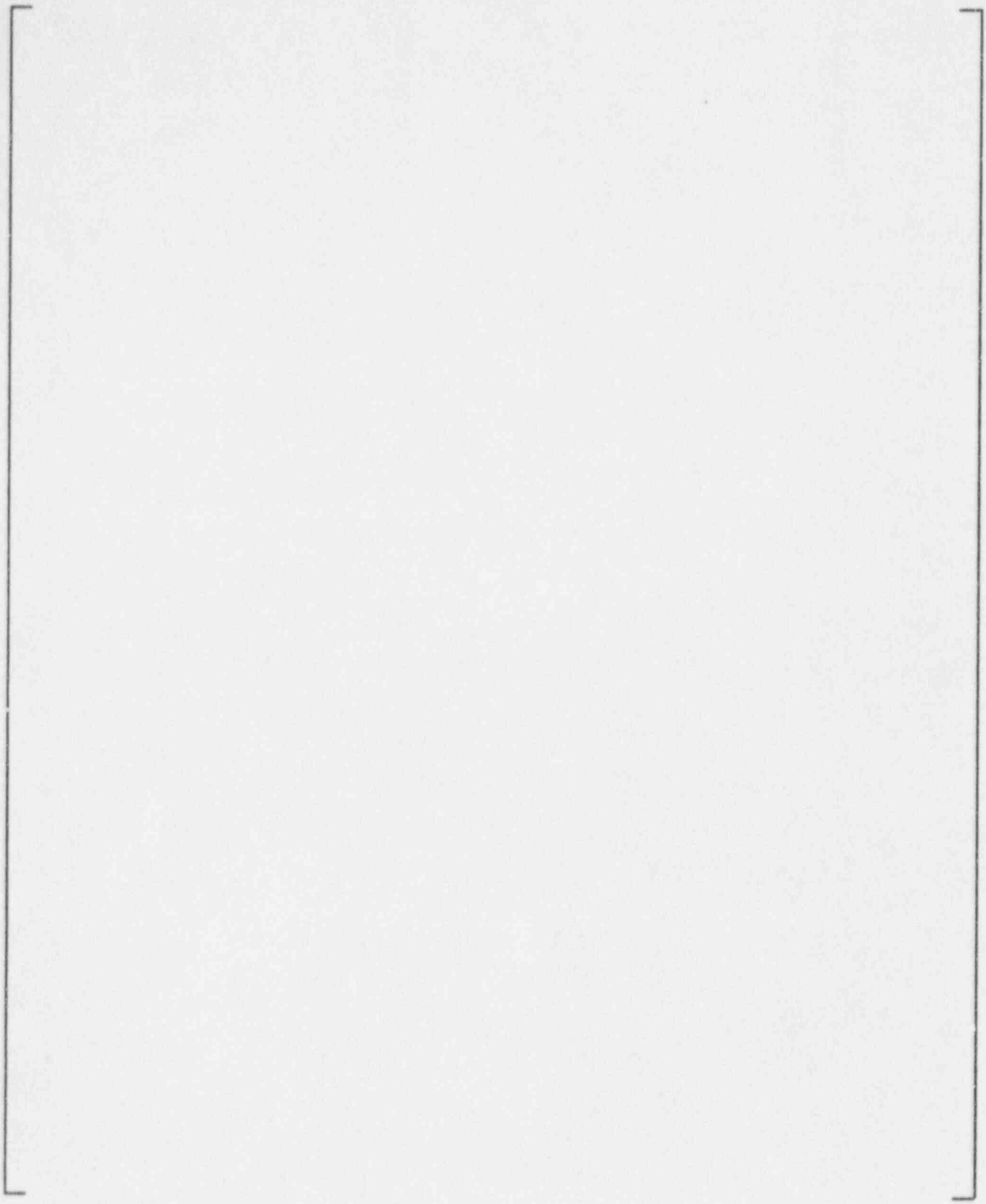

Figure 8-78 Measured and Lumped Parameter Predicted Air Pressure Ratios for Test 222.4B

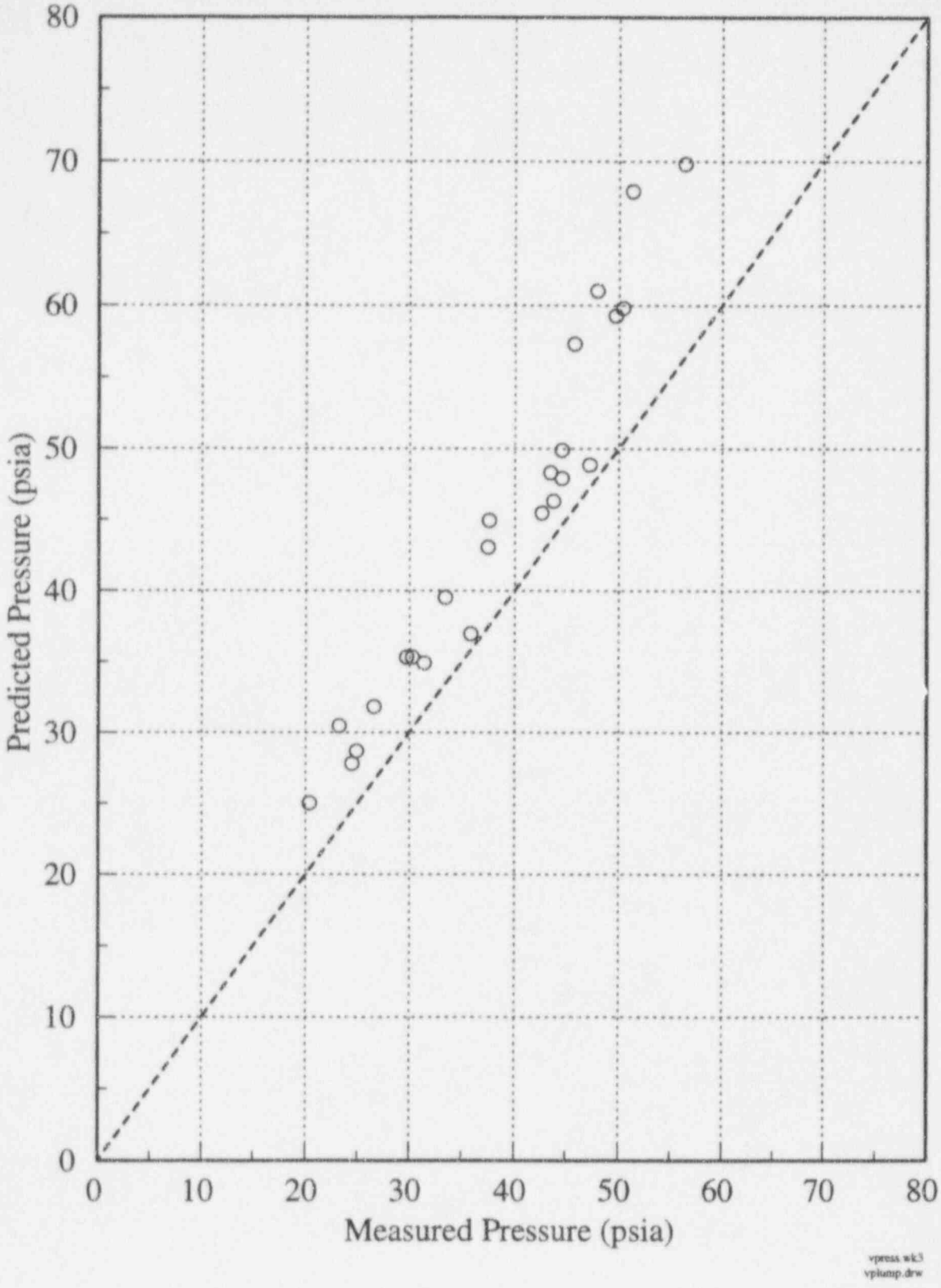

Figure 8-79 LST Lumped Parameter Predicted Versus Measured Steady-State Vessel Pressure

9.0 UNCERTAINTY OF WGOTHIC CALCULATION OF CONTAINMENT PRESSURE

This section addresses the uncertainties associated with the WGOTHIC code prediction of peak containment pressure during loss-of-coolant accident (LOCA) and main steam line break (MSLB) design basis accidents (DBAs). This section considers only those uncertainties, associated with the WGOTHIC code and its analytical models. Additional uncertainties, having to do with application to AP600, will be addressed in other documents. Section 9.4 identifies, but does not quantify, the uncertainties that must be considered for application of WGOTHIC to AP600. Uncertainties for application to AP600 will be addressed in a separate document.

The AP600 passive containment cooling system (PCS) differs from the active heat removal systems used in standard plants. Consequently, the performance and effect of the PCS must be evaluated and the uncertainties on performance evaluated. The PCS removes containment energy, mainly by the evaporation of water on the outside of the containment shell. Following a pipe break, the containment atmosphere heats and transfers energy into the internal heat sinks and the shell. Heat conduction through the shell has a time constant on the order of a few hundred seconds; therefore, events inside the containment are not influenced by the PCS for a few hundred seconds. During this initial time period, containment pressurization is no different than that of a typical dry containment plant, so standard analytical methods are acceptable. The LOCA blowdown pressure peaks at approximately 24 seconds for a LOCA event, and at approximately 200 seconds for a MSLB event. Both occur before the PCS can influence events inside the containment. Consequently, standard analytical methods, addressed in the AP600 *Standard Safety Analysis Report* (SSAR), (17) will be applied to the LOCA blowdown and the MSLB pressure peaks.

The WGOTHIC code and evaluation model are used to predict the LOCA peak containment pressure that occurs at 1000 to 2000 seconds, and the containment pressure at 24 hours after the event. A distributed parameter WGOTHIC evaluation model was developed to calculate the LOCA peak containment pressure, and a lumped-parameter evaluation model was developed to calculate the containment pressure at 24 hours. The containment pressure at both of these points is strongly influenced by PCS heat removal, and thus, by phenomena that are unique to AP600 (in contrast to standard plants).

9.1 Analytical Approach to Code Pressure Calculation Uncertainty

Distributed parameter evaluation model predictions were made for 20 large scale tests and lumped parameter model predictions were made for 22 large scale tests. This subsection discusses the analytical approach used to determine the code pressure calculation uncertainty for each evaluation model. The large-scale tests selected for comparisons were presented in Section 8.0.

The goal of this analysis is to define a multiplier, F_m, that, when multiplied by the WGOTHIC-predicted pressure, will produce a pressure, $P_{95\%}$, that exceeds the actual LST pressure 95 percent of the time. This is accomplished by calculating values of F_m for the second LOCA pressure peak and for the pressure at 24 hours. As shown in Sections 9.3 and 9.4, the WGOTHIC predictions for the

lumped parameter and distributed parameter evaluation models both show a consistent bias for overpredicting pressure. The parameters F_m and $P_{95\%}$ are related to the WGOTHIC pressure prediction $P_{WGOTHIC}$ by the following equation:

$$P_{95\%} = F_m P_{WGOTHIC} \tag{9-1}$$

The normalized error for test i is

$$e_i = \frac{P_i - M_i}{M_i} \tag{9-2}$$

where:

P_i = the pressure predicted for test i by WGOTHIC
M_i = the pressure measured in test i

The sample variance is

$$s^2 = \sum_{i=1}^{n} \frac{(\bar{e} - e_i)}{n} \tag{9-3}$$

where n is the number of tests in the sample population, and the bias is

$$\bar{e} = \sum_{i=1}^{n} \frac{e_i}{n} \tag{9-4}$$

The population variance is

$$\sigma^2 = s^2 \frac{n}{(n-1)} \tag{9-5}$$

The prediction multiplier is

$$F_m = \frac{1}{(1+\delta)} \tag{9-6}$$

where

$$\delta = \bar{e} - 1.645\sigma$$

It is expected that the difference between the predicted and measured pressures is proportional to the measured pressure. Thus, the statistical analyses were performed for the normalized error of each test prediction. It was also assumed that the normalized errors are normally distributed. Frequency distributions are presented in Sections 9.3 and 9.4 to verify this assumption.

9.2 Code Uncertainty Validation Range

Condensation mass transfer, evaporation mass transfer, and heat transfer to the subcooled external film were identified as the dominant transport phenomena in the PIRT.[2] The following are equations for internal condensation on the evaporating and subcooled surface areas:

$$\frac{\dot{m}_{cond}}{\dot{m}_{in}} = C_1 \frac{Gr^{n-1/3}}{Sc^{1-n}} \left(\frac{\Delta\rho}{\rho}\right)^{1/3} \frac{T_{in}}{T_{bl}} \ln\left(\frac{P_{nc,surf}}{P_{nc,ct}}\right) \frac{(\nu g)^{1/3} A}{Q_{in}} \tag{9-7}$$

where A is either the evaporating area or the subcooled area. The equation for external evaporation is

$$\frac{\dot{m}_{evap}}{\dot{m}_{in}} = \frac{0.023}{Sc^{2/3}} \frac{T_{in}}{T_{bl}} \frac{\ln(P_{nc,ri}/P_{nc,surf})}{R^{0.2}} \frac{v_{ri} A_{evap}}{Q_{in}} \tag{9-8}$$

where:

$\dot{m}_{cond}$ = condensation mass transfer rate
$\dot{m}_{in}$ = steam source mass flow rate
$\dot{m}_{evap}$ = evaporation mass transfer rate
C_1,n = coefficient and exponent on the free convection heat transfer correlation

$$Nu = C_1 Gr^n Pr^n$$

Gr = containment internal Grashof number based on height
Sc = Schmidt number
Pr = Prandtl number
Re = riser Reynolds number based on hydraulic diameter
$\Delta\rho$ = difference between the containment gas density and the gas at the liquid film surface
ρ = containment gas density
T_{in} = steam source temperature as it enters containment
T_{bl} = boundary layer temperature, defined as the average of the containment gas and the saturation temperature of the surface of the condensing film
$P_{nc,surf}$ = noncondensible gas partial pressure at the condensing or evaporating surface
$P_{nc,ct}$ = noncondensible gas partial pressure in containment
$P_{nc,ri}$ = noncondensible gas partial pressure in the riser

ν = the internal boundary layer kinematic viscosity
g = acceleration due to gravity
v_{ri} = riser bulk velocity
Q_{in} = steam source volumetric flow rate

Both equations result from normalizing the steady-state mass transport equations with the steam source mass flow rate. Table 9-1 lists dimensionless operating parameters for each test that can be used to characterize the condensation, evaporation, and subcooled mass transfer. The numerator of the last term in each equation is represented by Q in Table 9-1.

The Schmidt number and temperature ratios are limited in range (the SSAR will show that the LST range is approximately equal to the AP600 range) and, therefore, are not included in Table 9-1. The Schmidt number range inside the containment was $0.51 < Sc < 0.52$ for tests without helium and ranged up to $Sc = 0.72$ with helium. The temperature ratio for both groups is based on absolute temperatures and is limited in range to approximately $1.09 < T_{in}/T_{bl} < 1.36$ inside containment and 1.23 to 1.45 outside containment. The value of n and C_1 correspond to the coefficient and exponent on the free convection correlation chosen. The McAdams correlation values are 1/3 and 0.13, respectively. The characteristic parameters could only be determined for large-scale tests with internal noncondensible gas concentration measurements. Noncondensible measurements are not available for tests 202.2 and 214.1, so characteristic parameters could not be determined for those tests.

The evaluation model pressure uncertainty must account for individual pressure variations due to the following:

- Deviation of the LST pressure measurement from the actual pressure
- LST nodalization
- Test initial and boundary conditions
- Phenomenological model uncertainties
- Velocity, temperature and gas species concentration fields

The WGOTHIC predictions and measurements embody all of these contributions to the pressure uncertainty. Therefore, it can be stated that there is a 95-percent probability that the pressure for another LST, with parameters lying within the range of those in Table 9-1, will be less than $F_m P_{WGOTHIC}$. Predictions for another LST with parameters lying outside the range of those in Table 9-1, or for AP600 that differ in other respects from the LST test configuration and parameters, require consideration of additional uncertainties discussed in Section 9.6.

9.3 Pressure Uncertainty on Second LOCA Peak

A WGOTHIC distributed parameter evaluation model was developed and used to predict the vessel pressure for 20 LST data points discussed in Section 8.1. The 20 tests are identified and the predicted and measured pressures are compared in Table 9-2.

A statistical analysis of the distributed parameter WGOTHIC evaluation model predictions of the large scale tests was performed as discussed in Section 9.1 and the results are summarized in Table 9-3. The histogram of the normalized prediction error, presented in Figure 9-1, shows that the distribution is a reasonable approximation to a normal population. Consequently, the statistical analysis presented in Section 9.1 is appropriate.

The mean and 95 percent probability limit are compared to the data in Figure 9-2. The mean prediction is biased slightly higher than the measurements. The resulting net error is -0.043, so the value of the pressure multiplier is $F_m = 1.045$. Consequently the pressure at 95-percent probability is $P_{95\%} = 1.045P_{WGOTHIC}$.

9.4 Pressure Uncertainty at 24 Hours

A WGOTHIC lumped-parameter model was developed and used to predict the vessel pressure for 22 LST data points as discussed in Section 8.2. The 22 tests are listed in Table 9-4 with a comparison of the predicted and measured pressures.

A statistical analysis was performed on the lumped-parameter model predictions as discussed in Section 9.1 and the results are summarized in Table 9-5. The histogram of the normalized error is presented in Figure 9-3. The distribution shows that the assumption of a normal population is reasonable.

The mean and 95-percent probability limit are compared to the measurements in Figure 9-4. The mean prediction is biased well above the measurements, for reasons discussed in Section 5.3. The resulting net error is +0.030 and the pressure multiplier is $F_m = 0.974$. Consequently there is a 95-percent probability that the actual pressure is less than $0.975P_{WGOTHIC}$. In this case, the bias is so high that even with uncertainty, the predicted pressure is still 2.5 percent higher than the expected pressure.

9.5 Time Step Size and Convergence

Any errors due to time step size and convergence are already embodied in the code uncertainties presented in Sections 9.3 and 9.4, so it is not necessary to consider them separately. It is important, however, for confidence in the code predictions, to know that convergence and stability do not comprise significant errors.

A design review group (DRG), comprised of nationally recognized nuclear thermal-hydraulic code experts, was convened by Electric Power Research Institute (EPRI) to review GOTHIC Version 3.4d[33]. The expert review team concluded:

> "Based on the DRG test cases, reports by users, and the technical review, the DRG concludes that the solution technique of GOTHIC_S is stable and convergent."

To further evaluate GOTHIC convergence and stability, as well as to evaluate the convergence and stability of the code modifications embodied in WGOTHIC, the effect of the time step on the predicted pressure was examined by halving the time step for one of the large scale tests. LST 212.1 was analyzed with both the lumped-parameter and distributed parameter evaluation models, and the results were compared to the calculations using the standard time step. The comparisons showed that the largest change during the steady-state or transient portion, was less than 2 percent; for the distributed parameter evaluation model.

9.6 Application of Pressure Uncertainty to AP600 Calculations

The pressure uncertainties determined in Sections 9.3 and 9.4 were qualified to define their range of applicability. In general, the range of applicability was limited to the code version, noding option, momentum equation form, and heat transfer models selected, as well as the dominant non-dimensional parameters characterizing the test. The peak pressure calculation for AP600 requires that any differences between AP600 and the test basis be identified, and for each difference, any bias and uncertainty be evaluated and combined with the uncertainty considered in Sections 9.3 and 9.4.

The characteristics for which uncertainties should be considered are

- Internal Scale – AP600 is approximately 8 times larger than the LST.
- External Scale – The LST riser hydraulic diameter is 1/3 that of AP600 while the vertical scale is 1/8 that of AP600.
- Geometry – The LST had no flow communication between the simulated below-deck compartments and the steam generator compartment.
- Dimensionless Groups – The AP600 internal Grashof number is approximately 8^3 times that of the LST. The AP600 riser Reynolds number is 3.5 times the highest large scale test value.
- The LST internal heat sinks have little effect on the steady-state pressure, while in AP600 the internal heat sinks are significant until a few thousand seconds into the LOCA transient.

The identification and evaluation of the additional uncertainties for application of the WGOTHIC models to AP600 will be addressed separately.

TABLE 9-1
RANGE OF MEASURED LST OPERATING PARAMETERS FOR WGOTHIC DISTRIBUTED PARAMETER MODEL UNCERTAINTIES

	Condensation Parameters Inside Containment				Evaporation Parameters in Riser			Condensation Parameters to Subcooled Liquid			
Test	$\Delta\rho/\rho$	$\ln(P_{s2}/P_{s1})$	Gr	Q/Q_{in}	Re	$\ln(P_{s2}/P_{s1})$	Q/Q_{in}	$\Delta\rho/\rho$	$\ln(P_{s2}/P_{s1})$	Gr	Q/Q_{in}
212.1A	0.206	0.421	1.28e12	14.5	32200	0.214	1103	.307	.517	2.07e12	3.27
212.1B	0.235	0.508	1.94e12	11.3	32385	0.307	925	.357	.631	3.22e12	2.27
212.1C	0.260	0.634	2.95e12	8.62	31573	0.463	746	.405	.797	5.05e12	1.47
213.1A	0.209	0.422	1.27e12	17.6	32450	0.213	1338	.308	.516	2.02e12	1.17
213.1B	0.232	0.527	1.84e12	11.1	28289	0.347	792	.359	.665	3.10e12	0.87
216.1A	0.241	0.707	2.02e12	8.47	28806	0.477	632	0.392	0.901	3.58e12	1.80
216.1B	0.275	1.056	4.50e12	3.71	29416	0.968	329	0.452	1.344	8.02e12	0.79
217.1A	0.282	0.748	3.84e12	5.70	33100	0.586	541	.436	.938	6.51e12	1.09
217.1B	0.291	0.718	4.89e12	6.35	32884	0.630	623	.431	.889	7.86e12	1.26
218.1A	0.281	0.789	3.79e12	6.56	32557	0.623	612	.437	.990	6.46e12	1.03
218.1B	0.294	0.737	4.73e12	6.93	32148	0.651	666	.436	.919	7.61e12	1.16
219.1A	0.072	0.118	7.10e11	76.1	31861	dry	0	-	-	-	-
219.1B	0.072	0.128	8.03e11	81.4	29681	dry	0	-	-	-	-
219.1C	0.091	0.184	3.74e11	49.1	35529	0.059	3644	.066	.205	0.28e12	4.00
221.1A	0.155	0.264	7.46e11	33.6	32553	0.106	2422	.216	.314	1.10e12	1.25
221.1B	0.079	0.222	3.47e11	42.3	32209	0.081	3003	.045	.255	2.07e12	3.20
222.1	0.253	0.583	2.41e12	10.8	32956	0.379	930	.407	.741	4.30e12	1.75
224.1	0.166	0.193	3.69e12	27.3	34137	0.133	2590	.245	.224	5.94e12	9.57
224.2	0.219	0.358	6.05e12	15.2	32881	0.320	1500	.345	.433	10.7e12	4.51

TABLE 9-2
COMPARISON OF MEASURED AND WGOTHIC DISTRIBUTED PARAMETER MODEL PREDICTIONS OF LST PRESSURES

Large-Scale Test	Measured (psia)	Predicted (psia)	Pred Meas	Large-Scale Test	Measured (psia)	Predicted (psia)	Pred Meas
202.3	[ ] a,b	[ ] a,c	0.96	218.1A	[ ] a,b	[ ] a,c	1.00
212.1A	[ ]	[ ]	1.04	218.1B	[ ]	[ ]	1.05
212.1B	[ ]	[ ]	1.03	219.1A	[ ]	[ ]	1.02
212.1C	[ ]	[ ]	1.04	219.1B	[ ]	[ ]	1.05
213.1A	[ ]	[ ]	1.01	219.1C	[ ]	[ ]	1.16
213.1B	[ ]	[ ]	1.03	221.1A	[ ]	[ ]	1.10
214.1A	[ ]	[ ]	0.98	221.1B	[ ]	[ ]	1.12
214.1B	[ ]	[ ]	1.00	221.1C	[ ]	[ ]	1.02
216.1A	[ ]	[ ]	0.98	222.1	[ ]	[ ]	1.05
216.1B	[ ]	[ ]	1.01	224.2	[ ]	[ ]	1.07

TABLE 9-3
STATISTICS ON WGOTHIC DISTRIBUTED PARAMETER MODEL PREDICTIONS OF LST

Mean (Bias)	n	s	σ	1.645σ	δ	F_m
0.0362	20	0.0469	0.0482	0.0792	-0.0430	1.045

TABLE 9-4
COMPARISON OF MEASURED AND WGOTHIC
LUMPED PARAMETER MODEL PREDICTIONS OF LST PRESSURES

Large Scale Test	Measured (psia)	Predicted (psia)	Pred / Meas	Large-Scale Test	Measured (psia)	Predicted (psia)	Pred / Meas
202.3	[ ]a,b	[ ]a,c	1.07	217.1B	[ ]a,b	[ ]a,c	1.32
212.1A	[ ]	[ ]	1.15	218.1A	[ ]	[ ]	1.11
212.1B	[ ]	[ ]	1.17	218.1B	[ ]	[ ]	1.19
212.1C	[ ]	[ ]	1.20	219.1A	[ ]	[ ]	1.03
213.1A	[ ]	[ ]	1.13	219.1B	[ ]	[ ]	1.07
213.1B	[ ]	[ ]	1.18	219.1C	[ ]	[ ]	1.31
214.1A	[ ]	[ ]	1.03	221.1A	[ ]	[ ]	1.22
214.1B	[ ]	[ ]	1.12	221.1B	[ ]	[ ]	1.19
216.1A	[ ]	[ ]	1.11	222.1	[ ]	[ ]	1.18
216.1B	[ ]	[ ]	1.19	224.1	[ ]	[ ]	1.25
217.1A	[ ]	[ ]	1.06	224.2	[ ]	[ ]	1.24

TABLE 9-5
STATISTICS ON WGOTHIC LUMPED
PARAMETER MODEL PREDICTIONS OF LST

Mean (Bias)	n	s	σ	1.645σ	δ	F_m
0.1610	22	0.0800	0.0819	0.1347	+0.0264	0.974

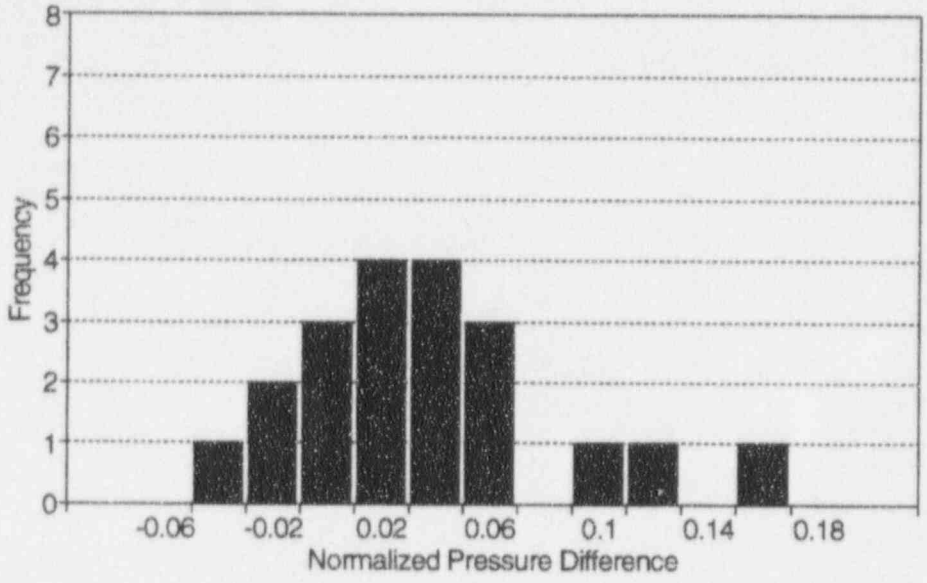

Figure 9-1 Frequency Distribution in Distributed Parameter WGOTHIC Predictions for LST

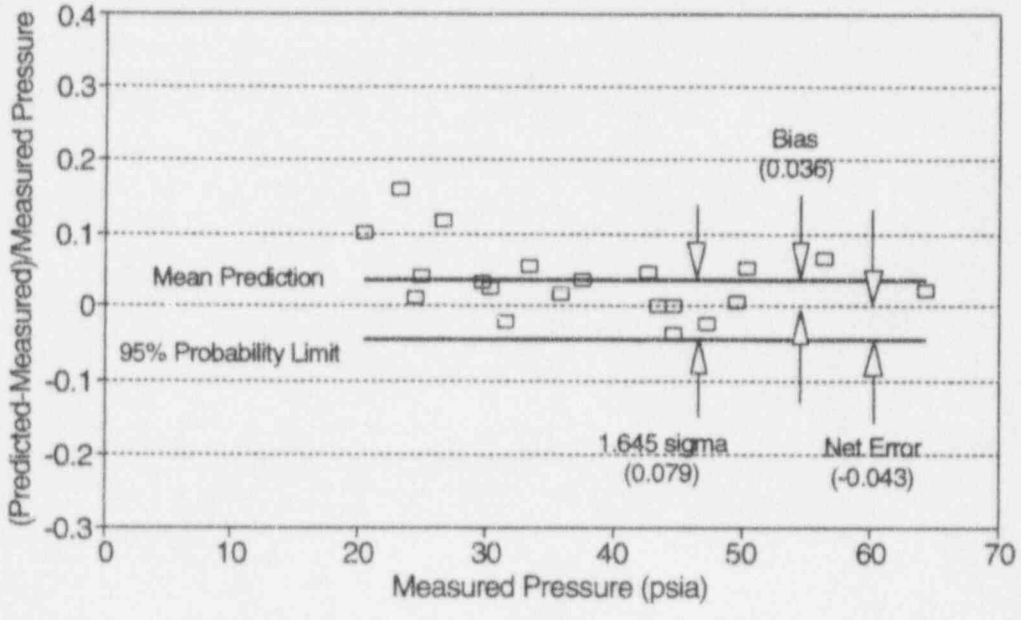

Figure 9-2 WGOTHIC Distributed Parameter Model Predictions of LST Measured Pressures

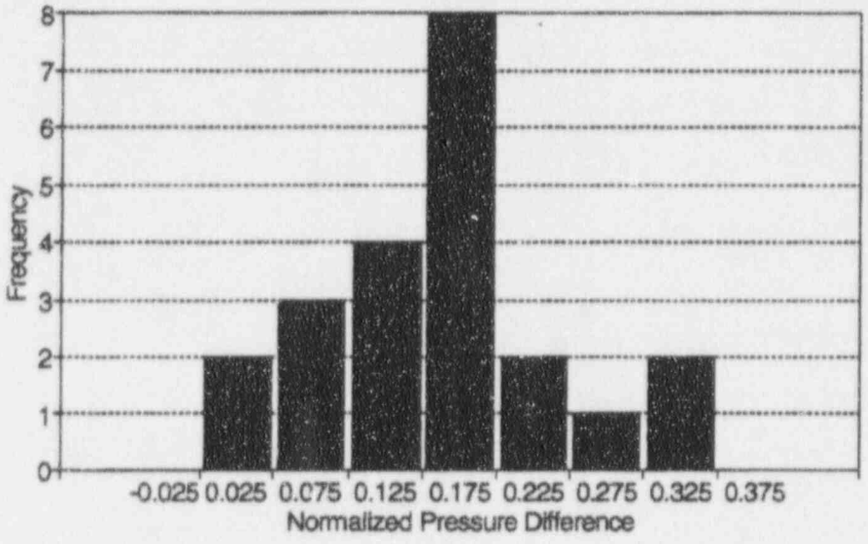

Figure 9-3 Frequency Distribution for WGOTHIC Lumped Parameter Predictions of LST

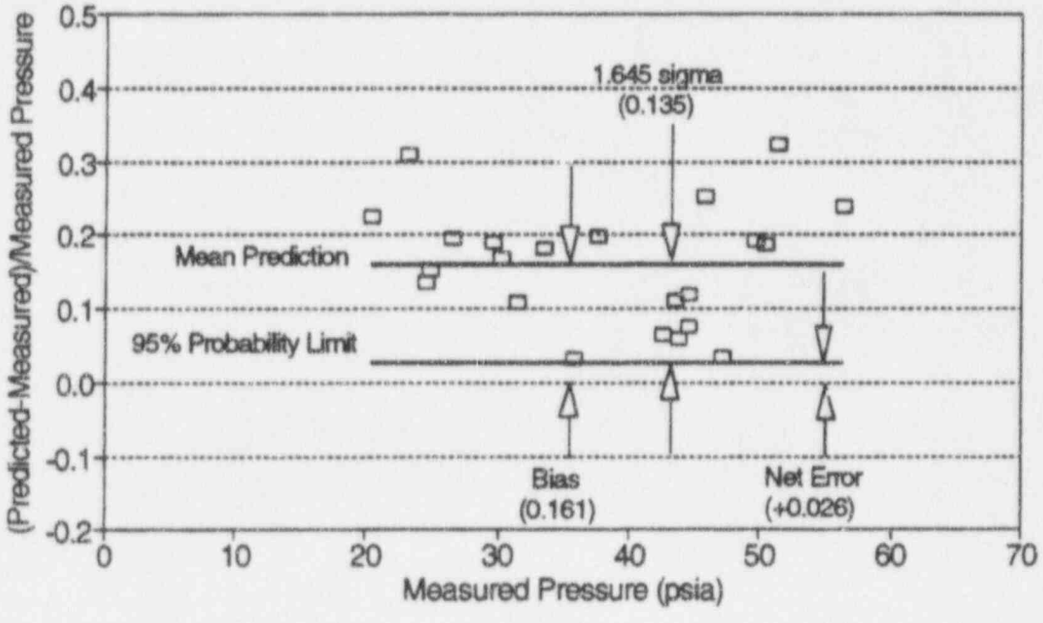

Figure 9-4 WGOTHIC Lumped Parameter Model Predictions of Measured LST Pressures

10.0 CONCLUSIONS

The containment pressurization during the blowdown phase of both the loss-of-coolant accident (LOCA) and main steam line break (MSLB) design basis accidents is not impacted by operation of the passive containment cooling system (PCS), so standard analytical methods are acceptable for calculating the pressure response over these periods. The calculation of the long-term containment pressure response during operation of the PCS requires a coupled solution of the equations for conduction, heat and mass transfer, and wall-to-wall radiant heat transfer. The PCS calculational methodology was developed and added to the GOTHIC code to create the Westinghouse-GOTHIC (WGOTHIC) code.

The heat and mass transfer correlations, the Clime solution methodology, and the lumped and distributed parameter noding structures that are used in the WGOTHIC code to model the heat transfer from the AP600 containment by the PCS have been validated using test data from laboratory-scale tests (for modeling local, separate effects heat and mass transfer) and from the large-scale PCS tests (for integral testing of the PCS heat and mass transfer). A number of separate effects heat and mass transfer tests utilizing geometries representative of the AP600 have been examined. These tests cover the range of expected conditions for heat and mass transfer within the AP600. The WGOTHIC code results were compared with measured data from these separate effects tests to validate the correlations and Clime solution methodology. The correlations were found to yield acceptable results with mean predicted-to-measured heat and mass transfer ratios near 1.0 over the expected range of dimensionless parameters during design basis accident (DBA) events in the AP600.

The WGOTHIC lumped and distributed parameter noding structures to be used in the DBA evaluation model were validated using data from the large-scale PCS tests. The distributed parameter model was found to yield acceptable results in all of the important validation parameters (pressure, local temperatures, local velocities, noncondensible gas concentrations, etc.). The lumped parameter model causes compensating errors with respect to velocity and the noncondensible gas distribution and as a result over-predicts the global pressure.

The uncertainties on the WGOTHIC distributed parameter and lumped parameter evaluation models were determined for the prediction of the large-scale PCS tests. Within the range of parameters characterizing the large-scale PCS tests, the pressure at 95 percent confidence is 1.037 times the pressure predicted by the distributed parameter evaluation model and 0.975 times the pressure predicted by the lumped parameter model.

11.0 REFERENCES

1. Tagami, Takasi, Interim Report on Safety Assessments and Facilities Establishment Project in Japan for Period Ending June, 1965 (No. 1).

2. Spencer, D. R., *Scaling Analysis for AP600 Passive Containment Cooling System,* WCAP-14190, October 1994, Westinghouse Electric Corporation, Proprietary.

3. Spencer, D. R., *ACRS Thermal-Hydraulics Subcommittee Meeting on AP600 PCS,* March 29, 1995, Westinghouse Electric Corporation, Proprietary.

4. George, T. L., *GOTHIC Containment Analysis Package Technical Manual,* Version 3.4, NAI 8907-06 , July 1991.

5. McAdams, W. H., *Heat Transmission*, Third Edition, McGraw-Hill, 1954.

6. Vliet, G. C., "Natural Convection Local Heat Transfer on Constant-Heat Flux Inclined Surfaces," *Journal of Heat Transfer*, November 1969, pp. 511-516.

7. Colburn, A. P., "A Method of Correlating Forced Convection Heat Transfer Data and a Comparison With Fluid Friction," *Transactions of the AIChE*, Vol. 29 1933, p. 174.

8. Boelter, L. M. K., G. Young, and H. W. Iverson, NACA TN 1451, 1948.

9. Burmeister, L. C., *Convective Heat Transfer*, John Wiley & Sons, 1983.

10. Schlichting, H., *Boundary Layer Theory*, Sixth Edition, McGraw-Hill.

11. Churchill, S. W., "Combined Free and Forced Convection Around Immersed Bodies" (Section 2.5.9) and "Combined Free and Forced Convection in Channels" (Section 2.5.10), *Heat Exchanger Design Handbook*, Hemisphere Publishing Corp., 1983.

12. Eckert, E. R. G. and A. J. Diaguila., "Convective Heat Transfer for Mixed, Free, and Forced Flow Through Tubes," *Transactions of the ASME*, May, 1954, pp. 497-504.

13. Chun, K. R., and R. A. Seban, "Heat Transfer to Evaporating Liquid Films," *J. Heat Transfer*, Vol. 93C, pp. 391-396, November 1971.

14. George, T. L., et al., *GOTHIC Containment Analysis Package Programmer's Manual for GOTHIC_S,* Version 3.4, NAI 8907-10, June 1991.

15. Wiles, L. E., et al., *GOTHIC Containment Analysis Package Qualification Report for GOTHIC_S*, NAI 8907-09, June 1991.

16. Ofstun, R. P., *Experimental Basis for the AP600 Containment Vessel Heat and Mass Transfer Correlations,* WCAP-14326, March 1995.

17. *AP600 Standard Safety Analysis Report* (SSAR).

18. Stewart, W. A., A. T. Pieczynski, and L. E. Conway, *Test of Heat Transfer and Water Film Evaporation on a Heated Plate Simulating Cooling of the AP600 Reactor Containment*, WCAP-12665 (WCAP-13341, Nonproprietary).

19. Huhtiniemi, I., A. Pernsteiner, and M. L. Corradini, *Condensation in the Presence of a Noncondensible Gas: Experimental Investigation*, WCAP-13308, April 1991 (published as WCAP in April 1992, Nonproprietary).

20. *Final Data Report for PCS Large-Scale Tests, Phase 2 and Phase 3*, WCAP-14135, July 1994.

21. Peters, F., AP600 1/8th Large-Scale Passive Containment Cooling System Heat Transfer Test Baseline Data Report, WCAP-13566, October, 1992.

22. Holman, J. P., Heat Transfer, 3rd Edition, McGraw-Hill, 1972, p. 91.

23. G. Hugot, "Study of the Natural Convection Between Two Planes, Vertical, Parallel and Isothermal Plates," Derived from Doctoral Dissertation University of Paris, 1972, Translated by D.R. de Boisblanc, EBASCo Services Incorporated, June, 1991.

24. Siegel, R. and R. H. Norris, "Test of Free Convection in a Partially Enclosed Space Between Two Heated Vertical Plates," Transaction of the ASME, Journal of Heat Transfer, April 1957.

25. Peterson, P. F., V. E. Schrock, T. Kageyama, "Diffusion Layer Theory for Turbulent Vapor Condensation with Noncondensible Gases," *Journal of Heat Transfer*, November 1993, Vol. 115, pp. 998-1003.

26. Jakob, M., *Heat Transfer*, John Wiley & Sons, 1967.

27. Gilliland, E. R. and T. K. Sherwood, "Diffusion of Vapors into Air Streams," *Industrial and Engineering Chemistry*, Vol. 26, No. 5, pp. 516-523.

28. *Heavy Water Reactor Facility (HWRF) Large Scale Passive Containment Cooling System Baseline Test Data Report*, HWRF-RPT-92-004, Feb. 1993.

29. Narula, J. S., and Woodcock, J., *Westinghouse - GOTHIC Distributed Parameter Modeling of HDR Test E11.2*, The Third International Conference on Containment Design and Operation, Volume 1, Toronto, Ontario, October 19-21, 1994.

30. Woodcock, J., et. al., *Westinghouse-GOTHIC: A Computer Code for Analyses of Thermal Hydraulic Transients for Nuclear Plant Containments and Auxiliary Buildings*, WCAP-13246.

31. Ofstun, R. P., and Spencer, D. R., *Large-Scale Test Data Evaluation*, PCS-T2R-050, May 1995.

32. Letter NTD-NRC-94-4260, N.J. Liparulo to Borchardt (NRC), EPRI Report TR-103053-V1, "GOTHIC Containment Analysis Package", Version 3.4e, Volume 1: Technical Manual; Volume 2: User's Manual; Volume 3: Qualification Report, August 10e, 1994.

33. Letter NTD-NRC-95-4462, N.J. Liparulo to T.R. Quay (NRC), EPRI Report RA-93-10, "GOTHIC Design Review, Final Report", May 15, 1995.

34. Rowe, D., Corradini, M., McFadden, J., Slaughterbeck, D., and Paulsen, D., "GOTHIC Design Review Final Report," Prepared for the Electric Power Research Institute by the Design Review Group, RA-93-10, September, 1993.

3.8 References

1. G. Hugot, "Study of the Natural Convection Between Two Planes, Vertical, Parallel and Isothermal Plates," Derived from Doctoral Dissertation University of Paris, 1972, Translated by D.R. de Boisblanc, EBASCo Services Incorporated, June, 1991.

2. Eckert, E.R.G., and R.M. Drake, *Analysis of Heat and Mass Transfer, McGraw-Hill*, 1972.

3. Chun, K.R., and R.A. Seban, "Heat Transfer to Evaporating Liquid Films," *J. Heat Transfer*, Vol. 93C, pp. 391-396, November 1971.

4. Collier, J.G., *Convective Boiling and Condensation*, McGraw-Hill, 1981, Second Edition.

5. George, T.L., et al., *GOTHIC Containment Analysis Package Programmer's Manual for GOTHIC_S*, Version 3.4, NAI 8907-10, June 1991.

4.2 References

1. Wiles, L. E., T. L. George, W. W. Claybrook, M. J. Thurgood, and C. L. Wheeler, *GOTHIC Containment Analysis Package Qualification Report for GOTHIC_S*, June 1991.

2. *Experimental Basis for the AP600 Containment Vessel Heat and Mass Transfer Correlations*, WCAP-14326 (WCAP-14327, Nonproprietary), March 1995.

3. Steward, W. A., A. T. Pieczynski, and L. E. Conway, *Test of Heat Transfer and Water Film Evaporation on a Heated Plat Simulating Cooling of the AP600 Reactor Containment*, WCAP-12665 (WCAP-13341, Nonproprietary).

4. Huhtiniemi, I., A. Pernsteiner, and M. L. Corradini, *Condensation in the Presence of a Noncondensible Gas: Experimental Investigation*, WCAP-1337, April 1991 (published as a WCAP in April 1992, Westinghouse Proprietary Class 2).

5. Huhtiniemi, I., A. Pernsteiner, and M. L. Corradini, *Condensation in the Presence of a Noncondensible Gas: Experimental Investigation*, WCAP-13308, April 1991 (published as WCAP in April 1992, Nonproprietary).

6. *PCS Water Distribution Test Phase II Test Data Report*, WCAP-13296 (WCAP-13296, Nonproprietary).

7. *Passive Containment Cooling System Water Distribution Test*, Rev. 0, WCAP-13290 (WCAP-13291, Nonproprietary).

8. *Test of Air Flow for Cooling the AP600 Reactor Containment*, Rev. 0, WCAP-13328 (WCAP-13329, Nonproprietary).

9. *Tests of Heat Transfer and Water Film Evaporation from a Simulated Containment to Demonstrate the AP600 Passive Containment Cooling System*, Rev. 1, WCAP-1!267 (WCAP-13340, Nonproprietary).

10. *Passive Containment Cooling System Water Distribution Phase I Test Data Report*, Rev. 0, WCAP-13353 (WCAP-13354, Nonproprietary).

11. *AP600 Standard Safety Analysis Report* (SSAR).

2.1 References

1. Spencer, D. R., *Scaling Analysis for AP600 Passive Containment Cooling System,* WCAP-14190, October 1994, Westinghouse Electric Corporation, Proprietary.

2. Spencer, D. R., "ACRS Thermal-Hydraulics Subcommittee Meeting on AP600 PCS," March 29, 1995, Westinghouse Electric Corporation, Proprietary.

9.7 References

1. D. R. Spencer, *Scaling Analysis for AP600 Passive Containment Cooling System,* WCAP-14190, October, 1994, Westinghouse Electric Corporation.

2. D. Rowe, M. Corradini, J. McFadden, D. Slaughterbeck, D. Paulsen, "GOTHIC Design Review Final Report", Prepared for the Electric Power Research Institute by the Design Review Group, RA-93-10, September, 1993.

APPENDIX A

Validation of WGOTHIC Detailed Distributed Parameter Large-Scale Test Model

APPENDIX A

VALIDATION OF WGOTHIC DETAILED DISTRIBUTED PARAMETER LARGE-SCALE TEST MODEL

A.1 Introduction

A detailed distributed parameter model of the phase-2 large-scale test (LST) has been developed. The noding methodology and comparisons to test data are discussed. It will be shown that this model accurately predicts the vessel pressure response, as well as axial gradients in noncondensable concentration and vessel-wall heat flux.

A.2 Model Description

A.2.1 Noding Methodology

The noding for the distributed parameter model discussed within this appendix was developed based on noding studies completed on the baseline large-scale dry tests (see Section 5.2.6) and taking into consideration differences between the baseline large-scale test and the phase 2 large-scale test configuration.

The detailed distributed parameter model has the following noding characteristics:

- The model is a 1/2-symmetry representation of the LST, dividing the facility through the 0-degree to 180-degree plane (Figure A-1).

- The vessel is modeled with two volumes having a total of approximately 550 subdivided nodes using the distributed parameter formulation of the code. Above- and below-deck volumes are modeled with the distributed-parameter code formulation.

- The air annulus is modeled using the lumped-parameter volume. [ ]^{a,c} volumes are used to model the air annulus and chimney.

Figure A-2 shows an elevation view of the LST model. Figures A-3, A-4, and A-5 are plan views of the model. Figure A-3 is the general plan view of the vessel. Figure A-4 illustrates how the nodes are divided among the compartments below the operating deck. The solid lines show the walls between the compartments. The hatched area shows the location of the steam inlet diffuser. Figure A-5 illustrates the lumped parameter noding in the air annulus.

A.2.2 Code Input

Once the geometry and noding are set, the code input includes boundary and initial conditions, loss coefficients, and a Prandtl mixing length for the anisotropic turbulence model.

The initial and boundary conditions vary for each test and are input into the code as reported in WCAP-14135.[1] The boundary conditions are steam flow rate, enthalpy and pressure; ambient pressure, temperature, and humidity; external applied water flow rate and temperature, and coverage; and air flow rate. The initial conditions are the ambient pressure, temperature, and humidity; the

vessel pressure, temperature, and humidity; and the heat sinks, vessel wall, and baffle wall initial temperatures.

A single loss coefficient was used inside the vessel for the loss across the operating deck grating. The grating loss coefficient is [ ]^{a,c} based on the unblocked area. The total air flow loss in the annulus and chimney is [ ]^{a,c} based on the air flow area.

The viscous and turbulent shear and diffusion options were activated for the subdivided vessel. A Prandtl mixing length of [ ]^{a,c} was specified.

The loss coefficients and Prandtl mixing length are the same for every test.

A.3 Code Comparison Results

Comparisons of predicted values with measured data from large-scale test 212.1 (run number 48) and 222.1 (run number 61). The large-scale test instrumentation elevations, which will be referenced throughout this section, are shown in Figure A-6.

The following parameters are compared:

- Global comparisons
  - Vessel pressure
  - Condensate flow rate
  - Excess external passive containment cooling system (PCS) water flow rate

The excess external PCS water flow rate is an indirect measurement of the total evaporation rate from the vessel.

- Local parameters

  - Noncondensible gas concentrations

    Up to four gas sample locations were used to measure the noncondensible gases:

    1. F-0°-6": The location is at elevation F at the 0-degree azimuthal position taken approximately 6 inches from the inside of the vessel wall.

    2. E-90°-6": The location is at elevation E at the 90-degree azimuthal location taken approximately 6 inches from the inside of the vessel wall.

    3. A-270°-6": The location is at elevation A at the 270-degree azimuthal location taken approximately 6 inches from the inside of the vessel wall.

4. DO-90°-63"-3": The location is in the dome at a height corresponding to a 63 in. radius at the 90-degree azimuthal location. The noncondensable measurement was taken approximately 3 inches from the inside of the vessel wall.

Gas sampling was taken at only two locations for test 212.1 (F-0°-6" and DO-90°-63"-3").

The measurements and predictions are compared on an air pressure ratio basis. The air pressure ratio is defined as the air partial pressure divided by the total vessel pressure. (Neither of the tests had helium.)

- Velocity inside vessel

Five velocity sensors (vane-type anemometers) were used within the vessel to monitor the flow of gas. The locations are listed below. The elevation is listed followed by the azimuthal position in degrees.

- DO-42"-165° directional output available (Hontzsch sensor)
- A-90° directional output available (Hontzsch sensor)
- DO-42"-345° (Pacer sensor)
- D-180° (Pacer sensor)
- E-30° (Pacer sensor)

During testing, functional output was not always available from some of the velocity sensors. The Pacer velocity meter performance was degraded by exposure to the steam environment; however, the measurements obtained give an indication of the local bulk velocity along the wall. The velocity meters are used in the WGOTHIC validation to show that the code is predicting the proper range of velocities along the vessel wall.

- ΔT through vessel wall

At the LST instrumentation elevations, the temperature difference through the vessel wall at several azimuthal locations is measured. An average temperature difference through the vessel wall at each elevation is used in the comparison.

A.3.1 Test 212.1

Large-scale test 212.1 was a constant flow test conducted by establishing a constant steam flow rate and maintaining the flow until the vessel arrived at a constant pressure with the air cooling fan on and with water cooling to the vessel exterior. After the vessel reached a constant pressure, the steam flow was increased and maintained until the vessel again reached a steady pressure. The steam flow was increased to a third level and was allowed to come to a third and final steady pressure. The PCS water coverage was measured at each of the steady-state periods. For the first and second

steady-states, the water coverage was [ ].[a,b] For the third steady-state, measured water coverage was measured to be[ ][a,c]. More details on the test are in WCAP-14135.[1]

The global comparisons are shown in Figures A-7, A-8, and A-9. Good agreement between the code predictions and the measurements were obtained for all the global comparisons.

Several local comparisons were made. The first of these is the noncondensable concentration measured at two locations: F-0°-6" below the operating deck and DO-90°-63"-3" near the top of the dome.

The noncondensible gas concentrations expressed as air pressure ratios are shown in Figures A-10 and A-11. There was very good agreement between the measured and predicted values. This supports the assertion that there is enough detail in the noding to model the mixing within the vessel.

The internal average velocity measurements for test 212.1 indicated the following:

[ ][a,b] at DO-42"-165°

[ ][a,b] at A-90°

[ ][a,b] at DO-42"-345°

- Anemometers at D-180° and E-30° have either failed or the velocities are below the sensor threshold.

Figures A-12 through A-19 show the velocity field predicted by WGOTHIC. Each figure shows the velocity field in the plane indicated on the figure from the bottom to the top of the vessel. In the lower left corner of the velocity vector figure, Vmax is specified. Vmax is the maximum velocity in the figure. The largest arrow in the figure has the velocity Vmax. All other arrows are scaled linearly. Thus, the size of the arrow is representative of the magnitude of the velocity.

The predicted velocity is shown for a specific time during the first steady-state. A similar flow field is predicted for the second and third steady-states.

The velocity field shows that during steady-state the steam comes out of the steam generator compartment, flows up to the dome, turns, and flows down the vessel walls. Flow also enters the steam generator compartment from the above-deck containment atmosphere. Since the steam exiting the steam generator is a buoyant plume and there is no communication between the steam generator compartment and other compartments below deck as the hot steam air mixture exits the steam generator compartment, cooler gas from above the deck replaces the air entrained into the plume.

As shown in Figures A-18 and A-19, the velocities downward along the wall are approximately [ ]^{a,c}; therefore, the predicted velocities along the vessel wall are consistent with the measured wall velocities of [ ]^{a,b}.

The average vessel wall temperature differences for the instrumentation elevations are shown in Figures A-20 through A-28. The temperature differences were predicted very well. The most significant discrepancy between the measured and predicted values occurred at DO-21. This discrepancy is due to the location of the PCS water film distributor and the way in which it is modeled.

Location DO-21 is between the two sets of J-tube rings through which the water is supplied to the vessel (Figure A-29). In the model, all the water is applied to the top center of the vessel; however, in reality, the full water flow rate is not applied until after the second set of J-tube rings [ ]^{a,b}. Therefore, the vessel at DO-21 is not 100 percent wet (or [ ]^{a,b} wet for the third steady-state); however, it is modeled as 100 percent wet ([ ]^{a,b} wet for third steady-state), resulting in a higher predicted heat flux.

The surface area effected by this modeling limitation is small (less than 1 percent of total surface area) and has a negligible impact on the overall results.

Good agreement between the measured and predicted results for both the global and local parameters were obtained. Comparison with several independent parameters supports that the code is calculating the vessel pressure agreement for the right reasons.

A.3.2 Test 222.1

Large-scale test 222.1 was conducted by providing a steam flow of approximately 5.5 lb/sec. for 15 seconds. The flow was then reduced to approximately 3 lb/sec. for 30 seconds and then reduced to 0.5 lb/sec. for the remainder of the test until the vessel arrived at a constant pressure with the air cooling fan on and with water cooling to the vessel set at a predetermined level. The vessel was initially [ ]^{a,b} wet. At steady-state, the water coverage was measured to be [ ]^{a,b} Additional details on the test are provided in WCAP-14135[1].

As recommended in WCAP-14135,[1] the condensate flow was used for the steam-flow rate boundary condition during the steady-state because the vortex meter consistently read a value of 8 to 12 percent lower flow than indicated by the condensate. For the initial blowdown, the steam-flow rate measured by the vortex meter was used.

The global comparisons are shown in Figures A-30, A-31, and A-32. During steady-state, the code overpredicted the measured pressure by approximately 5 percent. The variation in the predicted vessel pressure as a function of time, particularly between 8000 seconds and 12,000 seconds, is due to the variation in condensate flow that was used for the steam flow rate (Figure A-31).

The dips in the measured vessel pressure at around 9000 seconds and 11,300 seconds (Figure A-30) are due to a direct discharge of condensate that had backed up into the test vessel. The vessel pressure transducer is closely coupled with the vessel sight gage line and was reacting to the localized decrease in pressure.

The predicted vessel pressure was underpredicted from approximately 400 seconds to 700 seconds (Figure A-30). The prediction reaches a minimum pressure at approximately 550 seconds, at which time it is 13 percent underpredicted. This discrepancy between the measurement and prediction is attributed to the uncertainty in the vortex meter measurement. The lower limit on the vortex meter's applicable range is 0.45 lb/sec. The vortex meter reading is significantly below its applicable range (0.05 lb/sec. to 0.1 lb/sec.) for approximately 5 minutes following the blowdown.

A sensitivity run was made in which the steam flow rate during the period that the meter was below its minimum range was set at 0.4 lb/sec. This increased the predicted pressure between 400 seconds and 700 seconds, resulting in a maximum underprediction of 1.4 percent at approximately 550 seconds.

Several local comparisons were made. Noncondensibles were measured at the four sample locations: F-0°-6", E-90°-6", A-270°-6", and DO-90°-63"-3". The measured and predicted air pressure ratios are shown in Figures A-33, A-34, A-35, and A-36. Good agreement between the code and the measurements were obtained. This supports the assertion that there is enough noding detail to model the mixing within the vessel.

The internal velocity meter measurements for test 222.1 indicated the following:

[ ]^{a,b} at DO-42"-165°
[ ]^{a,b} at A-90°
[ ]^{a,b} at DO-42"-345°
[ ]^{a,b} at D-180°
[ ]^{a,b} at E-30°

At steady-state, the velocity field for test 222.1 is similar to that of test 212.1, so the velocity vector plots will not be shown. The average steady-state velocities predicted for each of the measurement locations are as follows:

- Predicted velocity is [ ]^{a,c} at [ ]^{a,c}
- Predicted velocity is [ ]^{a,c} at [ ]^{a,c}
- Predicted velocity is [ ]^{a,c} at [ ]^{a,c}
- Predicted velocity is [ ]^{a,c} at [ ]^{a,c}
- Predicted velocity is [ ]^{a,c} at [ ]^{a,c}

The predicted velocities along the vessel wall are consistent with the measured wall velocities.

The average wall temperature differences for the instrumentation elevations are shown in Figures A-37 through A-45. There was good agreement between the measured and predicted delta temperature through the vessel wall. As in test 212.1, the most significant discrepancy between the measured and predicted results occurs at DO-21 (Figure A-45). As explained in the code comparison section for test 212.1, the reason for the discrepancy is due to the location of the PCS water film distributer and the way in which it is modeled. The surface area affected was small (less than 1 percent of total surface area) and had a negligible impact on the overall results.

The trend in the wall temperature difference after 2000 seconds had the same trend as the condensate flow, which was used as the steam flow into the vessel.

For all elevations, the temperature difference was underpredicted immediately following the blowdown. The vessel pressure was underpredicted immediately following the blowdown also. This further supports the conclusion that the steam flow measured and input into the code during this time is too low.

Good agreement between the measured and predicted results for both the global and local parameters were obtained.

A.4 Conclusions

The detailed distributed parameter large-scale test model has been compared to tests 212.1 and 222.2. Comparisons were made to several independent global and local parameters. The global comparisons show that the primary parameter, vessel pressure, was predicted well and that the total heat transfer was correct. The local comparisons show good agreement for many independent parameters, which supports the vessel pressure predicted results.

A.5 References

1. WCAP-14135, *Final Data Report for PCS Large-Scale Tests*, Phase 2 and 3, July 1994.

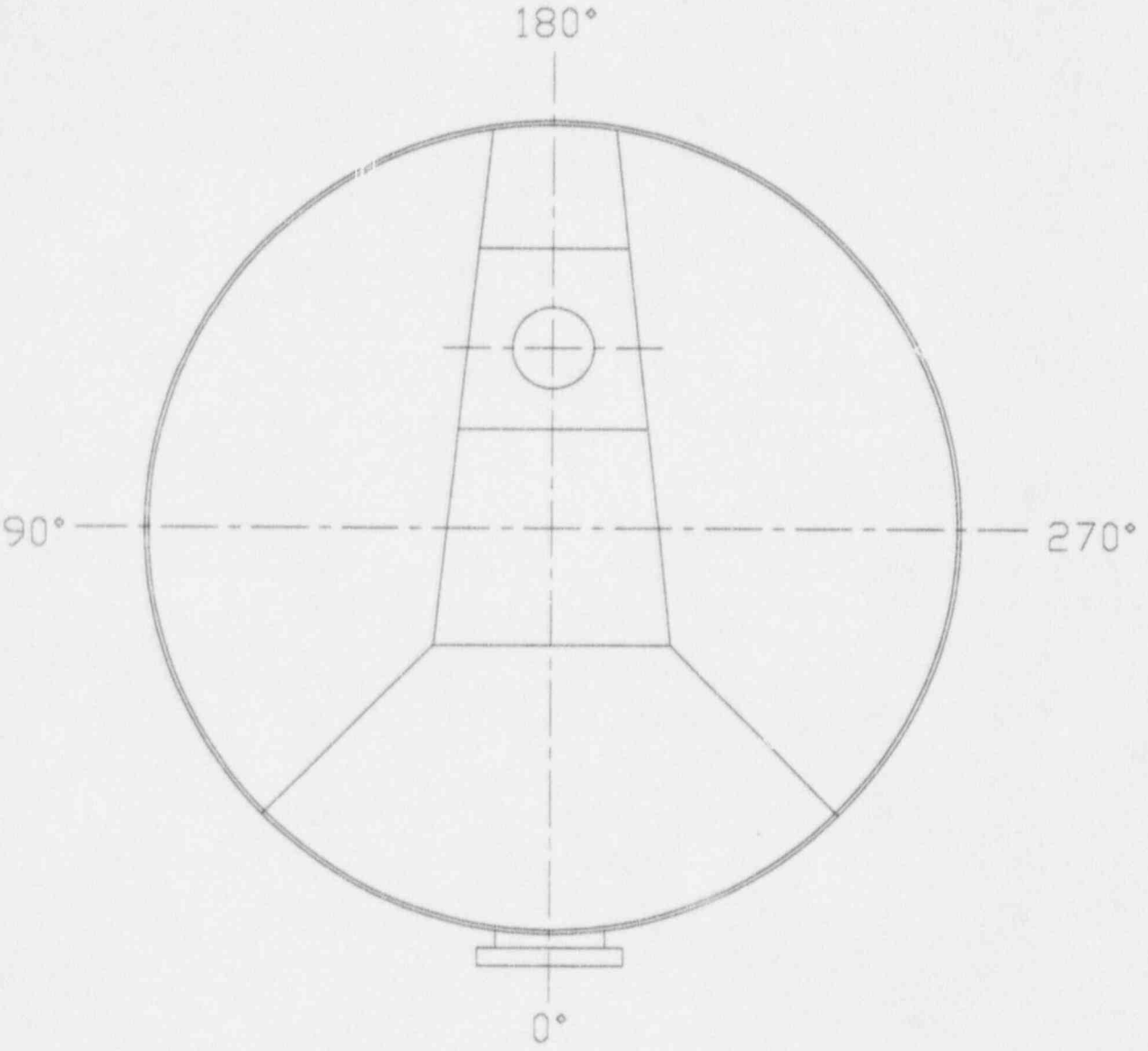

Figure A-1 Cross-Section Orientation Convention

Figures A-2 through A-5 are proprietary and are, therefore, not included in the Class 3 version of the report.

These figures are contained in the Class 2 version of the report.

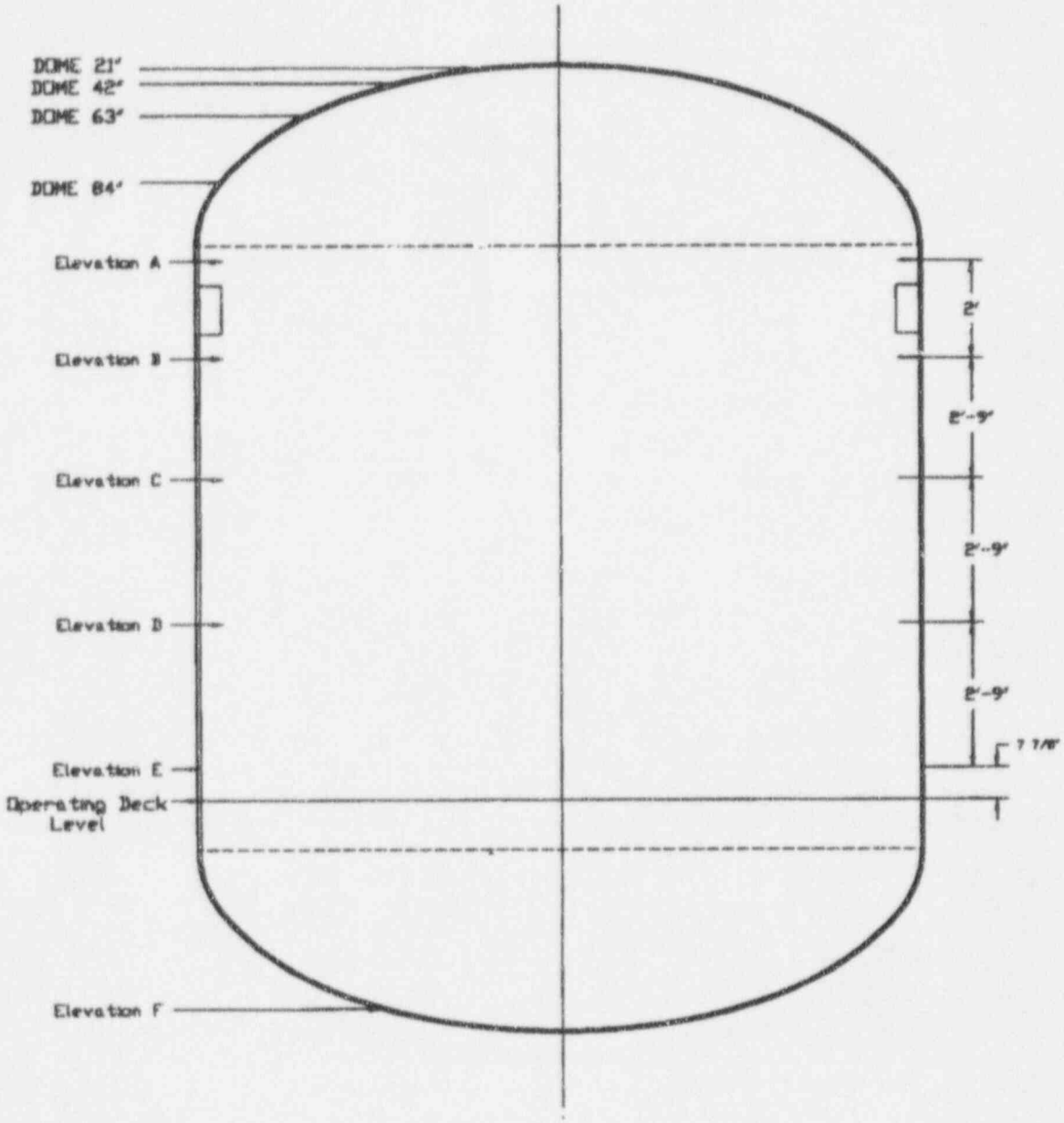

Figure A-6 Large-Scale PCS Instrumentation Elevations

Figures A-7 through A-45 are proprietary and are, therefore, not included in the Class 3 version of the report.

These figures are contained in the Class 2 version of the report.

APPENDIX B

Blind Test

APPENDIX B

BLIND TEST

B.1 Introduction and Background

The blind large-scale test (LST), test number 220.1, is part of the Phase 2 LST series. After the Westinghouse test matrix was defined, the U.S. Nuclear Regulatory Commission (NRC) chose this test to be the blind test. Only the boundary and initial conditions were given to the Westinghouse analysis group. Other measured data were held by the Westinghouse test engineering group until the WGOTHIC lumped parameter and distributed parameter input decks were frozen, documented, and a pretest prediction performed.

The frozen input decks and the pretest WGOTHIC predictions have been documented in Westinghouse's internal calculation note and letter log systems. The pretest mass and energy releases were provided to the U.S. NRC in March 1995.[1] The frozen lumped and distributed parameter models used for the analysis are the same models that were used for the priority tests (Section 6.0 through 6.3.2).

After the pretest predictions were made, the post-test data were then obtained from the AP600 test engineering group. The post-test condensation rate data showed that the average steam flow used for the pretest prediction was too low and that significant dips seen in the pretest steam flows, taken from the vortex meter, were in error. A modified steam flow rate was used for the post-test WGOTHIC simulation with the lumped and distributed parameter models. The modified steam flow rate was provided to the U.S. NRC.[2]

The post-test predictions for the distributed parameter and lumped parameter evaluation models are shown in this Appendix.

B.2 Test Description

The LST facility is described in Section 3.1.3. The steam inlet configuration for the blind test is the steam diffuser located below the operating deck (Figure 3-1).

Test 220.1[3] is a blowdown test in which the maximum flow of steam attainable was provided to the test vessel for a 20- to 30-second period. The flow was then reduced to approximately 0.5 lb/sec., for the remainder of the test, until the vessel arrived at a constant pressure. Air cooling in the annulus was provided by the fan. Water cooling was supplied to the outside of the vessel. The outside of the vessel was initially [ ]^{a,b} wet. Ten minutes after the steam flow was introduced into the vessel, the water coverage was [ ]^{a,b}. At steady-state, an [ ]^{a,b} water coverage was measured.

B.3 WGOTHIC Formulation

Version 1.2 of the WGOTHIC solver (WGOTHIC_S) was used for the analysis. WGOTHIC_S solves the conservation equations for mass, momentum, and energy. It also includes heat and mass transfer

correlations used to model the passive containment cooling system (PCS). These correlations are given in Sections 2.2 and 2.3.

Two WGOTHIC formulations were used to model the thermal-hydraulic behavior of containment atmospheres and structures: the lumped parameter and the distributed parameter formulation. In the lumped parameter formulation, the momentum equations are simplified by eliminating the convective terms and stress terms. The gravity terms are retained so that buoyancy dominated flows may be determined. At the same time, the mass and energy conservation diffusion terms are eliminated because there are no velocity gradients available for their calculation. The distributed parameter approach retains all of the above terms in the momentum equation. Further details on the lumped and distributed parameter formulations are given in Section 5.0.

B.4 Large-Scale Test Input Model Description

The distributed and lumped parameter LST input models for the blind test analysis are the same as the evaluation models described in Sections 6.0 through 6.3.2.

These models were used for the pretest and post-test predictions. As discussed in Section B.1, the only difference between the pretest and post-test input is the steam flow rate.

The condensate flow and the steam flow meter's applicable range were used to determine the post-test steam flow rate.[2] There are no reliable condensate flow measurements prior to 6950 seconds so the steam flow rate for the initial 1209 seconds (from 5741 seconds to 6950 seconds) can not be verified with any other steam flow measurement device. In summary, the following changes were made to the pretest steam flow rate to get the post-test steam flow rate. (The steam enters the containment at 5741 seconds.)

1. The steam flow rate was set to 0.45 lbm/sec. (the minimum value in the vortex meter's applicable range) when the vortex meter reading falls below its range, except at the end of the test when the steam is being shut off.

2. The time-averaged condensate flow is used from 6950 seconds to 13,819 seconds.

3. The steam flow rate after 13,820 seconds was unchanged from what was used in the pretest prediction.

The resulting post-test steam flow rate is shown in Figure B-1. Figures B-2 through B-5 show post-test steam flow rate during specific time intervals. The steam flow rate significantly influences the vessel pressure response, so having the correct flow rate is important.

B.5 Comparison of Measured and Predicted Results

Measured data will be compared to the distributed parameter and lumped parameter model predictions. More detailed comparisons will be made to the distributed parameter model to show its ability to model the LST. The distributed parameter model is expected to provide a better representation of the LST than the lumped parameter model.

The lumped parameter model is expected to overpredict the vessel pressure. The model was conservatively biased by eliminating one of the competing effects (Section 5.3).

B.5.1 Distributed Parameter Results

Several global and local comparisons are made to the distributed parameter model. The LST instrumentation elevations, which are referenced throughout this section, are shown in Figure B-6.

The following global parameters are compared:

- Vessel pressure
- Condensate flow rate
- Excess external water flow rate

The following local parameters are compared:

- Noncondensible concentrations
- Temperature difference through the vessel wall at LST instrumentation elevations

Vessel Pressure

The post-test predicted vessel pressure will be compared to the measured vessel pressure in the same time frames as the post-test steam flow rate described earlier. This will illustrate how the vessel pressure trends relate to the steam flow rate trends.

The measured and predicted vessel pressures during the blowdown and shortly thereafter are shown in Figure B-7. The measured and the predicted initial rate of pressure increase were in agreement. The predicted vessel pressure for the remainder of the time was very close to the measured vessel pressure; however, the predicted vessel pressure followed the trend of the steam flow rate. The dip in steam flow rate from 5840 to 5940 seconds (Figure B-2) caused vessel pressure prediction to dip also. There was no verification as to whether this dip in steam flow rate was as significant as shown. This is a point where the vortex meter dropped below its applicable range and the minimum steam flow rate was assumed to be 0.45 lbm/sec.

The predicted and measured vessel pressures from 6100 seconds to 7000 seconds are shown in Figure B-8. There was a dip in the measured and predicted vessel pressures at approximately 6500 seconds,

which corresponds with the dip in steam flow in Figure B-3; however, it is more pronounced in the predictions. The magnitude of the dip in steam flow rate at approximately 6500 seconds can not be verified. This is also a point where the vortex meter dropped below its applicable range and the minimum steam flow rate was assumed to be 0.45 lbm/sec.

During the time interval in Figure B-8 and a portion of the time interval shown in Figure B-9, the predicted vessel pressure was lower than the measured pressure. This may be due to a lower steam flow rate input into the code than there actually was from 5840 to 5940 seconds and 6390 to 6640 seconds.

The predicted and measure vessel pressure both came to a steady-state pressure (Figure B-10) until the steam flow was turned off at the end of the test. Although it appears that the predicted vessel pressure started to decrease at an earlier time than the measured vessel pressure, this was not the case. It appears that way because the code output was only printed every 100 seconds.

The full transient for the measured and predicted vessel pressure is shown in Figure B-11. The average steady-state vessel pressure was less than 1 percent underpredicted; however, there were some discrepancies between the measured and predicted pressure earlier in the transient. These discrepancies are due to the uncertainty in the steam flow rate from 5741 seconds to 6950 seconds.

Condensate Flow Rate

The condensation rate comparison is shown in Figure B-12. The measured and predicted values were in agreement, except at around 6500 seconds. The measured condensate rates during a transient were not reliable because the condensate measurements were not instantaneous. Even though the measured condensate flow shows a higher value at approximately 6500 seconds, this measured condensate flow rate corresponds to a steam flow rate from a previous time. The predicted values did not have such a lag time between the steam flow and the condensate flow.

Excess External Water Flow Rate

The excess PCS water flow rate is an indirect measurement of the total evaporation rate from the vessel. The excess external water flow rate is shown in Figure B-13. Although it appears that the predicted excess external water flow rate during the first 1000 seconds is underpredicted, it is not. The discrepancy appeared because during the first 5000 seconds when there was not yet any steam in the vessel, the user specified that the code only output information every 1000 seconds. After 5000 seconds, the print interval was decreased so that output would be printed more often.

During the transient, the measured and predicted values were in agreement. At longer term, the excess external water was overpredicted, indicating that the evaporation rate was underpredicted.

Noncondensible Concentrations

Four gas sample locations were used to measure the noncondensible gas concentrations:

- F-0°-6": The location is at elevation F at the 0° azimuthal position taken approximately 6 inches from the inside of the vessel wall.

- E-90°-6": The location is at elevation E at the 90° azimuthal location taken approximately 6 inches from the inside of the vessel wall.

- A-270°-6": The location is at elevation A at the 270° azimuthal location taken approximately 6 inches from the inside of the vessel wall.

- DO-90°-63"-3": The location is in the dome at a height corresponding to a 63" radius at the 90° azimuthal location. The noncondensible measurement was taken approximately 3 inches from the inside of the vessel wall.

The measurements and predictions were compared on an air-pressure ratio basis. The air pressure ratio is defined as the air partial pressure divided by the total vessel pressure.

The measurements were taken at steady-state. The steady-state air pressure ratios as a function of vessel height are shown in Figure B-14.

Both the measurements and the code predictions show that the vessel is air-rich at elevation F. The measured and predicted values were in agreement.

Temperature Difference Through the Vessel Wall

The temperature difference through the vessel wall at several azimuthal locations for each instrumentation elevation in the LST facility was measured. The average azimuthal temperature difference through the vessel wall at each elevation was used in the comparison. The average temperature includes the wet and dry portions of the test vessel. The test was initially [ ]^{a,b} wet. At approximately 6350 seconds, the water coverage was [ ]^{a,b} At steady-state, the water coverage was [ ]^{a,b}

Figures B-15 through B-24 show the measured and predicted vessel wall temperature differences for each elevation. The predictions were within 2°F of the measurements for all the elevations, except DO-21 and DO-42.

The discrepancy at DO-21 was due to the location of the PCS water film distributor and the way in which it was modeled. Location DO-21 is in between the two sets of J-tube rings through which the water was supplied to the vessel (see Figure 8-68). In the model, all the water was applied to the top center of the vessel; however in reality, the full water flow rate was not applied until after the second

set of J-tube rings at [ ]^{a,b} This results in a higher predicted heat flux at location DO-21. The surface area affected by this modeling limitation was small (less than 1 percent of total surface area).

B.5.2 Lumped Parameter Results

The predicted vessel pressure will be compared to the measured vessel pressure in the same manner as the distributed parameter model. The predictions and measurements from 5700 seconds to 6100 seconds are shown in Figure B-25. The vessel pressure was overpredicted during the blowdown. The predicted vessel pressure follows a similar trend as the steam flow rate shown in Figure B-2.

Figure B-26 shows the measured and predicted vessel pressures between 6100 seconds and 7000 seconds. Again, the predicted vessel pressure has a similar trend as the steam flow rate (Figure 5-3). The predicted pressure is both under and overpredicted during this time range.

The predicted vessel pressure is overpredicted from 7000 seconds to 13,820 seconds (Figure B-27). The predicted and measured pressure continue to increase during this time, although the predicted pressure is increasing at a faster rate. This may be due to less steam flow introduced into the model than in the test from 5840 to 5940 seconds and 6390 to 6640 seconds. The predicted vessel pressure comes to a steady state at a later time and at a pressure higher than the measured pressure (Figure B-28).

The total measured and predicted vessel pressure transients are shown in Figure B-29.

Detailed comparisons were not be made for the lumped parameter model because, as previously acknowledged, the lumped parameter model does not predict the internal flow field or noncondensible gas concentrations accurately (Section 5.3). The free convection heat and mass transfer correlation with overmixing of noncondensibles overpredicts the heat and mass transfer and hence overpredicts pressure.

B.6 Conclusions

The blind test process, which includes freezing the input decks, making pretest predictions, and post-test predictions, has been completed. The distributed parameter and lumped parameter model predictions have been compared with the blind test (test number 220.1). The results were consistent with other LST using the same WGOTHIC model (Section 8.0). The blind test showed that the modeling approach did not require test specific tuning.

B.7 References

1. Letter NTD-NRC-95-4422, N. J. Liparulo to Borchardt (NRC), *Mass and Energy Release for AP600 PCS Large-Scale Test 220.1*, March 27, 1995.

2. Letter NTD-NRC-95-4456, N. J. Liparulo to T. R. Quay (NRC), *Revised Mass and Energy Tables for AP600 Large-Scale Containment Test 220.1*, May 8, 1995.

3. *Final Data Report For PCS Large-Scale Tests, Phase 2 and Phase 3*, WCAP-14135, July 1994.

Figures B-1 through B-29 are proprietary and, therefore, are not included in the Class 3 version of the report.

These figures are contained in the Class 2 version.

APPENDIX C

Clime Numerical Solution Method

APPENDIX C

CLIME NUMERICAL SOLUTION METHOD

C.1 Introduction

The Clime numerical solution matrix equation is of the form a,c

[ ]

The numerical solution method for each of the three boundary equations is described in this appendix. The Clime nodal representation is shown in Figure C-1. The terms used in this appendix were defined in Section 2.5.

C.2 Wall/Film Boundary Equation

a,c

[ ]

a,c

a,c

a,c

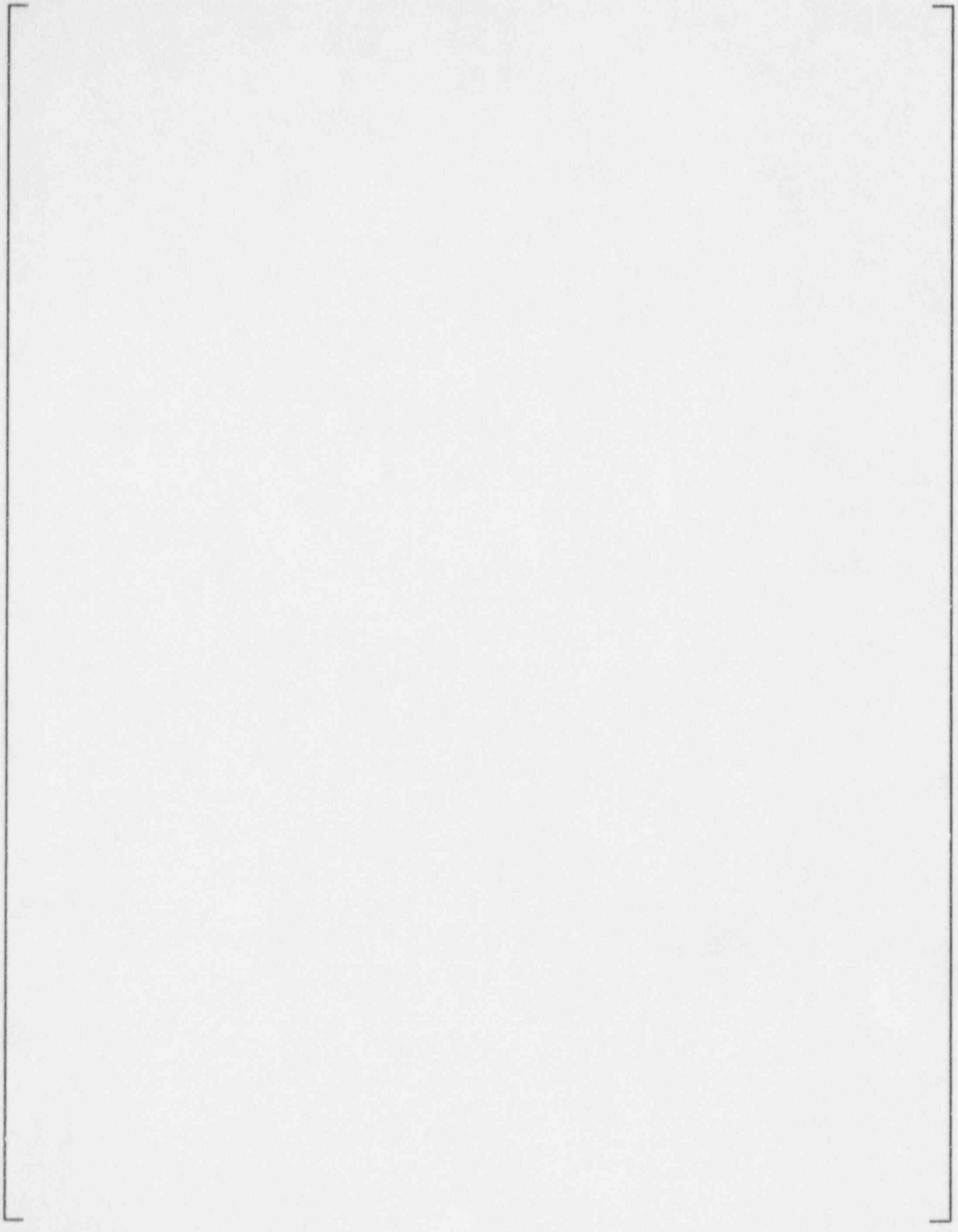

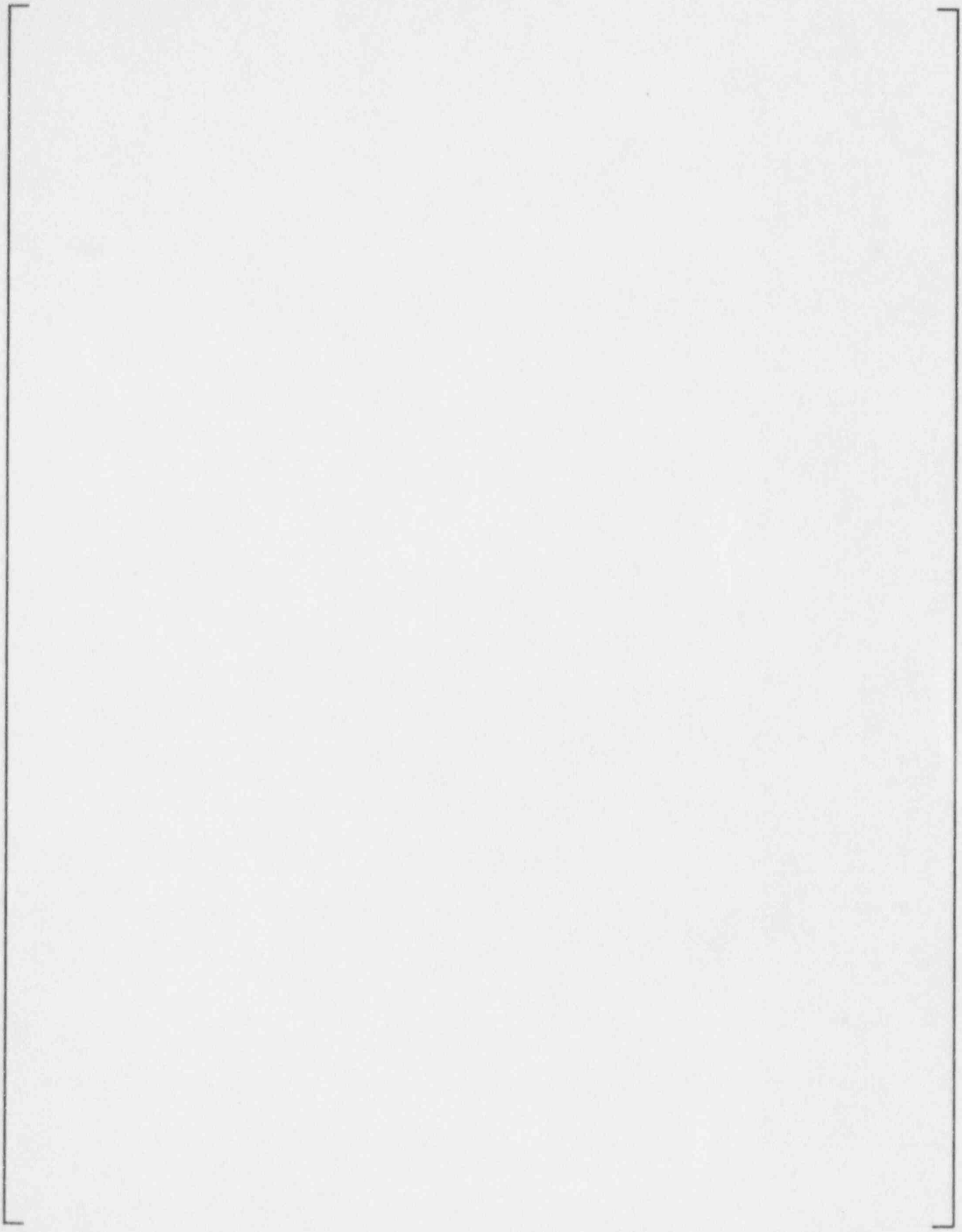

a,c

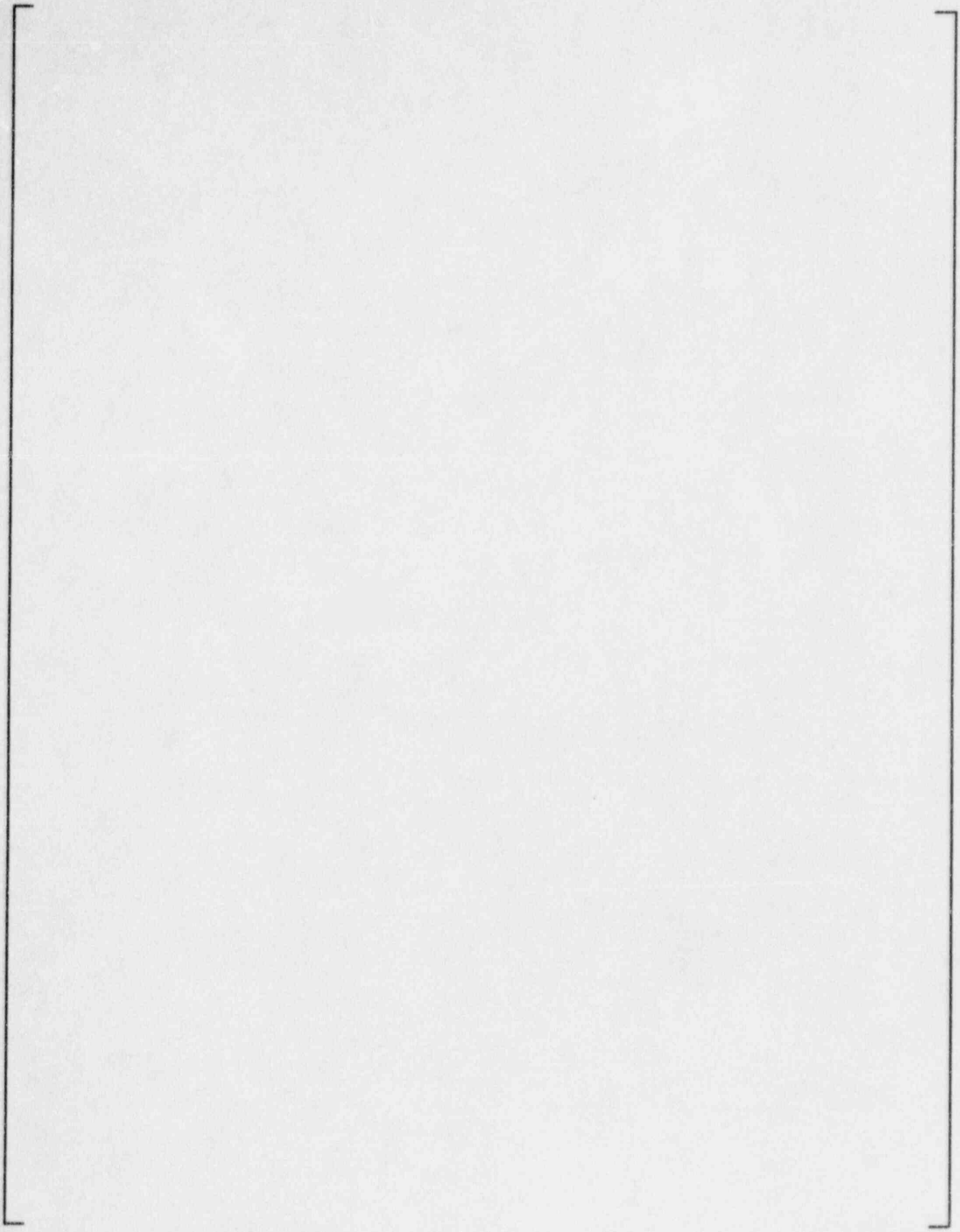

a,c

a,c

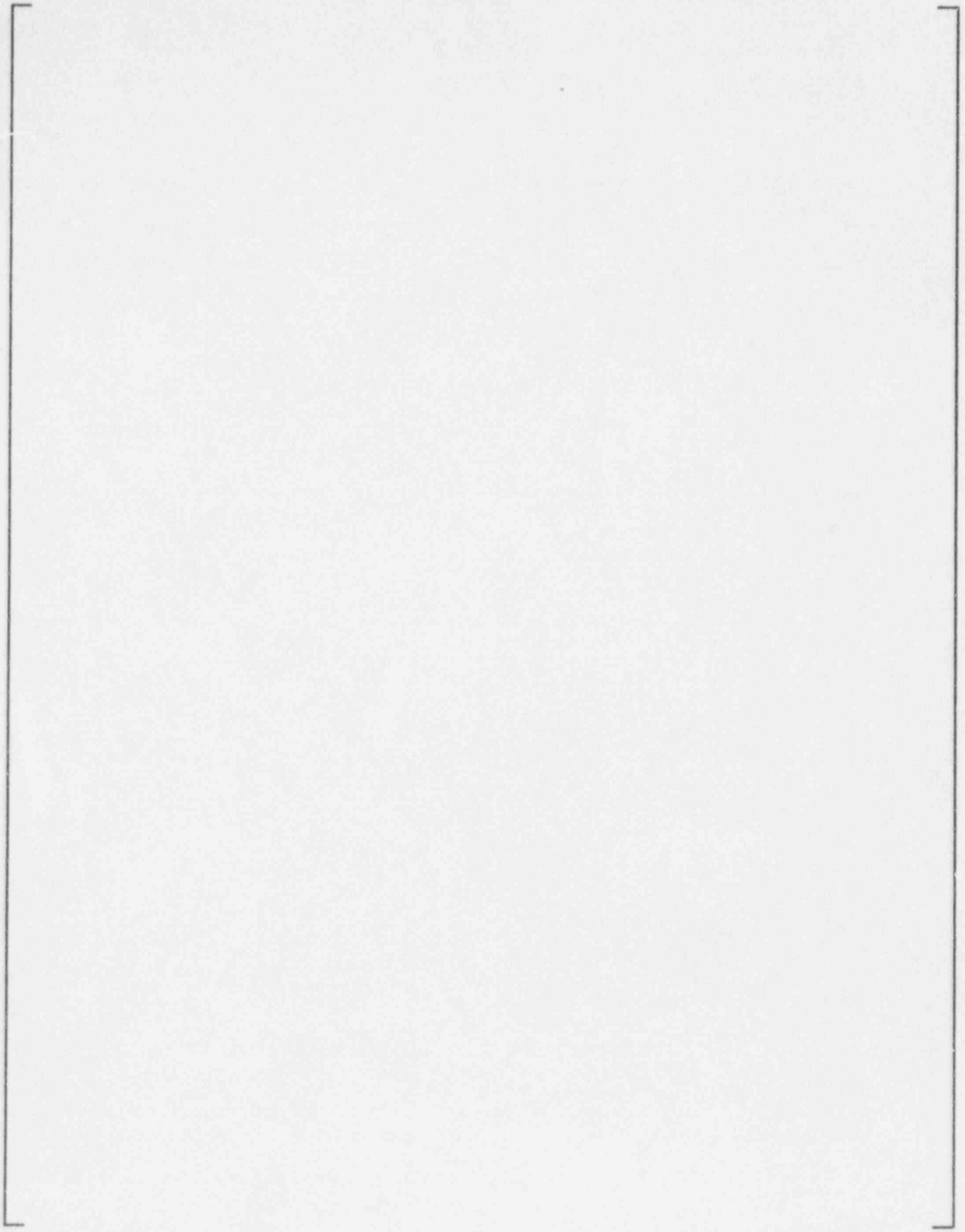

a,c

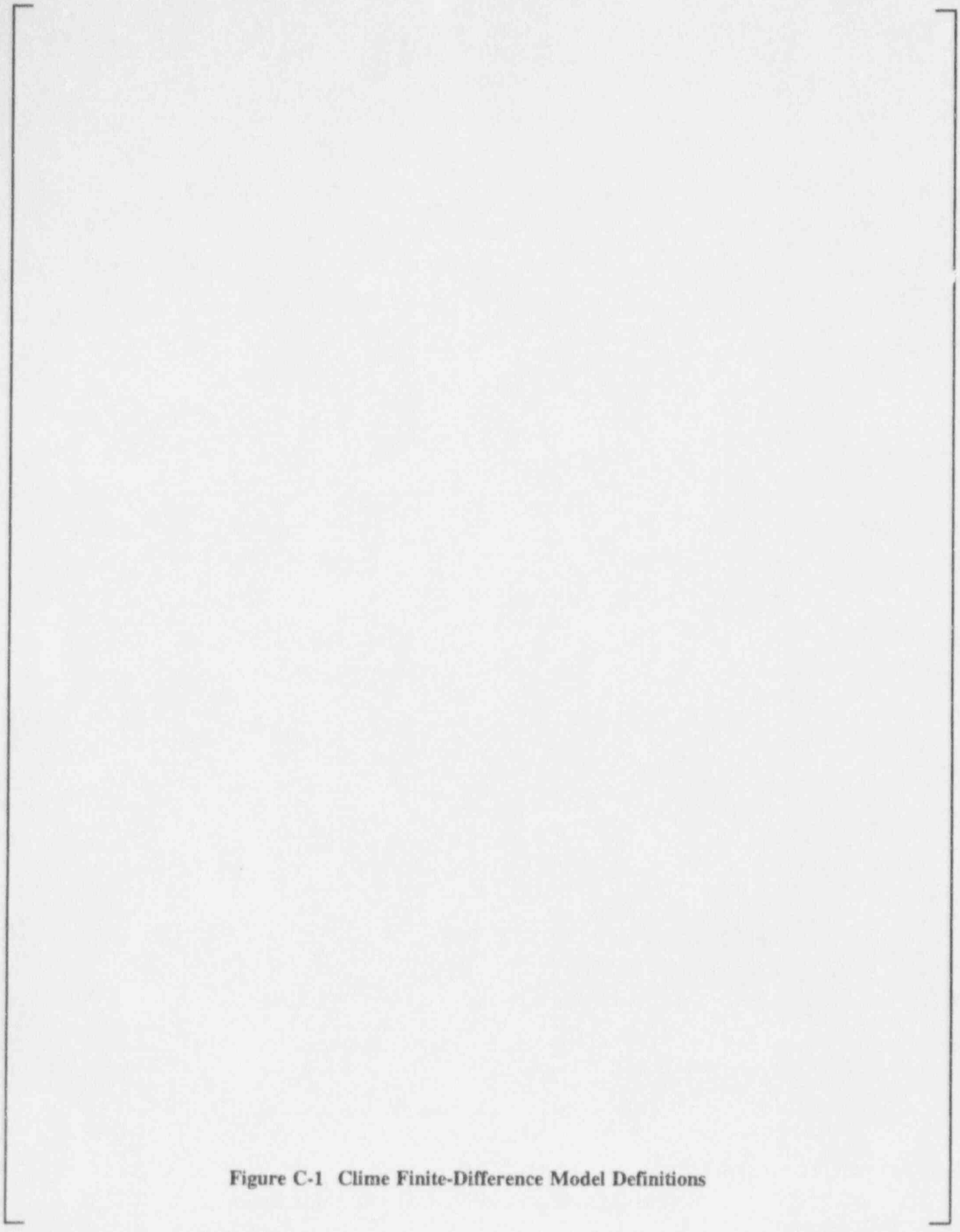

Figure C-1 Clime Finite-Difference Model Definitions

APPENDIX D

GOTHIC Validation Tests Using WGOTHIC

APPENDIX D

GOTHIC VALIDATION TESTS USING WGOTHIC

After compiling and installing the GOTHIC code on the Westinghouse computer workstations, the entire set of GOTHIC validation tests was run to determine if changes in the computer platform or compiler would affect the results. No significant differences were observed in any of the parameters that were compared, so the GOTHIC code was placed under the Westinghouse configuration control system.

In performing this initial testing, certain tests were discovered to be more sensitive than others to changes in the computer platform, compiler and/or the numerical solution time step. These 6 tests are listed below.

Battelle-Frankfurt Test D-16
Blowdown transients, subcompartment pressurization, wall differential pressures

Battelle-Frankfurt Test D-20
Hydrogen transport by convection and diffusion

Marviken Full-Scale Containment Test 17
Full-scale steam/water blowdown, condensation, multi-compartment mass/energy transport

HDR Test T31 Steam blowdown with helium injection

Carolinas Virginia Tube Reactor Test 3
Pressurized, high temperature steam blowdown

LACE Test LA-5 Severe accident response to sudden containment failure

Changes were made to the GOTHIC code (as described in Section 2.0) to incorporate the PCS models for condensation, evaporation and wall-to-wall radiant heat transfer. The revised code, called Westinghouse-GOTHIC and abbreviated as WGOTHIC, was tested using the subset of sensitive GOTHIC validation tests described above. These tests were run with the same input options selected in the original validation calculation (i.e., the PCS models were not exercised) to determine if any of the code changes made to incorporate the PCS models would affect the transient results.

The comparison plots for these six tests are shown in Figures D-1 through D-41. The GOTHIC-calculated response is shown on the top plot and the WGOTHIC-calculated response is shown on the bottom plot. A visual comparison of the plots shows that in all cases, the GOTHIC- and WGOTHIC-calculated responses are nearly identical. The minor difference in the calculated transient hydrogen concentration in Battelle-Frankfurt test D-20 (Figures D-14 through D-16) is believed to be caused by differences in the machine roundoff errors which affected the calculated time step size. Therefore, since the WGOTHIC-calculated response to these six tests was nearly identical to the GOTHIC-calculated response, the changes made to incorporate the Clime heat and mass transfer models did not affect the GOTHIC portion of the WGOTHIC code.

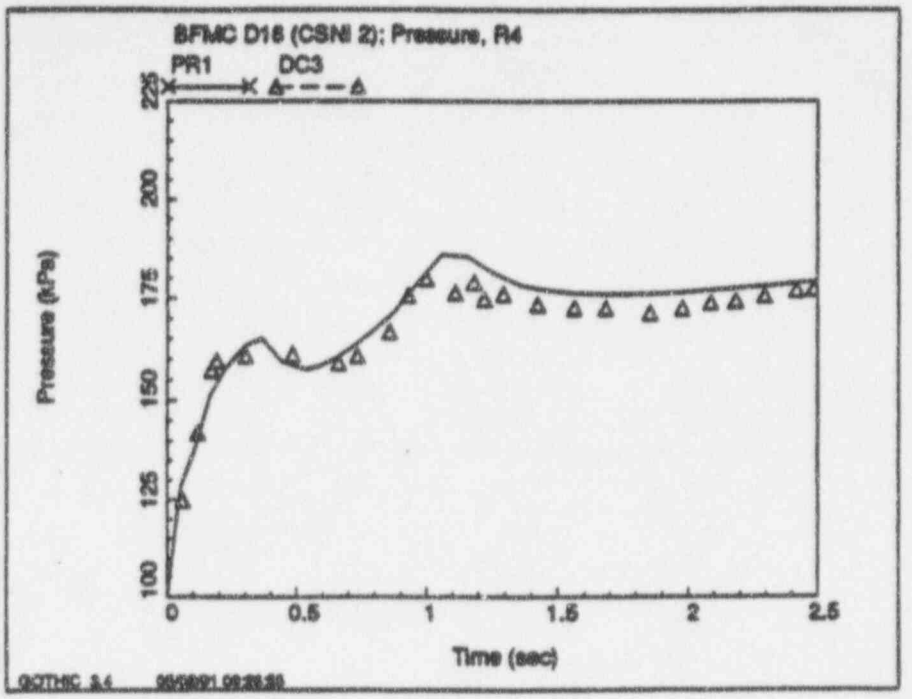

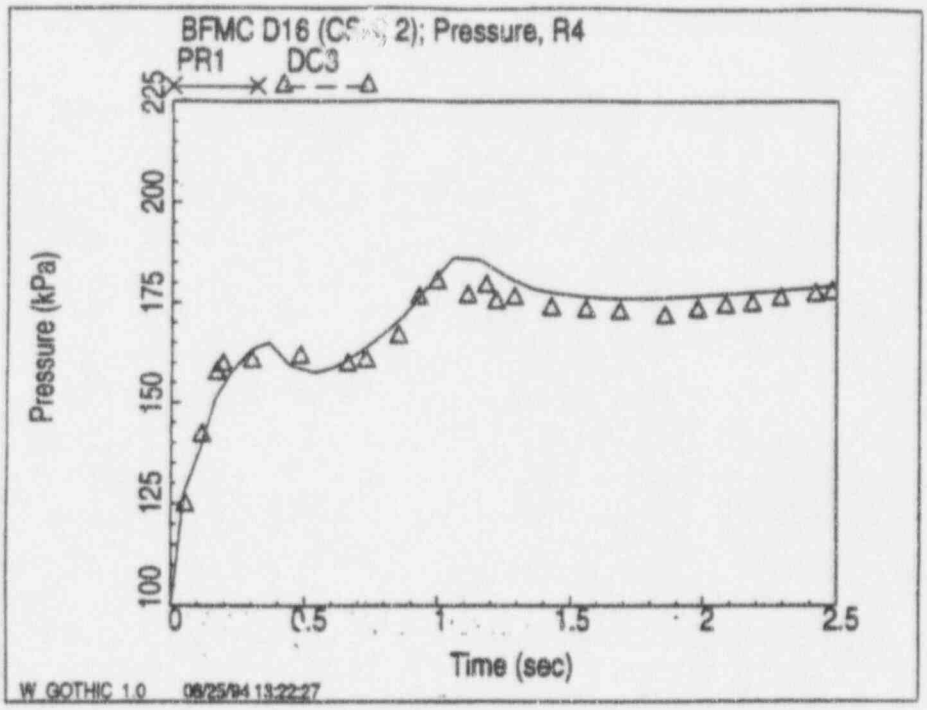

Figure D-1 Pressure in Room R4; BFMC Test D-16, 0-2.5 Seconds

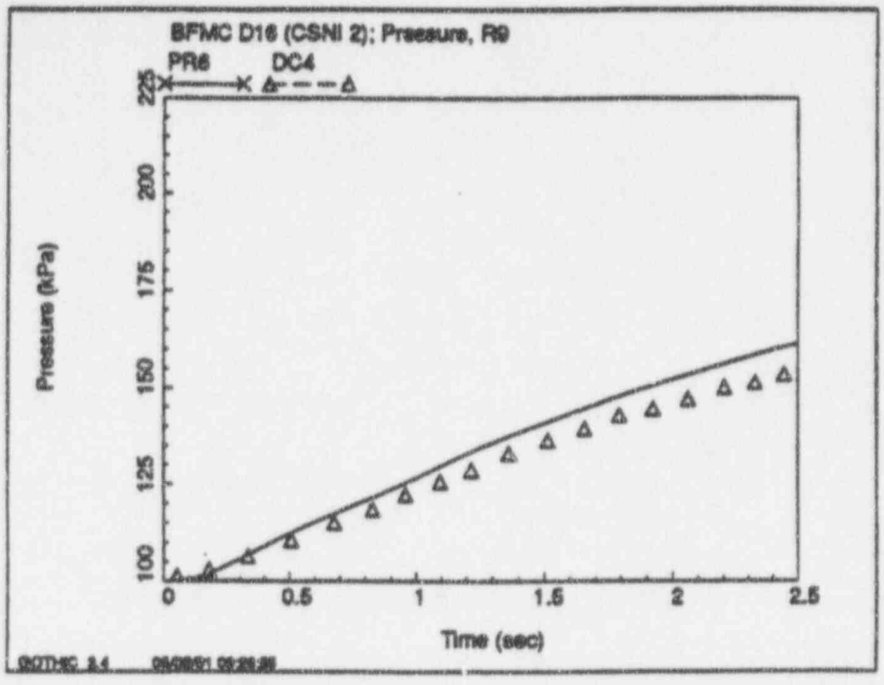

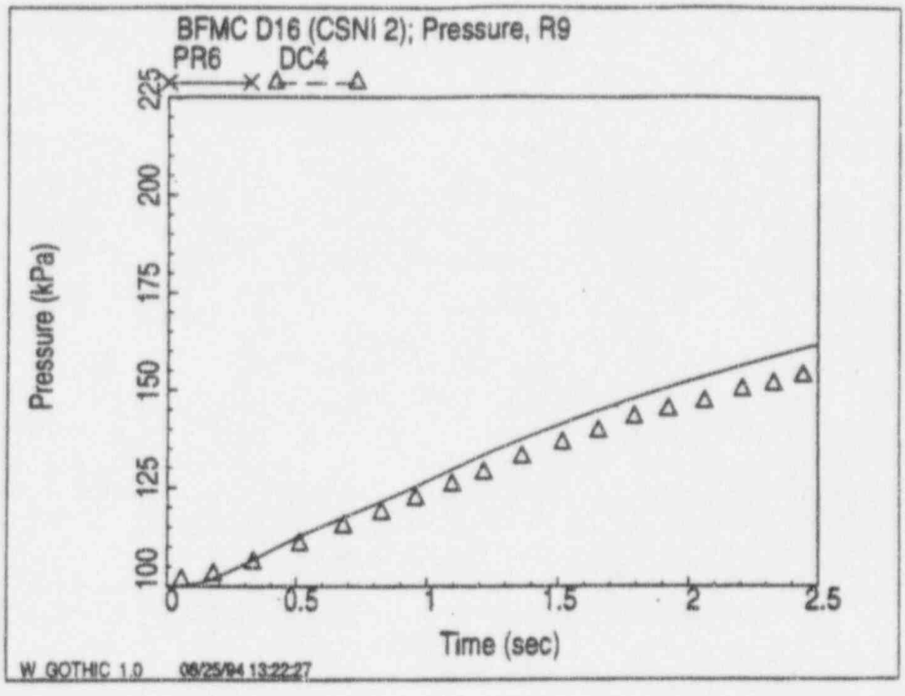

Figure D-2 Pressure in Room R9; BFMC Test D-16, 0-2.5 Seconds

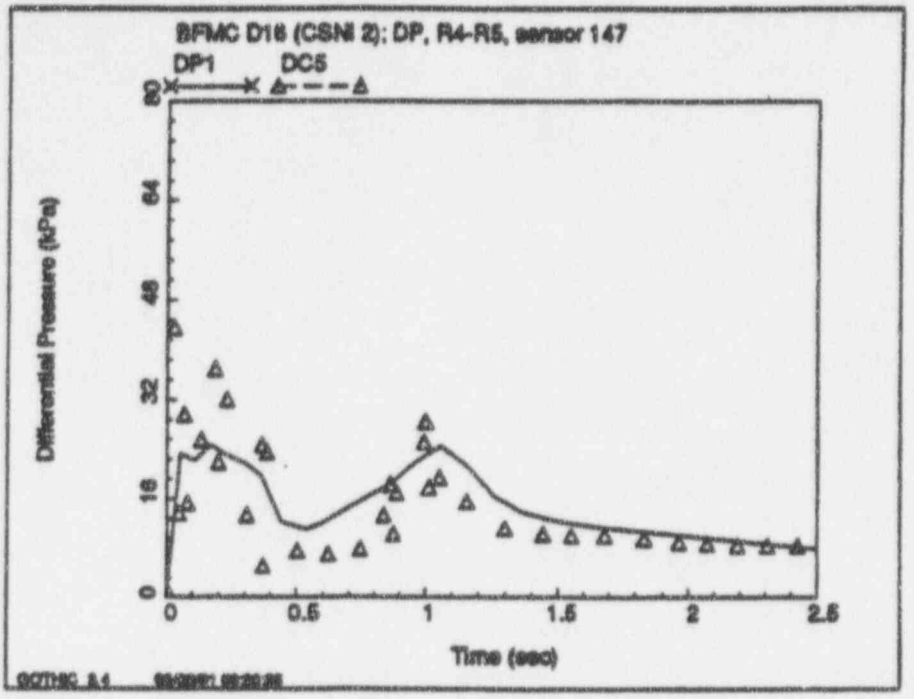

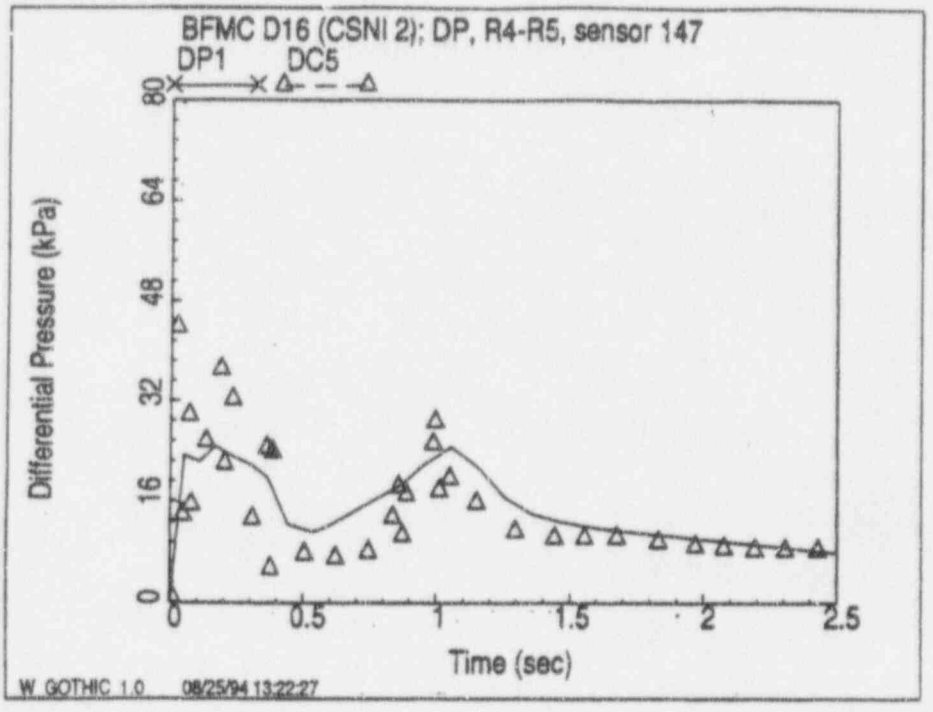

Figure D-3 Differential Pressure, R4 to R5; BFMC Test D-16

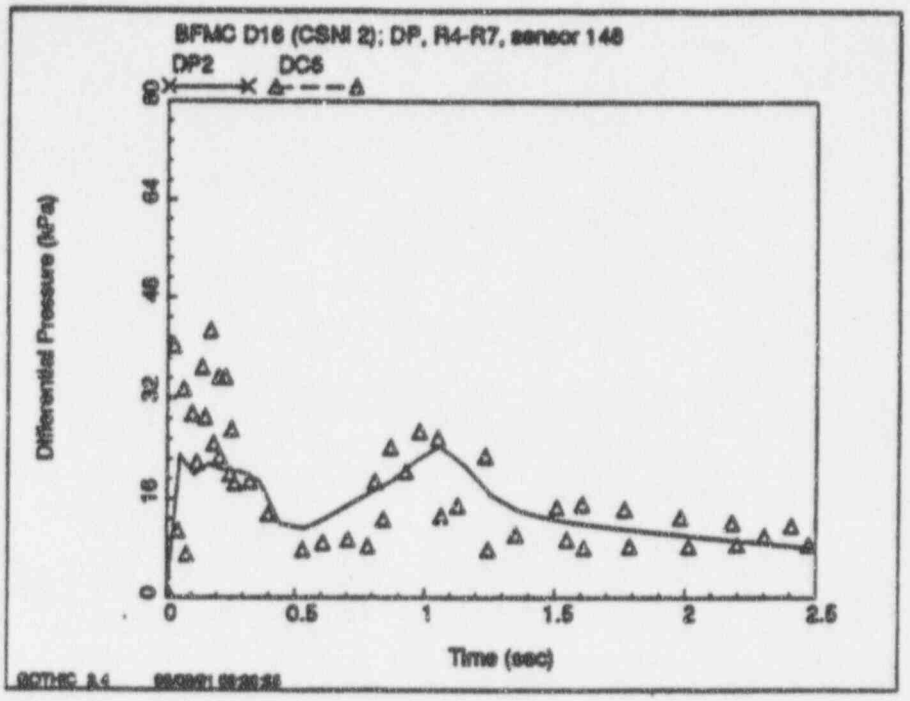

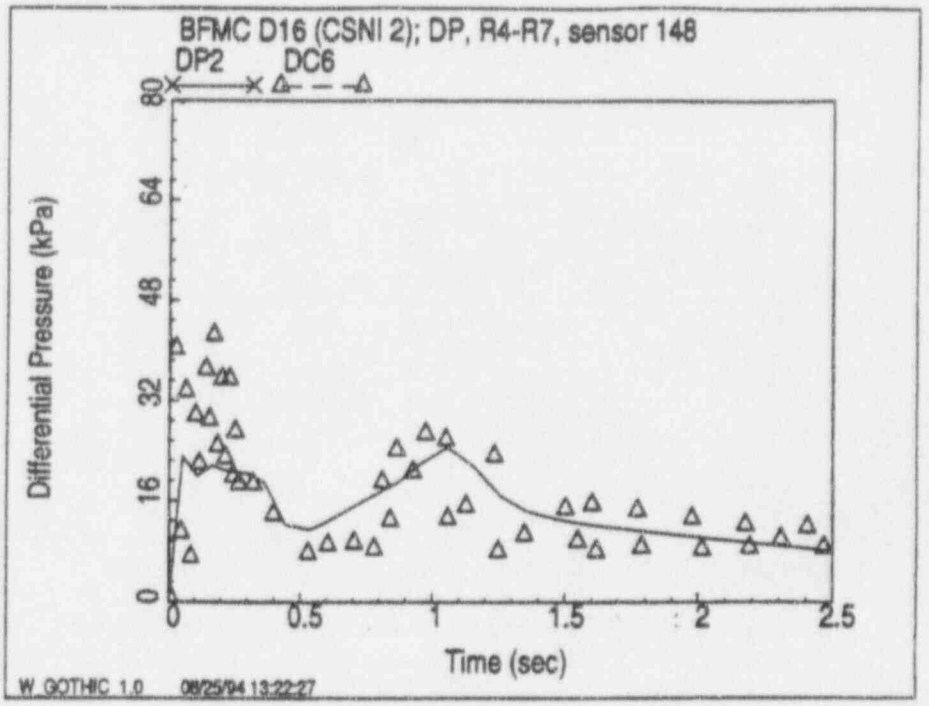

Figure D-4 Differential Pressure, R4 to R7; BFMC Test D-16

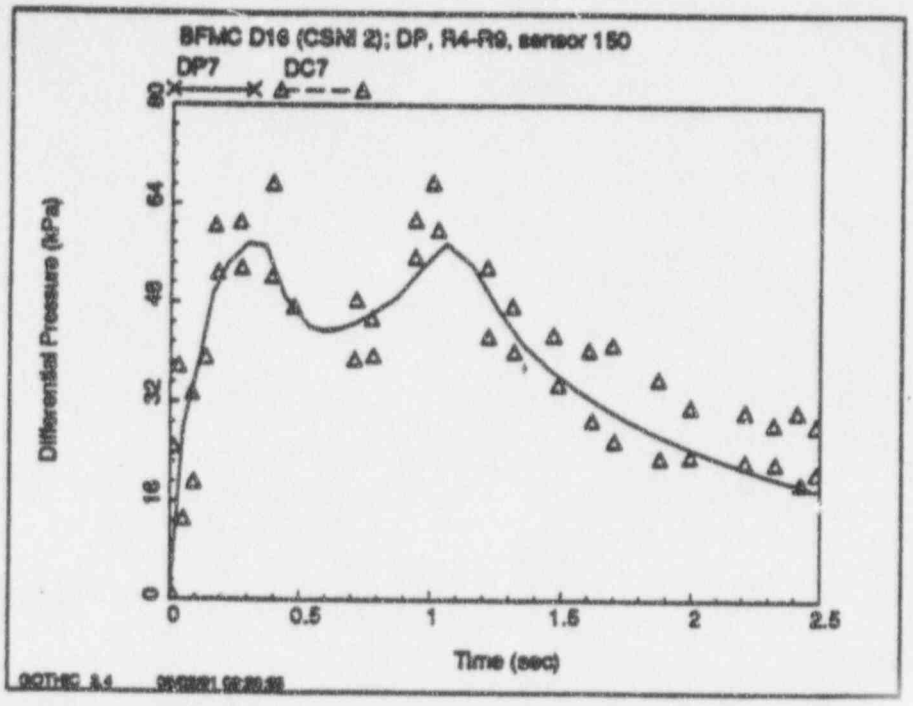

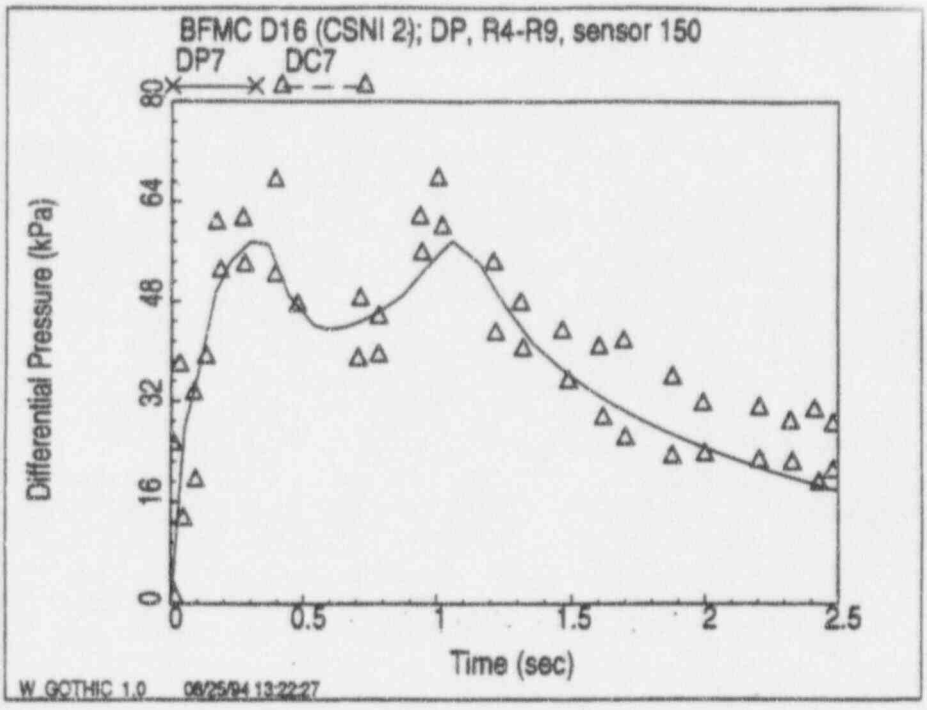

Figure D-5 Differential Pressure, R4 to R9; BFMC Test D-16

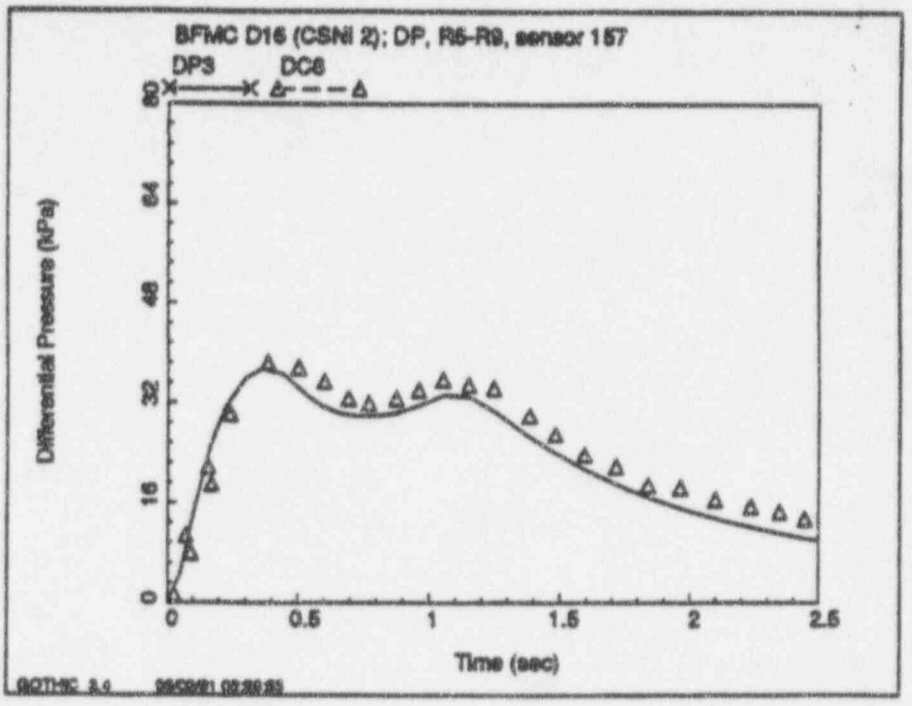

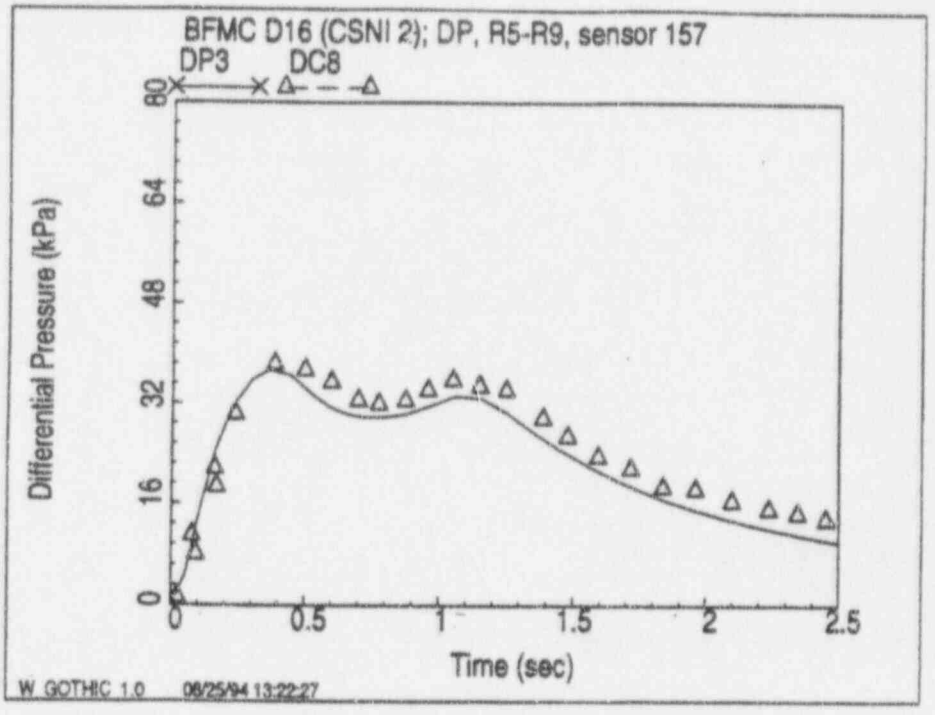

Figure D-6 Differential Pressure, R5 to R9; BFMC Test D-16

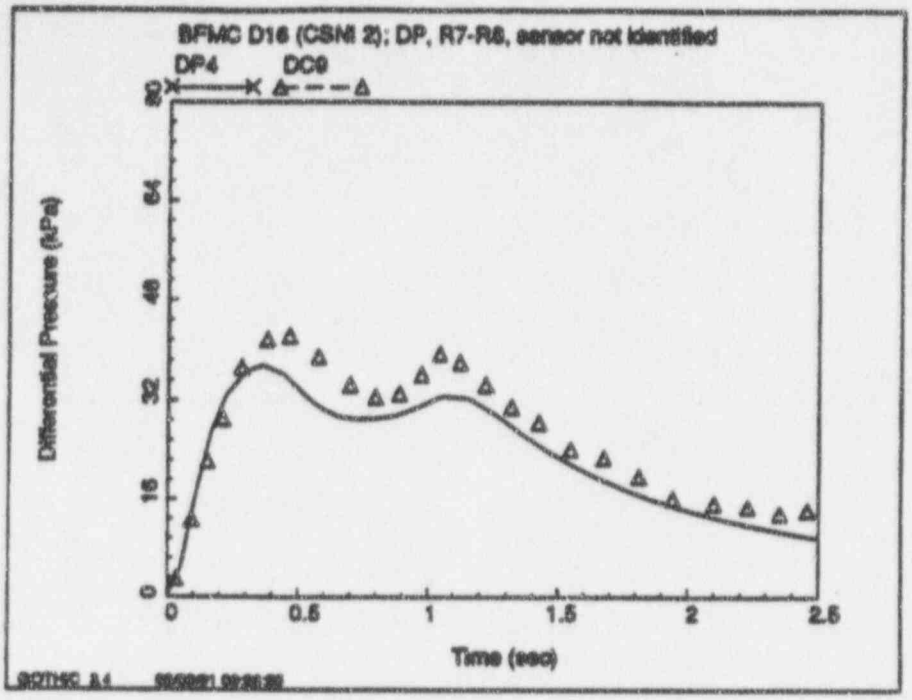

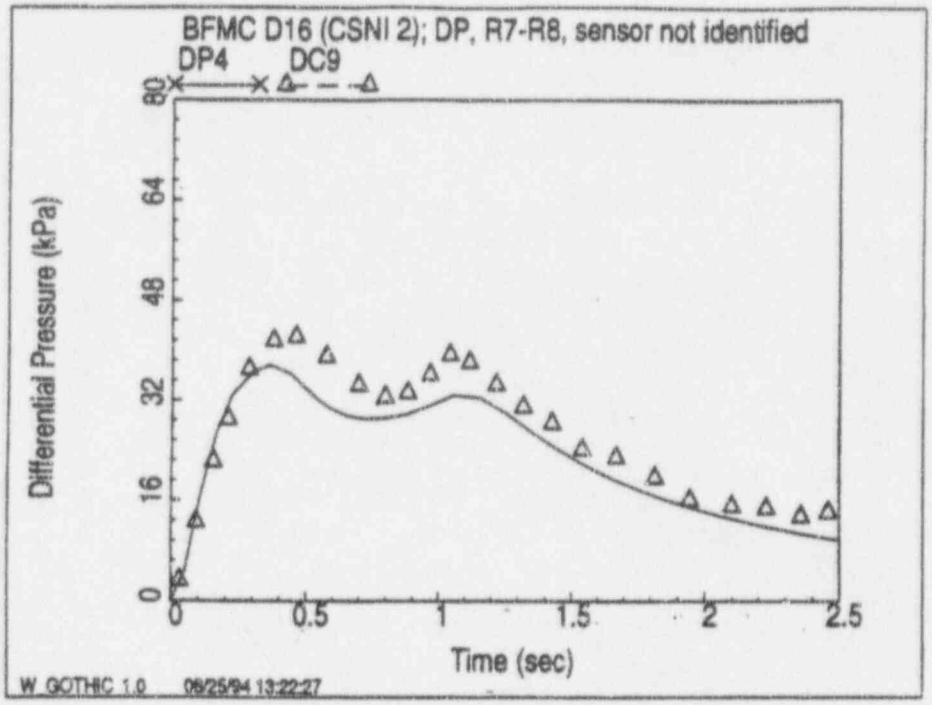

Figure D-7 Differential Pressure, R7 to R8; BFMC Test D-16

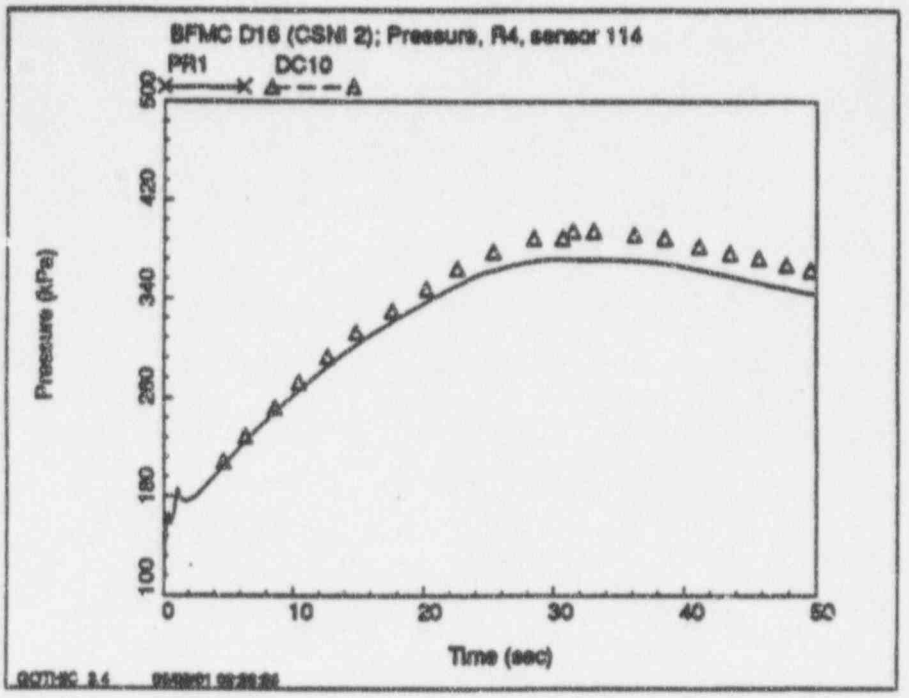

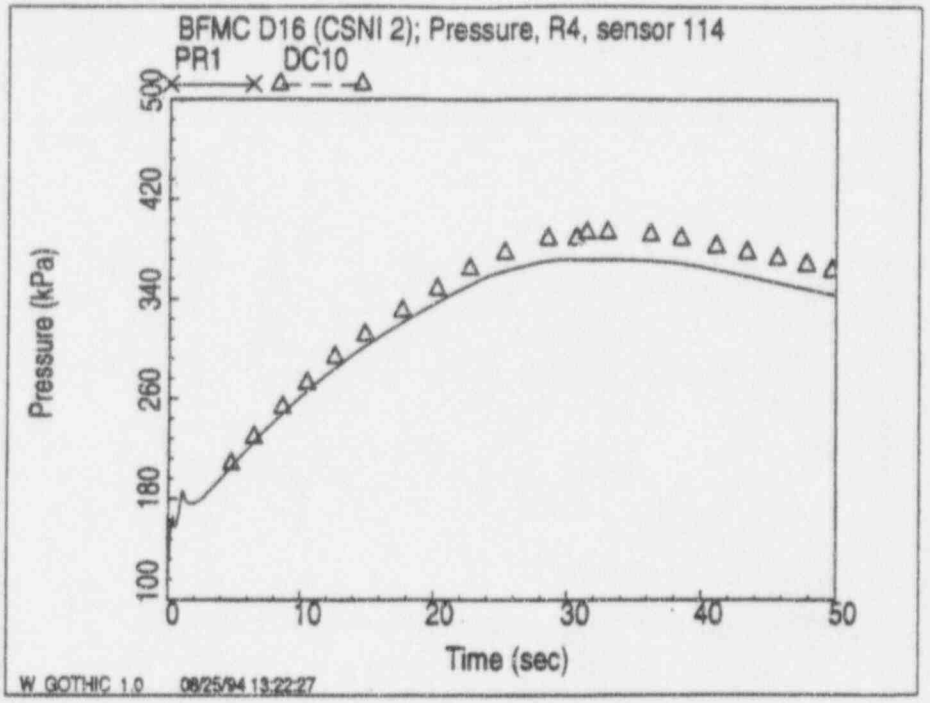

Figure D-8 Pressure in Room R4; BFMC Test D-16, 0-50 Seconds

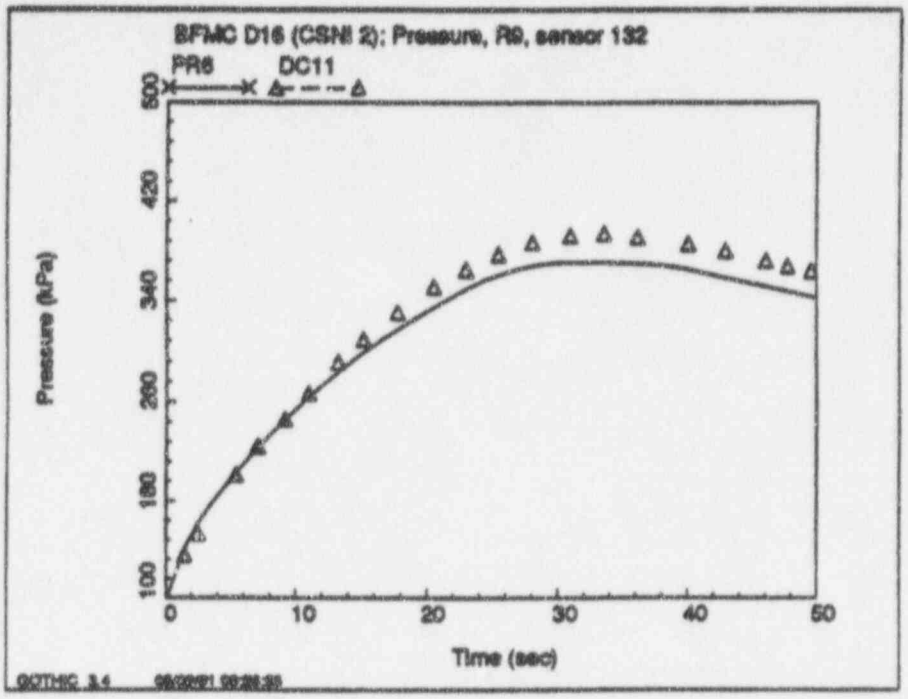

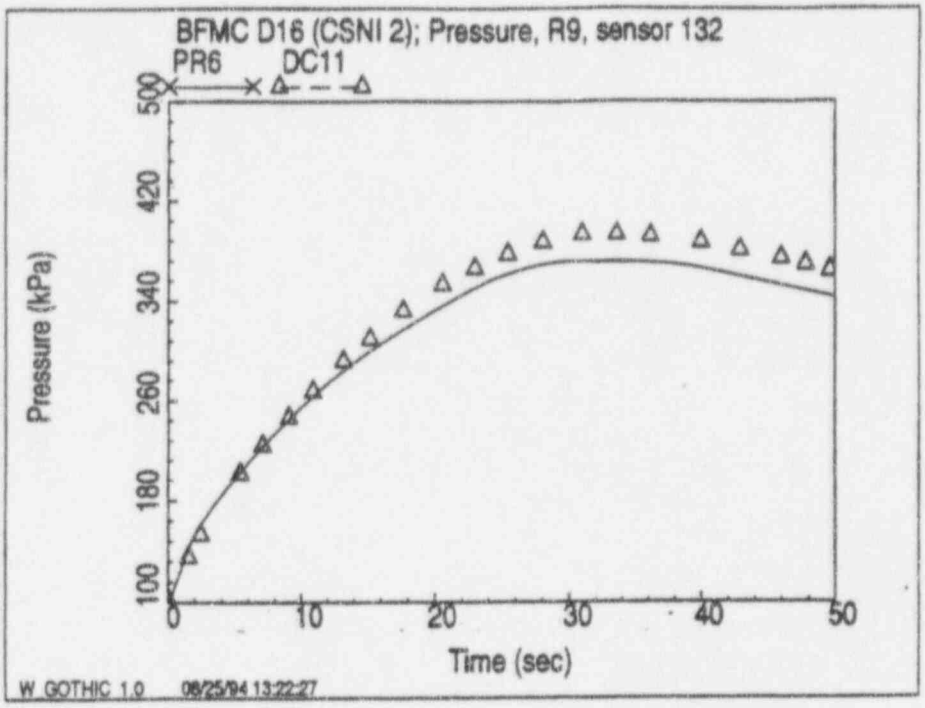

Figure D-9 Pressure in Room R9; BFMC Test D-16, 0-50 Seconds

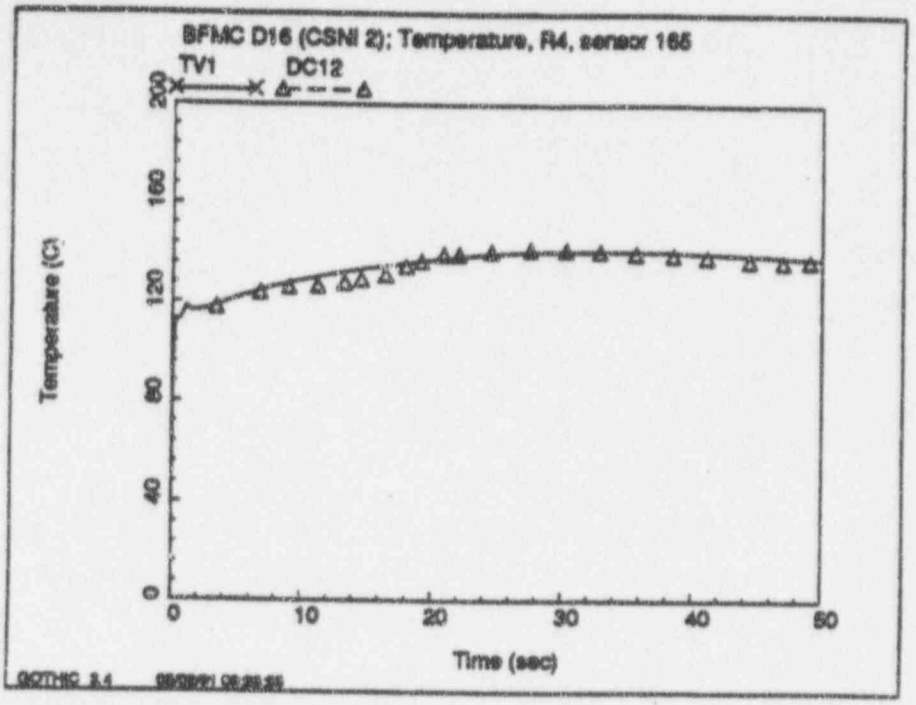

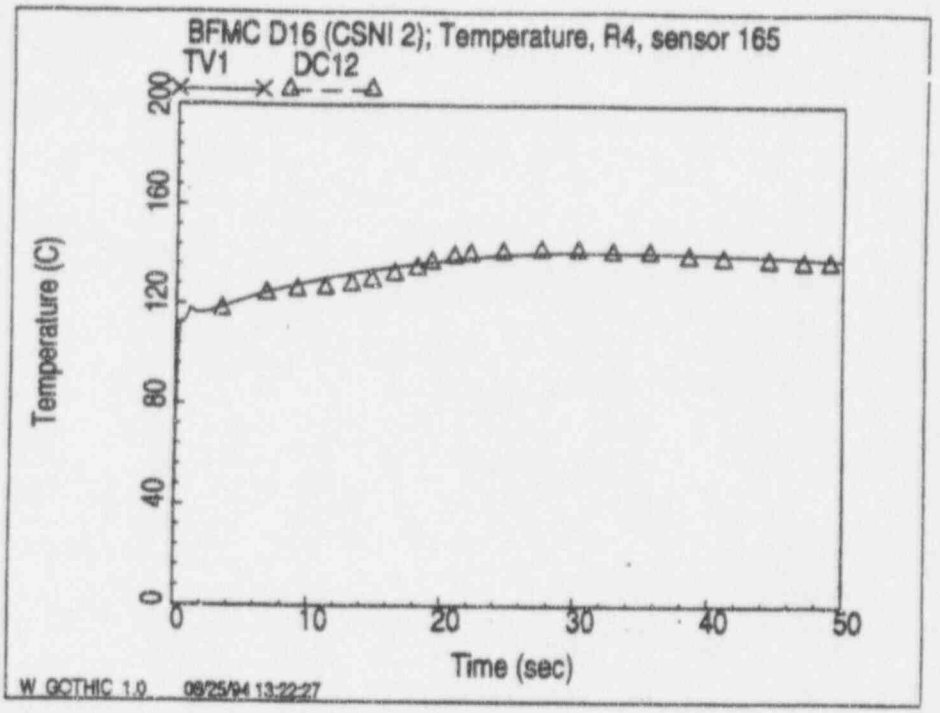

Figure D-10 Temperature in Room R4; BFMC Test D-16

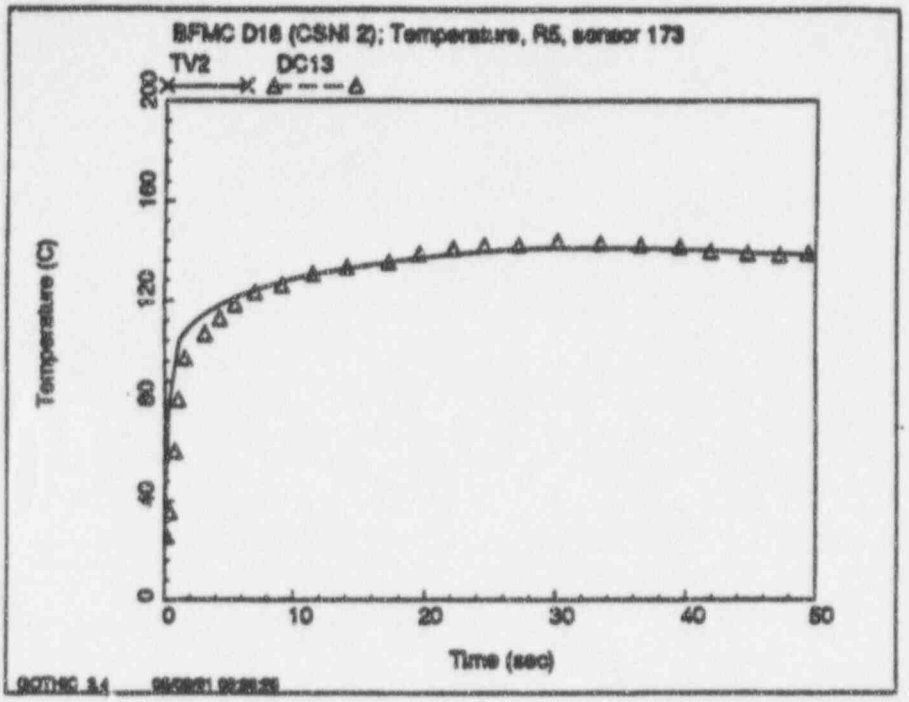

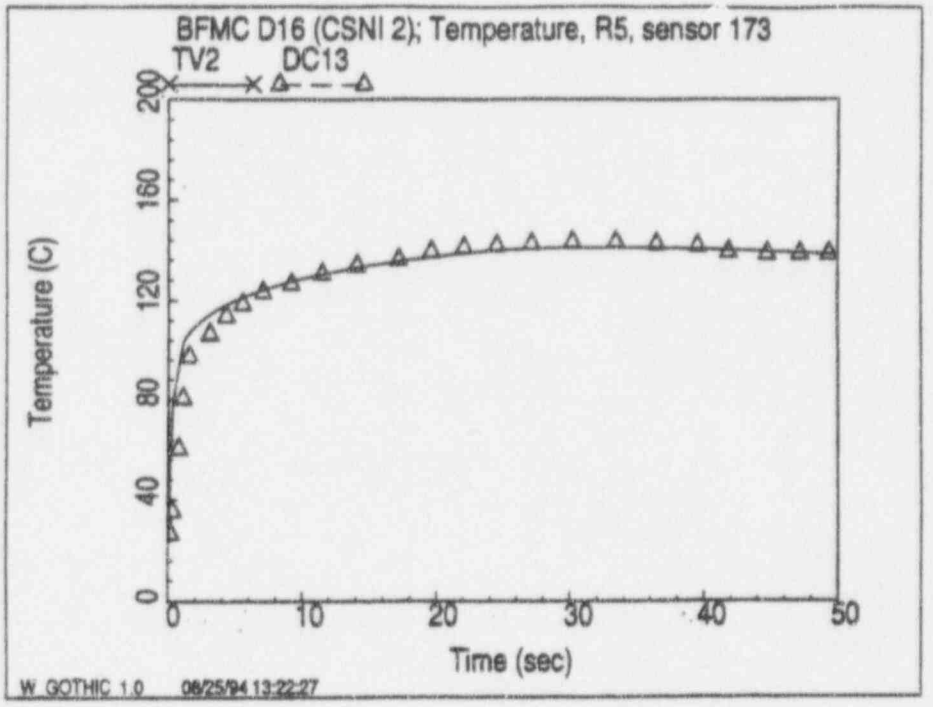

Figure D-11 Temperature in Room R5; BFMC Test D-16

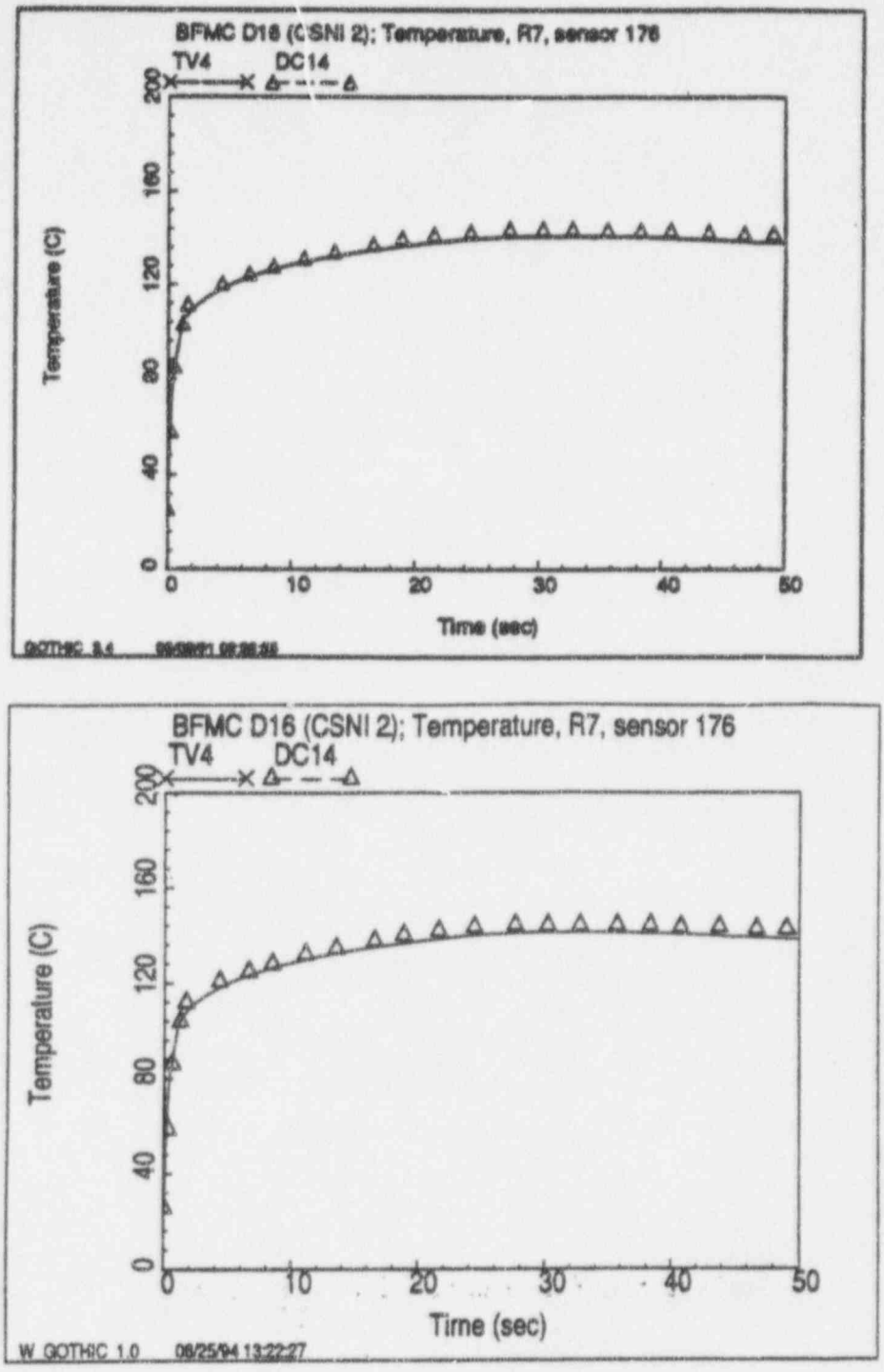

Figure D-12 Temperature in Room R7; BFMC Test D-16

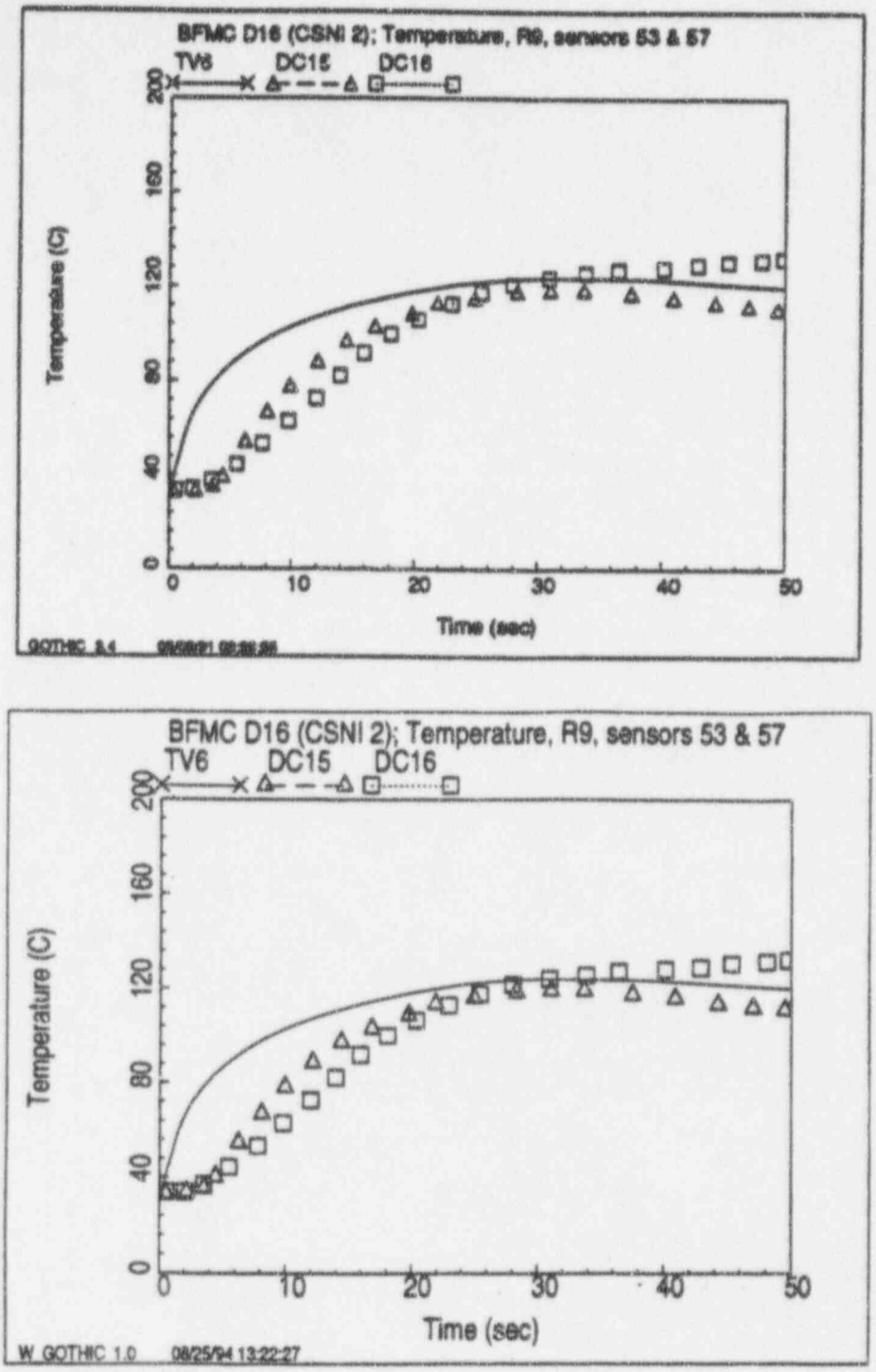

Figure D-13 Temperature in Room R9; BFMC Test D-16

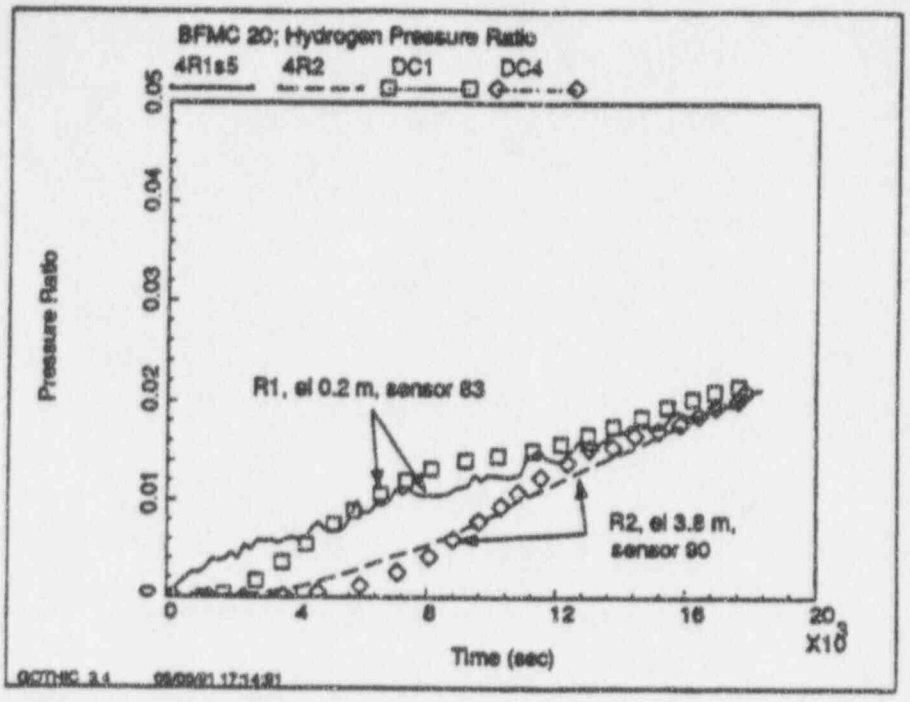

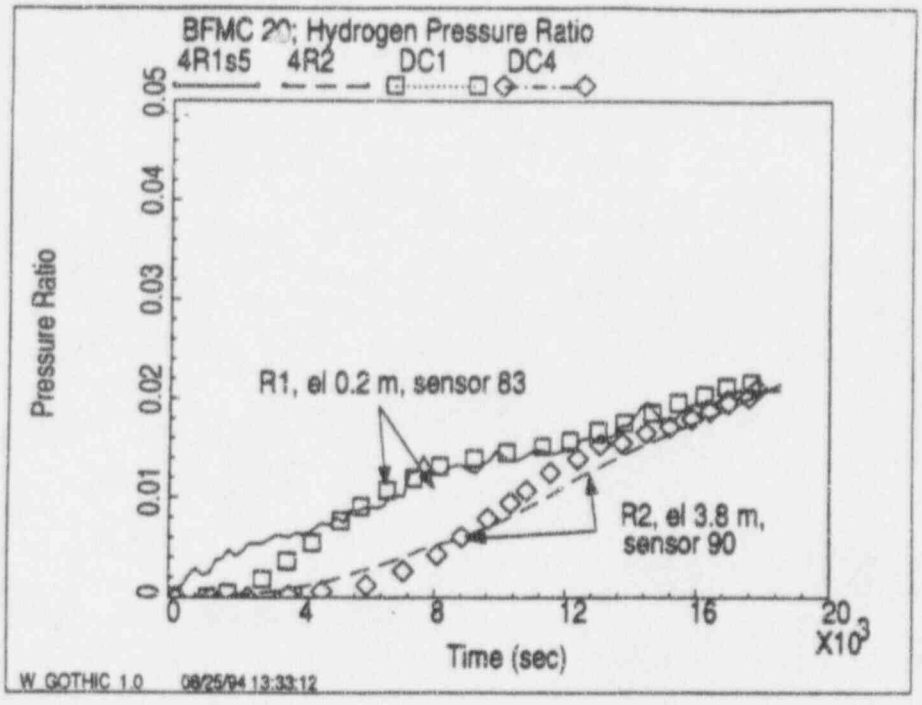

Figure D-14 Hydrogen Concentration in Rooms R1 and R2; BFMC Test D-20

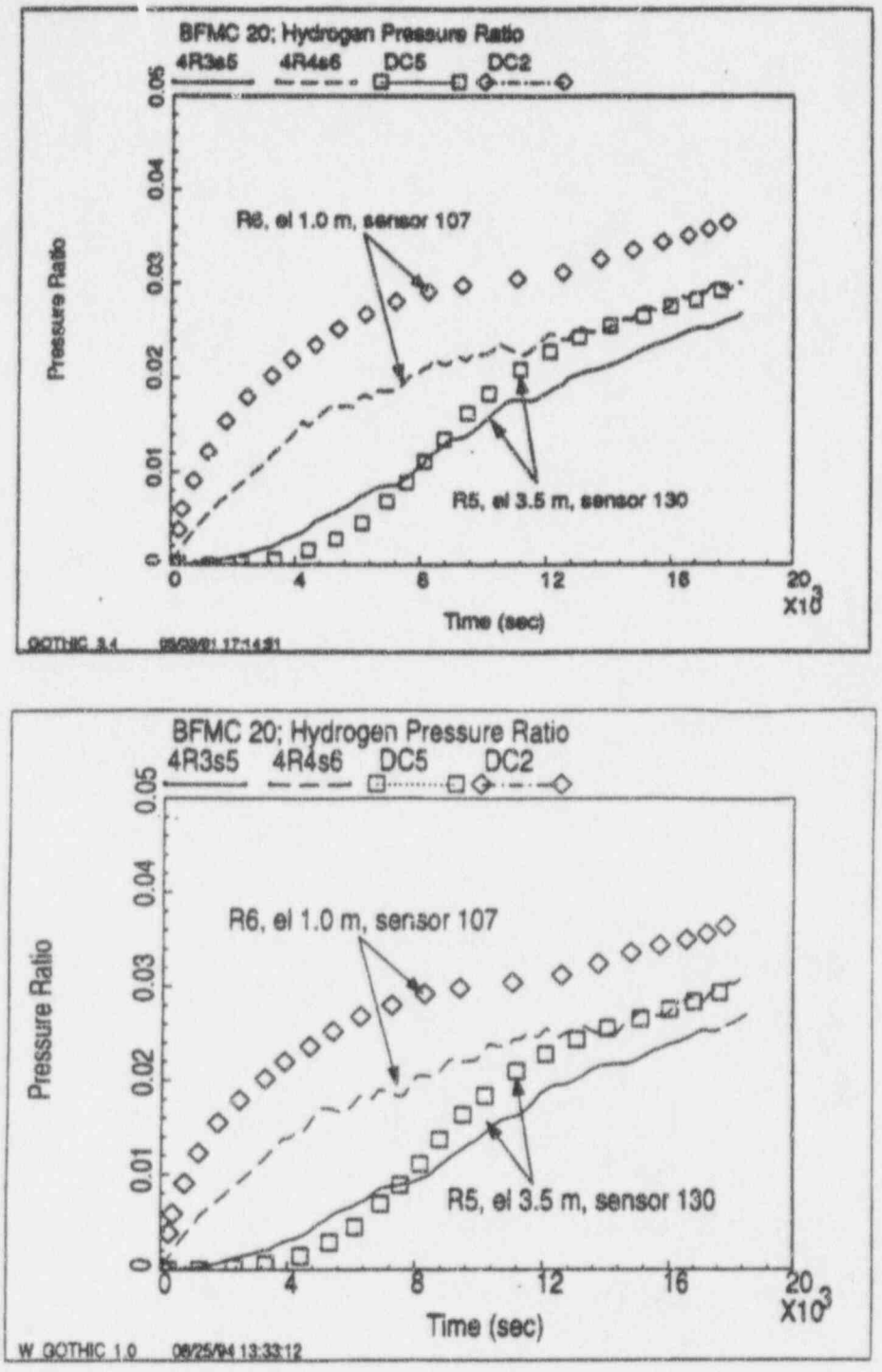

Figure D-15 Hydrogen Concentration in Rooms R5 and R6; BFMC Test D-20

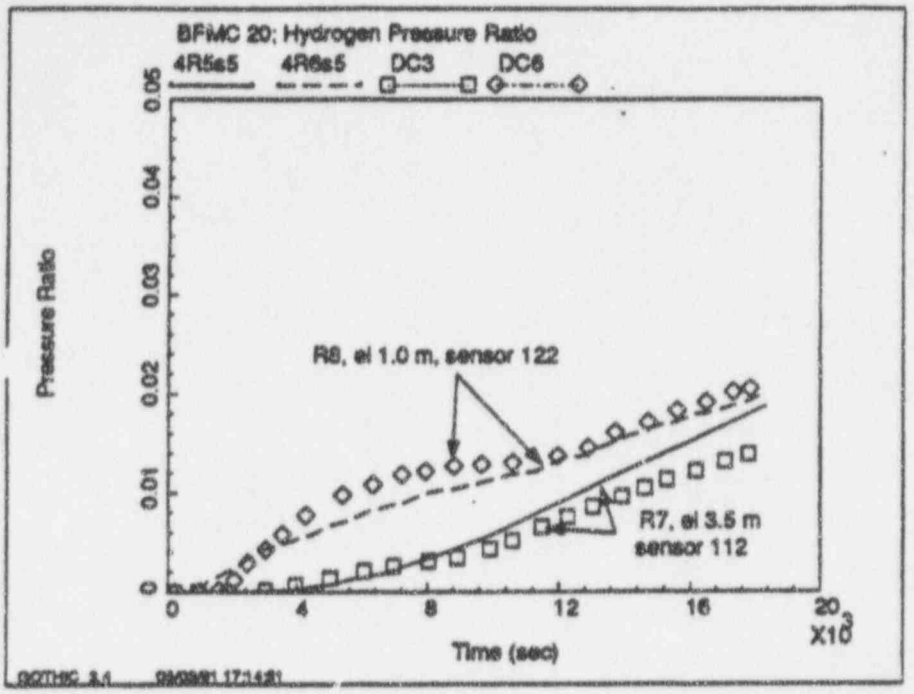

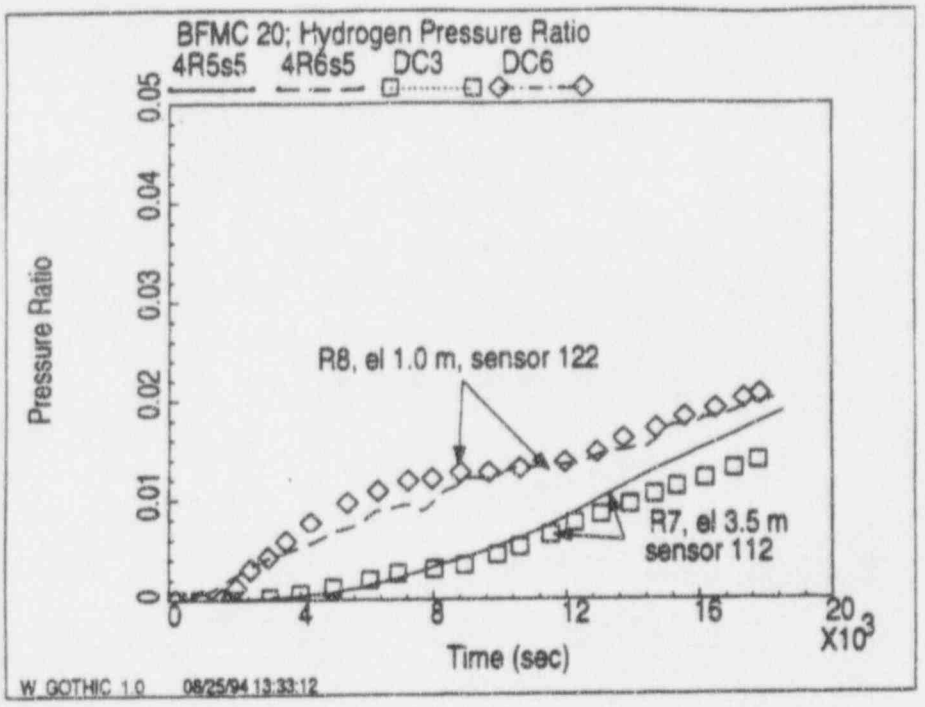

Figure D-16 Hydrogen Concentration in Rooms P.7 and R8; BFMC Test D-20

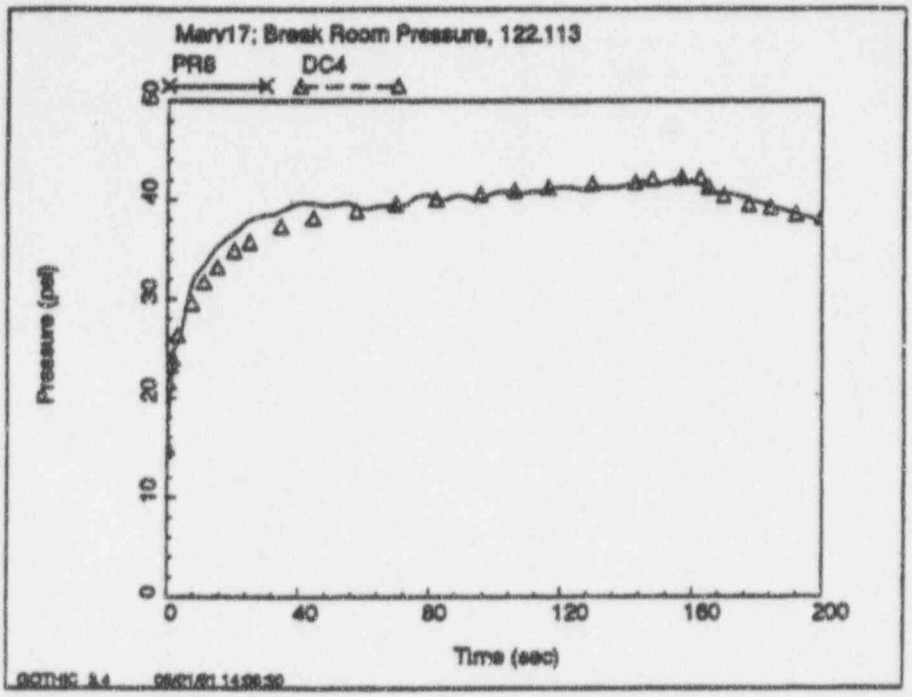

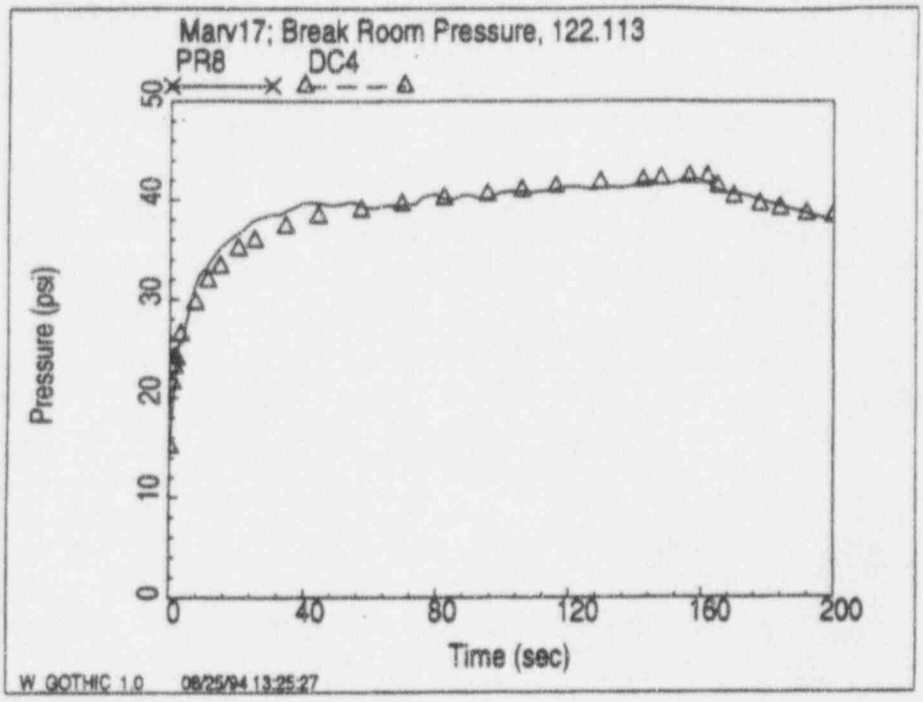

Figure D-17 Break Room Pressure; Marviken Test 17

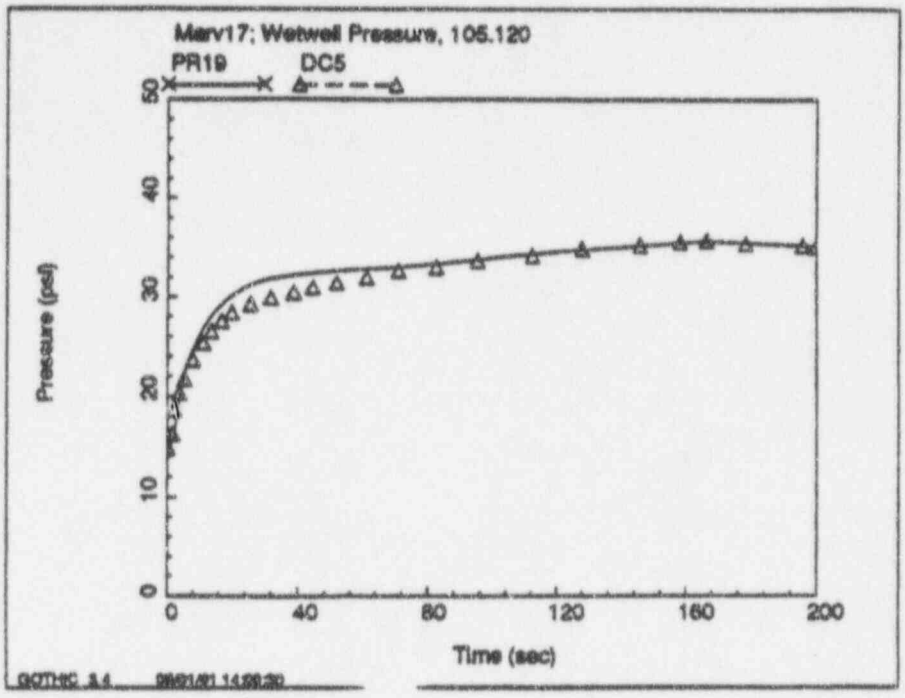

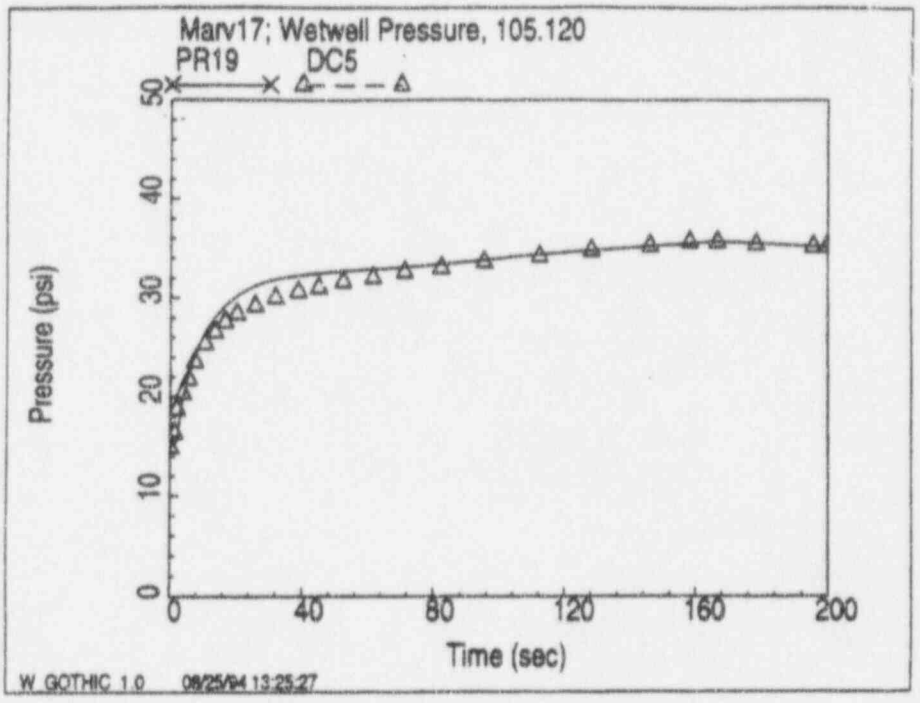

Figure D-18 Wetwell Pressure; Marviken Test 17

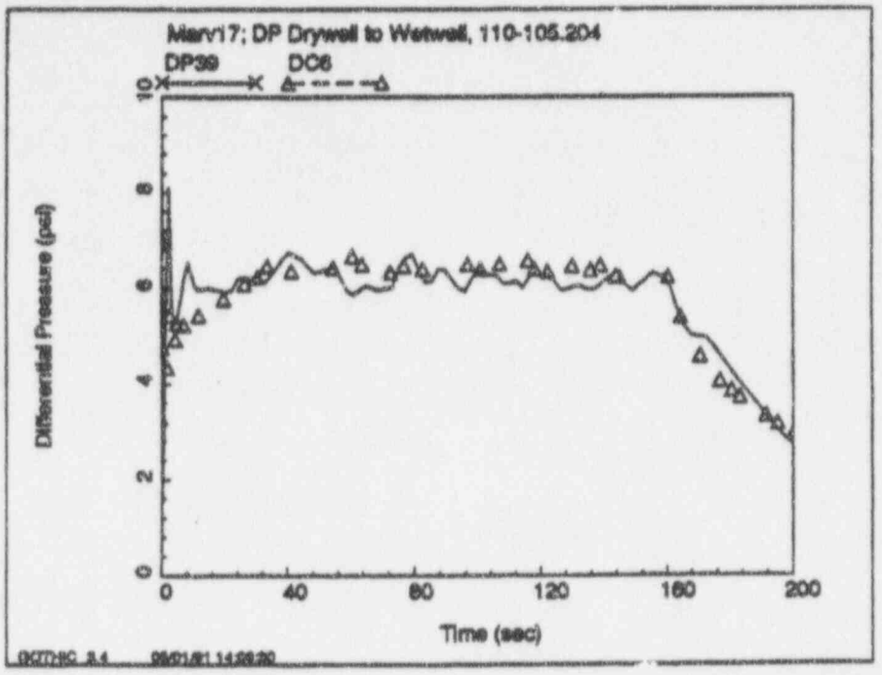

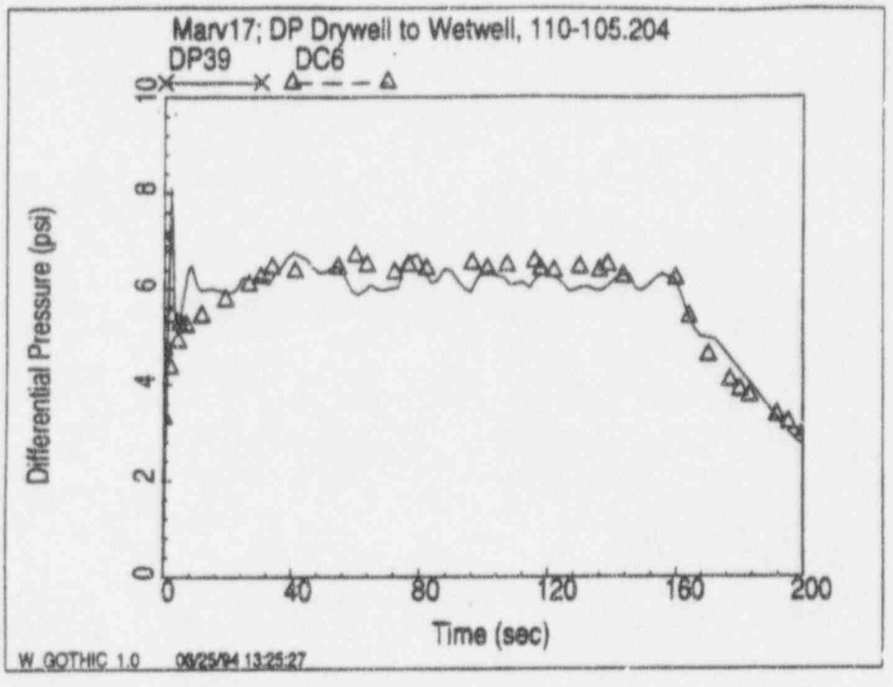

Figure D-19 Differential Pressure, Junction 39; Marviken Test 17

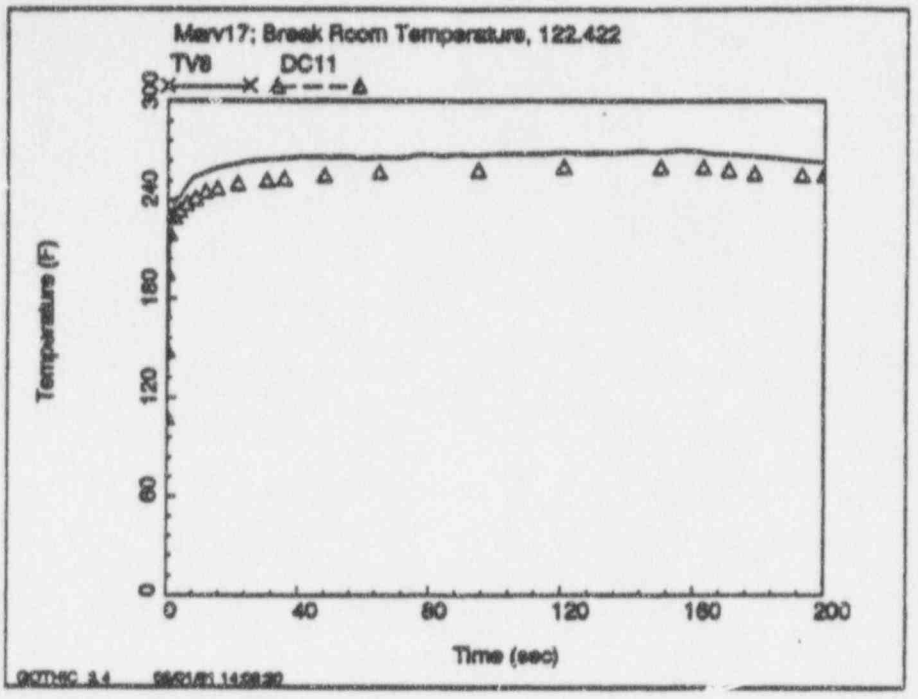

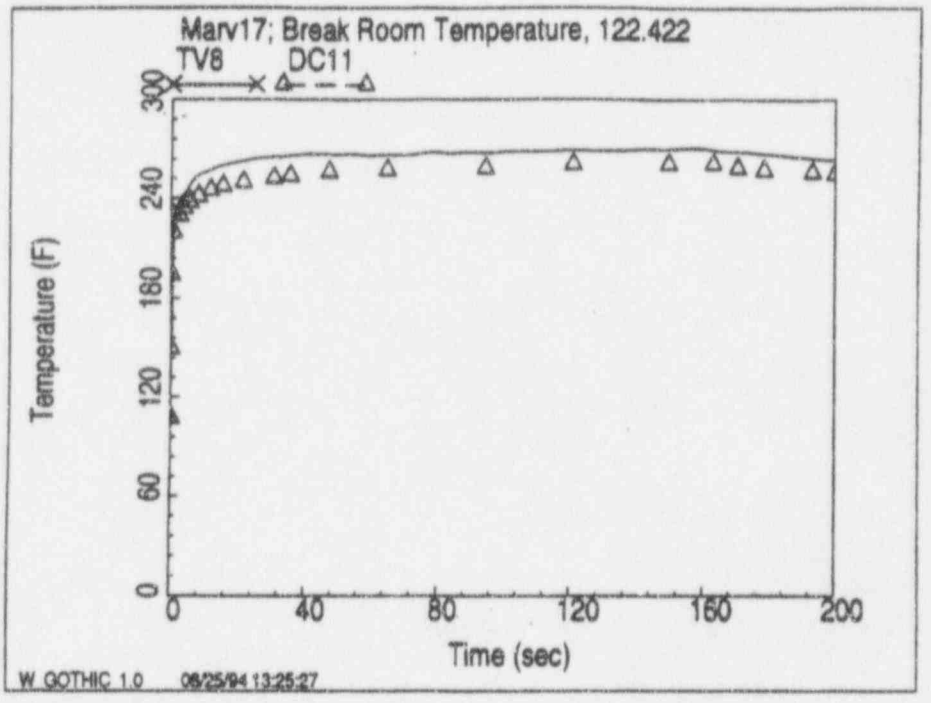

Figure D-20 Break Room Temperature; Marviken Test 17

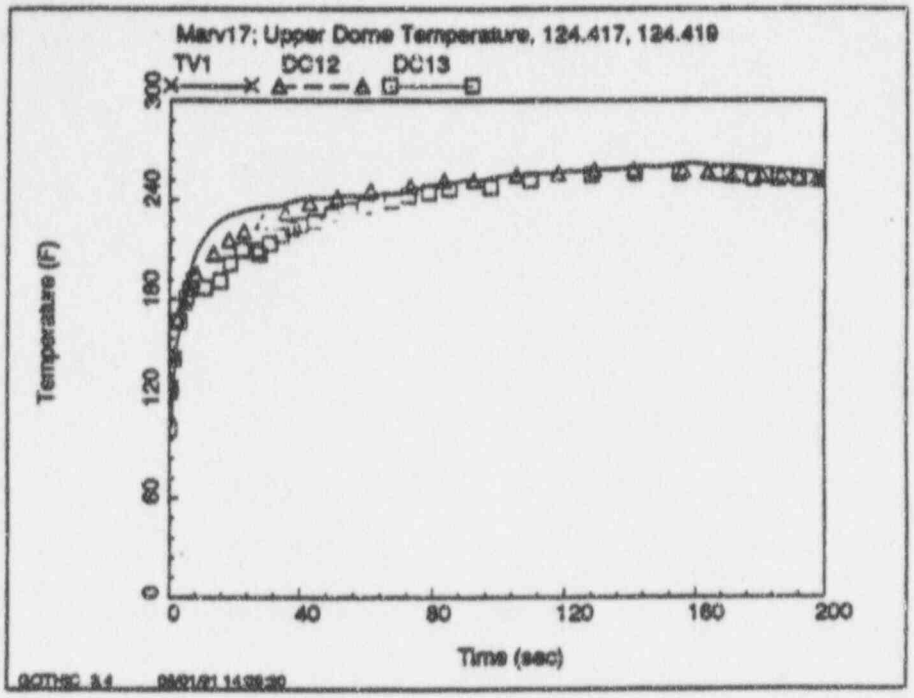

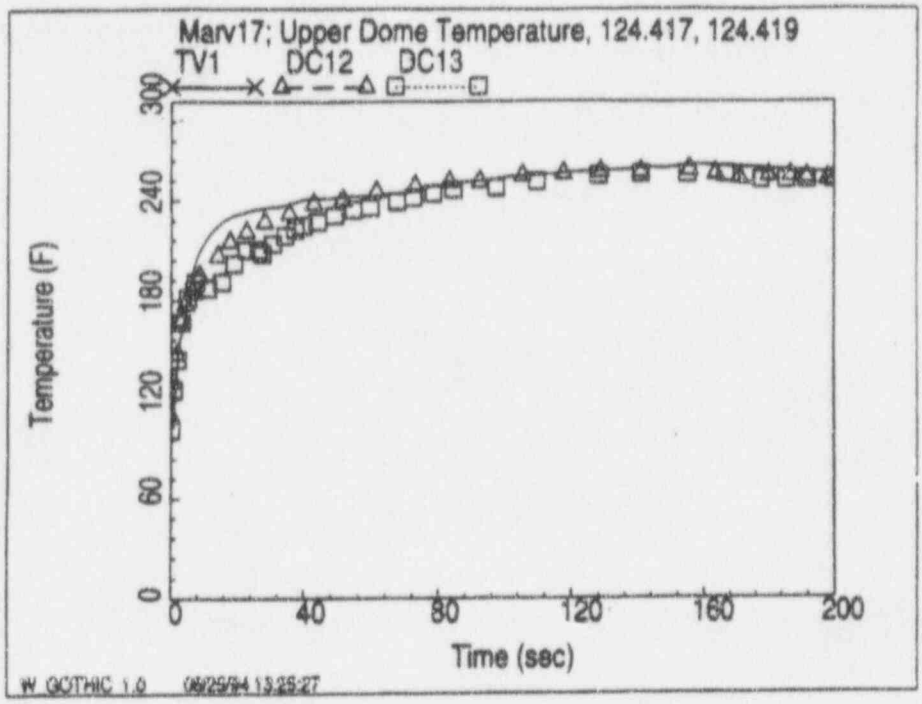

Figure D-21 Upper Dome Temperature; Marviken Test 17

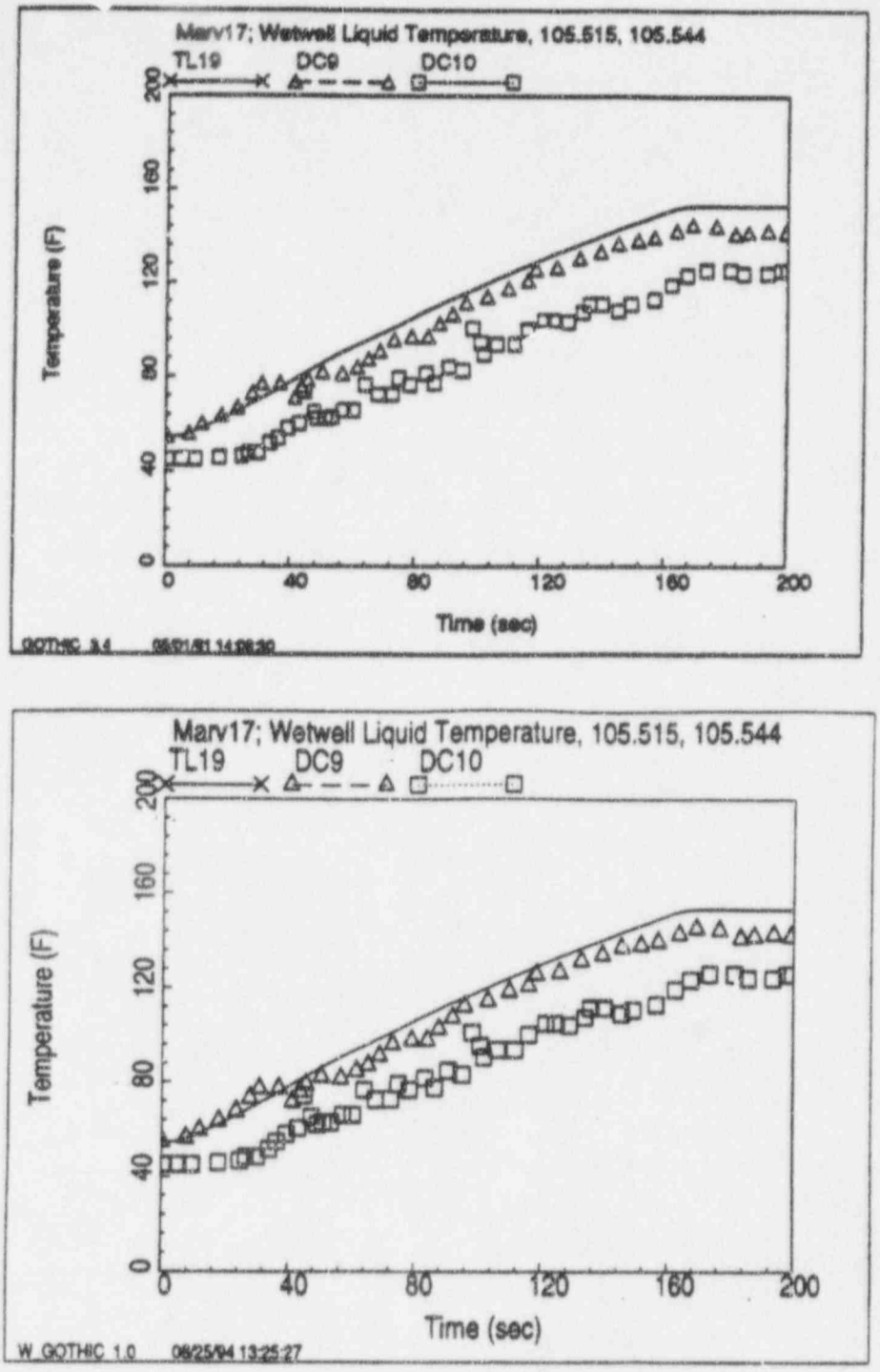

Figure D-22 Wetwell Liquid Temperatures; Marviken Test 17

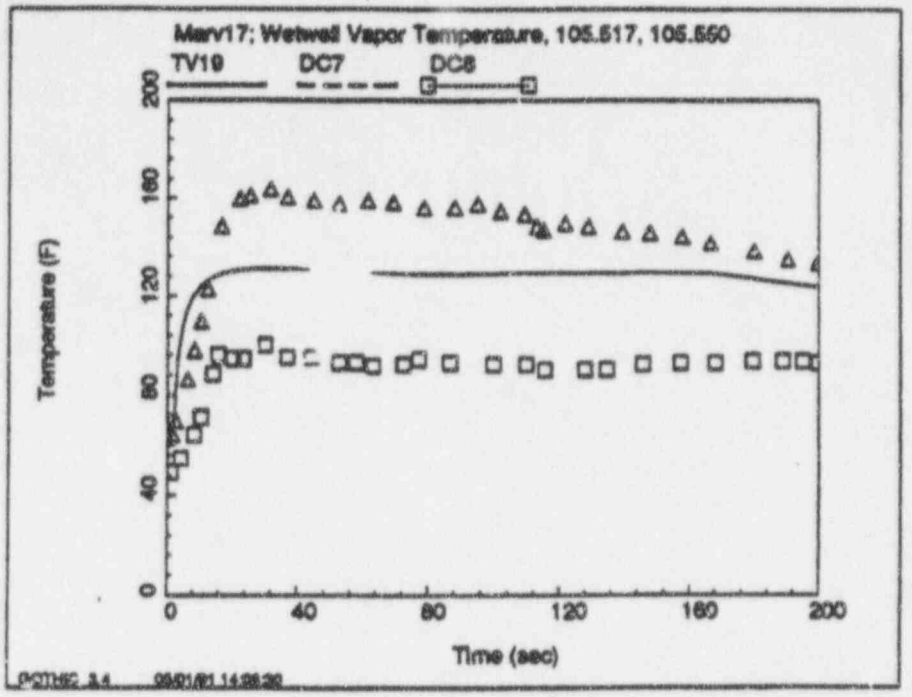

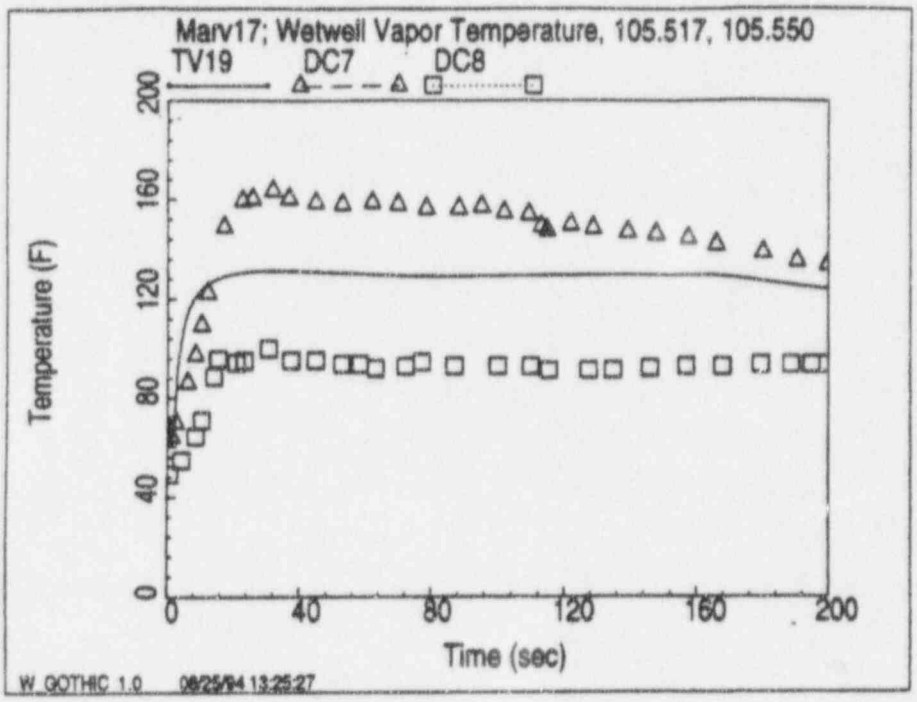

Figure D-23 Wetwell Vapor Temperatures; Marviken Test 17

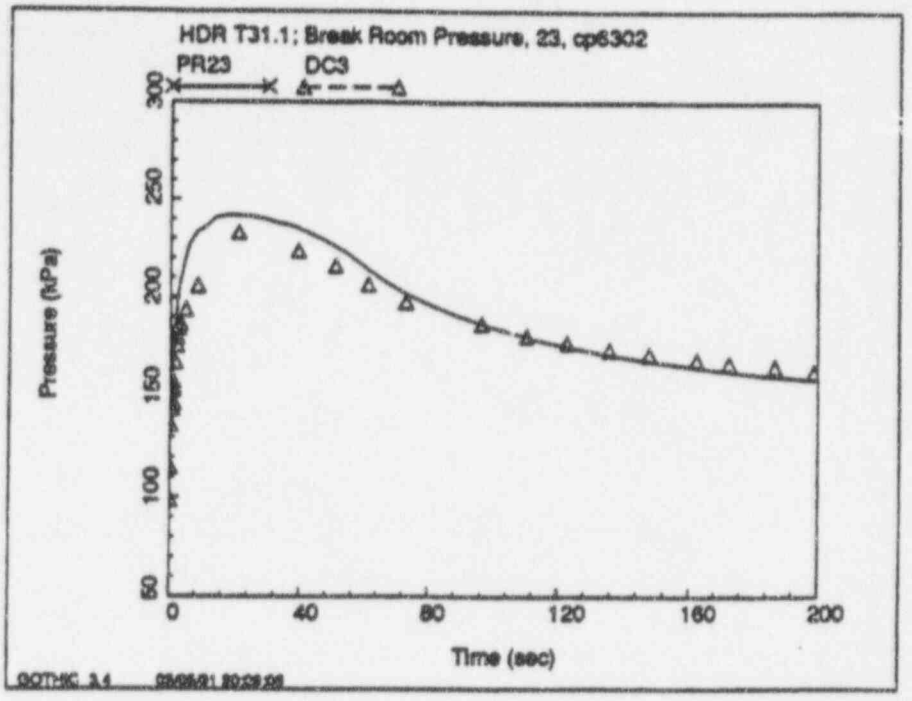

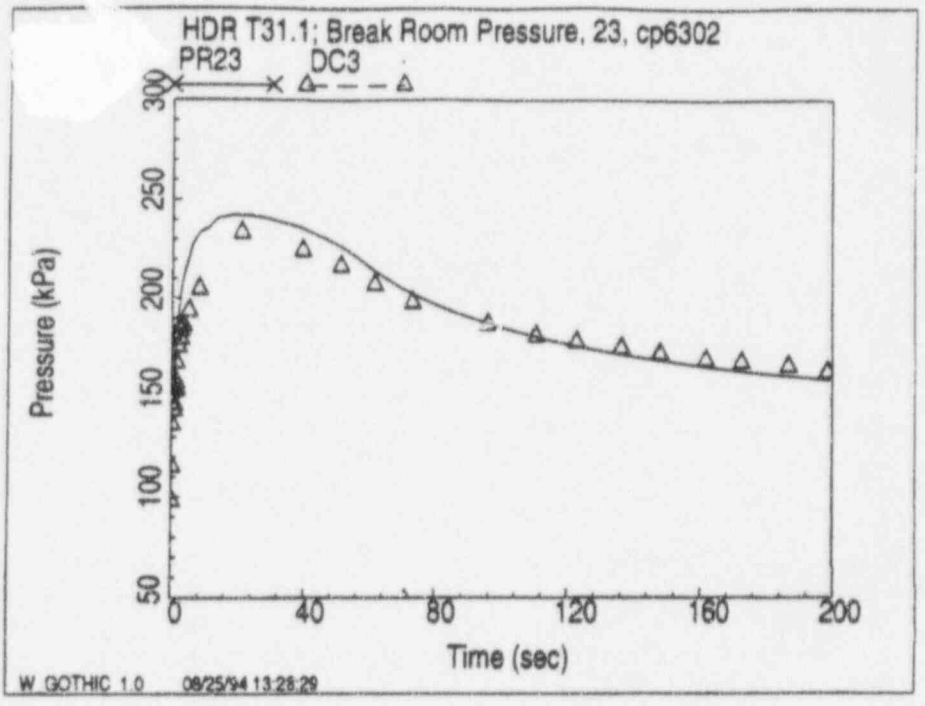

Figure D-24 Break Room Pressure; HDR T31.1

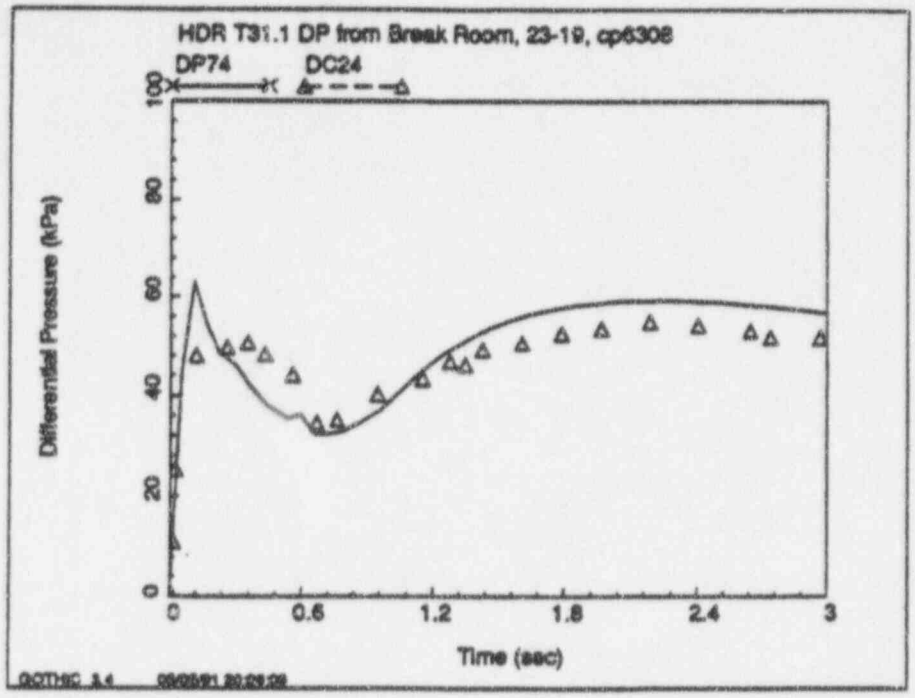

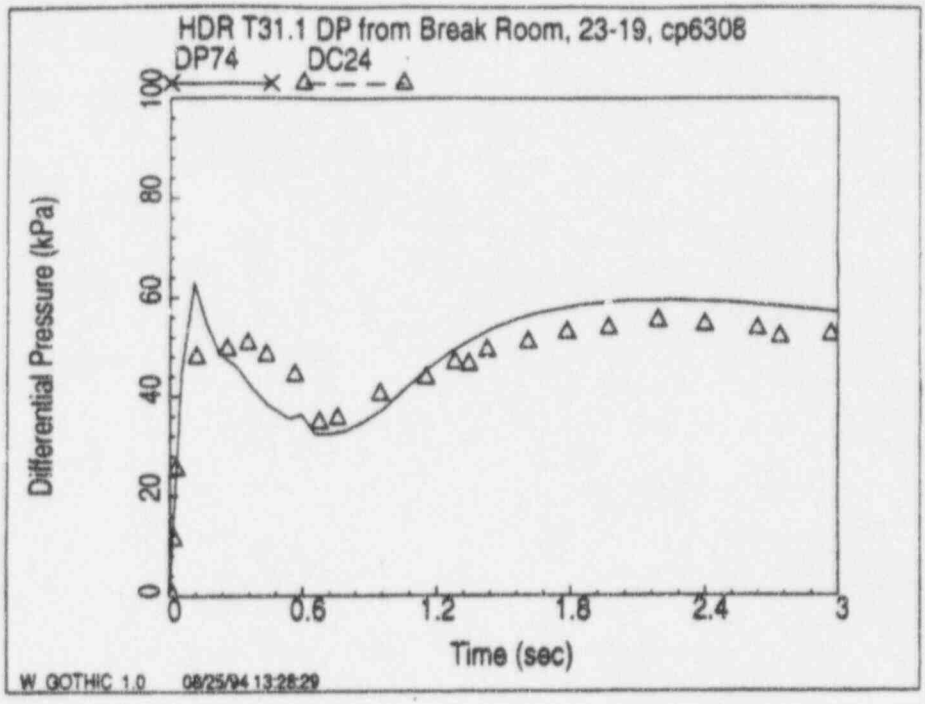

Figure D-25 Differential Pressure from the Break Room; HDR T31.1

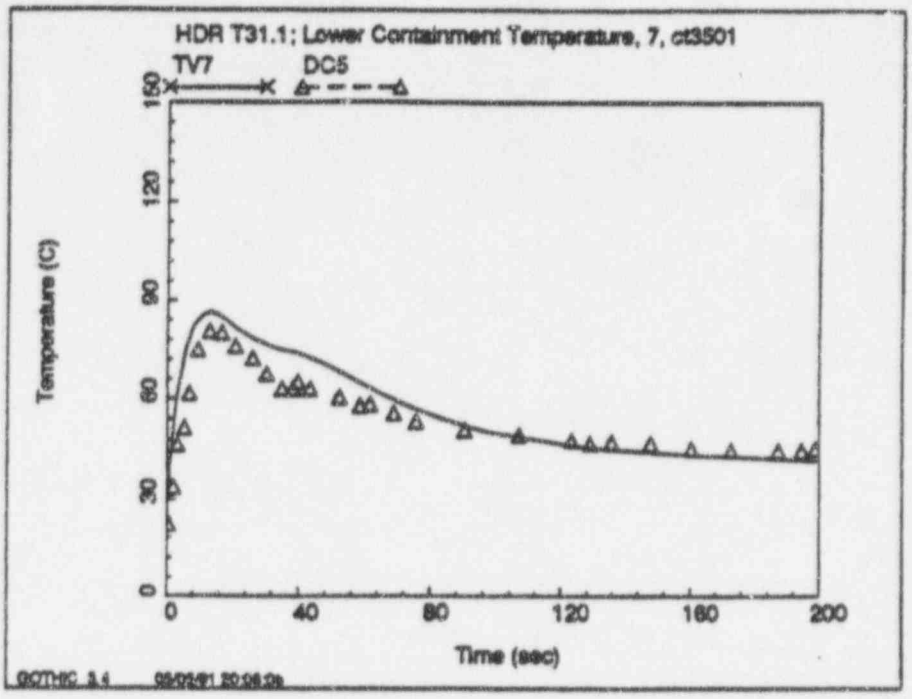

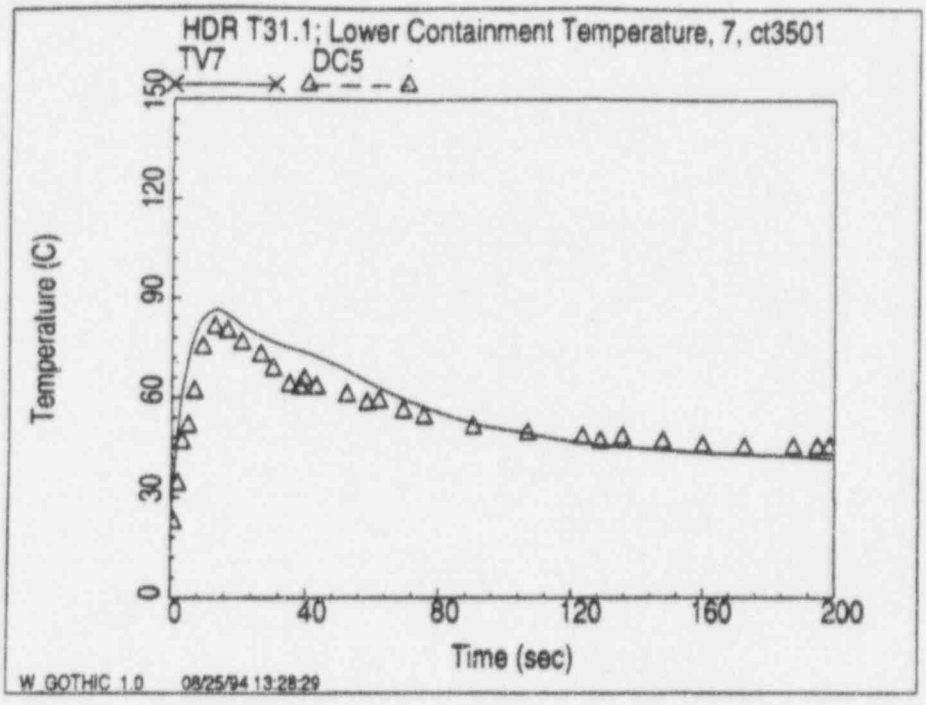

Figure D-26 Lower Containment Vapor Temperature, Volume 9; HDR T31.1

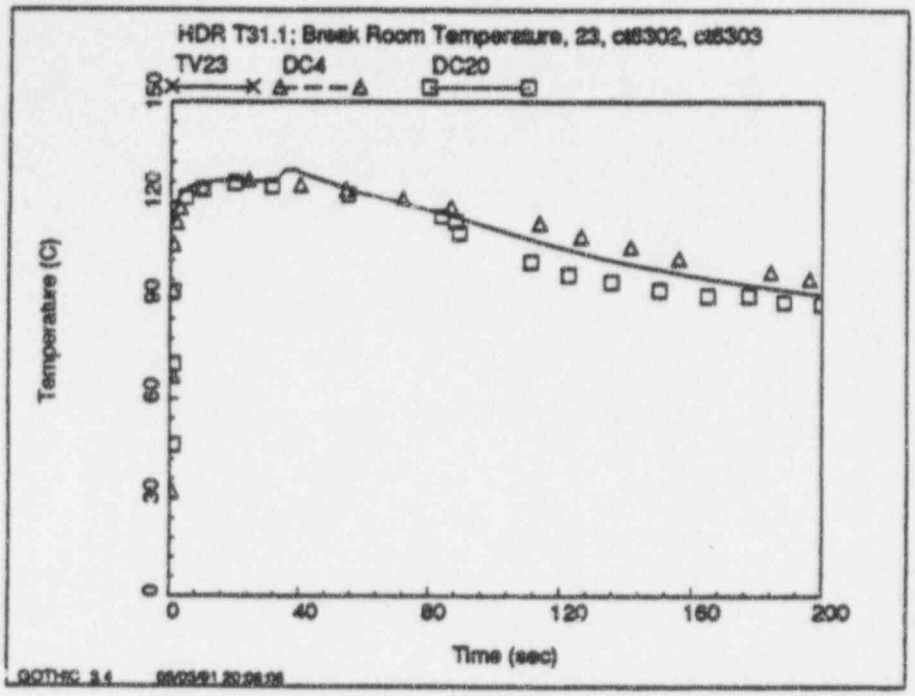

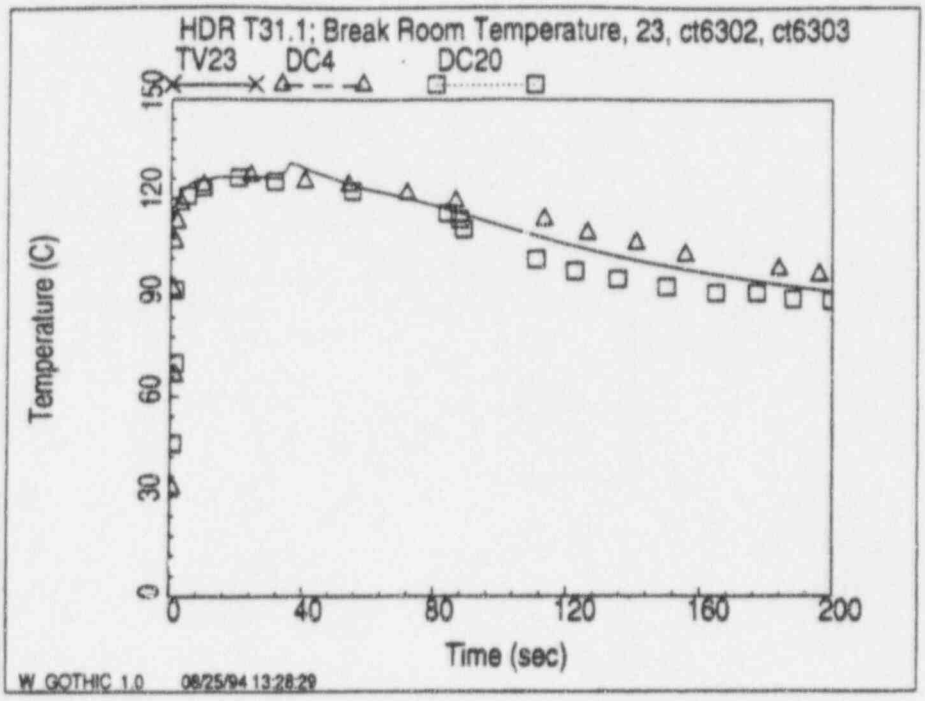

Figure D-27 Break Room Vapor Temperature, Volume 23; HDR T31.1

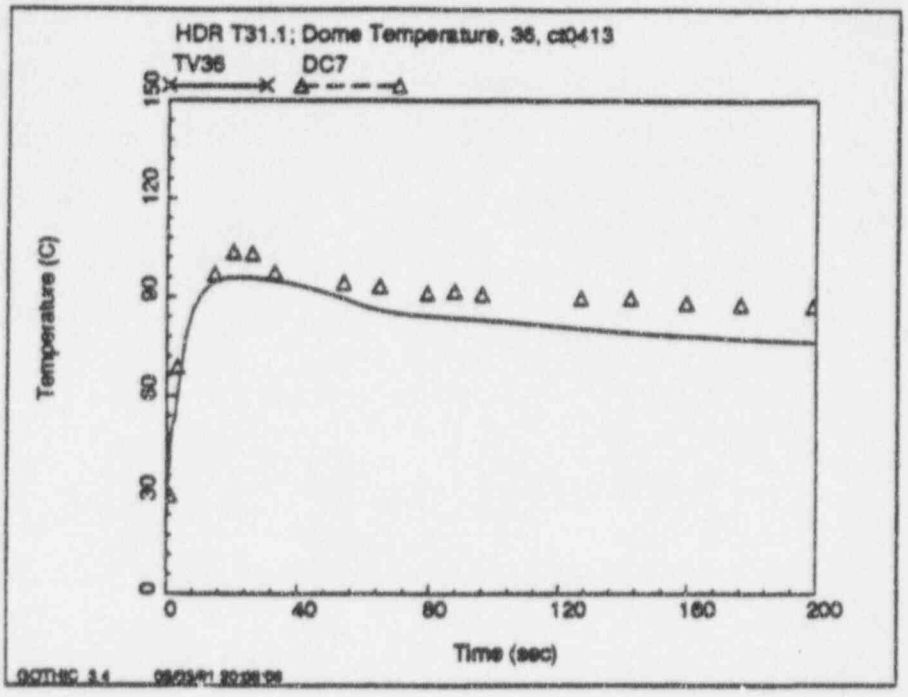

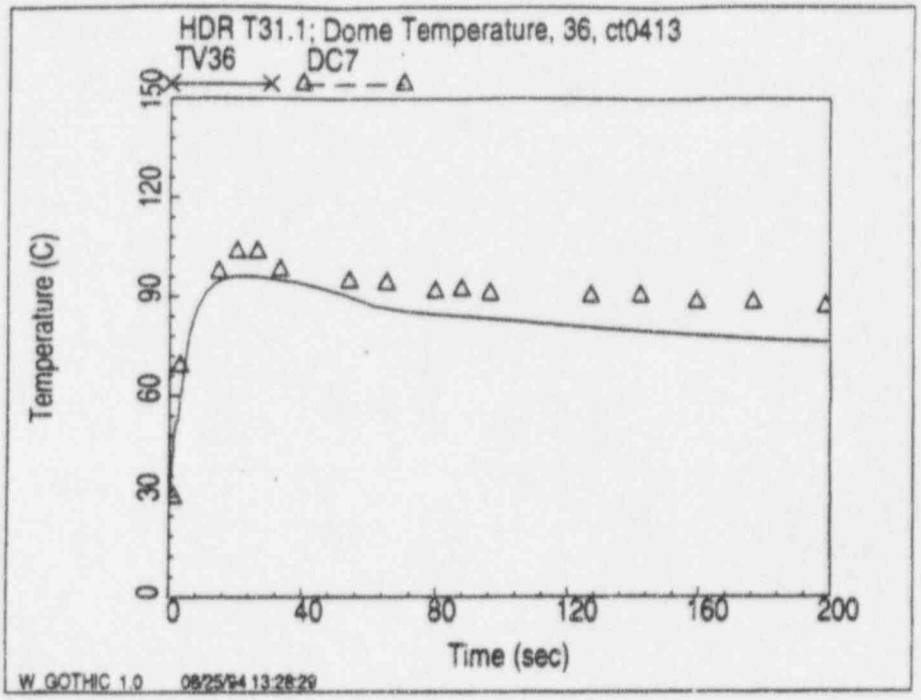

Figure D-28 Dome Vapor Temperature, Volume 36; HDR T31.1

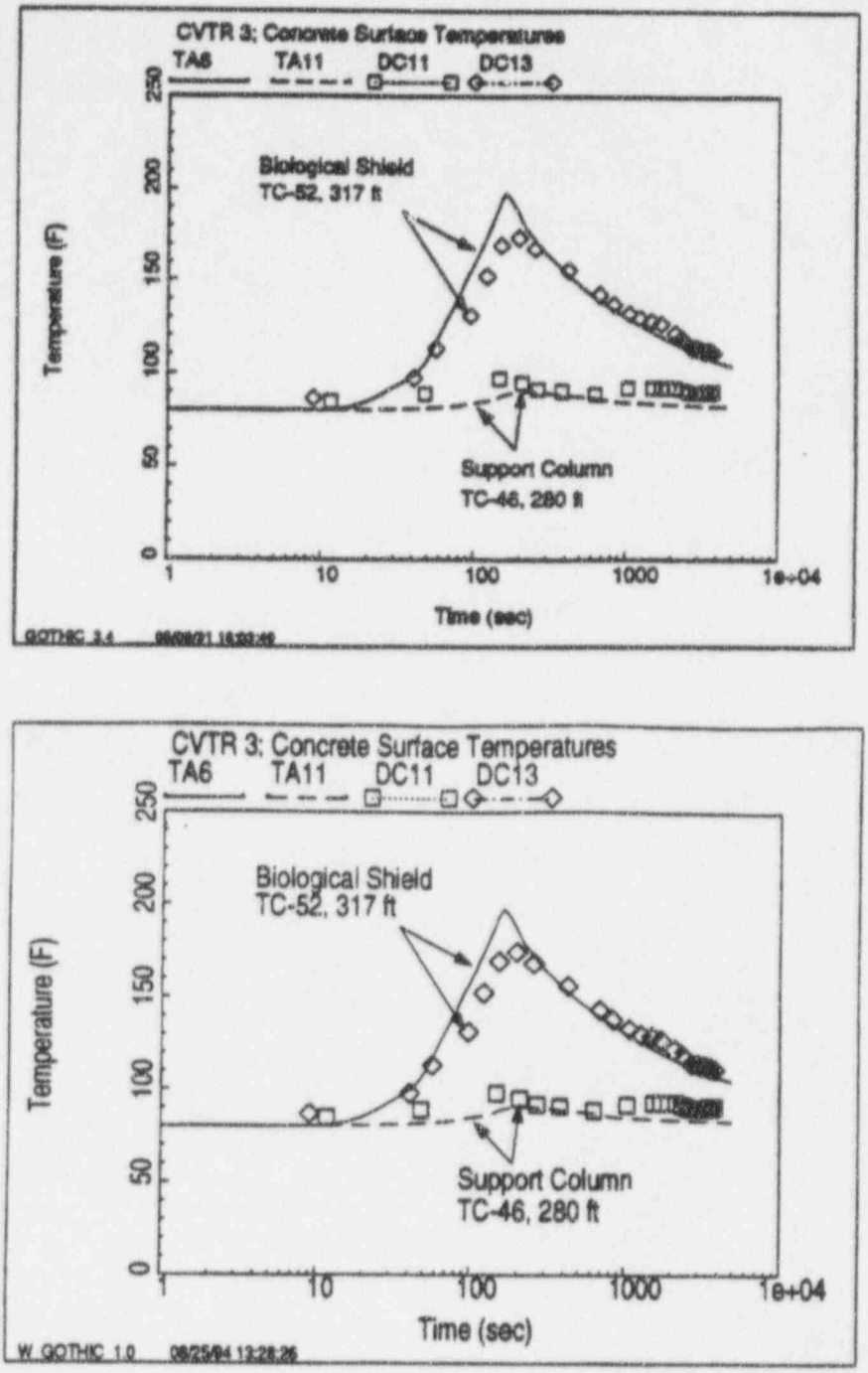

Figure D-29 Concrete Surface Temperatures in Lower Containment; CVTR Test 3

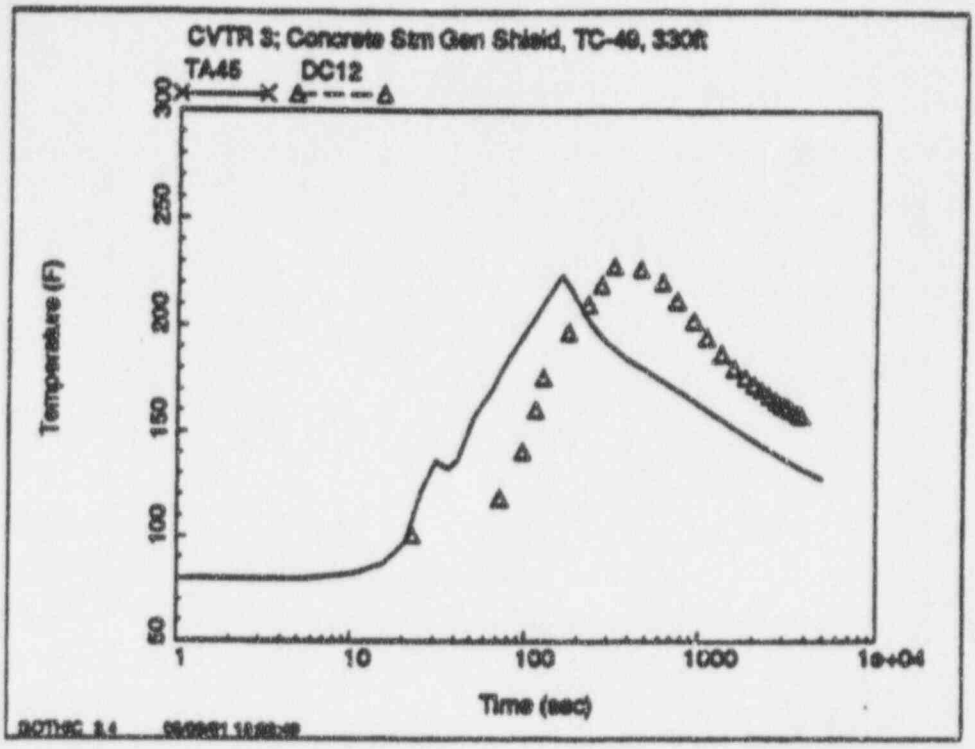

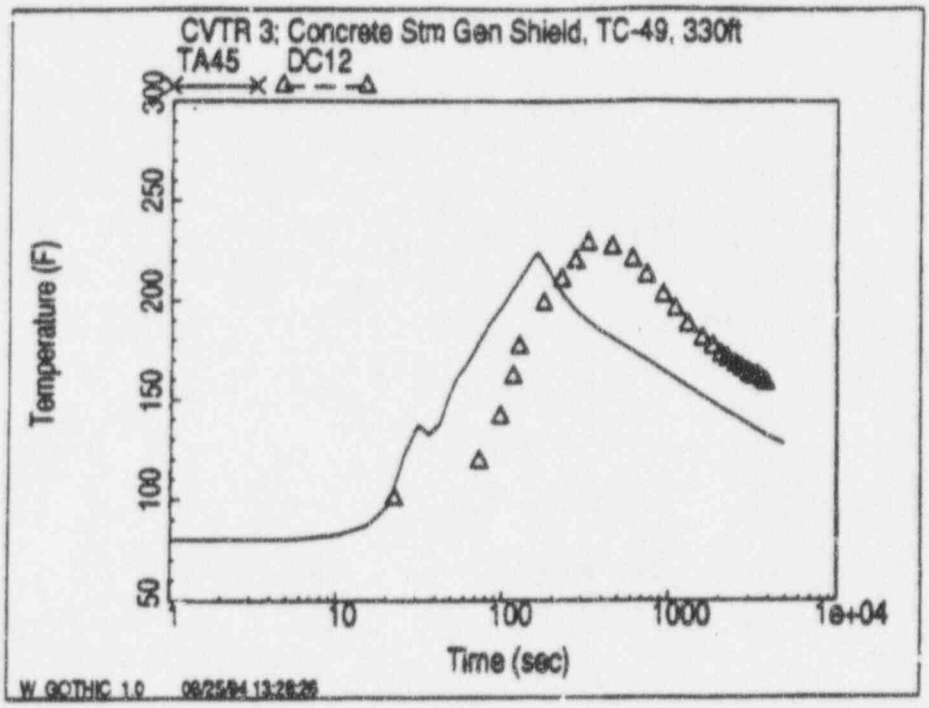

Figure D-30 Concrete Surface Temperatures in Upper Containment; CVTR Test 3

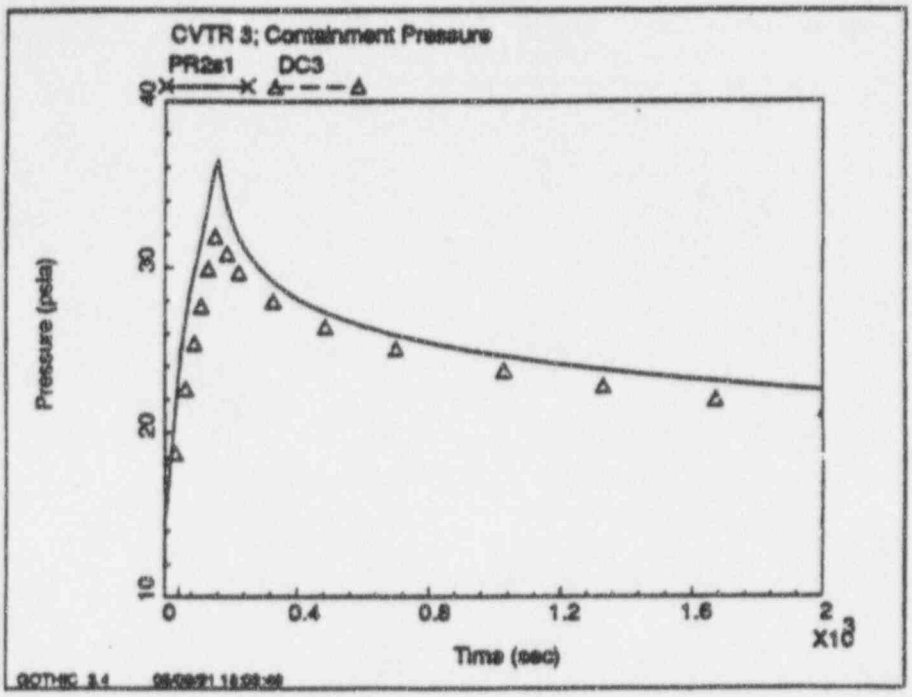

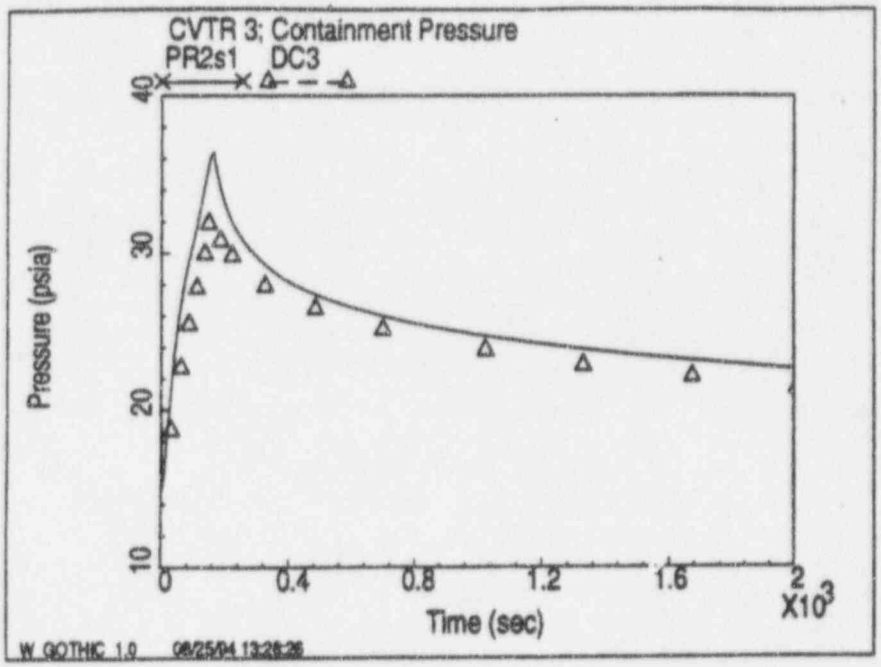

Figure D-31 Containment Pressure; CVTR Test 3

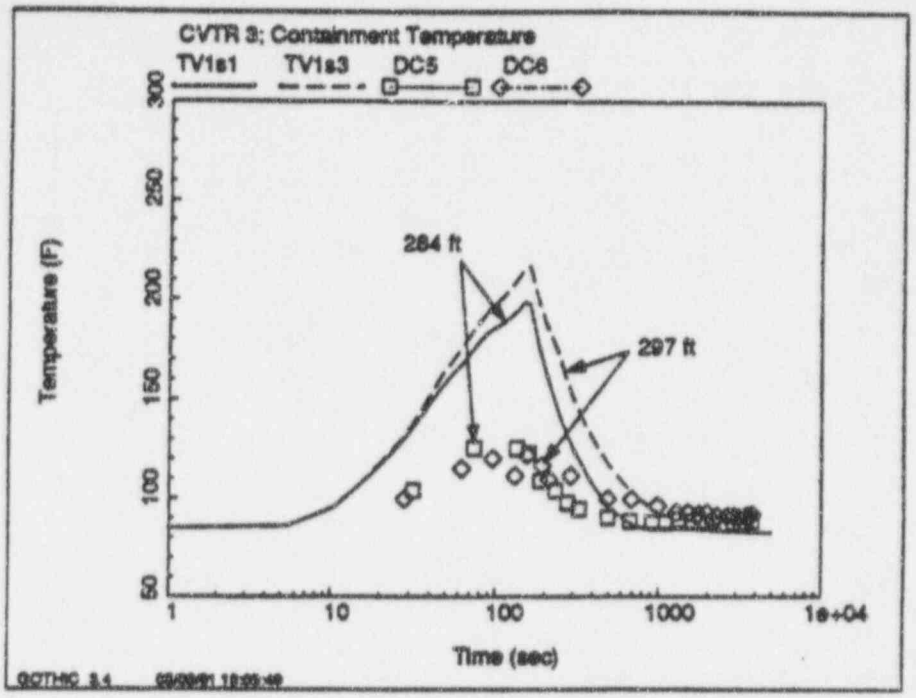

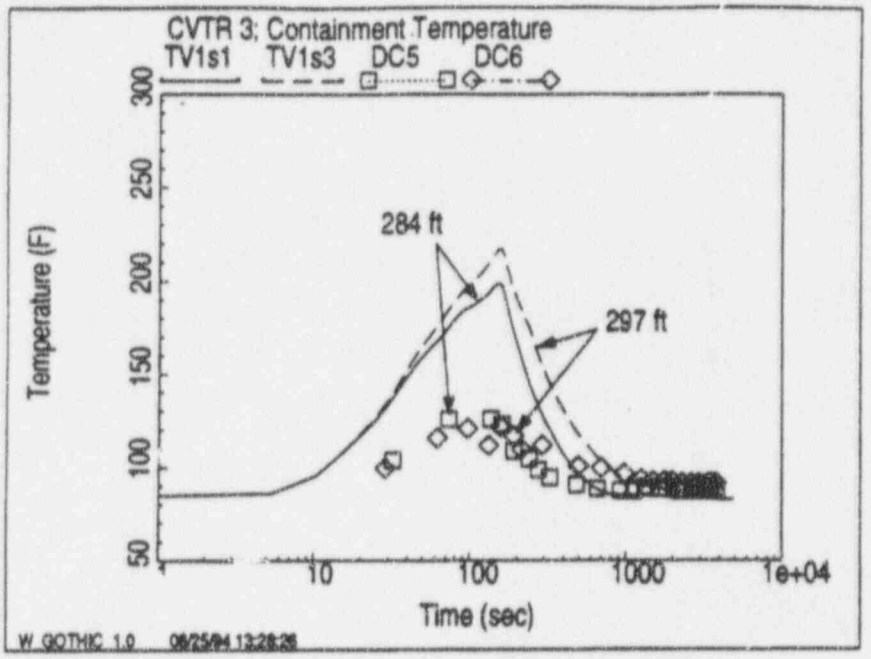

Figure D-32 Containment Temperatures; CVTR Test 3

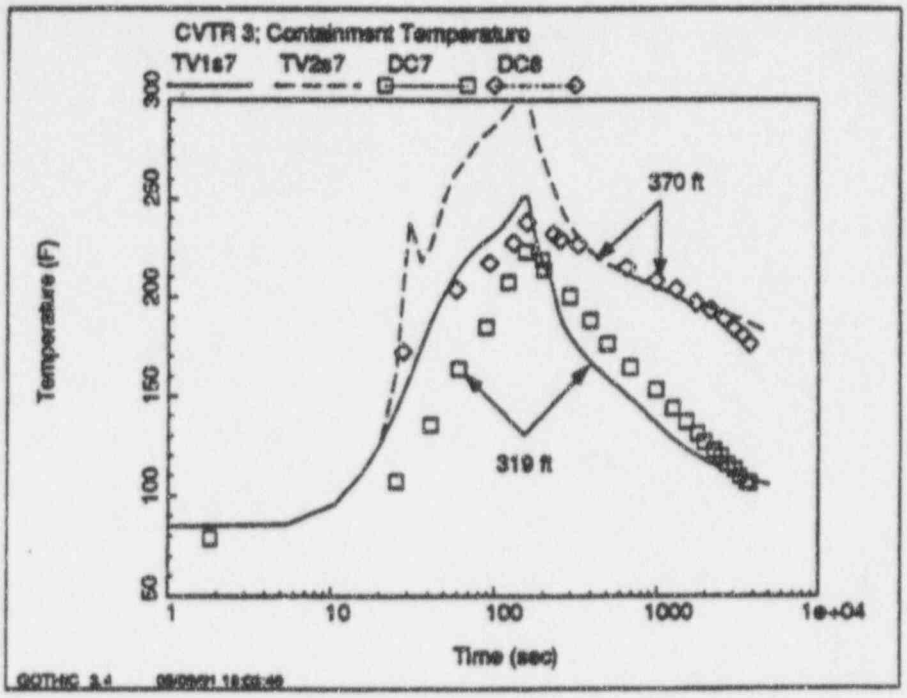

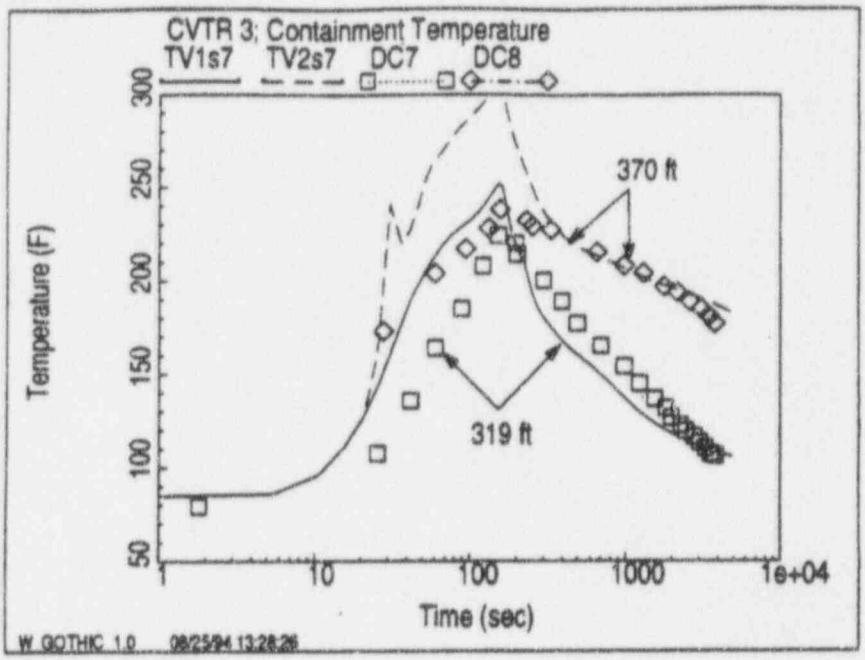

Figure D-33 Containment Temperatures; CVTR Test 3

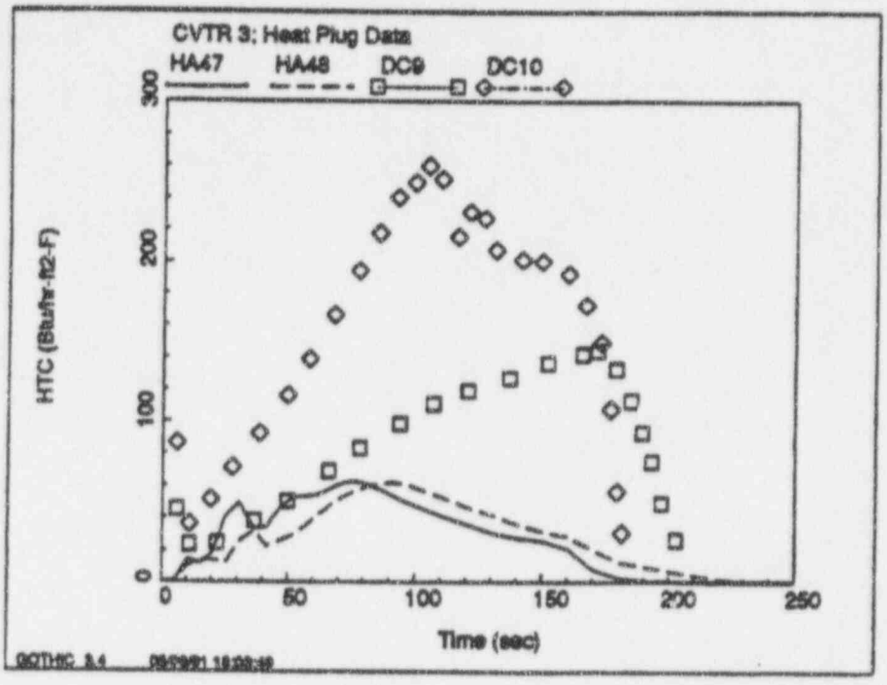

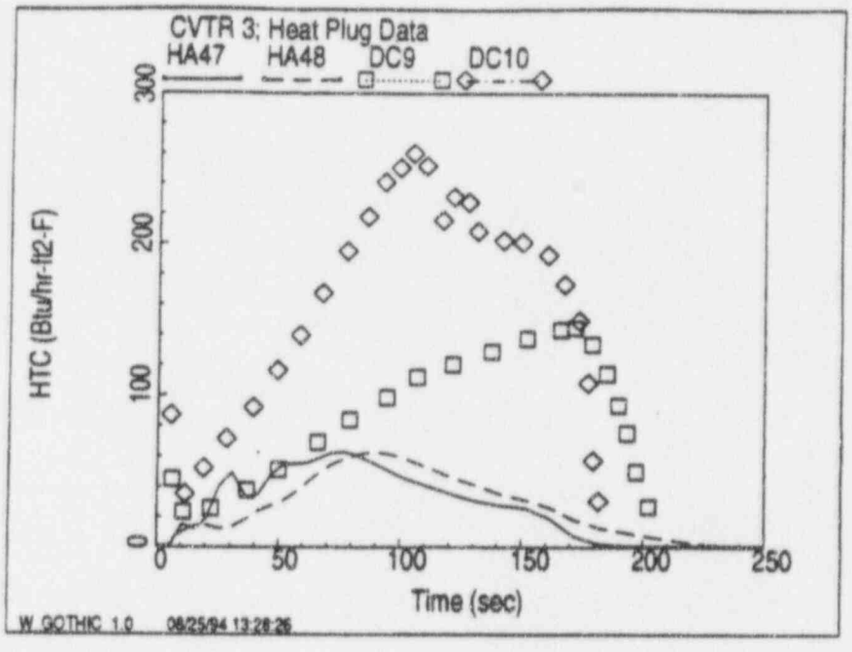

Figure D-34 Heat Transfer Coefficients; CVTR Test 3

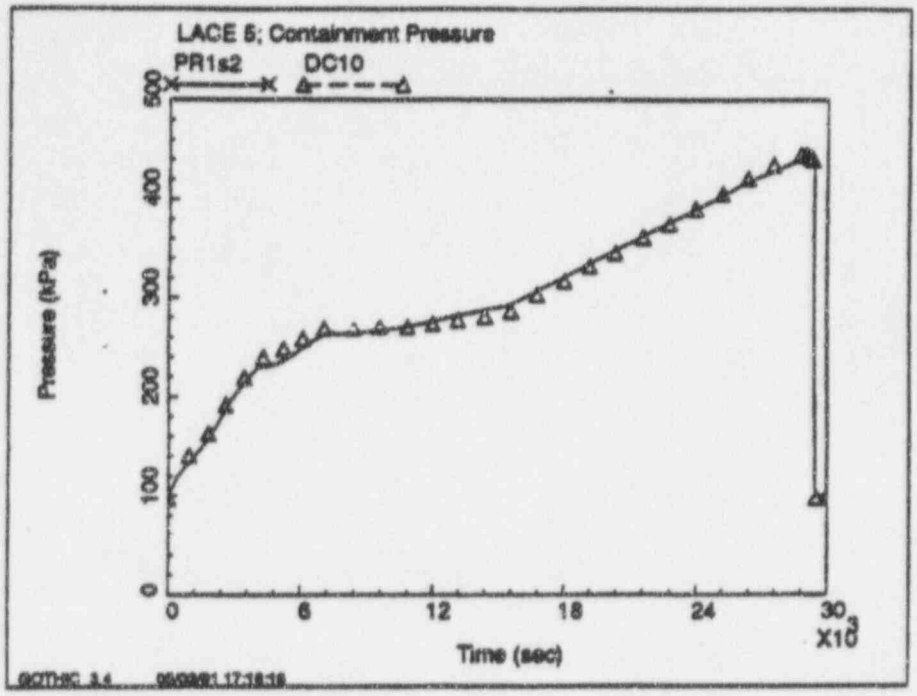

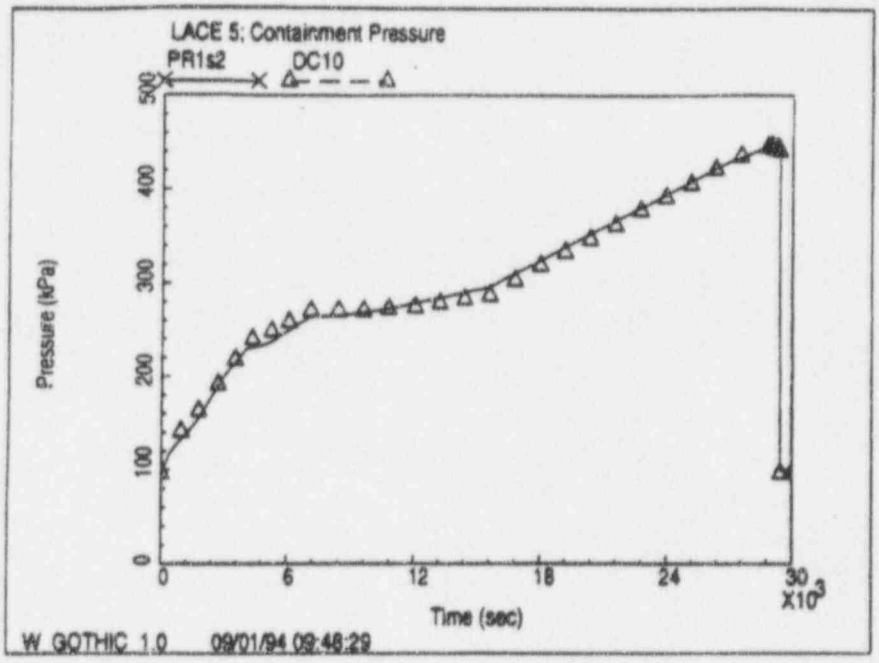

Figure D-35 Containment Pressure for LACE Test LA-5

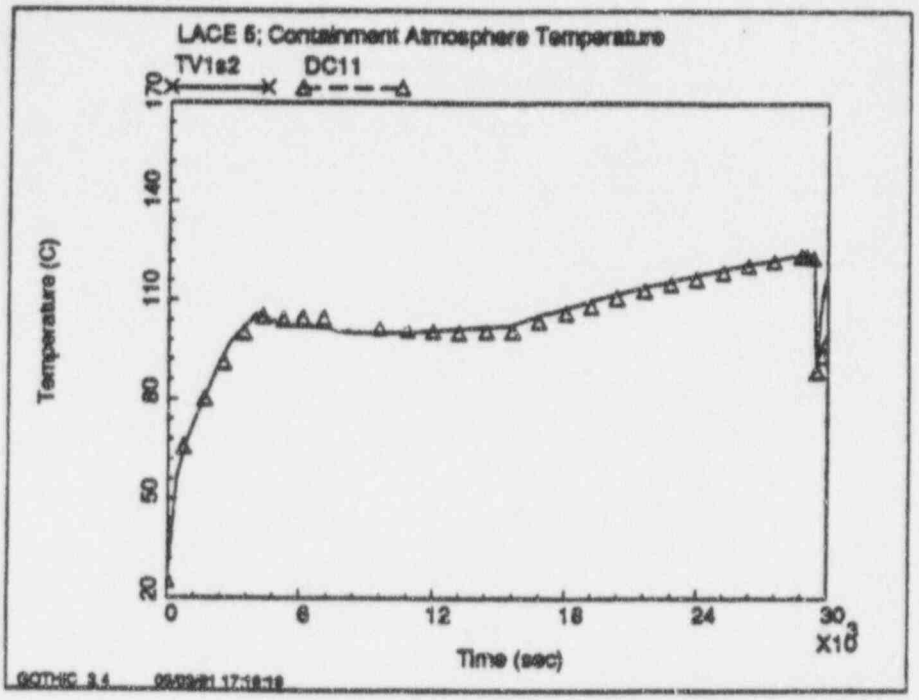

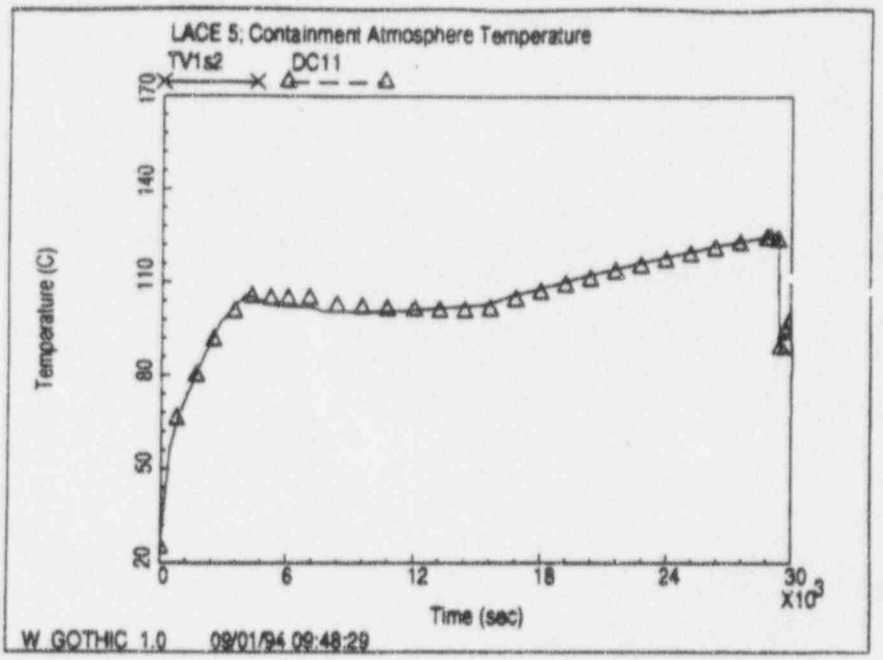

Figure D-36 Containment Atmosphere Temperature for LACE Test LA-5

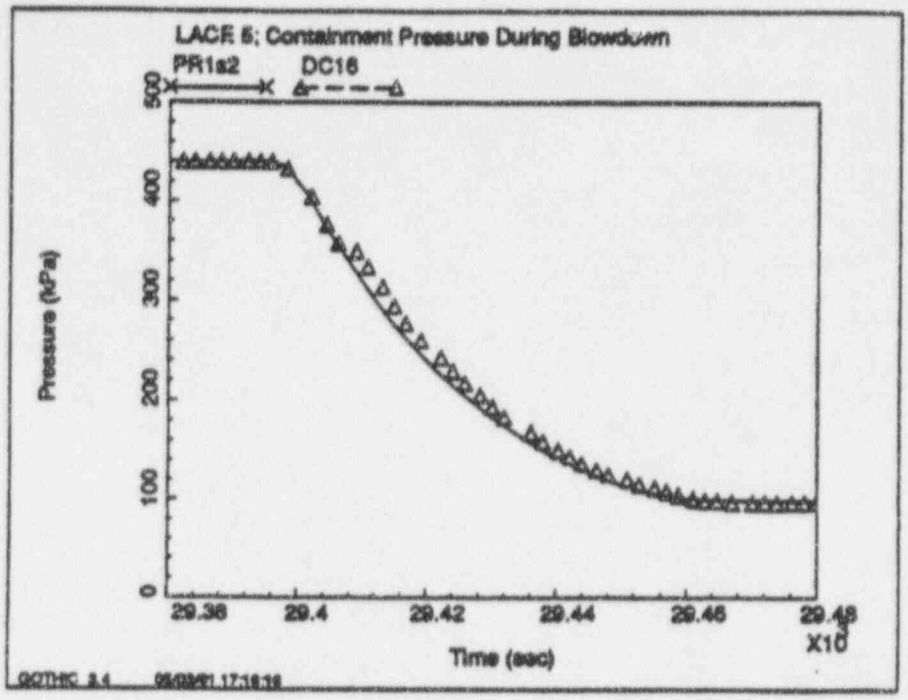

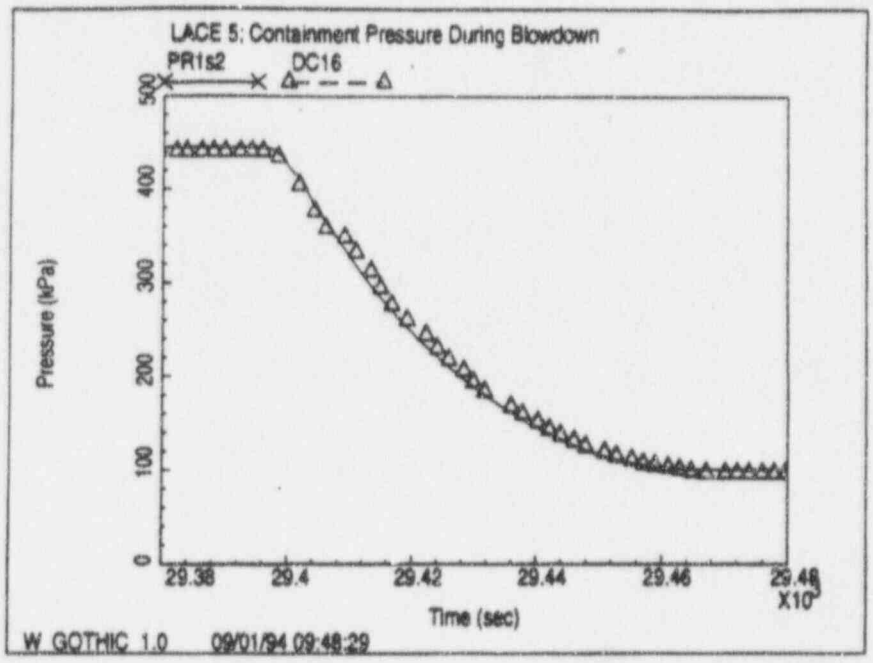

Figure D-37 Containment Atmosphere Temperature During Blowdown for LACE Test LA-5

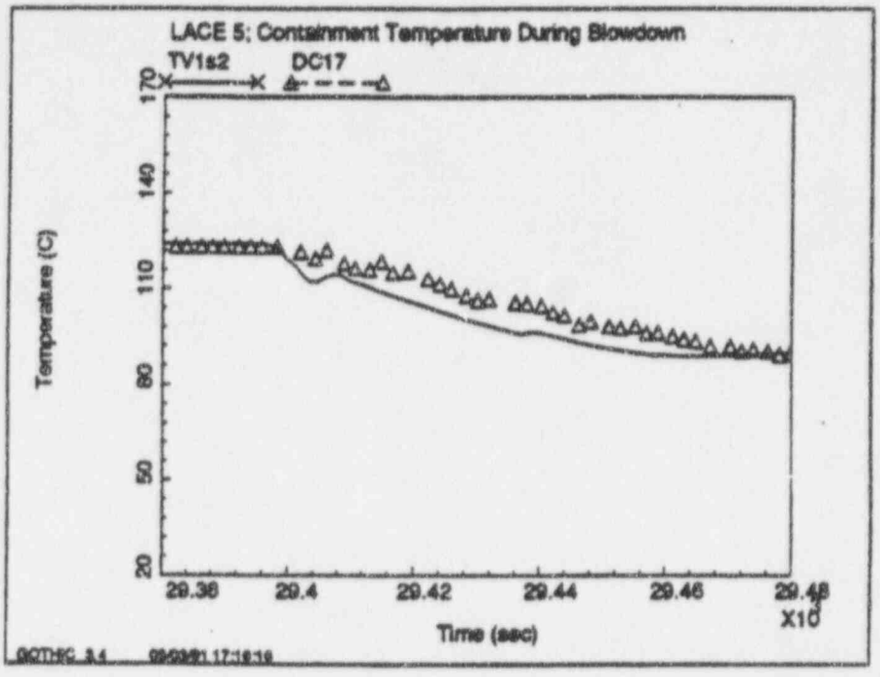

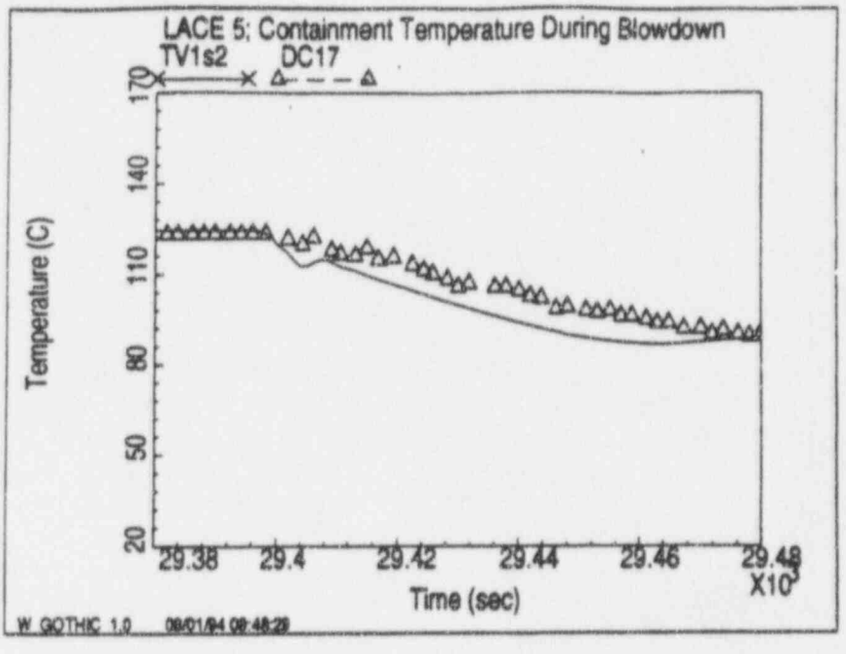

Figure D-38 Containment Atmosphere Temperature During Blowdown for LACE Test LA-5

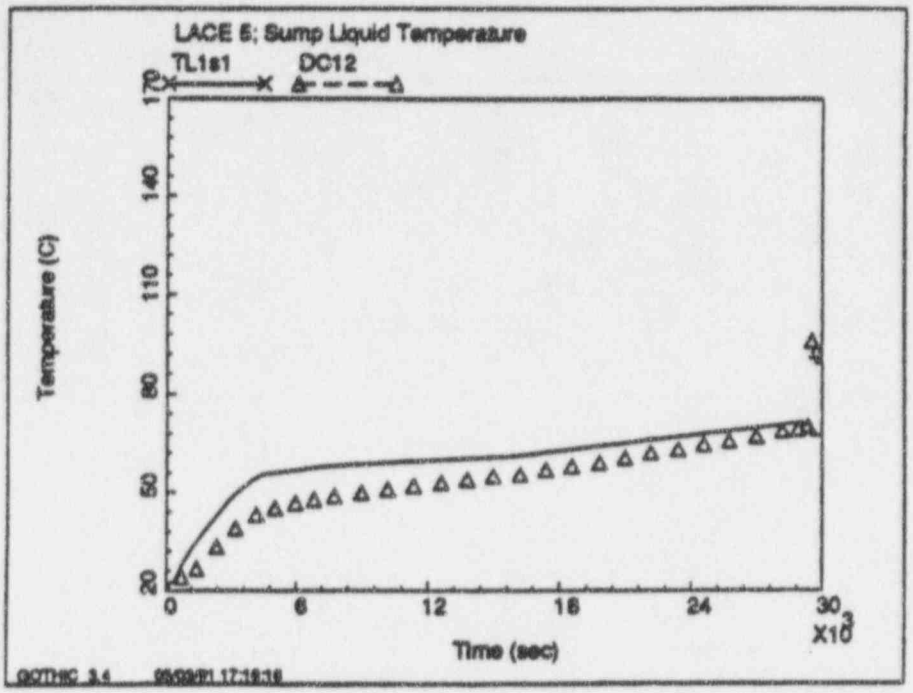

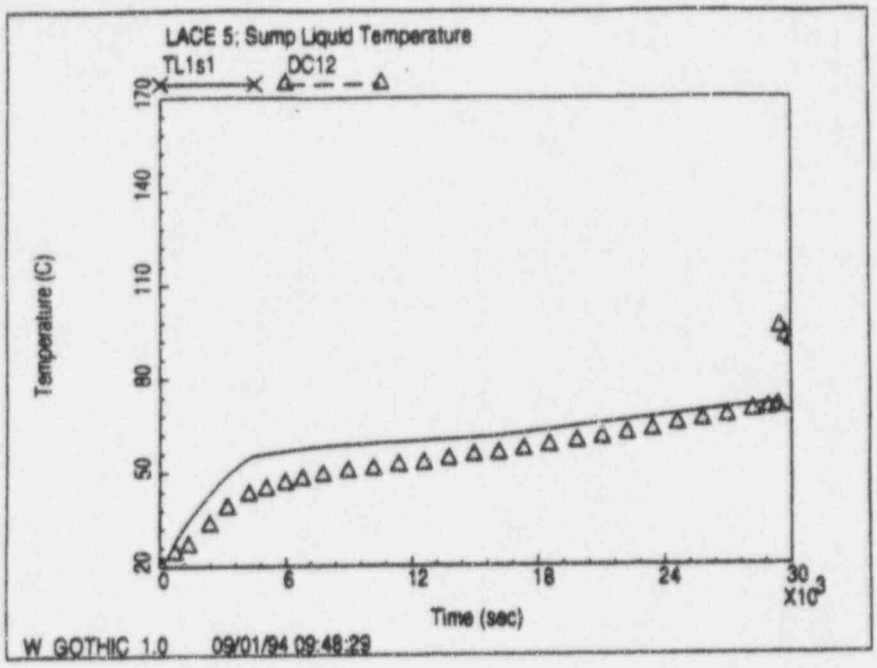

Figure D-39 Sump Liquid Temperature for LACE Test LA-5

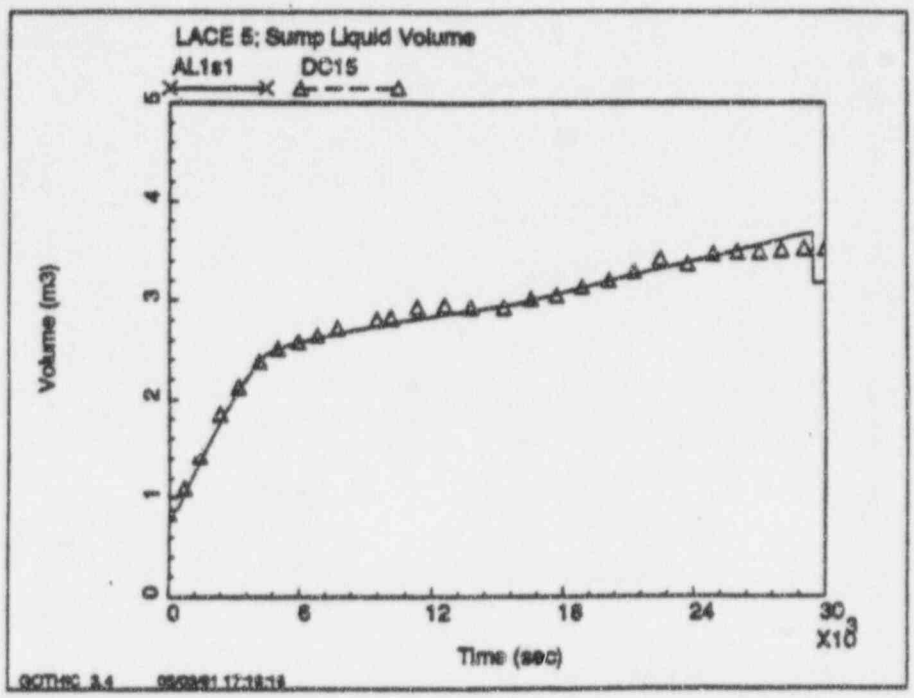

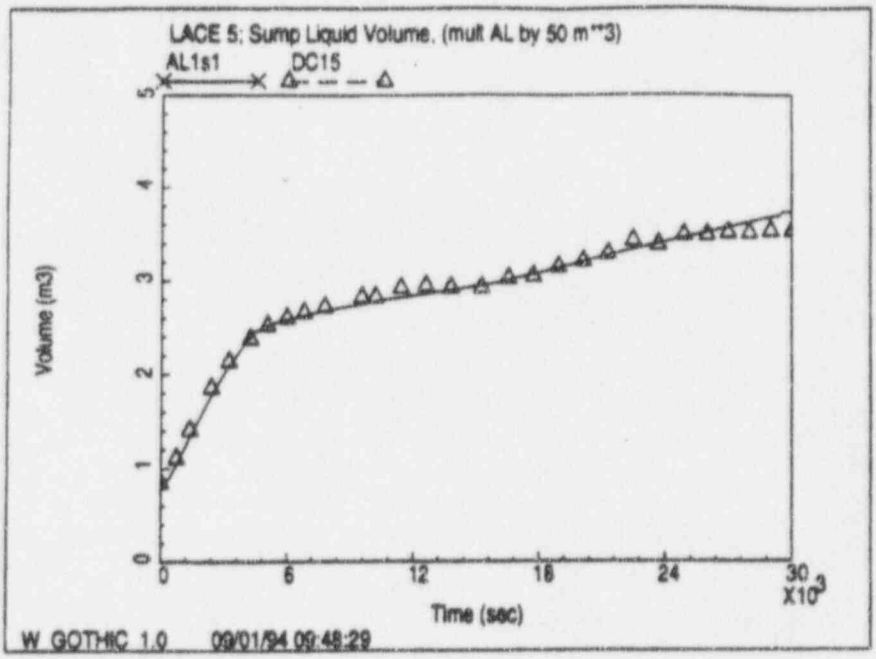

Figure D-40 Sump Liquid Volume for LACE Test LA-5

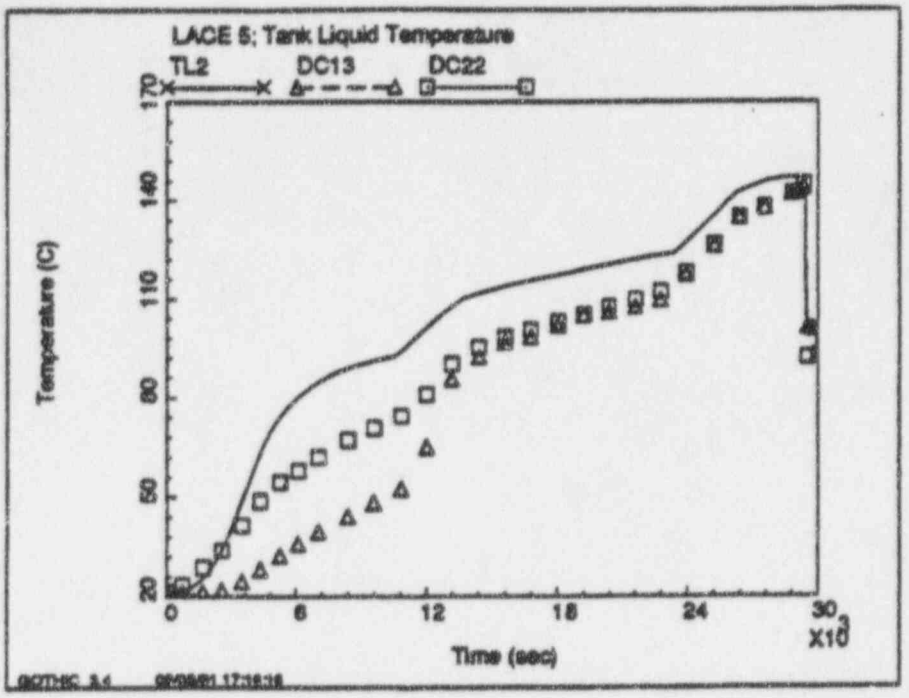

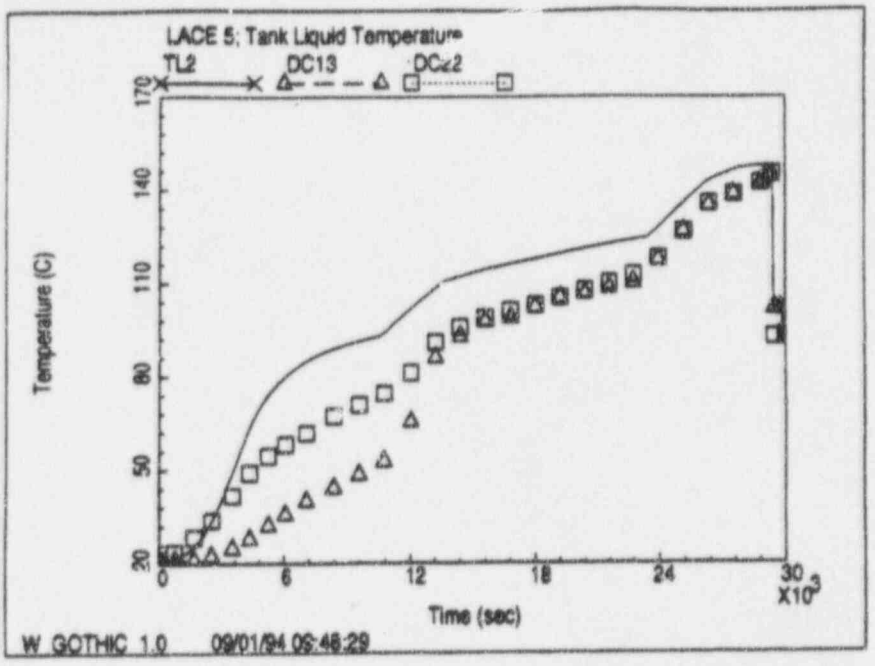

Figure D-41 Tank Liquid Temperature for LACE Test LA-5